The identification and classification of variability in stellar sources observed with SuperWasp

Thesis

The Identification and Classification of Variability in Stellar Sources Observed with SuperWasp

A thesis submitted in partial fulfilment of the requirements for the Open University's Doctor of Philosophy Degree in Physics & Astronomy

Stanley G. Payne MSc. BSc. (Honours), FIAP
M3875063
September-2012

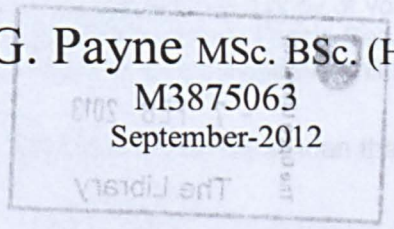

DATE OF SUBMISSION: 29 SEPTEMBER 2012

DATE OF AWARD : 21 JANUARY 2013

IMAGING SERVICES NORTH
Boston Spa, Wetherby
West Yorkshire, LS23 7BQ
www.bl.uk

CONTAINS CD

Abstract

The purpose of this thesis was to create an automated classifier for periodic stellar objects in the Wide-Angle Search for Planets Survey (SuperWASP) and to use the classified stars to investigate three phenomena: differentiation of Beta Lyrae and W UMa eclipsing binary stars using eclipse-depth ratio; identification of RR Lyrae stars exhibiting the Blazhko effect; and, the presence of the Oosterhoff dichotomy in the Milky Way.

During this work, period/amplitude ranges and distribution maps were created for the classified stars in stellar classes Algol, Beta Lyrae, W UMa, Delta Scuti and RR Lyrae (RRAB) and comparison made with published equivalents. SuperWASP objects known in the General Catalogue of Variable Stars (GCVS) were also assessed to identify differences.

The automated system contained three neural networks (NNs) that processed parameters defining the shape of the phase-folded light-curve and they were trained with representative sets of eclipsing binary, pulsating and sinusoidal-like stars. The system, installed at Leicester University processed 4.3 million object/periods from the SuperWASP database, of which 1.1 million were given prospective classifications. From these, approximately 64 thousand objects consisting of eclipsing binary and pulsating stars were assessed manually to confirm the given period/classifications and roughly half were classified correctly. The reasons for the misclassifications were identified and recommendations made on improving the results.

The manually confirmed objects consisted of 12,882 Algols, 5,226 Beta Lyrae, 2,875 W UMa, 1,979 Delta Scutis and 8,322 RR Lyraes (RRAB), where significant numbers of each were unknown in SIMBAD or the GCVS. Many objects had periods and/or amplitudes outside published ranges with the surprising result that the majority of Beta Lyraes had periods shorter than published.

A separation range for eclipse-depth ratio was identified but a cross-over point existed where differentiation was not possible. A number of new RRAB Blazhko stars were identified and the amplitude range between peaks calculated. The presence of the Oosterhoff dichotomy in the Milky Way galaxy was supported, but the causative factors could not be confirmed.

Comparison of the SuperWASP periods with the GCVS resulted in 649 variable stars being added to the GCVS catalogue where the period was unknown in the GCVS and also revision of the variability period of 194 GCVS variable stars was suggested. For comparison of classification, sub-classes were suggested for 333 unconfirmed objects in the GCVS (e.g. CEP:, EA:, RR etc.) and re-classification was suggested for 197 GCVS objects with suspected incorrect classes.

---------- o ----------

Acknowledgements

Completing this PhD has been one of the most character-building tasks I have every undertaken... and one of the most enjoyable.

I could not have achieved this task without the help of some special people. Firstly, I would like to thank those who have supervised me over the years: Andrew Norton at the Open University, Peter Wheatley at the University of Warwick and Richard West at the University of Leicester. Without their support and guidance, I would have tied myself up in knots. Their enthusiasm at our face-to-face meetings was awesome and I felt more enthused after each meeting. Thanks guys.

One other person deserves a special mention: my wife Siân. Not only did she keep me fed and watered through the years (well, wined really), she also kept me sane. At times when I was about to throw in the towel, she provided discussion, persuasion and on occasion, the 'whip'. I am really grateful for the proof reading that she did, but she could have chosen a different colour pen – pink just doesn't suit me. Thanks for the support Tipsy; I couldn't have done it without you.

I'd also like to thank my children Deryth, Rhydian and Geraint for leaving me alone over the years. They must have thought they were from a single-parent family. You've got your father back now kids – remember me! Thanks for your support, and Rhydian – thanks for the heated debates on certain astronomical concepts.

Next, to two people without whom, there would have been no degree, masters or doctorate: to my Mum (Eunice) and Dad (Kenneth). They instilled in me at an early age an inquisitive nature and a level of persistence that I have put to good use over the years. I'm sure they would be proud of me – I certainly am of them. Thank you both.

I am grateful to the SuperWASP consortium[1] for providing the observational data necessary for me to perform this research.

I am also grateful to the General Catalogue of Variable Stars (GCVS[2], Samus+ 2004) for providing the background information which formed the basis of my research proposal.

This research has made use of the 'Set of Identifications, Measurements, and Bibliography for Astronomical Data' database (SIMBAD[3], SIMBAD4 1.194 - 26-Apr-2012), operated at CDS, Strasbourg, France.

---------- o ----------

[1] *SuperWASP is a consortium of: Queen's University Belfast, University of Cambridge, Isaac Newton Group of Telescopes (La Palma), University of Keele, University of Leicester, Open University, and the University of St Andrews*
[2] *http://www.sai.msu.su/gcvs/gcvs/*
[3] *http://simbad.u-strasbg.fr/simbad/*

Contents

List of Figures

List of Tables

List of Equations

List of Abbreviations

Abbreviation	Meaning
ASAS	All Sky Automated Survey
BMA	Binned Magnitude Amplitude
Detrend	The de-trending technique run on the object before the period is calculated
DSCT	Pulsating star - Delta Scuti-type
EA	Eclipsing Binary star – Algol-type
EB	Eclipsing Binary star – Beta Lyrae-type
EW	Eclipsing Binary star – W UMa-type
GCVS	General Catalogue of Variable stars (http://www.sai.msu.su/gcvs/gcvs/)
HNS	Human nervous system
MLP	Multiple-layer Perceptron neural network
NN	Neural network
PFlag	A flag given to the calculated period for each object in the SuperWASP archive. The flag indicates a 'caution' level i.e. 0 means a period not matched to the rotation of the Earth and thereby it is a 'good' period. PFlag 1 means that the period is between 0.9 and 1.3 days and may therefore not be a true period. Many other flags are present and they can be seen in Chapter 5.
RM	Rotational Modulation Star (also known as Sinusoidal-type star)
RRAB	Pulsating star - RR Lyrae-type (type AB)
RRC	Pulsating star - RR Lyrae-type (type C)
SIMBAD	The 'Set of Identifications, Measurements, and Bibliography for Astronomical Data' database (http://simbad.u-strasbg.fr/simbad/)
SLP	Single-layer Perceptron neural network
SOM	Self-organising map neural network
SuperWASP	All-sky survey 'Wide-Angle Search for Planets'
UCAC2	Second U.S. Naval Observatory CCD Astrograph Catalog (Zacharias et al. 2004)
2MASS	2 Micron All-Sky Survey (Skrutskie et al. 2006)

Note: This thesis is supported by two DVD's that contain supplementary information if the reader is interested.

At the appropriate point in each chapter, the reader is directed to the relevant location on the required DVD. Additionally, each DVD has a 'ReadMe.txt' file in the root directory explaining the contents of each DVD. The file can be opened with any basic ASCII text editor.

Chapter 1 Introduction

We have it on good authority from Douglas Adams that "Space is big. In fact, you just won't believe how vastly, hugely, mind-bogglingly big it is". Nobody knows this better than a researcher looking for the elusive stellar objects that they require for their work. This research has brought together principles of astronomy and neural network technology in order to identify and classify variable stellar objects in large astronomical surveys in order to support these researchers.

1.1. History

Paczynski (1997) argued that a complete inventory of variable stars would improve our understanding of stellar evolution and Galactic structure. He suggested that cataloguing detached eclipsing binaries would improve the measurement of the distance scale and the value of the Hubble constant, and hence the age of the oldest stars.

Wide-field sky surveys can now capture variability information across the whole sky, allowing us to complete a census of variable stars and therefore realise Paczynski's ideals. The data from these surveys allow us ultimately to improve the cosmic distance scale (Bird et al. 2009) and study Galactic structure using distance indicators (Prior et al. 2009). It also allows us to study stellar distribution (Maciel & Costa, 2008), stellar structure (Bono et al. 2011), stellar evolution (Feast, 2008) and stellar activity and rotation (Biazzo et al. 2009a). We can also look at system parametrics using eclipsing binaries (Zasche, 2008, Zasche et al. 2008, 2009) and investigate anomalies like the Blazhko effect (Blazko, 1907, Kovács, 2009) and the Oosterhoff Dichotomy (Oosterhoff, 1939).

Since 1997, a number of large surveys have been introduced to obtain a phenomenal amount of data to help realise these objectives. For instance, the 'All Sky Automated Survey' (ASAS) (Pojmański, 1997) captured data for 100 million stars brighter than

magnitude 14 all over the sky, with the ultimate goal of the project being the detection and investigation of any kind of photometric variability. The Robotic Optical Transient Search Experiment (ROTSE) (Akerlof et al. 2000) has a primary goal to achieve observations in optical light of Gamma-Ray Bursts, but other interests include the detection of variable stars. The Amateur Sky Survey (TASS) (Richmond et al. 2000) in 1996-1998 studied bright objects across large sections of the sky. They created a catalogue of 206 million observations of over 10 million stars. In addition to these, a number of institutions or consortia have initiated long term projects searching for transiting extra-solar planets e.g. the Hungarian-made Automated Telescope (HAT) (Bakos et al. 2002); the XO Project (McCullough et al. 2005); the Trans-Atlantic Exoplanet Survey (TrES) (O'Donovan & Charbonneau, 2007); the University of New South Wales Extrasolar Planet Search (Christiansen et al. 2007); the RApid Temporal Survey (RATS) (Ramsay & Hakala, 2005, Ramsay et al. 2006); and the Wide-angle Search for Planets (SuperWASP) (Pollacco et al. 2006).

1.2. Objectives

The main problem with these large surveys is that they contain literally millions of stars, and the time taken to identify the variable stars and to classify them is prohibitive. Only automated processing methods are able to digest and process this amount of data. The primary objective of this research was therefore to create an automated classifier for variable stars that provided preliminary classifications for all the periodic stars in a given survey i.e., SuperWASP (Pollacco et al. 2006). This allowed two secondary objectives. Firstly, to manually confirm the following pulsating and eclipsing variables: Delta Scuti-type (DSCT), RR Lyrae-type (RRAB), Algol-type (EA), Beta Lyrae-type (EB) and W UMa-type (EW), and secondly, to create stellar catalogues for each of these classes of

objects. This was done to test that the proposed method of classification was acceptable for use and to provide objects for the following tertiary objectives:

- Reviewing the periodicity and classification of SuperWASP identified stars known in the General Catalogue of Variable Stars (GCVS, Samus+, 2004). This provided good classified stars to train and test the NNs with and also gave mutual confirmation that the automated classifier was identifying known stellar objects and that the GCVS had the correct period and class.
- Identifying period and amplitude ranges for the eclipsing and pulsating stars indicated above and comparing them against published ranges.
- Creating distribution maps for the eclipsing and pulsating stars indicated above.
- Investigating the use of the eclipse-depth ratio to differentiate between the eclipsing classes EB and EW.
- Calculating distances for the identified RRAB stars and using them to create a 3D map of our galaxy.
- Investigating the Blazhko effect in the identified RRAB stars.
- Investigating the Oosterhoff Dichotomy in the identified RRAB stars.

This research made use of the data from the SuperWASP archive[4], whose primary aim is the discovery of extra-solar planets using the transit method. In this research, the suitability of the very large dataset in the SuperWASP survey (10^{11} observations) was assessed to identify the periodic variable stars and then provide a classification for them through the use of an automated classifier. The automated classifier created was limited to photometric observations made in the visible band, and the classification method involved the use of the period, amplitude and shape of the light-curve. This meant that the classification obtained was only a preliminary one, but this was necessary in order to provide an automated method that could be used with the data from any survey. Processing all the data in the SuperWASP survey minimised the size of the dataset used for the secondary and tertiary objectives.

[4] *The WASP archive contains all the light curve data and images for a large number of stars in both the Northern and Southern hemispheres. Butters et al. (2010) describes the contents of the archive available to the public, but this research used the data from the private archive prior to release to the public.*

1.3. Motivation

I have been interested in astronomy since childhood, but career choice and family pressures steered my direction of study away from my passion. Having completed formal study over the past 20 years and reaching a comfortable position, I am now able to return to my passion - with a vengeance.

As soon as I heard of the SuperWASP collaboration project, I realised this provided an opportunity for me to combine the knowledge I gained over the years in Neural Network Technology with my passion for astronomy to help analyse the SuperWASP data and provide a baseline for other researchers.

As previously mentioned, identification and classification of variable stars is a time consuming and tedious task for researchers. Use of artificial neural networks (NN) can speed up the classification process by identifying those stellar variables that are similar to a given training set of variables based on the class of the object (e.g. Cepheids, Algols, Beta Lyrae, W UMa, RR Lyrae etc.). The pattern-matching capabilities of NNs are well known and allow millions of stellar objects to be scanned and given a 'prospective' classification for researchers to perform follow-up investigations to confirm the class. Use of NNs enables researchers to concentrate on a far smaller set of objects and therefore reduce the time taken and overall cost of the research.

In order to construct NNs for automated classification of stellar variables, observational data for a number of variables of known 'stellar class' were required to train and test the NNs. The SuperWASP detection program (Pollacco et al. 2006) collects observational data for stellar objects in both hemispheres of the sky and the archive provides access to this

data. The archive is cross-referenced with the GCVS[5], which is one of the main repositories of variable objects. This allowed SuperWASP objects to be selected and retrieved by the GCVS class and provided an ideal opportunity to model a set of neural networks that use the shape of the phase-folded light-curve as an input (along with certain other parameters).

1.4. Description of SuperWASP

SuperWASP[6] is the UK's leading extra-solar planet detection program comprising of a consortium of eight academic institutions. SuperWASP consists of two robotic observatories. The first, SuperWASP-North, is at the Isaac Newton Group of telescopes located on the island of La Palma in the Canaries. The second, SuperWASP-South, is located at the site of the South African Astronomical Observatory (SAAO), just outside Sutherland, South Africa. The observatories are identical and consist of 8 wide-angle cameras that simultaneously capture the magnitude of stellar objects. Each camera consists of a 2048 × 2048 pixel thinned Marconi CCD and a Canon 200mm f/1.8 lens. This combination gives each camera a 7.8 x 7.8 square degrees field of view for a total of nearly 500 square degrees of sky coverage, in a magnitude range of approximately 7 to 15. The pixel size of 13.5μm means that the plate scale is 16.7 arcsec per pixel (Pollacco et al. 2006).

The data is processed through an automated pipeline to confirm that the raw data is consistent between observing sessions and also converts a series of sky images into light curves for many individual objects. The Vmag values used in this research were obtained from the SuperWASP pipeline as described in Pollacco et al. (2006). The instrumental magnitude is converted into the SuperWASP V magnitude by calibrating and removing

[5] http://www.sai.msu.su/gcvs/gcvs/
[6] *http://www.superwasp.org (01-Aug-2012)*

four main trends in the photometry using extinction coefficients determined from an iterative least-squares fit to the variation of raw magnitude with air mass through the night for a sample of stars with colours defined in the Tycho-2 catalogue. Once the instrumental magnitudes have been corrected to a standard air mass near the middle of the observed range, a linear equation for the instrumental colour response and zero point of each camera is used to transform the instrumental magnitudes to a system defined by the Tycho-2 V bandpass. Their standardised magnitudes as determined over a few photometric nights are subsequently used to define the "WASP V" magnitude system for the field concerned. The night-to-night variations using this system are <0.002 mag and are therefore deemed reliable.

The observations for each stellar object and their variability period, determined using the method of Norton & Payne et al. (2007) are stored in a database (known as the SuperWASP archive in this research). Currently (Nov. 2012) 321,144,914,057 data points are held in the archive covering 30,874,261 unique objects. This data can be retrieved across the Internet for further analysis (Butters et al. 2010) via a simple web based interface at www.wasp.le.ac.uk/public/ – such as for classification by a neural network.

The naming convention for each object in the SuperWASP archive follows IAU conventions, so each object is assigned a unique name based on their first, best measured co-ordinates. For objects measured by catalogue-driven photometry, the co-ordinates are taken directly from the USNO B-1.0 counterpart (Monet et al. 2003). The form of the SuperWASP catalogue name is therefore as follows:

1SWASP Jhhmmss.ss±ddmmss.s

It is an unfortunate property of the USNO B-1.0 catalogue in that it is quite common for catalogue entries to be degenerate, i.e. contain multiple entries for a single celestial object.

Neither the SuperWASP pipeline nor the archive has made any attempt to rectify this situation, and as a consequence the catalogue contains multiple, uniquely-named objects which are records for the same, single celestial object. For this reason when searching objects that are in the GCVS, more than one (genuinely) matching SuperWASP object may be retrieved.

1.5. Understanding variability

Variability in stellar objects simply means the change in magnitude of light over a period of time. To explain, take a star like HD209458 (in the constellation Pegasus) observed continuously over a period of 3.5 days, we would see the light from the star vary periodically. This is because we suspect that there is a planet the size of Jupiter orbiting the star and obscuring a fraction of the surface on each orbit as shown in Figure 1-1.

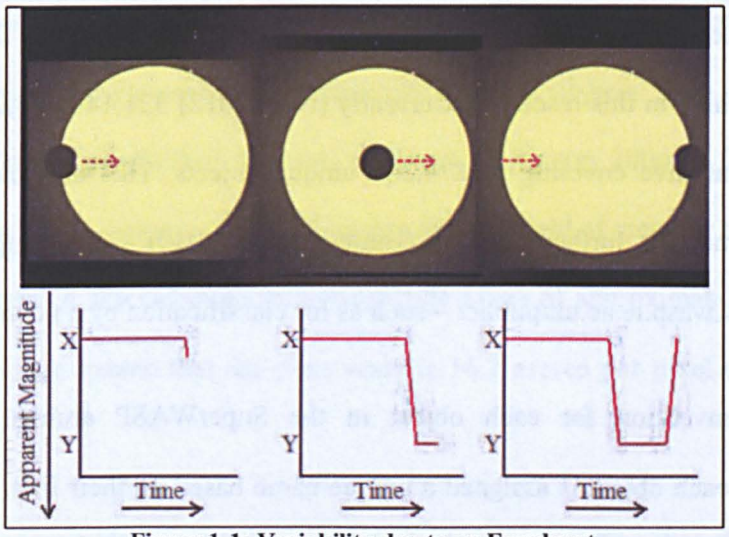

Figure 1-1: Variability due to an Exoplanet

The light-curve below the three images tracks the apparent magnitude coming from the star as the planet moves in front of it. The final light-curve shape can be seen in panel (a) in Figure 1-4.

To pick another example - if we look at a star like Algol (in the constellation Perseus) constantly over a period of 68.75 hours, it would also vary periodically. This is because it

is not one star, it is actually two stars (known as a binary star) and they periodically eclipse one another as shown in Figure 1-2.

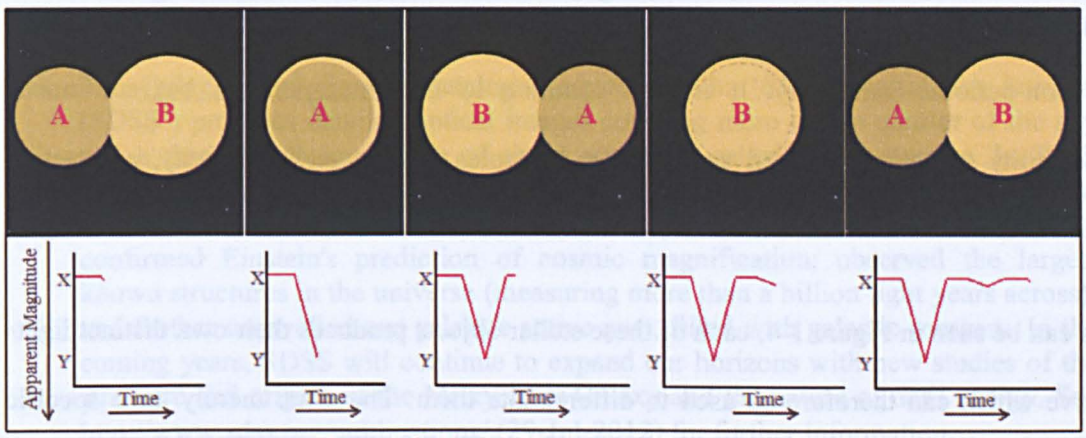

Figure 1-2: Variability due to a binary star

As a final example - looking at SN1987A (in the Large Magellanic Cloud) today, all we will see is a remnant of a star. This is because the star went supernova in 1987 - producing as much light output as usually given by a galaxy as shown in Figure 1-3. The first picture shows the star at its usual magnitude, the second picture shows a far greater magnitude during the supernova explosion and the third picture shows a far lower magnitude after the explosion.

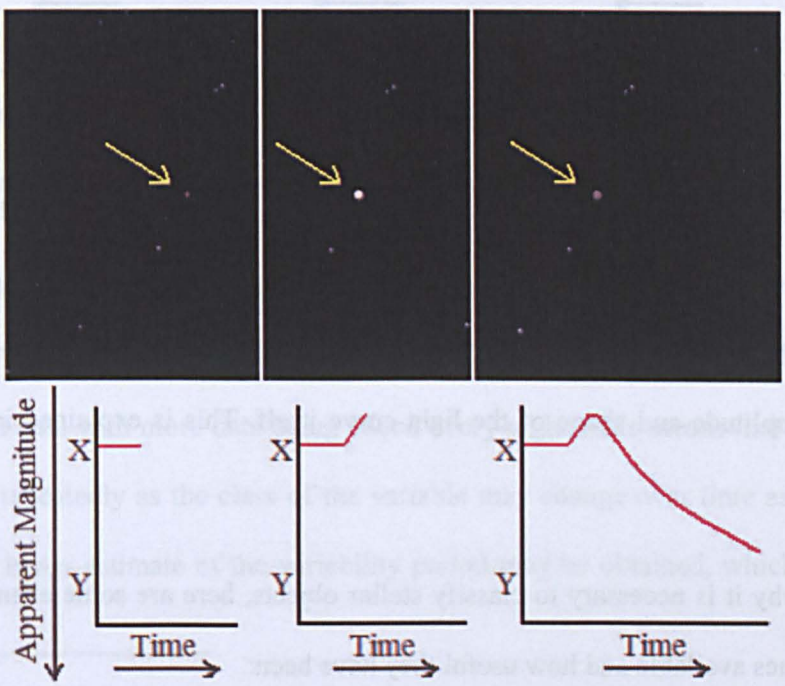

Figure 1-3: Variability due to a supernova

These three relatively common examples of variability show how the light output from stars can vary. The first two examples are known as periodic variability, as they are repetitive in nature, i.e. 3.5 days and 68.75 hours respectively. The third example is known as non-periodic variability. It is also common to have non-periodic but continuous variability (usually described as "noise"); examples include stellar activity, and active galactic nuclei.

As can be seen in Figure 1-4, each of these stellar objects produces their own distinct light-curve which can therefore be used to differentiate them. These are merely three specific examples of variability out of many possibilities – the first two of which may be characterised as extrinsic, and the last as intrinsic, to the stellar system. Further types of variability of both kinds will be described in Chapter 2 (section 2.1).

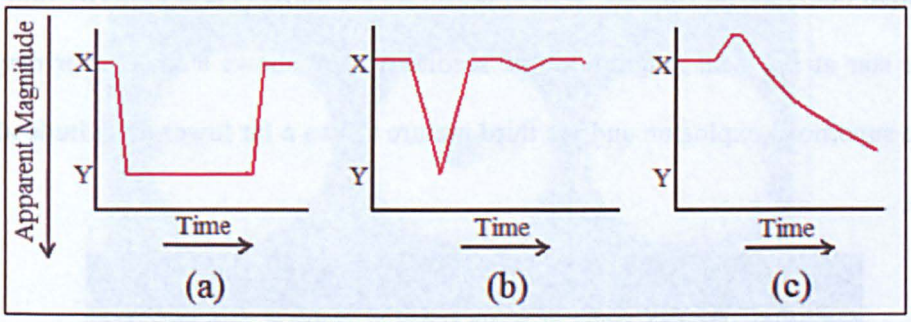

Figure 1-4: Comparison of light-curves
(a) Exoplanet, (b) binary star, (c) supernova

For this research, the work was limited to 'periodic' variability, so the method used to classify these stellar objects was based on that provided by the GCVS, which involved looking at the light-curve for each object and matching it to the criteria given in the GCVS e.g. period, amplitude and shape of the light-curve itself. This is explained in Chapter 2 (section 2.2).

To illustrate why it is necessary to classify stellar objects, here are some examples of the public catalogues available and how useful they have been:

- Eclipsing binaries (and other variables) e.g. the catalogue of short-period variables and catalogue of variable stars I, II, III, IV and V in the 'All Sky Automated Survey' (ASAS) (Pojmański, 1997, Pojmański et al. 2006). This survey has catalogued 50,000+ variable stars for use by researchers and has discovered comets, novae and dwarf novae.

- The Galaxies and Quasars catalogue created by the 'Sloan Digital Sky Survey' (SDSS[7]) provides detailed optical images covering more than a quarter of the sky and a three-dimensional map of about a million galaxies and quasars. In 2006, SDSS advanced mankind's understanding of the universe with several new discoveries. The survey found new dwarf companion galaxies to the Milky Way; confirmed Einstein's prediction of cosmic magnification; observed the largest known structures in the universe (measuring more than a billion light years across); and further unravelled our galaxy's active past, filled with galactic mergers. In the coming years, SDSS will continue to expand our horizons with new studies of the structure and origins of the Milky Way Galaxy and the nature of dark energy. See http://www.sdss.org/publications/ (29-Jul-2012) for further information.

- The Supernovae catalogue created by the Supernova Cosmology Project (Perlmutter et al. 1997) studied high-redshift supernovae that can be used to measure cosmological parameters.

- The catalogue of micro-lensing events created by the Optical Gravitational Lensing experiment (OGLE) (Pietrzynski & Udalski, 1999) regularly monitored 130 million stars in the Galactic Bulge and 33 million stars in the Magellanic Clouds. More than 500 lensing events were detected during each Bulge season (year). They have catalogues of Red Giants, Eclipsing binaries, RR Lyrae stars and Population II Cepheids. All these catalogues/surveys help to calculate stellar distances and map the universe.

Basically, these surveys help us to answer large-scale questions like how the universe began, how it is developing and how is it going to end. Chapter 2 (section 2.3) provides detailed examples of the work performed by other researchers.

The variables identified in these surveys are held in various catalogues, such as the GCVS, Hipparcos, and TYCHO catalogues, and these surveys provide an abundance of observational data with more data being added every night. This means that the data must be analysed repeatedly as the class of the variable may change over time as more data is added e.g. a better estimate of the variability period may be obtained, which may change

[7] *http://www.sdss.org/ - 29-Jul-2012*

the object class for classifications that depend on the difference in period, for instance DSCT and RRAB stars. Performing 'repeat' analyses manually would take many lifetimes therefore automated methods must be introduced. One method of achieving this classification is employing the pattern-matching abilities of neural networks, which are introduced in the next section.

1.6. Understanding neural networks

Neural networks can be described as mathematical models, used for analysing patterns of data (Picton, 1994). There are many different types, but they all follow the same principles as discussed in Chapter 3. A general example of how NNs were used to classify stellar variables in this research is shown in Figure 1-5.

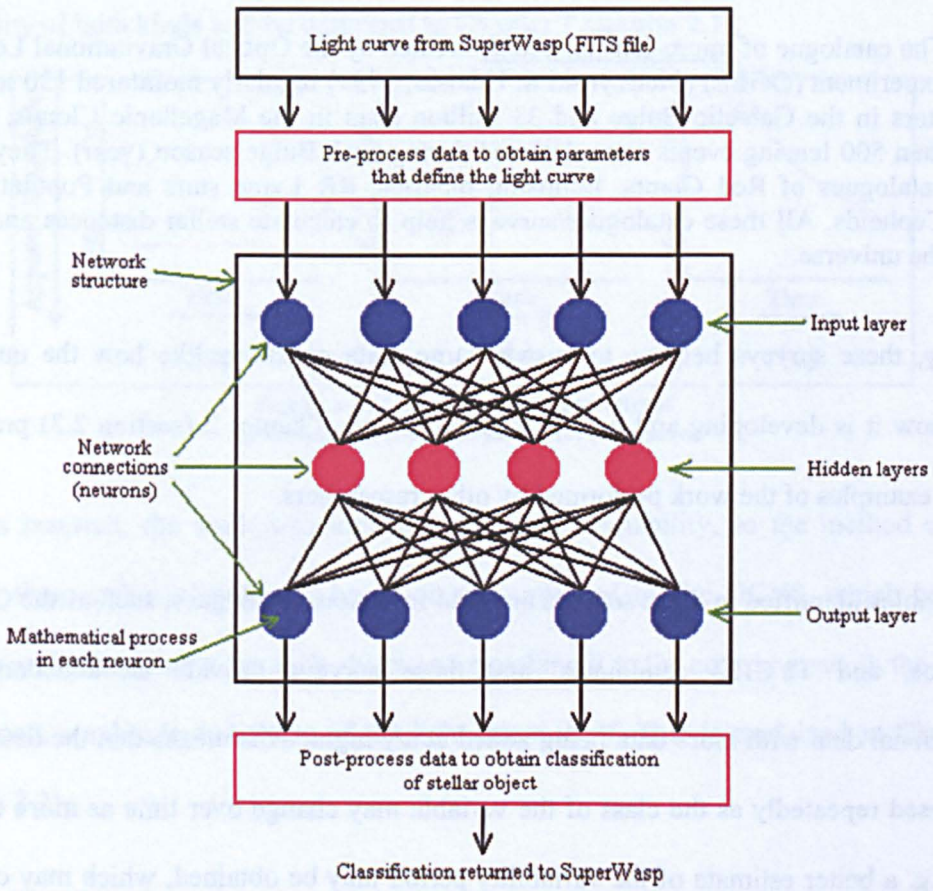

Figure 1-5: Model of a neural network describing its basic principles

Observational data were downloaded from the SuperWASP archive and pre-processed to obtain a set of parameters that represented the light-curve. These parameters were termed light-curve 'patterns' because NNs are known as pattern-matching tools. The NN was trained by repeatedly presenting many examples of 'known' patterns (i.e. classes) to it.

During training, the network 'learned' the different patterns, so that when a test pattern was presented to the trained network, it would indicate which training pattern it was the most similar to. As the training patterns covered all the likely outcomes (i.e. variability class) of the test data and the NN knew the variability class of each of the training patterns, the NN would identify the 'best' pattern match and hence the expected class.

A useful feature of NNs is their ability to generalise, meaning that the training set does not need to contain exact matches for the patterns being tested, in order to identify them. A test pattern that is identical to a training pattern would give a result with a high degree of confidence and a test pattern which was similar to a training pattern would still be identified, but with a lower level of confidence. This type of analysis is 'fuzzy' in nature as there are no definite limits that define a given pattern. A good analogy of this is describing how you feel in hot weather conditions i.e. you say that you feel hot, warm or cold, not that you feel 25°C. There is no precise temperature where you suddenly say that you are hot – it happens gradually. This characteristic of NNs makes them ideal for analysing and classifying stellar variables, as the data generated in the test can be easily transformed into patterns as discussed in Chapter 3.

Although NNs are good at generalising, the level of confidence of the output depends on the quality of the training and test patterns. These patterns must represent all classes to be encountered in the data set and they must be chosen to allow differentiation between each

of the classes. The training patterns must be tested to ensure their suitability to enable 'separability' of the classes. This is described in Chapter 3.

NNs have previously been used to classify stellar variables (see Chapter 2 section 2.4), but these tended to use complex datasets requiring high levels of pre-processing. The method used in this research employed a relatively simple mapping of the light-curve for the object under test and was therefore processed quickly. As the light-curve is based only on visible light, the class assigned by the NNs is preliminary, so any objects classified by this method must be confirmed using other methods such as manual review of the phase-folded light-curve or spectrophotometry. This is a very useful method of initial classification for researchers, as it means they can concentrate on a smaller sub-set of classified objects.

1.7. Proposed method of classification

The set of object classes selected for classification in this research were Cepheid, Delta Scuti, Algols (with a double-eclipse), Algols (with a single-eclipse), Beta Lyrae, W UMa, Sinusoidal-type stars, and RR Lyrae sub-classes RRAB and RRC. They are all described fully in Chapter 2.

The objects required to train and test the NNs needed to be robust representatives of these selected classes with regards to light-curve shape and variability period, therefore a manual review was required for each of the objects to confirm their fitness for purpose. This process is described in Chapter 4, where sixty objects were pre-processed to obtain phase-folded light-curves and modified phase-folded light-curves as shown in panel (a) and (b) respectively of Figure 1-6 to Figure 1-15. The modified phase-folded light-curves were necessary to provide a standard shape light-curve to be processed by a set of NNs. This is fully described in Chapter 3 (section 3.4).

The light-curves were manually reviewed to confirm that they belonged to the required classes and then the patterns required for entry into the NNs were obtained from the modified phase-folded light-curves. Thirty objects for each class were used to train the NNs and the other thirty were used to test them.

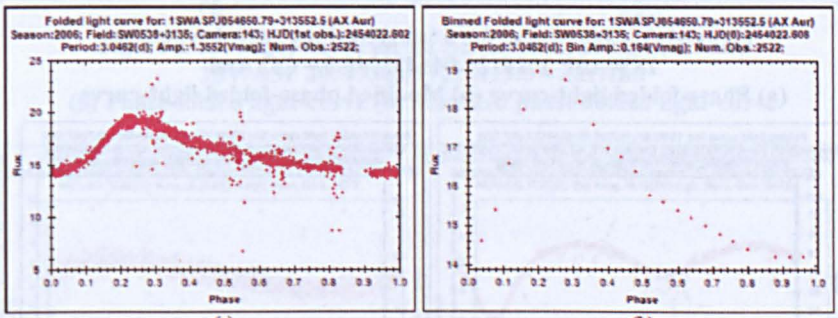

Figure 1-6: Light-curve for a Cepheid-type star
1SWASPJ054650.79+313552.5 - AX Aur
(a) Phase-folded light-curve (b) Modified phase-folded light-curve

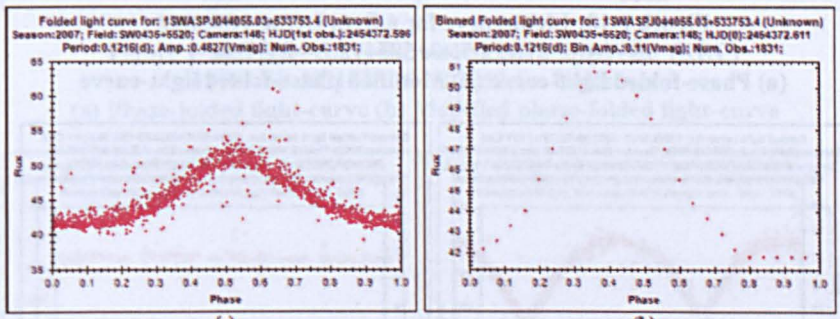

Figure 1-7: Light-curve for a Delta Scuti-type star
1SWASP J044055.03+533753.4 - Unknown
(a) Phase-folded light-curve (b) Modified phase-folded light-curve

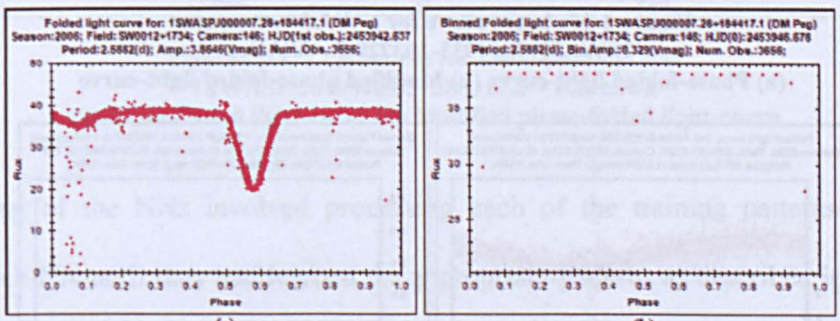

Figure 1-8: Light-curve for a 'double-eclipse' Algol-type star
1SWASP J000007.28+184417.1 – DM Peg
(a) Phase-folded light-curve (b) Modified phase-folded light-curve

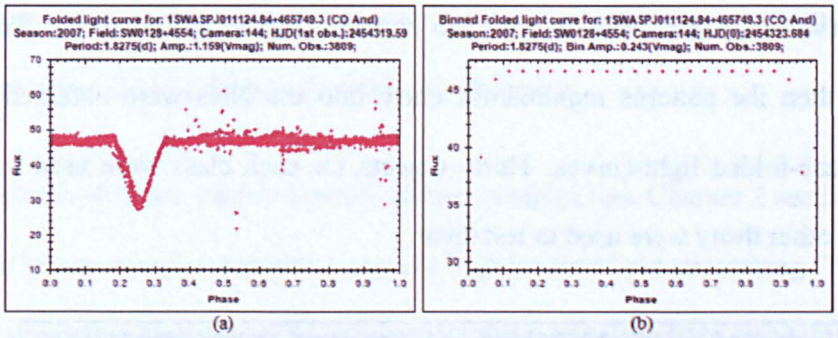

Figure 1-9: Light-curve for a 'single-eclipse' Algol-type star 1SWASP J011124.84+465749.3 – CO And
(a) Phase-folded light-curve (b) Modified phase-folded light-curve

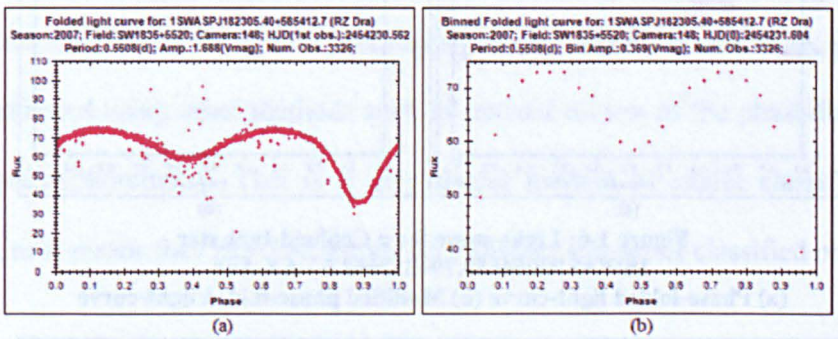

Figure 1-10: Light-curve for a Beta Lyrae-type star 1SWASP J182305.40+585412.7 – RZ Dra
(a) Phase-folded light-curve (b) Modified phase-folded light-curve

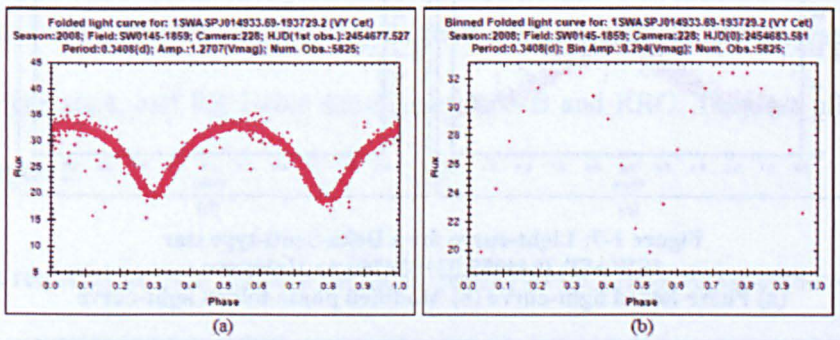

Figure 1-11: Light-curve for a W UMa-type star 1SWASP J014933-193729.2 – VY Cet
(a) Phase-folded light-curve (b) Modified phase-folded light-curve

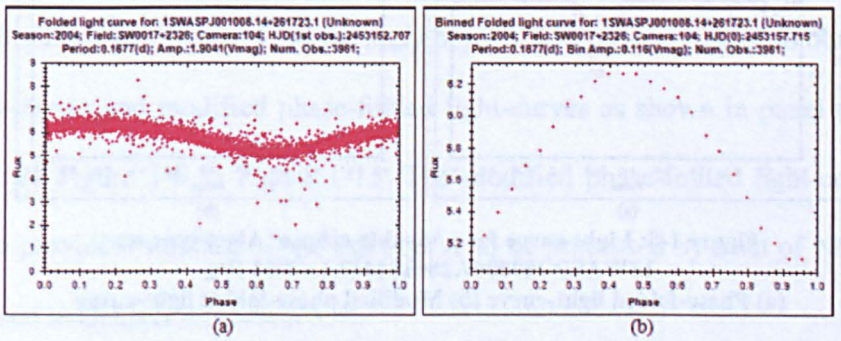

Figure 1-12: Light-curve for a Sinusoidal-type star 1SWASP J001008.14+261723.1 – Unknown
(a) Phase-folded light-curve (b) Modified phase-folded light-curve

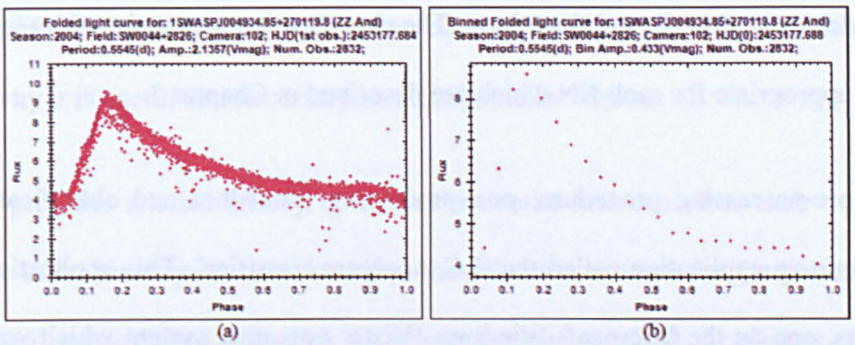

Figure 1-13: Light-curve for an RR Lyrae-type star (RRAB)
1SWASP J004934.85+270119.8 – ZZ And
(a) Phase-folded light-curve (b) Modified phase-folded light-curve

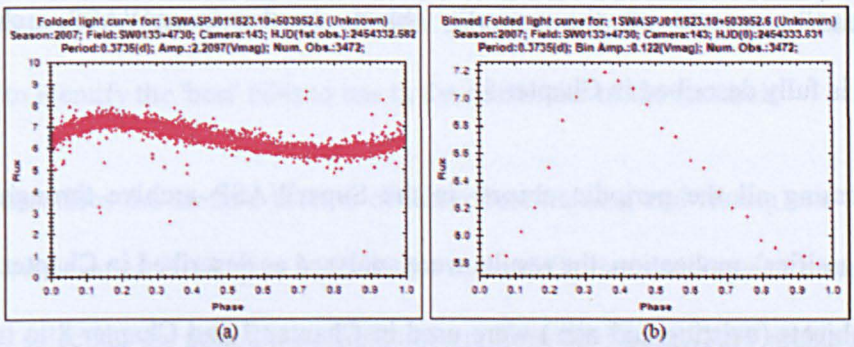

Figure 1-14: Light-curve for an RR Lyrae-type star (RRC)
1SWASP J011823.10+503952.6 – Unknown
(a) Phase-folded light-curve (b) Modified phase-folded light-curve

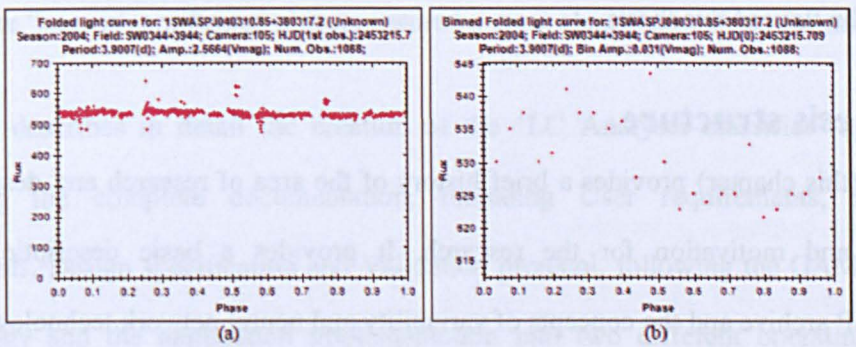

Figure 1-15: Light-curve for a non-periodic star
1SWASP J040310.85+380317.2 – Unknown
(a) Phase-folded light-curve (b) Modified phase-folded light-curve

The training of the NNs involved processing each of the training patterns repeatedly through each NN until they had learned the appropriate patterns as described in Chapter 5. Testing involved processing each of the test objects through each NN on one occasion and obtaining the output value for each node of each NN. Post-processing occurred using the output values for each node, which were compared against a threshold value for each NN,

which was determined in the training phase. The classification was assigned by following a set of rules appropriate for each NN which are described in Chapter 5.

The NNs, pre-processing procedure, post-processing procedure and classification rules were built into an application called the 'LC Analyser classifier'. This application existed in two forms, one on the Microsoft Windows 'Vista' operating system which was used to train and test the NNs and a second version on the Linux operating system which was used to automatically process all the periodic objects in the SuperWASP archive. The application is fully described in Chapter 5.

After processing all the periodic objects in the SuperWASP archive through the 'LC Analyser classifier' application, the results were analysed as described in Chapter 6 and the identified objects (existing and new) were used in Chapter 7 and Chapter 8 to investigate some topical interests in eclipsing and pulsating stars respectively. The next section described the flow of this thesis.

1.8. Thesis structure

Chapter 1 (this chapter) provides a brief history of the area of research and describes the objectives and motivation for the research. It provides a basic description of the SuperWASP archive and the concepts of variability and neural network technology. It then concludes with a brief introduction of the proposed method of classification. This chapter prepares the reader for their journey through the subsequent chapters.

Chapter 2 provides a more detailed description of the causes of variability, separating them into 'intrinsic' causes (for pulsating, eruptive and cataclysmic stars), 'extrinsic' causes (for eclipsing and rotating stars) and those that have both 'intrinsic and extrinsic' causes. It discusses the classification of variability in general before describing the proposed method of classification and some of the problems that were encountered. It goes on to describe the

use of neural network technology in the classification of variable stars and finally, discusses why it is useful and necessary to classify stellar objects.

Chapter 3 provides a brief history of neural networks and describes their components, architecture and characteristics. It describes the selection process for the parameters used in each neural network and describes the pre-processing required for objects entered into the NNs and the post-processing required for the output from the NNs. It then describes the testing performed on the NNs with relation to training and testing sets obtained from Chapter 4, to identify the 'best' NNs to use in the remainder of the research.

Chapter 4 describes the method used to obtain robust training and testing sets to use with the three NNs selected in Chapter 3. Here, the more definitive training and testing set was obtained by selecting the periodic variable objects from the SuperWASP archive that were known in the GCVS and manually reviewing them to confirm the variability period and class. These 'known', confirmed objects ensured a good classification rate for the NNs.

Chapter 5 describes in detail the creation of the 'LC Analyser classifier' application, comprising the complete documentation, including User requirements, Functional requirements, Design specification and Validation protocol, following the GAMP5 (2008) methodology and the application implementation into two different operating systems (Microsoft Vista and Linux). It also describes the processing of all the periodic objects in the SuperWASP archive and discusses the problems identified along the way.

Chapter 6 describes the interpretation of results from processing all periodic objects in the SuperWASP archive with the 'LC Analyser classifier' application. In effect, the chapter shows how effective the proposed method of classification is. In the chapter, the classified objects were reviewed and after removal of the non-classified and misclassified objects,

individual catalogues of Algol-type, Beta Lyrae-type, W UMa-type, Delta Scuti-type, and RR Lyrae-type stars were created for use in Chapter 7 and Chapter 8. The non-classified and misclassified objects were also investigated and recommendations made to improve the quality of the results. These are described in Chapter 10.

Chapter 7 assesses the eclipsing binary stars Algol-type, Beta Lyrae-type and W UMa-type that were catalogued in Chapter 6. It provides statistics on the number of objects identified and how many were known in SIMBAD and the GCVS. It also provides statistics on the period and amplitude ranges obtained and compares them against those published in other surveys. Each class is then shown on distribution maps. Finally, the eclipse-depth ratio was used to show differentiation between Beta Lyrae-type and W UMa-type classes.

Chapter 8 assesses the pulsating stars Delta Scuti-type, and RR Lyrae-type catalogued in Chapter 6, providing statistics on the number of objects identified and how many were known in SIMBAD and the GCVS. It also presents statistics on the period and amplitude ranges obtained and displays them on distribution maps. RR Lyrae-type stars are further analysed in three ways. Firstly by using a published absolute magnitude to calculate their distances and creating a three-dimensional map of the galaxy using these stars; secondly, a search is made for RR Lyrae-type stars that exhibit the Blazhko effect, and thirdly, the periods for the RR Lyrae-type population are plotted on a graph to look for evidence of the Oosterhoff Dichotomy. The distances to the DSCT stars are also calculated using their Period-Luminosity relationship.

Chapter 9 provides a summary of the results obtained from this research and as already mentioned above, Chapter 10 describes further work required before the full SuperWASP stellar catalogues can be created.

---------- o ----------

Chapter 2 Variable stars - their causes and classification

This chapter provides an overview of variability in stars. This research was limited to the assessment of periodic variability only, but non-periodic objects are also mentioned in this chapter in order to place them into context with the classification methods available. In section 2.1, the causes of variability are described as a prelude to describing the methods of classification in section 2.2. Section 2.3 discusses why we classify stars, and finally, the use of neural networks in automated classification is described in section 2.4.

2.1. Causes of variability

As described in Chapter 1, variability simply means the change in magnitude of light of a stellar object over a period of time. The light itself does not have to be in the visible spectrum as in the SuperWASP survey. It can be in Infra-red (e.g. The Spitzer Space Telescope Mission[8], Werner et al. (2004)); Gamma rays (e.g. Compton Gamma Ray Observatory[9], Kniffen et al. (1991)); X-rays (e.g. Chandra[10], Weisskopf et al. (2000)); Ultraviolet (e.g. EUVE[11], Craig et al. (1997)); Microwaves (e.g. COBE[12], Boggess et al. (1992)) or even a combination e.g. visible light and X-rays.

At the basic level, variability of stellar objects can be broadly classified as 'intrinsic' (variability internal to the system) or 'extrinsic' (variability due to an obstruction) and within these broad areas the stellar objects can be described in terms of their physical processes. Table 2-1 illustrates the split of some well-known variables into these different process areas. Note that only those processes that are detected in the visible spectrum are shown as this is the area this research applies to.

---

[8] *NASA's Great Observatories Program, (formerly SIRTF, the Space Infrared Telescope Facility): www.spitzer.caltech.edu/spitzer/index.shtml*
[9] *NASA's CGRO Mission: http://heasarc.gsfc.nasa.gov/docs/cgro/*
[10] *NASA's Chandra X-ray Observatory: www.chandra.harvard.edu*
[11] *Extreme Ultraviolet Explorer Space Telescope: http://science.nasa.gov/missions/euve/*
[12] *Cosmic Background Explorer: http://www.nasa.gov/topics/universe/features/cobe_20th.html (Sept. 2012)*

		Intrinsic				Extrinsic		
Stellar class type	Abbrev.	Eruptive	Cataclysmic	Pulsating	Accreting	Eclipsing	Rotating	Micro-lensing
Alpha2 Canum Venaticorum	ACV	✓					X	
Beta Cephei	BCEP			✓				
BY Draconis	BY			✓			X	
Cepheid	CEP			✓				
Detached binary	D binary					✓		
Delta Cephei	DCEP			✓				
Delta Scuti	DSCT			✓				
Rotating ellipsoidal	ELL						X	
Exoplanet	Exoplanet					✓		
FK Comae Berenices	FKCOM						X	
FU Orionis	FU Ori	X			X			
Gamma Cas	G Cas	✓						
Gamma-ray burst afterglow	GRB Ag	X						
Gamma-ray burst Hypernova	GRB Hyp.		X					
Gamma-ray burst Neutron star	GRB Neut.		X					
Irregular	Irr	X						
Long period variable	LPV			✓				
Micro-lensing	Micro-lensing							X
Novae	Novae		X					
Optically variable pulsars	PSR						X	
R Coronae Borealis	R Cor Bor	X		X				
Recurrent novae	Rec. Nova	✓						
RR Lyrae	RR (B)			✓				
RR Lyrae	RRAB			✓				
RR Lyrae	RRC			✓				
RS Canum Venaticorum	RS CVn	✓						
RV Tauri	RV Tauri			✓				
S Doradus	S Dor	X						
Semi-detached binary	SD binary				✓	✓		
Semi-regular	Semi-reg.			X				
Supernova Ia	SN Ia		X					
Supernova Ib	SN Ib		X					
Supernova II	SN II		X					
Superhump	Superhump	X			X			
SX Arietis	SXARI						X	
T-Tauri	T-Tauri	X		✓				
U Geminorum	U Gem		X					
UV Ceti	UV Ceti	X						
VY Sculptoris	VY Scl	X						
Contact binary (W UMa)	W UMa				✓	✓		
Overcontact binary	W UMa				✓	✓		
W Virginis	W Vir			✓				
Wolf-Rayet	WR	X						
Z Andromedae	Z And		X					
Z Camelopardalis	Z Cam		X					

Table 2-1: Split of intrinsic and extrinsic variables.

In Table 2-1, a ✓ or an x indicates the process causing the variability in the stellar class. A ✓ indicates a periodic variable and an x indicates a non-periodic variable. Objects shown inside a yellow cell are those included in the automated classification in this research.

Occasionally, an object appears in more than one process area as it exhibits more than one physical process, for instance, R Cor Bor appears in both Eruptive and Pulsating processes (both intrinsic properties and both non-periodic) and a SD binary object can show intrinsic and extrinsic properties (i.e. accreting and eclipsing).

The following sections describe the physical processes and provide examples that were used in this research to illustrate the ideas. Note the characteristics of the objects given below are heavily paraphrased from the descriptions given in the GCVS and AAVSO as the main objective of this research was to identify new objects based on their classification characteristics. For a complete review, the reader should visit the GCVS[13] and AAVSO[14] websites. Additional information has been gathered from other sources and specific references have been given when this occurs. All phase-folded light-curves displayed in this chapter were obtained from observations in the SuperWASP archive and created by the 'LC Analyser Classifier' application designed and created in Chapter 5.

In the descriptions that follow, the nomenclature used is that described by the GCVS e.g. DCEP, CEP, RRAB etc. A full list can be seen on the GCVS web-site and this GCVS nomenclature was used throughout this research.

[13] *http://www.sai.msu.su/gcvs/gcvs/. Descriptors for the stellar classes are on http://www.sai.msu.su/gcvs/gcvs/iii/vartype.txt*
[14] *http://www.aavso.org/*

2.1.1 Intrinsic causes of variability

This type of variability is caused by variation of the internal mechanisms of the stellar systems themselves. As the stars continually evolve, their variability will change over time as they follow their life-cycle through the Hertzprung-Russell (H-R) diagram. Figure 2-1 has been adapted from Cooper & Walker (1989) to show the location of some examples of intrinsic variables in the H-R diagram. As the stars move through the classes they exhibit one or more of these intrinsic physical processes, which are described below: Pulsations; Eruptions; Cataclysms; Accretion.

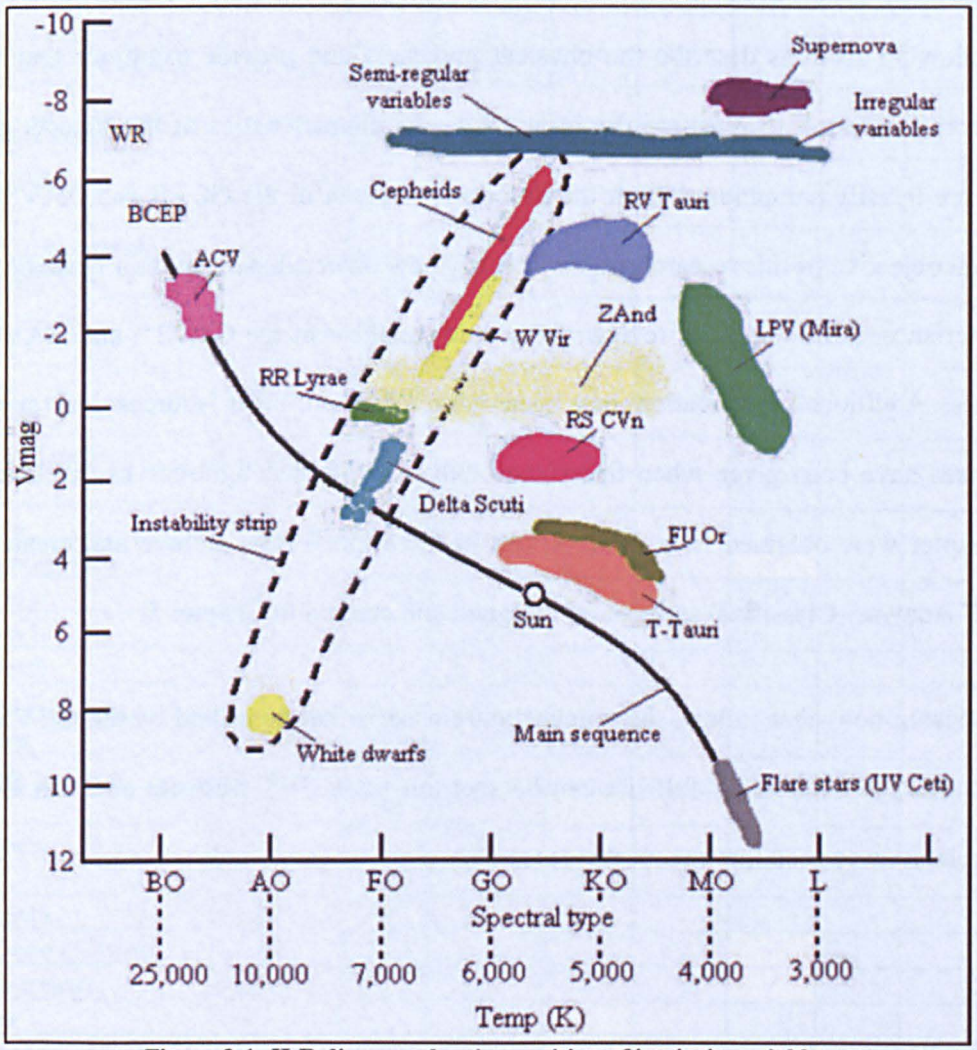

Figure 2-1: H-R diagram showing position of intrinsic variables

2.1.1.1 Pulsating stars

Pulsating variables are stars showing periodic expansion and contraction of their surface layers, where their pulsations may be radial or non-radial. A radially pulsating star remains spherical in shape, while non-radial pulsations periodically deviate from a sphere, and even neighbouring zones of its surface may have opposite pulsation phases. In a pulsating star, if the pressure outwards exceeds the gravitational force inwards, the outer layers will expand outwards following the Kappa mechanism shown in Figure 2-2.

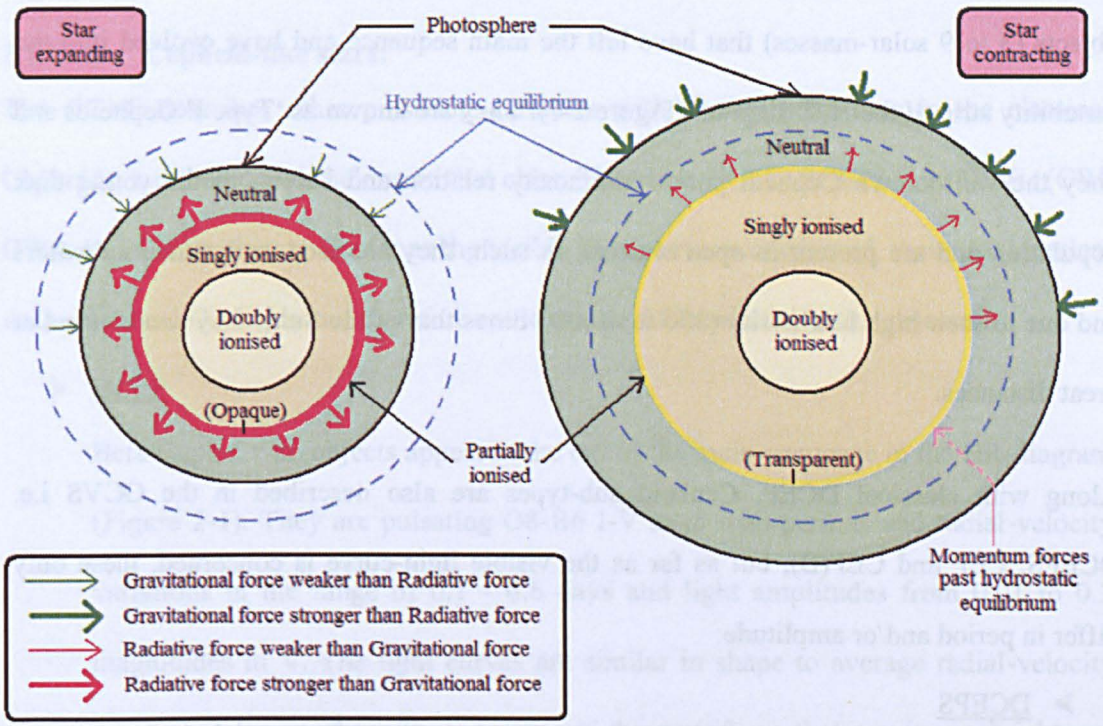

Figure 2-2: Pulsation process in Pulsating stars

As the star is compressed, the energy that normally heats the star mostly increases the ionisation. This increases the opacity of the partially ionised zone (see 'Star expanding' in Figure 2-2), trapping radiation more efficiently and resulting in a large outward pressure. The zone is therefore driven outwards towards hydrostatic equilibrium where the gas pressure force is equivalent to the gravitational force. However, the outwardly moving layers still have momentum and are carried past the equilibrium position (see 'Star contracting' in Figure 2-2). Eventually, gravitational force becomes greater than the gas

pressure force and the outer layer of the star also starts cooling. The cooling results in recombination of the ionised material in the partially ionised zone, which leads to a sudden decrease in the opacity and a decrease in outward pressure. The zone therefore drops back to its original position (again, due to momentum) and the cycle repeats. Examples of pulsating stars that were assessed in this research are:

2.1.1.1.1 Cepheid stars:

The classical Delta Cephei type variables (DCEP) are comparatively young massive objects (3 to 9 solar-masses) that have left the main sequence and have evolved into the instability strip of the H-R diagram (Figure 2-1). They are known as 'Type I' Cepheids and obey the well-known Cepheid period-luminosity relation and belong to the young disk population and are present in open clusters, as such, they are used as distance indicators and due to their high luminosity (300 to 40,000 times that of the Sun), they can be used at great distances.

Along with classical DCEP, Cepheid sub-types are also described in the GCVS i.e. DCEPS, CEP and CEP(B), but as far as the visible light-curve is concerned, these only differ in period and/or amplitude:

- DCEPS

  This is a subclass of DCEP variables that have light amplitudes <0.5 magnitudes in V and almost symmetrical light curves. As a rule, their periods do not exceed 7 days. They are probably first-overtone pulsators and/or are in the first transition across the instability strip after leaving the main sequence.

- CEP

  These objects are radially pulsating, high luminosity variables (classes Ib-II) with periods in the range of 1-135 days and amplitudes from several hundredths to 2

magnitudes in V. Their spectral types are F-K (maximum to minimum light) and the longer the period of light variation, the later the spectral type.

- CEP(B)

  This sub-class displays the presence of two or more simultaneously operating pulsation modes, usually the fundamental tone with the period P0 and the first overtone P1. The periods P0 are in the range from 2 to 7 days, with the ratio P1/P0 approximately 0.71.

2.1.1.1.2 Cepheid-like stars:

The GCVS describes other pulsating variables with similar properties to the classical Cepheids, but they do not belong to that class. These are BCEP, BCEPS, and W Vir (CW, CWA and CWB) objects. As far as the visible light-curve is concerned, these are identical to the classical Cepheids and therefore could not be differentiated in this research:

- BCEP

  Beta-Cephei type objects appear at the top of the main-sequence in the HR-diagram (Figure 2-1). They are pulsating O8-B6 I-V stars with periods and radial-velocity variations in the range of 0.1 - 0.6 days and light amplitudes from 0.01 to 0.3 magnitudes in V. The light curves are similar in shape to average radial-velocity curves but lag in phase by a quarter of the period, so that maximum brightness corresponds to maximum contraction, i.e., to minimum stellar radius. The majority of these stars probably show radial pulsations, but some (e.g. V649 Per) display non-radial pulsations; multi-periodicity is characteristic of many of these stars.

- BCEPS

  These are a short-period group of BCEP variables where the periods are an order of magnitude smaller than the normally observed ones (0.015 - 0.04 days). The spectral types are B2-B3 IV-V.

- W Vir

These are old, low mass stars (around 1 solar-mass) which have evolved away from the main sequence, up the giant branch (as hydrogen fusion ends), down to the horizontal-branch (after helium fusion switches on), back up the asymptotic giant branch (as helium fusion ends), but are experiencing helium flashes as helium burning briefly switches on again. This shifts the star to higher temperature and over to the instability strip, where the 'Type II' Cepheid variations occur (see Figure 2-1). It is often impossible to differentiate between these and DCEP (Type I) on the basis of the light curves for periods in the range 3 to 10 days. One of the significant spectral differences between W Vir stars and Cepheids is the presence of hydrogen-line emission in the former and of CaII, H, and K emission in the latter. W Vir type stars (CW) have periods of approximately 0.8 to 35 days and amplitudes from 0.3 to 1.2 magnitudes in V and obey a period-luminosity relation different to that for DCEP. For an equal period value, the W Vir variables are fainter than the DCEP stars by 0.7 to 2 magnitudes. The light curves of W Vir variables for some period intervals differ from those of DCEP for corresponding periods either by amplitudes or by the presence of humps on their descending branches, sometimes turning into broad flat maxima. It was seen as a possibility in this research that W Vir stars could be differentiated from other Cepheid-type stars due to these slight differences in light-curve and examples are included in the following chapters. However, the NNs were not trained to specifically look for them in this research. W Vir subclasses CWA and CWB have periods longer or shorter than 8 days respectively.

2.1.1.1.3 RR Lyrae stars

These 'Population II' stars are a type of yellow giant star that changes in brightness with a regular period of a few days. The variability is caused by the star radially pulsating due to it burning helium into carbon through nuclear fusion processes very similar to that shown in Figure 2-2. They are generally much older than our Sun, with a little over half the mass. Their luminosity is about 80 times that of the Sun and they are much hotter, with an average temperature of about 7000 Kelvin. They are found in the galactic halo and globular clusters and one of the main features of RR Lyrae stars is that they lie in the horizontal branch of the H-R diagram (see Figure 2-1). As such, they all have (roughly) the same luminosity and therefore can be used to calculate distances. Three subtypes are described in the GCVS:

- RRAB

  These RR Lyrae stars pulsate in the fundamental tone and their periods are 0.3 to 1.2 days, with amplitudes from 0.5 to 2.0 magnitude in V. They all have approximately the same absolute magnitude (+/- 0.5) which makes them valuable distance indicators for mid-range distances.

- RRC

  These RR Lyrae stars pulsate in the first overtone and their periods are from 0.2 to 0.5 days with amplitudes no greater than 0.8 magnitudes in V.

- RR(B)

  These are double-mode RR Lyrae stars which pulsate in the fundamental mode and in the first overtone with a period ratio of 0.74 and a fundamental period near 0.5 days (or in the first and second overtones with a period ratio of 0.80). These are called RRD in AAVSO.

2.1.1.1.4 Delta-Scuti stars

Sometimes called Dwarf Cepheids, these are variable stars that exhibit variations in their luminosity due to both radial and non-radial pulsations of the star's surface. They lay in the instability strip, just off the main sequence (Figure 2-1). Typical brightness fluctuations are from 0.003 to 0.9 magnitudes in V over a period of a few hours, although the amplitude and period fluctuations can vary greatly. The stars are usually A0 to F5 giant or main sequence stars. The high amplitude Delta Scuti variables are also called AI Velorum stars. They are a very common variable source in the Milky Way.

Other pulsating classes described in the GCVS and AAVSO that will not be included in this research are: Alpha Cygni type (ACYG), Mira type (M), RV Tauri type (RV, RVA and RVB), PV Telescopii type (PVTEL), SX Phoenicis type (SXPHE), and ZZ Ceti (ZZ, ZZA and ZZB). Along with these are also the Semi-regular types (SR, SRA, SRB, SRC and SRD) and Slow Irregular types (L, LB and LC). These classes were not included in this research because sufficient 'good' representatives could not be obtained from the SuperWASP archive, but it should be noted that, as the phase-folded light-curves of these objects are similar to those described above, it is possible that they were detected by the NNs as Cepheid-type stars and would be available for manual review.

2.1.1.2 Eruptive stars

Eruptive variables are stars varying in brightness due to violent processes and flares occurring in their chromospheres and coronae. The changes are usually accompanied by shell events or mass outflow in the form of stellar winds of variable intensity and/or by interaction with the surrounding interstellar medium. They occur throughout the stellar life-cycle as described by the examples below. These objects were not included in the automated classification in this research as they are non-periodic in nature:

2.1.1.2.1 Proto-stars

These are young, hot pre-main sequence stars that are usually embedded in nebulosity. They have irregular periods with amplitudes of several magnitudes. Two examples are:

- T Tauri type

  These variables are pre-main sequence stars approaching the main sequence in the H-R diagram (Figure 2-1). They are of spectral type Fe to Me and they are characterised by spots on the stellar surface and gas-dust clumps orbiting in the circumstellar disks. The feature specific to this type of star is the presence of the fluorescent emission lines Fe II 4046, 4132 A, emission lines [Si II] and [O I], as well as the absorption line Li I 6707 A.

- FU Ori type

  FU Orionis variables are of spectral type A through G and are possibly an evolutionary phase in the life of T Tauri stars. They are characterized by gradual increases in brightness of about six magnitudes over several months, followed by either constant output for years or by a slow decline of one to two magnitudes. All presently known FU Ori variables are coupled with reflecting cometary nebulae.

2.1.1.2.2 Main Sequence stars

The main sequence is a continuous and distinctive band of stars that appear on the H-R diagram as shown in Figure 2-1. The stars on the main sequence are in hydrostatic equilibrium, where the outward thermal pressure from the hot core is balanced by the inward gravitational pressure from the overlying layers, as such, these stars seldom exhibit eruptions. Two examples in this region that do show variability are:

- Wolf-Rayet stars (WR)

  These are super-massive hot stars (around 30,000°K) that are located at the top of the main-sequence where it joins the Super Giants (Figure 2-1). They undergo periodic mass ejections causing them to brighten irregularly, but by 0.1 magnitudes

on average. They exhibit broad emission line spectra with He I and He II as well as C II-C IV, O II-O IV, and N III-N V lines.

- Flare stars (UV Ceti stars)

  These are very faint stars, which undergo regular flares. They increase in brightness from tenths of a magnitude up to six magnitudes in just a few seconds, and then fade back to normal brightness in half an hour or less. The amplitude is considerably greater in the ultraviolet spectral region.

2.1.1.2.3 Giant and Supergiant stars

These large stars lose their matter relatively easily and therefore, eruptions are fairly common. Two examples are:

- S Dor type

  Variables of the S Dor type are stars showing irregular photospheric pulsations and sometimes cyclic light changes with amplitude in the range 1 to 7 magnitudes with time scales of hundreds to thousands of days. They belong to the brightest Luminous Blue Variable stars (LBV) of their parent galaxies and as a rule they are connected with diffuse nebulae and surrounded by expanding envelopes.

- G CAS

  Gamma Cassiopeiae variables are BIII-IVe type stars that fluctuate irregularly by up to 1.5 magnitudes due to the ejection of matter at their equatorial regions caused by a fast rotational speed. The formation of equatorial rings or disks is often accompanied by temporary brightening or fading depending on the facing side of the star (polar or equator).

As previously mentioned, eruptive stellar objects were not included in the NN classification for this research, however it was possible that similarities in the phase-folded light-curve caused them to be given preliminary classifications based on the visible light-

curve e.g. T Tauri stars although eruptive in nature, may also have a sinusoidal curve-shape that may give a RM star classification.

2.1.1.3 Cataclysmic stars

Cataclysmic variables (CV) are binary systems consisting of a (degenerate) white dwarf star accreting via Roche lobe overflow from a low mass, main sequence, companion star (usually stellar type K or M). This category is subdivided into the following types:

2.1.1.3.1 Novae

These are CVs in which thermonuclear runaway burning occurs on the surface of the white dwarf as a result of the material it has accreted from the K- or M-star companion. The event may be one-off, or more likely recurrent with timescales of tens of thousands of years. Recurrent novae are merely those where the recurrence timescale is amenable to human observation (typically 80-90 years).

Novae are close binary systems with orbital periods from 0.05 to 230 days. One of the components of these systems is a hot dwarf star that suddenly, during a time interval from one to several dozen or several hundred days, increases its brightness by 7 to 19 magnitudes in V then returns gradually to its former brightness over several months, years, or decades.

Sub-types of Novae are NA, which are fast novae displaying rapid light increases, then fading by 3 magnitudes in 100 or fewer days; NB, which are slow novae that fade after maximum light by 3 magnitudes in >= 150 days; NC, which are novae with a very slow development and remaining at maximum light for more than a decade, then fading very slowly; NL, which are nova-like variables that have spectra that look like old novae, but for which no nova explosion has yet been seen; and NR, which are recurrent novae, which

differ from typical novae by the fact that two or more outbursts have been observed, separated by 10 to 80 years.

2.1.1.3.2 Other cataclysmic stars

- U Geminorum stars (U Gem)

  These are quite often called dwarf novae. They are close binary systems consisting of a dwarf or sub-giant K-M star that fills the volume of its inner Roche lobe and a white dwarf surrounded by an accretion disk. The eruption in these CV stars is due to a quasi-periodic thermal-viscous instability in the accretion disc around the white dwarf. Orbital periods are in the range 0.05 to 0.5 days, and these systems are frequently sources of X-ray emission. Some of these systems are also eclipsing (**Ramsay et al. 2012**). According to the characteristics of the light changes, U Gem variables may be subdivided into three types: SS Cyg-type (UGSS), SU UMa-type (UGSU), and Z Cam-type (UGZ).

- Z Andromedae type (Z And)

  These are symbiotic variables of the Z Andromedae type. They are close binaries where the donor is a giant star rather than a main sequence dwarf star and the mode of accretion is via wind rather than via Roche lobe overflow, but otherwise they are similar to Cataclysmic Variables. The source of variability is accretion onto the white dwarf. The combined brightness displays irregular variations with amplitudes up to 4 magnitudes in V.

These cataclysmic stellar objects were not included in the NN classification in this research as they are non-periodic objects.

2.1.1.4 Accreting stars and disc instability

Variability in accreting systems is caused by the larger star of a close-binary system taking material from its companion due to the effect of its larger gravity e.g. UZ Tau (**Mathieu,**

2007). The transfer of material causes an increase in the light output of the system. The process also occurs in active galactic nuclei, proto-planetary discs, and gamma ray bursts. These will not be progressed any further in this research. Variability in systems with disc instability is caused by thermal-viscous instability in a thin disc e.g. Z. And, U Gem, and Z Cam. This is one of the theories proposed for planet formation (Janson et al. 2012).

2.1.1.5 Supernova events

These stars increase in brightness by 20 magnitudes or more as a result of a final explosion, then fade slowly. The spectrum is characterized by the presence of very broad emission bands, their widths being several times greater than those of the bright bands observed in the spectra of novae. The expansion velocities of supernovae envelopes are in thousands of km/s. According to the light curve shape and the spectral features, supernovae are subdivided into the following types: SNI (a, b and c), SNII (a, b, d and n); SNII-L and SNII-P. SN1a are believed to arise in "accretion induced collapse" of a white-dwarf star that accretes enough mass to exceed the Chandrasekhar limit. The other classes of supernovae are believed to be due to "core collapse" of a massive (single) star at the end of its life when its core is composed of Fe-Ni-Co and unable to undergo any more energy-releasing fusion reactions.

2.1.2 Extrinsic causes of variability

Extrinsic variability is caused by some external reason, such as rotation, orbital motion, or partial obscuration of the star. The stars exhibit one or more of the following physical processes, which are described below: Eclipsing; Rotating; and Micro-lensing.

2.1.2.1 Eclipsing stars

These binary stars show variability due to eclipsing of one another while the orbital plane is almost parallel with the observers line of sight. Consequently, the observer finds changes of the apparent combined brightness of the system with the period coincident with that of

the components' orbital motion. Three sets of nomenclature exist for eclipsing binaries in the GCVS, each depending on the properties of the stars i.e. classification using the light-curve shape (EA/EB/EW), classification using magnitude-colour properties (GS/PN/RS CVn/WD/WR), and classification using the amount of fill in the Roche lobe of each component of the system (Detached/Semi-detached/Contact). These are described more fully in section 2.2.2.

2.1.2.2 Rotating

These are variable stars that have non-uniform surface brightness and/or ellipsoidal shapes. The variability is caused by axial rotation with respect to the observer. The non-uniformity of surface brightness distributions may be caused by the presence of spots (which could be argued is an 'intrinsic' property) or by some thermal or chemical inhomogeneity of the atmosphere caused by a magnetic field whose axis is not coincident with the rotation axis. These stars are subdivided into the following types, which vary on their star size and spectral properties: Alpha2 Canum Venaticorum variables (ACV and ACVO); BY Draconis-type variables (BY); Rotating ellipsoidal variables (ELL); FK Comae Berenices-type variables (FKCOM); Optically variable pulsars (PSR); and SX Arietis-type variables (SXARI).

In this research these would all be represented by a sinusoidal-like light-curve and as such, are termed 'Rotational Modulation' (RM) stars. They are pre-main sequence and main-sequence stars and the light variability is caused by axial rotation of the stars and the presence of surface spots and chromospheric activity. Some RM stars also show flares as described in section 2.1.1.2.1. These stars display a light-curve that is sinusoidal in nature, e.g. BY Draconis and the Orion variables of the T Tauri type:

- BY

  BY Draconis-type variables show quasi-periodic light changes with periods from a fraction of a day to 120 days and amplitudes from several hundredths to 0.5 magnitudes in V.

- T Tauri

  Stars are assigned to this type on spectroscopic criteria, and so cannot be differentiated from other RM Stars in this research. These are classified simply as RM in nature and follow-up work would be required to identify them as T Tauri.

2.1.2.3 Micro-lensing

AAVSO describes the micro-lensing event as symmetric brightening of a star caused by the presence of a separate gravitational influence intervening in line of sight. It may last from seconds to years. Micro-lensing events are a type of extrinsic variable that, like supernovae, are a once in a lifetime event, for example: GSC 3656-1328 (AAVSO designation: VSX J000921.8+543943) (Fukui et al. 2007).

2.1.3 Combined Intrinsic and Extrinsic causes of variability

As indicated in section 2.1, many of the systems described contain more than one type of variability. For example, NY Virginis (NY Vir) is an Algol type (EA), but consists of a main sequence dwarf M-star (dM) and a sub dwarf B-star (sdB) with a stripped core. The system is therefore eclipsing, but the sdB star also exhibits pulsations (Hu et al. 2007). This is an important system as it enables independent determination of stellar parameters from the two processes that can be compared with each other for confirmation. A second example is the OGLE object, OGLE-BLG-RRLYR-02792 described by Pietrzynski et al. (2012). This is the only RR Lyrae star found in an eclipsing binary so could be enormously important as a means of testing stellar models.

2.2. Classification of variability

As this research was performed using observations in the visible spectrum, only those stellar objects shown in this section were used in the initial NN classification scheme described in subsequent chapters. The classification approach that was taken in the automated system was based on that provided by the GCVS, as described below. The classification method used in this research was based around the shape of the phase-folded light-curve, along with the period and amplitude. The following sections describe the shape of the phase-folded light-curves obtained from each stellar class. These formed the basis of the input to the NNs in subsequent chapters.

2.2.1 Pulsating variables

2.2.1.1 CEP and CEP-like

As mentioned above, this research confined the identification and classification of stellar objects to the visible spectrum. Therefore the proposed classification system could not differentiate between the classical Cepheid DCEP and the other sub-types described in sections 2.1.1.1.1 and 2.1.1.1.2. For instance, the phase-folded light-curve of a typical Cepheid is shown in Figure 2-3 and an example of a W Vir star is shown in Figure 2-4 (note the hump on the downward facing phase).

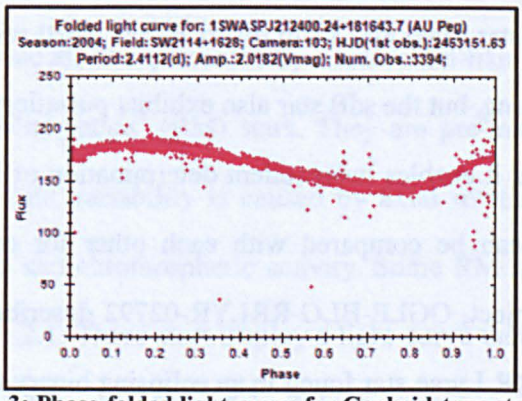

Figure 2-3: Phase-folded light-curve for Cepheid-type star (CEP) (1SWASP J212400.24+181643.7 → AU Peg)

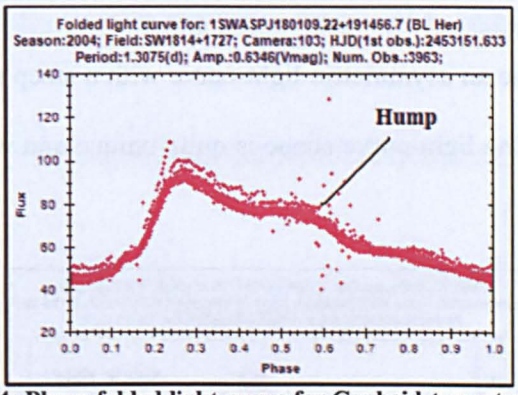

Figure 2-4: Phase-folded light-curve for Cepheid-type star (W Vir)
(1SWASP J180109.22+191456.7 → BL Her)

During the proposed automated classification method, a binned version of the phase-folded light-curve was created in order to obtain the parameters necessary to classify the object. Unfortunately, the training set for the neural networks did not differentiate between Cepheid and W Vir stars, i.e. the training set did not contain any W Vir objects. Therefore the 'bump' in the W Vir object was absorbed into the Cepheid classification and therefore they were unable to be differentiated from other Cepheid-type objects.

2.2.1.2 DSCT

The shape of DSCT type objects as shown in Figure 2-5 is very similar to the Cepheid-type objects, but the difference in period range allows them to be differentiated easily.

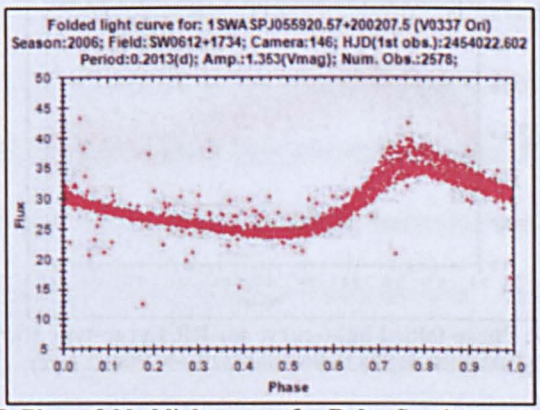

Figure 2-5: Phase-folded light-curve for Delta-Scuti-type star (DSCT)
(1SWASP J055920.57+200207.5 → V0337 Ori)

2.2.1.3 RRAB

These RR Lyrae stars have an asymmetric light-curve with a steep rise and gentler decline as shown in Figure 2-6. The light-curve shape is quite unique and was easy to represent in the NNs:

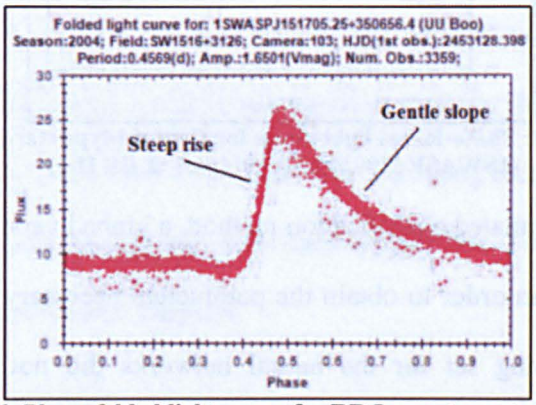

Figure 2-6: Phase-folded light-curve for RR Lyrae-type star (RRAB) (1SWASP J151705.25+350656.4 → UU Boo)

2.2.1.4 RRC

The shape of RRC objects is as shown in Figure 2-7, where they are nearly sinusoidal in shape. There was some difficulty in differentiating these stars from others as described later in section 2.2.3.

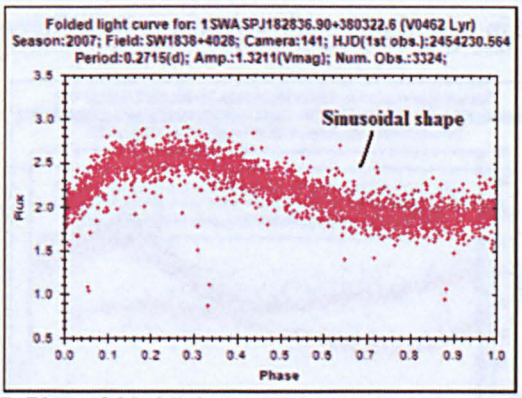

Figure 2-7: Phase-folded light-curve for RR Lyrae-type star (RRC) (1SWASP J182836.90+380322.6 → V0462 Lyr)

2.2.1.5 Sinusoidal stars (RM Stars)

The shape of RM Stars as shown in Figure 2-8 is very close to a sine-wave and is quite similar to the RR Lyrae class RRC objects in section 2.2.1.4. As such, there was some

difficulty in separating them from each other. This will be fully explored in subsequent chapters.

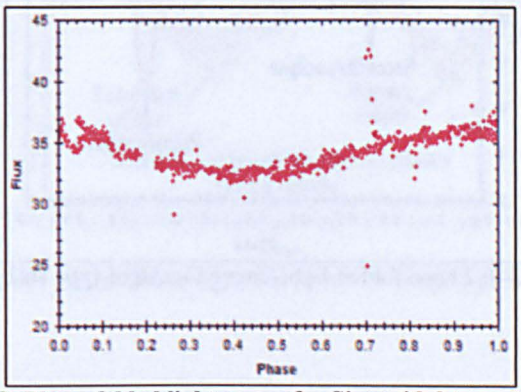

Figure 2-8: Phase-folded light-curve for Sinusoidal-type stars (RM)

2.2.2 Eclipsing binary variables

Three methods of classifying eclipsing binaries are described in the GCVS as shown here:

2.2.2.1 Method 1

This method uses the shape of the phase-folded light-curve and was the method used in this research. Three classes exist in this method:

- EA

  These are Beta Persei type eclipsing systems, better known as Algol systems. Looking at the phase-folded light-curve in Figure 2-9, it was possible to specify the moments of the beginning and end of the eclipses. Between eclipses the light remains almost constant or varies insignificantly because of reflection effects, slight ellipsoidality of the components, or physical variations are negligible. Note that the secondary minima may be absent (i.e. a single-eclipse). An extremely wide range of periods is observed, from 0.2 to >=10000 days. Light amplitudes are also quite different and may reach several magnitudes.

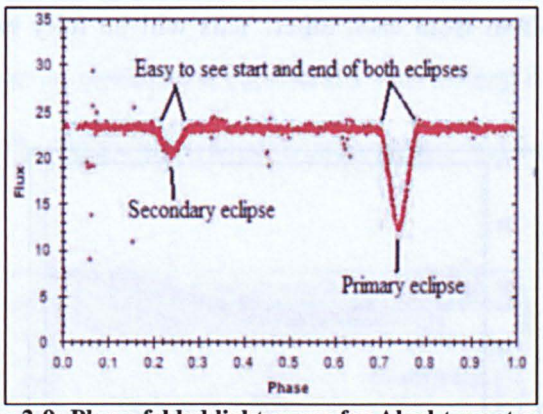

Figure 2-9: Phase-folded light-curve for Algol-type star (EA)

- EB

These are Beta Lyrae-type eclipsing systems. From the light-curve (Figure 2-10), it is not possible to specify the exact times of onset and end of eclipses and the secondary minimum is observed in all cases. The depth of the secondary minimum is usually considerably smaller than that of the primary minimum. Periods are mainly longer than 1 day and light amplitudes are usually <2 magnitude in V.

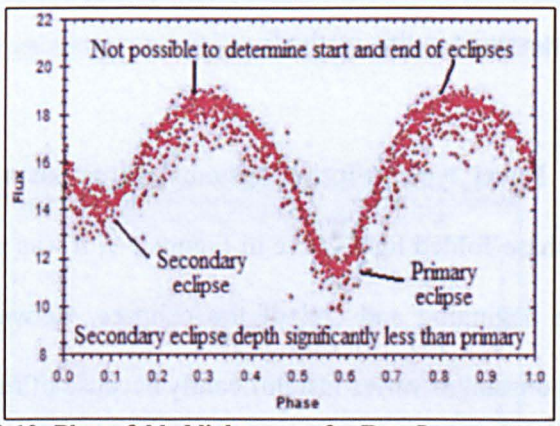

Figure 2-10: Phase-folded light-curve for Beta Lyrae-type star (EB)

- EW

These are W Ursae Majoris-type eclipsing variables. From the light-curve (Figure 2-11), it is not possible to specify the exact times of onset and end of eclipses. The depths of the primary and secondary minima are almost equal or differ insignificantly. They have periods shorter than 1 day and light amplitudes usually <0.8 mag in V.

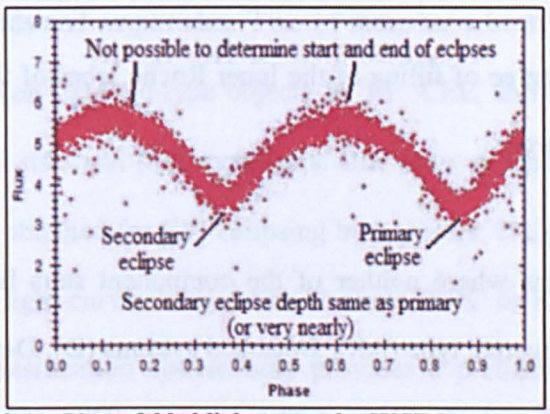

Figure 2-11: Phase-folded light-curve for W UMa-type star (EW)

2.2.2.2 Method 2

This method uses the positions of the binary-system components in the Colour-Magnitude diagram. Five classes exist for this method:

- GS

  These are systems containing one or both giant and supergiant components. One of the components may be a main sequence star.

- PN

  These are Systems having nuclei of planetary nebulae among their components (e.g. UU Sge).

- RS CVn

  These are RS Canum Venaticorum-type systems where the systems have the presence of strong CaII, H, and K emission lines of variable intensity in their spectra, indicating increased chromospheric activity. They are also characterized by the presence of radio and x-ray emissions.

- WD

  These are systems containing white-dwarf components.

- WR

  These systems have Wolf-Rayet stars among their components (e.g. V 444 Cyg).

2.2.2.3 Method 3

This method uses the degree of filling of the inner Roche lobes of the binary stars. Three classes exist in this method:

- Detached

  These are systems where neither of the component stars have their Roche lobe filled, e.g. AR Lacertae type (AR), Detached systems (D), Detached main-sequence systems (DM), Detached systems with a sub-giant (DS), and systems similar to W UMa, but not in contact (DW).

- Semi-detached

  These are systems where the surface of the less massive component is close to its inner Roche lobe.

- Contact (sometimes termed Over-contact)

  These are systems where both components fill their inner Roche lobes, e.g. Contact systems (K), Contact systems of early spectral type (KE) and Contact systems of the W UMa type (KW). These systems coincide well with the EW class in method 1 in that phase-folded light-curve describes a close binary system.

The full classification described in the GCVS amalgamates all three methods e.g. the combination of the above three classification methods for eclipsing systems result in the assignment of multiple classifications for object types. These are separated by a solidus ("/") in the data field. Examples are: E/DM (for eclipsing detached main-sequence system), EA/DS/RS (for Algol with a sub-giant in an eruptive system), EB/WR (for Beta-Lyrae with Wolf-Rayet star), and EW/KW (for W UMa with ellipsoid components), etc.

2.2.3 Difficulties in classifying variables using only the light-curve

The main difficulties that were encountered using the proposed method of automated classification were due to the similarities of the light-curve shape and objects that have

similar variability periods and amplitudes. Two of these have been introduced previously, i.e. the similarity between Cepheid-type objects DCEP, CEP, and BCEP and W Vir etc., and between Sinusoidal stars and RRC-type stars. One other expected difficulty was when incorrect periods were obtained for EW eclipsing binary stars. If they were half or double the correct period, the light-curves looked like Cepheid, RRC or Sinusoidal stars. This is why the automated classification system only provides a preliminary classification that must be confirmed using other techniques. The main advantage of the proposed automated system is that it is extremely fast and can be used with light-curves from any survey without re-training the NNs.

2.3. Why classification of stars is useful

The material that follows demonstrates the value of classifying the stellar objects described above, but in order to perform this work, we need to find and classify the objects. This was one of the main objectives of this research.

2.3.1 RR Lyrae stars

Examples of work performed on RR Lyrae stars over the past few years show extensive activity in the areas of *distance calculations*, *distributions*, *stellar structure* and *various anomalies*.

A significant amount of work has been performed with regard to distance calculations, Bono et al. (2008) determined the relative distances to the two globular clusters Omega Centauri and 47 Tucanae using a novel method and then used the distance to the RR Lyrae stars to confirm their results. In the same year, Feast (2008) summarised the findings of the Variable Star Project and estimated the distance to the Large Magellanic Cloud using RR Lyrae and Cepheid stars. Cáceres & Catelan (2008) on the other hand used data from the Sloan Digital Sky Survey to provide the first detailed study of the period-luminosity

relationship in RR Lyrae stars in the 'ugriz' filter bandpasses. This allowed them to obtain precise absolute magnitudes to improve their distance calculations. Like Feast (2008) above, Szewczyk et al. (2008) also calculated the distance to the Large Magellanic Cloud, but they used infrared band observations from the Araucaria Project instead. Similarly, in the same project, Pietrzynski et al. (2008) used similar techniques to obtain the distance to the Sculptor Dwarf Galaxy. Using observations from the revised Hipparcos data, Feast et al. (2008) calculated the infra-red and optical absolute magnitudes for two type II Cepheids and also obtained phase-corrected magnitudes for 142 RR Lyrae stars using 2MASS (Skrutskie et al. 2006) data. This allowed them to calculate the distance to the Galactic Centre. Trying a different approach, this time using period-luminosity-colour and period-colour-colour relations in the multi-band 'uvby' Stroemgren system, Cortés & Catelan (2008) created a theoretical calibration of RR Lyrae to help in distance calculations. Looking at Population-II Cepheids and RR Lyrae stars from the OGLE-II and III surveys, Groenewegen et al. (2008) determined K-band magnitudes for them and used them to obtain the period-luminosity relation and hence the distance modulus to the Galactic Centre. Last, but not least, Prior et al (2009) explored the extent of the Virgo Stellar Stream using RR Lyrae Stars from the SEKBO survey.

Investigating distribution of RR Lyrae stars in the Milky Way was an area looked at by Kunder & Chaboyer (2008) who analysed the metallicity of the galactic bulge RR Lyrae stars, and Silva Aguirre et al. (2008) investigated some RR Lyrae stars with high period change rates to see if they were zero-age horizontal branch stars (pre-ZAHB stars). Catelan & Cortés (2008) used theoretical models to form a relationship between the absolute magnitude of RR Lyrae stars and their periods and Stroemgren pseudo-colour. This allowed them to show an 'over-luminosity' of the star RR Lyr. Looking at the halo of the

Milky Way, Morrison et al. (2009) used a sample of 248 metal-poor stars (including RR Lyrae) to describe its structure.

Investigating distribution outside the Milky Way, Bernard et al. (2008) studied the radial distribution of RR Lyrae stars in the Tucana Dwarf Galaxy using data from the ACS LCID Project.

A number of projects looked at the stellar structure of RR Lyrae stars. For instance, in 2008, Moskalik & Kolaczkowski (2008) used RR Lyrae stars as a comparator for multimode Cepheid pulsators in the Large Magellanic Cloud, and in 2008, Vivas et al. (2008) used samples of RR Lyrae stars from the QUEST survey in a spectroscopic study to look at metallicity in Virgo. In the following year, Subramanian & Subramanian (2009) used RR Lyrae stars to estimate the 'line of sight' depths of the Large and Small Magellanic Clouds to show that the halo of the Large Magellanic Cloud has a larger depth compared to the disk/bar. This indicated the existence of an inner halo.

Finally, two anomalies were investigated, the Blazhko effect and the Oosterhoff dichotomy:

2.3.1.1 Blazhko effect

Blazko (1907) discovered long-period modulation in the star RW Dra due to a variation in the period and amplitude. This is clearly seen in the phase-folded light-curve in Figure 2-12.

Moskalik & Olech (2008) investigated multi-periodic RR Lyrae stars in Omega Centauri noting higher levels of RR Lyrae stars showing the Blazhko effect than in other population studies. Wils et al. (2008) also investigated the Blazhko effect in the RRC star LS Her, and Hurta (2008) investigated the relation between the pulsation and modulation periods of the

RR Lyrae star RV UMa, which also shows the Blazhko effect. The Blazhko effect was investigated further in this research and the results are discussed in chapter 8.5.2.

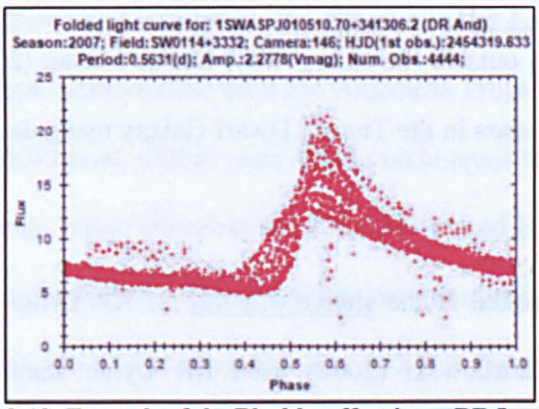

Figure 2-12: Example of the Blazhko effect in an RR Lyrae star (1SWASP J010510.70+341306.2 → DR And)

2.3.1.2 Oosterhoff Dichotomy

Oosterhoff (1939) showed that there was a definite correlation between period and amplitude of RR Lyrae variables in three globular clusters and that the periods fell into two groups (currently known as OoI and OoII). Szczygiel et al. (2009) performed a substantial meta-analysis of work performed by other researchers on the Oosterhoff dichotomy and this is further examined in this research in chapter 8.5.1.

2.3.2 Cepheid-type stars

Looking at examples of work performed on Cepheid stars over the past few years' shows activity in similar areas to RRAB, i.e. *distance calculations*, *distributions*, *stellar structure* and *Blazhko effect*. With regard to distance calculations, Feast (2008) used Classical Cepheids, Type II Cepheids and RR Lyrae stars to calculate the distances to the Large Magellanic Cloud and the Galactic Centre as well as the value of the Hubble Constant. Feast et al. (2008) also derived infrared and optical absolute magnitudes for type II Cepheids using revised Hipparcos parallaxes. In other work, Groenewegen et al. (2008) established an independent distance to the Galactic Centre using Population II Cepheids discovered in the OGLE-II and OGLE-III surveys and Bird et al. (2009) used Cepheids to

extend the cosmic distance ladder to 100 Mpc and beyond. Researching distributions, Maciel et al. (2008) used the abundances of planetary nebulae' to study the chemical evolution of the Galactic bulge. They computed three classes of models for the Galactic bulge. Looking at stellar structure, Romaniello et al. (2008) investigated the influence of chemical composition on the properties of Cepheid stars, and investigated the Blazhko effect, Moskalik & Kolaczkowski (2009) observed the effect in double-mode Cepheids and Molnár et al. (2012) determined if turbulent convective variations could drive the Blazhko cycle. Their findings suggested that the convective cycle model was not well suited as a standalone mechanism behind the Blazhko-effect.

2.3.3 Sinusoidal (Rotational Modulation) stars

Looking at examples of work performed on RM stars over the past few years shows that the visible, ultraviolet and magnetic spectra have all been under scrutiny. Biazzo et al. (2009a) presented preliminary results of a study based on photometric and spectroscopic observations of young weak-line T Tauri and post-T Tauri stars just arriving on the Zero Age Main Sequence. Biazzo et al. (2009b) also presented preliminary results on a study based on contemporaneous photometric and spectroscopic observations of the young K0-1V star SAO 51891. Also, Lobel (2008) presented detailed semi-empiric models for rotational modulations observed in ultraviolet wind lines of B0.5 supergiant HD64760, and Arentoft et al. (2008) carried out a multi-site campaign to measure oscillations in the F5 star Procyon A. They obtained high-precision velocity observations and interpreted them as being due to rotational modulation from active regions on the stellar surface. Jardine et al. (2008) assessed a surface magnetogram of a moderately-accreting T Tauri star (V2129 Oph) and used it to extrapolate the geometry of its large-scale field. Finally, Donati et al. (2008) reported the detection of Zeeman signatures on the classical T Tauri star BP Tau using observations collected with the ESPaDOnS and NARVAL spectropolarimeters.

2.3.4 Eclipsing binary stars

The key science made available by the study of eclipsing binaries is determination of stellar parameters, especially masses and radii of stars, as this simply cannot be measured directly in single stars. Dynamical measurements of eclipsing binaries can allow the masses and radii to be measured directly then compared with model predictions for testing their validity. This underlies all our understanding of stellar structure and evolution. Specific research areas are:

2.3.4.1 Semi-detached eclipsing binary systems

A literature review of work performed on semi-detached binaries over the past few years showed far less activity than on detached or contact binaries. The work appears to cover three distinct areas: *Identification of triple and quadruple systems*, *System parametrics* and *System evolution*. Zasche et al. (2008) selected six semi-detached Algol-type binaries to test for the presence of a third body. Zasche (2008) also examined three Algol-type binaries in the Cygnus constellation. Mennickent et al. (2008) investigated the nature of one of the Double Periodic Variables recently found in the Magellanic Clouds and Van Rensbergen et al. (2008) proposed a method whereby higher mass-ratio Algols can survive longer.

2.3.4.2 Detached eclipsing binary systems

A literature review of work performed on detached binaries over the past few years showed that work appears to only cover two of the three distinct areas also covered by semi-detached binaries: *Identification of triple and quadruple systems* and *System parametrics*. Pribulla et al. (2008) discovered the tightest quadruple system to-date, and Grundahl et al. (2008) determined an accurate age of open cluster NGC6791 using accurate masses and radii of the components of detached eclipsing binary V20. Torres et al. (2008) obtained improved absolute dimensions of the detached, circular, 0.84-day period, double-lined

eclipsing binary system CV Boo for the purpose of testing various aspects of theoretical modelling and Bilir et al. (2008) obtained corrected absolute magnitude calibrations for the detached binary systems with main-sequence components.

2.3.4.3 Contact binary systems

A vast amount of work has been performed on contact binaries over the past few years. This appears to cover the same three distinct areas as semi-detached binaries: *Identification of triple and quadruple systems*, *System parametrics* and *System evolution*. In 2006, Li & Zhang (2006) investigated the dynamical stability of W UMa-type systems. In 2008, Pribulla et al. (2008) identified triple and quadruple systems using radial-velocity measurements, and period analysis was undertaken by Zasche (2008). Rucinski & Pribulla (2008) identified the shortest period contact binary and Nef & Rucinski (2008) estimated the frequency of occurrence of contact binaries in the SMC and LMC based on their luminosity function. Also in 2008, Gazeas & Stepien (2008) presented an alternative scenario of evolution in contact binaries and Li et al. (2008) investigated the evolutionary status and dynamical evolution of W UMa systems. In 2009, Pribulla et al. (2009) discovered the tightest quadruple system to-date and Eker et al. (2009) analysed parallaxes of W UMa stars in the Hipparcos catalogue to re-calibrate the Period–Luminosity–Colour (PLC) relation of W UMa stars. Finally, in 2011, Norton & Payne et al. (2011) identified 53 candidates for short period eclipsing binary stars identified by SuperWASP, which are important for understanding the evolution of low mass stars and to allow investigation of the cause of the period cut-off.

In summary, in order to confirm and/or extend the work described above, it is necessary to obtain many more examples of each stellar class from the many surveys that are underway or have been completed. Surveys are usually performed with specific targets in mind e.g. the main task for SuperWASP is to look for Exoplanets, but while doing this, many other

objects are also recorded and will remain undiscovered until automated systems are created to trawl the stored data efficiently. This is where the system developed in this research will be applied.

2.4. Use of neural networks in classification

Neural networks have been successfully applied to many application areas, such as financial prediction (Zirilli, 1996), inventory control (Bansal et al. 1998), signal analysis and processing (Byung-Su et al. 2001), process control (Kovárová-Kovar et al. 2000), classification (Blonda et al. 1993), speech synthesis (Thompson, 1994), medical diagnosis (Willoughby et al. 1996), e-commerce (Ryan and Silva, 2003) and many others.

They have also become very useful in analysis of large surveys of astronomical data, such as the OGLE survey that provided a census of 2768 eclipsing binaries in the Large Magellanic Cloud (Wyrzykowski et al. 2003, Graczyk et al. 2011). The system used an image recognition neural network to classify the eclipsing binaries into three classes: detached (68.0%), semi-detached (25.9%) and overcontact (6.1%). Another system created by Prŝa et al (2008) trained a neural network to determine principal parameters for eclipsing binaries in a study they were analysing. Blomme et al. (2010) used a supervised neural network to classify the variables in the Kepler survey, which is similar to the method proposed in this research. They identified three independent frequencies for every star, which were used to make a harmonic best-fit to the trend-subtracted time series. They then used a multi-stage tree in each node to decide which stars they want to distinguish. The authors state that the method was good at classifying existing stars and identifying new ones, but did not quantify the results. Debosscher et al. (2011) also analysed the data in the Kepler survey using the same supervised neural network, but the authors added a new extractor method to detect the presence of eclipses when other variability was present in the light curves.

As mentioned in Chapter 1, the method in this research used a representation of the phase-folded light-curve along with the period and amplitude. This method had difficulty in providing a definite class for certain types, but reported a general 'preliminary' class. The major benefits of this method were that it was very fast and could be applied to any periodic variable that could be trained in the NNs.

It should be noted that other automated systems exist that do not depend on neural networks, such as that used by Devor et al. (2008), where the authors used an automated pipeline on a subset of the Trans-Atlantic Exoplanet Survey dataset to identify and model 773 eclipsing binary systems. The method employed fitting each light-curve to a geometric model of a detached EB and then using a ten-step procedure to analyse the data. The authors state that some manual work is required in the final classification.

2.5. Chapter summary

This chapter provided an overview of the variability in stars, and allowed a selection to be made of the various classes of stars that were to be included in the automated classification method described in Chapter 3. The selected classes were:

- Eclipsing binaries: Algol-type (EA), Beta Lyrae-type (EB) and W UMa-type (EW);
- Pulsating stars: Cepheid-type (BCEP, CEP and DCEP), Delta Scuti-type (DSCT), RR Lyrae-type (RRAB and RRC)
- Sinusoidal-type stars, also known as Rotational Modulation (RM) Stars.

Chapter 3 describes the selection and construction of the neural networks that were employed in this research and also describes their training and testing.

---------- o ----------

Chapter 3 NN: Selection, Construction, Training and Testing

This chapter provides a general introduction to Neural Networks (NN) and describes the work performed in selecting the NNs used to classify all the periodic variables in the SuperWASP archive as discussed in Chapter 5.

Functionally, according to Picton (1994), NNs are modelled on the human nervous system (HNS) and are designed to mimic the way the human brain learns and classifies objects. The model of the HNS given by Bowsher (1988) has been adapted in Figure 3-1 to show the similarities between communication in a neuron and communication between human nerve-cells. The model explains the general functionality of NNs and the remaining sections discusses the components of NNs and indicates which models were selected for classification of SuperWASP stellar objects in this research.

3.1. Basic components of a neural network

The black text in Figure 3-1 indicates the terms used for the nervous system and the red text indicates the equivalent term for NNs.

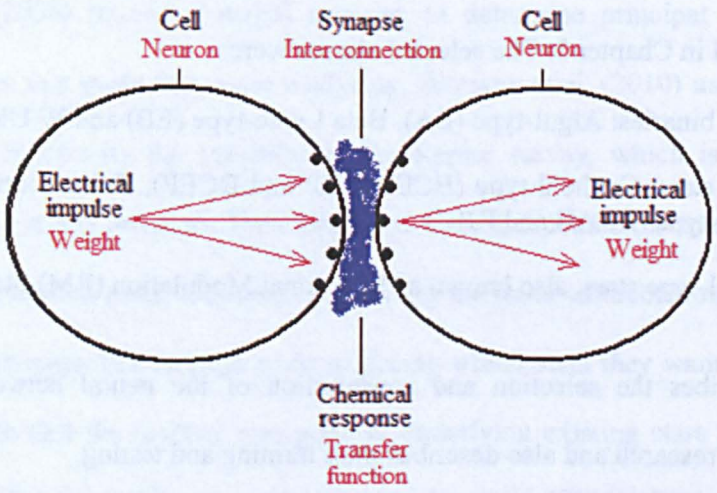

Figure 3-1: Similarities between a neural network and a human nerve cell

In human nerve cells, a cell communicates with adjacent cells by generating an electrical impulse. The impulse causes receptors in the cell to 'fire' i.e. to produce a chemical

response. The size of the response varies on the strength of the impulse and only if the strength of the impulse is greater than the threshold level of the cell, will a response be elicited. The stimulating chemical is released into the connecting synapse and when detected by a neighbouring cell, it is reconverted into an electrical impulse in that cell.

In NNs, a neuron communicates with adjacent neurons by generating a weight value (the equivalent of the electrical impulse). The size of the weight will vary depending on the size of the weights coming from other connecting neurons (the equivalent of the strength of the impulse). This weight is compared against a threshold value (based on the transfer function) and if larger than this value, it causes the neuron to 'fire' i.e. pass its weight value onto the next neuron.

3.2. Brief history of neural networks

In order to describe the functionality of NNs and the complexity they must overcome when used for classification, it is important to understand how they were developed. Development of NNs started in 1943, when McCulloch & Pitts (1943) published the first mathematical model of a biological neuron. It was based on 'excitatory' and 'inhibitory' inputs to a neuron being summed and the sum being compared against a threshold. If the sum was greater than the threshold, a value of 1 was passed on to the next neuron otherwise 0 was passed on.

The single neuron raised much interest at the time because it could be used to perform basic Boolean logic such as 'A AND B', 'A OR B' and 'NOT A' as shown in Figure 3-2, which was adapted from Picton (1994). As the outputs for each of these Boolean functions were different (i.e. 2, 1 and 0), they can successfully differentiate between 'AND', 'OR' and 'NOT'.

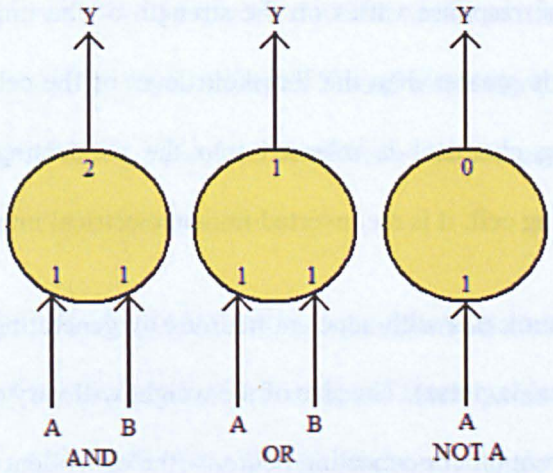

Figure 3-2: Use of single neuron to differentiate Boolean 'AND', 'OR' and 'NOT'

The first attempt to implement a model of this neuron in software was achieved by Rosenplatt (1958) and it was called the perceptron. It contained a single-layer of multiple neurons which was used for optical pattern recognition, but was later found to clearly demonstrate the above Boolean logic. Later, Minsky & Papert (1989) proved the inability of the perceptron to model the Boolean 'exclusive-or' function (XOR). This is clearly demonstrated in the right-hand circle of Figure 3-3, where two lines are needed to isolate the crosses from the dots. This diagram has been expanded from Johnson & Picton (1995).

A	B	A AND B	A OR B	NOT A	A XOR B
0	0	0	0	1	0
1	0	0	1	0	1
0	1	0	1	1	1
1	1	1	1	0	0

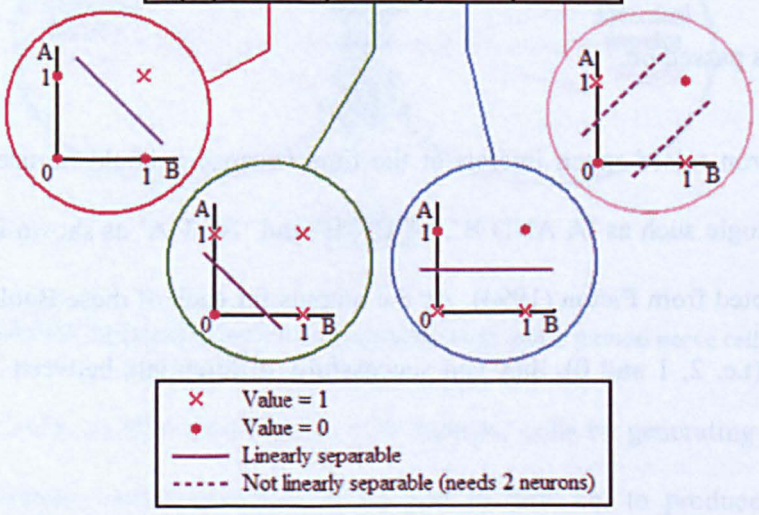

Figure 3-3: Linear separability of the Boolean functions using a single neuron

In Figure 3-3, a single straight line separates the 0's (dots) from the 1's (crosses) in the 'A AND B', 'A OR B' and 'NOT A' functions, demonstrating that they are separable from each other mathematically in the perceptron (Tajine & Elizondo, 2002). This was termed linear separability, which was used in section 3.4.2 to explore the suitability of the Single-layer perceptron (SLP) networks for classifying stellar objects. The non-linear function 'A XOR B' however, cannot be separated this way. This observation by Minsky & Papert (1989) made many researchers lose interest in NNs for a number of years, until the observation was made that the XOR function could be implemented if a number of perceptrons were used together as shown in Figure 3-4.

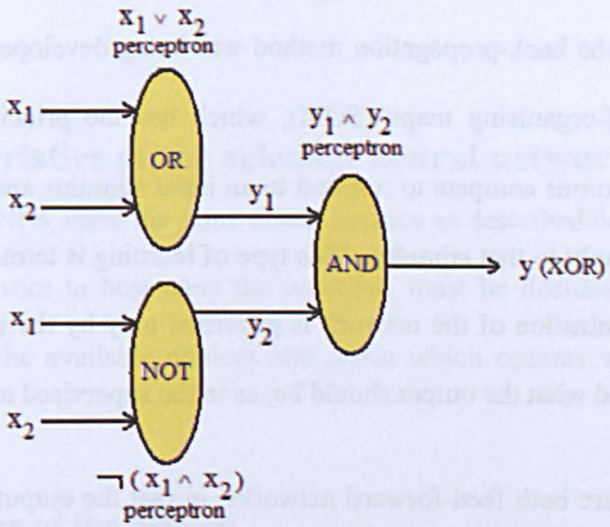

Figure 3-4: Implementation of the XOR function using Multiple Perceptrons

Although a number of SLPs working together solved the XOR problem, this only solved two-dimensional data such as the Boolean functions above. In order to differentiate higher dimensions (like classification of stellar variables) a different method was required which contained multiple layers.

The first multiple-layer perceptron (MLP) to be constructed was the 'back-propagation' NN. This had the ability to implement all of the Boolean functions (including XOR) and it could implement higher-dimensions of data. This ability was realised by implementing

three new features: **incorporating a hidden layer** between the input and output layers; **connecting the output** of every neuron in one layer to the input of every neuron in the next layer (i.e. a fully connected network); and **using a sigmoid function** as the delimiter in each neuron. These new features allowed any error (i.e. the difference between the values in the output layer and the expected output) to be 'back-propagated' through the network for re-processing to minimise this error (hence the name of the network, 'back-propagation'). In order to calculate this error in the output, the MLP needs to know what the expected output is and these values must be given to the network during training. This is termed supervised learning.

At the same time as the back-propagation method was being developed, Kohonen (1990) was working on self-organising maps (SOM), which has the principle of competitive learning, in which neurons compete to respond to an input stimulus and the winner adapts to respond more strongly to that stimulus. This type of learning is termed unsupervised, in that the internal organization of the network is governed only by the input stimuli (i.e. it has not been instructed what the output should be, as in the supervised model).

The MLP and SOM are both feed-forward networks, in that the outputs of the neurons in one layer lead to the input of the neurons in the next layer. Hopfield (1982) proposed the first 'feed-back' network, which took the outputs from some neurons and fed them back in to the inputs of neurons in a previous layer. The objective was to be able to store a number of input/output associations in one matrix, but, like the SLP, the network could only be used for linear-separable functions i.e. its use was also restricted to value of 0 and 1.

Today, there are a vast number of different NN types available based on the type of learning, topology and type of data they accept. Although the number of networks seemed

to be never-ending, with new networks springing up frequently, they are all based on the same core concepts of supervised/unsupervised' and 'feed-forward/feed-back'.

From all the NNs reviewed in the literature, the main observation was that there were many ways to achieve the same end. An SLP can classify linear data, an MLP can classify multi-dimensional data and a SOM can classify data without being supervised. All the other network types provide small improvements to the basic models. It was therefore decided to assess only the 'supervised' models in this research (i.e. SLP and MLP networks) as there was sufficient information available to provide the known outcomes required for supervised training. The unsupervised training method, SOM will be examined in future work.

3.3. Characteristics of the selected neural network models

The SLP and MLP NNs share the same characteristics as described below. When creating NNs, the characteristics to best meet the objective must be decided upon. This section describes some of the available choices and states which options were selected in this research.

3.3.1 Structure of the neuron

The neuron is the most basic building block of all NNs (see Figure 3-5). The neuron receives input values from a set of neurons in a previous layer (x_0 to x_n in the diagram), multiplies them by the weights stored for each input and then sums the result. This becomes the new weight for the neuron. The result is then converted by a transfer function (section 3.3.2) to provide a suitable output for the neurons in the next layer. This process continues through to the output layer (section 3.3.4).

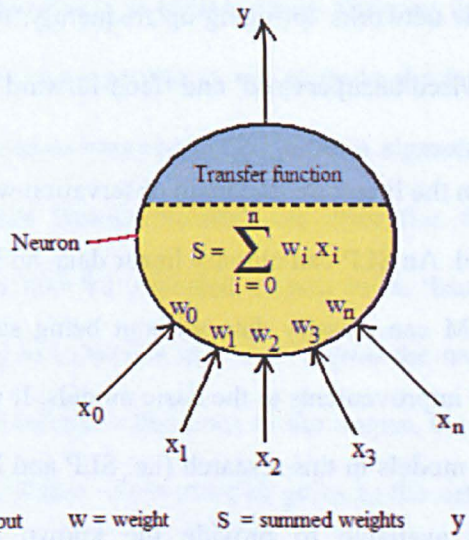

Figure 3-5: Structure of a single neuron in a neural network

3.3.2 Transfer function

As shown in Figure 3-5, the sum S is modified by a transfer function and the modified value is passed to each neuron in the next layer. The reason for modifying the output is to keep the output limited to the required domain. The literature shows many types of transfer function: '**Sigmoid' function** as used by Turner (1997), where the function is a continuous monotonic mapping of the input to a value between 0.0 and 1.0; '**TanH' function** (Hyperbolic Tangent), where the output is very similar to the sigmoid function, but it maps to the range -1.0 to 1.0; '**Linear' function** as used by Mahapatra et al. (1999), where the output of the transfer function is just the sum of the neuron i.e. no change takes place; '**Sine' function**, where the output takes the trigonometric sine of the input; '**Brain-State-in-a-Box' (BSB)** as described by Vandenberghe and Vandewalle (1989), where there is a linear mapping of input to output modified by the value of the recall portion of the appropriate learning and recall schedule; and the '**Bi-Directional Associative Memory' (BAM)** as described by Picton (1994), where the output is 1 if the sum is > 0, the Sum itself if the Sum is 0, or –1 if the sum is < 0. As well as these 'general' transfer functions, there are also 'network specific' transfer functions, such as '**Radial Basis' function** as

used by Sanchez et al. (1996) and the **'Boltzmann machine'** network as described by Hertz et al. (1991). These transfer functions make use of values generated by the architecture of the network.

Of the many options used for the transfer function, the two most common, tried and tested methods were selected for this research: 'Sigmoid' and 'TanH'. Both functions are graphically displayed in Figure 3-6.

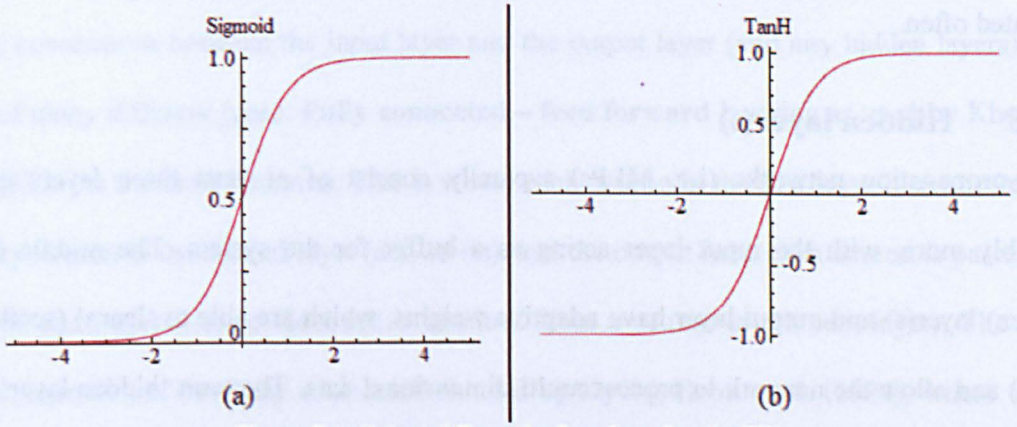

Figure 3-6: Selected Transfer functions for the NNs

3.3.3 Input layer

The input layer is simply a set of neurons that accept the pre-processed input values from the user and stores them ready to pass on to the next layer. In this work, three NN models were created with 28, 27 and 53 input neurons respectively. They are fully described in section 3.4.1.

3.3.4 Output layer

Each neuron in the output layer holds the response of the network to a given input. In some network types (e.g. the MLP), a neuron in the output layer calculates a scaled local error (i.e. the difference between the expected output and the current weight), and then calculates a delta weight to back-propagate through the network. The weights in each neuron in the network are altered by adding the delta weight to the corresponding previous

weight values. In this way, the NN converges to a solution in the pattern space. The solution obtained by NNs then usually requires post-processing in order to interpret the results of the network (section 3.4.3).

For the three NN models used in this research, the back-propagation networks were selected as they are more robust than the alternatives. They are known to be slow to train, but this is not a problem for classification of stellar objects as the training phase will not be repeated often.

3.3.5 Hidden layer(s)

Back-propagation networks (i.e. MLPs) typically consist of at least three layers and possibly more, with the input layer acting as a buffer for the system. The middle (or hidden) layer(s) and output layer have adaptive weights, which are able to 'learn' (section 3.3.8) and allow the network to process multi-dimensional data. The term 'hidden layer' is used as neither the inputs or the outputs of this layer can be seen by the outside world.

The number of hidden layers is not limited but typically, there would be one or two. General consensus (Cybenko, 1989; Hecht-Nielsen, 1989; and Hornik et al. 1989) indicates that one hidden layer is sufficient for most NNs. Two hidden-layers may improve the training slightly, but it increases the length of time required for training (Chester, 1990). In this research, the decision was made to use one hidden layer only.

3.3.6 Number of neurons in the Hidden layer

A number of heuristic rules have been stated in the literature to identify the number of neurons to use in the hidden layer, such as **not more than twice the number in the input layer** (Berry & Linoff, 1997 and Swingler, 1996); or **somewhere between the size of the input layer and output layer** (Blum, 1992); or more complicated scenarios like **as many hidden nodes as dimensions needed to capture 70-90% of the variance of the input**

data (Boger & Guterman, 1997). Whichever method is chosen, it is usually the starting point for the NN and further work is then required in a 'trial-and-error' fashion to obtain the best number of neurons.

For this research, the second heuristic rule above was selected and a range of numbers chosen to test in the trial-and-error fashion (section 3.5).

3.3.7 Layer connections

The connections between the input layer and the output layer (and any hidden layers) can be of many different types. **Fully connected – feed forward** layering as used by Khaw et al. (1995) is the most common. This is where each neuron in the first layer is connected to every neuron in the second layer (and so on), and the output from each neuron is passed on to the next layer (i.e. no feedback is obtained from a neuron in the next layer). The next most common is **Partially connected** as used by Kyung-Hoon et al. (1994), where some neurons are not connected to all the neurons in the next layer. Other types of layer connections occurring in the literature are: **Bi-directional** as described by Picton (1994, pages 79 to 81), where an additional set of connections carry the output of the neurons in the second layer into the neurons in the first layer (i.e. feed-forward and feed-back in the same network); **Resonance** as used by Williamson (1996), where a bi-directional network continually sends signals between the layers until a given condition is reached; **Recurrent** as used by Werbos (1990), where neurons within a layer are fully or partially connected (intra-layer connections) and a joint decision is reached before communication with the next layer is concerned; and **On centre/Off surround**, where a neuron within a layer has connections to itself and its immediate neighbours. The group of neurons activate itself or other groups and passes the active output to the next layer. There are many others available.

In addition to the way the layers are connected, the NN can be either hetero-associative or auto-associative. This describes the link between types of input and output data. If the desired output of the NN is different to the input data, then the network is said to be hetero-associative, otherwise, it is auto-associative.

For this research, 'Fully connected – feed forward layering' and 'Partially connected layering' was selected, both types being auto-associative. These are the most common methods available.

3.3.8 Learning method

The information presented to the NN is used to update the connection weights at each layer. The methods used to achieve this are termed learning methods and they can be classified into three forms. The first form is termed **unsupervised learning**, where neurons in the hidden layer(s) must find a way to organize themselves without help from the outside world. In this approach, no sample outputs are provided to the network against which it can measure its predictive performance. The second form is termed **supervised learning** (or reinforcement learning), where learning is reinforced from the outside world. The connections among the neurons in the hidden layer are randomly arranged then the weights adjusted as the network is told how close it is to solving the problem. The third form is an extension of the supervised method and it is termed **back-propagation.** The method has proven highly successful in training of multi-layered NNs. The network is not just given reinforcement for how it is doing on a task, as information about errors is also filtered back through the system and is used to adjust the connections between the layers, thus improving performance. For this research supervised back-propagation learning was selected as there was sufficient information available to provide the known outcomes required for supervised training and the back-propagation method is known to provide better classification.

3.3.9 Learn rule

There are a variety of learning rules that are in common use. These rules are mathematical algorithms used to update the connection weights, and most are some sort of variation of the best-known and oldest learning rule that was described by Hebb (1949). **Hebb's rule** described a situation where a connection weight entering a neuron is incremented if both the input is high and the desired output is high. He modelled this on the biological term where a neural pathway is strengthened each time an activation occurs on each side of the synapse. Modifications to this rule lead to others, such as **Hopfield's rule** (Hopfield, 1982), which is similar to Hebb's Rule, with the exception that it specifies the magnitude of the strengthening or weakening of the interaction. It states, "if the desired output and input are both active, or both inactive, then increment the connection weight by the learning rate (section 3.3.10), otherwise decrement the weight by the learning rate". Another rule is the **Delta rule** (Widrow & Hoff, 1960), which is a further variation of Hebb's Rule, and it is one of the most commonly used. The rule is based on the idea of continuously modifying the strengths of the weights to reduce the difference (i.e. delta) between the desired output value and the actual output of a neuron. The error is back propagated into previous layers one layer at a time until the first layer is reached. Three other rules based on the Delta rule, are the **Norm-Cum-Delta Rule**, **Delta-bar-delta rule** (Jacobs, 1988) and **Extended Delta-bar-delta** (as employed by Minai & Williams, 1990). The Norm-Cum-Delta-Rule accumulates changes to the weights and only updates the weights at the end of an *epoch*, thus normalising them so the learning rate is independent of epoch size. The Delta-bar-delta and Extended Delta-bar-delta rules attempt to increase the speed of convergence by using heuristic rules. This involves using past values of the gradient, to infer the curvature of the local error surface and then using this information to perform intelligent steps in the weight space using a number of simple rules. Two other

variations are, the **Quick-prop** (Fahlman, 1988) and **Maxprop** rules (Burgess et al. 2006). They use a quadratic estimation heuristic to determine direction and step size.

For this research the Delta, Norm-cum-delta, Delta-bar-delta, Extended Delta-bar-delta, Quick-prop and Maxprop rules were selected. The main reason for this was that the Delta rule is the most commonly used learning method and it is suitable for use with the SLP and MLP. The other rules are variations of this method, which may improve the network.

3.3.10 Learn rate and Momentum

Learning in NNs takes time. The time taken to learn is termed 'time to converge to a solution' and the convergence time increases with the complexity of the system. One of the problems of learning is setting an appropriate learning rate that will cause the network to converge to a 'global' solution in the fastest time possible, while avoiding the 'local' solutions (see Figure 3-7).

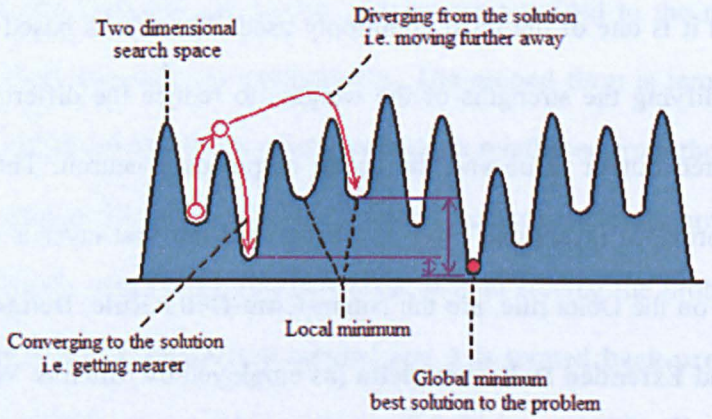

Figure 3-7: Finding the 'global' solution

In order to avoid these 'local' solutions, the function 'momentum' was introduced. Momentum provides the network with the facility to 'jump' out of a 'local' minimum and continue the search for a 'global' minimum (i.e. best solution). This is achieved by adding a portion of the previous delta weight to the current delta weight. Obtaining the 'best' learn rate and 'momentum' is usually done by trial and error. For this research, a value of 0.4

was selected for all networks as this value was used in similar NNs for other non-related projects in unpublished work.

In summary of this section, the following NN models and internal components were selected, to test in 'trial-and-error' scenarios using the NN parameters discussed in the next section (3.4)…

Component	Selection
Neural network structure	SLP; MLP
Input neurons	Based on the input parameter set (section 3.4)
Hidden layers	1
Hidden neurons	Based on the input parameter set (section 3.4)
Output neurons	9
Transfer function	Sigmoid; TanH
Layer connections	Fully connected – Feed forward; Partially connected
Learn method	Supervised Back-propagation
Learn rule	Delta; Norm-Cum-Delta; Delta-Bar-Delta; Extended Delta-Bar-Delta; Quick-prop; Maxprop
Momentum	0.4

Table 3-1: Network components to be tested

The justification for this selection was three-fold: they are the most widely used network components from the 'supervised' network lists; the algorithms were easily obtainable for inclusion in the application that was created in Chapter 5 (section 5.1); and, in order to identify if stellar variables can be classified by NNs, it is advisable to use the most basic, well-documented models available.

3.4. Selection of parameters to be used in the neural networks

The parameters selected for training and testing the NNs were designed to represent the shape of the binned phase-folded light-curve for each star. The light-curves were created from observations obtained from the SuperWASP archive and the following parameters calculated from the curve using the 'LC Analyser classifier' application created and fully described in Chapter 5 (section 5.1):

3.4.1 Parameters used and pre-processing ready for analysis

Variability period: This was one of the parameters already calculated and stored for each stellar object in the SuperWASP archive. The 'LC Analyser classifier' application retrieved this value directly from the SuperWASP archive database. The period was calculated using the method described by Norton et al. (2007), where the method selected data for a given object on a 'per camera', 'per site', 'per year' basis. This restricted the light-curve to ~100 days maximum length. It then removed the upper and lower 1% of data points and removed the remaining flux spikes/dropouts based on extreme excursions from the running mean. A two-stage period finding process was then used, where the first stage involved identification of the variability period through period folding and the second stage involved calculation of the variability period through creation of a power spectrum. The periods that were common to both stages were stored in the SuperWASP archive. This method sometimes provided multiple variability periods for each stellar object, which were usually harmonics or daily aliases of each other. For this research, all SuperWASP periods were manually assessed to obtain the most appropriate period for each object (see Chapter 4). The best period was identified by reviewing the folded light-curve created with each period. When two folded light-curves were similar in shape, the period that gave the shortest string length was used (the string-length being the length of the binned folded light-curve as calculated by Dworetsky (1983)).

Once the best period had been obtained for the object, it was compared against the list in Table 3-2, to obtain the period bin to be used in the NNs.

Period bin	Period range (days)
1	0.0000 to 1.0000
2	1.0001 to 10.0000
3	10.0001 to 50.0000
4	50.0001 to 100.0000
5	100.0001 to 500.0000
6	500.0001 to 999999.0

Table 3-2: Period bin ranges

This was required to bring the period parameter into a range that would not force the neuron values outside their Min-Max ranges. For instance, a period of 100 days would have a more significant effect on the weight values of a NN than a period of 2.5 days, simply due to the magnitude of the value in relation to the sum of the neuron, especially if both objects were the same object class (e.g. EA). Note that the period range in Table 3-2 shows values up to 500 days, even though SuperWASP data only supports periods up to 100 days. This is to make the 'LC Analyser classifier' application scalable over time i.e. the application will not need to be re-built to re-train neural networks at a later time.

X-axis and Y-axis bin values: The data retrieved from the SuperWASP archive was pre-processed by the 'LC Analyser classifier' application prior to creating the folded light-curves. Firstly, observations from selected cameras were excluded when a camera was known to be producing data subject to large uncertainties. Observations were also excluded where the blend flags were greater than 1 (Pollacco et al. 2006). The blend flag was determined by the SuperWASP pipeline and indicated when light-curves were potentially contaminated by a nearby star. Next, satellite trails were excluded by removing observations where magnitude values were within the top and bottom 0.1% range of all observations (from all cameras). Erratic observations were removed if the change in brightness between successive observations was greater than 0.01 magnitudes per second. Finally, the observations to create the folded light-curve were selected from the camera that had the most observations (thus eliminating between camera variability). For objects that had >500 observations remaining, the 'LC Analyser classifier' application created a folded light-curve using the pre-processed observations and the period from the SuperWASP archive as shown in Figure 3-8.

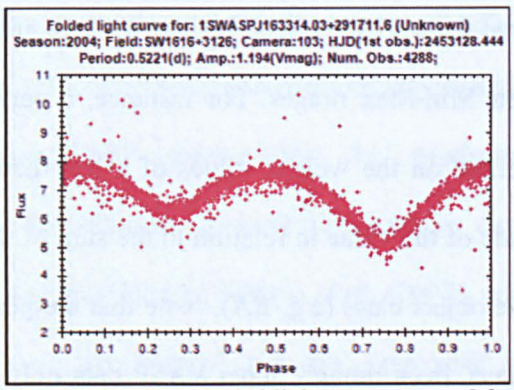

Figure 3-8: Example of a phase-folded light-curve created from flux values (1SWASP J163314.03+291711.6)

A second '25-bin' light-curve was created from the original folded light-curve by creating an average curve from the multiple observations in each bin (see Figure 3-9).

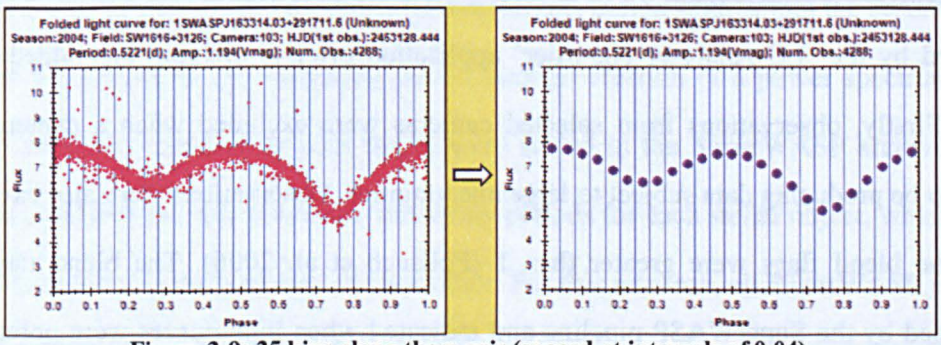

Figure 3-9: 25 bins along the x-axis (spaced at intervals of 0.04), then the average flux is taken for each bin, thus removing spurious observations

The binned light-curve was then expanded in the y-axis (see Figure 3-10) and the light-curve moved along the x-axis until the lowest flux was at position 0 so that it was standardised for a given class (see Figure 3-11).

To obtain the inputs for the NN, the binned light-curve was split into 25 bins on the y-axis and the average flux values placed in the relevant bins as shown in Figure 3-12 and Figure 3-13.

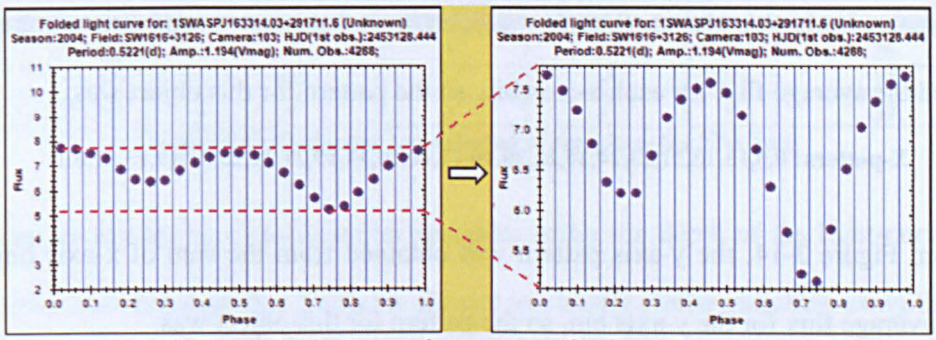

Figure 3-10: Expanded in the y-axis to remove the dependence on amplitude

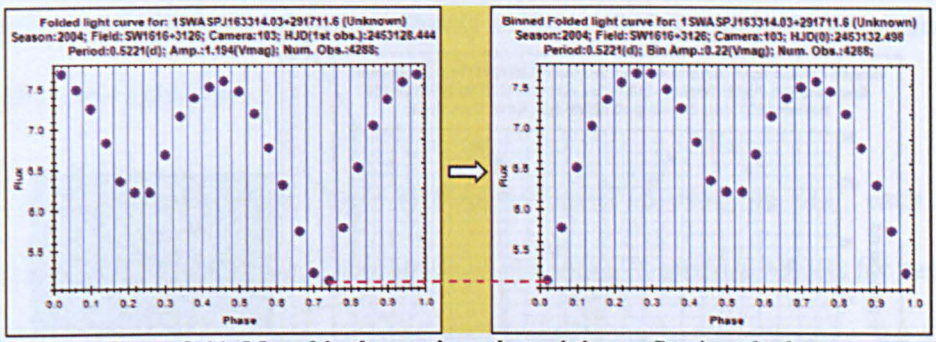

Figure 3-11: Moved in the x-axis so that minimum flux is at 0-phase – this standardises the shape of the light-curve

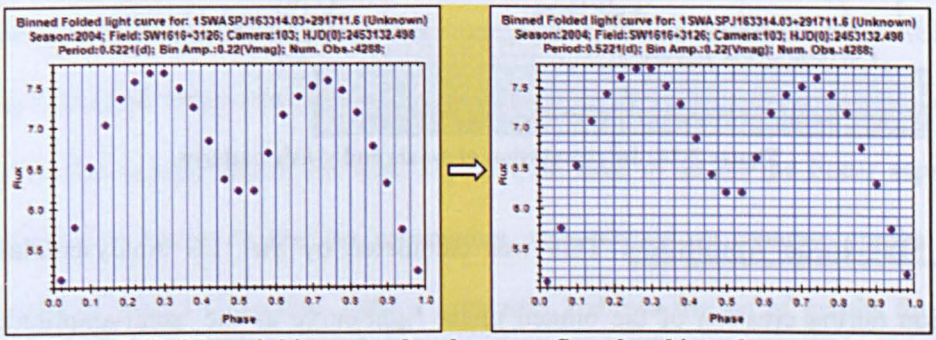

Figure 3-12: 25 y-axis bins created and average flux placed into the correct bins

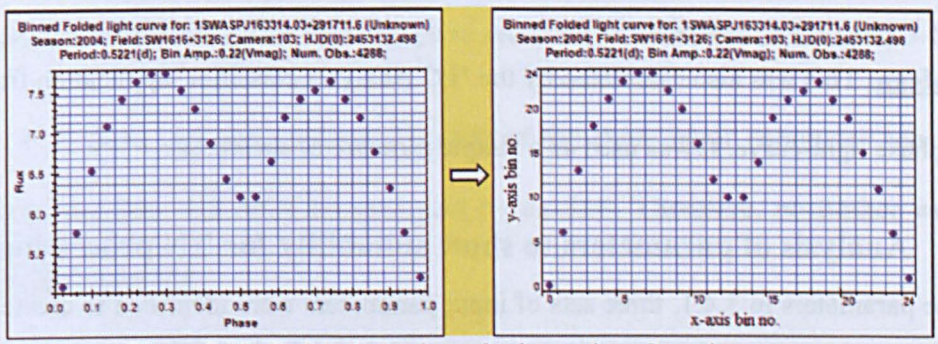

Figure 3-13: Re-labelled axis to obtain x-axis and y-axis pattern

From Figure 3-14, the x-axis pattern was obtained from the y-axis bin number that contained the average flux for each x-axis bin, so the pattern for this object was:

X-pattern: 0,6,13,18,21,23,24,24,22,20,16,12,10,10,14,19,21,22,23,21,19,15,11,6,1

Also from Figure 3-14, the y-axis pattern was obtained from the sum of x-axis bins that have an average flux for the y-axis bin, so the pattern for this object was:

Y-pattern: 1,1,0,0,0,0,2,0,0,0,2,1,1,1,1,1,1,0,1,2,1,3,2,2,2

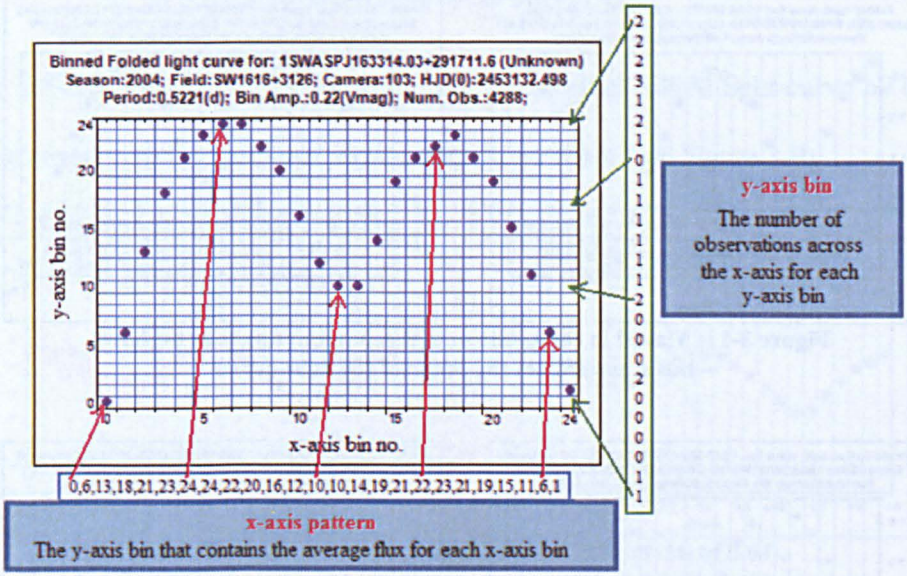

Figure 3-14: Interpretation of x-axis and y-axis patterns

Binned Magnitude Amplitude: This was calculated by the 'LC Analyser classifier' application during creation of the binned phase light-curve as the 'semi-amplitude' (i.e. half the peak-to-peak amplitude). Objects were rejected if the BMA was 0.01 or less.

Mode-Mean: This was also calculated by the 'LC Analyser classifier' application from the binned phase light-curve. It was used as a simple measure of skewness.

3.4.2 Analysis of parameters to show suitability for NN processing

From the parameters in 3.4.1, three sets of input parameters were identified to create 3 NN models, as shown in Table 3-3:

Set	X-axis pattern	Y-axis pattern	Period bin	Mode-mean	BMA	No. Input neurons
1	N/A	✓	✓	✓	✓	28
2	✓	N/A	✓	✓	N/A	27
3	✓	✓	✓	✓	✓	53

Table 3-3: Parameter sets selected to train/test the NNs with

Set 1 was an attempt to classify stellar variables using the depth of the light-curve along with period and skewness. Set 2 was an attempt to classify stellar variables using the width and shape of the light-curve along with period and skewness. Set 3 used all the available parameters and therefore attempted to classify stellar variables with both the general shape and depth of the light-curve.

To see if these parameter sets were able to be classified using an SLP, each set was assessed for **linear separability**. This involved obtaining 20 random objects for each of the classes CEP, DSCT, EA (Double eclipse), EA (Single eclipse), EB, EW, RM, RRAB, RRC and 'No variability' (i.e. no class) and using the 'LC Analyser classifier' application to calculate the parameters shown in section 3.4.1. Appendix 1 shows the SuperWASP object Id's and calculated values obtained – note that only the first 20 objects in each class were used due to the complexity of the test. The method used to assess the linear separability was graphical in nature in that the parameters were plotted on separate graphs and the convex hull identified (Elizondo, 2006). Appendix 2 shows the set of graphs for each of the three input parameter sets and the convex hull for each class was then extracted from these graphs and plotted on the same graph to see if they overlapped (see Figure 3-15).

Figure 3-15 show that the patterns for each of the three input parameter sets overlap indicating that they will NOT be separated by an SLP. Therefore, no further work was undertaken on the SLP.

Zhao et al. (2000) described the use of Euclidean distances as a comparative measure to show that results from an MLP were acceptable.

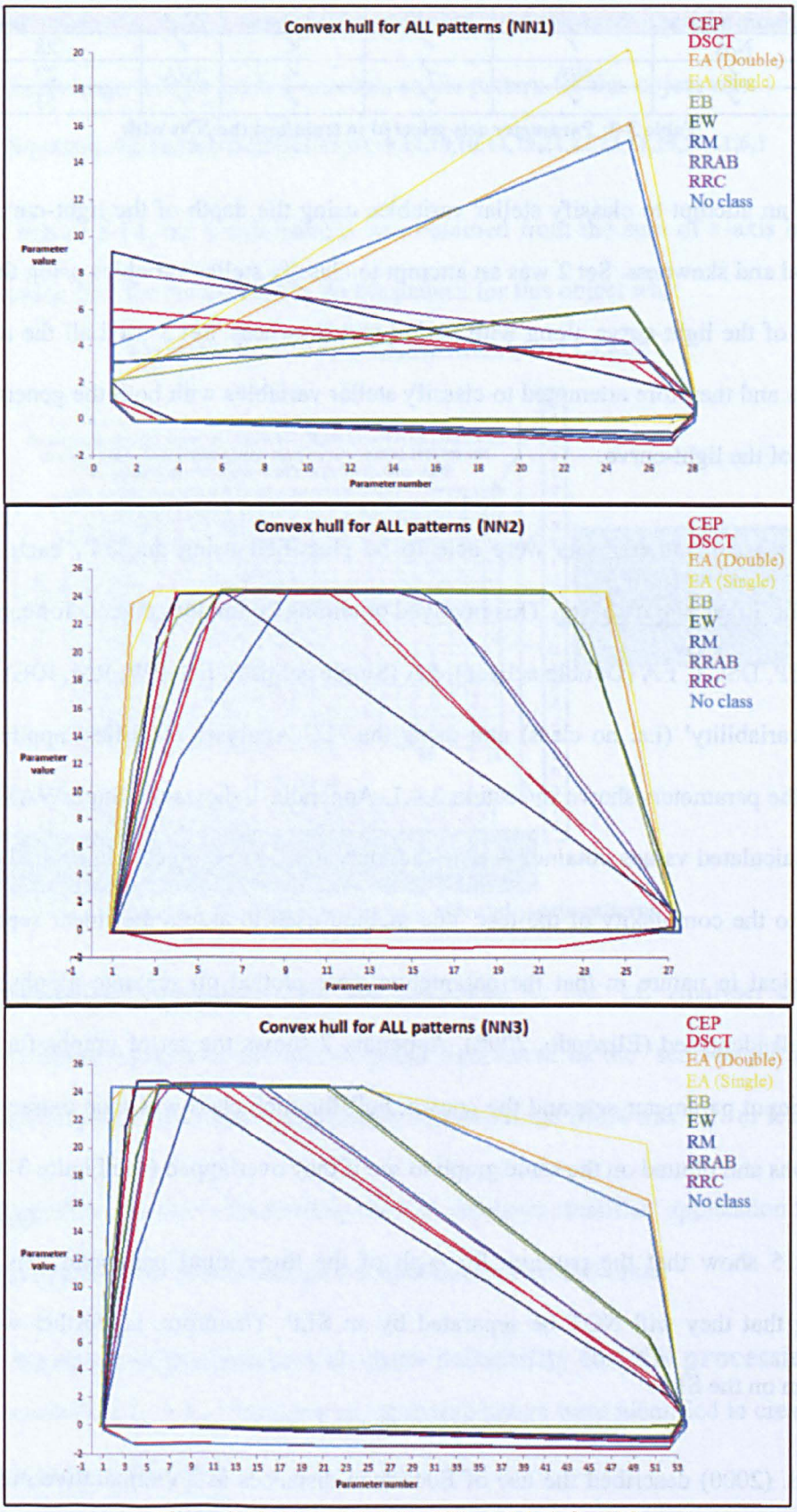

Figure 3-15: Convex hull for NN models 1, 2 and 3 indicating that the parameters overlap one-another and therefore cannot be separated by a SLP

The results indicated that Euclidean Distances, calculated using Equation 3-1, allowed data to be separated using an MLP.

$$D_e = \sqrt{(a_1 - b_1)^2 + (a_2 - b_2)^2 + (a_3 - b_3)^2 + ... + (a_n - b_n)^2}$$

where a_x = object 1 values and b_x = object 2 values

Equation 3-1: Calculation of the Euclidean distance for 'within' and 'between' patterns

The authors used this method to confirm the results of the MLP, so it should be possible to use the method as a 'pre-test' in this research to see if the data can be analysed successfully using an MLP. The method used was: if the median of the 'between-pattern' Euclidean distances was greater than the median of the 'within-pattern' Euclidean distances, then the data would be separable by an MLP. As an example, Figure 3-16 shows the median graph of Euclidean distances obtained for the CEP class using the data for input parameter Set 1. The first column of data (in red) contains the 'within-CEP' distances' i.e. the Euclidean distance between each CEP object, while the other columns show the distances between each object class and the CEP class. The black line connects the median of each dataset…

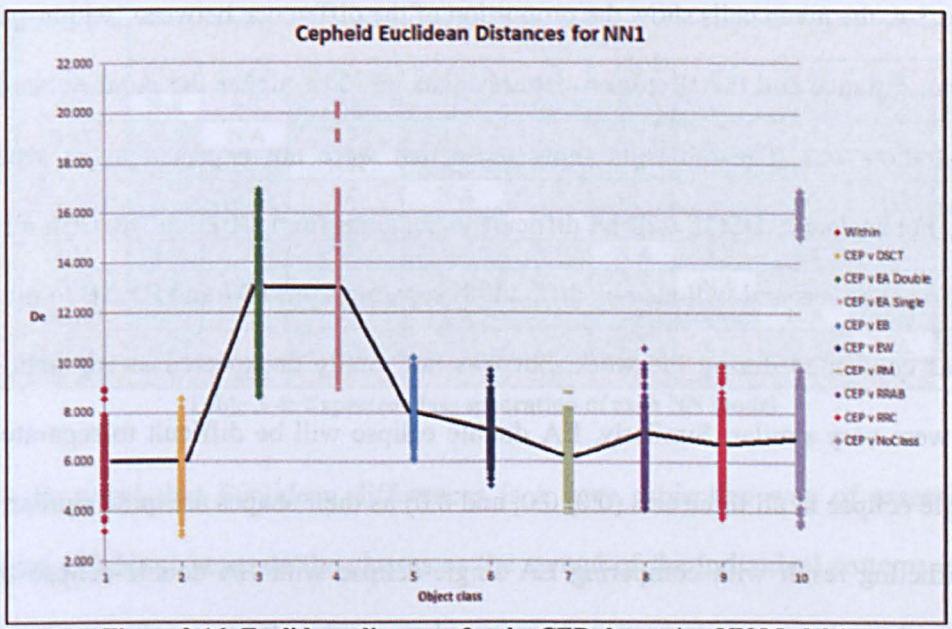

Figure 3-16: Euclidean distances for the CEP class using NN Model 1

The full set of median graphs for all three parameter sets can be seen in Appendix 3 and graphs for the individual objects in each class (plus all Euclidean values) can be seen in the supplementary data on the accompanying DVD in the following location…

Supplementary data	
NN1 Euclidean distances	X:\Chapter03\NN1\EucSet1.xlsm
NN2 Euclidean distances	X:\Chapter03\NN2\EucSet2.xlsm
NN3 Euclidean distances	X:\Chapter03\NN3\EucSet3.xlsm

Where X is DVD-1 in the DVD-drive

From each of the median graphs, the percentage differences were calculated between the median value of each 'between-class' object and the 'within class' object set and the results can be seen in Table 3-4 (below). By scanning down the columns in each table, the results indicate which classes were likely to be separated by an MLP model, with the exception of the 'No class' objects, due to their large spread of values obtained from their random observations. Note that due to the method of calculation (i.e. plotting 'between' values against 'within' values), the results are not associative. The results must be read down the column, not across the rows.

In Table 3-4, the green cells show the proportion of the difference between 'within-pattern' Euclidean distance and the 'Between-pattern' distance. The higher the number, the better the separation was. The red cells show those that were not expected to be separated cleanly. For instance, DSCT will be difficult to separate from CEP and RCC in all three input parameter sets and will also be difficult to separate from RM and RRAB in model 1. This was confirmed during the work, but was not totally unexpected as the light-curve shapes were very similar. Similarly, EA double eclipse will be difficult to separate from EA single eclipse in all three sets (0.0, 0.0, and 0.0) as their shapes are quite similar. Note the conflicting result with comparing EA single-eclipse with EA double-eclipse though (0.2, 0.7 and 0.3). This conflicted with the former results but the values are quite low, so poor separation would be expected. The remainder of the red cells fail to separate in only

one of the parameter sets, so this indicated that it will be necessary to use all three parameter sets for the classification in three different NNs and to amalgamate their results. Therefore, this was the approach taken for the research.

Model 1		D_e (Between)									
	Class	CEP	DSCT	EA Double	EA Single	EB	EW	RM	RRAB	RRC	No class
D_e (Within)	CEP	N/A	0.0	1.2	1.2	0.3	0.3	0.0	0.2	0.2	0.2
	DSCT	0.2	N/A	1.4	1.4	0.6	0.4	0.2	0.2	0.0	0.4
	EA Double	0.4	0.4	N/A	0.2	0.2	0.2	0.3	0.6	0.3	0.3
	EA Single	0.3	0.3	0.0	N/A	0.1	0.1	0.2	0.3	0.2	0.0
	EB	0.3	0.3	0.8	1.2	N/A	0.0	0.0	0.5	0.3	0.8
	EW	0.2	0.2	1.0	1.2	0.0	N/A	0.0	0.3	0.2	0.7
	RM	0.2	0.0	1.0	1.2	0.2	0.2	N/A	0.3	0.2	0.7
	RRAB	0.2	0.0	1.3	1.5	0.5	0.3	0.2	N/A	0.2	0.7
	RRC	0.2	0.0	1.2	1.3	0.3	0.3	0.0	0.2	N/A	0.7
	No class	0.0	0.0	0.0	0.1	0.0	0.0	0.0	0.0	0.0	N/A

Model 2		D_e (Between)									
	Class	CEP	DSCT	EA Double	EA Single	EB	EW	RM	RRAB	RRC	No class
D_e (Within)	CEP	N/A	0.0	1.3	1.3	1.0	1.0	0.3	0.3	0.3	0.8
	DSCT	0.5	N/A	2.5	2.3	1.8	2.0	0.5	0.8	0.5	1.5
	EA Double	3.3	3.3	N/A	0.7	1.3	2.0	2.7	3.7	3.3	2.0
	EA Single	2.3	2.3	0.0	N/A	0.5	1.3	1.5	2.8	2.0	1.5
	EB	2.3	2.3	1.0	1.0	N/A	0.7	2.3	3.0	3.0	2.0
	EW	2.7	2.7	1.7	1.7	0.7	N/A	2.7	2.7	3.0	2.0
	RM	1.3	1.3	2.7	2.0	2.0	2.7	N/A	2.7	1.0	2.0
	RRAB	1.3	1.3	4.0	4.0	3.3	3.0	2.7	N/A	2.0	2.7
	RRC	0.2	0.0	1.3	1.2	1.0	1.0	0.0	0.7	N/A	0.7
	No class	0.0	0.0	0.0	0.0	0.0	0.0	0.0	0.0	0.0	N/A

Model 3		D_e (Between)									
	Class	CEP	DSCT	EA Double	EA Single	EB	EW	RM	RRAB	RRC	No class
D_e (Within)	CEP	N/A	0.0	1.3	1.3	0.8	0.8	0.3	0.3	0.3	0.8
	DSCT	0.5	N/A	2.5	2.3	2.0	2.0	0.5	1.0	0.5	1.5
	EA Double	2.5	2.5	N/A	0.3	0.5	1.3	2.0	2.8	2.5	1.8
	EA Single	2.3	2.3	0.0	N/A	0.5	1.0	1.3	2.8	1.8	1.3
	EB	2.7	2.7	1.0	1.3	N/A	0.7	2.0	3.0	2.7	2.0
	EW	2.7	2.7	2.0	2.0	0.7	N/A	2.7	2.7	3.0	2.0
	RM	1.3	1.0	3.0	2.3	2.3	2.7	N/A	2.7	1.3	2.0
	RRAB	1.3	1.3	4.0	4.0	3.3	2.7	2.7	N/A	2.0	3.0
	RRC	0.2	0.0	1.3	1.2	1.0	1.2	0.0	0.7	N/A	0.8
	No class	0.0	0.0	0.0	0.0	0.0	0.0	0.0	0.0	0.0	N/A

Table 3-4: Expected class separation of each NN model

It must be noted that Euclidean differences is a very subjective way of assessing the suitability of NNs to separate the classes as the spread of the individual patterns within a class can be very large and therefore overlap other classes, even if the median of each class

is different. However, the results obtained indicated that it was certainly worth continuing with the MLP in this research.

3.4.3 Neural network output and post-processing

Investigation into the method of post-processing had to take into consideration the fact, that the three NNs were being used as a complimentary set to determine the class of each object. This meant that the networks had to receive the same inputs during training and testing and the output had to be in the same domain. In order to achieve this, each NN was set up to accept bi-polar input and to use a Min-Max table. This ensured that the values being input to the networks were mapped between a bi-polar range of −1 to +1 and each value was scaled between the minimum and maximum values of the input pattern (which were held in the Min-Max table). The output values from each NN were then re-scaled back to the 'real world' values before analysis.

To assess the results of the individual NNs, a 'scoring' method was created that allowed easy comparison of the networks. The method employed compared the output values of each test pattern against a threshold value. The following rules were applied:

1. If the pattern expected a positive state (i.e. a known class) and a value greater than or equal to the threshold was obtained, then a score of 1 was awarded to 'Correct classification'
2. If the pattern expected a positive state and a value less than the threshold was obtained, then a score of 1 was awarded to 'No classification'
3. If the pattern expected a negative state (i.e. no class) and a value greater than the threshold was obtained, then a score of 1 was awarded to 'Misclassification'

The scores were summed and the categories 'percentage classified correctly', 'percentage misclassified' and 'percentage not-classified' were calculated. These values were used to compare each of the test NNs to identify the best model. The scores were also compared against a number of threshold values to obtain an optimum threshold for each NN. This helped to assess the sensitivity of each network. The thresholds used were: 0.1, 0.2, 0.3, 0.4, 0.5, 0.6, 0.7, 0.8, 0.9 and 1.0.

3.4.4 Selection of training criteria

Chapter 4 discusses the selection of both Training and Test sets in depth. Although NNs can generalise (Picton, 1994, pages 34 to 42), they are very poor at extrapolating. Assessing the whole domain of variable objects was not possible in the time given, so a subset was selected containing 30 objects for each of the following classes: Cepheid (CEP), Delta-Scuti (DSCT), Algol-type (EA) double eclipse, Algol-type (EA) single eclipse, Beta-Lyrae type (EB), W-UMa type (EW), Rotational Modulation (RM) stars, RR Lyrae classes RRAB and RRC. These object classes were representative of pulsating and eclipsing classes and the SuperWASP object Id's for each of the training objects can be seen in Appendix 1.

3.4.5 Selection of testing criteria

Like the training data, test data for NNs must cover the domain being tested and the objects must be different from the training set. The test data for this research used 30 objects for each of the classes in the training set. The SuperWASP object Id's can be seen in Appendix 1.

3.5. Investigation of a Multiple-Layer Perceptron

The three parameter sets identified in section 3.4.2 were processed through 90 NNs in total as indicated in this section. All NNs were created using 'NeuralWorks Professional II/Plus'

software created by NeuralWare[15], which was kindly provided by the Open University. Each NN was trained with the required Training set (from Chapter 4) and then both the required Test and Training sets were processed through each NN. The output obtained from each NN was then scored using the method in section 3.4.3 and the results then compared in order to identify the best NN for the parameter set.

3.5.1 Neural Network Model 1

NN Model 1 was created to process the first parameter set shown in section 3.4.2 (Table 3-3). The parameter set comprised the following values calculated from the light-curve: **Y-axis pattern**, **Period bin**, **Amplitude** and **Mode-Mean**. 30 NNs were created as indicated in Table 3-5 in order to identify the best structure.

Neural Network 1								
Test No.	Input	Hidden	Output	Learn-rule	Transfer	Momentum	Connect prior	No. iterations
1	28	15	9	Delta-Rule	TanH	0.40	No	100,000
2	28	15	9	Delta-Rule	Sigmoid	0.40	Yes	100,000
3	28	15	9	Norm-Cum-Delta	TanH	0.40	Yes	100,000
4	28	15	9	Norm-Cum-Delta	Sigmoid	0.40	No	100,000
5	28	15	9	Delta-Bar-Delta	TanH	0.40	No	100,000
6	28	15	9	Delta-Bar-Delta	Sigmoid	0.40	Yes	100,000
7	28	15	9	Ext DBD	TanH	0.40	Yes	100,000
8	28	15	9	Ext DBD	Sigmoid	0.40	No	100,000
9	28	15	9	Quick-Prop	TanH	0.40	No	100,000
10	28	15	9	Quick-Prop	Sigmoid	0.40	Yes	100,000
11	28	15	9	MaxProp	TanH	0.40	Yes	100,000
12	28	15	9	MaxProp	Sigmoid	0.40	No	100,000
13	28	17	9	Delta-Rule	TanH	0.40	Yes	100,000
14	28	17	9	Delta-Rule	Sigmoid	0.40	No	100,000
15	28	17	9	Norm-Cum-Delta	TanH	0.40	No	100,000
16	28	17	9	Norm-Cum-Delta	Sigmoid	0.40	Yes	100,000
17	28	17	9	Delta-Bar-Delta	TanH	0.40	Yes	100,000
18	28	17	9	Delta-Bar-Delta	Sigmoid	0.40	No	100,000
19	28	17	9	Ext DBD	TanH	0.40	No	100,000
20	28	17	9	Ext DBD	Sigmoid	0.40	Yes	100,000
21	28	17	9	Quick-Prop	TanH	0.40	Yes	100,000
22	28	17	9	Quick-Prop	Sigmoid	0.40	No	100,000
23	28	17	9	MaxProp	TanH	0.40	No	100,000
24	28	17	9	MaxProp	Sigmoid	0.40	Yes	100,000
25	28	10	9	Delta-Rule	TanH	0.40	Yes	75,000
26	28	10	9	Delta-Rule	TanH	0.40	Yes	200,000
27	28	17	9	Delta-Rule	TanH	0.40	Yes	75,000
28	28	17	9	Delta-Rule	TanH	0.40	Yes	200,000
29	28	20	9	Delta-Rule	TanH	0.40	Yes	75,000
30	28	20	9	Delta-Rule	TanH	0.40	Yes	200,000

Table 3-5: NN models tested for parameter set 1

[15] http://www.neuralware.com

The number of input and output neurons in each NN was kept constant due to the number of input parameters and expected output classes. The first 24 NNs used 15 or 17 neurons in the hidden layer as it seemed a sensible workspace to separate the 28 inputs. They also varied the learn-rule, transfer function and connection-type. The NN with the best results from the first 24 NNs was further tested in the remaining 6 NNs, to see if there was any improvement with varying the number of hidden neurons and number of iterations.

During the training of the NNs, two tools were used to track the process: Root-Mean-Squared error (RMS) and Correlation coefficient. Both these indicated how under-trained or over-trained the NN was. These values were included in the results and used as part of the analysis.

In order to analyse the results efficiently, a Microsoft Excel spreadsheet was created that took the output from each NN and performed the scoring method shown in section 3.4.3. An example of the output can be seen in Table 3-6 where the raw NN output for the 30 CEP Test objects for Test No. 1 has been placed into the 'Output values' section in the spreadsheet.

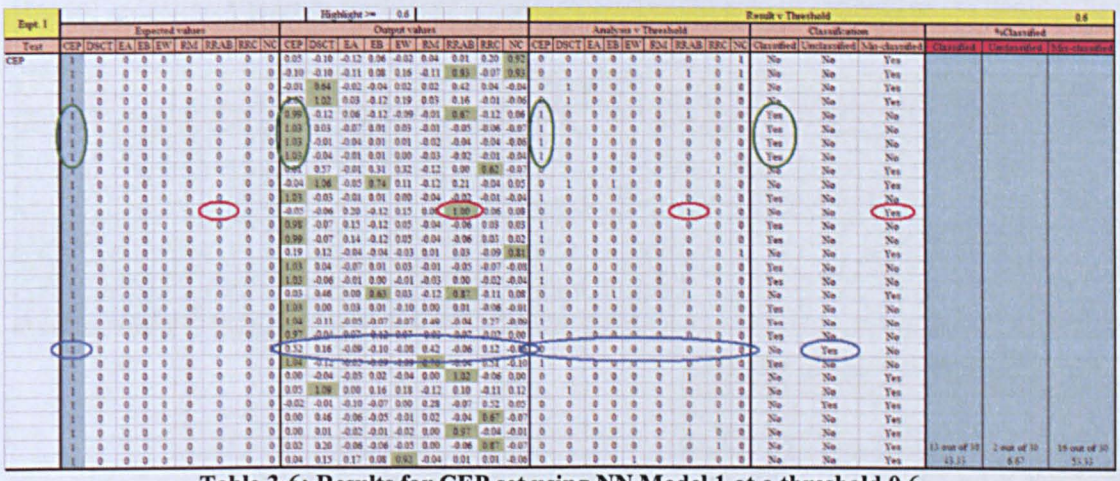

Table 3-6: Results for CEP set using NN Model 1 at a threshold 0.6

The 'Output values' were automatically compared against the threshold in the top right of the grid (i.e. 0.6 in this instance) and the cells highlighted when they were above the threshold. The 'Analysis v Threshold' section updated the scores as indicated in section 3.4.3 and the 'Classification' section used the 'Analysis v Threshold' and 'Expected values' sections to calculate the result and flag the object as 'Classified' (see green ovals), 'Unclassified' (see blue ovals) or 'Misclassified' (see red ovals). The last three columns provided the summary of results for this class. All other classes (e.g. DSCT, EA (Double eclipse), EA (Single eclipse) etc.) were calculated in a similar way in the same worksheet and a second identical worksheet contained the results for the 30 Training objects for each class.

A separate worksheet collated the results for each threshold (0.1 to 1.0) for the NN under test and placed them into a summary grid for easy comparison as shown in Table 3-7.

Expt. 1	Percentage of training data correctly classified																							
Threshold ==>	0.3			0.4			0.5			0.6			0.7			0.8			0.9			1.0		
Classified ==>	%C	%U	%M	%C	%U	%M	%C	%U	%M	%C	%U	%M	%C	%U	%M	%C	%U	%M	%C	%U	%M	%C	%U	%M
CEP	96.67	0.00	3.33	96.67	0.00	3.33	96.67	0.00	3.33	96.67	0.00	3.33	96.67	0.00	3.33	96.67	0.00	3.33	96.67	3.33	3.33	60.00	40.00	3.33
DSCT	100.00	0.00	0.00	100.00	0.00	0.00	100.00	0.00	0.00	100.00	0.00	0.00	100.00	0.00	0.00	100.00	0.00	0.00	83.33	16.67	0.00	36.67	63.33	0.00
EA Double	100.00	0.00	0.00	100.00	0.00	0.00	100.00	0.00	0.00	100.00	0.00	0.00	100.00	0.00	0.00	100.00	0.00	0.00	100.00	0.00	0.00	0.00	100.00	0.00
EA Single	100.00	0.00	0.00	100.00	0.00	0.00	100.00	0.00	0.00	100.00	0.00	0.00	100.00	0.00	0.00	100.00	0.00	0.00	100.00	0.00	0.00	0.00	100.00	0.00
EB	100.00	0.00	0.00	100.00	0.00	0.00	100.00	0.00	0.00	100.00	0.00	0.00	100.00	0.00	0.00	96.67	3.33	0.00	96.67	3.33	0.00	0.00	100.00	0.00
EW	100.00	0.00	0.00	100.00	0.00	0.00	100.00	0.00	0.00	100.00	0.00	0.00	96.67	3.33	0.00	96.67	3.33	0.00	83.33	16.67	0.00	60.00	40.00	0.00
RM	100.00	0.00	0.00	100.00	0.00	0.00	100.00	0.00	0.00	100.00	0.00	0.00	100.00	0.00	0.00	100.00	0.00	0.00	100.00	0.00	0.00	3.33	96.67	0.00
RRAB	100.00	0.00	0.00	100.00	0.00	0.00	100.00	0.00	0.00	100.00	0.00	0.00	100.00	0.00	0.00	96.67	3.33	0.00	96.67	3.33	0.00	30.00	70.00	0.00
RRC	100.00	0.00	0.00	100.00	0.00	0.00	100.00	0.00	0.00	100.00	0.00	0.00	100.00	0.00	0.00	100.00	0.00	0.00	90.00	10.00	0.00	33.33	66.67	0.00
No class	96.67	0.00	3.33	93.33	3.33	3.33	90.00	6.67	3.33	90.00	6.67	3.33	90.00	6.67	3.33	86.67	10.00	3.33	80.00	16.67	3.33	40.00	60.00	3.33
Total	99.33	0.00	0.67	99.00	0.33	0.67	98.67	0.67	0.67	98.67	0.67	0.67	98.33	1.00	0.67	97.33	2.00	0.67	92.67	7.00	0.67	26.33	73.67	0.67

Expt. 1	Percentage of test data correctly classified																							
Pass mark ==>	0.3			0.4			0.5			0.6			0.7			0.8			0.9			1.0		
Classified ==>	%C	%U	%M	%C	%U	%M	%C	%U	%M	%C	%U	%M	%C	%U	%M	%C	%U	%M	%C	%U	%M	%C	%U	%M
CEP	46.67	0.00	53.33	46.67	0.00	53.33	46.67	0.00	53.33	43.33	6.67	53.33	43.33	16.67	53.33	43.33	16.67	53.33	43.33	26.67	53.33	30.00	56.67	53.33
DSCT	60.00	0.00	40.00	60.00	0.00	40.00	60.00	0.00	40.00	56.67	6.67	40.00	46.67	20.00	40.00	46.67	30.00	40.00	40.00	43.33	40.00	23.33	73.33	40.00
EA Double	80.00	0.00	20.00	80.00	3.33	20.00	80.00	6.67	20.00	80.00	6.67	20.00	80.00	6.67	20.00	76.67	10.00	20.00	76.67	20.00	20.00	0.00	100.00	20.00
EA Single	90.00	0.00	10.00	90.00	0.00	10.00	90.00	0.00	10.00	90.00	0.00	10.00	86.67	3.33	10.00	80.00	13.33	10.00	76.67	23.33	10.00	0.00	100.00	10.00
EB	66.67	3.33	30.00	66.67	10.00	30.00	66.67	10.00	30.00	66.67	10.00	30.00	60.00	23.33	30.00	56.67	30.00	30.00	46.67	43.33	30.00	0.00	93.33	30.00
EW	80.00	0.00	20.00	80.00	0.00	20.00	80.00	0.00	20.00	76.67	3.33	20.00	70.00	16.67	20.00	63.33	26.67	20.00	56.67	40.00	20.00	40.00	60.00	20.00
RM	10.00	0.00	90.00	10.00	0.00	90.00	3.33	20.00	90.00	3.33	36.67	90.00	3.33	50.00	90.00	0.00	66.67	90.00	0.00	76.67	90.00	0.00	86.67	90.00
RRAB	76.67	0.00	23.33	76.67	3.33	23.33	76.67	6.67	23.33	76.67	6.67	23.33	76.67	10.00	23.33	70.00	16.67	23.33	56.67	40.00	23.33	26.67	73.33	23.33
RRC	53.33	0.00	46.67	50.00	3.33	46.67	50.00	6.67	46.67	46.67	13.33	46.67	36.67	26.67	46.67	30.00	46.67	46.67	23.33	53.33	46.67	10.00	73.33	46.67
No class	50.00	0.00	50.00	50.00	0.00	50.00	50.00	0.00	50.00	50.00	3.33	50.00	50.00	10.00	50.00	50.00	10.00	50.00	33.33	30.00	50.00	16.67	83.33	50.00
Total	61.33	0.33	38.33	61.00	2.00	38.33	60.33	5.00	38.33	59.00	9.33	38.33	55.33	18.33	38.33	51.67	26.67	38.33	45.33	39.67	38.33	14.67	80.00	38.33

Expt. 1	Number of 'Test' variables classified as object type (N=30)							
Threshold ==>	0.3	0.4	0.5	0.6	0.7	0.8	0.9	1.0
CEP	14	14	14	13	13	13	13	9
DSCT	18	18	18	17	14	14	12	7
EA Double	24	24	24	24	24	23	23	0
EA Single	27	27	27	27	26	24	23	0
EB	20	20	20	20	18	17	14	0
EW	24	24	24	23	21	19	17	12
RM	3	3	1	1	1	0	0	0
RRAB	23	23	23	23	23	21	17	8
RRC	16	15	15	14	11	9	7	3
No class	15	15	15	15	15	15	10	5

Table 3-7: Summary of results for NN Model 1 – Test number 1

The spreadsheet automatically identified the 'best' threshold (highlighted red) as the set with the highest Total %Classified (%C) and lowest Total %Misclassified (%M) i.e. threshold 0.3 for Test No. 1.

In Table 3-7, the top grid shows the results obtained when processing the Training set through the NN. The middle grid shows the results from processing the Test set and the bottom grid shows the number of Test objects that were classified correctly for each class. The individual results and summaries for each of the 30 Model 1 NNs can be seen in the supplementary data on the accompanying DVD in the following location…

Supplementary data	
NN1 Experiment 1 Summary data	X:\Chapter03\NN1\NN_01_Expt01.xlsm
to	to
NN1 Experiment 30 Summary data	X:\Chapter03\NN1\NN_01_Expt30.xlsm

Where X is DVD-1 in the DVD-drive

When all 30 NNs were completed, the data from each summary was extracted and collated into one table so that the 'best' NN could be selected. Table 3-8 shows the overall summary for NN Model 1.

	Results from Best neural network									Results from Best neural network								
	Training statistics		Threshold	Training set classification			Test set classification			Number correct in the Test data set (out of 30)								
Test No.	RMS error	Correlation	Train / Test	%C	%U	%M	%C	%U	%M	CEP	DSCT	EA Double	EA Single	EB	EW	RM	RRAB	RRC	No class
1	0.1005	0.9795	0.3 / 0.3	99.33	0	0.67	61.33	0.33	38.33	14	18	24	27	20	24	3	23	16	15
2	0.1165	0.7579	0.3 / 0.3	85.67	5.00	12.00	56.00	9.33	40.67	13	12	26	28	22	23	1	24	10	9
3	0.3146	0.7773	0.3 / 0.3	83.00	9.33	13.67	52.33	18.33	41.33	8	12	27	29	14	23	3	22	5	14
4	0.1508	0.5497	0.3 / 0.3	39.67	55.00	27.67	24.67	66.67	45.00	1	0	29	29	4	0	1	0	0	10
5	0.3785	0.6041	0.3 / 0.3	59.00	29.67	30.00	37.00	43.33	47.67	6	3	28	27	9	0	4	19	0	15
6	0.1642	0.4448	0.3 / 0.3	33.00	53.00	47.00	25.00	53.33	61.67	0	2	28	29	2	2	2	7	0	3
7	0.2270	0.8796	0.3 / 0.3	93.67	1.33	6.00	60.67	5.00	38.67	13	13	24	29	27	26	0	22	16	12
8	0.1004	0.8268	0.3 / 0.3	90.67	2.00	8.67	60.33	7.67	38.67	13	12	24	29	23	29	1	24	14	12
9	0.4857	0.44	0.4 / 0.3	47.33	18.00	52.67	37.33	12.67	62.67	0	27	28	29	0	0	4	11	1	12
10	0.1358	0.6517	0.3 / 0.3	73.00	13.00	21.00	48.00	23.33	46.67	3	7	27	29	13	20	8	22	4	11
11	0.7474	0.0519	0.3 / 0.3	73.00	13.00	21.00	48.00	23.33	46.67	3	7	27	29	13	20	8	22	4	11
12	0.2980	-0.001	0.6 / 0.3	21.00	0.33	79.00	20.67	0.00	79.33	0	0	30	30	0	0	0	0	0	2
13	0.1267	0.9674	0.6 / 0.3	99.67	0.00	0.33	59.00	4.00	39.33	12	20	22	28	23	22	1	25	12	12
14	0.0746	0.9107	0.3 / 0.3	95.67	0.00	4.33	65.33	1.00	34.67	14	16	27	29	26	30	0	25	16	13
15	0.4253	0.4621	0.3 / 0.3	35.33	52.00	49.67	26.00	56.33	61.00	1	0	22	28	1	24	0	0	0	2
16	0.1319	0.6737	0.3 / 0.3	78.67	9.00	18.00	51.67	17.67	43.67	7	8	28	29	18	20	9	21	4	11
17	0.3368	0.7055	0.3 / 0.3	78.67	10.33	18.00	51.33	16.67	43.67	6	10	28	29	17	20	7	21	5	11
18	0.1860	0.1694	1.0 / 0.3	0.00	100.00	80.00	0.00	100.00	80.00	0	0	0	0	0	0	0	0	0	0
19	0.5297	0.2403	0.3 / 0.3	34.33	62.00	53.00	26.33	65.67	61.00	0	0	25	29	17	0	0	0	0	8
20	0.1274	0.6985	0.3 / 0.3	82.67	7.33	15.00	54.33	11.67	42.00	8	12	27	29	20	21	6	23	7	10
21	0.3208	0.6871	0.3 / 0.3	79.67	5.67	18.33	54.00	7.67	43.00	3	7	24	29	24	24	10	23	8	10
22	0.1537	0.5349	0.3 / 0.3	32.33	62.33	36.67	26.00	63.67	53.00	0	0	29	29	6	0	0	5	0	9
23	0.6249	0.0055	0.3 / 0.3	8.00	0.00	92.00	13.33	0.00	86.67	9	8	0	1	9	0	12	0	0	1
24	0.3251	-0.0321	0.8 / 0.3	10.00	1.67	90.00	10.00	0.00	90.00	0	30	0	0	0	0	0	0	0	0
25	0.1526	0.9516	0.5 / 0.3	99.67	0.00	0.33	57.67	4.33	40.67	11	19	23	28	19	27	0	25	11	10
26	0.1514	0.9521	0.5 / 0.3	99.67	0.00	0.33	57.67	4.00	41.00	11	19	23	28	20	27	0	24	11	10
27	0.1272	0.9672	0.6 / 0.3	99.67	0.00	0.33	59.33	4.00	39.00	12	20	22	28	23	23	1	25	12	12
28	0.1250	0.9681	0.6 / 0.3	99.67	0.00	0.33	58.33	4.33	40.00	12	19	22	28	22	22	1	25	12	12
29	0.1235	0.9701	0.6 / 0.3	99.67	0.00	0.33	60.67	2.67	38.67	14	18	24	29	25	27	0	24	11	10
30	0.1210	0.9710	0.6 / 0.3	99.67	0.00	0.33	60.00	2.33	39.67	14	19	24	29	24	27	0	23	11	9

Table 3-8: Summary of all test results for NN Model 1

The results in Table 3-8 show that the best NN for model 1 was used in Test 27 with a threshold of 0.6. The RMS error and Correlation shows that the NN was not over or under-trained and 99.67% of the training set was classified correctly and only 0.33% was misclassified. The test data shows that 59.33% was classified correctly and 39% was misclassified. The NN did very well on eclipsing binaries and RRAB, but very poor with CEP, RM and RRC. This was lower than expected but is understandable for patterns that were created from the Y-axis as the depth of eclipse can vary significantly between objects within a class and between classes of the same shape.

The selected NN for Model 1 can be seen in Figure 3-17. This was the first NN selected for use in the remainder of the research.

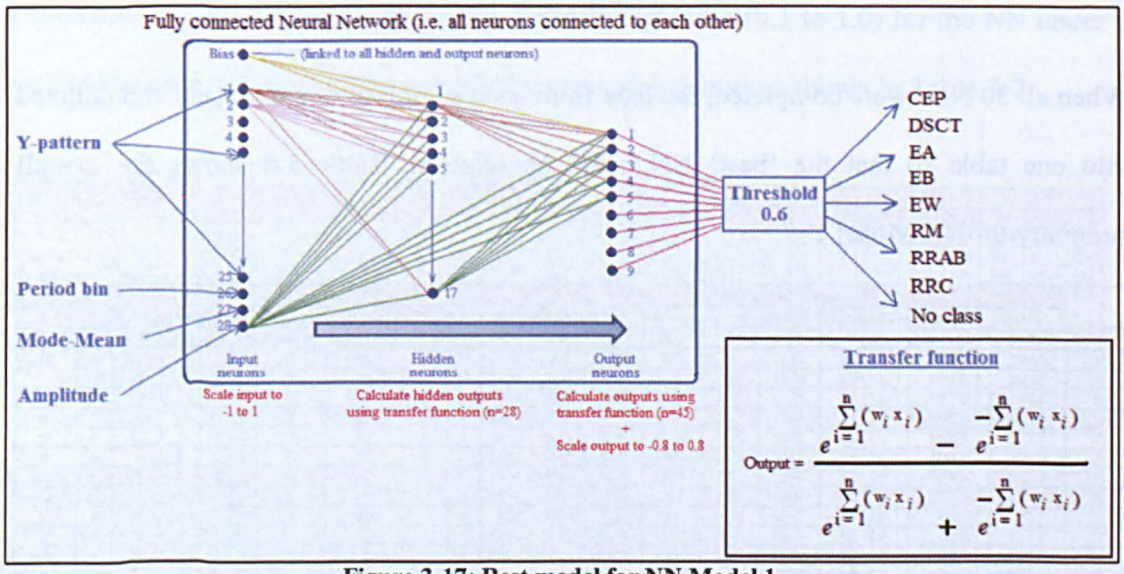

Figure 3-17: Best model for NN Model 1

3.5.2 Neural Network Model 2

NN Model 2 was created to process the second parameter set shown in section 3.4.2 (Table 3-3). The parameter set comprised the following values calculated from the light-curve: **X-axis pattern**, **Period bin** and **Mode-Mean**. 30 NNs were created to identify the best structure as indicated in Table 3-9.

The method of identifying the best NN for this parameter set was identical to that of the first parameter set in section 3.5.1 except for the number of input and hidden neurons. There were 27 input neurons for this NN instead of 28 and therefore the hidden neurons were reduced to 16 and 14 for the first 24 tests to reflect the reduced number of inputs. Tests 25 to 30 were used to fine-tune the best NN obtained in the first 24 tests, by varying the number of hidden neurons and iterations.

Neural Network 2								
Test No.	Input	Hidden	Output	Learn-rule	Transfer	Momentum	Connect prior	No. iterations
1	27	16	9	Delta-Rule	TanH	0.40	No	100,000
2	27	16	9	Delta-Rule	Sigmoid	0.40	Yes	100,000
3	27	16	9	Norm-Cum-Delta	TanH	0.40	Yes	100,000
4	27	16	9	Norm-Cum-Delta	Sigmoid	0.40	No	100,000
5	27	16	9	Delta-Bar-Delta	TanH	0.40	No	100,000
6	27	16	9	Delta-Bar-Delta	Sigmoid	0.40	Yes	100,000
7	27	16	9	Ext DBD	TanH	0.40	Yes	100,000
8	27	16	9	Ext DBD	Sigmoid	0.40	No	100,000
9	27	16	9	Quick-Prop	TanH	0.40	No	100,000
10	27	16	9	Quick-Prop	Sigmoid	0.40	Yes	100,000
11	27	16	9	MaxProp	TanH	0.40	Yes	100,000
12	27	16	9	MaxProp	Sigmoid	0.40	No	100,000
13	27	14	9	Delta-Rule	TanH	0.40	Yes	100,000
14	27	14	9	Delta-Rule	Sigmoid	0.40	No	100,000
15	27	14	9	Norm-Cum-Delta	TanH	0.40	No	100,000
16	27	14	9	Norm-Cum-Delta	Sigmoid	0.40	Yes	100,000
17	27	14	9	Delta-Bar-Delta	TanH	0.40	Yes	100,000
18	27	14	9	Delta-Bar-Delta	Sigmoid	0.40	No	100,000
19	27	14	9	Ext DBD	TanH	0.40	No	100,000
20	27	14	9	Ext DBD	Sigmoid	0.40	Yes	100,000
21	27	14	9	Quick-Prop	TanH	0.40	Yes	100,000
22	27	14	9	Quick-Prop	Sigmoid	0.40	No	100,000
23	27	14	9	MaxProp	TanH	0.40	No	100,000
24	27	14	9	MaxProp	Sigmoid	0.40	Yes	100,000
25	27	10	9	Delta-Rule	TanH	0.40	Yes	75,000
26	27	10	9	Delta-Rule	TanH	0.40	Yes	200,000
27	27	17	9	Delta-Rule	TanH	0.40	Yes	75,000
28	27	17	9	Delta-Rule	TanH	0.40	Yes	200,000
29	27	20	9	Delta-Rule	TanH	0.40	Yes	75,000
30	27	20	9	Delta-Rule	TanH	0.40	Yes	200,000

Table 3-9: NN models tested for parameter set 2

The individual results and summaries for each of the 30 Model 2 NNs can be seen in the supplementary data on the accompanying DVD in the following location…

Supplementary data	
NN2 Experiment 1 Summary data	X:\Chapter03\NN2\NN_01_Expt01.xlsm
To	To
NN2 Experiment 30 Summary data	X:\Chapter03\NN2\NN_01_Expt30.xlsm

Where X is DVD-1 in the DVD-drive

The overall summary for all 30 NNs are presented in Table 3-10 and this shows that the best NN for model 2 was created in Test 13 with a threshold of 0.4. The RMS error and Correlation shows that the NN was not over or under-trained and 99.33% of the training set was classified correctly and 0.67% were misclassified. The test data shows that 75% were classified correctly and 24.67% were misclassified (as opposed to 59.55% classified and 39% misclassified for NN Model 1). This was much better than NN Model 1 in that it did very well with eclipsing binaries and RRABs, but it also did much better with RM objects. However, it still shows difficulty with classifying CEP and RRC objects.

	Results from Best neural network									Results from Best neural network									
	Training statistics		Threshold	Training set classification			Test set classification			Number correct in the Test data set (out of 30)									
Test No.	RMS error	Correlation	Train / Test	%C	%U	%M	%C	%U	%M	CEP	DSCT	EA Double	EA Single	EB	EW	RM	RRAB	RRC	No class
1	0.1325	0.9622	0.3 / 0.3	99.33	0.00	0.67	70.67	2.33	29.00	12	26	22	28	28	29	27	27	10	16
2	0.0866	0.8722	0.3 / 0.3	90.33	0.67	9.67	74.67	0.00	25.33	12	23	22	29	29	30	29	27	9	14
3	0.2390	0.8748	0.3 / 0.3	91.33	0.33	8.33	73.33	2.33	25.67	12	25	22	29	27	29	26	26	12	12
4	0.1316	0.6779	0.3 / 0.3	71.67	5.67	26.33	63.33	7.33	35.00	5	17	28	29	10	30	30	28	0	13
5	0.3301	0.7152	0.3 / 0.3	80.67	4.00	17.67	67.33	7.33	29.67	8	22	26	29	14	30	29	27	2	15
6	0.1512	0.5454	0.3 / 0.3	52.33	24.67	35.33	49.00	24.00	43.00	3	1	30	29	0	30	25	28	0	1
7	0.1465	0.9513	0.4 / 0.3	98.33	0.00	1.67	75.67	0.00	24.33	14	26	21	29	29	30	27	27	7	17
8	0.0918	0.8555	0.3 / 0.3	89.67	0.00	10.33	75.33	0.00	24.67	12	24	23	29	28	30	29	27	12	12
9	0.2425	0.8512	0.4 / 0.3	88.67	1.33	10.67	75.33	0.00	24.67	11	21	23	29	28	30	24	28	19	13
10	0.1276	0.7016	0.3 / 0.3	80.33	2.00	19.00	68.00	2.67	32.00	10	24	27	29	12	30	30	28	1	13
11	0.7121	0.0499	0.5 / 0.3	10.33	2.00	89.67	10.33	0.00	89.67	1	0	0	0	0	0	0	30	0	0
12	0.3000	-0.0013	0.6 / 0.3	21.67	0.00	78.33	21.00	0.00	79.00	0	0	30	30	0	0	0	0	0	3
13	0.1206	0.9680	0.4 / 0.3	99.33	0.00	0.67	75.00	0.33	24.67	13	24	21	28	27	29	26	27	6	11
14	0.0799	0.8925	0.3 / 0.3	92.00	0.00	8.00	77.00	0.00	23.00	15	24	22	29	28	30	28	27	12	16
15	0.2270	0.8772	0.3 / 0.3	91.67	1.00	8.33	74.33	1.33	25.33	12	25	23	29	26	29	29	27	8	15
16	0.1240	0.7215	0.3 / 0.3	80.67	0.67	19.00	70.33	1.67	29.67	8	24	27	30	18	30	29	28	3	14
17	0.3190	0.7435	0.3 / 0.3	85.33	1.00	14.00	70.00	4.00	28.67	10	23	24	30	20	30	29	27	4	13
18	0.1744	0.4230	0.3 / 0.3	20.00	72.67	65.00	19.67	71.00	66.00	0	0	30	29	0	0	0	0	0	0
19	0.1904	0.9025	0.3 / 0.3	94.67	0.00	5.33	75.67	0.00	24.33	14	22	22	29	29	30	26	27	14	14
20	0.1164	0.7601	0.3 / 0.3	86.67	0.67	13.00	71.33	1.67	28.00	10	26	26	28	23	30	29	27	3	12
21	0.2533	0.8487	0.3 / 0.3	88.67	0.33	11.00	75.00	0.33	24.67	16	18	21	29	28	30	23	28	19	13
22	0.1361	0.6510	0.3 / 0.3	65.67	11.67	33.33	59.33	8.33	39.33	0	19	28	29	1	30	30	28	1	12
23	0.7061	0.0194	0.4 / 0.3	10.33	0.00	89.67	11.00	0.00	89.00	0	0	1	2	1	1	24	0	4	0
24	0.3178	-0.0706	0.8 / 0.3	10.00	7.00	90.00	10.00	0.00	90.00	0	0	0	0	30	0	0	0	0	0
25	0.1529	0.9484	0.4 / 0.3	98.33	0.00	1.67	70.33	1.00	29.67	11	25	22	29	26	29	26	27	6	10
26	0.1298	0.9636	0.4 / 0.3	99.33	0.00	0.67	70.67	2.33	29.00	13	24	21	28	27	29	26	27	6	11
27	0.1253	0.9663	0.4 / 0.3	99.00	0.33	1.00	71.00	1.33	28.67	14	25	19	29	29	30	25	26	6	10
28	0.1223	0.9678	0.4 / 0.3	99.33	0.00	0.67	71.67	1.33	28.00	14	25	20	29	29	30	26	26	6	10
29	0.1267	0.9659	0.4 / 0.3	98.67	0.00	1.33	72.33	1.67	27.33	11	26	21	29	28	30	26	27	8	11
30	0.1231	0.9676	0.4 / 0.3	99.00	0.00	1.00	72.33	1.33	27.33	12	26	21	29	28	30	25	27	8	11

Table 3-10: Summary of all test results for NN Model 2

The selected NN for Model 2 is shown in Figure 3-18. This was the second NN selected for use in the remainder of this research.

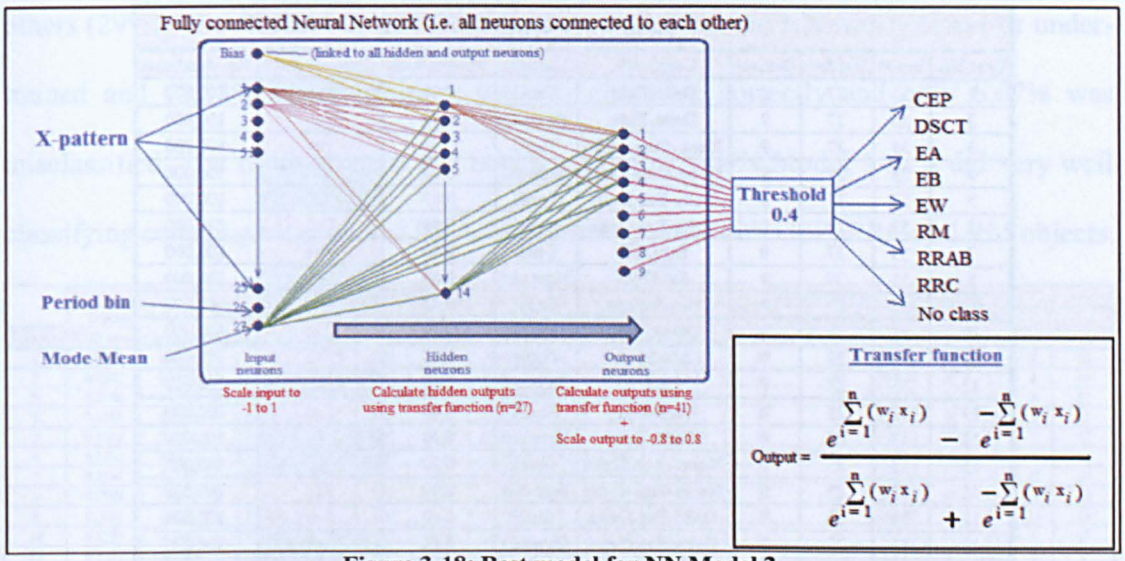

Figure 3-18: Best model for NN Model 2

3.5.3 Neural Network Model 3

NN Model 3 was created to process the third parameter set shown in section 3.4.2 (Table 3-3). The parameter set comprised the following values calculated from the light-curve: **X-axis pattern**, **Y-axis pattern**, **Period bin**, **Mode-Mean** and **Amplitude**. As in the first two NN models, 30 NNs were created to identify the best structure as indicated in Table 3-11 (below).

Again, the method of identifying the best NN for this parameter set was identical to that of the first parameter set in section 3.5.1 except for the number of input and hidden neurons. There were 53 input neurons for this NN instead of 28 and therefore the hidden neurons were increased to 27 and 25 for the first 24 tests to reflect the increased number of inputs. Tests 25 to 30 were used to fine-tune the best NN obtained in the first 24 tests by varying the hidden neurons and iterations.

The individual results and summaries for each of the 30 Model 3 NNs can be seen in the supplementary data on the accompanying DVD in the following location…

Neural Network 3								
Test No.	Input	Hidden	Output	Learn-rule	Transfer	Momentum	Connect prior	No. iterations
1	53	27	9	Delta-Rule	TanH	0.40	No	100,000
2	53	27	9	Delta-Rule	Sigmoid	0.40	Yes	100,000
3	53	27	9	Norm-Cum-Delta	TanH	0.40	Yes	100,000
4	53	27	9	Norm-Cum-Delta	Sigmoid	0.40	No	100,000
5	53	27	9	Delta-Bar-Delta	TanH	0.40	No	100,000
6	53	27	9	Delta-Bar-Delta	Sigmoid	0.40	Yes	100,000
7	53	27	9	Ext DBD	TanH	0.40	Yes	100,000
8	53	27	9	Ext DBD	Sigmoid	0.40	No	100,000
9	53	27	9	Quick-Prop	TanH	0.40	No	100,000
10	53	27	9	Quick-Prop	Sigmoid	0.40	Yes	100,000
11	53	27	9	MaxProp	TanH	0.40	Yes	100,000
12	53	27	9	MaxProp	Sigmoid	0.40	No	100,000
13	53	25	9	Delta-Rule	TanH	0.40	Yes	100,000
14	53	25	9	Delta-Rule	Sigmoid	0.40	No	100,000
15	53	25	9	Norm-Cum-Delta	TanH	0.40	No	100,000
16	53	25	9	Norm-Cum-Delta	Sigmoid	0.40	Yes	100,000
17	53	25	9	Delta-Bar-Delta	TanH	0.40	Yes	100,000
18	53	25	9	Delta-Bar-Delta	Sigmoid	0.40	No	100,000
19	53	25	9	Ext DBD	TanH	0.40	No	100,000
20	53	25	9	Ext DBD	Sigmoid	0.40	Yes	100,000
21	53	25	9	Quick-Prop	TanH	0.40	Yes	100,000
22	53	25	9	Quick-Prop	Sigmoid	0.40	No	100,000
23	53	25	9	MaxProp	TanH	0.40	No	100,000
24	53	25	9	MaxProp	Sigmoid	0.40	Yes	100,000
25	53	10	9	Ext DBD	Sigmoid	0.40	No	75,000
26	53	10	9	Ext DBD	Sigmoid	0.40	No	200,000
27	53	17	9	Ext DBD	Sigmoid	0.40	No	75,000
28	53	17	9	Ext DBD	Sigmoid	0.40	No	200,000
29	53	20	9	Ext DBD	Sigmoid	0.40	No	75,000
30	53	20	9	Ext DBD	Sigmoid	0.40	No	200,000

Table 3-11: NN models tested for parameter set 3

Supplementary data	
NN3 Experiment 1 Summary data	X:\Chapter03\NN3\NN_01_Expt01.xlsm
To	To
NN3 Experiment 30 Summary data	X:\Chapter03\NN3\NN_01_Expt30.xlsm

Where X is DVD-1 in the DVD-drive

The overall summary for all 30 NNs can be seen in Table 3-12 (below).

The best NN for model 3 was created in Test 1, but in this case, Test 8 was selected instead with a threshold of 0.4. The reason for this is that NN model 1 and 2 both used the Delta-rule with TanH transfer rule and Connect-prior. Test 1 for NN model 3 used identical parameters but had a low %Classified value for the test set (69%) and high %Misclassification value (31%). The NN in Test 8 was selected as it had a different set of parameters (Extended Delta-bar-delta, Sigmoid and not connect-prior) and gave a higher level of %Classified for the Test set (71%) and a similar level of %Misclassified as the

others (29%). The RMS error and Correlation showed that the NN was not over or under-trained and 93.33% of the training set was classified correctly and only 6.67% was misclassified. The results for the test data was similar to NN Model 1 as it did very well classifying eclipsing binaries and RRABs, but it was poor with CEP, RRC and RM objects.

	Results from Best neural network									Results from Best neural network									
	Training statistics		Threshold	Training set classification			Test set classification			Number correct in the Test data set (out of 30)									
Test No.	RMS error	Correlation	Train / Test	%C	%U	%M	%C	%U	%M	CEP	DSCT	EA Double	EA Single	EB	EW	RM	RRAB	RRC	No class
1	0.0710	0.9896	0.7 / 0.3	100.00	0.00	0.00	69.00	0.33	31.00	12	21	22	29	24	29	19	26	9	16
2	0.0842	0.8840	0.3 / 0.3	95.33	0.33	4.67	71.67	0.00	28.33	11	23	22	29	29	30	28	27	6	10
3	0.2566	0.8760	0.3 / 0.3	91.33	3.33	6.67	70.67	3.00	28.33	11	24	23	28	25	30	21	25	8	17
4	0.1261	0.7090	0.3 / 0.3	80.67	3.67	16.67	67.67	4.67	31.33	3	17	27	29	19	30	30	28	3	17
5	0.3106	0.7525	0.3 / 0.3	85.33	2.67	12.67	69.33	4.67	29.00	6	19	27	29	20	30	28	27	5	17
6	0.1436	0.5976	0.3 / 0.3	62.33	15.33	31.67	56.33	13.33	41.00	1	13	28	30	5	27	22	28	1	14
7	0.1084	0.9785	0.5 / 0.3	99.33	0.33	0.67	71.33	0.33	28.67	13	20	22	29	28	29	18	26	12	17
8	0.0899	0.8647	0.4 / 0.3	93.33	0.00	6.67	71.00	0.67	29.00	10	22	23	29	28	30	24	27	8	12
9	0.2401	0.8772	0.3 / 0.3	87.67	1.00	12.33	69.00	1.00	30.33	6	18	24	29	28	29	5	28	25	15
10	0.1223	0.7315	0.3 / 0.3	84.67	1.00	15.00	68.00	3.33	31.33	4	21	27	29	17	30	27	28	4	17
11	0.7743	0.0664	0.6 / 0.3	10.67	1.00	89.33	7.33	0.00	92.67	0	13	0	0	7	1	1	0	0	0
12	0.3353	0.0027	0.7 / 0.3	10.00	0.00	90.00	9.67	0.00	90.33	0	0	0	0	0	0	0	0	0	29
13	0.1028	0.9798	0.7 / 0.3	100.00	0.00	0.00	65.33	1.67	34.33	9	23	22	26	28	30	19	22	8	9
14	0.0535	0.9557	0.4 / 0.3	98.33	0.33	1.67	73.67	0.00	26.33	13	24	23	29	28	30	23	26	9	16
15	0.2785	0.8190	0.3 / 0.3	85.33	0.00	14.67	65.67	0.67	34.33	6	22	24	29	26	26	19	25	7	13
16	0.1118	0.7805	0.3 / 0.3	88.67	0.33	11.33	69.67	1.67	30.00	7	21	24	29	22	30	26	28	6	16
17	0.2844	0.8023	0.3 / 0.3	86.67	1.00	13.33	68.67	1.33	31.33	9	17	23	29	22	29	24	28	8	17
18	0.1728	0.4433	0.3 / 0.3	20.00	68.00	58.67	19.67	65.33	59.33	0	0	30	29	0	0	0	0	0	0
19	0.1818	0.9576	0.3 / 0.3	96.67	0.67	3.33	70.00	2.00	29.00	11	16	22	29	27	30	22	28	15	10
20	0.1058	0.8058	0.3 / 0.3	92.67	0.67	7.00	70.00	0.33	30.00	10	22	24	29	23	30	26	27	5	14
21	0.2635	0.8298	0.3 / 0.3	82.33	9.33	12.33	65.33	11.33	31.00	17	11	24	29	26	30	15	26	2	16
22	0.1423	0.6198	0.3 / 0.3	57.67	20.00	36.67	51.67	23.33	41.00	0	7	30	29	0	30	28	28	1	2
23	0.6957	0.0031	0.4 / 0.3	4.00	0.00	96.00	6.00	0.00	94.00	0	8	0	0	6	0	2	1	0	1
24	0.3673	0.0497	0.7 / 0.3	18.00	0.00	82.00	20.00	0.00	80.00	0	0	0	1	8	0	30	10	1	10
25	0.0916	0.8569	0.3 / 0.3	93.00	0.67	7.00	74.00	0.33	26.00	11	23	23	29	29	30	27	26	8	16
26	0.0652	0.9329	0.4 / 0.3	97.00	0.67	3.00	74.33	0.33	25.67	13	25	24	29	27	30	24	28	8	15
27	0.0986	0.8312	0.3 / 0.3	91.00	0.67	9.00	70.33	0.67	29.33	10	22	24	29	25	30	25	27	7	12
28	0.0682	0.9260	0.3 / 0.3	96.67	0.00	3.33	71.67	0.33	28.33	13	22	22	29	28	30	24	28	6	13
29	0.0983	0.8330	0.3 / 0.3	92.00	1.33	8.00	71.67	0.33	28.33	9	23	24	29	26	30	25	27	6	16
30	0.0633	0.9369	0.3 / 0.3	97.00	0.00	3.00	71.67	0.00	28.33	12	24	22	29	28	30	24	26	6	14

Table 3-12: Summary of all test results for NN Model 3

The selected NN for Model 3 can be seen in Figure 3-19. This was the third NN selected for use in the remainder of this research.

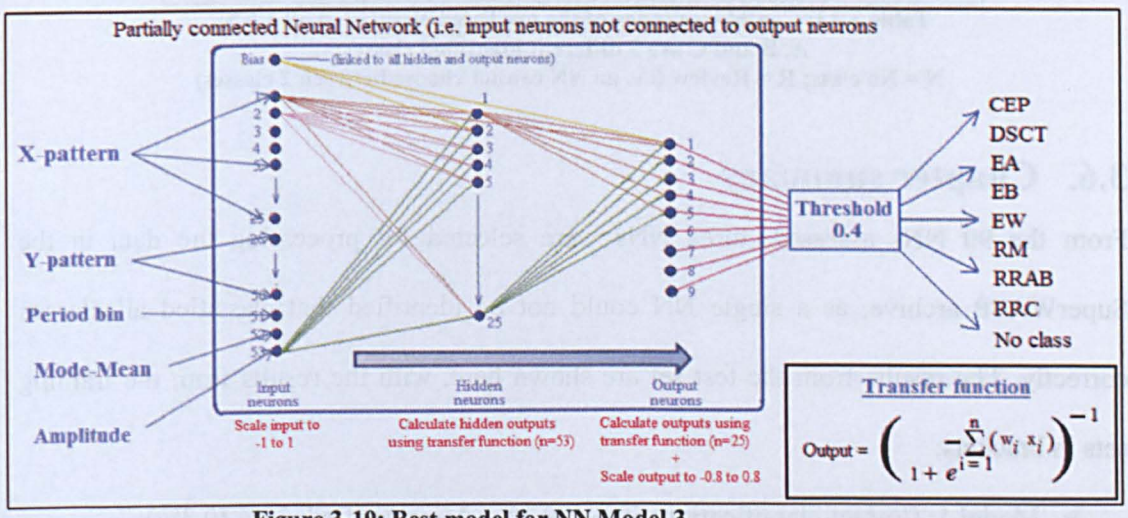

Figure 3-19: Best model for NN Model 3

3.5.4 Final processing

Each of the selected NN models was very good at classifying eclipsing binaries and RR Lyraes and model 2 was good at identifying RM stars. None of the NNs were very efficient at identifying CEP, DSCT and RRC, but this was expected due to the results from the linear separability and Euclidean distance tests in section 3.4.2. To enhance the ability of the NNs to identify these classes, it was decided to use all three NNs together to confirm the class. The final class for the object pattern under test was obtained as shown in Table 3-13 and a 'confidence index' level was assigned. Using this method, researchers would be able to search for objects appropriate to their needs. If objects of a specific class are required then confidence index 1 objects can be retrieved. This will provide a lower number of objects, but they are likely to be of the expected class. If general pulsating objects are required, then a lower confidence index can be used. This will provide a higher number of objects but they may be of mixed class like CEP, DSCT, RRC or RM.

NN1 result	NN2 result	NN3 result	Final class	Confidence
A	A	A	A	1
A	A	N	A	2
A	A	R	A	3
A	N	N	A	4
A	R	N	R	5
A	R	R	A	6
A	A	B	A	7
A	B	C	R	8

Table 3-13: Confidence index of the predicted class using all 3 NNs
A, B and C are 3 different identified classes;
N = No class; R = Review (i.e. an NN cannot choose between 2 classes)

3.6. Chapter summary

From the 90 NNs assessed, three NNs were selected for processing the data in the SuperWASP archive, as a single NN could not be identified that classified all classes correctly. The results from the test set are shown here, with the results from the training sets in brackets:

- Model 1: Correct classification: 59% (99.7%); Misclassified: 39% (0.3%);
- Model 2: Correct classification: 75% (99.3%); Misclassified: 25% (0.7%);

- Model 3: Correct classification: 71% (93.3%); Misclassified: 29% (6.7%);

By using all three NNs together with the method in section 3.5.4, it was possible to increase the confidence index of the result.

The structure of the NNs and the weights from the trained NNs were then extracted from the 'NeuralWorks' software so that they could be implemented in a new application created to automatically process objects from the SuperWASP archive. This is fully described in Chapter 5.

---------- o ----------

Chapter 4 Establishing a 'training' set

In the first part of Chapter 3, NN model structure was described and a number of NN models proposed that could be used to classify all periodic variables in the SuperWASP archive. In order to select the best NNs to use from these and to ensure a high classification rate, the objects used to train and test the NNs needed to be good representatives of each of the classes defined in the NN output i.e. CEP, DSCT, EA double-eclipse, EA single-eclipse, EB, EW, RM, RRAB and RRC. The objects also needed to have correct variability periods. This chapter describes the selection of the objects for the training and test sets that were used in the second part of Chapter 3 to obtain the neural network parameters for the creation of the 'LC Analyser classifier' application in Chapter 5.

To obtain the new improved training sets, the data in the SuperWASP archive was assessed for the following reasons...

- The data is designed to search for extra-solar planets and transient objects, there is therefore a need to assess the systemic effects in the un-de-trended SuperWASP data due to the temperature sensitivity of the optics and the aggressive use of de-trending needed for the planet search.
- If there were any objects in a training or test class that were not of that class then the NNs would either not be able to be trained or they would have a high misclassification rate when testing.

For the assessment, all objects in the SuperWASP archive were obtained that had a variability period and their period values were compared against the GCVS. The classification was performed in two ways: firstly, a direct comparison of the SuperWASP-calculated periods against the known periods in the GCVS; secondly, the objects were processed by the 'LC Analyser classifier' application (see Chapter 5, section 5.1) in order to obtain phase-folded light-curves and binned phase-folded light-curves using the SuperWASP-calculated period and the GCVS-calculated period. These were then manually reviewed to confirm the periods and to obtain the classifications.

From the confirmed objects, 60 were obtained for each class and the three NNs re-trained and re-tested to obtain the parameters for use in the full SuperWASP archive scan.

4.1. Selection of Stellar Classes to use with the NNs

The data used for the assessment was taken from the SuperWASP archive (seasons 2004 to 2008). To confirm the SuperWASP-calculated periods and classifications, objects were obtained from the SuperWASP archive where they had a known period and/or classification in the GCVS. The SuperWASP archive was cross-matched with the GCVS by comparing the position of each SuperWASP object against a 4 arc-second match-radius of the GCVS objects. During this process, objects were removed from the dataset when more than one match was found for a given object. For this study, the subset of classes shown in Table 4-1 was investigated as they covered Pulsating, Eclipsing and Sinusoidal-like periodic variables.

Variability type	GCVS abbreviation	WASP abbreviation	Class name type
Pulsating	BCEP	Cepheid-like	Beta Cephei
	CEP		Cepheid
	DCEP		Delta Cephei
	CWA		W Virginis (type A)
	CWB		W Virginis (type B)
	RRAB	RRAB	RR Lyrae (asymmetric light-curve)
	RRC	RRC	RR Lyrae (near symmetric light-curve)
	DSCT	DSCT	Delta Scuti
	SXPHE		Resemble Delta Scuti
Eclipsing	EA	EA	Algol (Beta Persei) type
	EB	EB	Beta Lyrae type
	EW	EW	W Ursae Majoris type
Sinusoidal like	ACV	Rotational Modulation stars (RM)	Alpha2 Canum Venaticorum
	BY		BY Draconis type
	ELL		Rotating ellipsoid variables
	UV		UV Ceti type

Table 4-1: List of abbreviations for the objects used

In Table 4-1 the 'GCVS abbreviation' column indicates the class as defined in the GCVS, while the 'WASP abbreviation' column indicates what the NNs will classify these objects as. The reason for this revision of class is as follows.

Chapter 2 discusses the differences in variability classes in detail, but this chapter is solely concerned with phase-folded light-curve shapes. The GCVS classification is based on multiple observational parameters, such as spectral type, luminosity class, radial velocity and multiband photometry, whereas the SuperWASP data provides only photometric observations made in the visible band. This meant that the only parameters that could be used for the SuperWASP classification were the variability periods and parameters taken from the shape of the light-curves. This makes it difficult for certain classes of objects to be differentiated from each other e.g. BCEP, CEP, DCEP, CWA and CWB all have the same shape light-curve. As such, Table 4-1 shows the grouping of the GCVS classes into those classes that SuperWASP can identify. The following section describes the classification scheme that was adopted.

4.1.1 Pulsating periodic variables

Pulsating stars are intrinsic variables where their variation in brightness is due to physical changes within the star. Pulsating classes were included in this work as identification of stars in these classes will support researchers in four main areas: *distance indicators*, *stellar distribution*, *stellar structure* and *stellar evolution*. These have all been discussed in Chapter 2. For this study, the following GCVS classes were assessed:

4.1.1.1 Cepheid-like stars:

Four main classes of Cepheid-like stars are described in the literature: Delta-Cephei type (DCEP), Cepheid type (CEP), Beta-Cephei type (BCEP) and W Virginis type (CWA and CWB). As the shape of the light-curves for all four classes are very similar (see Figure 4-1), they cannot be differentiated using only the visible light-curves, therefore further classification criteria would be needed to finalise their classification. In this particular case, it was possible to differentiate BCEP and DCEP using the amplitudes and periods of the pulsations, but the other classes could not be separated. However, as the binned phase-

folded light-curves created by the 'LC Analyser classifier' application were stretched along the y-axis so as to keep a consistent shape (see Chapter 3, section 3.4.1) the amplitude of the light-curve itself, did not play a big part in the neural network classification. The calculated amplitude value was successful in aiding classification for NN1 and NN3 but this parameter was not included in NN2 (see Table 3-3 in chapter 3.4.2). Amplitude values are fully assessed in Chapter 7 and Chapter 8, but for this study, all of these classes were included into one class and called 'Cepheid-like' stars.

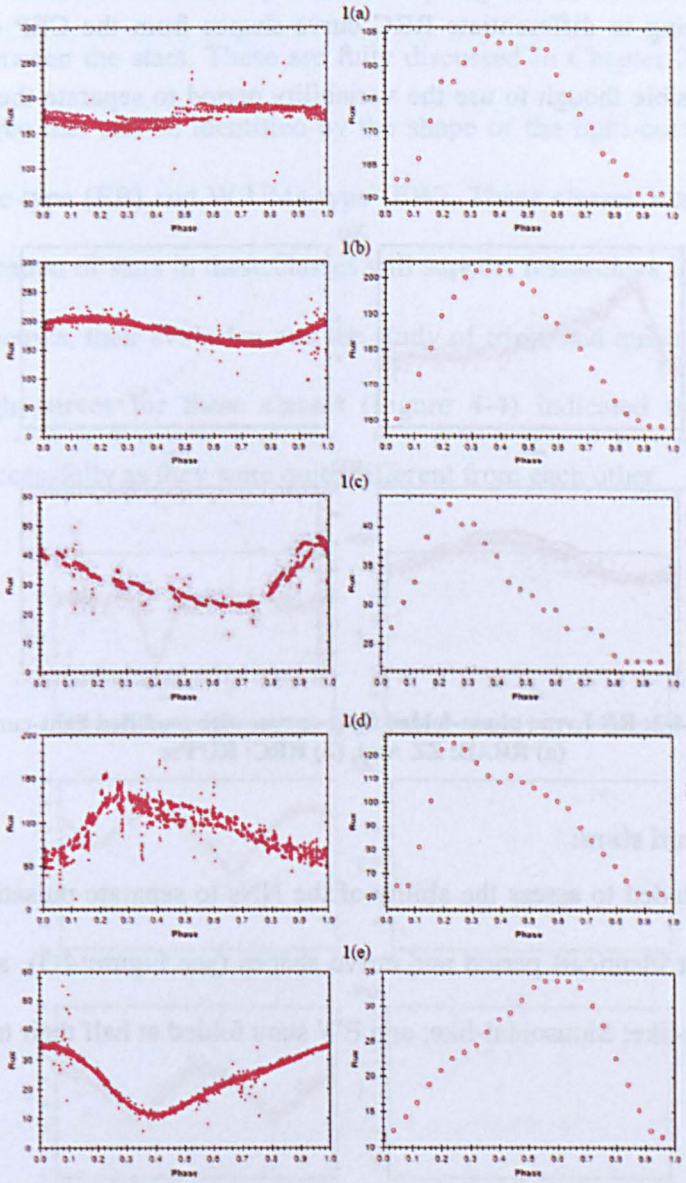

Figure 4-1: Similarity of Cepheid-like phase-folded light-curves shown alongside their modified light-curves
(a) BCEP: V0792 Cas, (b) CEP: AU Peg, (c) DCEP: VY Per, (d) CWA: ST Pup, (e) CWB: HR Aur

Note that the modified curves in Figure 4-1 were binned and repositioned so that the lowest flux is at the 0-point on the x-axis. This made the light-curve shape consistent between objects of the same class.

4.1.1.2 RR Lyrae stars:

There are two types of light-curve for these stars as shown in Figure 4-2, i.e. RRAB and RRC. The classes are described fully in Chapter 2, but as we can see here, it was possible to differentiate between the two as they are clearly of a different shape. However, difficulty did arise when trying to differentiate RRC curve-shapes from the CEP class in section 4.1.1.1. It was possible though to use the variability period to separate the CEP and RRC classes.

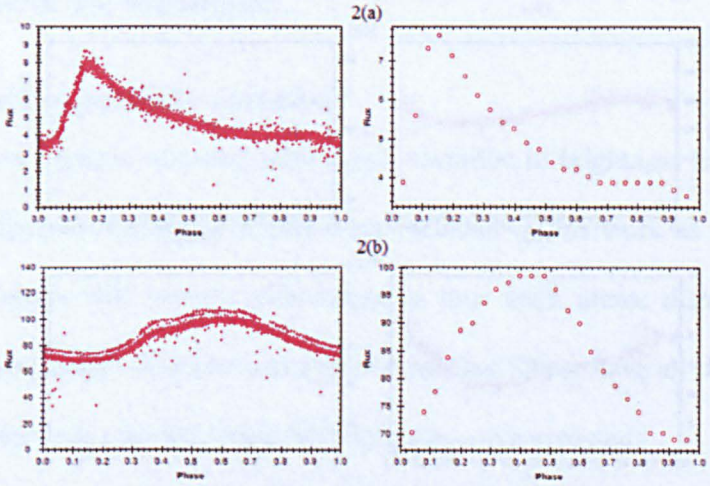

Figure 4-2: RR Lyrae phase-folded light-curves with modified light-curves (a) RRAB: ZZ And, (b) RRC: RU Psc

4.1.1.3 Delta Scuti stars:

This class was included to assess the ability of the NNs to separate pulsating classes with similar (though not identical) period and curve shapes (see Figure 4-3), as they are very similar to: Cepheid-like; Sinusoidal-like; and EW stars folded at half their true period.

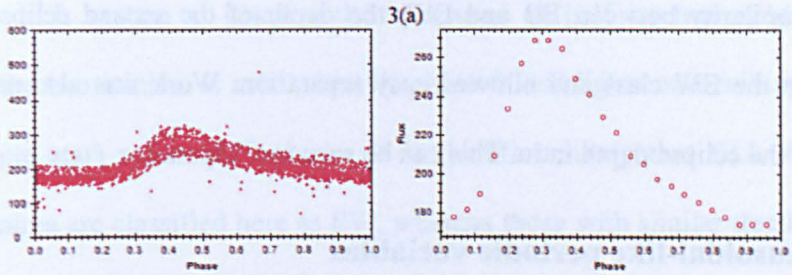

Figure 4-3: Delta Scuti phase-folded light-curve with modified light-curve (a) DSCT: SZ Lyn

4.1.2 Eclipsing periodic variables

Eclipsing binary stars show variability due to eclipsing of one another and may involve mass transfer between the stars. These are fully discussed in Chapter 2. Many sub-types exist, but the three that can be identified by the shape of the light-curve are: Algol-type (EA), Beta Lyrae-type (EB) and W UMa-type (EW). These classes were included in this study as identification of stars in these classes will support researchers in the identification of system parametrics, their evolution and the study of triple and quadruple systems. The phase-folded light-curves for these classes (Figure 4-4) indicated that they could be differentiated successfully as they were quite different from each other.

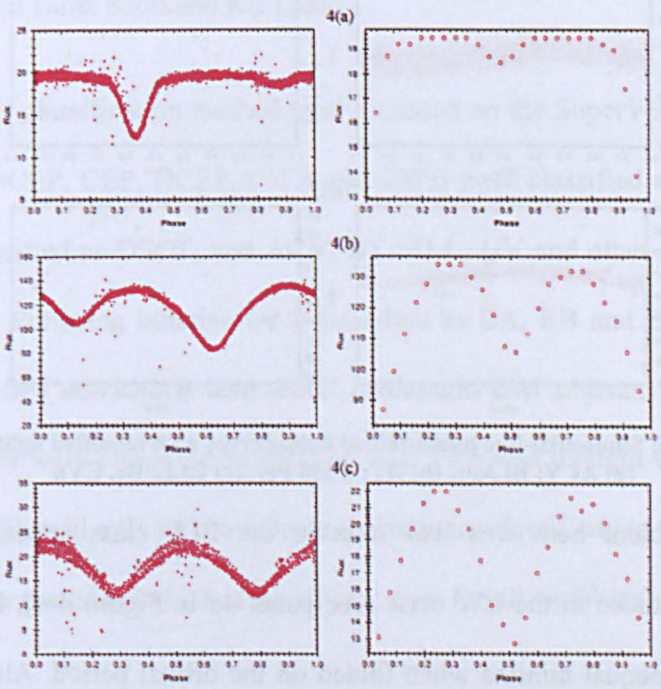

Figure 4-4: Eclipsing binary phase-folded light-curves with modified light-curves (a) EA: V834 Cas, (b) EB: CN And, (c) EW: V366 Cas

Despite the similarity between EB and EW, the depth of the second eclipse was more pronounced in the EW class and allowed easy separation. Work was also performed on assessment of the eclipse depth ratio. This can be seen in Chapter 7.

4.1.3 Sinusoidal-like periodic variables

Variability in Sinusoidal-like stars can be caused by axial rotation of the star and presence of surface spots and chromospheric activity. This class was included in this study as identification of these stars will support researchers in studying stellar activity, rotation and evolution. For example, the classes ACV and BY are axial-rotation stars and the ELL class is a close binary rotational object. However, these objects all show similar light-curves as shown in Figure 4-5.

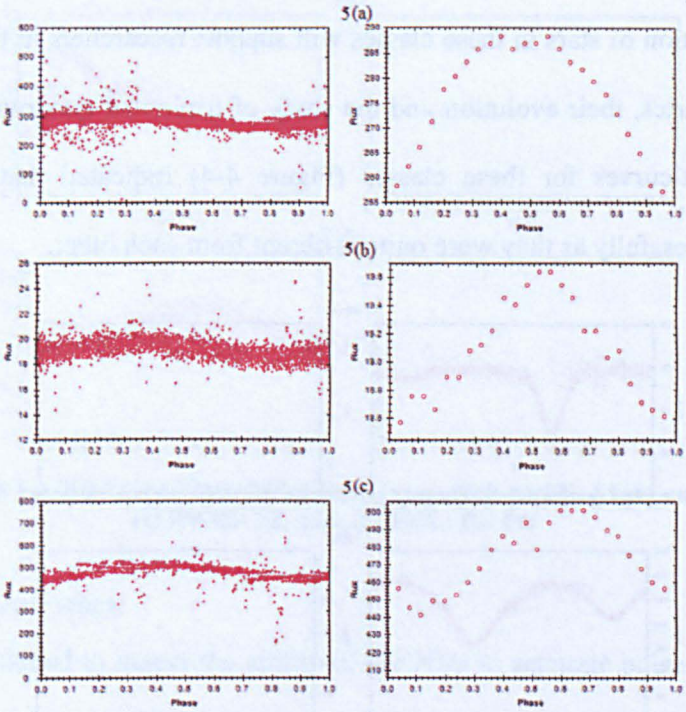

Figure 4-5: Sinusoidal-like phase-folded light-curves with modified light-curves (a) ACV: BI Mic, (b) BY: V530 Per, (c) ELL: BL CVn

An additional problem here was that stars in the ELL class appeared very similar photometrically to those in the EW class (see panel 4c in Figure 4-4), having two equal maxima and two unequal minima when folded on the orbital period. Alternatively, if the

period of an ELL system is (incorrectly) measured at half its true value, when the difference in the two minima is small, then its phase-folded light-curve will appear similar to other (single star) rotational systems. It is therefore likely that ELL systems with dissimilar minima are classified here as EW, whereas those with similar depth minima are classified as Sinusoidal-like, but with half their true period.

4.2. Classification Limitations

As the analysis uses only the period, amplitude (for NN1 and NN3), and shape of the phase-folded light-curve to classify objects, some classes would not be separated without further classification criteria. For instance, both Delta Cep and W Vir stars are quite often called Cepheids because it is often impossible to discriminate between them on the basis of the light-curves for periods in the range 3 - 10 days (see Figure 4-1 above). Similarly, the light-curves of Delta Scuti stars are very similar to RR Lyrae stars. However, they are distinct groups of entirely different objects in different evolutionary stages. They can only be separated by including spectral differences like hydrogen-line emission or variability period in the case of Delta Scuti and RR Lyrae.

For this reason, the classification method used focussed on the SuperWASP classes shown in Table 4-1 i.e. BCEP, CEP, DCEP, CWA and CWB were classified as CEP. DSCT and SXPHE were classified as DSCT, and ACV, BY, ELL, UV and other rotating stars were classified as RM. Eclipsing binaries were classified as EA, EB and EW, and RR Lyrae stars were classified as RRAB and RRC, although EW objects with an incorrect half/double periods were classified as RRC or RM. This was thought to be an acceptable approach as the NNs will only be providing a preliminary classification that will need to be confirmed by other methods (which is usually the case for all variables).

4.3. Assessment Method

All the selected objects were processed as indicated below and the resulting variability periods and folded light-curves were manually assessed to confirm the classification:

4.3.1 Period search

As indicated in Chapter 3, section 3.4.1, a search for periodic variability was performed on all objects in the SuperWASP archive using the method described by Norton et al. (2007). This method sometimes provided multiple variability periods for each stellar object, due to harmonics or daily aliases of each other. In this analysis, all SuperWASP periods were manually assessed to obtain the most appropriate period for each object. The best period was identified by reviewing the phase-folded light-curve created with the periods. When two folded light-curves were grossly different as shown in the top pair of images in Figure 4-6, the period was chosen that gave the 'cleanest' curve, but when they were similar in shape as shown in the bottom pair of images, the period that gave the shortest phase-length was selected (i.e. 7.636 in these images): the phase-length being the length of the binned phase-folded light-curves as calculated by Dworetsky (1983). Note that Dworetsky calls it 'string-length' in his work.

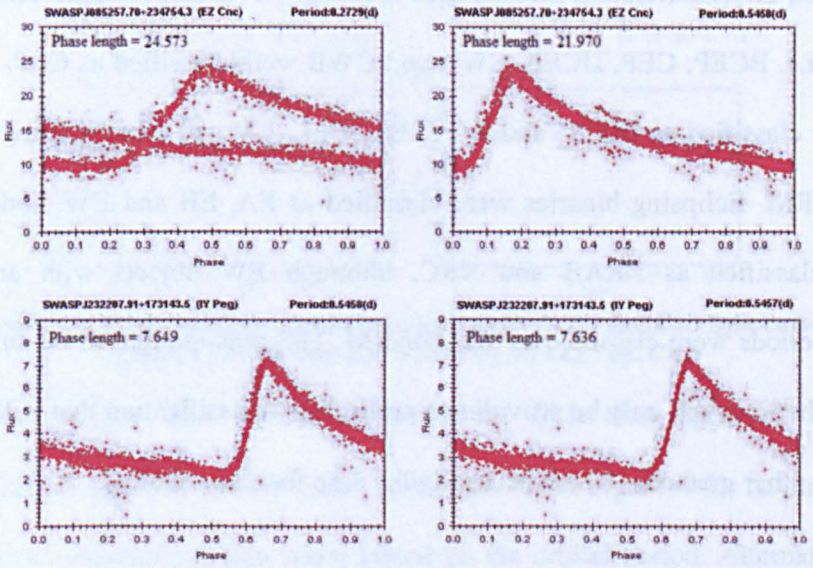

Figure 4-6: Phase-length comparison in grossly different folded light-curves (top) and similar light-curves (bottom)

It was not possible to use the phase-length method for gross differences in curve shape as they can give similar values (as shown in the top 2 images in Figure 4-6). On many occasions, the phase-length was actually smaller on the poorer light-curve, leading to the incorrect period being selected.

4.3.2 Folded light-curve creation

Data retrieved from the SuperWASP archive (for each object) was processed through the 'LC Analyser classifier' application as indicated in Chapter 3 (section 3.4.1). This pre-processed the observations to remove spurious flux values. For all objects that had >500 observations remaining, the 'LC Analyser classifier' application created a phase-folded light-curve as shown in the first diagram of Figure 4-7 and then created a second 'binned' phase-folded light-curve as shown in the second diagram of Figure 4-7. The binned phase-folded light-curve was formed as an average curve from the multiple observations, expanding the graph in the y-axis and then moving the start position of the light-curve in the x-axis so that it was standardised for a given class (i.e. moving the start position of the light-curve in the x-axis so that the minimum flux of the binned phase-folded light-curve falls at phase 0). Each pair of phase-folded light-curves was created twice for each object: once using the SuperWASP-calculated period and once using the known GCVS period and the pairs were then compared manually.

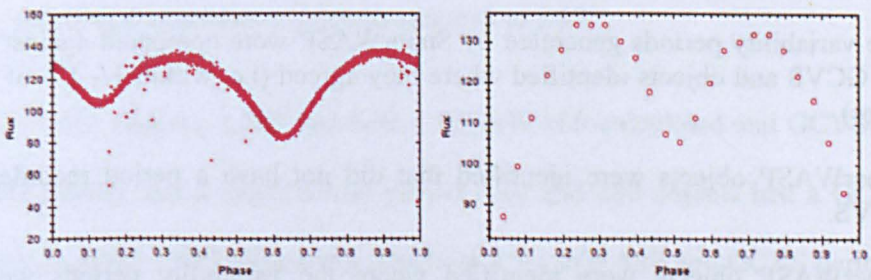

Figure 4-7: Modified phase-folded light-curve (EB-class CN And)

4.3.3 Light-curve classification

The binned phase-folded light-curve of each object was manually compared against the 'typical' curve for each object class (see Chapter 2) and a class assigned. The un-binned phase-folded light-curve was then reviewed to see if the suggested class was appropriate.

During the study, two problems were observed: Firstly, the shape of the binned phase-folded light-curve for Cepheid-like, RRC, Sinusoidal-like and EWs folded at half their true period were very similar. Secondly, the depths of the secondary eclipses of EB and EW were very subjective i.e. there was no numerical cut-off in the literature to decide between EB and EW classes. This was explored further in Chapter 7.

It was accepted that NN classification using the light-curve alone was only going to produce a preliminary classification. However, motivation in this research was to develop a system that could make a useful classification of SuperWASP variables based on light curve shape alone (since that is all that was available). These could then be further assessed by researchers using other methods.

4.3.4 Data analysis

In summary, the following tests were performed on the retrieved data:

- A general census was made of the number of known GCVS periodic objects that exist in the SuperWASP archive.
- The variability periods generated by SuperWASP were compared against those in the GCVS and objects identified where they agreed (i.e. within +/- 1% of the each other).
- SuperWASP objects were identified that did not have a period recorded in the GCVS.
- SuperWASP objects were identified where the variability periods were more accurate than the GCVS periods.
- The period and amplitude values calculated for SuperWASP observations were compared against the ranges given for the classes by the GCVS.
- SuperWASP objects were identified that classified differently to the GCVS.

4.4. Results

Data analysis was performed in two stages, period search and classification. The results are presented here, but it should be noted that presenting data and two light-curves for 3,048 objects would take up a significant amount of space. Therefore, the results for the first 20 objects are shown in tables as examples in the main body of the text and the full lists are included as Adobe 'pdf' files on the accompanying DVD. Similarly for light-curves, a full page of examples are presented in appendices, while each complete set have been placed in Adobe 'pdf' files on the DVD. For each set of results, the exact location of the files where the results can be seen has been provided.

4.4.1 Variability Period results

A total of 3,048 objects were retrieved from the SuperWASP archive where they were known in the GCVS. Comparison of the retrieved objects showed two areas where there were significant differences between SuperWASP and the GCVS periods. Firstly, the long period variables differed (Mira, RV and Semi-regulars SR and sub-classes) due to the limitation on the length of the SuperWASP data range (maximum period search was 50 days). Secondly, a band of variables across the 1-day period range showed a large number of probable false periods for the SuperWASP long period variables. The 424 long-period variables Mira, RV, SR, SRA, SRB, SRC, SRD and the 1-day aliases were therefore removed, reducing the number of objects assessed to 2,621.

From these 2,621 objects, 1,683 had both a SuperWASP-calculated and GCVS-calculated period, 649 objects had a SuperWASP period only and 289 objects had a GCVS period only. Analysis of the 1,683 objects that had both a SuperWASP and GCVS period, showed that 1,472 (87.5%) agreed within +/-1% and only 211 (13%) disagreed.

Figure 4-8 shows a correlation of SuperWASP-calculated and known GCVS variability periods for the 1,683 objects. It can be seen that the majority of objects correlate well, but some are located on the half or double-period lines. The phase-folded light-curves for these objects were examined to find the best period.

The periods that lay well outside the half/double period lines did not show any particular class trend i.e. they appeared to be EA, EB, BCEP, DCEP, CW and RRAB. They were therefore likely to be due to errors in the SuperWASP-calculated or known GCVS period. Again, the phase-folded light-curves were examined to find the best period.

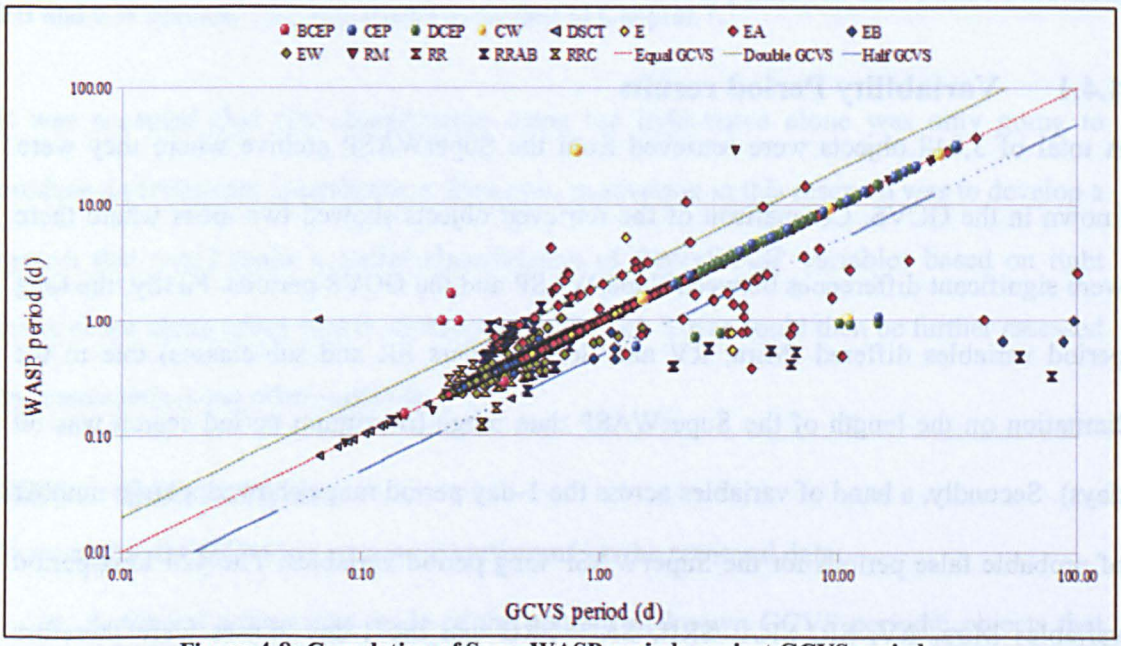

Figure 4-8: Correlation of SuperWASP periods against GCVS periods

Figure 4-9 shows that the majority of periods (i.e. 1,472) lay within +/-1% of each other, with the majority of these lying between +/-0.1%. Table 4-2 lists the first 20 of these objects and Appendix 4 shows the phase-folded light-curves for the first six objects. The complete list of data and phase-folded light-curves can be found on the supplementary DVD in the following location…

Supplementary data	
Object data within +/-1% of GCVS	X:\Chapter04\Table1_data.pdf
Phase-folded light-curves	X:\Chapter04\Table1_images.pdf

Where X is DVD-1 in the DVD-drive

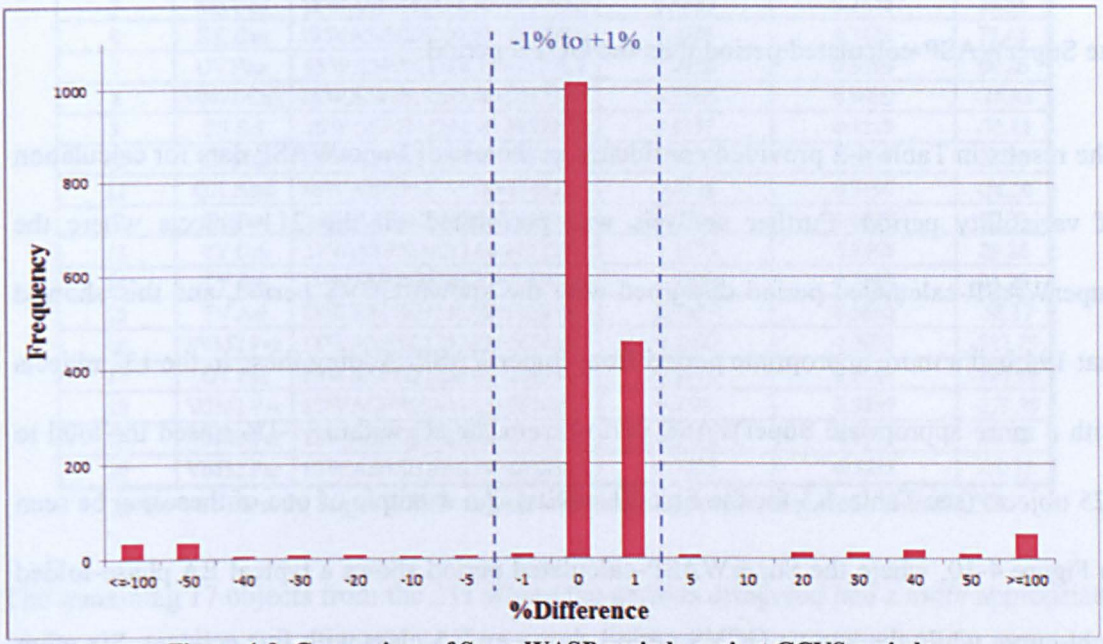

Figure 4-9: Comparison of SuperWASP periods against GCVS periods. This shows that the majority of periods agree within a tolerance of +/-1%

No.	Name	WASP Id	GCVS period (d)	WASP period (d)	%Diff
1	GM And	1SWASPJ000003.66+352146.1	0.7068	0.7066	0.03
2	DM Peg	1SWASPJ000007.28+184417.1	2.5890	2.5878	0.05
3	SW Phe	1SWASPJ000030.01-393729.1	2.5531	2.5530	0.00
4	TZ Scl	1SWASPJ000049.23-284900.4	0.5829	0.5831	-0.03
5	RU Scl	1SWASPJ000248.10-245643.1	0.4933	0.4934	-0.01
6	TW And	1SWASPJ000318.22+325045.0	4.1228	4.1170	0.14
7	EY Cas	1SWASPJ000322.62+574454.5	0.4820	0.4819	0.02
8	UU Cet	1SWASPJ000405.10-165951.5	0.6061	0.6061	0.00
9	IX Cas	1SWASPJ000450.82+501405.5	9.1534	9.1435	0.11
10	AM And	1SWASPJ000507.48+482705.2	8.8505	8.8325	0.20
11	WW Scl	1SWASPJ000601.94-365414.7	0.7866	0.7848	0.23
12	SX Scl	1SWASPJ000658.70-293624.7	0.5294	0.5294	0.00
13	NP And	1SWASPJ001039.85+340656.4	0.3244	7.0466	0.00
14	V0337 Cas	1SWASPJ001322.33+581233.2	7.0466	0.3139	0.00
15	MT Cas	1SWASPJ001443.56+544012.5	0.3139	4.0782	-0.17
16	SY Cas	1SWASPJ001509.81+582527.4	4.0711	0.3208	-0.01
17	SZ Scl	1SWASPJ001546.65-310544.3	0.3208	3.3729	0.05
18	V0544 Cas	1SWASPJ001602.78+485505.4	3.3747	3.0946	-0.04
19	GU Cas	1SWASPJ001625.00+562046.7	3.0934	0.4627	0.02
20	CN And	1SWASPJ002030.54+401333.8	0.4628	0.9814	-0.06

Table 4-2: First 20 SuperWASP periods within +/- 1% of the GCVS period

With regard to the light-curves in Appendix 4 and the supplementary data, four light-curves are displayed on each row. The pair on the left is the phase-folded light-curve and

binned phase-folded light-curve generated from the known GCVS period and the pair on the right is generated from the SuperWASP-calculated period. Manual review of these light-curves showed that 131 objects had a slightly better phase-folded light-curve using the SuperWASP-calculated period than the GCVS period.

The results in Table 4-2 provided confidence in the use of SuperWASP data for calculation of variability period. Further analysis was performed on the 211 objects where the SuperWASP-calculated period disagreed with the known GCVS period, and this showed that 194 had a more appropriate period from SuperWASP. Adding these to the 131 objects with a more appropriate SuperWASP period from the set within +/-1% raised the total to 325 objects (see Table 4-3 for the first 20 results). An example of one of these can be seen in Figure 4-10, where the SuperWASP-calculated period shows a typical EA phase-folded light-curve while the known GCVS period shows an EA class with five eclipses. Six other examples can be seen in Appendix 5 and the complete list of data and phase-folded light-curves can be found on the supplementary DVD in the following location…

Supplementary data	
Object data more appropriate period from SuperWASP	X:\Chapter04\Table2_data.pdf
Phase-folded light-curves	X:\Chapter04\Table2_images.pdf

Where X is DVD-1 in the DVD-drive

Not all the differences in the light-curves of Appendix 5 (and the supplementary data) were this pronounced, some of them were simply improved by having a smaller phase-length.

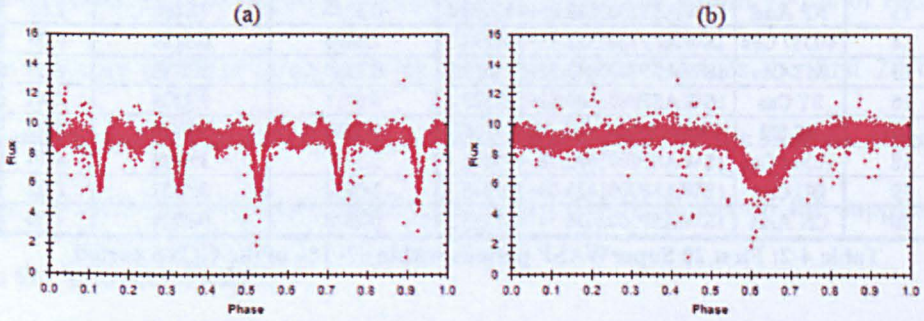

Figure 4-10: IQ Vel with a more appropriate period from SuperWASP data (a) Created using the GCVS period, (b) Using the SuperWASP period

No.	Name	WASP Id	GCVS period (d)	WASP period (d)	%Diff
1	GV Peg	1SWASPJ000035.58+263949.6	0.5669	1.3068	-130.51
2	UU Scl	1SWASPJ000122.50-263524.1	3.4470	0.7736	77.56
3	DO And	1SWASPJ001057.17+420639.5	0.6720	1.3479	-100.58
4	MR Cas	1SWASPJ001142.00+580423.9	0.3529	0.4352	-23.32
5	BH Cas	1SWASPJ002121.36+590905.2	0.5000	0.3372	32.56
6	HK Cas	1SWASPJ005720.01+552620.4	2.4996	0.7128	71.48
7	UV Phe	1SWASPJ011210.74-411326.1	2.0190	0.3986	80.26
8	V0471 Cas	1SWASPJ013220.46+551220.1	0.3360	0.4009	-19.32
9	SS Scl	1SWASPJ014211.46-295920.6	0.4187	0.7219	-72.41
10	YZ Phe	1SWASPJ014225.87-455703.7	0.3052	0.2347	23.09
11	QX And	1SWASPJ015757.78+374822.4	0.4118	0.5197	-26.20
12	SV For	1SWASPJ015825.21-242244.4	87.2400	0.6679	99.23
13	YY Cet	1SWASPJ020012.04-181228.1	1.1175	0.7905	29.26
14	TY Ari	1SWASPJ020840.25+251306.6	0.4800	0.3298	31.29
15	TV Ari	1SWASPJ021108.68+202659.9	0.3667	0.5800	-58.17
16	V0352 Per	1SWASPJ021337.01+563414.2	0.2200	0.9850	-347.73
17	DV Per	1SWASPJ023236.68+530931.3	0.8071	1.6147	-100.06
18	V0362 Per	1SWASPJ023411.45+582419.7	0.2594	0.9839	-279.30
19	V0449 Per	1SWASPJ025733.45+351400.9	0.9462	0.4731	50.00
20	V0432 Per	1SWASPJ031010.79+425209.2	0.3215	0.3833	-19.22

Table 4-3: First 20 SuperWASP objects with more appropriate periods than GCVS

The remaining 17 objects from the 211 where the periods disagreed had a more appropriate period in the GCVS. These can be seen in Table 4-4 and the first six light-curves can be seen in Appendix 6. The complete list of data and phase-folded light-curves can be found on the supplementary DVD in the following location:

Supplementary data	
Object data more appropriate period from GCVS	X:\Chapter04\Table3_data.pdf
Phase-folded light-curves	X:\Chapter04\Table3_images.pdf

Where X is DVD-1 in the DVD-drive

When assessing the above objects, the more appropriate period between GCVS and SuperWASP was determined by creating a phase-folded light-curve for these objects with both the SuperWASP and GCVS periods and comparing them by eye for gross differences. For minor differences, the phase-length of each phase-folded light-curve was calculated as shown in section 4.3.1 and used to identify the period with the shortest phase-length.

No.	Name	WASP Id	GCVS period (d)	WASP period (d)	%Diff
1	GT Cas	1SWASPJ001330.10+581700.7	2.9898	1.4939	50.03
2	WX And	1SWASPJ004537.33+284459.9	3.0011	1.5015	49.97
3	UW Psc	1SWASPJ012325.29+224818.1	2.4908	1.6626	33.25
4	RW Cas	1SWASPJ013714.02+574533.2	14.7949	0.9324	93.70
5	XZ Ari	1SWASPJ023224.14+280304.8	0.2655	0.2343	11.74
6	CC Eri	1SWASPJ023422.56-434746.8	1.5615	0.7777	50.20
7	GO Cas	1SWASPJ023505.76+592302.9	3.2390	0.7643	76.40
8	MZ And	1SWASPJ023805.21+431822.6	0.3622	0.3066	15.36
9	UU Cnc	1SWASPJ080230.89+151041.9	96.7100	1.0097	98.96
10	TY Lyn	1SWASPJ081823.23+461607.6	4.3317	0.3843	91.13
11	V0337 Tel	1SWASPJ192627.70-454526.7	0.4234	0.2117	50.00
12	V0438 Cyg	1SWASPJ201854.31+400352.1	11.2111	0.9224	91.77
13	V1320 Cyg	1SWASPJ202122.17+391956.8	40.9000	1.0232	97.50
14	BZ Cyg	1SWASPJ204559.79+451825.0	10.1419	0.9343	90.79
15	V0392 And	1SWASPJ233848.72+442445.3	4.0463	2.0221	50.03
16	HH And	1SWASPJ234155.04+441039.0	120.0000	0.3326	99.72
17	CS Cas	1SWASPJ235014.28+512358.8	14.7360	1.0709	92.73

Table 4-4: GCVS objects with more appropriate periods than SuperWASP

From the remainder of the objects, 649 had period values calculated by SuperWASP that were not present in the GCVS. Table 4-5 shows the first 20 objects and the first twelve light-curves are shown in Appendix 7. The complete list of data and phase-folded light-curves can be found on the supplementary DVD in the following location…

Supplementary data	
Object data for SuperWASP periods not in the GCVS	X:\Chapter04\Table4_data.pdf
Phase-folded light-curves	X:\Chapter04\Table4_images.pdf

Where X is DVD-1 in the DVD-drive

No.	Name	WASP Id	WASP period (d)
1	UY Scl	1SWASPJ001445.75-391435.5	0.3644
2	MW Cas	1SWASPJ001649.86+550501.1	0.4809
3	BM Phe	1SWASPJ001845.86-394038.1	0.4136
4	CK Cet	1SWASPJ002256.95-203923.6	0.7673
5	V0860 Cas	1SWASPJ002649.08+494035.7	1.0839
6	CL Cet	1SWASPJ002904.06-171300.8	0.3108
7	BD Scl	1SWASPJ003225.22-245234.4	0.4411
8	V0516 Cas	1SWASPJ003521.83+525953.4	0.4040
9	DZ Psc	1SWASPJ003627.94+213214.4	0.3663
10	AT Psc	1SWASPJ005828.47+314044.8	3.7859
11	CP Psc	1SWASPJ005845.91+320620.3	0.6840
12	VV Psc	1SWASPJ010144.87+304814.1	0.5036
13	AS Scl	1SWASPJ010534.58-265718.4	1.0346
14	AP Scl	1SWASPJ010555.69-264344.0	1.0355
15	CT Cet	1SWASPJ010945.77-201259.5	0.2565
16	TZ Phe	1SWASPJ010958.35-420743.6	0.6156
17	FP And	1SWASPJ011649.48+350332.0	0.2914
18	V0830 Cas	1SWASPJ011826.65+504018.4	0.3735
19	BE Scl	1SWASPJ012132.95-290752.6	0.4229
20	V0588 Cas	1SWASPJ012238.01+542308.4	0.9910

Table 4-5: First 20 SuperWASP objects that do not have GCVS periods

289 objects had periods calculated by GCVS only. This was due to SuperWASP not having sufficient data to compute the period for these objects or the brightness of each variable was outside the range of SuperWASP.

It should be noted that if the period of the object is revised from that given in the GCVS to that determined from the SuperWASP data, this does not necessarily imply a change in the object's classification. That decision is determined on an object by object basis, which is discussed in the next section. Table 4-6 shows the number of objects with consistent periods per class and Table 4-7 shows a complete summary of the variability period analysis.

Variability type	GCVS Class	WASP Class	GCVS/WASP periods within +/- 1%	GCVS/WASP periods outside +/-1%	Total
Pulsating	BCEP	Cepheid-like	1	4	5
	CEP		10	5	15
	DCEP		43	5	48
	CWA		2	1	3
	CWB		2	1	3
	RRAB	RRAB	581	49	630
	RRC	RRC	78	26	104
	RR	RR	16	5	21
	DSCT	DSCT	13	3	16
Eclipsing	E	E	5	3	8
	EA	EA	468	55	523
	EB	EB	114	9	123
	EW	EW	124	38	162
Sinusoidal-like	RM	RM	15	7	22
		Total	1472	211	1683

Table 4-6: Number of objects per class from the period analysis

Variability period analysis								
Total objects		2,621						
==>	Objects have both a WASP-calculated and GCVS-calculated period	1,683	==>	WASP agree with GCVS	1,472			
				Disagree	211	==>	WASP better	194
							GCVS better	17
==>	Objects have a WASP period only (i.e. new periods)	649						
==>	Objects have a GCVS period only	289		WASP better = 194 + 131 from the agreed periods	325			

Table 4-7: Summary of variability period analysis
The arrows indicate the split of data e.g. 1,683 objects split into 1,472 and 211 etc.

4.4.2 Classification

Using the GCVS data as a comparison of the 2,621 objects that had a known class in the GCVS, 2,050 (78%) of the SuperWASP phase-folded light curves agreed with the GCVS classification. Table 4-8 shows the first 20 objects and Appendix 8a to Appendix 8j shows up to twelve phase-folded light-curves for CEP (105), DSCT (40), E (3), EA (705), EB (141), EW (233), RM (64), RR (19), RRAB (653) and RRC (86) respectively. The numbers in brackets indicate how many objects were identified for that class. The complete list of data and phase-folded light-curves can be found on the supplementary DVD in the following location…

Supplementary data	
Object data that agree with the GCVS class	X:\Chapter04\Table5_data.pdf
Phase-folded light-curves CEP	X:\Chapter04\Table5a_images.pdf
Phase-folded light-curves DSCT	X:\Chapter04\Table5b_images.pdf
Phase-folded light-curves E	X:\Chapter04\Table5c_images.pdf
Phase-folded light-curves EA	X:\Chapter04\Table5d_images.pdf
Phase-folded light-curves EB	X:\Chapter04\Table5e_images.pdf
Phase-folded light-curves EW	X:\Chapter04\Table5f_images.pdf
Phase-folded light-curves RM	X:\Chapter04\Table5g_images.pdf
Phase-folded light-curves RR	X:\Chapter04\Table5h_images.pdf
Phase-folded light-curves RRAB	X:\Chapter04\Table5i_images.pdf
Phase-folded light-curves RRC	X:\Chapter04\Table5j_images.pdf

Where X is DVD-1 in the DVD-drive

No.	Name	WASP Id	GCVS class	WASP class	Period (d)	Data set
1	GM And	1SWASPJ000003.66+352146.1	RRAB	RRAB	0.7066	WASP v GCVS (WASP)
2	DM Peg	1SWASPJ000007.28+184417.1	EA/D:	EA	2.5878	WASP v GCVS (WASP)
3	SW Phe	1SWASPJ000030.01-393729.1	EA/SD	EA	2.5530	WASP v GCVS (WASP)
4	GV Peg	1SWASPJ000035.58+263949.6	RRAB	RRAB	1.3068	WASP v GCVS (WASP)
5	RU Scl	1SWASPJ000248.10-245643.1	RRAB	RRAB	0.4934	WASP v GCVS (WASP)
6	TW And	1SWASPJ000318.22+325045.0	EA/SD	EA	4.1170	WASP v GCVS (WASP)
7	EY Cas	1SWASPJ000322.62+574454.5	EW/KW	EW	0.4819	WASP v GCVS (WASP)
8	UU Cet	1SWASPJ000405.10-165951.5	RRAB	RRAB	0.6061	WASP v GCVS (WASP)
9	IX Cas	1SWASPJ000450.82+501405.5	CWA	CWA	9.1435	WASP v GCVS (WASP)
10	AM And	1SWASPJ000507.48+482705.2	EA/DS	EA	8.8325	WASP v GCVS (WASP)
11	WW Scl	1SWASPJ000601.94-365414.7	RRAB	RRAB	0.7848	WASP v GCVS (WASP)
12	RY Psc	1SWASPJ001141.10-014455.2	RRAB	RRAB	0.5297	GCVS only
13	MR Cas	1SWASPJ001142.00+580423.9	EW/KW	EW	0.4352	WASP v GCVS (WASP)
14	V0337 Cas	1SWASPJ001322.33+581233.2	EA/DM	EA	7.0466	WASP v GCVS (WASP)
15	GT Cas	1SWASPJ001330.10+581700.7	EA/SD	EA	2.9898	WASP v GCVS (GCVS)
16	FM Cas	1SWASPJ001428.24+561510.5	DCEP	CEP	5.8093	GCVS only
17	MT Cas	1SWASPJ001443.56+544012.5	EW/KW	EW	0.3139	WASP v GCVS (WASP)
18	SY Cas	1SWASPJ001509.81+582527.4	DCEP	CEP	4.0782	WASP v GCVS (WASP)
19	SZ Scl	1SWASPJ001546.65-310544.3	EW/KW	EW	0.3208	WASP v GCVS (WASP)
20	V0544 Cas	1SWASPJ001602.78+485505.4	EA/SD	EA	3.3729	WASP v GCVS (WASP)

Table 4-8: First 20 SuperWASP objects where class agrees with the GCVS

The classes E and RR have been included in this data because a manual review of the phase-folded light-curves could not justify a clear EA, EB, EW, RRAB or RRC class. In these cases, the SuperWASP class supported the GCVS 'query' class.

333 (13%) of the 2,621 objects were able to be classified as a subclass from the general class e.g. general class E into EA, EB or EW and general class RR into RRAB or RRC. Table 4-9 shows the first 20 objects and Appendix 9a to Appendix 9h shows up to twelve phase-folded light-curves for CEP (4), DSCT (4), EA (61), EB (22), EW (19), RM (17), RRAB (174) and RRC (32) respectively. The numbers in brackets indicate the number of objects identified for that class. The complete list of data and phase-folded light-curves can be found on the supplementary DVD in the following location…

Supplementary data	
Object data moving unconfirmed GCVS class into a subclass	X:\Chapter04\Table6_data.pdf
Phase-folded light-curves CEP	X:\Chapter04\Table6a_images.pdf
Phase-folded light-curves DSCT	X:\Chapter04\Table6b_images.pdf
Phase-folded light-curves EA	X:\Chapter04\Table6c_images.pdf
Phase-folded light-curves EB	X:\Chapter04\Table6d_images.pdf
Phase-folded light-curves EW	X:\Chapter04\Table6e_images.pdf
Phase-folded light-curves RM	X:\Chapter04\Table6f_images.pdf
Phase-folded light-curves RRAB	X:\Chapter04\Table6g_images.pdf
Phase-folded light-curves RRC	X:\Chapter04\Table6h_images.pdf

Where X is DVD-1 in the DVD-drive

No.	Name	WASP Id	GCVS class	WASP class	Period (d)	Data set
1	TZ Scl	1SWASPJ000049.23-284900.4	RR	RRAB	0.5831	WASP v GCVS (WASP)
2	UU Scl	1SWASPJ000122.50-263524.1	E	EA	0.7736	WASP v GCVS (WASP)
3	SX Scl	1SWASPJ000658.70-293624.7	RR	RRAB	0.5294	WASP v GCVS (WASP)
4	DO And	1SWASPJ001057.17+420639.5	E/SD	EA	1.3479	WASP v GCVS (WASP)
5	BH Cas	1SWASPJ002121.36+590905.2	EW:	EW	0.3372	WASP v GCVS (WASP)
6	CL Cet	1SWASPJ002904.06-171300.8	RRC:	RRC	0.3108	WASP only
7	RW Phe	1SWASPJ003016.31-462758.6	E	EA	5.4138	WASP v GCVS (WASP)
8	V0516 Cas	1SWASPJ003521.83+525953.4	RR	RRAB	0.4040	WASP only
9	ST Cet	1SWASPJ004904.31+022515.7	RR	RRAB	0.5265	GCVS only
10	VV Psc	1SWASPJ010144.87+304814.1	RR	RRAB	0.5036	WASP only
11	AS Scl	1SWASPJ010534.58-265718.4	ELL:	RM	1.0346	WASP only
12	UV Phe	1SWASPJ011210.74-411326.1	RR	RRC	0.3986	WASP v GCVS (WASP)
13	FP And	1SWASPJ011649.48+350332.0	RR	RRC	0.2914	WASP only
14	RX Scl	1SWASPJ012624.36-273000.1	RR	RRAB	0.5445	WASP v GCVS (WASP)
15	TV Tri	1SWASPJ013311.01+323539.8	RR:	RRAB	0.7056	WASP only
16	RY Scl	1SWASPJ013323.38-302952.6	RR:	RRC	0.1589	WASP only
17	V0473 Cas	1SWASPJ013452.24+563909.6	E	EB	0.4155	WASP only
18	SS Scl	1SWASPJ014211.46-295920.6	RR	RRC	0.7219	WASP v GCVS (WASP)
19	ST Scl	1SWASPJ014236.41-300138.4	RR	RRAB	0.5146	WASP v GCVS (WASP)
20	AC Phe	1SWASPJ015648.96-442105.6	RR	RRAB	0.5827	WASP only

Table 4-9: First 20 SuperWASP objects where a GCVS sub-class is confirmed

The classification for 204 objects (8%) disagreed with the GCVS. These can be seen in Table 4-10 for the first 20 objects and Appendix 10a to Appendix 10k shows up to six phase-folded light-curves for CEP (3), DSCT (1), E (6), EA (50), EB (42), EW (37), RM (12), RR (4), RRAB (26), RRC (22) and '???' (1), the numbers in brackets indicating how many objects were identified for that class. The complete list of data and phase-folded light-curves can be found on the supplementary DVD in the following location…

Supplementary data	
Object data that disagreed with the GCVS class	X:\Chapter04\Table7_data.pdf
Phase-folded light-curves EA	X:\Chapter04\Table7d_images.pdf
Phase-folded light-curves EB	X:\Chapter04\Table7e_images.pdf
Phase-folded light-curves EW	X:\Chapter04\Table7f_images.pdf
Phase-folded light-curves RM	X:\Chapter04\Table7g_images.pdf
Phase-folded light-curves RRAB	X:\Chapter04\Table7i_images.pdf
Phase-folded light-curves RRC	X:\Chapter04\Table7j_images.pdf

Where X is DVD-1 in the DVD-drive

The '???' object was classed as 'EA/DS' in the GCVS, but it was unable to be classified using SuperWASP data.

No.	Name	WASP Id	GCVS class	WASP class	Period (d)	Data set
1	UY Scl	1SWASPJ001445.75-391435.5	RRC:	EW	0.3644	WASP only
2	MW Cas	1SWASPJ001649.86+550501.1	EA	EB	0.4809	WASP only
3	CN And	1SWASPJ002030.54+401333.8	EW/KW	EB	0.4627	WASP v GCVS (WASP)
4	NU Cas	1SWASPJ003224.64+570151.9	EB/KE	EA	0.7667	WASP v GCVS (WASP)
5	BD Scl	1SWASPJ003225.22-245234.4	EB	EW	0.4411	WASP only
6	KL Cas	1SWASPJ005141.49+585151.8	EB/SD	EA	2.4499	WASP v GCVS (WASP)
7	MM Cas	1SWASPJ005434.96+542636.4	EA/SD	EB	1.1586	WASP v GCVS (WASP)
8	CP Psc	1SWASPJ005845.91+320620.3	EB:	EA	0.6840	WASP only
9	DQ And	1SWASPJ005934.46+452424.2	CWB:	RRAB	3.1992	WASP v GCVS (WASP)
10	RV Psc	1SWASPJ011941.07+311205.0	EA/DW	EW	0.5540	WASP v GCVS (WASP)
11	SU Psc	1SWASPJ012924.39+193740.6	EB/D:	EA	2.6808	WASP v GCVS (WASP)
12	WW Phe	1SWASPJ013106.81-435934.8	EA	EB	0.7199	WASP v GCVS (WASP)
13	SV For	1SWASPJ015825.21-242244.4	SRD	EB	0.6679	WASP v GCVS (WASP)
14	CC Per	1SWASPJ015937.02+555922.2	EB/SD	EA	2.4700	WASP v GCVS (WASP)
15	KW Per	1SWASPJ015959.97+531324.9	EB/SD	EA	0.9312	WASP v GCVS (WASP)
16	XZ Cet	1SWASPJ020016.63-162046.0	RRAB	RRC	0.8232	WASP v GCVS (WASP)
17	RU Tri	1SWASPJ020021.16+351713.1	EB/D	EA	3.2696	WASP v GCVS (WASP)
18	XZ For	1SWASPJ020118.74-370452.1	EW	EB	0.3081	WASP only
19	BX And	1SWASPJ020903.42+404739.1	EW/DW:	EB	0.6101	WASP v GCVS (WASP)
20	DK Per	1SWASPJ022345.58+575923.6	EB/SD	EA	0.8987	WASP v GCVS (WASP)

Table 4-10: First 20 SuperWASP objects where class disagrees with the GCVS

Of the 204 objects that disagreed, 197 should be reviewed further by the GCVS to see if the classification should be changed (see Table 4-11).

In Table 4-11, the first column indicates the GCVS class, while the other columns (with the yellow heading) are the SuperWASP classes. From the list, the 27 EBs were reclassified as EW based on the shape of the phase-folded light-curve, not the variability period. The other seven objects where the classifications disagreed were variables of CWA, CWB, SXPHE and ZAND types that showed sinusoidal-like light-curves – they were not included in the above table.

GCVS class	CEP-like	DSCT	E	EA	EB	EW	RM	RR	RRAB	RRC
CEP				1					1	
CST							4			
CWA	2						3			
CWB	1			1			1		7	
DSCT							1			
E				1					3	2
EA			4		21	4			1	
EB			2	41		27			2	
EW				3	19					1
RM				1						
RR										1
RRAB				1				4		18
RRC		1				3			5	
SR				1		1			6	
SRD					2					

Table 4-11: 197 objects where manually identified class differs with the GCVS

The remaining 34 objects whose classifications did not agree with those in the GCVS or which could not be reclassified had erratic light-curves that were not representative of their classes. These can be seen in Table 4-12 for the first 20 objects and Appendix 11 shows six examples of the phase-folded light-curves. The complete list of data and phase-folded light-curves can be found on the supplementary DVD in the following location…

Supplementary data	
Object data with erratic light-curves	X:\Chapter04\Table8_data.pdf
Phase-folded light-curves EA	X:\Chapter04\Table8_images.pdf

Where X is DVD-1 in the DVD-drive

No.	Name	WASP Id	GCVS class	WASP class	Period (d)	Data set
1	V0588 Cas	1SWASPJ012238.01+542308.4	DCEP:	?	0.9910	WASP only
2	V0362 Per	1SWASPJ023411.45+582419.7	BCEP:	?	0.9839	WASP v GCVS (WASP)
3	V0917 Ori	1SWASPJ060827.35+135551.1	BCEP	?	0.2889	WASP v GCVS (WASP)
4	V0378 Aur	1SWASPJ062033.21+465000.6	RRAB	?	0.5022	WASP only
5	UU Cnc	1SWASPJ080230.89+151041.9	EB/GS	?	96.7100	WASP v GCVS (GCVS)
6	CW Lyn	1SWASPJ084026.28+445418.3	EB:	?	0.8121	WASP only
7	EY UMa	1SWASPJ090220.75+494909.8	RRAB	?	0.5497	WASP only
8	DK Leo	1SWASPJ101419.17+210429.4	BY	?	8.0122	WASP v GCVS (WASP)
9	V0581 Cen	1SWASPJ115757.23-360611.4	EW/KW	?	0.3462	WASP v GCVS (WASP)
10	GW Com	1SWASPJ121628.85+313743.6	E:	?	16.0984	WASP only
11	V0450 Cen	1SWASPJ124004.63-341616.8	RR	?	0.4655	WASP v GCVS (WASP)
12	BZ Boo	1SWASPJ133821.39+271713.5	DSCTC	?	0.9860	WASP v GCVS (WASP)
13	NY Vir	1SWASPJ133848.16-020149.3	EA+RPHS	?	0.1010	WASP only
14	AZ Boo	1SWASPJ135318.27+152833.3	RRAB	?	0.4897	WASP v GCVS (WASP)
15	V0345 Ser	1SWASPJ151621.88+113002.1	SR:	?	0.1862	WASP only
16	RX CrB	1SWASPJ151749.42+293953.2	CST:	?	1.0111	WASP only
17	BO Lib	1SWASPJ152741.55-222448.8	RRAB	?	0.6062	WASP v GCVS (WASP)
18	IR Lib	1SWASPJ152926.87-285052.3	EW:	?	0.2744	WASP only
19	V0944 Oph	1SWASPJ175853.67+071920.0	RRAB	?	0.2734	WASP v GCVS (WASP)
20	V0480 Lyr	1SWASPJ184023.43+435621.6	EB:	?	1.0088	WASP only

Table 4-12: First 20 SuperWASP objects unable to obtain a classification

Table 4-13 shows a complete summary of the variability classes after the long period variables RV, Mira, SR and its sub-classes were removed.

Variability class analysis					
Class	Agrees with GCVS	Confirm a GCVS sub-class	Change a GCVS class	Erratic light-curves	
CEP	105	4	3		
DSCT	40	4	1		
E	3		6		
EA	705	61	50		
EB	141	22	42		
EW	233	19	35		
RM	64	17	9		
RR	19		4		
RRAB	653	174	25		
RRC	86	32	22		
???	1		7	34	
Total	2,050	333	204	34	2,621

Table 4-13: Number of objects where manually identified class agrees with GCVS

4.5. Training and Testing of the selected Neural Networks

From the objects identified in the above section where the variability period and classification was confirmed, 60 objects for each of the classes CEP, DSCT, EA double-eclipse, EA single-eclipse, EB, EW, RM, RRAB and RRC were randomly selected and used to train and test ALL the NNs in the later sections of Chapter 3, so as to identify the

most appropriate neural networks for processing all the periodic objects in the SuperWASP archive. The method of processing the objects through each neural network and the results obtained have already been discussed in Chapter 3 (section 3.5) and the results (reproduced below) showed that three NNs were required to classify all the selected objects:

- Model 1: Correct classification: 59% (99.7%); Misclassified: 39% (0.3%);
- Model 2: Correct classification: 75% (99.3%); Misclassified: 25% (0.7%);
- Model 3: Correct classification: 71% (93.3%); Misclassified: 29% (6.7%);

The required parameters were then extracted from the three selected NNs and placed into the 'LC Analyser classifier' application. This is fully described in the next chapter.

4.6. Chapter summary

In this chapter, the suitability of SuperWASP data was assessed to confirm that it was suitable for classification of stellar objects. This assessment was required because the data from the SuperWASP project was designed to search for extra-solar planets and transient objects and as such the data may not have been suitable for classification purposes. During the suitability assessment, the variability period of 1,472 variable stars in the GCVS was confirmed by showing that the SuperWASP-calculated periods agreed with the GCVS, and revision of the variability period of 194 GCVS variable stars was suggested where SuperWASP disagreed and had more appropriate phase-folded light-curves. 649 variable stars were added where the period was not known in the GCVS. This provided confidence that the SuperWASP data could be used successfully to calculate the variability period.

With regard to classification, it was shown that 2,050 SuperWASP objects agreed with the GCVS class and sub-classes were suggested for 333 objects in the GCVS that were unconfirmed classes (e.g. CEP:, EA:, RR etc.). Also, re-classification was suggested for 197 GCVS objects with suspected incorrect classes. Again, this provided confidence that the SuperWASP data was suitable for identifying a preliminary classification.

At this point, 60 'confirmed' objects for each of the classes CEP, DSCT, EA double-eclipse, EA single-eclipse, EB, EW, RM, RRAB and RRC objects were randomly selected and used to train and test the NNs as described in Chapter 3 (section 3.5). The method used to classify the SuperWASP objects was based on the period and the shape of the binned phase-folded light-curves of photometric data in the visible band. This meant that a 'final' classification could not be made using SuperWASP data, but it was possible to obtain preliminary classifications that would reduce the search space of the SuperWASP archive so that researchers can spend more of their time confirming the classes of these objects, rather than searching for the classes that they require for their work.

As a check on the SuperWASP calculated periods and manual classifications, the output was cross-checked against the known periods and classifications listed in the GCVS. The GCVS was chosen as the comparator because it uses a variety of sources to decide on the period and classification, such as spectral type, luminosity class, radial velocity data and multiband photometry.

Although the SuperWASP classification cannot differentiate between objects with similar light-curves (like BCEP, CEP and DCEP), this method of classification is still useful to perform a fast scan of a large dataset to identify potential objects for further study. For instance, if a researcher is interested in DCEP objects, they can examine all CEP-like objects identified by the 'LC Analyser classifier' application and determine which of the objects meets their need by using confirmatory tests. This will still be less work for the researcher than searching the whole archive for candidate DCEPs. Therefore, in Chapter 5 an automated system is created to extract data from the SuperWASP archive, pre-process it into the correct format and then process it through the three NNs created in Chapter 3 that have been trained and tested with the data identified in this chapter.

In summary, this study using SuperWASP data has shown that the data are reliable for calculating variability periods and classifying objects. Additionally, it has highlighted many objects where the GCVS can be updated with new and corrected periods and classifications. The SuperWASP data and objects are made available for classification by other authors/teams that wish to confirm these conclusions.

Chapter 5 discusses the design, creation, validation and implementation of an automated system that will use the NNs from Chapter 3 and the training/testing data from this chapter to prime the application. The application is then used to process all data in the SuperWASP archive.

---------- o ----------

Chapter 5 Neural Network analysis of SuperWASP data

This chapter describes the design, creation, validation and implementation of the 'LC Analyser classifier' application following the GAMP5 (2008) methodology. The application is used to classify periodic variable objects from the SuperWASP archive and this chapter also discusses the results obtained from the SuperWASP archive analysis and some problems identified along the way.

5.1. User Requirements for the 'LC Analyser classifier' application

The two main objectives of the 'LC Analyser classifier' application were to support creation of training and testing sets for the neural networks, as described in Chapter 4, and to process all periodic objects in the SuperWASP archive. The latter aspect is described in this chapter. The following user requirements allowed these objectives to be met. The expected functional detail can be seen in section 5.2:

1. The following methods of inputting SuperWASP objects to the application must be provided:
    a. Using individual SuperWASP object Id's, where specific objects are selected to train the NNs in Chapter 4. This method allows objects to be analysed on a single PC for processing low numbers of objects (see section 5.2.1.1).
    b. Using SuperWASP Season and Field, where all periodic variables in the SuperWASP archive are processed automatically on multiple processors at Leicester University. This method supports processing of large numbers of objects (see section 5.2.1.2).
2. Objects must be pre-processed through a series of rules to remove spurious observations (see section 5.2.2).

3. Various calculations must be performed on observations from the object to support decision making throughout the project (see section 5.2.3).
4. A binned and an un-binned phase-folded light-curve must be created to help the selection of objects for training/testing the NNs (see section 5.2.4).
5. The binned phase-folded light-curve must be pre-processed to obtain parameters for entry into the NNs (see section 5.2.5).
6. The three NNs described in Chapter 3 must be created (see section 5.2.6).
7. The NN parameters from requirement 5 must be passed through the three NNs in requirement 6 to obtain a classification (see section 5.2.7).
8. The calculations and results must be written to output files for further analysis (see section 5.2.8).

5.2. Functional Requirements for the 'LC Analyser classifier' application

The functional requirements required to meet the user requirements in section 5.1 are described below. Figure 5-1 shows the top level design of the application. As indicated in user requirement 1, two methods of inputting objects to the application are required and therefore the input routine is set outside the application environment. Once the 'LC Analyser classifier' application completes processing, the output files are also analysed outside the application environment.

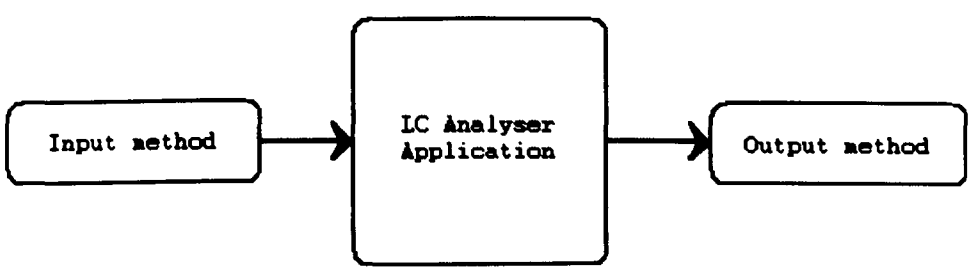

Figure 5-1: Top level design for 'LC Analyser classifier' application

5.2.1 Requirement 1 (Input methods)

Two input methods are required as follows:

5.2.1.1 Batch Processing using individual SuperWASP object Id's

An input file must be created manually by running a query on the SuperWASP archive to obtain the required objects. The fields in Table 5-1 must be obtained…

Field name	Description	Range	Example	Required for
WASP Id	Unique identifier for the object	N/A	1SWASPJ 000003.66+352 146.1	Uniquely identifying a specific object/period
Season	Season the observations were made	2004 to 2011	2006	
Field	The name of the field (generally in the form SWhhmm±ddmm)	N/A	SW0016+3126	
Camera	DAS camera identifier	N/A	145	
PFlag	Period warning flag	0 = good; >0 = harmonic (e.g. 1 day)	0	
Period	Detected period in seconds	N/A	61064.1	
Detrend	De-trending technique applied before running the period search	NONE, TAMUZ, TFA	TAMUZ	Labelling the de-trend method
GCVS class	Type of variability	BCEP, CEP, DCEP, DSCT, EA, EB, EW, RM, RRAB, RRC, Unknown	RRAB	Labelling the phase diagrams and confirming the training/testing data
pm_ra	Proper motion (arcsec/yr)	N/A	0.018	To investigate classification using reduced proper-motion
pm_dec	Proper motion (arcsec/yr)	N/A	-0.006	
bmag	B magnitude	N/A	12.92	To investigate classification using colour
vmag	V magnitude	N/A	12.75	
jmag	J magnitude	N/A	12.151	
hmag	H magnitude	N/A	11.859	
kmag	K magnitude	N/A	11.815	

Table 5-1: Parameters obtained from SuperWASP archive

The output must be manually copied to a text file for entry into the 'LC Analyser classifier' application. Figure 5-2 shows an example of the expected input file…

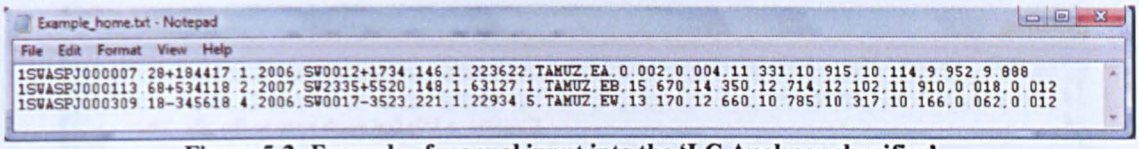

Figure 5-2: Example of manual input into the 'LC Analyser classifier'

For this research, all objects were retrieved from the SuperWASP archive where they had a known period and/or classification in the GCVS. The 'LC Analyser classifier' application must be started using a command-line argument such as the following for the above example:

LC Analyser "C:\LC Analyser\Example_home.txt"

5.2.1.2 Batch Processing using SuperWASP Season and Field

Again, an input file must be created manually by running a query on the SuperWASP archive, but in this case, only the field, camera, season, Detrend and PFlag parameters are retrieved as shown in Figure 5-3 where all the fields for PFlag 0 were selected (see Table 5-1 above for a definition of these parameters). Each line in this file is called a 'session' and controls the processing of all the objects in the field, camera and season.

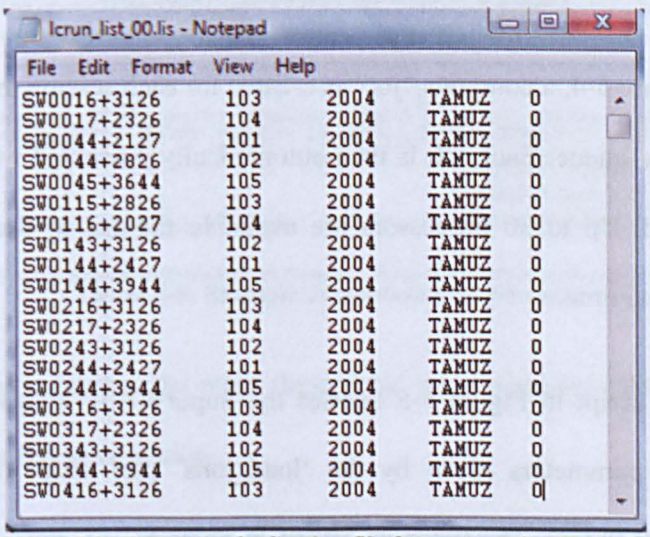

Figure 5-3: Example of a Session file for automatic processing in the 'LC Analyser classifier' application

The file must be transferred to the computer at Leicester University where the Perl batch job in Figure 5-4 must be started to automatically control the processing of all sessions in the file.

load_jobs.txt - Notepad

File Edit Format View Help

```
#!/usr/local/bin/perl
#

use English;
use strict qw(vars subs refs);

# Location of job logs and place to keep output permanently
my $logdir="/home/sgp/lcruns/logs";
my $outdir="/home/sgp/lcruns/out";

# Open the list of field/camera/season/detrend
open(FILE, "lcrun_list.lis")
    or die "Error opening lcrun_list.lis: $OS_ERROR";
while(my $line=<FILE>) {
   chomp($line);
   my ($field, $camera, $season, $detrend, $pflag)=split(/\s+/, $line);
   my $jobname="LCAnal_${field}_${camera}_${season}_${detrend}_${pflag}";
   my $outputDir="$outdir/$jobname";

   print "$jobname\n";

   # Open pipe to qsub to submit the job
   open(PIPE, "|qsub -N $jobname -e $logdir -o $logdir");

   print PIPE "#!/bin/tcsh

   cd \$TMPDIR
   /home/sgp/LCAnalyser/getclass $field $season $camera $detrend $pflag

   rm *.fits

   mkdir $outputDir
   cp -r \$TMPDIR/* $outputDir/

";

   close(PIPE);
}
close(FILE);
```

Creates a job for each row in the file. This job is called a 'Session'

Calls the perl script 'getclass' to prepare each object and call my LC Analyser application

Figure 5-4: Example of loading Session jobs

As indicated in Figure 5-4, a computer 'job' is created for each session in the input file and each job placed in a queue. Each job is then automatically processed when the 'getclass' perl script is called. Up to 30 processors are available for use so that 30 jobs can be processed at the same time.

The 'getclass' perl script in Figure 5-5 queries the SuperWASP archive for all periodic variables with the parameters given by the 'load_jobs' perl script (i.e. season, field, camera, Detrend and PFlag). The fields described in Table 5-1 are automatically retrieved for each object and they are saved to the text file 'objects.txt'. The 'getclass' script then downloads the FITS file containing the observational data for each of the objects in the

'objects.txt' file and then calls the 'LC Analyser classifier' application to process each object. The output is saved to directories on the server for downloading at a later time.

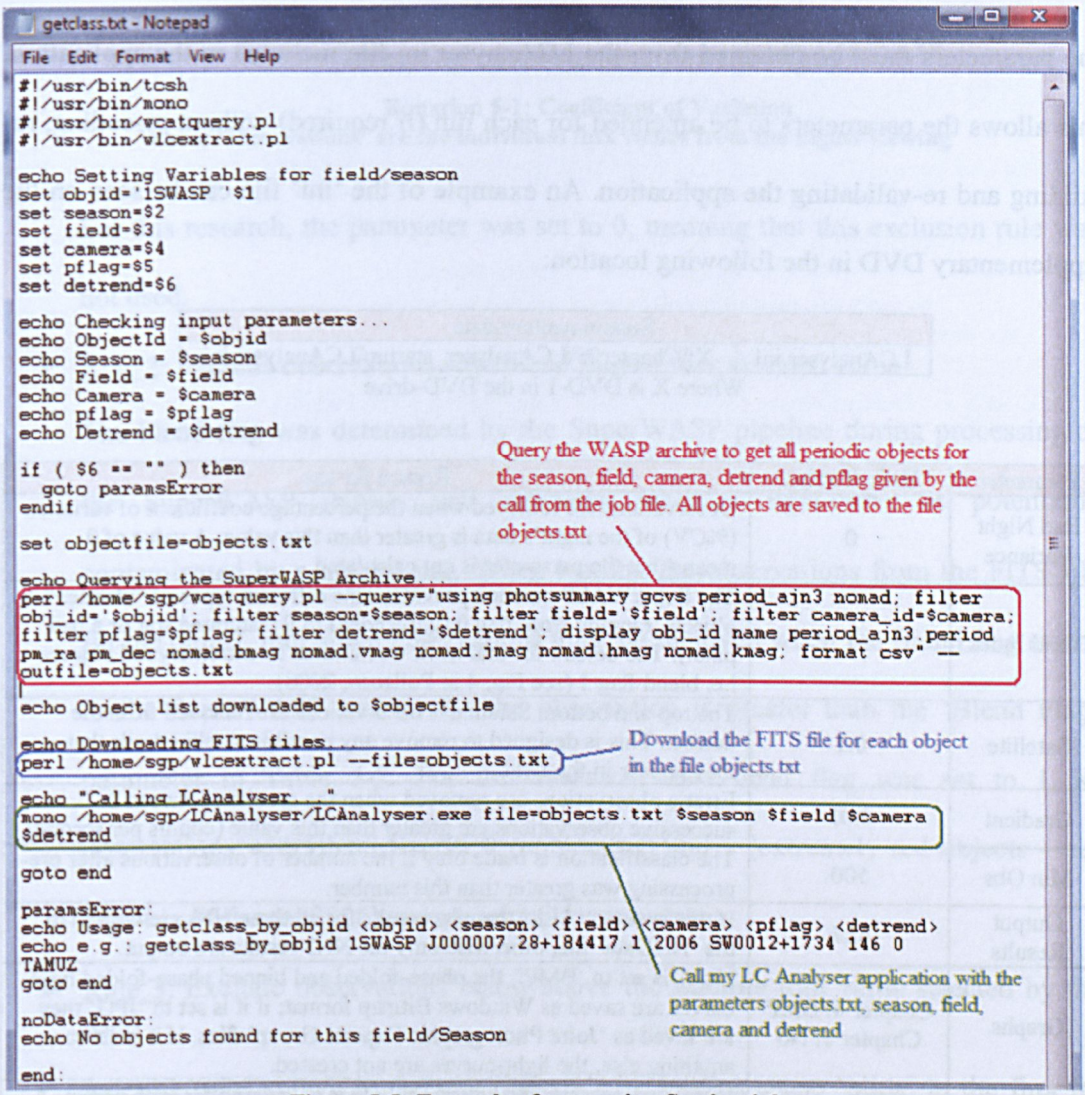

Figure 5-5: Example of processing Session jobs

When processing is complete, the main 'load_jobs' script removes all the FITS files from the server ready for the next session.

5.2.2 Requirement 2 (Remove spurious observations)

In order to ensure that there are no spurious observations in the dataset for each object, a set of 'exclusion' rules must be created. The 'LC Analyser classifier' application must first

be primed with the variable parameters shown in Table 5-2 ready for pre-processing the data.

The parameters must be obtained from the LCAnayser.ini file included in the application. This allows the parameters to be amended for each run (if required) without re-coding, re-building and re-validating the application. An example of the 'ini' file can be seen on the supplementary DVD in the following location:

Supplementary data	
LCAnalyser.ini	X:\Chapter05\LCAnalyser_startup\LCAnalyser.ini

Where X is DVD-1 in the DVD-drive

Parameter	Default value	Reason for use
Bad Night Variance	0	Observations are removed when the percentage coefficient of variation (%CV) of the night's data is greater than this value. A value of 0 means that the parameter is not calculated.
Blend Index	1	The SuperWASP pipeline provides nine different types of "blended" objects, ranging from flag 0 (unblended) to 9 (saturated star or a bad pixel). The default for this work was limited to extremely red objects i.e. blend flag 1 (see Fig. 4 in Pollacco, 2006).
Satellite	0.1	The top and bottom Satellite% observations are removed from the dataset. This is designed to remove any possible satellite trails that may appear in the field.
Gradient	0.01	Erratic observations are removed when the gradient between 2 successive observations are greater than this value (counts per second).
Min Obs	500	The classification is made only if the number of observations after pre-processing was greater than this number.
Output Results	ALL	If this is set to 'ALL' then the results for all three NNs are written to the 'NNData' file, otherwise only the NN3 results are output.
Graphs	Chapter 4: BMP Chapter 5: No	If this is set to 'BMP', the phase-folded and binned phase-folded light-curves are saved as Windows Bitmap format; if it is set to 'JPG' they are saved as 'Joint Photographic Experts Group' files. If it is set to anything else, the light-curves are not created.
Lowest Bin Amplitude	0.01	During processing, the half-amplitude is calculated for each object. A query can be used in the database to retrieve all classified objects greater than this value.

Table 5-2: Parameters that control pre-processing of each object

The exclusion rules must be implemented as follows:

- Rule 1: Exclude observations for bad nights

  The percentage coefficient of variation (%CV) shown in Equation 5-1 identifies 'bad nights' when it shows large variation in the observations for a nights viewing. When loading the observations from the FITS file for the object, ALL observations

for a night must be removed when the %CV of a night's data was greater than the 'Bad Night Variance' parameter in Table 5-2.

$$\%CV = \left(\frac{SD\ of\ observations\ for\ the\ night}{Mean\ of\ observations\ for\ the\ night}\right) \times 100$$

Equation 5-1: Coefficient of Variation
Where 'observations' are the individual flux values from the nights viewing

For this research, the parameter was set to 0, meaning that this exclusion rule was not used.

- Rule 2: Exclude observations with blend flags > user selected value

  The blend flag was determined by the SuperWASP pipeline during processing of the SuperWASP images and indicates when a light-curve is potentially contaminated by a nearby star. When loading the observations from the FITS file for the object, individual observations must be removed when the Blend flag stored in the SuperWASP archive for the observation is greater than the 'Blend Flag' parameter in Table 5-2. For this research, the Blend flag was set to 1, so observations with blend flag of 0 (unblended) and 1 (extremely red objects – see Fig, 4 in Pollacco, 2006) were retained for analysis.

- Rule 3: Exclude observations below/above the satellite trail value selected by the user

  Satellite trails shown in the raw SuperWASP images cause 'blips' in the flux for the star. When loading the observations from the FITS file for the object, observations must be excluded when their flux values are within the top and bottom X percentage range of all observations (from all cameras), where X is the 'Satellite' parameter in Table 5-2. For this research, 0.1% was used.

- Rule 4: Exclude erratic observations

  Single erratic observations can occur in the dataset for any number of reasons. They are obvious outliers in the dataset and therefore need to be removed. The method to

be used must look at the gradient between successive observations as shown in Equation 5-2 and if it is greater than the 'Gradient' parameter in Table 5-2, then the more erratic point of the two observations must be removed. The more erratic observation is the one that is furthest from the running mean of all observations:

$$gradient = ABS\left(\frac{\left(\frac{\text{Abs(Next Flux} - \text{Current Flux)}}{\text{Current Flux}}\right)}{(\text{nextTime} - \text{currentTime})}\right) counts\ s^{-1}$$

Equation 5-2: Gradient calculation

For this research, a gradient of 0.01 was used.

- Rule 5: Obtain data for the camera with the most observations

  Due to the variance of flux values between cameras, only the observations from the camera with the most observations must be used. The observations from the other cameras must be excluded.

- Rule 6: Only process objects that have at least 500 observations

  In order to ensure that good light-curves are produced, only objects that have a number of observations greater than the 'Min Obs.' parameter in Table 5-2 must be processed. For this research, a minimum of 500 observations were required.

5.2.3 Requirement 3 (Perform various calculations)

The 'LC Analyser classifier' application must perform various calculations on each object to help the classification process. Two sets of statistics must be calculated: Firstly, in the 'Analysis' phase, statistics must be calculated after each exclusion rule is performed in order to see what effect the removal of observations have on the dataset. These values must be stored in the file Analysis.txt (see Table 5-3). Secondly, in the 'Classification' phase, (i.e. after removal of the spurious observations), statistics must be performed on the data used to construct the light-curves and the results must be stored in the file Stats.txt (see Table 5-5). Not all the statistics will be used in the final classification method used by the NNs, but they were assessed during the investigation stage of the classification method in

Chapter 4 to see if they were appropriate. Here are the values to be calculated by the 'LC Analyser classifier' application:

5.2.3.1 Calculations during Analysis phase

The parameters in Table 5-3 must be calculated during the analysis phase in order to identify those objects that do not meet the requirements for the neural networks to perform the classification. The calculations must be performed prior to analysis and after each exclusion rule is applied i.e. seven sets of output must be obtained per object:

Parameter	Explanation
Number of observations	The number of observations remaining after each of the exclusion rules is applied. One value is to be calculated for each stage: S1 to S7 inclusive.
Minimum flux	The minimum flux value of observations remaining after each of the exclusion rules is applied. One value is to be calculated for each stage: S1 to S7 inclusive.
Maximum flux	The maximum flux value of observations remaining after each of the exclusion rules is applied. One value is to be calculated for each stage: S1 to S7 inclusive.
Mean flux	The average flux value of observations remaining after each of the exclusion rules is applied. One value is to be calculated for each stage: S1 to S7 inclusive.
Median flux	The median flux value of observations remaining after each of the exclusion rules is applied. One value is to be calculated for each stage: S1 to S7 inclusive.
Flux range	The range between the minimum and maximum flux value after each of the exclusion rules is applied. One value is to be calculated for each stage: S1 to S7 inclusive.
RMS Error	The Root-Mean-Squared value of the flux errors for each of the observations after each of the exclusion rules is applied. One value is to be calculated for each stage: S1 to S7 inclusive.
S/N ratio	The Signal-to-noise ratio (i.e. Mean Flux / RMS Error) after each of the exclusion rules is applied. One value is to be calculated for each stage: S1 to S7 inclusive.
No. above Satellite trails	The number of observations above the satellite trails. One value is to be calculated for each stage: S1 to S4 inclusive.
No. below Satellite trails	The number of observations below the satellite trails. One value is to be calculated for each stage: S1 to S4 inclusive.
No. observations greater than Blend index	The number of observations above the blend index. One value is to be calculated for each stage: S1 to S3 inclusive.
Observations removed	The number of objects removed after each exclusion rule is applied. One value is to be calculated for each stage: S1 to S7 inclusive.

Table 5-3: Output values stored in the Analysis.txt file

5.2.3.2 Calculations during Classification phase

The calculations in Table 5-5 must be calculated during the classification phase in order to provide the values for the neural networks to perform the classification.

Parameter	Explanation
Observations analysed	The number of observations actually used in the classification i.e. those left after the exclusion process is performed.
Days analysed	The number of nights over which the observations are taken.
Total observations removed	The total number of observations removed in the exclusion process.
Period (d)	The period obtained from SuperWASP was in seconds. This is to be converted to the period in days.
Phase Length	The length of the binned phase-folded light-curve as calculated by Dworetsky (1983).
Mode/SD	Modal value of fluxes for all observations in the light curve divided by the Standard Deviation of all observations in the light-curve.
Time to process	Length of time taken to perform all calculations and classification of the object.
Period bin	The Period bin that the period value (in days) is in as indicated in Table 3-2, reproduced in Table 5-4.
Mean Flux	The average flux value of all observations.
Median Flux	The median flux value of all observations.
Minimum Flux	The minimum flux value of all observations.
Maximum Flux	The maximum flux value of all observations.
Flux Range	The range between the minimum and maximum flux value of all observations.
Mode-Mean	The modal flux value of all observations minus the mean flux value of all observations. This is calculated as a simple measure of skewness.
Flux Amplitude	The half-amplitude of flux values used in the light-curve.
All Magnitude Amplitude	The half-amplitude of magnitude values using all observations in the light-curve.
Binned Magnitude Amplitude	The half-amplitude of magnitude values using binned mean values in the light-curve.
Primary eclipse depth	The depth of the primary eclipse. This is only useful in eclipsing binaries but as the classification is not known, it is to be calculated for all objects.
Secondary eclipse depth	The depth of the secondary eclipse. Again, this is only useful in eclipsing binaries but as the classification is not known, it is to be calculated for all objects.
Eclipse ratio	The ratio of primary eclipse over secondary eclipse. This is only useful in eclipsing binaries but as the classification is not known, it is to be calculated for all objects.
Minimum Binned Magnitude	The minimum magnitude across all 25 bins.
Maximum Binned Magnitude	The maximum magnitude across all 25 bins.
Minimum Binned Flux	The minimum flux value across all 25 bins..
Maximum Binned Flux	The maximum flux value across all 25 bins.
HJD (1st observation)	The heliocentric Julian date of the earliest observation.
HJD (0 phase)	The heliocentric Julian date of the start of the phase for the object.
Binned Chi-Square	The Chi-squared value of the flux for each of the 25 bins.
Overall Chi-Square Flux	The overall Chi-squared value for all observations.

Period bin	Period range (d)
1	0.0000 to 1.0000
2	1.0001 to 10.0000
3	10.0001 to 50.0000
4	50.0001 to 100.0000
5	100.0001 to 500.0000
6	500.0001 to 999999.0

Table 5-4: Period bin ranges

Parameter	Explanation
Binned Skewness in Flux	The Skewness value of the flux for each of the 25 bins.
Overall Skewness in Flux	The overall Skewness value for all observations.
Binned Kurtosis in Flux	The Kurtosis value of the flux for each of the 25 bins.
Overall Kurtosis in Flux	The overall Kurtosis value for all observations.

Table 5-5: Output values stored in the Stats.txt file

5.2.4 Requirement 4 (Create two phase-folded diagrams)

Two phase-folded light-curves must be created in the 'LC Analyser classifier' application. The first must plot all remaining observations after the exclusion process as shown in Figure 5-6. The second must plot 'binned' observations where the lowest flux value is set at 'zero-phase' as shown in Figure 5-7.

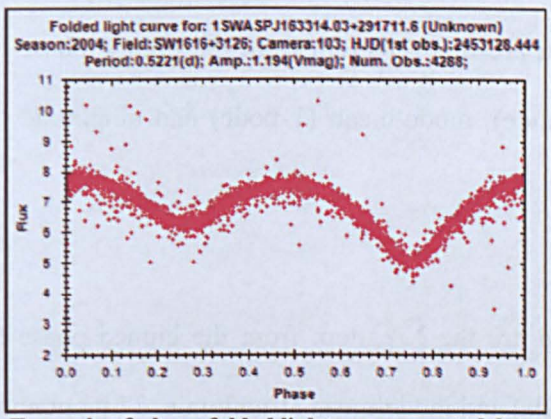

Figure 5-6: Example of phase-folded light-curve created from flux values

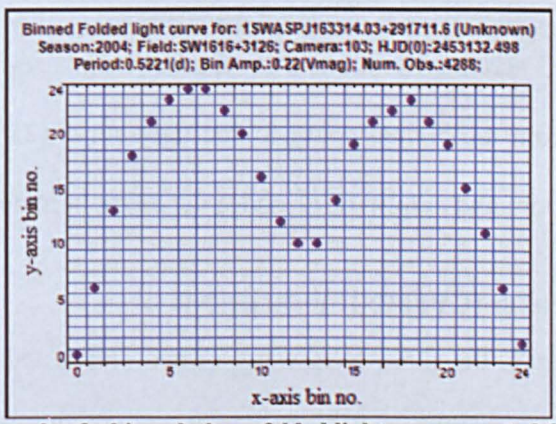

Figure 5-7: Example of a binned phase-folded light-curve created from flux values

The 'binned' phase-folded light-curve provides the parameters required for entry into the three NNs to obtain the classification of the object. The creation of these light-curves and obtaining the NN parameters is fully described in Chapter 3 (section 3.4.1).

5.2.5 Requirement 5 (Obtain parameters for entry into NNs)

After the spurious observations are removed from the object under test, the binned phase-folded light-curve must be used to obtain the parameters for entry into the NNs as indicated in Chapter 3 (section 3.4.1). The following parameters must be obtained for each object ready for processing through the neural network in order to obtain the output values for each object class:

5.2.5.1 NN Model 1

The parameters required are the Y-pattern from the binned phase-folded light-curve (25 nodes), period bin (1 node), mode-mean (1 node) and amplitude (1 node) i.e. 28 input nodes in all.

5.2.5.2 NN Model 2

The parameters required are the X-pattern from the binned phase-folded light-curve (25 nodes), period bin (1 node) and mode-mean (1 node) i.e. 27 input nodes in all.

5.2.5.3 NN Model 3

The parameters required are the Y-pattern from the binned phase-folded light-curve (25 nodes), the X-pattern from the binned phase-folded light-curve (25 nodes), period bin (1 node), mode-mean (1 node) and amplitude (1 node) i.e. 53 input nodes in all.

5.2.6 Requirement 6 (Create the three NNs)

As described in Chapter 3, the three NNs were trained and tested in the 'NeuralWorks Professional II/Plus' software (NeuralWare), which was kindly provided by the Open University. Once the decision had been made on which NNs were to be used, the

parameters shown in Table 5-6 were obtained from NeuralWorks for each of the trained NNs, in order to re-create them in the 'LC Analyser classifier' application. Note that the application will not train the NNs, it only processes objects through them using the defined NN structures. If the NNs require re-training at any point, they must be re-trained in the NeuralWorks software and the parameters re-imported into the application. This was deemed acceptable as the NNs only require re-training when new object classes are to be added or to increase the precision of the results when more data became available.

Parameter	Required for	Obtained from
Input range	The bounds within which each Input neuron was scaled	The 'I/O Parameters' form as indicated in the red border of Figure 5-8
Output range	The bounds within which each Output neuron was scaled	The 'I/O Parameters' form as indicated in the red border of Figure 5-8
NN range	Any output value outside this range was marked as 'out-of-range' in the application	Defined using the output of all the tests performed in Chapter 3 A fixed range of -0.13 to 1.13 was identified for all three NNs
Nodes	The number of nodes in the Bias, Input, Hidden and Output layers	Defined during creation of the NNs in Chapter 3
Bias MinMax	This is the default for back-propagation networks	Defined as 1 during creation of the NNs in Chapter 3
Input MinMax	Scaling the inputs and outputs of each neuron into an acceptable domain for the network	Obtained from the 'I/O MinMax Table' as indicated in the red border of Figure 5-9
Hidden Weights	Calculating the output of each hidden neuron	Obtained from the 'Load/Save Weights' function in NeuralWare
Output Weights	Calculating the output of each output neuron	Obtained from the 'Load/Save Weights' function in NeuralWare
Threshold	Decides which output neuron provides the classification	Defined in Chapter 3

Table 5-6: Parameters obtained from the trained and tested NNs

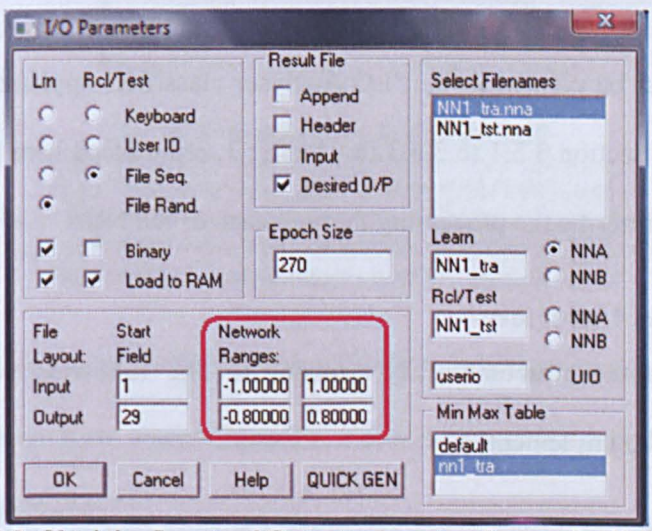

Figure 5-8: Obtaining Input and Output parameters from trained/tested NNs

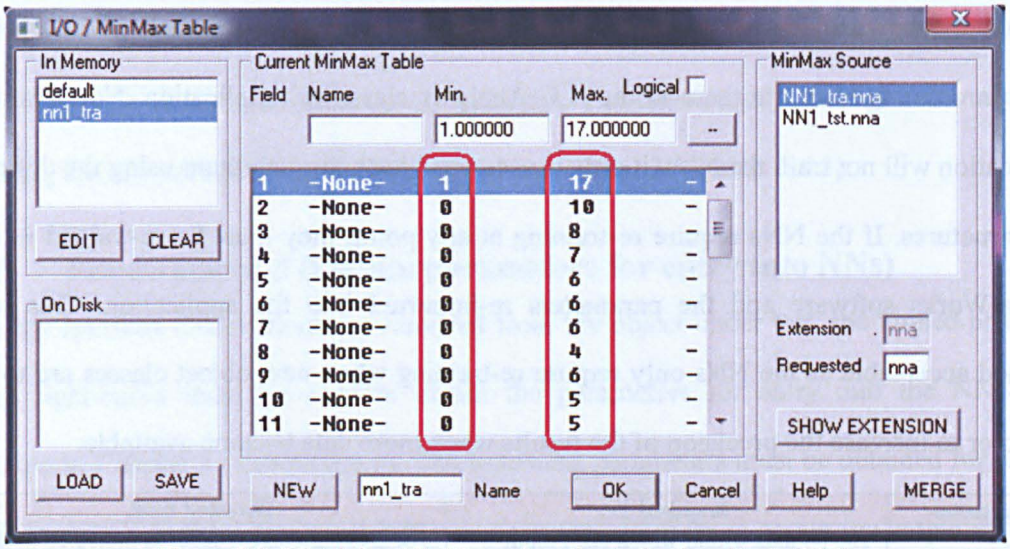

Figure 5-9: Obtaining MinMax values for trained and tested NNs

Each of the above parameters was stored in application files for each NN i.e. NNBase1.sgp for NN model 1, NNBase2.sgp for NN model 2 and NNBase3.sgp for NN model 3. This allows the application to be updated without re-coding and re-validating. Appendix 12 shows the structure of the file and an example of the data required for NN model 1. The complete file and the files for NN models 2 and 3 can be found on the supplementary DVD in the following location:

Supplementary data	
NNBase1.sgp	X:\Chapter05\LCAnalyser_NN\NNBase1.sgp
NNBase2.sgp	X:\Chapter05\LCAnalyser_NN\NNBase2.sgp
NNBase3.sgp	X:\Chapter05\LCAnalyser_NN\NNBase3.sgp

Where X is DVD-1 in the DVD-drive

The three NNs must be created in the 'LC Analyser classifier' application following the designs obtained in section 3.5.1 to 3.5.3 in Chapter 3, reproduced here for reference. The following sections describe the processing through each of the NNs:

5.2.6.1 NN Model 1 structure

Figure 5-10 shows the structure of NN model 1. The following steps describe the application flow to be implemented:

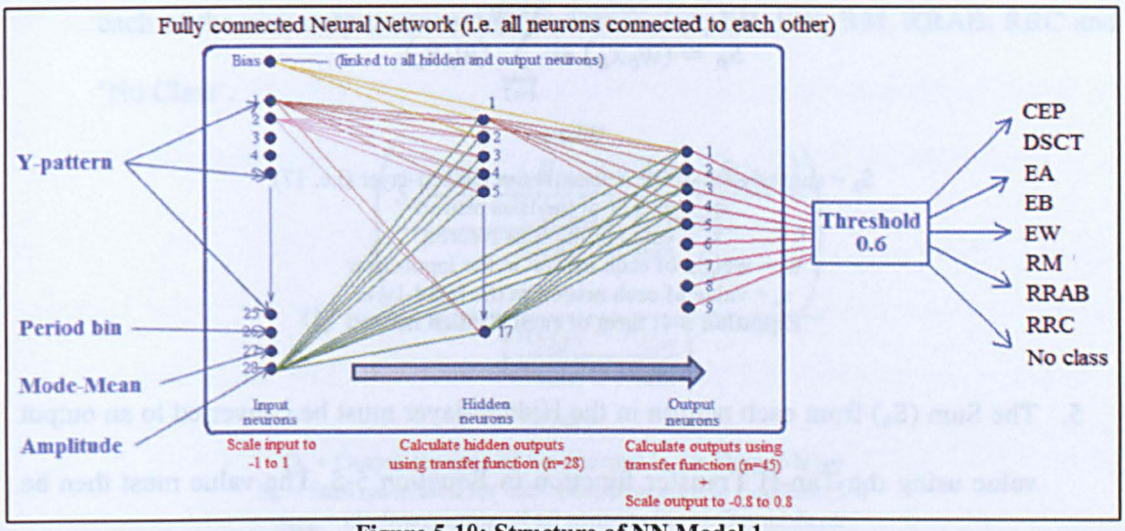

Figure 5-10: Structure of NN Model 1

1. The contents of the data file NNBase1.sgp must be loaded into the application. This inserts the parameters shown in Table 5-6 into the application ready for processing NN1.
2. The network structure must be created using the number of Bias, Input, Hidden and Output neurons indicated by the 'Nodes' parameter in Table 5-6 (i.e. 1, 28, 17 and 9 respectively).
3. The object parameters from section 5.2.5.1 must be seeded into the 28 neurons in the Input-layer and the values scaled using Equation 5-3.

$$x_i = x_i\left(\frac{R_{high} - R_{low}}{x_{max} - x_{min}}\right) + \left(\frac{(x_{max}R_{low}) - (x_{min}R_{high})}{(x_{max} - x_{min})}\right)$$

Where

x_i = value of each neuron in the Input-layer
X_{min} = minimum value of all neurons in the Input-layer
X_{max} = maximum value of all neurons in the Input-layer
R_{high} = high range value from 'Input range' parameter in Table 5-6
R_{low} = low range value from 'Input range' parameter in Table 5-6

Equation 5-3: Scaling input values to correct domain

4. The scaled values in the 28 Input neurons must be passed to each of the 17 neurons in the Hidden-layer where Equation 5-4 must be performed on each of them to obtain the sum (S):

$$S_h = (w_b x_b) + \sum_{i=1}^{n=28} (w_i\, x_i)$$

Where

S_h = sum of each of the neuron in the Hidden-layer (i.e. 17)
w_b = weight of the Bias neuron
x_b = value of the Bias Neuron
w_i = weight of each neuron in the Input-layer
x_i = value of each neuron in the Input-layer
Equation 5-4: Sum of each Hidden neuron

5. The Sum (S_h) from each neuron in the Hidden-layer must be converted to an output value using the Tan-H Transfer function in Equation 5-5. The value must then be passed to each neuron in the Output-layer.

$$O_h = \frac{e^{S_h} - e^{-S_h}}{e^{S_h} + e^{-S_h}}$$

Where

O_h = Output for each of the neurons in the Hidden-layer
S_h = Sum calculated for each Hidden neuron in Equation 5-4
Equation 5-5: Output of each Hidden neuron

6. As NN1 is a 'connect-prior' network, the weights from each neuron in the Input-layer must also be passed to the Output-layer. The output for each neuron in the Output-layer must then be calculated using Equation 5-6.

$$S_o = (w_b x_b) + \sum_{i=1}^{n=17} (w_i\, x_i) + \sum_{j=1}^{n=28} (w_j\, x_j)$$

Where

S_o = sum of each of the neurons in the Output-layer (i.e. 9)
w_b = weight of the Bias neuron
x_b = value of the Bias Neuron
w_i = weight of each neuron in the Hidden-layer
x_i = value of each neuron in the Hidden-layer
w_j = weight of each neuron in the Input-layer
x_j = value of each neuron in the Input-layer
Equation 5-6: Sum of each Output neuron

7. The output value (S_o) for each neuron in the Output-layer must then be scaled back to the 'real-world' values using Equation 5-7. This provides the calculated value for

each of the nine output neurons CEP, DSCT, EA, EB, EW, RM, RRAB, RRC and 'No Class'.

$$O_o = \frac{\left(S_o - \frac{(x_{max}R_{low}) - (x_{min}R_{high})}{(x_{max} - x_{min})} \right)}{\left(\frac{R_{high} - R_{low}}{x_{max} - x_{min}} \right)}$$

Where

O_h = Output for each of the neurons in the Output-layer
S_h = Sum calculated for each Output neuron in Equation 5-6
x_{min} = minimum value of all neurons in the Output-layer
x_{max} = maximum value of all neurons in the Output-layer
R_{high} = high range value from 'Output range' parameter in Table 5-6
R_{low} = low range value from 'Output range' parameter in Table 5-6

Equation 5-7: Output of each Hidden neuron

8. The output value (O_o) for each neuron in the Output-layer must then be used to classify the object as shown in section 5.2.7.

5.2.6.2 NN Model 2 structure

Figure 5-11 shows the structure of NN model 2.

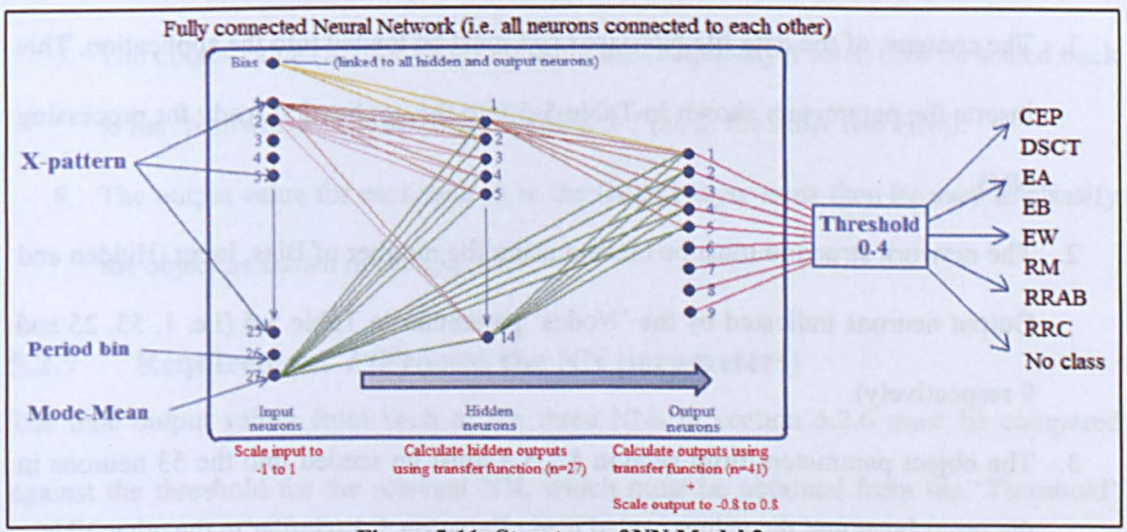

Figure 5-11: Structure of NN Model 2

NN2 is also a 'connect-prior' neural network therefore it follows exactly the same processing as NN1 in section 5.2.6.1. The only exceptions are:

a. The contents of the data file NNBase2.sgp must be used instead of NNBase1.sgp.

b. The number of Input and Hidden neurons is 27 and 14 respectively.

5.2.6.3 NN Model 3 structure

Figure 5-12 shows the structure of NN model 3. This NN is not a 'connect-prior' network, so the processing steps are slightly different. The following steps indicate the design:

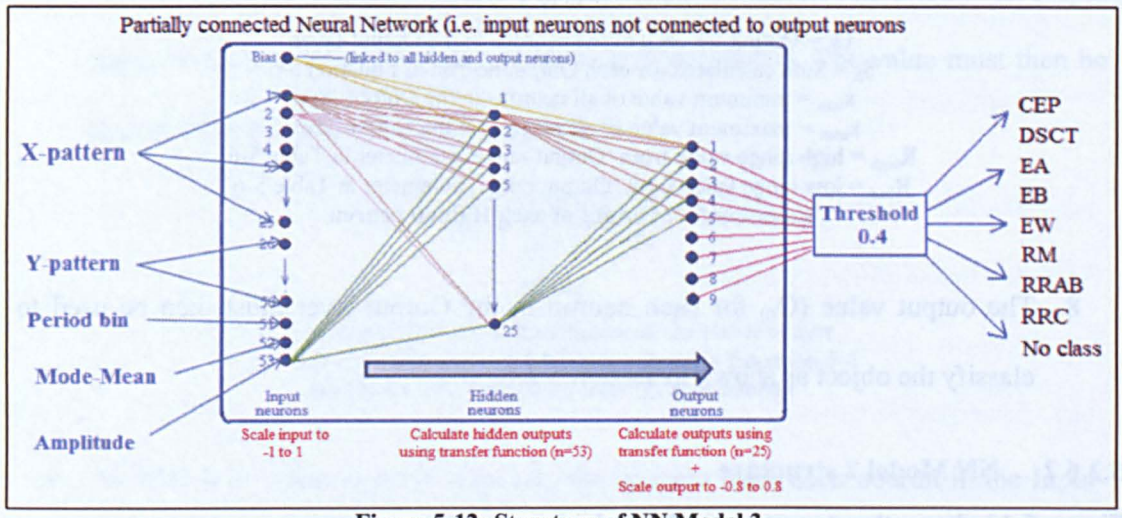

Figure 5-12: Structure of NN Model 3

1. The contents of the data file NNBase3.sgp must be loaded into the application. This inserts the parameters shown in Table 5-6 into the application ready for processing NN3.
2. The network structure must be created using the number of Bias, Input, Hidden and Output neurons indicated by the 'Nodes' parameter in Table 5-6 (i.e. 1, 53, 25 and 9 respectively).
3. The object parameters from section 5.2.5.3 must be seeded into the 53 neurons in the Input-layer and the values scaled using Equation 5-3 (similar to the other NNs).
4. The scaled values in the 53 Input neurons must be passed to each of the 25 neurons in the Hidden-layer where Equation 5-4 must be performed on each of them (again, similar to the other NNs).

5. The Sum (S_h) from each neuron in the Hidden-layer must be converted to an output value using the Sigmoid Transfer function in Equation 5-8 (instead of Tan-H for the other NNs) which must then be passed to each neuron in the Output-layer.

$$O_h = 1 + e^{S_h}$$

Where
O_h = Output for each of the neurons in the Hidden-layer
S_h = Sum calculated for each Hidden neuron in Equation 5-4
Equation 5-8: Output of each Hidden neuron in NN3

6. As NN3 is not a 'connect-prior' network, only the weights from each neuron in the Hidden-layer must be passed to the Output-layer. The output for each neuron in the Outer-layer must then be calculated using Equation 5-9.

$$S_o = (w_b x_b) + \sum_{i=1}^{n=25} (w_i x_i)$$

Where
S_o = sum of each of the neurons in the Output-layer (i.e. 9)
w_b = weight of the Bias neuron
x_b = value of the Bias Neuron
w_i = weight of each neuron in the Hidden-layer
x_i = value of each neuron in the Hidden-layer
Equation 5-9: Sum of each Output neuron for NN3

7. The output value (S_o) for each neuron in the Output-layer must then be scaled back to the 'real-world' values using Equation 5-7 (as in the other two NNs).
8. The output value for each neuron in the Output-layer must then be used to classify the object as shown in section 5.2.7.

5.2.7 Requirement 7 (Process the NN parameters)

The nine output values from each of the three NNs in section 5.2.6 must be compared against the threshold for the relevant NN, which must be obtained from the 'Threshold' parameter from Table 5-6. The following process must be employed for each NN:

1. To obtain the classification from each of the three NNs, the nine output values of each NN must be compared against the threshold (0.6 for NN1 values, 0.4 for NN2 values and 0.4 for NN3 values) and the following rules applied:
    a. If a single output value is higher than the threshold, then the class must be assigned from this list: Output 1 = CEP; Output 2 = DSCT; Output 3 = EA; Output 4 = EB; Output 5 = EW; Output 6 = RM; Output 7 = RRAB; Output 8 = RRC; and Output 9 = 'No Class'.
    b. If no output values are greater than the threshold, then the 'No Class' class must be assigned.
    c. If more than one output value is greater than the threshold, then the class 'Review' must be assigned.
2. The final classification and its confidence index must be calculated using an amalgamation of the classes from all three NNs. This must be performed using the rules in Table 5-7:

NN1 class	NN2 class	NN3 class	Overall class	Confidence index
A	A	A	A	1
A	A	No class	A	2
A	A	Review	A	3
A	No class	No class	A	4
A	Review	No class	A	5
A	Review	Review	A	6
A	A	B	A	7
A	B	C	Review	8

Table 5-7: Assignment of Overall Class and confidence index to tested objects

In Table 5-7, A is an identified class, B is a second identified class and C is a third identified class. When obtaining the Overall Class and Overall Confidence index, the order of the individual classes does not matter i.e. the result [A, A, No Class] is equivalent to [A, No Class, A] and [No Class, A, A], so they give the same Overall class and Overall Confidence index. To implement this, the file 'Outcome.sgp' must be loaded into the application. The file provides all known outcomes for the amalgamation of the three

classes provided by NN1, NN2 and NN3, in the first three columns of the file. The remaining two columns provide the final classification and confidence index. An example of the file can be seen in Figure 5-13. The complete file can be found on the supplementary DVD in the following location:

Supplementary data	
Outcome.sgp	X:\Chapter05\LCAnalyser_NN\Outcome.sgp

Where X is DVD-1 in the DVD-drive

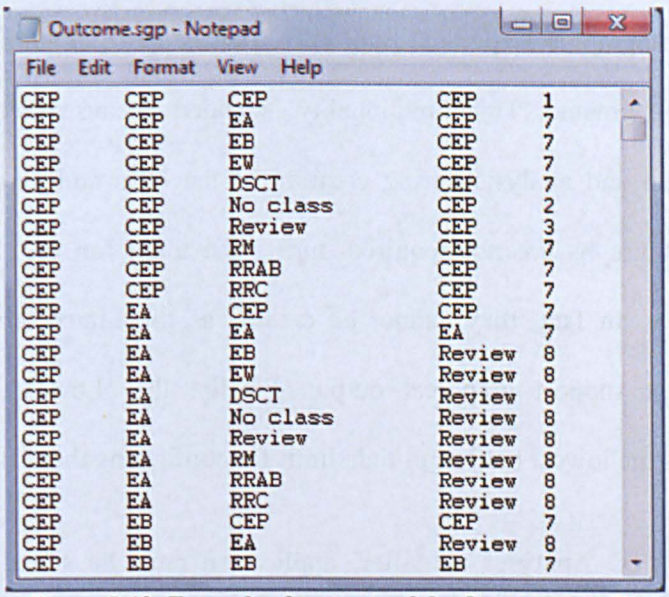

Figure 5-13: Example of contents of the Outcome.sgp file

The classification of the three NNs (e.g. CEP for NN1, CEP for NN2 and RM for NN3) must be automatically compared against every row in the file until a match is found. In this example, the final classification would be CEP and the confidence index would be 7. If the classification from the three NNs was CEP, CEP and CEP, then the final classification would be CEP with a confidence index of 1. The Overall Class obtained from the file is called 'Best class' and the confidence index is called 'Best confidence'.

5.2.8 Requirement 8 (Write calculations/results to files)

The parameters to be stored on completion of the analysis are defined in the LCAnalyser.ini file shown in Table 5-2. If the 'Output Results' parameter in the table is set to 'ALL' then the results for all three NNs must be written to the 'NNData.txt' file,

otherwise only the NN3 results are output. This functionality is provided in case the output from NN3 was sufficient to classify all objects by itself (see Chapter 3, section 3.4.2). The decision from Chapter 3 (section 3.5.4) was to use the results from all three NNs, so the default for this parameter must be set to 'ALL'. Also, the 'Graphs' parameter controls the output of the light-curves. If this is set to 'BMP', the phase-folded and binned phase-folded light-curves must be saved as Windows Bitmap format; if it is set to 'JPG' they must be saved as 'Joint Photographic Experts Group' files. If it is set to anything else, the light-curves must not be created. This functionality is added because the light-curves are required for creation and analysis during creation of the NNs and classification of the GCVS objects, but graphs are not required during the main run on all objects of the SuperWASP archive. In fact, they cannot be created as the Linux server used for the processing does not support graphical output. Finally, the 'Lowest Bin Amplitude' parameter identifies the lowest half-amplitude limit for confirming the class of the objects.

The data from the 'LC Analyser classifier' application must be stored in four files as shown in Table 5-8. The contents of each must be as follows:

Filename	Contents
NNData.txt	The classification output for the catalogue shown in section 5.2.8.1
Stats.txt	The results of the calculations performed in section 5.2.3.2
Analysis.txt	The results of the calculations performed in section 5.2.3.1
Session.txt	The number of objects processed and the number of objects with a classification

Table 5-8: Output files from 'LC Analyser classifier'

An example of the output can be seen on the supplementary DVD in the following location:

Supplementary data	
NNData.txt	X:\Chapter05\LCAnalyser_output\NNData.txt
Stats.txt	X:\Chapter05\LCAnalyser_output\Stats.txt
Analysis.txt	X:\Chapter05\LCAnalyser_output\Analysis.txt
Session.txt	X:\Chapter05\LCAnalyser_output\Session.txt

Where X is DVD-1 in the DVD-drive

5.2.8.1 NNData.txt output

In many ways, this is the most important file as it must contain the classification results for each object. The values stored in this file are shown in Table 5-9.

Field	Contents
Season	Unique identifier for the object i.e. an object can have a class for different seasons, fields, cameras and detrends, depending on when the observations were made
Field	
Camera	
Detrend	
Period (s)	
Object Id	
GCVS Name	The GCVS name if it is a known star
Obs. analysed	The number of observations used in the analysis
Days analysed	The number of nights the observations were taken over
HJD(0 phase)	The starting time of the light-curve
Output values for NN1	The 9 output values from NN1 and the calculated class i.e. CEP, DSCT, EA, EB, EW, RM, RRAB, RRC, No Class, NN1_Class
Output values for NN2	The 9 output values from NN2 and the calculated class
Output values for NN3	The 9 output values from NN3 and the calculated class
Overall class	The Overall class for the object
Overall confidence	The Overall confidence index in the result
Binned Mag Amplitude	The half-amplitude of the binned phased light-curve used for the classification
Colour values	The B mag, V mag, J mag, H mag and K mag colour values if the star has an existing classification (taken from NOMAD 1.0 catalogue)
x-axis values to plot	Used to reconstruct the binned phased light-curve (if required)
y-axis values to plot	
Num 0 chi-sqr	The number of bins in the binned phase light-curve that have a zero value
Num consec 0 chi-sqr	The number of consecutive bins in the binned phase light-curve that have a zero value
Below min amplitude	The number of bins in the binned phase light-curve that are below the minimum acceptable half-amplitude
Graph name (P)	The name of the binned phased light-curve (if plotted)

Table 5-9: Output data from the 'LC Analyser classifier' stored in the NNData.txt file

It is envisaged that this data will be stored in the SuperWASP archive to allow researchers to retrieve objects based on their classification. This can be done in a number of ways:

- Retrieve objects based on the Overall class and Overall confidence index:

  For example: retrieve all objects where the overall class = 'EA' and overall confidence index < 2. This query would provide all EA objects where the class was EA in all three NNs. Making overall confidence index < 4 would provide all EA objects where two or more NNs gave an EA result.

- Retrieve objects based on the weight of the output:

For example: retrieve all objects where the NN3 EA value >= 0.6. This would provide all EA objects where NN3 neuron 3 gave a value >= 0.6. Overall confidence index could also be added into the query if required. Similarly, 'Num 0 chi-sqr', 'Num consec 0 chi-sqr' and/or 'Below min amplitude' parameters could also be added to narrow the search.

5.2.8.2 Analysis.txt output

This file must hold the output for the Analysis phase during pre-processing of the objects. These values are fully described in section 5.2.3.1 (Table 5-3). An example of the output can be seen on the supporting DVD at:

Supplementary data	
Analysis.txt	X:\Chapter05\LCAnalyser_output\Analysis.txt

Where X is DVD-1 in the DVD-drive

5.2.8.3 Stats.txt output

This file must hold the output for the Statistics phase during processing of the objects. These are fully described in section 5.2.3.2 (Table 5-5). An example of the output can be seen on the supporting DVD at:

Supplementary data	
Stats.txt	X:\Chapter05\LCAnalyser_output\Stats.txt

Where X is DVD-1 in the DVD-drive

5.2.8.4 Session.txt output

This file must contain the number of objects classified in each session.

5.2.8.5 Phase-folded light-curves

If the 'Graphs' parameter in the LC Analyser file (Table 5-2) is set to 'BMP' or 'JPG', then the phase-folded light-curve and binned phase-folded light-curves must be saved as bitmap or jpg files respectively.

Now that the User and Functional Requirements have been described, the next section indicates the design necessary to implement them.

5.3. Design of the 'LC Analyser classifier' application

The 'LC Analyser classifier' application is designed in a modular fashion to make it easier to add extra features as the work progressed.

Figure 5-14 shows the main design for the 'LC Analyser classifier' application. The diagram shows the main flow through the application and each of the code modules and input files are discussed in detail below.

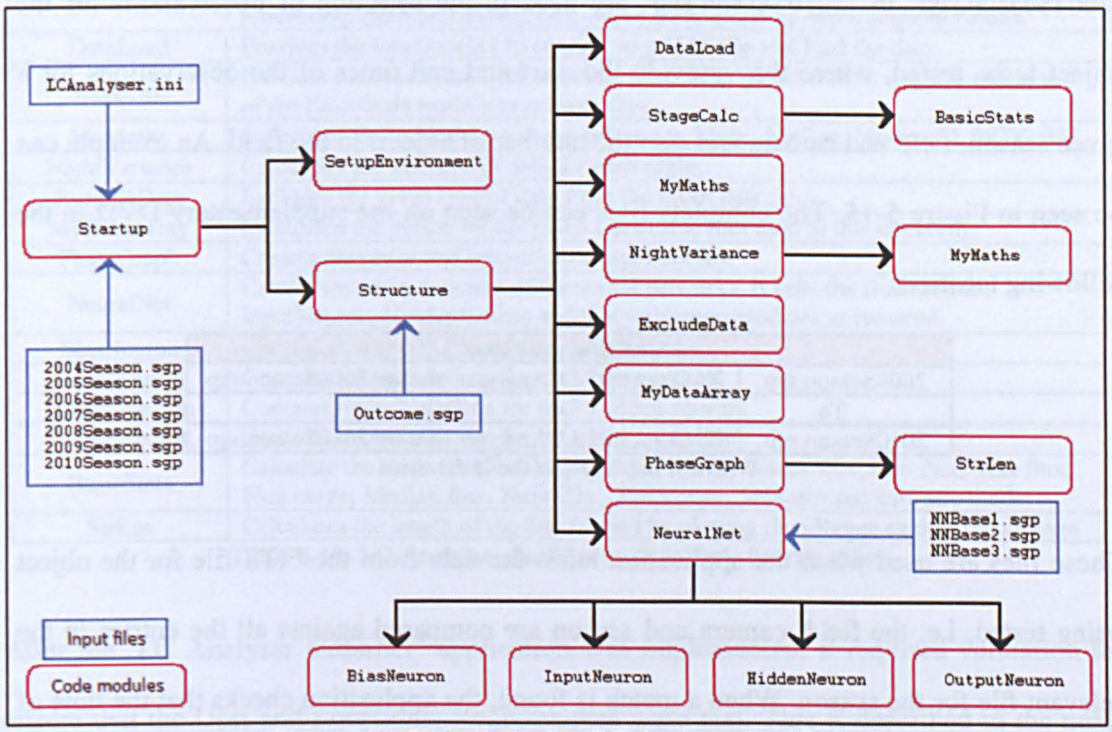

Figure 5-14: Main design for 'LC Analyser classifier'

The completed program can be found on the supplementary DVD in the following location:

Supplementary data	
Application files	X:\Chapter05\LC Analyser v19_1_0

Where X is DVD-1 in the DVD-drive

This design has been implemented and the application modules are liberally commented to help understand the code in the application. The files can be read with any text editor,

though Microsoft Visual Studio will highlight the text in different colours for easier reading (e.g. comments, commands, data constructs etc.).

5.3.1 Input files

The LCAnalyser.ini, NNBaseX.sgp and Outcome.sgp files have already been discussed in detail.in sections 5.2.2 (removing spurious observations), 5.2.6 (creating the three NNs) and 5.2.7 (processing the NN parameters) respectively. The remaining files '2004Season.sgp' to '2010Season.sgp' are used in the selection of observations for the object to be tested, where they provide the start and end times of the observations for a given season, field and camera and also the number of objects in the field. An example can be seen in Figure 5-15. The complete files can be seen on the supplementary DVD in the following location:

Supplementary data	
2004Season.sgp	X:\Chapter05\LCAnalyser_startup\2004Season.sgp
To	To
2010Season.sgp	X:\Chapter05\LCAnalyser_startup\2010Season.sgp

Where X is DVD-1 in the DVD-drive

These files are used when the application loads the data from the FITS file for the object being tested, i.e. the field, camera and season are compared against all the entries in the relevant file for the season. When a match is found, the application checks that the time of the observation is within the given range. If it is within the time range, the observation is loaded into the application for analysis, if it is not, the observation is ignored.

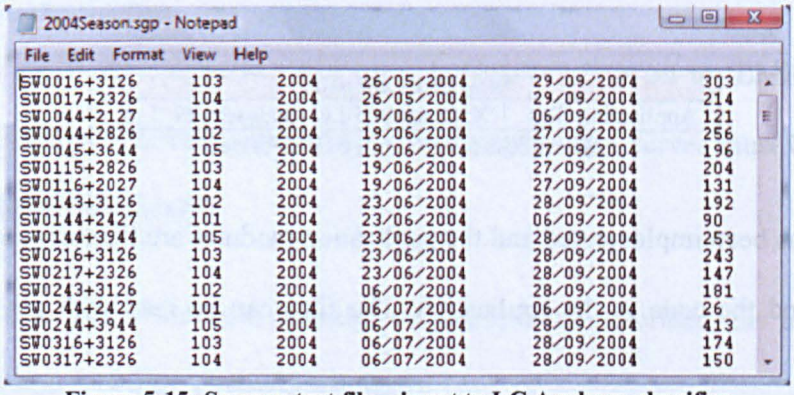

Figure 5-15: Seasons text file – input to LC Analyser classifier

5.3.2 Code modules

The code modules contain the functions required to process an object. Figure 5-14 (above) shows the flow of data and module interaction. Their main purpose is described in Table 5-10.

Module	Main functionality
Startup	Checks the consistency of the data file with the objects in, calls the 'SetupEnvironment' module and then repeatedly calls the 'Structure' module for each object.
SetupEnvironment	Creates the directory structure to hold the output of the session being processed.
Structure	Controls all the work. It calls all the modules below as required during the pre-processing, main processing, post-processing, graphing and storage of results.
DataLoad	Provides the functionality to connect to a FITS file and load the data.
StageCalc	Provides the functionality to calculate the details required for a stage. It makes use of the BasicStats module to achieve this.
MyMaths	Calculates Basic Maths on an ArrayList e.g. Mean, Median, Mode, SD, %CV, RM.
NightVariance	Calculates the variance of data for each night.
ExcludeData	Excludes the given type of data from the given data set.
MyDataArray	Calculates the period for the given DataTable (not used in this research).
PhaseGraph	Creates the phase and binned phase light-curves.
NeuralNet	Creates the main structure of the neural networks. It calls the BiasNeuron, InputNeuron, HiddenNeuron and OutputNeuron modules as required.
BiasNeuron	Contains the calculations for each Bias neuron.
InputNeuron	Contains the calculations for each Input neuron.
HiddenNeuron	Contains the calculations for each Hidden neuron.
OutputNeuron	Contains the calculations for each Output neuron.
BasicStats	Calculate the basic stats for the given data set i.e.: Mean flux, Min flux, Max flux, Flux range, Median flux, Num Obs., RMS error, SNRatio and half-amplitude.
StrLen	Calculates the length of the line formed by plotting the yRange against the xRange

Table 5-10: LC Analyser classifier code module functionality

After the 'LC Analyser classifier' application was implemented, it required validation to ensure that the User and Functional Requirements were met. This is described in the next section.

5.4. Validation of the 'LC Analyser classifier' application

The validation of the 'LC Analyser classifier' application involved taking 50 objects with known classification and processing them through each of the three NNs in the NeuralWare software where the NNs were created. This provided values for each of the neurons in the Output-layer for each object and these became the 'gold-standard' that had to be met in the application.

The NN calculations from section 5.2.6 were modelled in Microsoft Excel to confirm that the output was identical to the 'gold-standard'. This meant that the following values were correctly derived:

- Scaled values for each neuron in the Input layer
- Final value of each neuron in the Hidden layer
- Final value of each neuron in the Output layer

The equations were then implemented in the 'LC Analyser classifier' application. The 50 objects were then processed through the 'LC Analyser' code and debug statements were used to output the results of the three calculations shown above, during processing. The results were compared against the 'gold standard' and they were shown to be identical. This indicated that the calculations in the 'LC Analyser classifier' were implemented correctly.

The exclusion rules were validated by viewing the output in the Analysis.txt file. Each object that was removed displayed which rule it failed in this file. The observations for a selection of these objects (covering all rules) were manually reviewed to ensure that the relevant observations were removed.

The values calculated in the Analysis phase (Table 5-3) were compared against similar calculations created in Microsoft Excel for the same objects. These were shown to be identical.

The values calculated in the Classification phase (Table 5-5) were similarly compared against the same calculations created in Microsoft Excel for the same objects. These were again shown to be identical.

The phase-folded light-curves created in the 'LC Analyser classifier' application were compared against graphs created in Microsoft Excel using the same data that was used in the application. These graphs were also identical.

5.5. Implementation of the 'LC Analyser classifier'

Two versions of the 'LC Analyser classifier' application were required for this research: One for analysis of the objects with known GCVS class on a single PC (i.e. at home) in a 'supervised' mode, with limited numbers of objects as proof of principle for the NNs; the second for analysis of all periodic variables in the SuperWASP archive at Leicester University using multiple processors in an 'unsupervised' mode with large numbers of objects.

5.5.1 Create Windows' Vista version of application

This version of the application was used on a single PC (at home) for proof-of-principle of the NNs. This version was designed as indicated in section 5.2, validated as in section 5.4 and confirmed that the NNs were fully functional for use in this research. The application was created with Microsoft Visual Studio (version 8.0.50727.867) in the Microsoft .Net Framework (version 2.0.50727 SP2). The main programming language was C#.Net (C-sharp), but a couple of VB.Net (Visual Basic) commands were used where C# functions were not available, also some mathematical functions used the Microsoft Excel DLL (Dynamic Linked Library) as they were readily available.

5.5.2 Create Linux version of application

This version of the application was used at Leicester University for analysing all periodic variables in the SuperWASP archive. This version was built with MonoDevelop (version 2.1.0) using C# as the main programming language. The computer system used at Leicester employs the Linux operating system and Linux does not support the Windows Visual Studio environment, therefore the Windows version of the application (Visual Studio) was

imported into the Linux version where automatic conversion was provided for 98% of the code. The areas that could not be converted were listed in a 'conversion error' report and these were manually amended to use the same code, but different MonoDevelop functions. The Linux application was transferred to Leicester University and validated by processing 10 random objects (of different class) in both the Windows Vista version and the Linux version. The results from each application were compared to ensure that the same classification was given and that the output for each neuron in the Output layer was identical. An analysis of all the outputs in the files NNData.txt, Analysis.txt, and Stats.txt was made to ensure they were identical. This confirmed that the Linux version of the application yielded identical outputs to the Windows Vista version and therefore was acceptable for use to analyse all periodic variables in the SuperWASP archive.

5.6. Processing all data in the SuperWASP archive

Processing all the objects with known GCVS class was discussed in Chapter 4. This section briefly discusses the results of testing ALL periodic objects in the SuperWASP archive. It indicates the number of each class identified by the 'LC Analyser classifier' application. Due to the large amount of data provided by the application, the decision was made at this point to continue the study of the eclipsing binaries EA, EB and EW and the pulsating variables DSCT and RRAB only. These are fully assessed in Chapter 7 and Chapter 8.

The results presented in Table 5-11 provides an overview of the number of objects classified. There were 4,280,740 object/period combinations analysed automatically by the 'LC Analyser classifier' application and classifications were obtained for 3,913,807 object/period combinations. The remaining 366,933 objects were rejected due to insufficient observations after pre-processing. A review of the 4,280,740 objects showed

that there were 3,214,104 unique objects, the others being the same object with multiple periods.

Analysis of All objects				Neural Network Results				
	Total to	Total tested		1	2	4	All	
pFlag	be tested	Duplicates	Unique	NN	NN	NN	NN	Period location (from SuperWASP)
0	433,438	433,437	212,100	44,266	43,790	56,708	144,764	Good periods
1	1,872,278	1,698,674	1,357,796	111,695	161,512	273,383	546,590	Between 0.9d and 1.3d
2	714,567	643,468	570,036	28,817	31,845	43,389	104,051	Close to 1/2 sidereal day
3	605,218	544,559	511,724	34,543	40,694	61,566	136,803	Close to 1/3 sidereal day
4	237,815	216,978	209,736	20,637	23,290	29,167	73,094	Close to 1/4 sidereal day
5	111,874	101,541	97,014	10,178	12,055	13,401	35,634	Close to 1/5 sidereal day
6	78,619	71,118	67,121	7,019	8,901	8,630	24,550	Close to 1/6 sidereal day
7	54,308	49,087	46,056	4,998	6,409	5,722	17,129	Close to 1/7 sidereal day
8	29,301	26,388	25,145	2,727	3,420	2,891	9,038	Close to 1/8 sidereal day
9	17,075	15,206	14,700	1,690	2,081	1,537	5,308	Close to 1/9 sidereal day
10	14,333	12,940	12,591	1,381	1,761	1,432	4,574	Close to 1/10 sidereal day
11	9,110	5,499	5,462	578	675	540	1,793	Close to 1/11 sidereal day
12	5,716	5,166	4,856	583	651	518	1,752	Close to 1/12 sidereal day
13	3,362	2,861	2,668	302	351	282	935	Close to 1/13 sidereal day
14	1,892	1,607	1,421	169	192	154	515	Close to 1/14 sidereal day
15	973	846	722	86	86	84	256	Close to 1/15 sidereal day
16	1,608	1,466	1,335	119	174	153	446	Close to 1/16 sidereal day
20	7,795	7,219	6,543	314	374	871	1,559	Close to n x 1d (n>1)
31	2,109	1,888	1,522	300	154	351	805	Between 177800 - 182000 sec (~49h - 51h)
32	1,667	1,513	1,260	162	180	318	660	Between 278600 - 285100 sec (~77h - 79h)
33	4,815	4,224	3,341	343	356	878	1,577	Between 380000 - 407400 sec (~105h - ~113h)
87	12,420	11,004	8,726	848	1,005	2,216	4,069	Close to 1/4 month
88	10,206	9,222	7,539	613	743	2,221	3,577	Close to 1/3 month
89	16,628	15,105	12,959	630	1,207	4,187	6,024	Close to 1/2 month
91	32,279	31,602	30,630	1,748	2,252	6,531	10,531	Close to 1 month
92	1,327	1,182	1,094	62	165	303	530	Close to 2 months
93	7	7	7	0	0	2	2	Close to 3 months
Total	4,280,740	3,913,807	3,214,104	274,808	344,323	517,435	1,136,566	

Table 5-11: Summary of number of objects tested and classified

From these 3,214,104 unique periodic objects, 274,808 had a classification assigned by the 'LC Analyser classifier' application that agreed in all three NNs (i.e. confidence index 1). 344,323 objects had a class assigned that agreed in only two of the NNs (the other being 'No class' i.e. confidence index 2) and 517,435 of them had a classification assigned by one NN (the other two being 'No class' i.e. confidence index 4). Table 5-11 shows the results split across each PFlag. It should be noted that PFlag 0 objects are likely to be objects with true periods, but all the other PFlags may contain large numbers of false periods due to rotation of the Earth. The main point is that of the 3,913,807 object/period combinations, the 'LC Analyser classifier' application provided a preliminary

classification for 274,808 of them with a high confidence, thus narrowing down the number of objects a researcher has to examine to find objects of interest. Table 5-12 shows the number of objects obtained for each class that have a confidence index of 1. This means that these are likely to be 'good' objects. In order to confirm this, the eclipsing binaries EA, EB and EW and the pulsating classes DSCT and RRAB are examined further in Chapter 7 and Chapter 8 respectively.

	Confidence 1									
pFlag	CEP	DSCT	EA	EB	EW	RM	RRAB	RRC	Total	Period location (from SuperWASP)
0	1,616	4,275	10,761	3,212	1,338	15,860	3,773	3,431	44,266	Good periods
1	12,920	15,807	21,383	2,562	143	54,139	3,280	1,461	111,695	Between 0.9d and 1.3d
2	31	6,363	4,113	1,607	77	10,703	4,902	1,021	28,817	Close to 1/2 sidereal day
3	40	7,216	7,288	816	120	12,490	3,850	2,723	34,543	Close to 1/3 sidereal day
4	37	4,852	3,946	626	43	7,332	2,203	1,598	20,637	Close to 1/4 sidereal day
5	14	2,471	1,596	300	7	3,648	1,316	826	10,178	Close to 1/5 sidereal day
6	8	1,977	782	148	2	2,648	737	717	7,019	Close to 1/6 sidereal day
7	7	1,547	516	91	3	1,982	432	420	4,998	Close to 1/7 sidereal day
8	5	931	228	21	1	1,034	236	271	2,727	Close to 1/8 sidereal day
9	0	656	85	12	2	590	115	230	1,690	Close to 1/9 sidereal day
10	3	560	90	15	2	489	61	161	1,381	Close to 1/10 sidereal day
11	1	316	24	6	0	149	14	68	578	Close to 1/11 sidereal day
12	0	285	9	2	0	195	14	78	583	Close to 1/12 sidereal day
13	0	176	3	1	0	83	0	39	302	Close to 1/13 sidereal day
14	0	91	6	0	0	54	1	17	169	Close to 1/14 sidereal day
15	1	45	1	0	0	26	2	11	86	Close to 1/15 sidereal day
16	0	62	1	0	0	40	1	15	119	Close to 1/16 sidereal day
20	70	3	110	1	1	128	1	0	314	Close to n x 1d (n>1)
31	15	1	204	6	0	73	1	0	300	Between 177800 - 182000 sec (~49h - 51h)
32	15	0	80	1	1	64	1	0	162	Between 278600 - 285100 sec (~77h - 79h)
33	36	1	116	8	0	178	4	0	343	Between 380000 - 407400 sec (~105h - ~113h)
87	84	14	227	13	0	506	2	2	848	Close to 1/4 month
88	66	3	244	6	0	292	2	0	613	Close to 1/3 month
89	125	3	207	0	1	292	1	1	630	Close to 1/2 month
91	537	33	791	2	2	379	3	1	1,748	Close to 1 month
92	8	0	17	0	0	36	1	0	62	Close to 2 months
93	0	0	0	0	0	0	0	0	0	Close to 3 months
Total	15,639	47,688	52,828	9,456	1,743	113,410	20,953	13,091	274,808	

Table 5-12: Summary of number of objects with conf. index 1 (by class)

Table 5-13 shows the number of objects obtained for each class that have a confidence index of 2. This means that they are less likely to be 'good' objects, but as two NNs agree, they are still worth investigating.

Table 5-14 shows the number of objects obtained for each class that have a confidence index of 4. This means that they are even less likely to be 'good' objects as the classification is only given by one NN. Further work is required here to see if any one NN is better than another in classifying these objects. For instance as NN3 incorporates inputs

for x-axis, y-axis and period bin, therefore it is expected that it will be better than NN1 (y-axis only) and NN2 (x-axis only). If this is correct, then a large number of these objects with confidence index 4 could be 'good' classifications.

	Confidence 2									
pFlag	CEP	DSCT	EA	EB	EW	RM	RRAB	RRC	Total	Period location (from SuperWASP)
0	3,373	4,850	1,688	3,532	1,508	22,735	2,243	3,861	43,790	Good periods
1	21,152	15,842	7,352	8,892	1,222	97,869	5,660	3,523	161,512	Between 0.9d and 1.3d
2	719	5,896	1,158	2,548	250	17,046	2,504	1,724	31,845	Close to 1/2 sidereal day
3	997	7,516	1,541	3,020	272	20,854	3,315	3,179	40,694	Close to 1/3 sidereal day
4	595	4,616	735	1,438	147	12,305	1,676	1,778	23,290	Close to 1/4 sidereal day
5	286	2,453	288	647	59	6,465	814	1,043	12,055	Close to 1/5 sidereal day
6	184	1,906	165	426	41	4,783	484	912	8,901	Close to 1/6 sidereal day
7	124	1,447	105	250	32	3,495	268	688	6,409	Close to 1/7 sidereal day
8	59	832	26	84	10	1,841	125	443	3,420	Close to 1/8 sidereal day
9	26	579	20	31	12	1,102	68	243	2,081	Close to 1/9 sidereal day
10	31	503	27	46	8	883	89	174	1,761	Close to 1/10 sidereal day
11	8	252	12	9	1	298	23	72	675	Close to 1/11 sidereal day
12	4	213	7	9	4	321	23	70	651	Close to 1/12 sidereal day
13	5	112	7	7	1	159	6	54	351	Close to 1/13 sidereal day
14	7	58	4	6	0	90	5	22	192	Close to 1/14 sidereal day
15	0	25	0	0	0	51	1	9	86	Close to 1/15 sidereal day
16	3	51	0	7	1	90	3	19	174	Close to 1/16 sidereal day
20	131	4	11	5	3	211	7	2	374	Close to n x 1d (n>1)
31	33	4	13	13	0	89	2	0	154	Between 177800 - 182000 sec (~49h - 51h)
32	28	3	13	12	3	101	19	1	180	Between 278600 - 285100 sec (~77h - 79h)
33	71	9	19	23	6	223	3	2	356	Between 380000 - 407400 sec (~105h - ~113h)
87	181	32	47	28	7	694	13	3	1,005	Close to 1/4 month
88	185	26	52	21	8	436	12	3	743	Close to 1/3 month
89	267	17	140	18	3	746	14	2	1,207	Close to 1/2 month
91	696	43	109	32	82	1,135	144	11	2,252	Close to 1 month
92	66	0	1	1	2	95	0	0	165	Close to 2 months
93	0	0	0	0	0	0	0	0	0	Close to 3 months
Total	29,231	47,289	13,540	21,105	3,682	194,117	17,521	17,838	344,323	

Table 5-13: Summary of number of objects with conf. index 2 (by class)

	Confidence 4									
pFlag	CEP	DSCT	EA	EB	EW	RM	RRAB	RRC	Total	Period location (from SuperWASP)
0	5,371	11,719	1,042	7,699	1,657	22,726	1,875	4,619	56,708	Good periods
1	29,124	39,417	5,612	41,478	8,824	116,552	15,273	17,103	273,383	Between 0.9d and 1.3d
2	1,261	8,400	686	7,682	1,405	17,059	2,919	3,977	43,389	Close to 1/2 sidereal day
3	1,572	11,187	906	10,556	1,872	24,669	4,382	6,422	61,566	Close to 1/3 sidereal day
4	867	5,484	367	3,987	978	12,399	2,154	2,931	29,167	Close to 1/4 sidereal day
5	493	2,518	160	1,656	461	5,774	1,026	1,313	13,401	Close to 1/5 sidereal day
6	323	1,704	110	945	268	3,813	498	969	8,630	Close to 1/6 sidereal day
7	228	1,140	70	591	153	2,585	297	658	5,722	Close to 1/7 sidereal day
8	93	644	28	243	87	1,269	162	365	2,891	Close to 1/8 sidereal day
9	58	313	24	107	43	714	63	215	1,537	Close to 1/9 sidereal day
10	57	319	13	122	38	631	74	178	1,432	Close to 1/10 sidereal day
11	25	102	12	26	12	255	30	78	540	Close to 1/11 sidereal day
12	27	108	10	33	10	242	23	65	518	Close to 1/12 sidereal day
13	11	62	4	27	7	113	20	38	282	Close to 1/13 sidereal day
14	1	33	5	14	4	82	2	13	154	Close to 1/14 sidereal day
15	1	14	1	5	4	44	1	14	84	Close to 1/15 sidereal day
16	0	34	0	19	5	70	15	10	153	Close to 1/16 sidereal day
20	152	136	11	65	18	414	34	41	871	Close to n x 1d (n>1)
31	49	52	9	86	7	122	6	20	351	Between 177800 - 182000 sec (~49h - 51h)
32	31	52	2	41	13	143	19	17	318	Between 278600 - 285100 sec (~77h - 79h)
33	106	134	12	157	32	356	19	62	878	Between 380000 - 407400 sec (~105h - ~113h)
87	182	377	43	385	71	996	67	95	2,216	Close to 1/4 month
88	265	413	33	264	68	998	60	120	2,221	Close to 1/3 month
89	668	775	44	243	76	2,188	64	129	4,187	Close to 1/2 month
91	1,088	1,028	76	264	362	2,906	378	429	6,531	Close to 1 month
92	112	30	3	6	10	134	3	5	303	Close to 2 months
93	0	1	0	0	0	1	0	0	2	Close to 3 months
Total	42,165	86,196	9,283	76,701	16,485	217,255	29,464	39,886	517,435	

Table 5-14: Summary of number of objects with conf. index 4 (by class)

Table 5-15 shows the number of objects obtained for each class that have a confidence index of 1, 2 or 4. It is included here for completeness as it is envisaged that if a researcher is looking for a class of objects to research, they will initially search for objects with a confidence index of 1, 2 or 4 as this will provide a large database for analysis. This table indicates the number of objects they would have to review (i.e. 1,136,566 objects).

	Confidence 1, 2 and 4									
pFlag	CEP	DSCT	EA	EB	EW	RM	RRAB	RRC	Total	Period location (from SuperWASP)
0	10,360	20,844	13,491	14,443	4,503	61,321	7,891	11,911	144,764	Good periods
1	63,196	71,066	34,347	52,932	10,189	268,560	24,213	22,087	546,590	Between 0.9d and 1.3d
2	2,011	20,659	5,957	11,837	1,732	44,808	10,325	6,722	104,051	Close to 1/2 sidereal day
3	2,609	25,919	9,735	14,392	2,264	58,013	11,547	12,324	136,803	Close to 1/3 sidereal day
4	1,499	14,952	5,048	6,051	1,168	32,036	6,033	6,307	73,094	Close to 1/4 sidereal day
5	793	7,442	2,044	2,603	527	15,887	3,156	3,182	35,634	Close to 1/5 sidereal day
6	515	5,587	1,057	1,519	311	11,244	1,719	2,598	24,550	Close to 1/6 sidereal day
7	359	4,134	691	932	188	8,062	997	1,766	17,129	Close to 1/7 sidereal day
8	157	2,407	282	348	98	4,144	523	1,079	9,038	Close to 1/8 sidereal day
9	84	1,548	129	150	57	2,406	246	688	5,308	Close to 1/9 sidereal day
10	91	1,382	130	183	48	2,003	224	513	4,574	Close to 1/10 sidereal day
11	34	670	48	41	13	702	67	218	1,793	Close to 1/11 sidereal day
12	31	606	26	44	14	758	60	213	1,752	Close to 1/12 sidereal day
13	16	350	14	35	8	355	26	131	935	Close to 1/13 sidereal day
14	8	182	15	20	4	226	8	52	515	Close to 1/14 sidereal day
15	2	84	2	5	4	121	4	34	256	Close to 1/15 sidereal day
16	3	147	1	26	6	200	19	44	446	Close to 1/16 sidereal day
20	353	143	132	71	22	753	42	43	1,559	Close to n x 1d (n>1)
31	97	57	226	105	7	284	9	20	805	Between 177800 - 182000 sec (~49h - 51h)
32	74	55	95	54	17	308	39	18	660	Between 278600 - 285100 sec (~77h - 79h)
33	213	144	147	188	38	757	26	64	1,577	Between 380000 - 407400 sec (~105h - ~113h)
87	447	423	317	426	78	2,196	82	100	4,069	Close to 1/4 month
88	516	442	329	291	76	1,726	74	123	3,577	Close to 1/3 month
89	1,060	795	391	261	80	3,226	79	132	6,024	Close to 1/2 month
91	2,321	1,104	976	298	446	4,420	525	441	10,531	Close to 1 month
92	186	30	21	7	12	265	4	5	530	Close to 2 months
93	0	1	0	0	0	1	0	0	2	Close to 3 months
Total	87,035	181,173	75,651	107,262	21,910	524,782	67,938	70,815	1,136,566	

Table 5-15: Summary of number of objects with conf. index 1, 2 and 4 (by class)

5.7. Problems encountered along the way

Regarding the effectiveness of the neural networks, it should be remembered that the objective of this research was to provide a fast method of assigning a preliminary classification to all the periodic objects in the SuperWASP archive. It is not possible to assign a final classification as SuperWASP only provides observations in visible light and this is not sufficient to determine the actual class. The effectiveness of the NNs is therefore limited for the following reasons:

5.7.1 Similarity of binned phase-folded light-curves

The main component of the NNs that aids differentiation between classes is the shape of the binned phase-folded light-curve. Unfortunately, certain classes have the same light-curve shape e.g. DSCT, RRC, CEP and EW at half or double period. An attempt was made to differentiate between these using the 'period-bin' parameter, but this was not successful because the period bins were not fine-tuned to the period range of each object. This area is one of the improvements that will be addressed in the future and is discussed in Chapter 10. In the case of misclassification of DSCT, RRC and CEP, this is not really a problem as they are identified as a class that must be confirmed using other methods e.g. spectral analysis. Attempts at separating these objects are discussed in Chapter 8.

Another difficulty is the similarity between EB and EW light-curves, i.e. they are only different in the depth of the secondary eclipse. These will be reviewed in Chapter 7 to try to establish a 'hard-limit' for the secondary eclipse to aid future classification.

5.7.2 Classification is highly dependent on the period

As indicated above with the eclipsing binary EW, if the period is half or double the true period value, it looks similar to an RRC or DSCT and could be classified as such. It is necessary to ensure that the correct period is selected for each object, but this is complex as the method that SuperWASP uses to calculate the period also identifies harmonics of the true period. This is discussed further in Chapter 8.

5.7.3 Large scatter in light-curves

Some of the objects classified by the NNs were shown to have large scatter in the observations due to the objects being faint. This causes a problem when the phase-folded light-curve is converted into its binned counterpart. This problem is discussed further in Chapter 7 and Chapter 8.

5.7.4 Very low amplitude light-curves

As with large-scatter light-curves, small amplitude light-curves can also lead to misclassification when the binned phase-folded light-curve is expanded in the y-axis. These are discussed further in Chapter 7 and Chapter 8.

5.7.5 SuperWASP period ranges (PFlag)

As indicated in Table 5-11, the majority of objects are from periods with PFlag > 0. These are periods that may be generated due to the rotation of the Earth rather than the period of the object. The only way to check these is to look at the original phase-folded light-curve. This is examined in Chapter 7 and Chapter 8 for a selection of eclipsing and pulsating objects respectively.

5.7.6 Period 'clumping'

Finally, plotting the periods of classified objects onto a scatter plot shows that there is some 'clumping' of periods. These are unexpected and are unlikely to be true periods. Again, these are further discussed in Chapter 7 and Chapter 8.

5.8. Chapter summary

This chapter described the creation of the 'LC Analyser classifier' application. It described in detail the creation of the 'LC Analyser classifier' application, comprising the complete documentation, including User requirements, Functional requirements, Design specification and Validation protocol, following the GAMP5 (2008) methodology and the application implementation into two different operating systems (Microsoft Vista and Linux). It also described the processing of all the periodic objects in the SuperWASP archive and discussed the problems identified along the way. The next chapter assesses the quality of the results for the eclipsing binary (EA, EB and EW) and pulsating stars (DSCT and RRAB).

---------- o ----------

Chapter 6 Interpretation of Neural Network Results

In Chapter 5, the 'LC Analyser classifier' application processed all the periodic variables in the SuperWASP archive and gave preliminary classifications to 1,136,566 unique objects using a confidence index of 1, 2 or 4 (see Table 5-15 in Chapter 5). In this chapter, the quality of the results for the eclipsing binary (EA, EB and EW) and pulsating stars (DSCT and RRAB) is assessed before using the results in Chapter 7 and Chapter 8. The remaining classes will not be assessed further in this research.

6.1. Analysis of Neural Network output

In order to confirm the quality of the NN results, the output files NNData.txt (Table 5-9 in Chapter 5) and Stats.txt (Table 5-5 in Chapter 5) were obtained from Leicester University where the SuperWASP objects were processed through the 'LC Analyser classifier' application. The required data was then extracted for each eclipsing and pulsating object from the files in order to assess the light-curves. The following sections describe the process used and discuss the results:

6.1.1 Creating binned phase-folded light-curves

Remember that the main run on the SuperWASP archive at Leicester University used a version of the application that created virtual binned phase-folded light-curves in order to obtain the parameters for the NNs. It was not possible to create the full phase-folded light-curves in the main run as graphics was not supported on the server. It was also not possible to 'manually' create light-curves for each of the eclipsing binaries and pulsating stars in the 3,913,807 duplicate objects due to the large numbers of objects as shown in Table 5-11 in Chapter 5. Therefore, a subset of objects was taken to investigate as shown in Table 6-1.

The number of unique objects to be assessed was taken from Table 5-15 in Chapter 5 (i.e. objects that have a classification confidence index of 1, 2 or 4), but the number of graphs

created was actually more than this as all duplicate results had to be graphed for each object in order to identify the best period. However, as there were so many DSCT objects, the number was limited to all confidence index 1 objects plus only the PFlag=0 objects for confidence index 2 and 4, hence the reduced number of graphs shown for DSCT in Table 6-1.

Class	Unique objects Conf. 1, 2, 4	Graphs created Conf. 1, 2, 4
DSCT	181,173	64,257
EA	75,651	90,757
EB	107,262	112,496
EW	21,910	23,088
RRAB	67,938	75,941
Total	453,934	366,539

Table 6-1: Number of objects graphed

To help produce the 366,539 graphs, an application was created in Microsoft Visual C#.Net called 'LCAGraphPlotter'. This application read in the x-axis and y-axis values for each object in the 'NNData.txt' files and automatically generated binned phase-folded light-curves for each object (see Figure 6-1 for an example of each class).

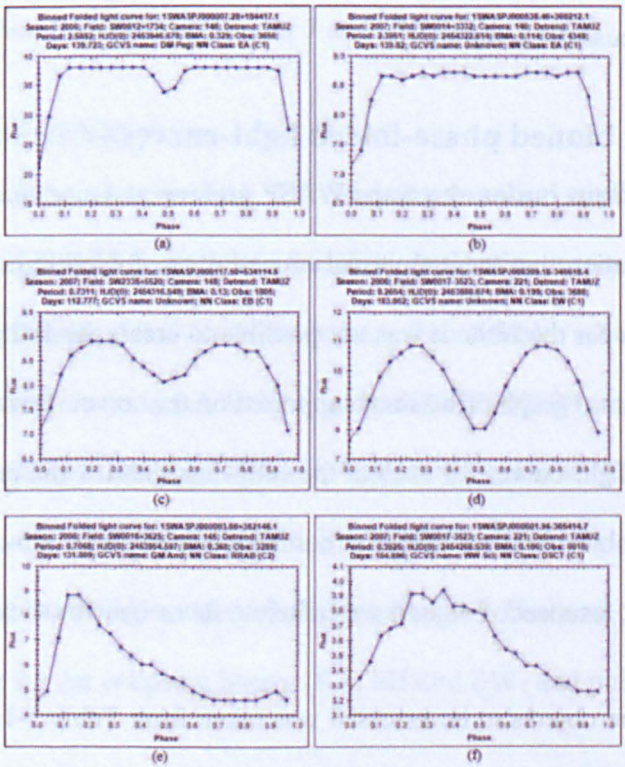

Figure 6-1: Example binned phase-folded light-curves for NN classes
(a) EA Double-eclipse; (b) EA Single-eclipse; (c) EB; (d) EW; (e) RRAB; (f) DSCT

The lines connecting the points on the graphs were displayed only to help visualise the object class. They could not be used to extrapolate information between points as the graphs contain discrete data.

During creation of the graphs, the application assigned filenames to them in the following format to allow processing of the duplicate objects in sections 6.1.3 and 6.1.4:

Object name_X_M.BMP
Where X starts at 1 and increments for each graph created for the 'duplicate' object name
e.g. objects with three periods would have the filenames:
1SWASPJ000003.93+313733.5_1M.BMP
1SWASPJ000003.93+313733.5_2M.BMP
1SWASPJ000003.93+313733.5_3M.BMP

The completed program can be found on the supplementary DVD in the following location:

Supplementary data	
Application files	X:\Chapter06\LCAGraphPlotter2

Where X is DVD-1 in the DVD-drive

6.1.2 Reassess the RRAB/DSCT objects

With the eclipsing binary objects, it was relatively simple to differentiate between EA, EB and EW classes due to the marked differences in the curve shape, but when it came to differentiating RRAB and DSCT classes, it was more difficult as their shapes were very similar (see Figure 6-1e and Figure 6-1f above). These classes could however be separated by the period as RRABs have a period range of 0.3 - 1.2 days and DSCT have a range of 0.01 - 0.2 days. At this point, it was realised that the period bin ranges for the NN classification was not sufficient to detect the differences in all cases, i.e. Table 6-2 shows that the period bin for all DSCT objects would be bin 1, but the period bin for RRAB would be 1 for periods up to 1.0 day and bin 2 for periods 1.0 to 1.2 days. This would lead to NN misclassification in some cases.

Period bin	Period range (days)
1	0.0000 to 1.0000
2	1.0001 to 10.0000
3	10.0001 to 50.0000
4	50.0001 to 100.0000
5	100.0001 to 500.0000
6	500.0001 to 999999.0

Table 6-2: Period bin ranges

One improvement that will be made to the application in the future is to re-train the NNs on a more appropriate period bin set once the period ranges for all SuperWASP objects (see Chapter 7 and Chapter 8) have been obtained. To overcome this issue, the confidence index levels used were re-assessed to identify the RRAB and DSCT objects. For instance, the NN classifications for RRAB and DSCT in Chapter 5 were based on confidence index 1, 2 or 4 which meant that the three NNs gave classes (in any NN permutation) as shown in Table 6-3:

Class	Confidence	NN1	NN2	NN3
RRAB	1	RRAB	RRAB	RRAB
	2	RRAB	RRAB	No class
	4	RRAB	No class	No class
DSCT	1	DSCT	DSCT	DSCT
	2	DSCT	DSCT	No class
	4	DSCT	No class	No class

Table 6-3: Key to confidence index 1, 2 and 4 for Pulsating stars

In order to overcome the underperformance, classifications were added for the additional confidence index shown in Table 6-4 (and their NN permutations) due to the overlap of period bin in the NNs:

Class	Confidence	NN1	NN2	NN3
RRAB	7	RRAB	RRAB	DSCT
	7	RRAB	DSCT	DSCT

Table 6-4: Additional Pulsating star confidence index levels to review

The number of extra RRAB and DSCT objects proved overwhelming for this research (53,009 RRAB and 178,647 DSCT), so the assessment was limited to all RRABs and DSCTs of PFlag=0 and all confidence index 1 objects across all PFlags. Table 6-1 above reflects this change in assessment, and indicates the number of DSCT assessed in this

research and included in the 'personal' catalogue. When the full catalogue becomes available, all DSCT objects will be included and their confidence index levels included in the catalogue.

6.1.3 Remove 'Within' PFlag duplicate objects

As already mentioned, the binned phase-folded light-curves created in section 6.1.1 contained many duplicate objects due to the same object being processed with different periods, seasons, fields and cameras. It was therefore necessary to identify the 'best' binned phase-folded light-curve for each object in order to obtain the best period. To achieve this, two further Microsoft Visual C#.Net applications were created called 'DuplicateChecker' and 'DuplicateAnalyser' to help process the large number of objects. The 'DuplicateChecker' application filtered the binned phase-folded light-curve files created in section 6.1.1 into a 'Duplicates' folder and a 'Unique' folder on the computer, depending on their filenames. The application obtained all files in the target directory for a given 'object_name' and when there was more than one file, they were all automatically moved to the 'Duplicates' folder, otherwise, they were automatically moved to a folder called 'Unique'. The 'DuplicateAnalyser' application was then used to display the set of binned phase-folded light-curves of each object in turn in the 'Duplicates' folder side-by-side so that the best light-curve could be identified (see Appendix 13). When the 'best' light-curve was selected in the application, it was automatically moved (i.e. added) to the 'Unique' folder while the others were moved to a new 'Duplicates' folder. The 'best' light-curve in this case was the one that looked more like a typical object class than the others. If more than one looked like a typical object class, then the light-curve with the shortest phase-length (Dworetsky, 1983) was selected. At the end of this process, the objects in the 'Unique' folder became the set for further analysis. Table 6-5 indicates the number of within-PFlag duplicate objects removed.

The completed programs can be found on the supplementary DVD in the following location:

Supplementary data - Application files	
DuplicateChecker	X:\Chapter06\DuplicateChecker v2
DuplicateAnalyser	X:\Chapter06\DuplicateAnalyser

Where X is DVD-1 in the DVD-drive

Class	Graphs created Conf. 1, 2, 4	Duplicates removed	Remaining objects
DSCT	64,257	652	63,605
EA	90,757	10,134	80,623
EB	112,496	2,339	110,157
EW	23,088	694	22,394
RRAB	75,941	5,164	70,777
Total	366,539	18,983	347,556

Table 6-5: Number of within-PFlag duplicate objects removed

6.1.4 Remove 'Between' PFlag duplicate objects

The duplicate objects in section 6.1.3 were duplicates 'within-PFlag' because the SuperWASP archive objects were processed by the 'LC Analyser classifier' application one PFlag at a time, starting with PFlag 0 and then incrementing on up to PFlag 93. In this section, the duplicate objects were identified between PFlags i.e. where the same object had large differences in the period e.g. object 1SWASPJ000413.16+494215.3 showed an EA class at period 0.6363 (PFlag=0), but an EW class at period 1.2753 (PFlag=1). The duplicates were identified in the same manner as the within-PFlag duplicates i.e. using the 'DuplicateChecker' and 'DuplicateAnalyser' applications. A total of 1,491 between-PFlag duplicate objects were removed.

6.1.5 Remove Duplicate objects by physical location

After removal of duplicate objects within-PFlag and between-PFlag, the duplicate objects that had a different SuperWASP identifier were removed. This situation can happen when an object is viewed from a different field or different camera and the SuperWASP pipeline does not recognise it as an existing object in the database. These duplicate objects were

removed by cross-matching the Right Ascension (RA) and Declination (Dec) for each object against all other objects as follows:

- All EA, EB, EW, DSCT and RRAB objects were placed into an Excel spreadsheet and ordered by declination.
- Objects were identified that were within +/- 1 arcmin of each other. This was achieved by looking at other objects within (dec+1 arcmin) and (dec-1 arcmin). Note that +/- 1 arcmin was selected for the radius as any objects outside this range would be guaranteed unique due to the accuracy of the SuperWASP cameras (Pollacco et al. 2006). However, when manually assessing the duplicates of an object within this range, any objects that gave a non-expected class were placed back into the dataset.
- The great circle separation distance was calculated for each identified pairs of objects as shown in Equation 6-1:

$$d = arccos\big((\sin dec1 \times \sin dec2) + (\cos dec1 \times \cos dec2 \times \cos(ra1 - ra2))\big)$$

Equation 6-1: Great circle separation distance between two locations ra1/dec1 and ra2/dec2

- When the great circle separation was less than 1 arcmin, all objects within the 1 arcmin were flagged as duplicates.

The 'best' object/period was selected for each duplicate and added to the unique object folder. A total of 3,091 duplicate objects were removed.

After removing all duplicates as indicated in the above sections, the outcome of this analysis produced 342,974 unique objects that required manual review of the binned phase-folded light-curves (i.e. 366,539 – 18,983 within-PFlag duplicates – 1,491 between-PFlag duplicates – 3,091 positional-duplicates).

6.1.6 Manual review of binned phase-folded light-curves

In order to assess the effectiveness of the NNs for classifying these 342,974 objects, all the binned phase-folded light-curves were manually reviewed. During the review, the EAs were split into double-eclipse and single-eclipse categories. Table 6-6 shows the number of good and unsuitable objects obtained for the eclipsing binaries, while Table 6-7 shows the same for the pulsating stars. The term 'Unsuitable' in the tables indicates that the phase-folded light-curve did not confirm the classification provided by the 'LC Analyser classifier' application.

Class	Unique	Good	Unsuitable
EA (Double eclipse)	73,267	4,894	47,695
EA (Single eclipse)		20,678	
EB	108,996	6,431	102,565
EW	22,011	3,089	18,922
All eclipsing	204,274	35,092	169,182

Table 6-6: Number of confirmed eclipsing binaries using binned phase-folded light-curves

Class	Unique	Good	Unsuitable
DSCT	63,605	22,525	41,080
RRAB	68,868	9,668	59,200
All pulsating	132,473	32,193	100,280

Table 6-7: Number of confirmed pulsating stars using the binned phase-folded light-curves

A total of 67,285 objects were confirmed as having a 'good' classification. There was an obvious concern in these results regarding the number of objects that were unsuitable (269,462). There were two main reasons for the 'unsuitable' objects. Firstly, the periods provided for the objects by SuperWASP were not always ideal (see section 6.2.1) and secondly, systemic errors in the SuperWASP pipeline gave values that mimicked the EA light-curve (see section 6.2.2).

6.2. Investigation of misclassified results

To investigate why the NNs classified the 269,462 objects as definite classes when they were actually unsuitable, a number of checks were performed as indicated in this section:

6.2.1 PFlag review

First, the number of objects for each PFlag (i.e. period range) were reviewed for each confidence index for each class, to see if a particular period range had more failures than others (e.g. due to harmonics of the actual period). Figure 6-2, Figure 6-3 and Figure 6-4 show the results of the analysis for EA confidence index 1, 2 and 4 respectively. The red bars in each graph indicate the unsuitable objects and as you can see, they are spread across the PFlag range.

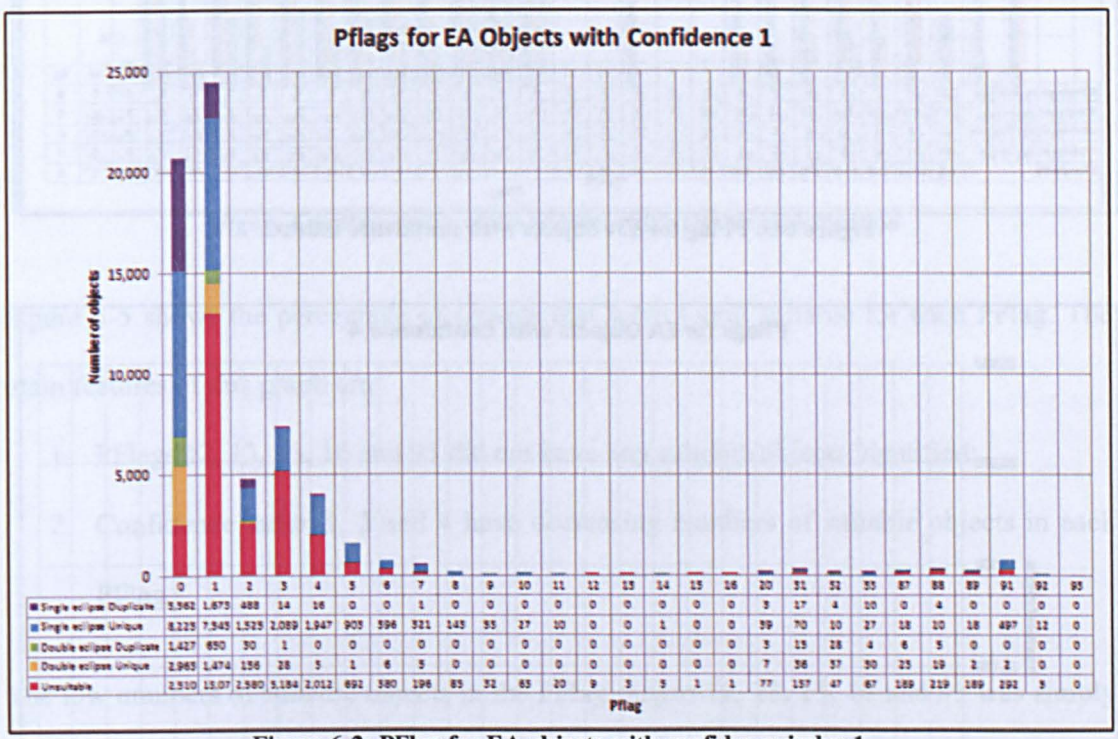

PFlag	0	1	2	3	4	5	6	7	8	9	10	11	12	13	14	15	16	20	31	51	55	87	88	89	91	92	95
Single eclipse Duplicate	5,562	1,673	488	14	16	0	0	1	0	0	0	0	0	0	0	0	0	3	17	4	10	0	4	0	0	0	0
Single eclipse Unique	8,225	7,343	1,525	2,089	1,947	905	396	321	145	55	27	10	0	0	1	0	0	39	70	10	27	18	10	18	497	12	0
Double eclipse Duplicate	1,427	650	30	1	0	0	0	0	0	0	0	0	0	0	0	0	0	3	13	28	4	6	5	0	0	0	0
Double eclipse Unique	2,965	1,474	156	28	5	1	6	5	0	0	0	0	0	0	0	0	0	7	36	37	30	25	19	2	2	0	0
Unsuitable	2,510	15,07	2,580	5,184	2,012	692	380	196	83	32	63	20	9	3	5	1	1	77	157	47	67	189	219	189	291	3	0

Figure 6-2: PFlag for EA objects with confidence index 1

Although PFlag 1 appears to have a large number of unsuitable objects in each graph, it shows the same (or better) percentage as the other PFlags that are greater than 1 (see Figure 6-6 below).

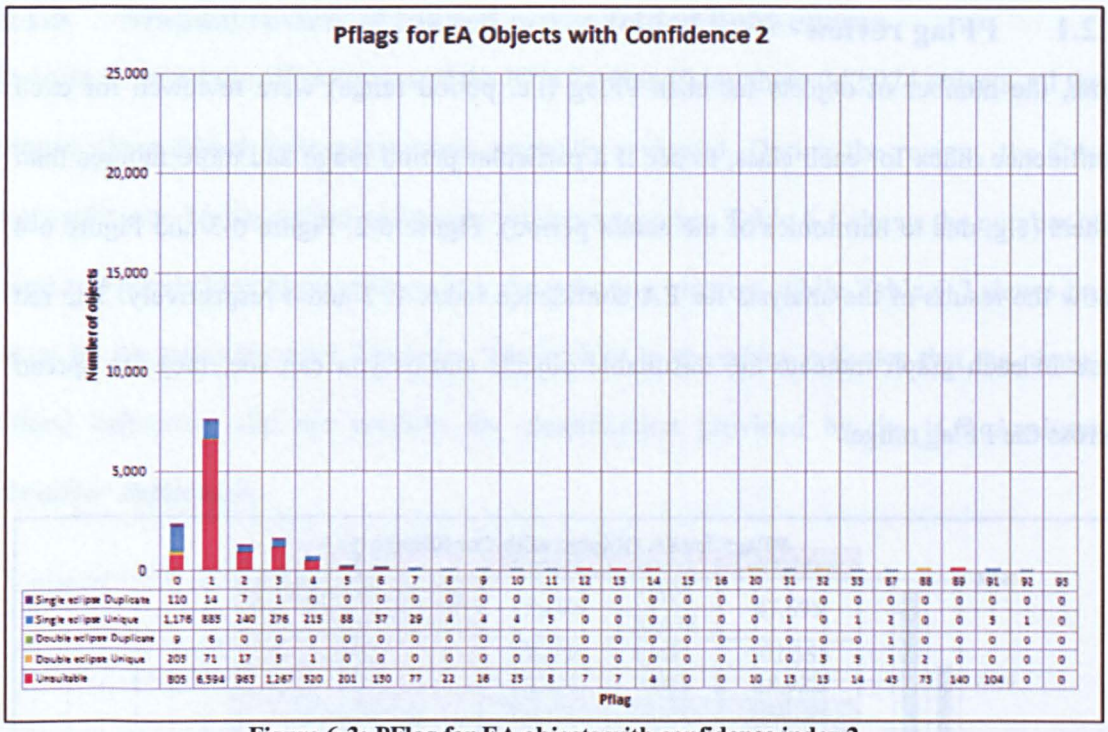

Figure 6-3: PFlag for EA objects with confidence index 2

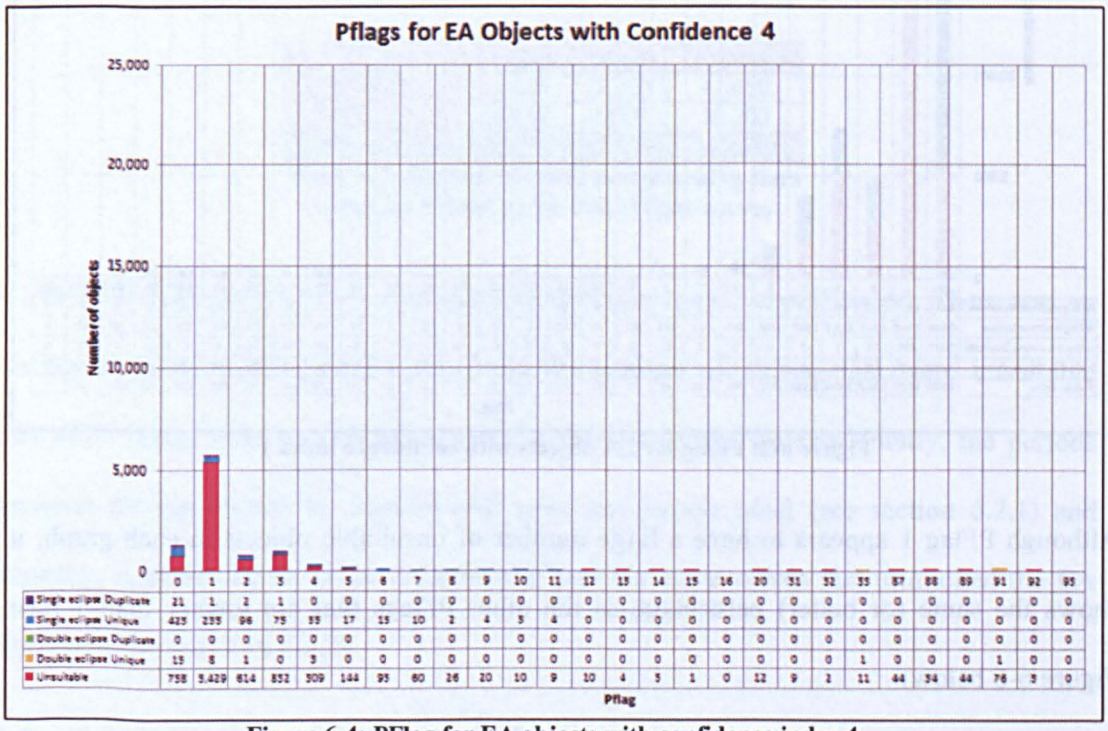

Figure 6-4: PFlag for EA objects with confidence index 4

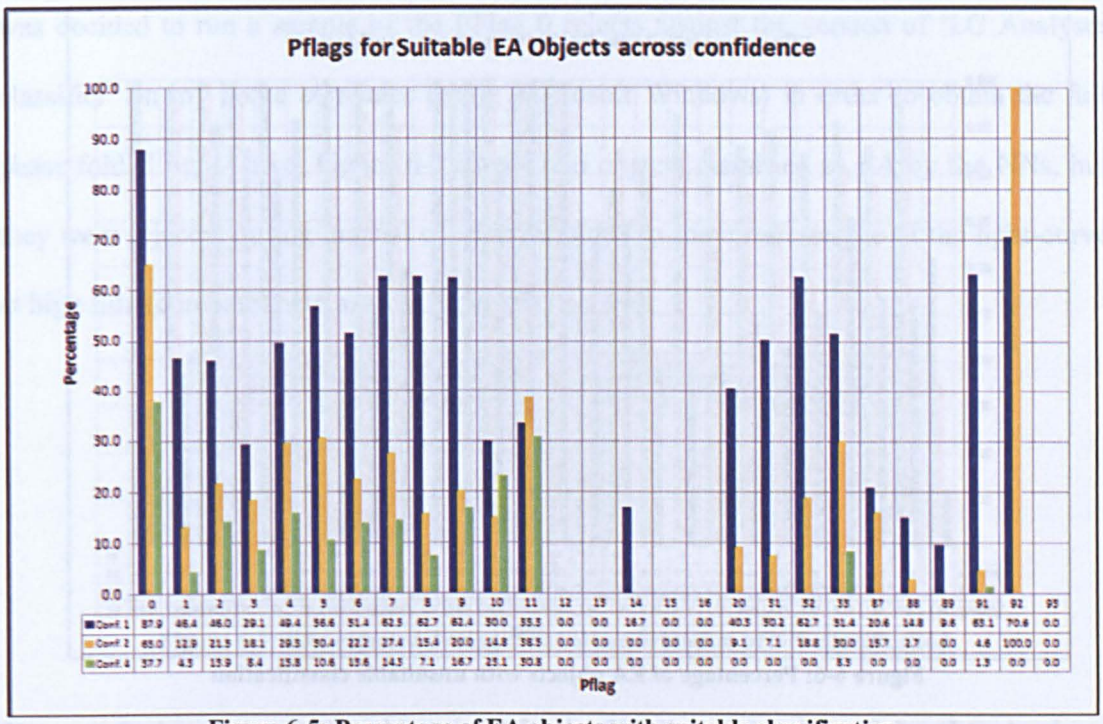

Figure 6-5: Percentage of EA objects with suitable classification

Figure 6-5 shows the percentage of objects that were found suitable for each PFlag. The main features of this graph are:

1. PFlags 12, 13, 15, 16 and 93 did not have any suitable objects identified;
2. Confidence index 1, 2 and 4 have decreasing numbers of suitable objects in each PFlag.

The low numbers of suitable objects in the PFlag ranges 12, 13, 15, 16 and 93 was simply due to the fact that not many objects were identified in these ranges in the SuperWASP archive. The significance of the decreasing numbers in the confidence index level supports the original expectation i.e. that as classes with confidence index 1 have the same class in all three NNs, confidence index 2 has the same class in two NNs, and confidence index 4 has the class in only 1 NN, then more significant classifications are going to be obtained in that order.

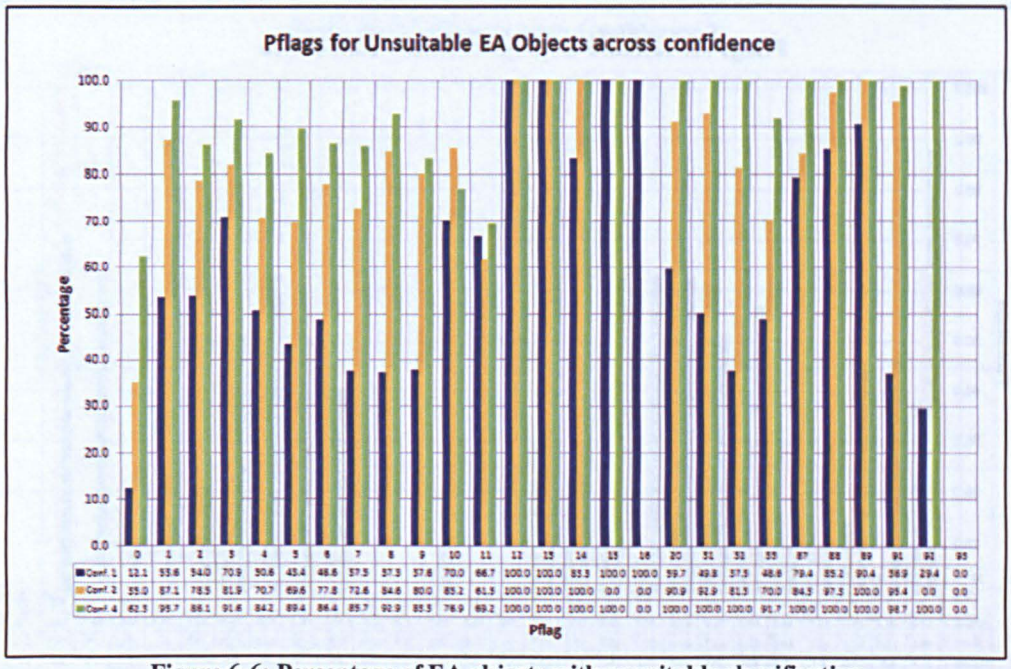

Figure 6-6: Percentage of EA objects with unsuitable classification

Figure 6-6 shows the percentage of objects that were found to be unsuitable. Again, it shows that the unsuitable objects appear in all PFlags, but in these cases, there appear to be a lot more in confidence index 2 and 4 than in the confidence index 1 objects. This confirms the observation in Figure 6-5.

Appendix 14 , Appendix 15 and Appendix 16 show similar graphs to the EA graphs above for the EB, EW and RRAB classes respectively. DSCT objects were not included in this analysis as the PFlag information was not available for the duplicate and unsuitable objects at the time. The results confirm the observations made in the EA class above, i.e. the PFlag ranges do not contribute to the incorrect classifications from the NNs.

6.2.2 Review instances of unsuitable light-curves

As mentioned above, the classifications given by the NNs were manually confirmed using the 'binned' phase-folded light-curves because that is what the NNs used for the classification and also they were the only data available from the main archive run at Leicester University. Due to the large number of objects that were manually rejected, it

was decided to run a sample of the PFlag 0 rejects against the version of 'LC Analyser classifier' on my home computer (using Microsoft Windows) in order to obtain the full phase-folded light-curve. Figure 6-7 shows two objects classified as EA by the NNs, but they were rejected during manual confirmation due to the erratic nature of the light-curve at high flux (compare them against Figure 6-1 above).

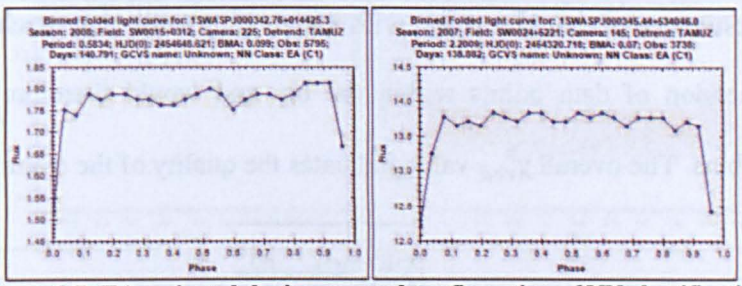

Figure 6-7: EAs rejected during manual confirmation of NN classification

Figure 6-8 shows these two objects run in the Windows' version of the 'LC Analyser classifier' application. The full phase-folded light-curve clearly shows them as single-eclipse EAs. Removing them from the dataset was therefore inappropriate. As there were probably a lot more of these in the 47,689 unsuitable EA objects and similar numbers in the other classes, a number of statistical methods were tried to distinguish between the good and rejected binned phase-folded light-curves. These included the methods in the following sections.

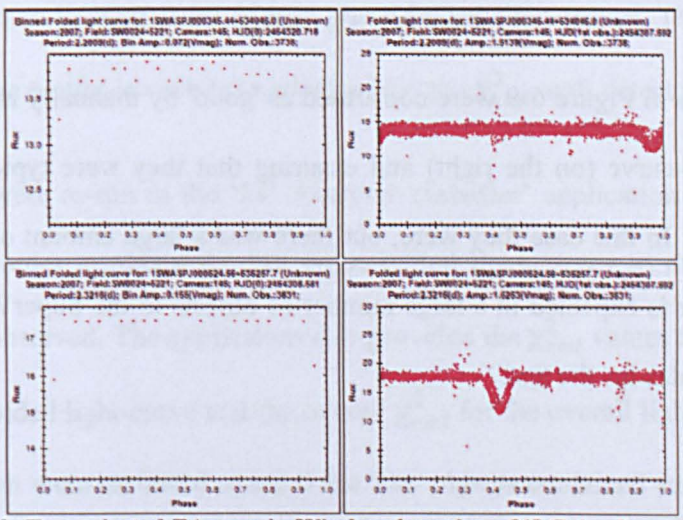

Figure 6-8: Two rejected EAs run in Windows' version of 'LC Analyser classifier'. Top pair is from Figure 6-7 (a) and Bottom pair is from Figure 6-7 (b)

6.2.3 Reduced chi-squared Test

This looked at identifying poor binned phase-folded light-curves by using Equation 6-2 to calculate the reduced chi-squared value (χ^2_{red}) for each of the 25 x-axis bins in the phase-folded light-curve plus an overall χ^2_{red} value. The hypothesis here was that bins with a low χ^2_{red} value (i.e. close to 1) have a low dispersion of data points within the bin and therefore would be good estimates of that bin. A bin with a high χ^2_{red} value (i.e. much more than 1) has a high dispersion of data points within the bin and would therefore indicate bad estimates of the bins. The overall χ^2_{red} value indicates the quality of the overall light-curve.

$$\chi^2_{red} = \frac{\sqrt{\sum_{i=1}^{n} \frac{(X_i - \bar{x})^2}{s_i^2}}}{(n-1)}$$

Equation 6-2: Calculation of reduced chi-square value

Where i = observation number in bin; n = max observations in the bin;
$\bar{x}$ = mean flux of bin; X_i = flux value in bin; s_i = standard deviation of observations in the bin

Six objects were selected to test this method: Three 'Good' class objects (Figure 6-9) and three 'Bad' class objects (Figure 6-10). The classifications obtained from the NNs were calculated on the binned phase-folded light-curves on the left hand side of each image. The full phase-folded light-curves on the right-hand side were used as a comparison to confirm the NN results

The 'good' images in Figure 6-9 were confirmed as 'good' by manually reviewing the full phase-folded light-curve (on the right) and ensuring that they were typical for the class given by the NNs. In this case they were, but there was a large amount of scatter in each bin. As this scatter is expected in a large number of objects in the SuperWASP data, they were good candidates for the test.

.

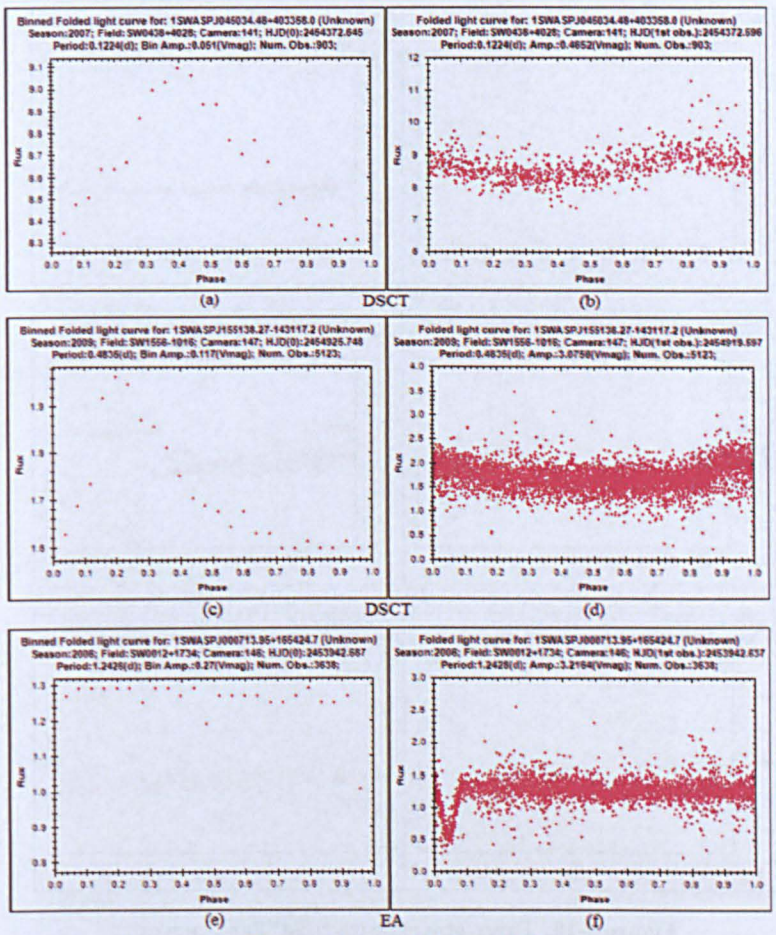

Figure 6-9: Three objects with 'good' light-curves.
Left images = Binned phase diagram; Right images = Full phase diagram

Looking at the full phase-folded light-curves for the 'bad' objects in Figure 6-10 shows that they did not have a variability class, but it was easy to see why the NNs classified them as DSCT when looking at the binned phase-folded light-curves. This was obviously caused by the large scatter in each bin and hopefully the χ^2_{red} will detect this.

The six objects were re-run in the 'LC Analyser classifier' application on the Microsoft Windows PC in order to obtain the full phase-folded light-curves so that the amount of scatter could be observed. The application also provided the χ^2_{red} values for each bin in the 'binned' phase-folded light-curve and the overall χ^2_{red} for the overall light-curve. The χ^2_{red} values for each bin were reviewed to see if the 'bad' objects contained values much greater than 1 and if the 'good' objects contained values around 1.

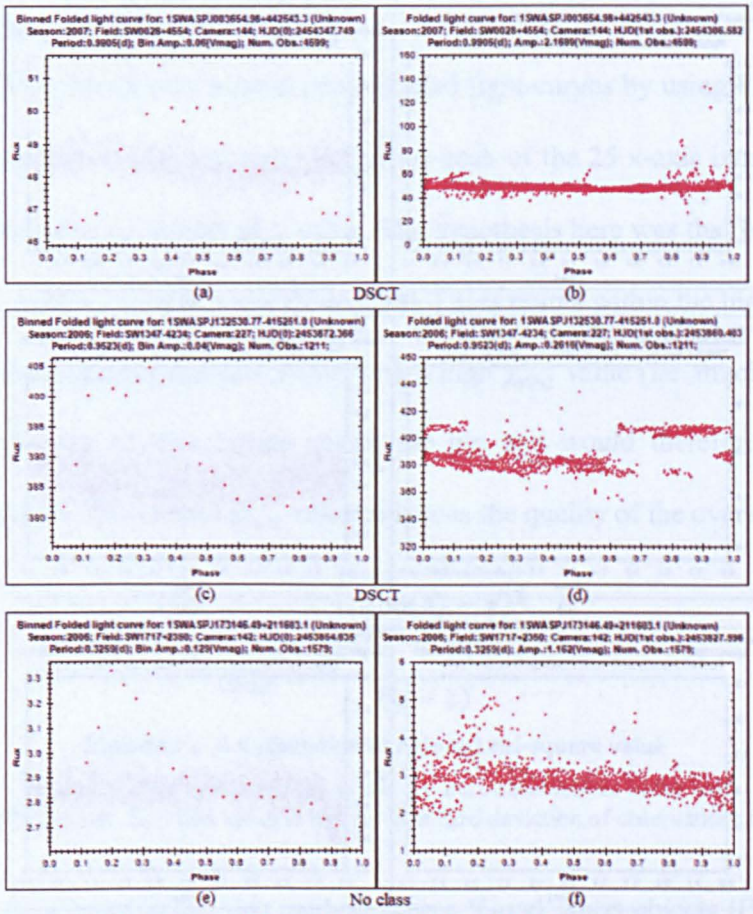

Figure 6-10: Three objects with 'bad' light-curves.
Left images = Binned phase diagram; Right images = Full phase diagram

The results showed that the χ^2_{red} values could not differentiate the 'good' objects from the 'bad' objects as proposed. However, if the χ^2_{red} test was implemented by comparing the χ^2_{red} value for each bin against a threshold value (in this case, the largest χ^2_{red} value from the bins in the 'good' objects), then it appeared to work well. For instance, the maximum χ^2_{red} value of the good objects in Table 6-8 was 0.2279. Comparing the χ^2_{red} value for each bin of the 'bad' objects against 0.2279 showed many values higher than this (all the red background cells). These indicated that they were bad objects. The challenge then, is to identify this threshold value to use. This is expected to be the RMS of the full-curve χ^2_{red} values of a large number of known 'good' objects.

LC Analyser Reduced Chi-Sqr method						
Bin	Good 1	Good 2	Good 3	Bad 1	Bad 2	Bad 3
1	0.1655	0.0726	0.2106	0.2439	1.2741	0.4279
2	0.1800	0.0716	0.2100	0.2973	1.6134	0.4009
3	0.1531	0.0904	0.0946	0.5263	1.1374	0.3903
4	0.1498	0.0771	0.1011	0.4408	1.0375	0.4213
5	0.1516	0.0769	0.0858	0.6830	0.7310	0.5226
6	0.1454	0.0726	0.0906	0.5314	0.6018	0.5233
7	0.1157	0.0790	0.0814	0.4997	0.5291	0.2371
8	0.1842	0.0742	0.0723	0.4242	0.5735	0.1674
9	0.1704	0.0770	0.0587	0.5431	0.4999	0.1717
10	0.1610	0.0710	0.0759	0.3627	0.5087	0.1409
11	0.1879	0.0787	0.0691	0.3080	0.3378	0.1665
12	0.1370	0.0677	0.0661	0.2306	0.7230	0.1726
13	0.1813	0.0652	0.0943	0.1889	0.5139	0.1487
14	0.2177	0.0705	0.0738	0.1944	0.5378	0.1238
15	0.1529	0.0694	0.0761	0.1277	0.4075	0.1708
16	0.1739	0.0702	0.0687	0.1051	1.6235	0.1637
17	0.2279	0.0761	0.0632	0.1343	3.2324	0.1224
18	0.1943	0.0729	0.0785	0.1593	3.0795	0.1796
19	0.2144	0.0774	0.0814	0.1508	1.0787	0.1335
20	0.1938	0.0739	0.0758	0.1096	1.4910	0.1161
21	0.1223	0.0690	0.0769	0.1777	1.3154	0.1684
22	0.1611	0.0806	0.0608	0.1374	0.8926	0.1445
23	0.1456	0.0830	0.0737	0.2640	0.3281	0.1744
24	0.1875	0.0807	0.0802	0.3314	0.6411	0.2180
25	0.1600	0.0715	0.0753	0.2705	1.1314	0.3221
Max	0.2279					

Table 6-8: Summary of reduced Chi-squared test results for 6 objects

The results for each individual object can be seen on the supplementary DVD at:

Supplementary data	
Reduced Chi-sqr results	X:\Chapter06\ChiSqr_check.xlsm

Where X is DVD-1 in the DVD-drive

Testing the χ^2_{red} was performed on a very small dataset, so on completion of this research, it will be included as part of the 'LC Analyser classifier' classification method and all periodic variables in the SuperWASP archive will be re-tested.

6.2.4 Skewness

In section 6.2.3, the χ^2_{red} test was used to look at scatter across the whole of each bin in the binned phase-folded light-curves. For instance, if we create a distribution graph of the flux values for all observations in a bin, we should get a normal curve (see Figure 6-11(a)), but

it was thought that looking at the tails of the distribution (i.e. the green circles in Figure 6-11(b)) would be a more appropriate test because any scatter in the bins would be seen as observations in the tails of the normal distribution and would therefore give higher or lower values in these regions. For example, these graphs show the distribution of flux values for Bin 15 in the Good object (on left) and Bin 13 in the Bad object (on right). The Good object shows a normal distribution, while the Bad object shows a skewed distribution with outliers shown in the green circles.

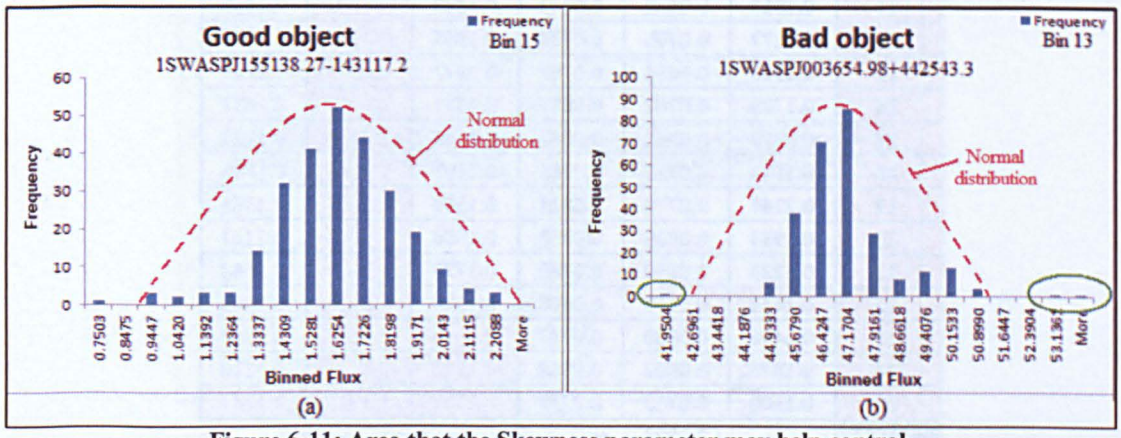

Figure 6-11: Area that the Skewness parameter may help control

The skewness parameter (G_1) as calculated in Equation 6-3 looks at the measure of asymmetry in a dataset and therefore achieves this goal. By taking an absolute value of the skewness, high values of skewness can be searched for to identify 'bad' light-curves.

$$G_1 = ABS\left(\frac{\sum_{i=1}^{n}(x_i - \bar{x})^3}{(n-1) \times s^3}\right)$$

Equation 6-3: Calculation of skewness value

Where i = observation number in bin; n = max observations in the bin;
$\bar{x}$ = mean flux of bin; x_i = flux value in bin; s = standard deviation of observations in the bin

For this study, the same six objects used in the χ^2_{red} test (section 6.2.3) were used so that three good objects and three bad objects could be compared. The results in Table 6-9 show that the skewness values could differentiate the 'good' light-curves from the 'bad' ones, but not as efficiently as the χ^2_{red} test. Note that the same method of identifying the 'bad' bins

was used, i.e. the maximum value of the good objects was 2.8302 and all the red background cells were above this value, indicating that they were bad objects.

ABS(Skewness)						
Bin	Good 1	Good 2	Good 3	Bad 1	Bad 2	Bad 3
1	0.1655	1.0557	0.3022	0.5646	0.8191	0.3167
2	1.3563	0.6825	0.2701	0.3716	1.2490	0.1547
3	0.2139	0.0256	2.7346	0.2424	1.3507	0.5415
4	0.1972	0.0984	0.2607	0.7736	1.6610	0.4919
5	0.5993	1.0090	1.4876	0.7871	0.2484	0.9125
6	0.0207	0.3631	0.1218	0.1729	1.3913	1.5698
7	0.3749	1.7630	0.2553	1.1992	1.4751	1.9599
8	0.3738	0.1032	0.7662	1.3371	0.5441	2.7306
9	0.0124	0.3033	1.0295	2.0300	0.5916	3.4317
10	0.7767	0.8119	0.2656	0.1686	0.2749	3.2034
11	1.0481	0.5050	0.3798	0.2447	0.8516	2.9238
12	0.9482	0.6186	1.3399	0.0393	3.2437	1.1584
13	1.1903	0.3836	2.8302	1.2762	5.0029	0.8517
14	1.0760	0.0069	0.1548	4.0465	1.3102	0.0676
15	0.1566	0.3003	1.2112	0.2774	3.0972	0.8134
16	0.1464	0.3681	0.0567	0.2462	0.7753	2.9337
17	0.6092	0.3743	0.1593	0.5369	0.2197	2.9286
18	2.1549	0.6583	0.4178	0.8684	1.4677	3.8975
19	1.9321	1.2774	0.1532	0.5025	0.0426	0.0265
20	1.7016	0.7417	0.6400	2.2995	2.6231	1.1704
21	2.1359	0.5982	0.6567	4.9421	2.0105	0.2359
22	1.8139	0.8126	0.1718	1.1259	3.1824	0.4091
23	0.8466	0.0706	0.7727	5.4555	0.0738	0.8527
24	0.3992	0.7521	0.8465	5.2409	1.4009	0.4425
25	0.1519	0.5239	0.3179	2.5759	0.7290	0.0332
Max	2.8302					

Table 6-9: Summary of the Skewness test results for six objects

The results for each individual object can be seen on the supplementary DVD at:

An example of the output can be seen on the supporting DVD at:

Supplementary data	
Skewness results	X:\Chapter06\Skewness_check.xlsm

Where X is DVD-1 in the DVD-drive

As with the χ^2_{red} test, it is also planned to include Skewness as part of the 'LC Analyser classifier' classification check for larger datasets and retest all periodic variable objects in the SuperWASP archive.

6.2.5 Kurtosis

Similar to Skewness, Kurtosis measures the shape of the distribution, but in this case, it measures the flatness of the tails. So, for similar reasons to skewness, an investigation was undertaken to see what happens at the tails of the distributions. The method used for calculating kurtosis in this research (Equation 6-4) provides a value of 3 for a normal distribution, but some systems like Microsoft Excel (Equation 6-5) includes a correction value in the equation so that the final kurtosis value equals 0. So for this research, values of <3 means that the tails are too thin and values > 3 means they are too fat. In this test however the comparison is made between the kurtosis of each individual bin and the kurtosis of the whole binned phase-folded light-curve, so the actual output of the equation did not make any difference and either equation could therefore be used.

$$kurtosis = \frac{\sum_{i=1}^{n}(x_i - \bar{x})^4}{n \times s^4}$$

Equation 6-4: Calculation of kurtosis using 'LC Analyser classifier'

Where i = observation number in bin; n = max observations in the bin;
$\bar{x}$ = mean flux of bin; x_i = flux value in bin; s = standard deviation of observations in the bin

$$kurtosis = \left\{\frac{n(n+1)}{(n-1)(n-2)(n-3)}\sum\left(\frac{x_i - \bar{x}}{s}\right)^4\right\} - \frac{3(n-1)^2}{(n-2)(n-3)}$$

Equation 6-5: Calculation of kurtosis value using Excel

Again, for this study, the same six objects used in the χ^2_{red} test (section 6.2.3) were used so that there were three good objects and three bad objects to compare. The results in Table 6-10 show that the kurtosis values could differentiate the 'good' light-curves from the 'bad' ones, but for two of the objects, it only flagged one of the bins as bad. This was because the same method of identifying the 'bad' bins was used as in the reduced chi-square and skewness tests, and therefore the largest value for the good objects (20.1712) was selected as the limit. This caused some of the bins in the bad objects to pass the test when they should not have (see the red background cells in Table 6-10). Like χ^2_{red} and Skewness

tests, the threshold value used to check each Kurtosis bin value against was obtained from only 3 light-curves. When implemented, the threshold will be obtained from a large dataset of 'good' light-curves. This should improve the quality of the threshold value. The Kurtosis test will also be implemented as part of the further work in Chapter 10.

Kurtosis						
Bin	Good 1	Good 2	Good 3	Bad 1	Bad 2	Bad 3
1	4.0710	5.0312	2.6617	3.0235	1.8406	2.2142
2	4.6455	3.9727	1.8180	3.6468	2.8890	2.5597
3	3.9713	4.6200	16.6360	4.1299	3.5147	3.1814
4	2.6830	2.9668	7.7820	7.8611	5.0429	2.8887
5	3.5827	7.6771	8.0255	5.3681	2.1297	2.5043
6	4.4405	4.3927	4.4015	4.6167	3.7707	3.7788
7	2.8427	9.9868	13.3368	6.7339	4.8592	6.6238
8	3.1328	3.6638	6.9828	8.6501	2.0174	11.7554
9	3.1657	3.5410	7.2430	15.0230	2.4641	18.4002
10	4.2509	7.4523	5.6989	5.2160	3.3000	14.5261
11	5.0559	4.4839	6.2042	6.2357	3.7917	16.1495
12	4.3169	3.4938	8.4859	7.4652	14.0918	4.9580
13	4.8375	6.3669	20.1712	6.1921	33.7473	3.9774
14	5.0556	4.4929	4.0236	26.6829	5.4241	3.2675
15	2.8207	4.1577	7.8672	3.7493	13.8176	3.1264
16	2.0420	4.4395	3.8355	2.8634	2.1869	13.1050
17	2.7609	3.7085	4.1569	2.4120	1.3795	18.2966
18	8.7963	4.7086	4.4195	3.4044	3.0555	21.2760
19	8.1806	7.9542	4.3516	3.0367	1.3287	2.9854
20	5.7546	4.4198	9.4422	15.5067	8.5380	5.0462
21	11.0548	5.1180	6.7825	30.9373	5.2545	3.5827
22	8.0001	7.9791	8.2734	17.3639	11.8482	2.7608
23	3.8581	4.3072	10.2667	44.3413	2.3660	3.5001
24	2.6577	4.4706	5.9910	30.6814	3.1221	2.1158
25	2.4630	5.3127	6.6316	11.0534	1.6452	1.8821
Max	20.1712					

Table 6-10: Summary of the Kurtosis test results

The results for each individual object can be seen on the supplementary DVD at:

Supplementary data	
Kurtosis results	X:\Chapter06\Kurtosis_check.xlsm

Where X is DVD-1 in the DVD-drive

6.2.6 Mean minus Median

The Mean-Median parameter was assessed as an alternative measure of skewness because it concentrates on the core of the distribution rather than the tails.

The same six objects as used in the χ^2_{red} test (section 6.2.3) were also used here so that the three good objects could be compared to the three bad objects. The results in Table 6-11 show that the mean-median values could differentiate the 'good' light-curves from the 'bad' ones, very efficiently.

Mean-Median						
Bin	Good 1	Good 2	Good 3	Bad 1	Bad 2	Bad 3
1	0.0331	0.0298	0.0412	0.6017	4.2464	0.0173
2	0.1009	0.0236	0.0507	0.3513	3.0410	0.0432
3	0.0070	0.0094	0.0095	0.6026	2.0617	0.0315
4	0.0196	0.0057	0.0267	0.1540	2.2722	0.1500
5	0.0120	0.0019	0.0284	0.0229	0.0930	0.3128
6	0.0236	0.0161	0.0122	0.1964	1.5772	0.2850
7	0.0041	0.0279	0.0047	0.0642	1.4218	0.1231
8	0.0164	0.0062	0.0081	0.0357	2.5830	0.0703
9	0.0097	0.0070	0.0113	0.0242	3.4146	0.0864
10	0.0219	0.0027	0.0063	0.1281	0.0485	0.0465
11	0.0382	0.0061	0.0036	0.2466	0.2727	0.0544
12	0.0128	0.0217	0.0083	0.2069	1.0038	0.0261
13	0.0601	0.0009	0.0164	0.2221	0.1196	0.0261
14	0.0326	0.0140	0.0037	0.4458	1.1177	0.0141
15	0.0009	0.0002	0.0147	0.0407	0.6228	0.0284
16	0.0085	0.0137	0.0010	0.0734	6.0004	0.0806
17	0.0695	0.0125	0.0023	0.2731	0.4799	0.0239
18	0.0471	0.0185	0.0031	0.3512	5.5967	0.0405
19	0.0874	0.0263	0.0172	0.0832	0.4615	0.0010
20	0.1329	0.0181	0.0012	0.1925	1.5899	0.0030
21	0.0158	0.0020	0.0030	1.3034	3.4421	0.0255
22	0.0282	0.0164	0.0101	0.3520	1.6369	0.0163
23	0.0188	0.0137	0.0003	1.3889	0.3713	0.0404
24	0.0059	0.0294	0.0162	2.9956	2.9256	0.0627
25	0.0100	0.0243	0.0002	0.5018	4.5742	0.0506
Max	0.1329					

Table 6-11: Summary of the Mode-mean test results

The Mean-Median parameter will be included as part of the **'LC Analyser classifier'** classification check on completion of this research and all the periodic variables in the SuperWASP archive will be retested.

The results for each individual object can be seen on the supplementary DVD at:

Supplementary data	
Mean-Median results	X:\Chapter06\Mean-Median_check.xlsm

Where X is DVD-1 in the DVD-drive

6.3. Plotting the period values for each class

A final check on the suitability of objects that were classified by the NNs involved creating period graphs for each class to observe where the objects lay in the period range. The following graphs show the calculated period for each object along with the expected range obtained from the GCVS (Samus+ 2004).

6.3.1 EA class

The graph of EA periods shown in Figure 6-12 was split into double-eclipse and single-eclipse objects to see if there was any difference in the distribution.

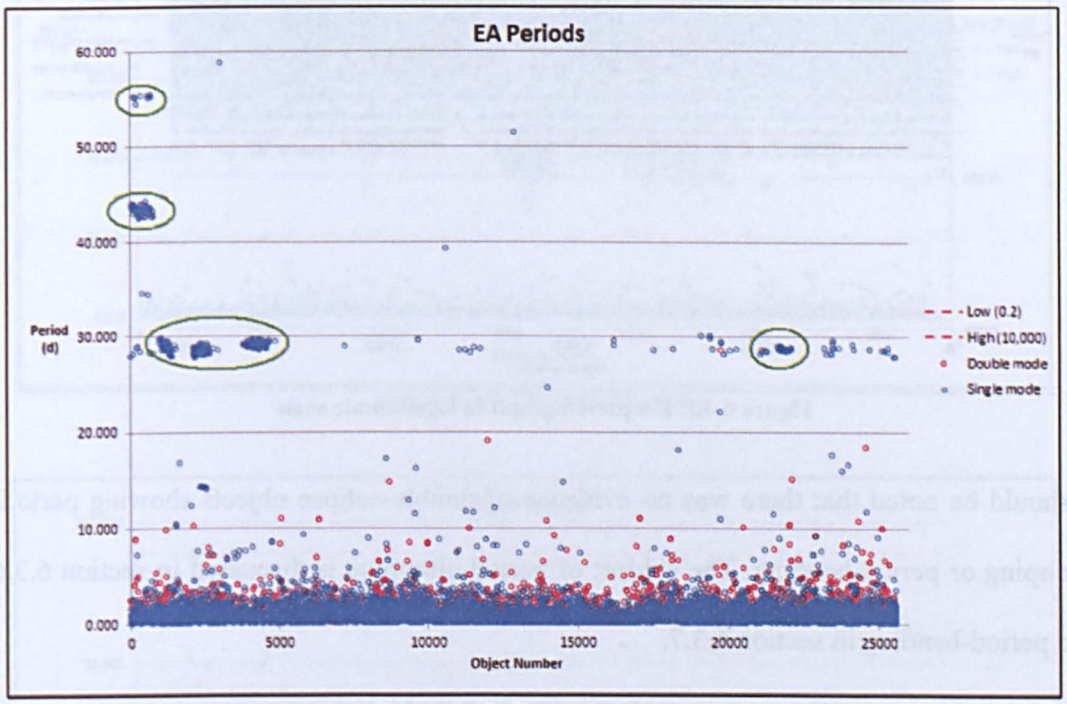

Figure 6-12: EA period graph

There was no difference, but that was not expected anyway. All the identified EA objects lay within the expected period range of 0.2 to 10,000 days, but as the maximum range of SuperWASP periods was around 50 days, it was unlikely that any of the periods would be outside the expected range. What was apparent though was the 'clumping' of single-eclipse objects as indicated by the green circles in the image. In order to look for period-clumping in the range 0.1 to 5 days, the graph was set to logarithmic scale (see Figure

6-13). No further period-clumping was seen, but a significant 'banding' effect was seen at period ranges 1.0, 0.5, 0.33, 0.25, 0.2, 0.167, 0.15, 0.125, 0.11 and 0.10 days. These occur at SuperWASP PFlags 1 to 10 respectively so are possibly caused by harmonics of the true period due to the rotation of the Earth.

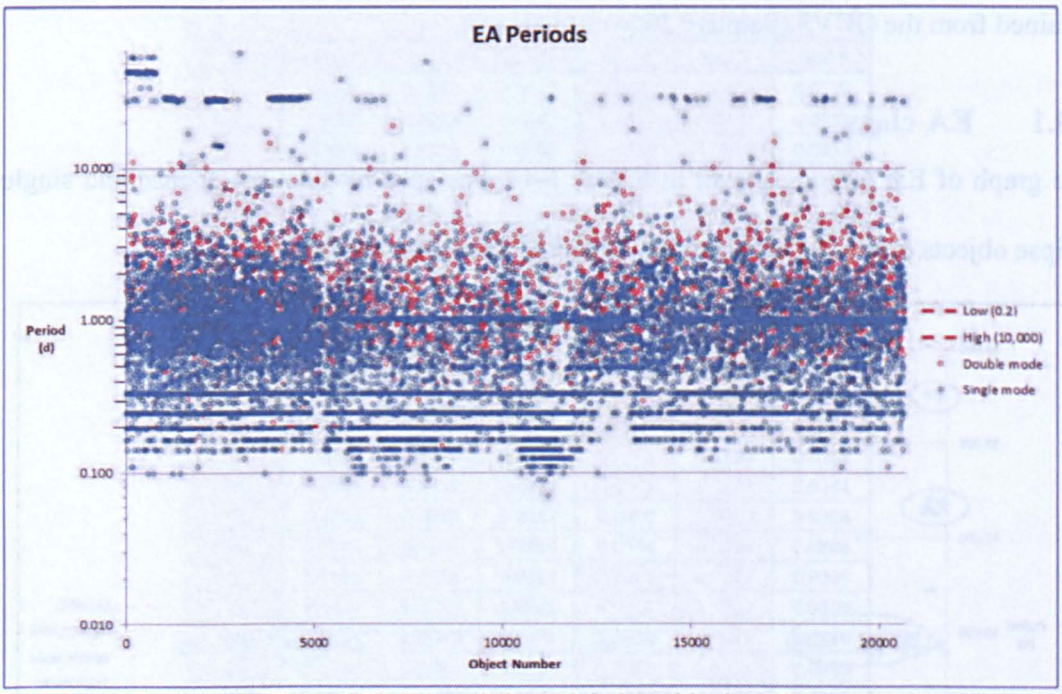

Figure 6-13: EA period graph in logarithmic scale

It should be noted that there was no evidence of double-eclipse objects showing period-clumping or period-banding. The subject of period-clumping is discussed in section 6.3.6 and period-banding in section 6.3.7.

6.3.2 EB class

The graph of EB periods is shown in Figure 6-14. Note that the 'High' period range was only set at 60 days because it was just above the maximum range of the SuperWASP period range of 50 days. The actual period range of EBs according to the GCVS is >1 day.

In order to compare the periods of the EB objects against the expected period range, the graph was changed to a logarithmic scale as shown in Figure 6-15. As stated previously,

the expected period of EBs is >1.0 days, but the period obtained from the SuperWASP EB objects showed that this was not the case. The lowest EB period in the set is 0.14 days and many objects lay below the 1 day limit. This is a concern that is investigated further in Chapter 7.

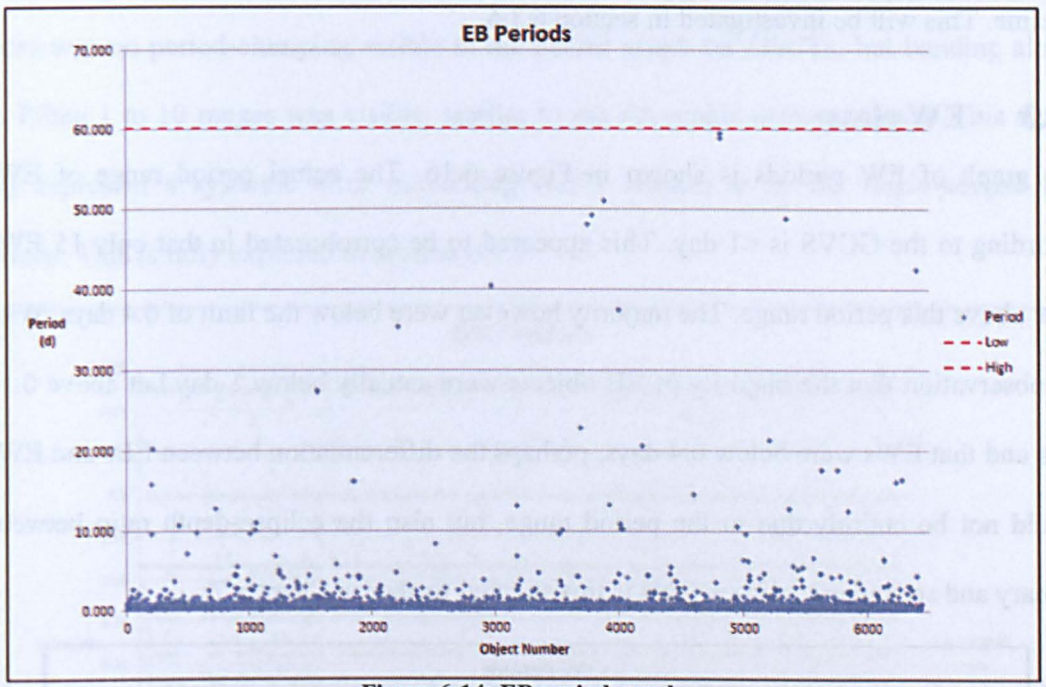

Figure 6-14: EB period graph

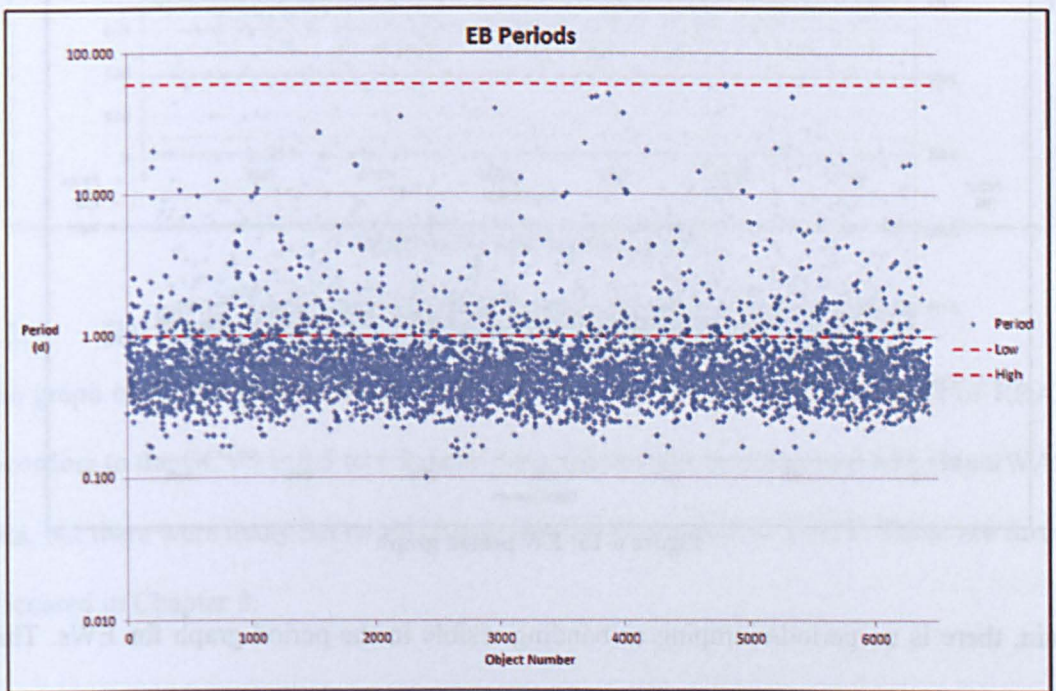

Figure 6-15: EB period graph in logarithmic scale

From the graph in Figure 6-15, there was no period-clumping or banding visible for EB objects. It should be noted that there was no period-clumping on double-eclipse EA objects either. Both of these are double-eclipse objects. This could be evidence that some of the single-eclipse EA objects are actually caused by systemic errors in the SuperWASP pipeline. This will be investigated in section 6.3.6.

6.3.3 EW class

The graph of EW periods is shown in Figure 6-16. The actual period range of EWs according to the GCVS is <1 day. This appeared to be corroborated in that only 15 EWs were above this period range. The majority however were below the limit of 0.4 days. With the observation that the majority of EB objects were actually below 1 day but above 0.14 days and that EWs were below 0.4 days, perhaps the differentiation between EBs and EWs should not be entirely due to the period range, but also the eclipse-depth ratio between primary and secondary eclipses. This is investigated further in Chapter 7.

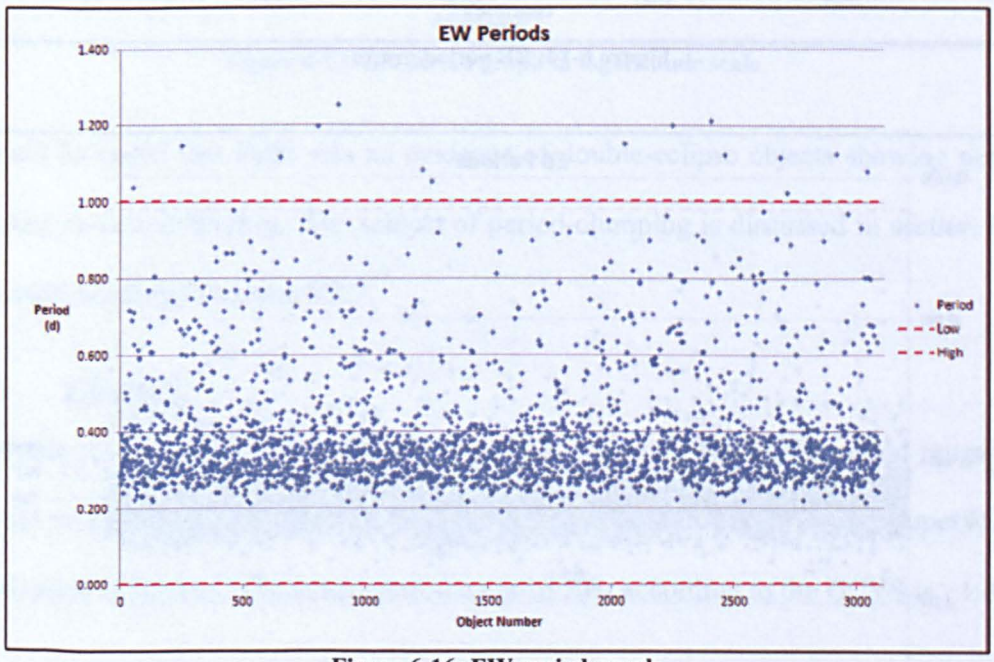

Figure 6-16: EW period graph

Again, there is no period-clumping or banding visible in the period graph for EWs. This supports the possibility of a systemic error mimicking single-eclipse periods.

6.3.4 DSCT class

The graph of DSCT periods is shown in Figure 6-17. The actual period range of DSCTs according to the GCVS is 0.01 to 0.2 days. This appeared to be supported with SuperWASP data, but the top range for SuperWASP DSCTs would be around 0.25 days.

There was no period-clumping visible in the period graph for DSCTs, but banding along the PFlag 1 to 10 ranges was visible, similar to the EA-single eclipse objects. This again may represent a systemic error mimicking DSCT objects as in the single-eclipse EA periods. This is fully explored in section 6.3.7.

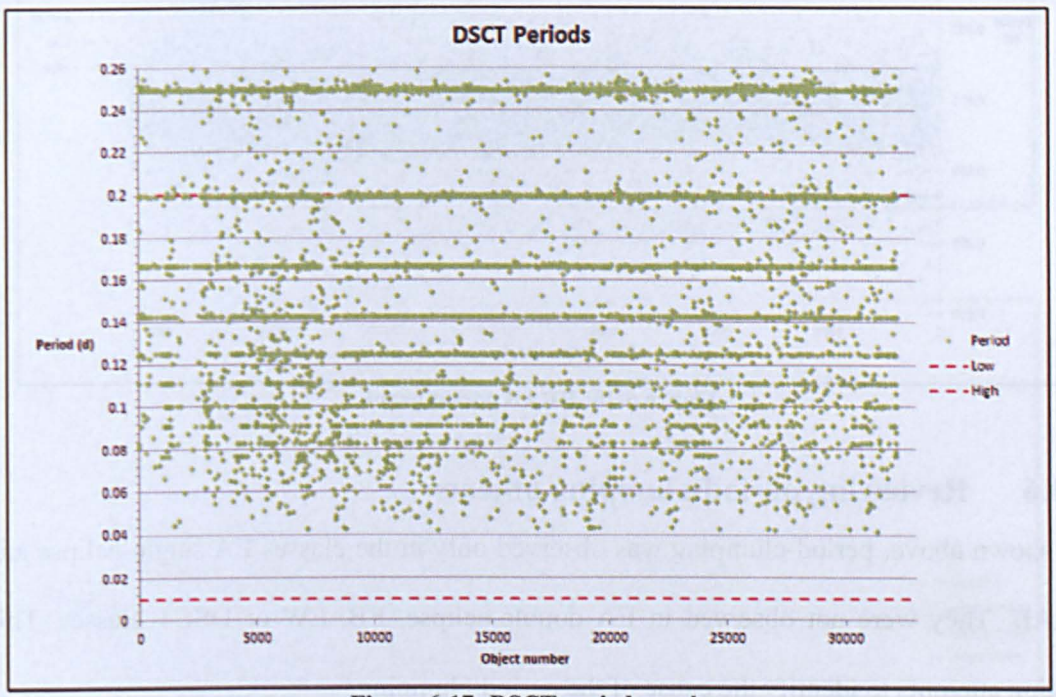

Figure 6-17: DSCT period graph

6.3.5 RRAB class

The graph of RRAB periods is shown in Figure 6-18. The actual period range of RRABs according to the GCVS is 0.3 to 1.2 days. This appeared to be supported with SuperWASP data, but there were many below this range that could possibly be DSCT. These are further discussed in Chapter 8.

Period-clumping was visible in the graph as shown by the green circles. There was also some period-banding at period 0.33 days (PFlag 3), which were probably false periods due to harmonics of the actual period. These will be discussed further in sections 6.3.6 and 6.3.7 respectively.

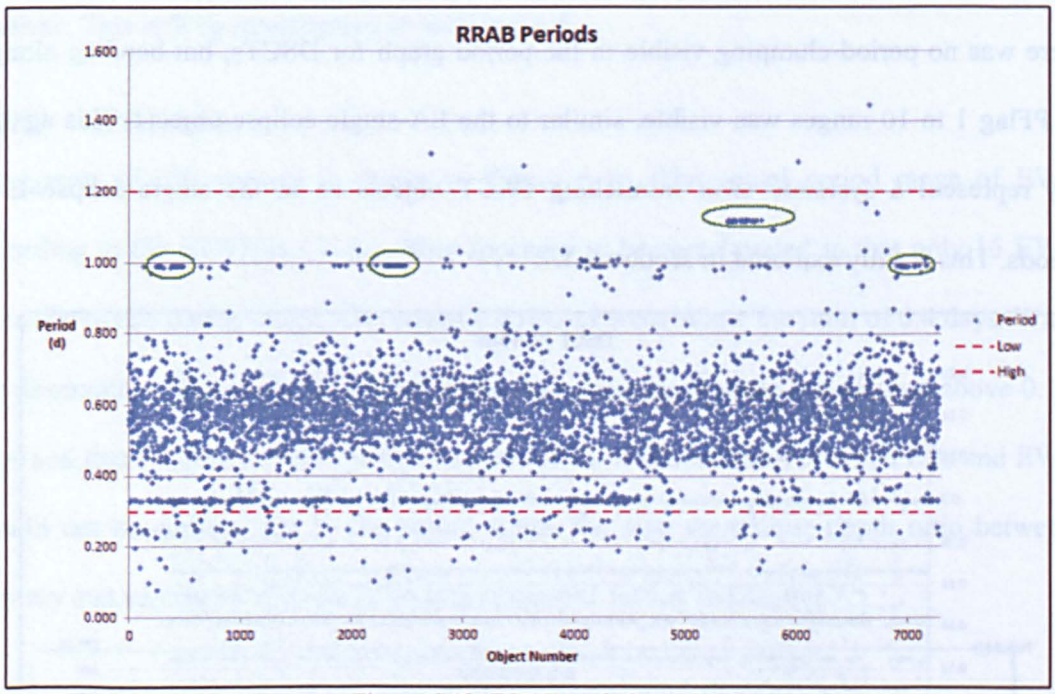

Figure 6-18: RRAB period graph

6.3.6 Reviewing period-clumping objects

As shown above, period-clumping was observed only in the classes EA single-eclipse and RRAB. They were not observed in EA double-eclipse, EB, EW or DSCT classes. This section attempts to identify the cause of the period-clumping.

6.3.6.1 EA class

From the EA period graph in Figure 6-13, the period axis was fine-tuned to identify the exact period ranges for the 'clumps' around 28 and 43 days. These can be seen in Figure 6-19 and Figure 6-20 respectively. For the 28 day period-clump, the actual period range was 27.9 to 30.0 days. There were 430 objects in this range, which showed 421 with PFlag

91 (i.e. period close to 1 lunar month) and 9 with PFlag 20 (period close to multiple of a single day).

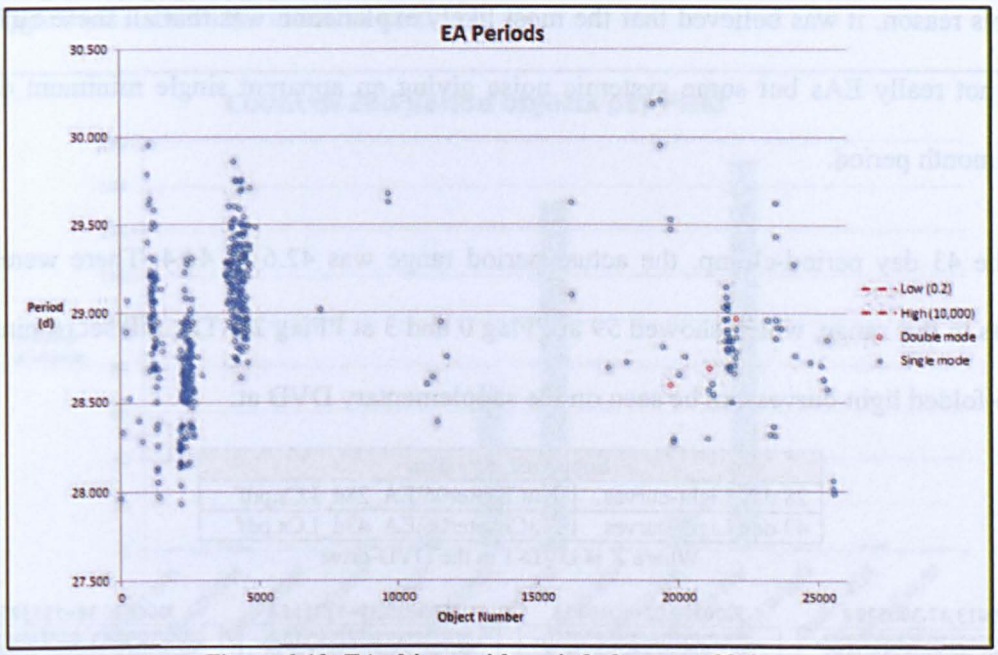

Figure 6-19: EA objects with period-clumps at 28 days

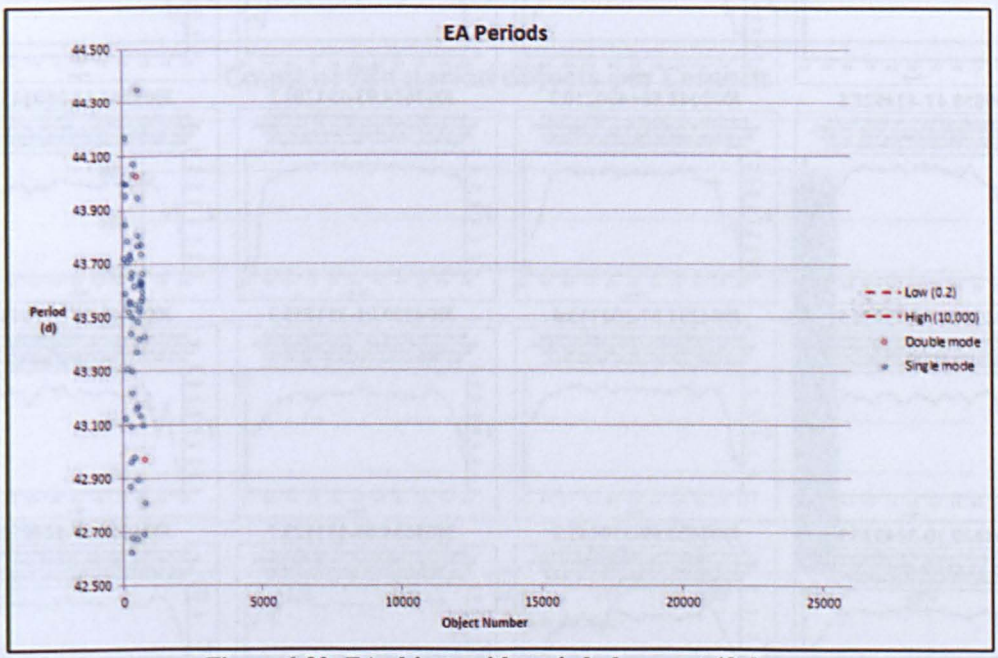

Figure 6-20: EA objects with period-clumps at 43 days

The binned phase-folded light-curves for these objects were not perfect EA shape (see Figure 6-21), but they could not be ruled out with the available information. As all the

objects showed single eclipses only, they were suspected as being false EAs because there was no reason to expect them to cluster at a period of 28 days for any real physical effect. For this reason, it was believed that the most likely explanation was that all these objects were not really EAs but some systemic noise giving an apparent single minimum on a lunar month period.

For the 43 day period-clump, the actual period range was 42.6 to 44.4. There were 62 objects in this range, which showed 59 at PFlag 0 and 3 at PFlag 20. The full set of binned phase-folded light-curves can be seen on the supplementary DVD at:

Supplementary data	
28 day Light-curves	X:\Chapter06\EA_28d_LCs.pdf
43 day Light-curves	X:\Chapter06\EA_43d_LCs.pdf

Where X is DVD-1 in the DVD-drive

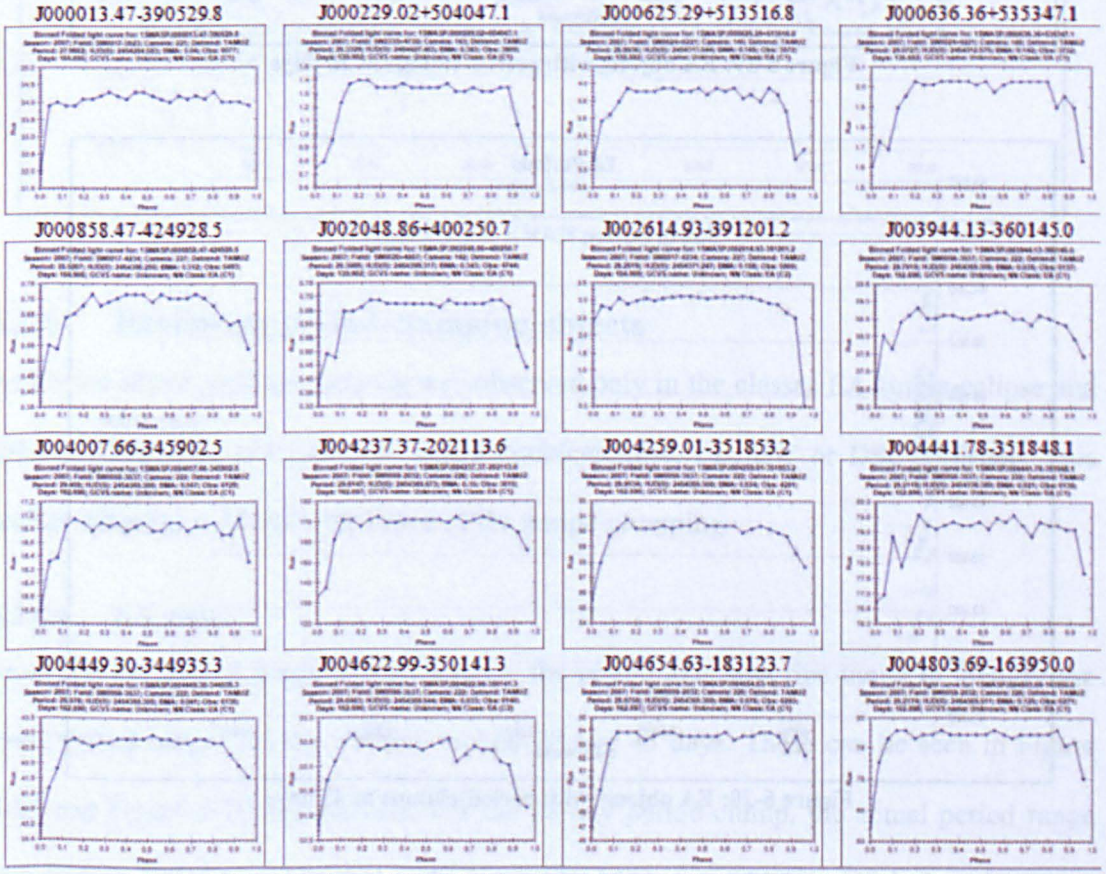

Figure 6-21: EA phase-folded light-curves for period-clumps at 28 and 43 days

At this point, the fields and cameras used were looked at for the EA period-clumps to see if there was a systemic error in any of them. Figure 6-22 shows the fields the objects were in and Figure 6-23 shows the cameras used.

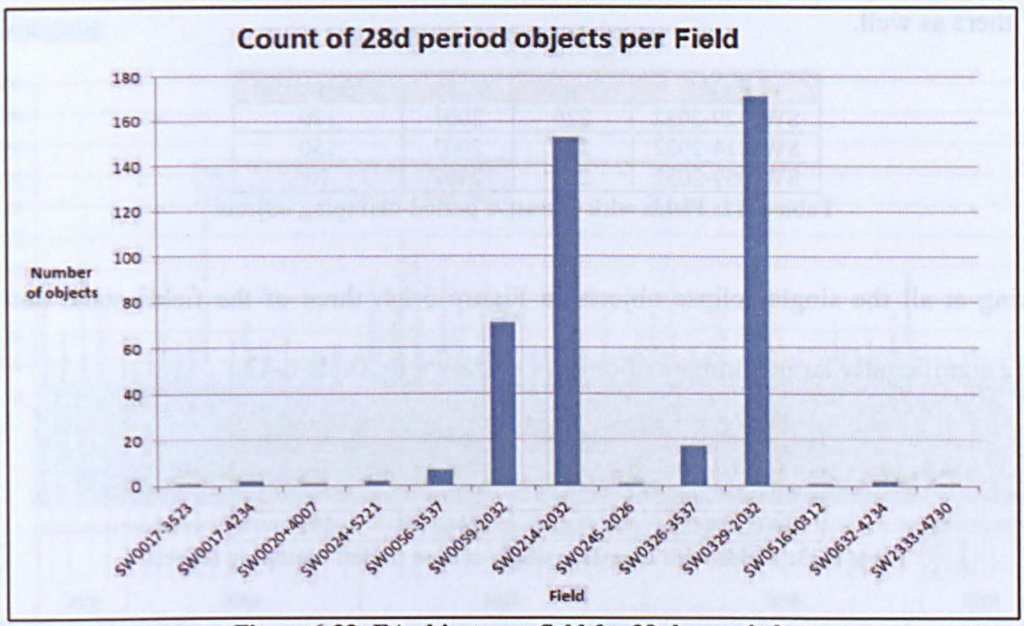

Figure 6-22: EA objects per field for 28-day periods

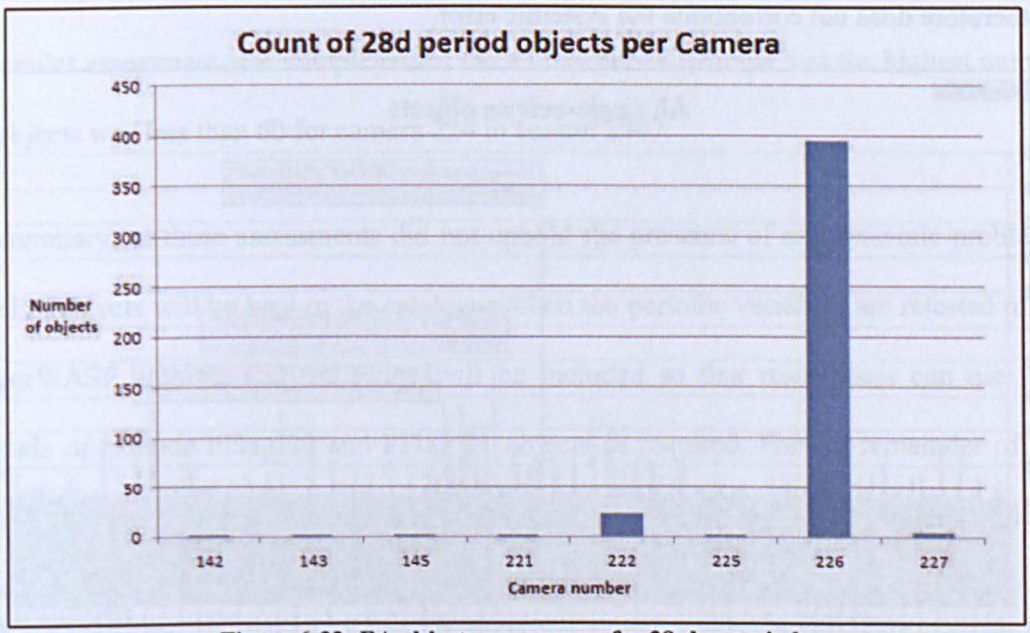

Figure 6-23: EA objects per camera for 28-day periods

Looking at the graphs for the above fields and cameras, we can see in Table 6-12 that three fields have more objects than any other field. This indicated that there may be a systemic

problem with camera 226 in season 2007. In order to confirm this, the same camera/field/seasons for all EA single-eclipse objects were looked at (see Figure 6-24). If there was a systemic problem, there should be large numbers for camera 226 in season 2007 there as well.

Field	Camera	Season	Object count
SW0329-2032	226	2007	170
SW0214-2032	226	2007	150
SW0059-2032	226	2007	70

Table 6-12: Fields with excessive period-clumping objects

Looking at all the single-eclipse objects in Figure 6-24, three of the fields stand out as having significantly large numbers of objects as shown in Table 6-13.

Field	Camera	Season	Object count
SW1635+5520	148	2007	953
SW0017-2822	224	2007	402
SW0517-4234	227	2007	301

Table 6-13: Fields with excessive single-eclipse period-clumping objects

These fields and cameras do not confirm the field and camera in the period-clump objects and therefore does not corroborate the systemic error.

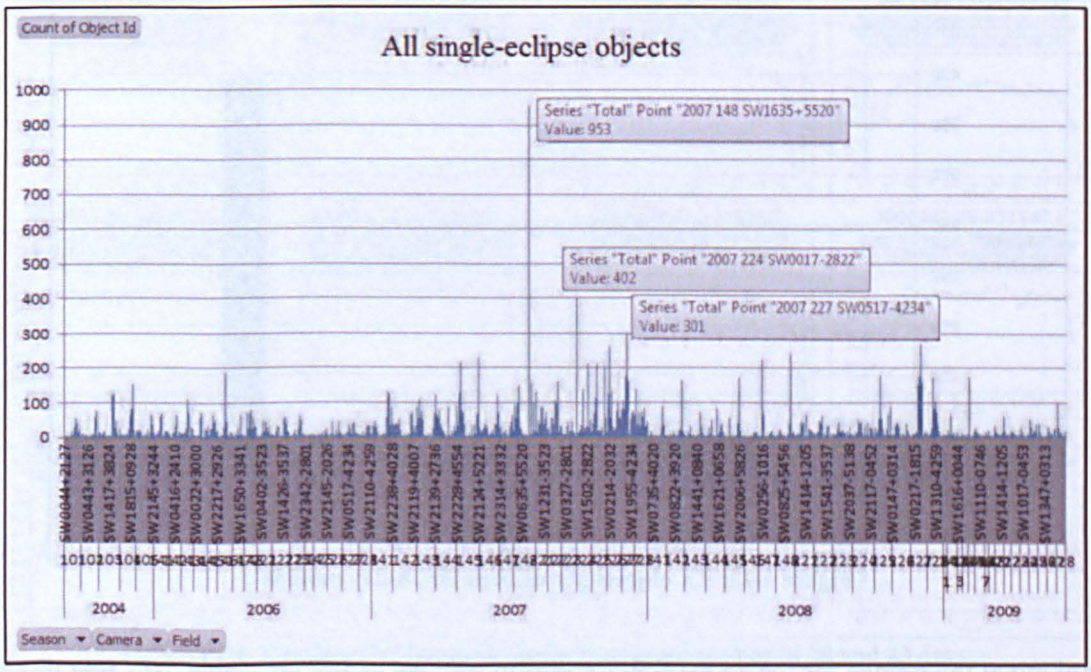

Figure 6-24: EA single-eclipse objects for each season, field and camera

As a comparison to the single-eclipse field/camera assessment, the double-eclipse objects were also examined in Figure 6-25. No problems were identified here as the highest number of objects for any given field and camera combination was less than 60.

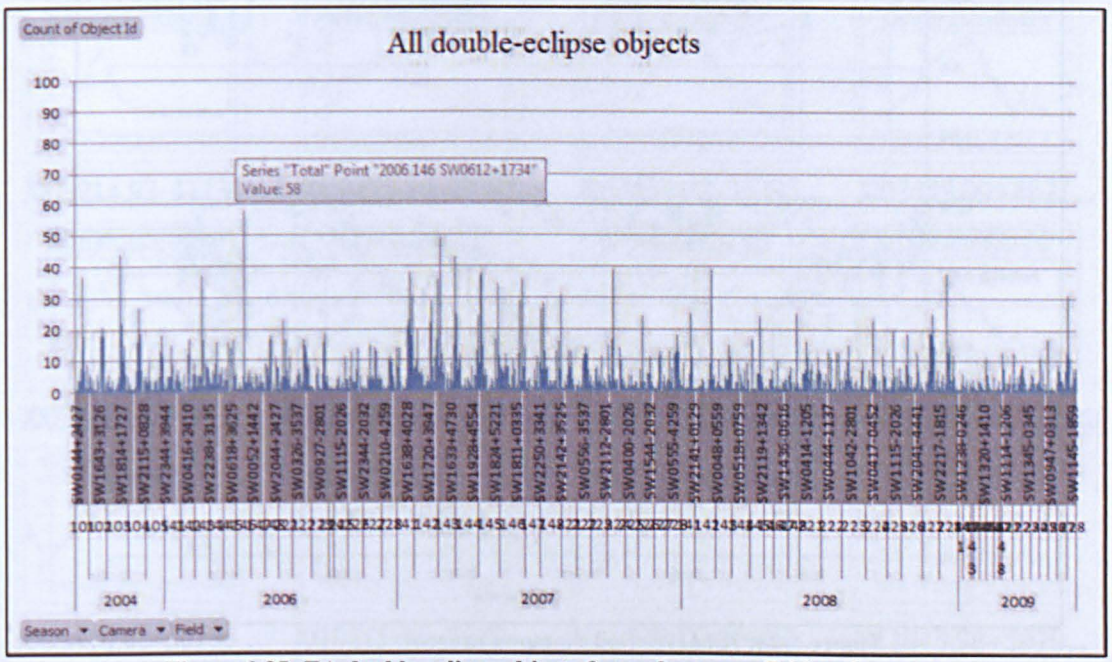

Figure 6-25: EA double-eclipse objects for each season, field and camera

A similar assessment was completed for the 43 day period-clumps, but the highest number of objects was less than 60 for camera 224 in season 2007.

In summary, as these assessments did not uphold the presence of any systemic problems, the EA objects will be kept in the catalogue when the periodic variables are retested in the SuperWASP archive, and the PFlag will be included so that researchers can use it to include or exclude PFlag 20 and PFlag 91 objects as required. For the remainder of this research, the 28-day and 43 day periods were removed to ensure high-confidence classifications were used in Chapter 7 and Chapter 8.

6.3.6.2 RRAB class

The RRAB period graph in Figure 6-18 above showed a number of areas with period-clumps similar to those found in the eclipsing binary objects. Figure 6-26 shows some of

the period-clumping regions circled in red, the remainder can be seen in Appendix 17. Appendix 18 shows similar graphs for the DSCT objects.

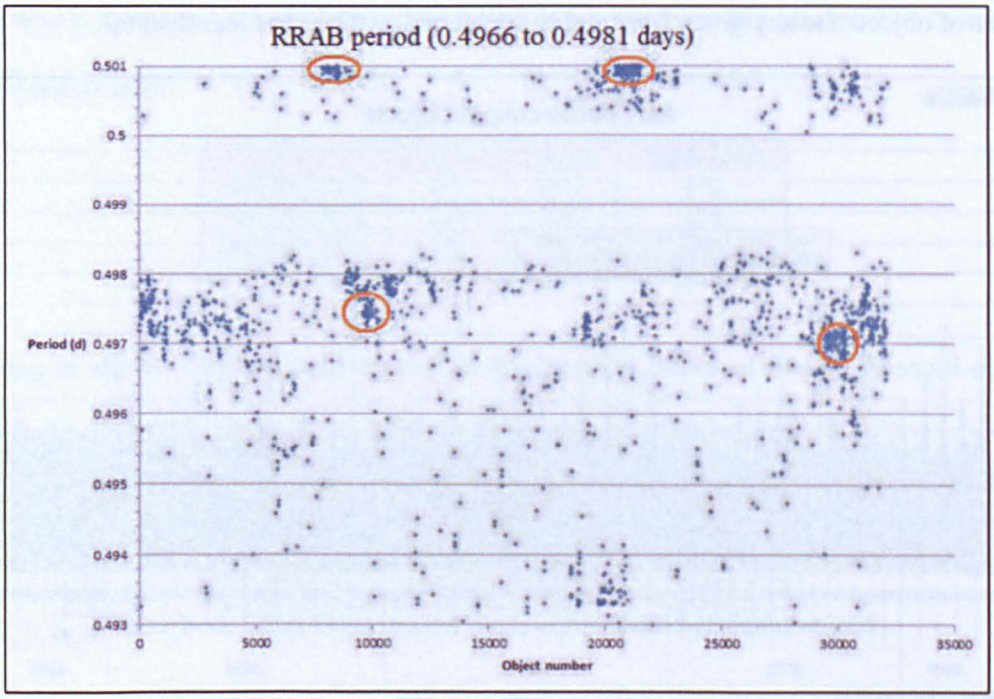

Figure 6-26: RRAB period-clumped ranges

In the case of the eclipsing binaries, it was thought that period-clumping was due to some form of systemic error that mimicked the binary curve, but this could not be confirmed. For the RRAB class, this was not the case as the phase-folded light-curves were definitely RRAB shape. See Figure 6-27 for some examples.

The results for each object can be seen on the supplementary DVD at:

Supplementary data	
RRAB light-curves	X:\Chapter06\RRAB_LCs.pdf

Where X is DVD-1 in the DVD-drive

Like the EAs, all the RRAB objects will be kept when the periodic variables are retested in the SuperWASP archive and the PFlag will be included so that researchers can use it to include or exclude the period-clumped objects as required. For the remainder of this

research though, the period-clumping objects were removed to ensure high-confidence classifications are used in Chapter 7 and Chapter 8.

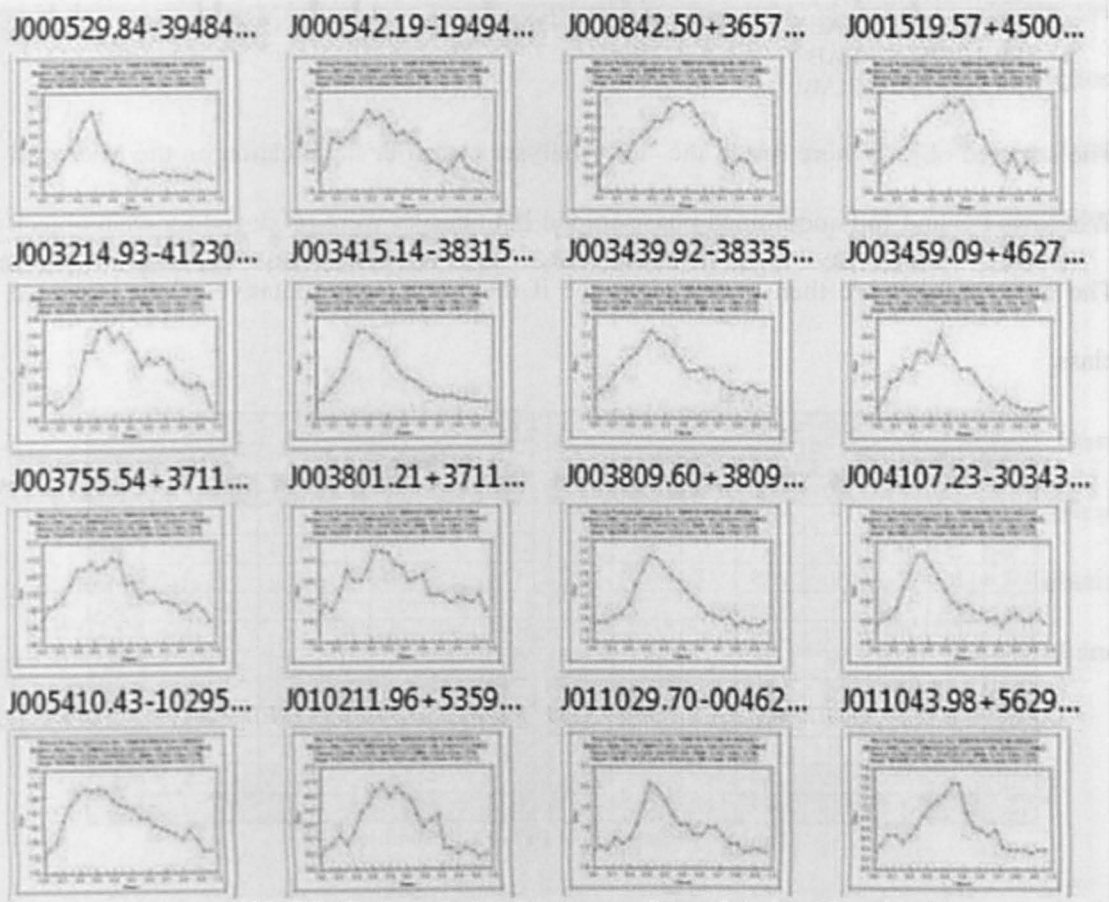

Figure 6-27: RRAB phase-folded light-curves for period-clumping objects

6.3.7 Reviewing period-banding objects

Period-banding was observed in the classes EA single-eclipse, DSCT and RRAB. They were NOT observed in EA double-eclipse, EB or EW, all of which are double-eclipse objects. This is indicative of a systemic error, but as indicated in the previous section the phase-folded light-curves look suitable for the classes. The systemic error must cause flux values that mimic these objects. To assess the period-banding, 5 EA objects, 5 DSCT objects and 5 RRAB objects were selected that had a good classification in all three NNs for each of the PFlags 1 to 10. Due to the similarity of DSCT light-curves to RRAB light-curves, the dataset also included the following NN classes (NN1/NN2/NN3):

- DSCT/DSCT/DSCT
- RRAB/DSCT/DSCT
- DSCT/RRAB/DSCT
- DSCT/DSCT/RRAB
- RRAB/RRAB/DSCT
- DSCT/RRAB/RRAB
- RRAB/DSCT/RRAB
- RRAB/RRAB/RRAB

The selected objects were run in the 'LC Analyser classifier' application on the Microsoft Windows PC and full and binned phase-folded light curves were produced for each object. The light-curves were then reviewed to see if they were representative of the expected class.

DSCT/RRAB							
Pflag	Good		Query		Bad		Total
	No.	%	No.	%	No.	%	
1	23	63.9	7	19.4	6	16.7	36
2	25	65.8	10	26.3	3	7.9	38
3	16	45.7	8	22.9	11	31.4	35
4	16	43.2	7	18.9	14	37.8	37
5	14	40.0	17	48.6	4	11.4	35
6	10	28.6	19	54.3	6	17.1	35
7	15	45.5	12	36.4	6	18.2	33
8	5	19.2	13	50.0	8	30.8	26
9	4	14.3	11	39.3	13	46.4	28
10	5	20.0	12	48.0	8	32.0	25
Total	133	40.5	116	35.4	79	24.1	328

EA							
Pflag	Good		Query		Bad		Total
	No.	%	No.	%	No.	%	
1	6	60.0	2	20.0	2	20.0	10
2	7	70.0	1	10.0	2	20.0	10
3	3	30.0	1	10.0	6	60.0	10
4	8	80.0	2	20.0	0	0.0	10
5	0	0.0	5	50.0	5	50.0	10
6	6	60.0	4	40.0	0	0.0	10
7	4	40.0	4	40.0	2	20.0	10
8	4	66.7	0	0.0	2	33.3	6
9	2	33.3	1	16.7	3	50.0	6
10	0	0.0	1	20.0	4	80.0	5
Total	40	46.0	21	24.1	26	29.9	87

Table 6-14: Results of PFlag 1 to 10 objects

Table 6-14 shows columns for 'Good' classification where the objects really should be included in the catalogue; 'Query' classification where the light-curve probably has a correct classification but it is being masked by other observations; and 'Bad' classification where there are random observations that are affecting the overall binned light-curve.

The results show that the majority of objects in the 'PFlag 1 to 10' range are either 'Good' or 'Query' classes. As such, they will be kept in the catalogue when all the periodic variables in the SuperWASP archive are retested and the PFlag will be included so that researchers can retrieve objects in or out of the period-banding regions. For the remainder of this research, objects in the PFlag 1 to 10 regions were removed.

6.4. Finalise the catalogues

Two catalogues will be available from the SuperWASP archive: firstly, a 'personal' catalogue, which was created from the 'good' objects in this research; and secondly, the complete 'SuperWASP' catalogue, which will become available shortly after completion of this research when all periodic variables in the SuperWASP archive will have been retested with the updated 'LC Analyser classifier' application. These catalogues are described here:

6.4.1 Personal catalogue

For the personal catalogue, the poor objects described in sections 6.1, 6.2 and 6.3 were removed so that it contained the 63,614 objects that have a good classification. These objects were processed through the 'LC Analyser classifier' application in order to obtain the full and binned phase-folded light-curves so that they could be manually reviewed and split into the categories shown in Table 6-15:

State	Comment
Good	Acceptable light-curve
Small amplitude	Good light-curve shape and scatter of observations is non-existent or small
Large scatter	Good light-curve shape, but there is a large scatter of observations due to the object being faint
Other class	Good light-curve shape, but classification does not agree with the neural networks
Half/Double/Multiple periods	Good light-curve shape, but more than one peak is shown
Bad period	Poor light-curve shape, but incorrect period is used
Weird	Poor light-curve shape, but something else is going on as well
Unclassified	No recognisable light-curve shape

Table 6-15: Categories for the 'personal' catalogue

Table 6-16 shows the number of objects that were obtained for each of the categories. Note that the classes CEP, RM and RRC were included in this table because during manual assessment of the EA, EB, EW, RRAB and DSCT phase-folded light-curves, some of them were classified as CEP, RM and RRC. The table shows that we have 28,393 'Good, Small amplitude, Large scatter and Other class objects', 4,990 'Half/Double/Multiple period, Bad

period and Weird objects' which required repeating using more appropriate periods, and 30,231 'Unclassified objects'.

The number of objects that were assigned 'unclassified' was surprising, but reviewing the full phase-folded light-curves showed that the scatter of observations around the main part of the curve in the prominent area for the class had a heavy influence on the binned light-curve. It was also noticed that binning the light-curves chopped the 'corners' off the EA class leading to an EB classification i.e. the 108 objects classified as EB by the neural networks were manually classed as EA.

Manual status	CEP	DSCT	EA	EB	EW	NoClass	Review	RM	RRAB	RRC	Totals
Good	0	1,446	7,490	4,258	2,454	0	0	11	5,541	6	21,206
SmallAmplitude	1	870	1,356	800	210	0	0	0	986	0	4,223
LargeScatter	0	1,520	915	135	44	0	0	1	197	1	2,813
OtherClass...	0	17	1	108	15	0	0	5	2	3	151
EA	0	0	0	108	15	0	0	2	0	1	126
EW	0	0	0	0	0	0	0	1	0	0	1
RM	0	17	1	0	0	0	0	0	0	0	18
RRAB	0	0	0	0	0	0	0	2	0	2	4
RRC	0	0	0	0	0	0	0	0	2	0	2
HDM period	0	0	2,867	13	1	0	0	0	0	0	2,881
Weird	0	0	871	16	1	0	0	0	0	0	888
Bad period	0	129	675	139	100	0	0	1	177	0	1,221
Unclassified	11	17,703	9,608	405	62	33	216	36	2,144	13	30,231
Totals	12	21,685	23,783	5,874	2,887	33	216	54	9,047	23	63,614

Table 6-16: Results of assessing Good, Large scatter and Small amplitude objects

In order to find the best periods to use in the catalogue for the 4,990 repeat objects, a total of 57,570 object/period combinations from the SuperWASP archive were re-run in the LC Analyser application and manually reviewed. Table 6-17 shows the results of repeating these objects and indicates that 2,573 of the repeat objects (2,313 + 252 + 8) could be added to the 28,393 confirmed 'good' objects to be placed in the 'personal' catalogue. It also shows that 823 objects needed to be repeated again due to the phase diagram showing half/double periods and 764 objects show definite variability. These objects should be run again using the SuperWASP period search (as extra data is added to the archive nightly).

The 30,231 unclassified objects, the 375 'weird' objects and the 455 unclassified objects from the repeats were dropped from the 'personal' catalogue. The 'weird' objects may be worth looking at in the future.

In Table 6-17, the 'Analysis of the 823 repeats' grid shows the breakdown after re-running the Half/Double/Multiple objects with periods of period/4, period/2, periodx2, periodx4. The analysis shows that 720 objects (719 + 1) would be added to the 'personal' catalogue. 21 objects needed to be added to the "bad periods' to re-run with the SuperWASP period search.

Main run analysis	
Good	28,393
To repeat	4,990
Unclassified	30,231
Total	63,614

→

Analysis of repeats	
Good	2,313
Small amplitude	252
Large scatter	8
HDM period	823
Weird	375
Bad period	764
Unclassified	455
Total	4,990

→

Analysis of repeats	
Good	719
Large scatter	1
HDM period	21
Bad period	82
Unclassified	0
Total	823

Table 6-17: Results of repeating Good, Large scatter and Small amplitude objects

Summing up, the 'personal' catalogue will hold 31,728 objects as shown in Table 6-18. The eclipsing binaries EA, EB, EW and the pulsating stars DSCT and RRAB will be analysed in depth in Chapter 7 and Chapter 8 respectively.

Overall totals	
Good	24,285
Large scatter	2,817
Other class	151
Small amplitude	4,475
Bad period	817
Unclassified	30,692
Weird	377
Total	63,614

→ → → →

Useable
31,728

→

NN class breakdown	
CEP	6
DSCT	1,574
EA	12,568
EB	5,433
EW	2,827
RM	36
RRAB	9,253
RRC	31
Total	31,728

Table 6-18: Number of objects available in the SuperWASP catalogue

6.4.2 Complete SuperWASP catalogue

The NNs in this research effectively reduced the millions of periodic variable objects in the SuperWASP archive to 1,136,566 unique objects that had a preliminary classification. These objects were assessed during this research to see how effective the classification was and the assessment has provided further parameters that can be included in the 'LC Analyser classifier' application as discussed in section 6.2. The main additions to the application will be:

1. Re-trained NNs with a more appropriate period bin and better defined training sets obtained from the 'personal' catalogue in 6.4.1. This will help differentiate the DSCT class from the RRAB.
2. Inclusion of the statistics χ^2_{red}, skewness and mean-median. This will help identify poor light-curves and also to identify the best period where objects have duplicates.

The catalogue will be stored at Leicester University and the information shown in Table 6-19 will be stored so that the catalogue can be searched in a number of ways depending on the needs of the researcher. For instance, as indicated in the previous sections, there may be objects included in the catalogue that have inappropriate classifications due to systemic errors in the SuperWASP archive. These can be removed by filtering the catalogue by PFlag, Field and/or Camera. It is envisaged that a researcher using the catalogue will retrieve all objects for a given class in the first instance and if too many objects are retrieved then they will use the other fields in Table 6-19 to reduce the numbers.

The 'unique identifier' section contains the information that uniquely identifies an object and all its duplicates due to season, field, camera, 'period range' (PFlag), and Detrend.

This allows a researcher to select (or not) a period range known to have period-clumping objects. The 'classification' section contains the class identified in the NNs.

Fields available in the catalogue			
Unique identifier	Object Id		
	Season		
	Field		
	Camera		
	Detrend		
	Period (sec)		
	PFlag		
Classification	Overall class name		
	Overall confidence value		
	NN1 class name	NN2 class name	NN3 class name
	NN1 Cep value	NN2 Cep value	NN3 Cep value
	NN1 DSCT value	NN2 DSCT value	NN3 DSCT value
	NN1 EA value	NN2 EA value	NN3 EA value
	NN1 EB value	NN2 EB value	NN3 EB value
	NN1 EW value	NN2 EW value	NN3 EW value
	NN1 RM value	NN2 RM value	NN3 RM value
	NN1 RRAB value	NN2 RRAB value	NN3 RRAB value
	NN1 RRC value	NN2 RRC value	NN3 RRC value
	NN1 No class value	NN2 No class value	NN3 No class value
Quality	Reduced chi-square value per x-axis bin (25)		
	Skewness value per x-axis bin (25)		
	Mean-median value per x-axis bin (25)		
	Number of 0 chi-sqr bins		
	Number of consecutive 0 chi-sqr bins		
	Below minimum amplitude (1=below, 0=Above or equal)		
	Chi-sqr binned flux		
	Chi-sqr overall flux		
Statistics calculated	Period (d)		Mode-mean
	Observations analysed		Flux amplitude
	Days analysed		Magnitude amplitude
	Total observations removed		Binned Magnitude amplitude
	Phase Length		Primary eclipse depth
	Period-bin		Secondary eclipse depth
	Mean flux		Eclipse depth ratio
	Median flux		Minimum binned magnitude
	Minimum flux		Maximum binned magnitude
	Maximum flux		HJD (1st obs.)
	Flux range		HJD (0 phase)
Link	GCVS Name		

Table 6-19: Information available in the SuperWASP catalogue

Here, the researcher can select objects using the 'Overall class' and 'Overall confidence index', where confidence index 1 gives the highest confidence in the class, e.g. this research has used confidence index levels 1, 2 and 4. An alternative approach to obtaining objects of a given class would be to use the individual values in the NNs, for instance, select all the objects where NN1 EA value > 0.6 and NN2 EA value > 0.2 and NN3 EA

value > 0.3. This would give all the EA objects. The 'quality' section contains data that suggests how robust the binned phase-folded light-curves are. The first three parameters are the ones that will be added to the 'LC Analyser classifier' application on completion of this research. The remaining five parameters indicate where zero chi-square values were obtained for the bins and allow the researcher to select objects using these criteria to avoid poor light-curves.

The 'statistics calculated' section provides information that was calculated during the classification process. They can be used to select objects, but they are more likely to be useful for analysis. The 'Link' section just provides a link to the GCVS table that is held in the SuperWASP archive. The GCVS name is stored for the objects if it is known.

6.5. Chapter summary

This chapter assessed the quality of the results obtained from the 'LC Analyser classifier' output produced in Chapter 5. The assessment showed that many duplicate objects existed which had to be removed and many poor classifications were observed due to period-clumping, period-banding, large-scatter of observations in the light-curve and small amplitudes of some of the objects. Various methods were identified to limit these poor objects in the next version of the 'LC Analyser classifier' application such as reduced-chi-square and skewness tests. A personal catalogue of 31,728 objects was then created as indicated in Table 6-18 and the EA, EB, EW, DSCT and RRAB objects extracted for use in the next two chapters. Chapter 7 assesses the eclipsing binary and Chapter 8 assesses the pulsating objects to see if they agree with the status quo and to investigate the use of 'eclipse-depth' ratio to distinguish between EB and EW classes, and to investigate the Blazhko effect and Oosterhoff dichotomy with the RR Lyrae stars.

---------- o ----------

Chapter 7 SuperWASP Eclipsing stars

In Chapter 5, all the periodic variables in the SuperWASP archive were processed with the 'LC Analyser classifier' application and gave preliminary classifications to 75,651 EA objects, 107,262 EB objects and 21,910 EW objects using a confidence index of 1, 2 and 4. In Chapter 6, the phase-folded light-curves for these objects were reviewed to identify those where the NN classification was manually confirmed. Once the 'bad period' objects highlighted in Chapter 6 were repeated with more appropriate periods, this provided 12,882 EA objects, 5,226 EB objects and 2,875 EW objects for assessment in this chapter, where their physical parameters were compared against published material and a quantitative approach to differentiating EB from EW objects is proposed, using an 'eclipse-depth ratio' parameter.

During the review of these 20,983 objects, they were split by eye into three categories based on the state of the light-curve, i.e. 'Good', 'Large scatter' and 'Small amplitude'. All three categories had binned phase-folded light-curves that were good representatives of the class, but they differed when looking at the full phase-folded light-curve as shown in Figure 7-1. This split was performed because less confidence was placed in the large scatter and small amplitude curves due to the difficulty in manually assigning the class, for instance the 'Large scatter' (i.e. faint) object in Figure 7-1 looked more like an EB than an EA when the full phase-folded light-curve was examined, but the NN classified it as an EA. Once the review had been completed, the physical parameters for each of the classes EA, EB and EW were assessed individually and as a group of 'eclipsing binaries'. The catalogue for each class and the supporting binned and full phase-folded light-curves can be seen on the supplementary DVD in the following locations:

Supplementary data – Catalogues	
EA catalogue	X:\Chapter07\Catalogues\EA.xlsm
EB catalogue	X:\Chapter07\Catalogues\EB.xlsm
EW catalogue	X:\Chapter07\Catalogues\EW.xlsm
Eclipsing catalogue	X:\Chapter07\Catalogues\Eclipsing.xlsm

Where X is DVD-1 in the DVD-drive

Supplementary data – Light-curves	
EA Double Good	X:\Chapter07\Light_curves\EA Double\Good
EA Double Large scatter	X:\Chapter07\Light_curves\EA Double\LS
EA Double Small amplitude	X:\Chapter07\Light_curves\EA Double\SA
EA Single Good	X:\Chapter07\Light_curves\EA Single\Good
EA Single Large scatter	X:\Chapter07\Light_curves\EA Single\LS
EA Single Small amplitude	X:\Chapter07\Light_curves\EA Single\SA
EB Good	X:\Chapter07\Light_curves\EB\Good
EB Large scatter	X:\Chapter07\Light_curves\EB\LS
EB Small amplitude	X:\Chapter07\Light_curves\EB\SA
EW Good	X:\Chapter07\Light_curves\EW\Good
EW Large scatter	X:\Chapter07\Light_curves\EW\LS
EW Small amplitude	X:\Chapter07\Light_curves\EW\SA

Where X is DVD-2 in the DVD-drive

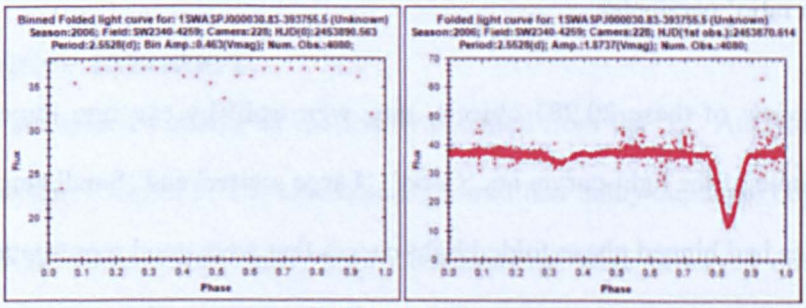

(a) 'Good' EA light-curve

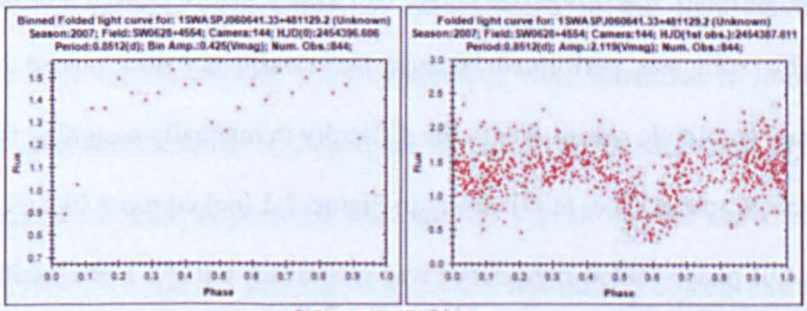

(b) 'Large scatter' EA light-curve

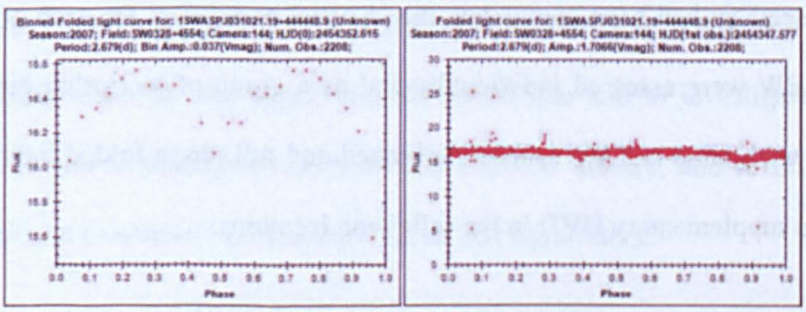

(c) 'Small amplitude' EA light-curve

Figure 7-1: EA: 'Good', 'Large scatter' (i.e. faint), 'Small amplitude' light-curves

During the analysis, each object was classified by manually reviewing the full phase-folded light-curve and the results compared against the classes obtained from the NNs to see how effective the NN classification was. A search was then made for each object in SIMBAD to identify the known objects, which was achieved by creating a number of files with the right-ascension and declination of each object and then submitting them to the SIMBAD web-site requesting objects within a 1-arcmin radius of each of the SuperWASP objects. An object was deemed as known if the nearest or second nearest match in SIMBAD was of the same or similar class. Graphs were created for variability period and amplitude to obtain the SuperWASP limits for these parameters and also for galactic location to show the distribution of the objects across the night sky. Finally, the eclipse-depth ratio for each object was graphed to assess the quantitative difference between EA, EB and EW to see if this could be used to separate them – particularly EB from EW.

7.1. Analysis of EA objects

The analysis was initially performed for 'All' 75,651 EA objects, but while plotting the period graph in section 7.1.3, it was noticed that period-clumping and period-banding were present as discussed in Chapter 6. The analysis was reworked on two occasions after identifying the PFlags associated with the anomalies. The first occasion was after removing both 'Large scatter (LS)' and 'Small amplitude (SA)' objects for the affected PFlags; and the second occasion was after removing all objects with the affected PFlags. The results of the analyses are discussed in the following sections.

7.1.1 Statistics

Table 7-1 shows the split between the number of double-eclipse and single-eclipse EA objects. Published figures for comparison of the numbers of double-eclipse and single-eclipse EA objects were not available at the time of this research, probably due to the fact that this parameter is very subjective as the light-curve can be affected by many situations,

e.g. the inclination of the binary system may not be 90°; physical parameters of the system may vary, such as the masses and separation of the stars, the brightness of each component, and the shape of the component stars; there may be reflection effects on the stars; the size of the stars can vary; the colour of the stars can vary; and of course, the calculated period may be half or double the actual period.

EA objects	Double-eclipse	Single-eclipse	Total
Good	5,697	5,111	10,808
Large scatter	17	900	917
Small amplitude	112	1,045	1,157
Total (N)	5,826	7,056	12,882
Total (%)	45.2	54.8	100

Table 7-1: EA: Number of Double-eclipse and Single-eclipse objects

The reason the 'double/single eclipse' parameter has been included here is because single-eclipse objects may indicate where both of the stars in the binary are of the same surface brightness (not necessarily same size) or are very different and this may be useful when assessing the distribution of eclipsing binaries. Although double/single eclipses cannot be confirmed using only the visible light-curve, this research is providing a method of identifying 'preliminary' object classes that will be fully explored using other techniques in the future. The Small amplitude – Single-eclipse objects were included as they may include low-mass eclipsing stars.

Table 7-2 shows that 96.74% of the EA objects that were classified by the NNs were confirmed by manual review.

EA Objects		Based on light-curve shape					
		All		LS/SA removed		G/LS/SA removed	
Light-curve quality	NN	No.	%	No.	%	No.	%
Good (G)	Agree	10,388	80.64	10,388	87.41	7,995	85.07
Large scatter (LS)	Agree	917	7.12	265	2.23	265	2.82
Small amplitude (SA)	Agree	1,157	8.98	811	6.82	811	8.63
Total	Agree	12,462	96.74	11,464	96.47	9,071	96.52
Good (G)	Disagree	420	3.26	420	3.53	327	3.48
Large scatter (LS)	Disagree	0	0.00	0	0.00	0	0.00
Small amplitude (SA)	Disagree	0	0.00	0	0.00	0	0.00
Total	Disagree	420	3.26	420	3.52	327	3.48
Overall total	All	12,882		11,884		9,398	

Table 7-2: EA: Statistics for identified objects

The 3.26% that disagreed were mainly 'Review' or 'No class' classes, as shown in Table 7-3, but some were also misclassified as EB or EW.

Class	Number
CEP	3
DSCT	2
EA	0
EB	156
EW	49
RM	8
RRAB	0
RRC	9
Review	177
No class	16
Total	420

Table 7-3: EA: NN class disagrees with manual class

Studying three of the misclassified objects (one EB, one EW and one CEP) explains why the NNs classified these as EA. Figure 7-2 shows the binned phase-folded light-curve on the left is quite rounded due to the scatter around the eclipses, thus indicating more of an EB shape than an EA. The disagreement probably arose due to a slightly incorrect period being used, which artificially spread out the folded data in the phase axis. The full phase-folded light-curve on the right shows that they are definitely flat and therefore EA class.

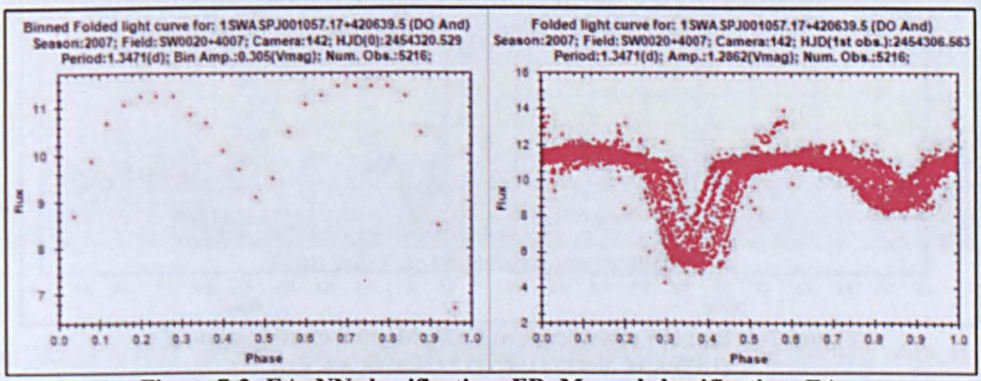

Figure 7-2: EA: NN classification: EB; Manual classification: EA (1SWASP J001057.17+420639.5 → DO And)

The scatter in the full phase-folded light-curve in Figure 7-3 caused the binned phase-folded light-curve to be more rounded and the deep second eclipse led the NNs to classify it as an EW. Also, the second eclipse does not return to the base line, possibly due to the

O'Connell effect (O'Connell, 1951) i.e. spots on one side of the star. The full phase-folded light-curve clearly shows this as an EA class.

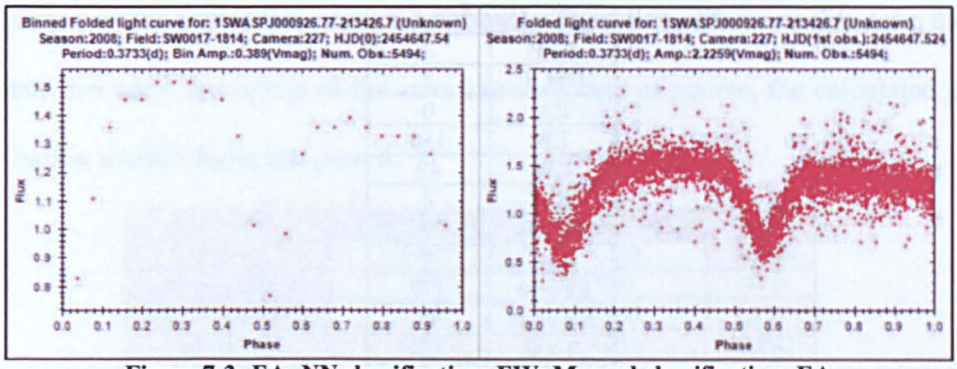

Figure 7-3: EA: NN classification: EW; Manual classification: EA (1SWASP J000926.77-213426.7)

Figure 7-4 has much of the light-curve missing and the binned phase-folded light-curve on the left is more CEP shape than EA. The other misclassified objects showed similar problems to these and indicates that a manual review of the preliminary classes provided by the NNs is essential. For the rest of this research, the manually obtained classes were used.

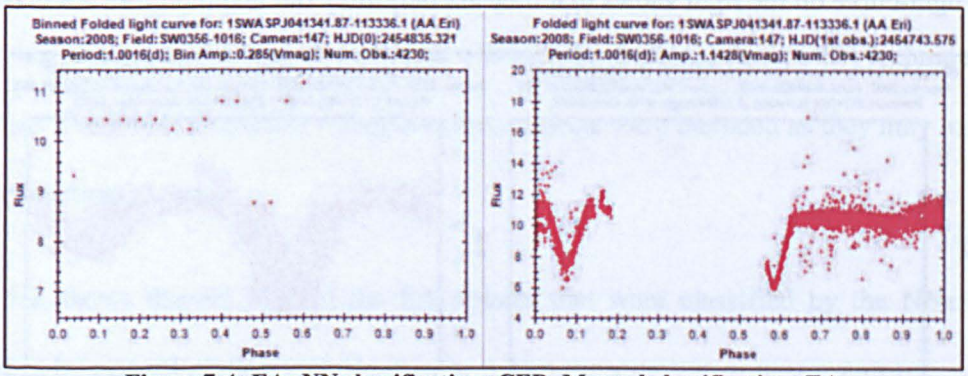

Figure 7-4: EA: NN classification: CEP; Manual classification: EA (1SWASP J041341.87-113336.1 → AA Eri)

7.1.2 Known objects

Two searches were made for all 12,882 EA objects to see if they were known i.e. SIMBAD and the GCVS. Table 7-4 shows the results of the search in SIMBAD for known objects.

Of the 12,882 EA objects, 3,807 had a nearest neighbour within 1 arc-min. Appendix 19 shows the breakdown of these per class. Of the 3,807 known objects, 1,060 confirmed the

NN **EA** class. 86 were **EB**, 6 were **EW** and 399 were **'other eclipsing'** classes (i.e. Eclipsing binary, Eclipsing binary candidate, Double star, Star in double system and Spectroscopic binary). The remaining 2,262 consisted of **pulsating objects** (i.e. Cepheid, Classical Cepheid, DSCT, RR, Horizontal Branch Star, Possible HB Star, Pulsating, W Vir, and Semi-regular pulsating Star); **Stars** (i.e. Star, High proper-motion Star, White Dwarf, Blue Straggler Star, and Low-mass star (M<1solMass)); and **'Other'** (i.e. Galaxy, Cluster of Galaxies, Galaxy in Cluster of Galaxies, HII (ionized) region, Quasar, Possible Quasar, Radio - Source, Unknown nature, Variable, and X-ray source). The pulsating stars were included in the total of 'known' objects as they could possibly be incorrect classifications in SIMBAD, but 'Star' and 'Other' classes were added to the overall total of 'unknown' stars, giving a preliminary total of 11,308 new EA eclipsing binaries.

EA objects (Overall total = 12,882)							
SIMBAD	Based on light-curve shape						
	Good		Large scatter		Small amplitude		Total
	NN agree	NN disagree	NN agree	NN disagree	NN agree	NN disagree	All
EA	998	34	11	0	17	0	1,060
EB	73	12	1	0	0	0	86
EW	6	0	0	0	0	0	6
Other eclipsing	339	24	19	0	17	0	399
Pulsating	18	1	2	0	2	0	23
Star	1,216	75	127	0	121	0	1,539
Other	545	40	53	0	56	0	694
Total known	3,195	186	213	0	213	0	3,807
Total unknowns							9,075
Total unknowns (including Star and Other categories)							11,308

Table 7-4: EA: Objects known in SIMBAD

As the SuperWASP archive was cross-matched with the GCVS, the known objects in the GCVS were identified at the time of 'LC Analyser classifier' data processing. 706 of the EA objects were known in the GCVS (539 double-eclipse objects and 167 single-eclipse objects). These were also known in SIMBAD.

7.1.3 Period

The period values for ALL the EA objects were plotted in Figure 7-5 to obtain an overview and to determine the period range. The 'expected' period range (0.2 to 10,000 days) was obtained from the GCVS and also plotted. The objects were plotted with 'Good', 'Large scatter' and 'Small amplitude' objects shown as different populations to see how they were distributed. These populations were also split by whether the NN-classifications agreed with the manual-classifications or not. The results in Figure 7-5 showed period-clumping and period-banding as discussed in Chapter 6, so the PFlags containing the affected objects were identified as shown in Table 7-5 and the 'Large scatter' and 'Small amplitude' objects were removed from the dataset and were re-plotted in Figure 7-6. Note that PFlag 91b in Table 7-5 indicates that they were PFlag 91 objects repeated due to the original periods being half or double the true period.

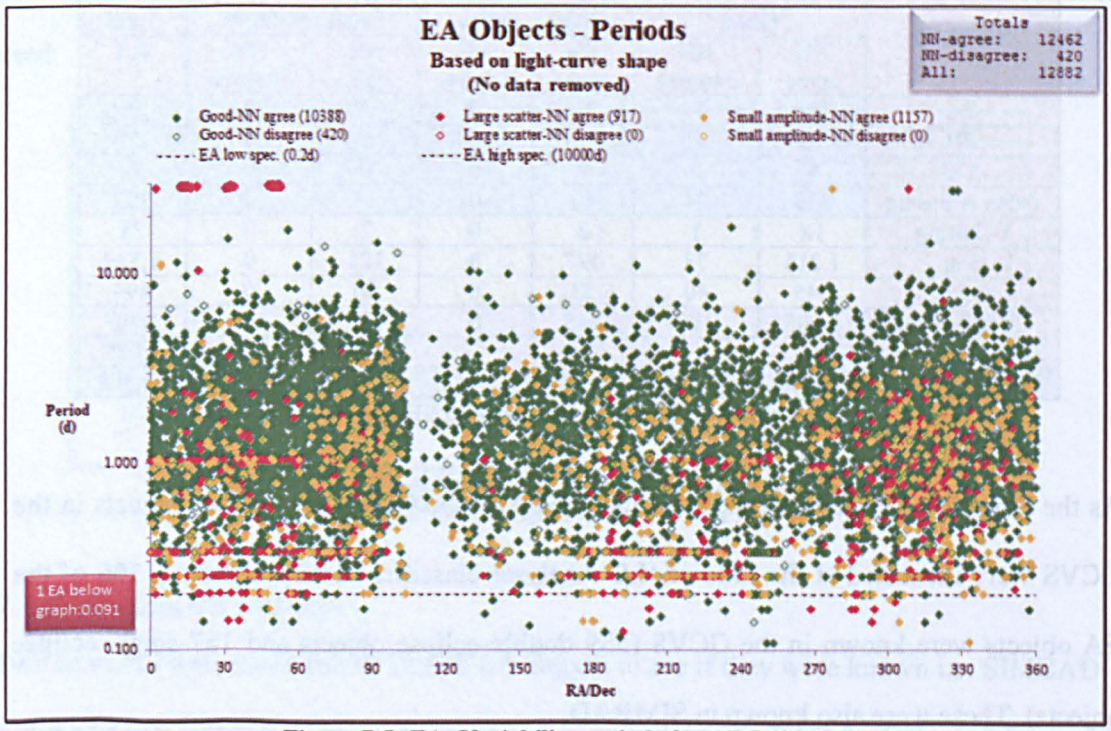

Figure 7-5: EA: Variability periods for All Objects

Periods to remove		
PFlags	Low	High
1	0.9	1.3
3	0.332	0.335
4	0.249	0.251
5	0.199	0.201
91b	28.00	30.00

Table 7-5: EA: PFlags containing clumped and banded periods

Figure 7-6 shows that all the period-clumping objects and a large number of the period-banding objects have been removed. However, as there was still some period-banding present, all objects with the PFlags in Table 7-5 were removed and the periods re-plotted in Figure 7-7. This removed all the clumped and banded periods and the remaining 9,398 objects became the dataset that was used to obtain the SuperWASP period and amplitude distributions.

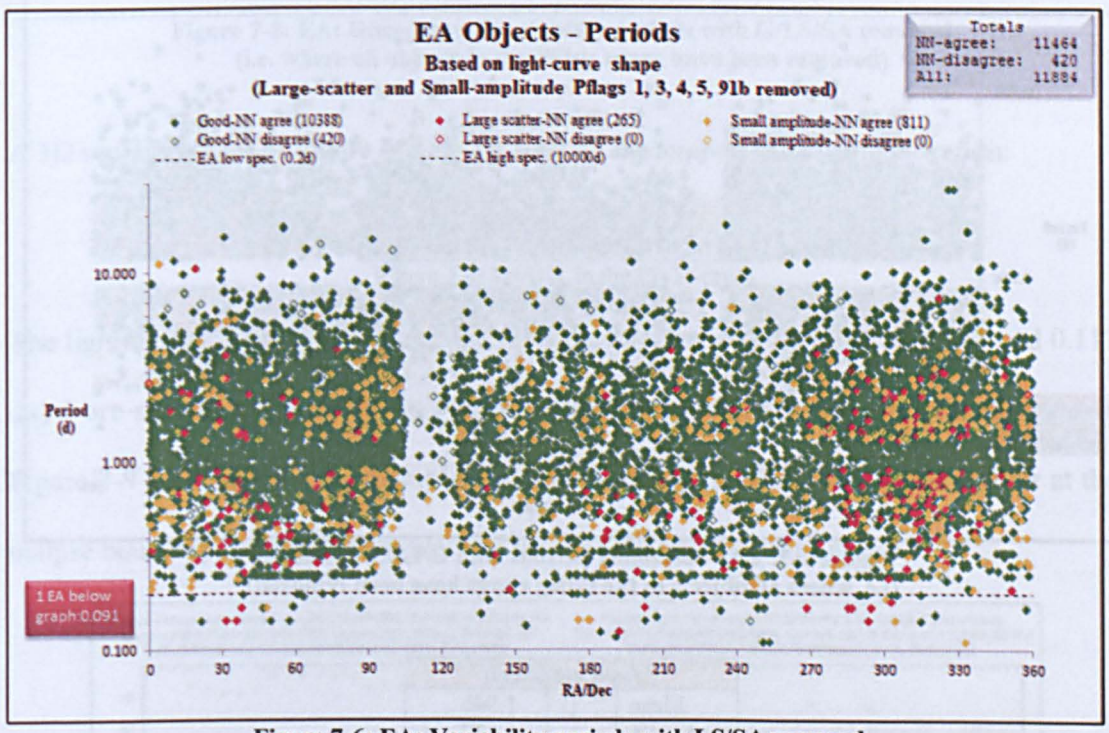

Figure 7-6: EA: Variability periods with LS/SA removed
(i.e. 'Large scatter' and 'Small amplitude' objects in the PFlag range have been removed)

To obtain the period range, a histogram of periods was created in Figure 7-8. The histogram contains a total of 9,398 EAs where 8,119 of them were 'unknown' and the rest were known in SIMBAD. The populations were displayed alongside one-another on the

same axis in order to see the distribution and it shows that there is an excess of short period objects in the 'unknown' object set. Table 7-6 shows that the range was 0.12 to 18.0 days with a median of 1.63 days and a modal value of 0.67 days. Figure 7-7 shows that 50 objects had a period less than the lower published period limit of 0.2 days (GCVS). The object-ids can be seen in Appendix 20 and the associated phase-folded light-curves can be seen on the support DVD at the location:

Light-curve output
X:\Chapter07\Outside_ranges\EA_P_below_0_2d

Where X is DVD-1 in the DVD-drive

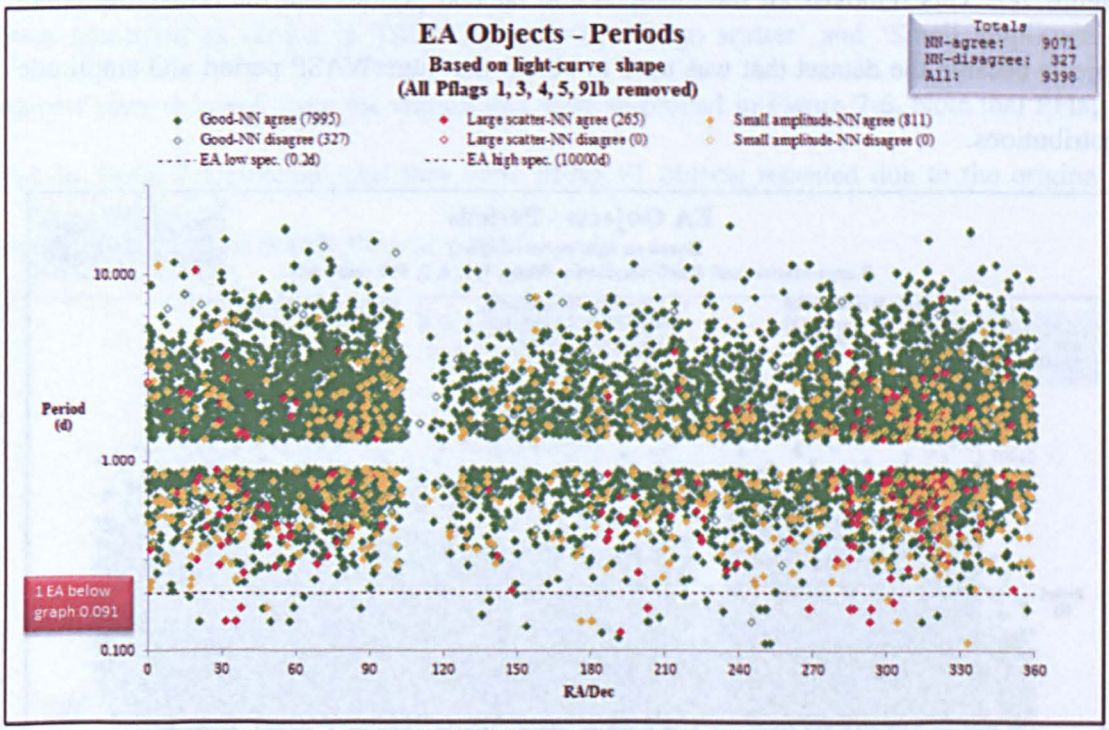

Figure 7-7: EA: Variability periods with G/LS/SA removed (i.e. where all objects in the PFlag range have been removed)

EA period (days)	
Mean	1.946
Median	1.627
Mode	0.664
Min	0.12 (0.091*)
Max	18.018
N	9,398
N < 0.2 days	50

Table 7-6: EA: Period statistics

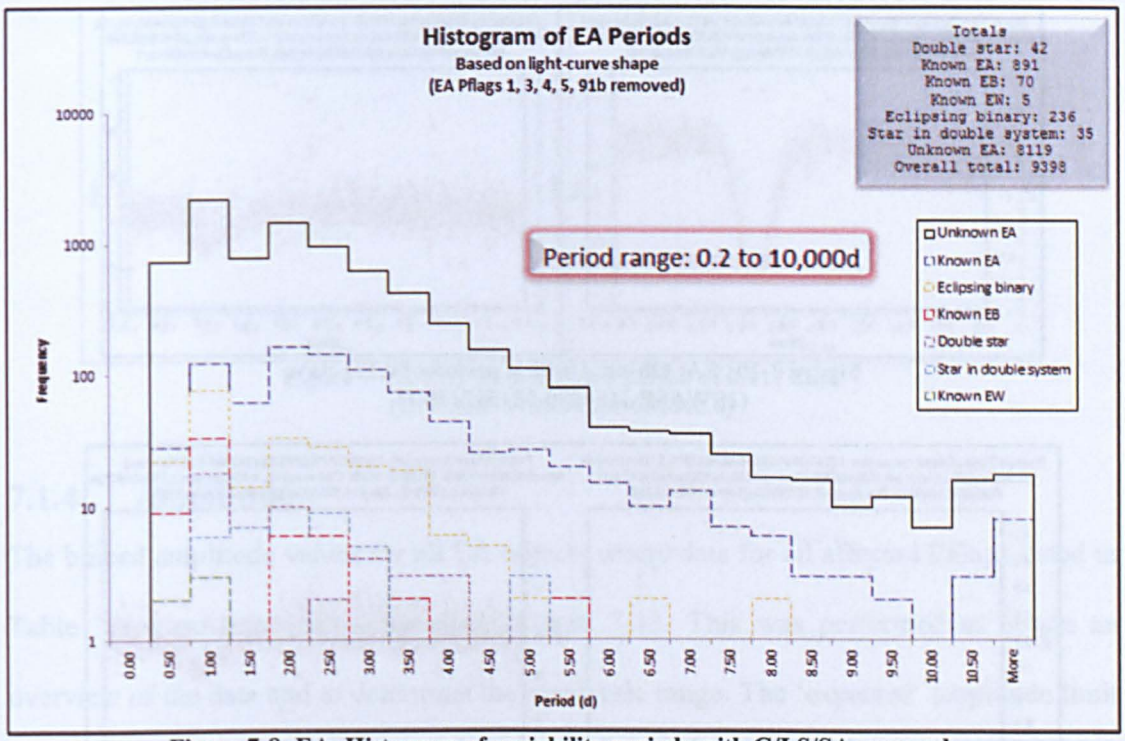

Figure 7-8: EA: Histogram of variability periods with G/LS/SA removed (i.e. where all objects in the PFlag range have been removed)

A 3D representation of Figure 7-8 can be seen on the support DVD at the location:

Light-curve output
X:\Chapter07\3D-hist\Fig_7-8.bmp

Where X is DVD-1 in the DVD-drive

The light-curves for the four objects with the shortest period (0.09, 0.111, 0.111 and 0.117 days) are shown in Figure 7-9 to Figure 7-12 respectively. The shortest period object in Figure 7-9 was classed 'Small amplitude' but also showed a large amount of scatter at the eclipse boundary. It was clear to see why the NNs classified this as an EA.

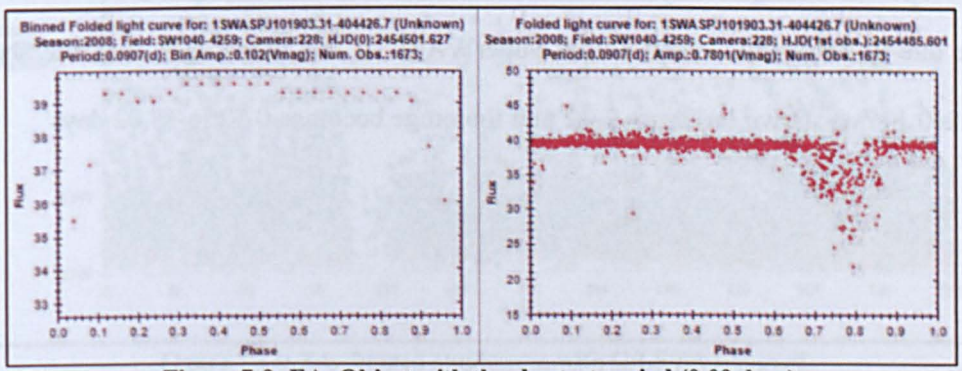

Figure 7-9: EA: Object with the shortest period (0.09 days) (1SWASP J101903.31-404426.7)

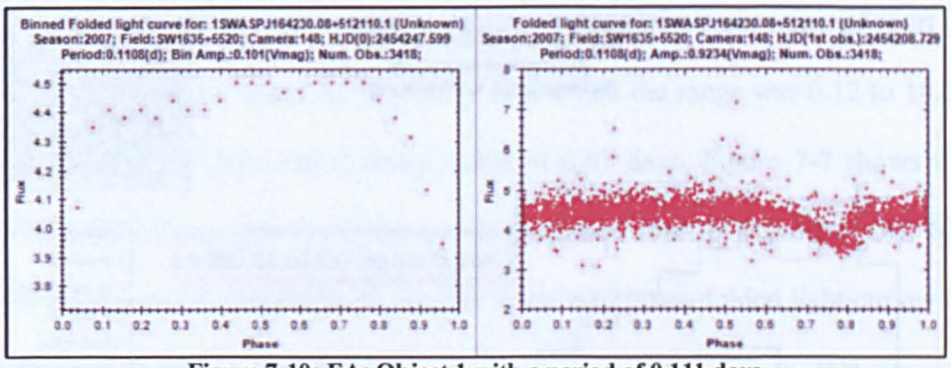

Figure 7-10: EA: Object 1 with a period of 0.111 days (1SWASP J164230.08+512110.1)

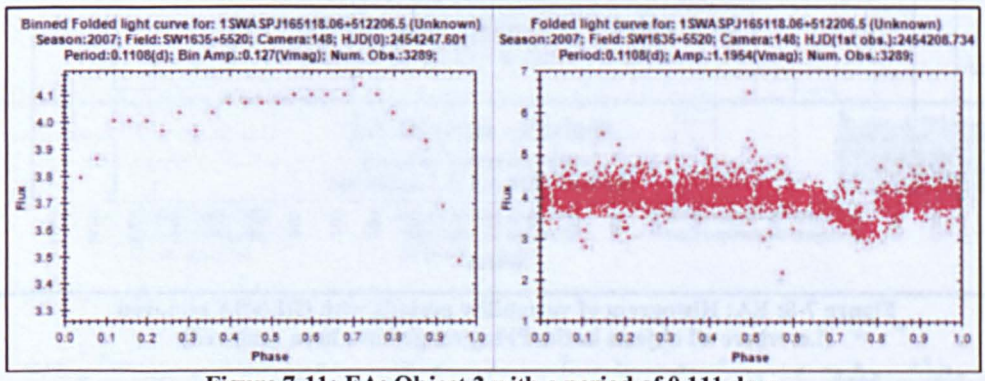

Figure 7-11: EA: Object 2 with a period of 0.111 days (1SWASP J165118.06+512206.5)

Figure 7-10 and Figure 7-11 look like good examples of EA objects, but it is possible that they are the same object with different SuperWASP object-ids as they have identical periods, almost identical light-curves, similar amplitudes and they are within a couple of degrees of each other in the sky (RA/Dec 250.625366/51.352810 and 252.825272/51.368484 respectively). Comparing all three objects together (Figure 7-9, Figure 7-10 and Figure 7-11) show a similar effect on the upward line of the eclipse and may be due to a systemic effect within SuperWASP. If this is the case, then the shortest period is 0.117 as shown in Figure 7-12 and the range becomes 0.12 to 18.02 days

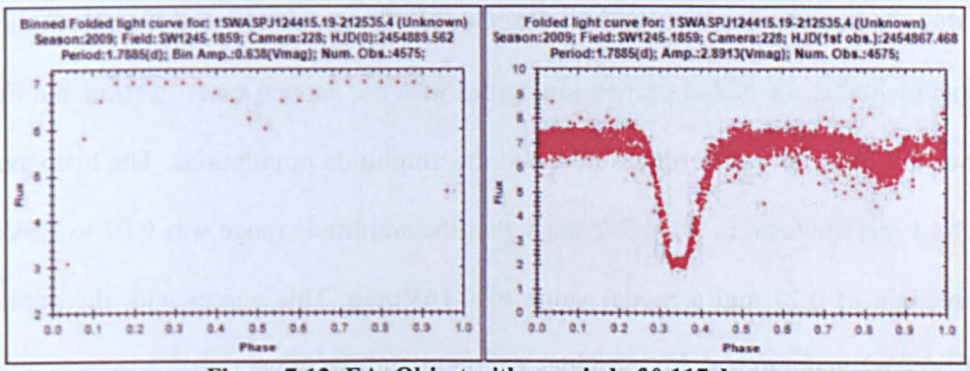

Figure 7-12: EA: Object with a period of 0.117 days (1SWASP J124420.23-084016.8)

7.1.4 Amplitude

The binned amplitude values for all EA objects where data for all affected PFlags listed in Table 7-5 were removed, is shown in Figure 7-13. This was performed to obtain an overview of the data and to determine the amplitude range. The 'expected' amplitude limit (several magnitudes) was obtained from the GCVS and included in the graph. A histogram of the amplitudes is shown in Figure 7-14. The histogram indicates that there are many objects with small amplitudes.

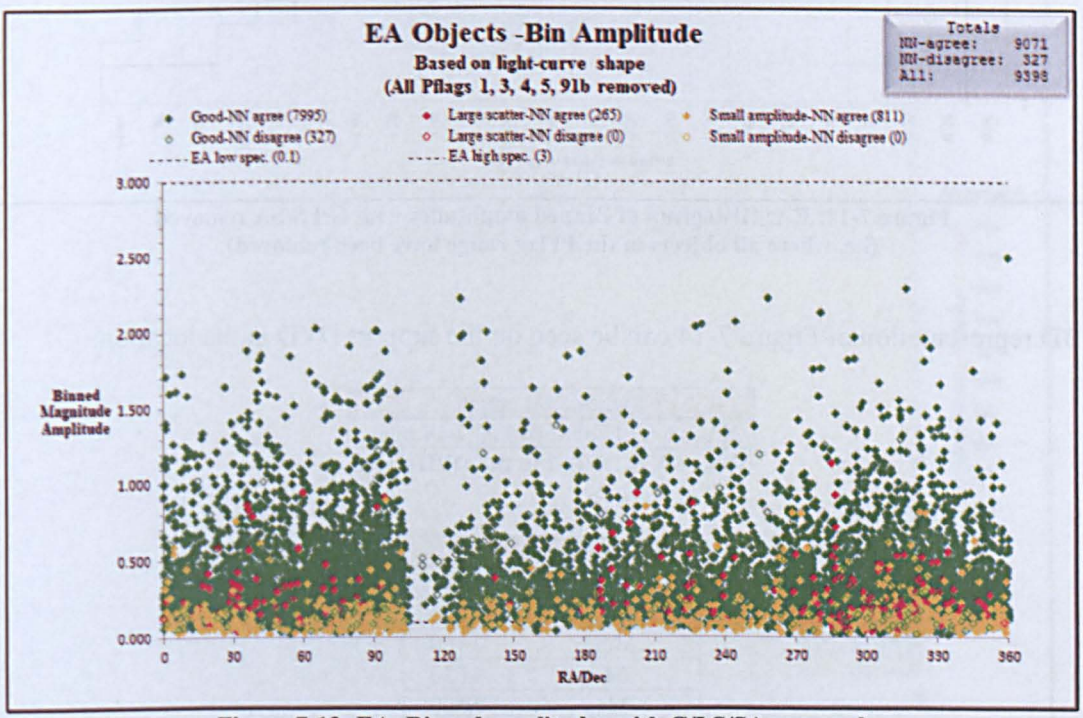

Figure 7-13: EA: Binned amplitudes with G/LS/SA removed (i.e. where all objects in the PFlag range have been removed)

Again, the graphs show the distributions for 'Good', 'Large scatter' and 'Small amplitude' objects and whether the NN-classification agrees with the manual-classification, but Figure 7-13 does not show any differences between the amplitude populations. The histogram in Figure 7-14 and the data in Table 7-7 show that the amplitude range was 0.02 to 2.5Vmag, with a median of 0.27 and a modal value of 0.16Vmag. This agrees with the published limit of 'several magnitudes', but provides a more definitive range.

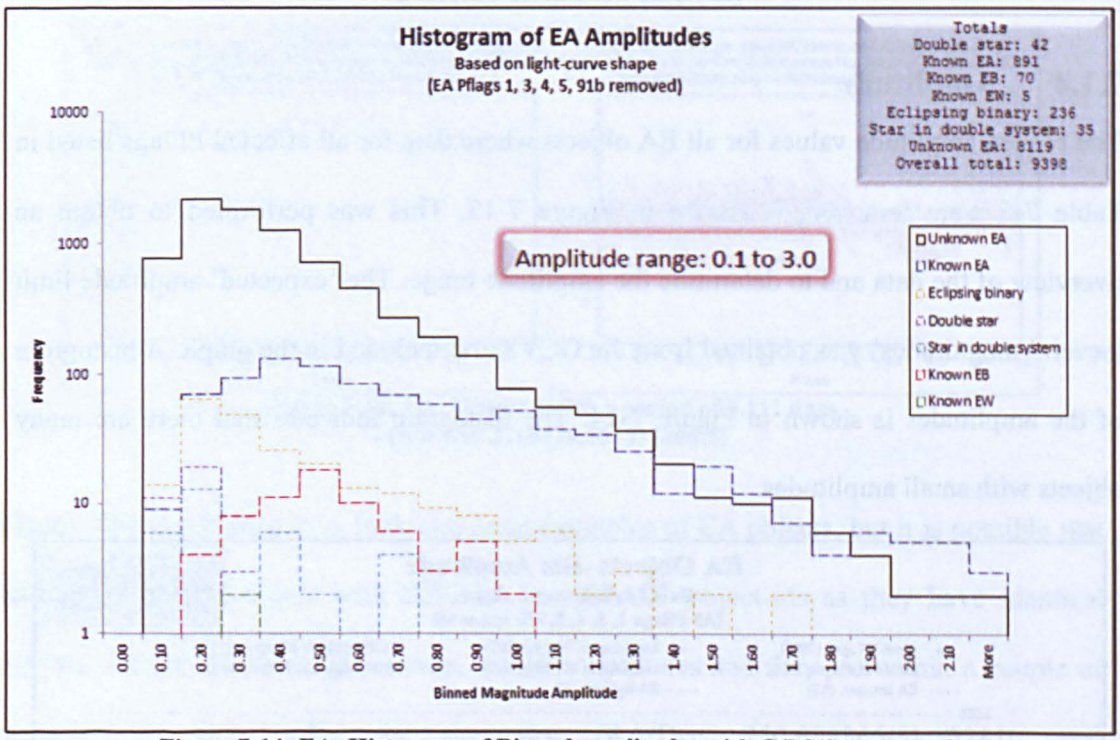

Figure 7-14: EA: Histogram of Binned amplitudes with G/LS/SA removed (i.e. where all objects in the PFlag range have been removed)

A 3D representation of Figure 7-14 can be seen on the support DVD at the location:

Light-curve output
X:\Chapter07\3D-hist\Fig_7-14.bmp

Where X is DVD-1 in the DVD-drive

EA amplitude (Vmag)	
Mean	0.357
Median	0.274
Mode	0.160
Min	0.020
Max	2.500
N	9,398
N > 3.0 Vmag	0

Table 7-7: EA: Amplitude statistics

Figure 7-15 shows the light-curve of the object with the highest amplitude.

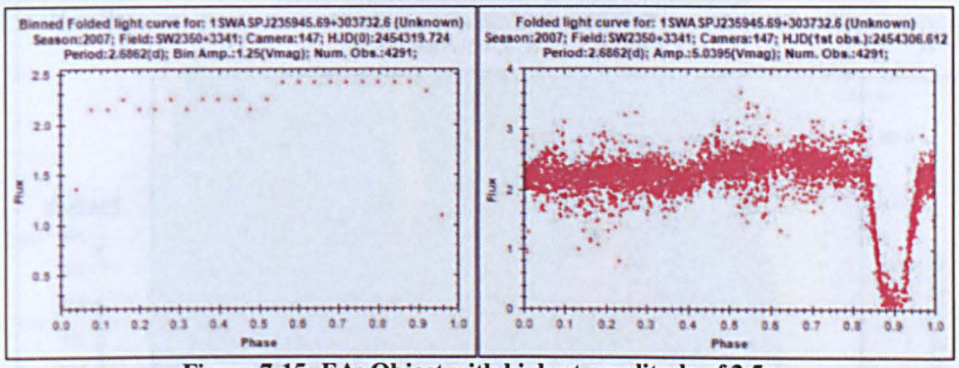

Figure 7-15: EA: Object with highest amplitude of 2.5v (1SWASP J235945.69+303732.6)

7.1.5 Period v Amplitude

Figure 7-16 shows a graph of Period v Amplitude for the EA objects and Figure 7-17 shows the range [Period 0:2, Amplitude 0:0.5] exploded in order to see the most active region of the graph. The graphs do not show any particular trend of amplitude with period, apart from the fact that the majority of 'Large scatter' and 'Small amplitude' objects having a period less than 4.0 days.

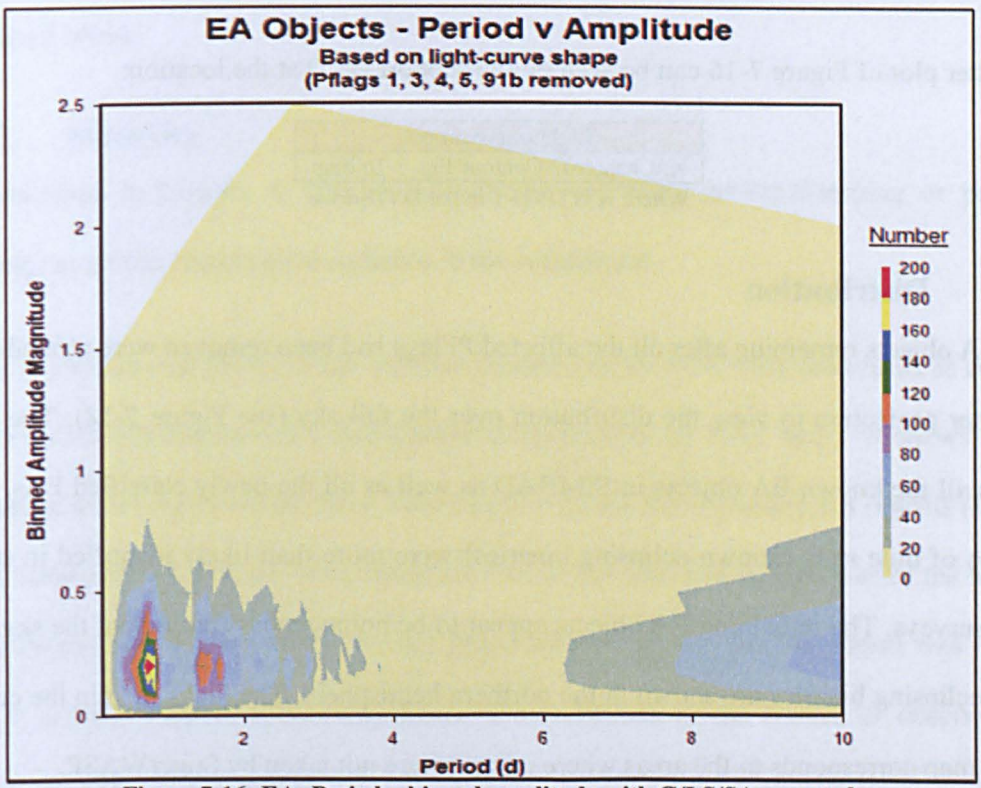

Figure 7-16: EA: Period v binned amplitude with G/LS/SA removed (i.e. where all objects in the PFlag range have been removed)

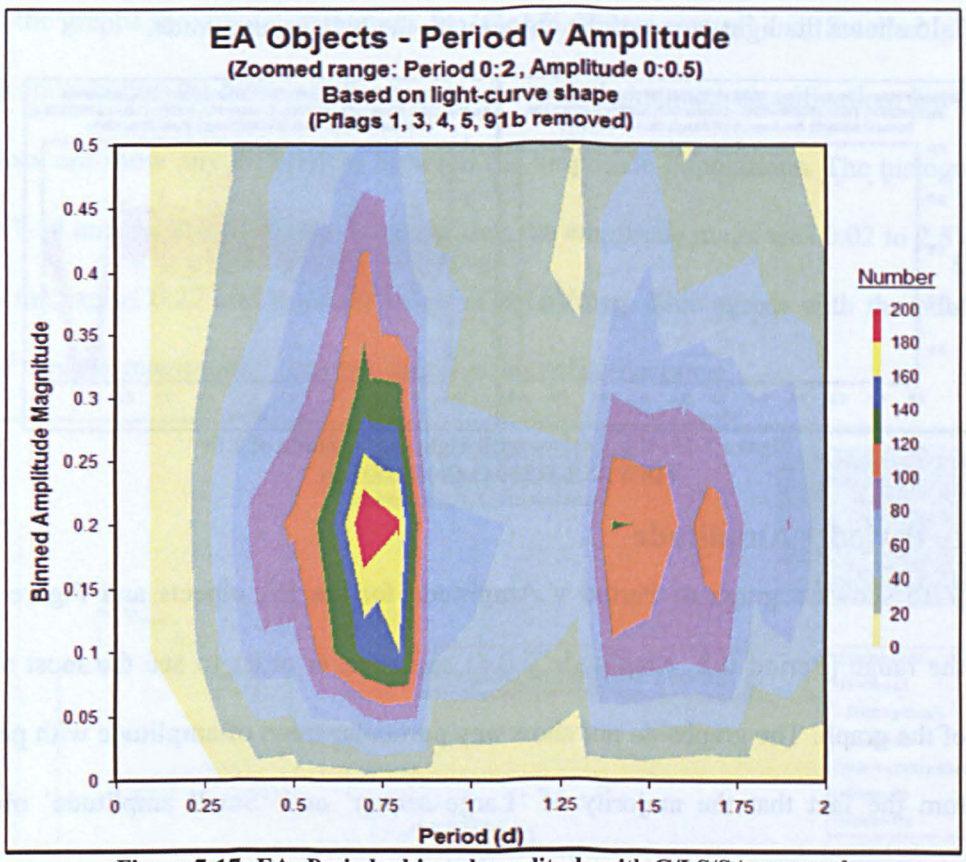

Figure 7-17: EA: Period v binned amplitude with G/LS/SA removed (Zoomed into range Period 0:2, Amplitude 0:0.5)

A scatter plot of Figure 7-16 can be seen on the support DVD at the location:

Light-curve output
X:\Chapter07\Contour\Fig_7-16.bmp

Where X is DVD-1 in the DVD-drive

7.1.6 Distribution

The EA objects remaining after all the affected PFlags had been removed were plotted on a Hammer projection to view the distribution over the full sky (see Figure 7-18). The map shows all the known EA objects in SIMBAD as well as all the newly classified EAs. The clumps of blue stars (known eclipsing binaries) were more than likely identified in small scale surveys. The remaining EA objects appear to be homogenous throughout the sky, but more eclipsing binaries are shown in the northern hemisphere. The blank area in the centre of the map corresponds to the areas where images were not taken by SuperWASP.

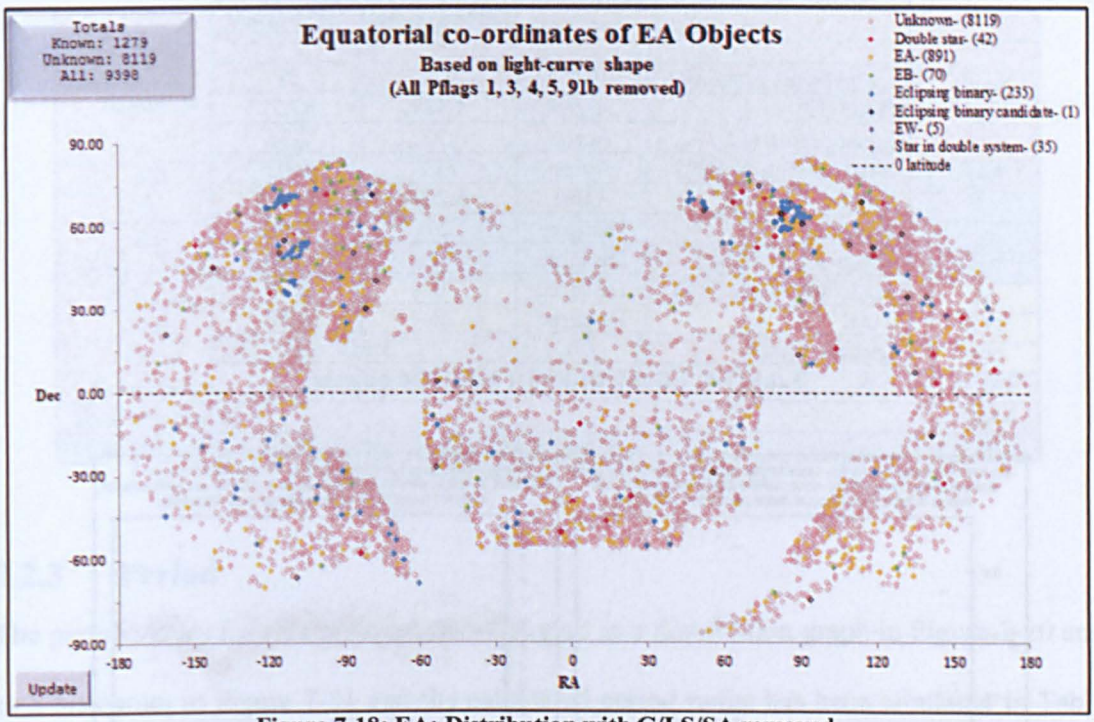

Figure 7-18: EA: Distribution with G/LS/SA removed
(i.e. where all objects in the PFlag range have been removed)

7.2. Analysis of EB objects

The analysis of EB objects followed the same process as for EA objects. The results are discussed below.

7.2.1 Statistics

As described in Chapter 6, the EB objects did not show period-clumping or period-banding, so all the objects were included in the assessment.

Table 7-8 shows that 99.5% of EB objects classified by the NNs were confirmed as correct by manual review and the 0.5% that disagreed consisted of 19 'EAs' and 7 'Reviews'. This was an excellent result for the NNs. Selecting one of the NN-classified EA objects (Figure 7-19) clearly shows why the NNs classified it as an EA the intra-eclipse part of the binned phase-folded light-curve is flat. The full phase-diagram shows that this object was in fact an EB and the flatness of the binned curve was caused by the scatter of observations around the start of the eclipse.

EB Objects		Based on light-curve shape	
		All	
Light-curve quality	NN	No.	%
Good (G)	Agree	4,558	87.22
Large scatter (LS)	Agree	123	2.35
Small amplitude (SA)	Agree	519	9.93
Total	Agree	5,200	99.50
Good (G)	Disagree	26	0.50
Large scatter (LS)	Disagree	0	0.00
Small amplitude (SA)	Disagree	0	0.00
Total	Disagree	26	0.50
Overall total	All	5,226	

Table 7-8: EB: Statistics for identified objects

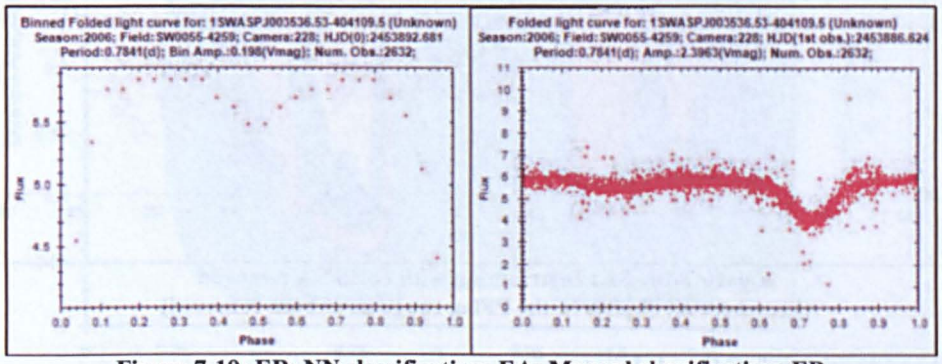

Figure 7-19: EB: NN classification: EA; Manual classification: EB (1SWASP J003536.53+404109.5)

7.2.2 Known objects

The same two searches were made for all 5,226 EBs that were performed for EAs in section 7.1.2. Of the 5,226 EB objects, 1,382 had a nearest neighbour within 1 arc-min. Appendix 21 shows the breakdown of these per class. Of the 1,382 known objects, 195 confirmed the NN EB class. 75 were EA, 72 were EW and 207 were 'other eclipsing' classes. The remainder consisted of pulsating objects; Stars; and 'Other'. The pulsating stars were included in the total of 'known' objects as they could possibly be incorrect classifications in SIMBAD, but 'Star' and 'Other' classes were added to the overall total of 'unknown' stars, giving a final total of 4,641 new EB eclipsing binaries.

As with the EAs, the known GCVS objects were identified at the time of 'LC Analyser classifier' data processing. 195 of the EB objects were known in the GCVS. These were also known in SIMBAD.

EB objects (Overall total = 5,226)							
SIMBAD	Based on light-curve shape						
	Good		Large scatter		Small amplitude		Total
	NN agree	NN disagree	NN agree	NN disagree	NN agree	NN disagree	All
EB	188	1	2	0	4	0	195
EA	70	3	1	0	1	0	75
EW	67	1	3	0	1	0	72
Other eclipsing	191	0	6	0	10	0	207
Pulsating	32	0	2	0	2	0	36
Star	470	0	8	0	49	0	527
Other	249	3	3	0	15	0	270
Total known	1,267	8	25	0	82	0	1,382
Total unknowns							3,844
Total unknowns (including Star and Other categories)							4,641

Table 7-9: EB: Objects known in SIMBAD

7.2.3 Period

The period values for all EB objects were plotted as a distribution graph in Figure 7-20 and as a histogram in Figure 7-21 and the calculated period range has been tabulated in Table 7-10. The 'expected' period limit (>1 day) was obtained from the GCVS and also plotted on the distribution graph.

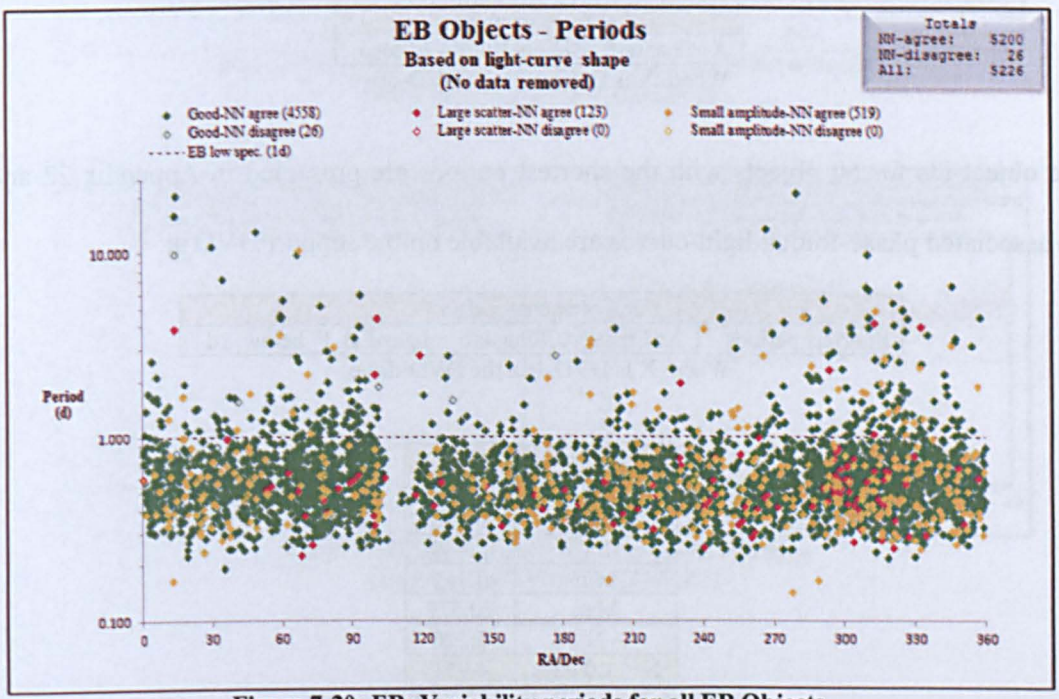

Figure 7-20: EB: Variability periods for all EB Objects

Figure 7-20 shows that no obvious differences were observed with regards to distribution, but the majority of objects had a period less than the published period limit of >1 day.

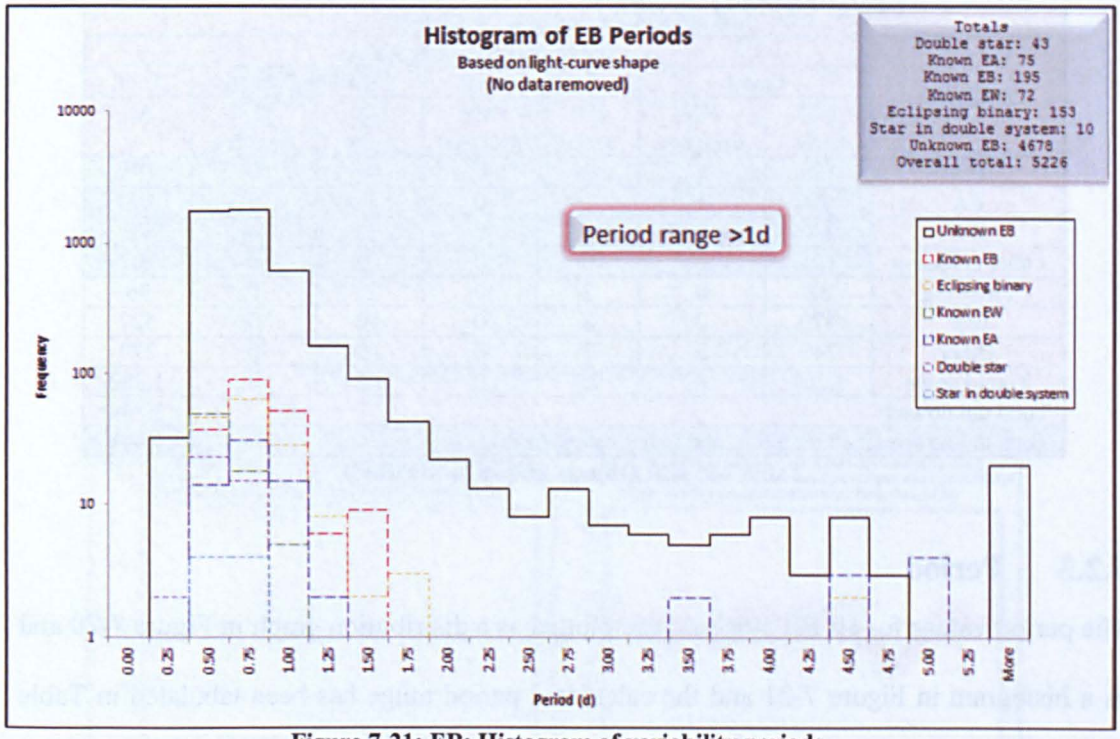

Figure 7-21: EB: Histogram of variability periods

A 3D representation of Figure 7-21 can be seen on the support DVD at the location:

Light-curve output
X:\Chapter07\3D-hist\Fig_7-20.bmp

Where X is DVD-1 in the DVD-drive

The object-ids for 50 objects with the shortest periods are presented in Appendix 22 and the associated phase-folded light-curves are available on the support DVD at:

Supplementary data	
Shortest periods	X:\Chapter07\Outside_ranges\EB_P_below_1d

Where X is DVD-1 in the DVD-drive

EB period (days)	
Mean	0.694
Median	0.560
Mode	0.480
Min	0.142
Max	20.572
N	5,226
N < 1.0 days	4,751

Table 7-10: EB: Period statistics

The histogram in Figure 7-21 contains a total of 5,226 EBs where 4,678 were 'unknown' and the remainder were known in SIMBAD. Table 7-10 shows that the period range was

0.14 to 20.57 days with a median of 0.56 days and a modal value of 0.48 days. Of the objects that lay below the published period limit, the three objects with the shortest period (0.14, 0.16 and 0.19 days) were selected and the light-curves presented in Figure 7-22, Figure 7-23 and Figure 7-24 respectively. These are all good examples of EB objects and therefore confirm the period range for EB objects using SuperWASP data is 0.14 to 20.58 days. This research proposes that the period of the object should not be used to classify EBs, but the ratio of the eclipse depths in the phase-folded light-curve itself. This is discussed further in section 7.6.

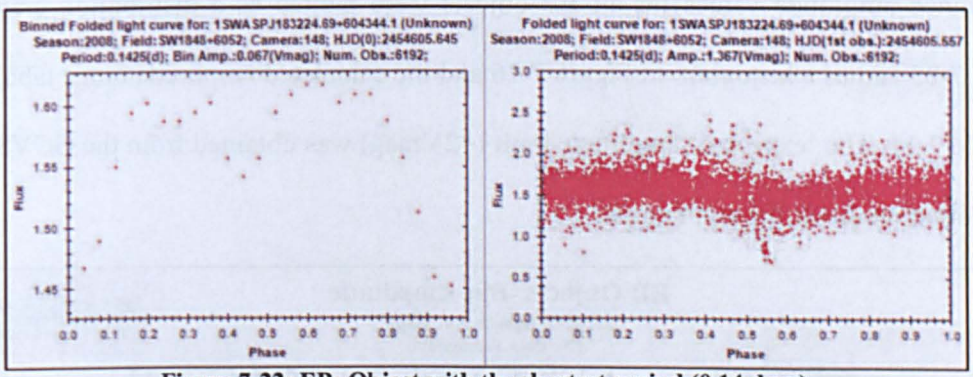

Figure 7-22: EB: Object with the shortest period (0.14 days) (1SWASP J183224.69+604344.1)

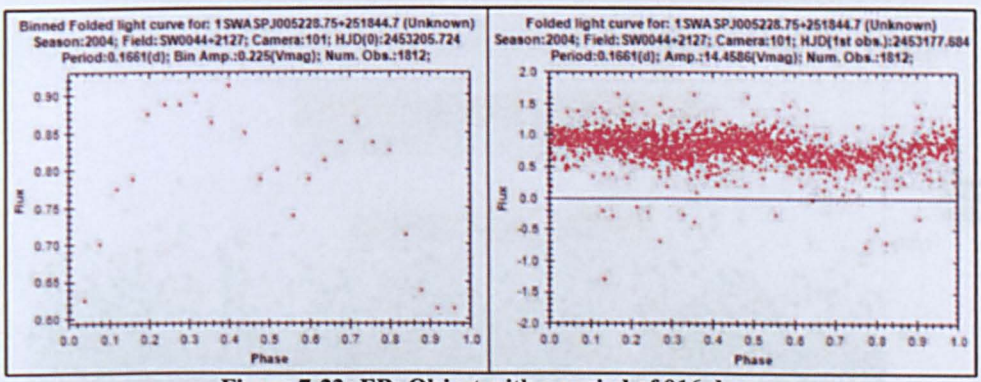

Figure 7-23: EB: Object with a period of 016 days (1SWASP J005228.75+251844.7)

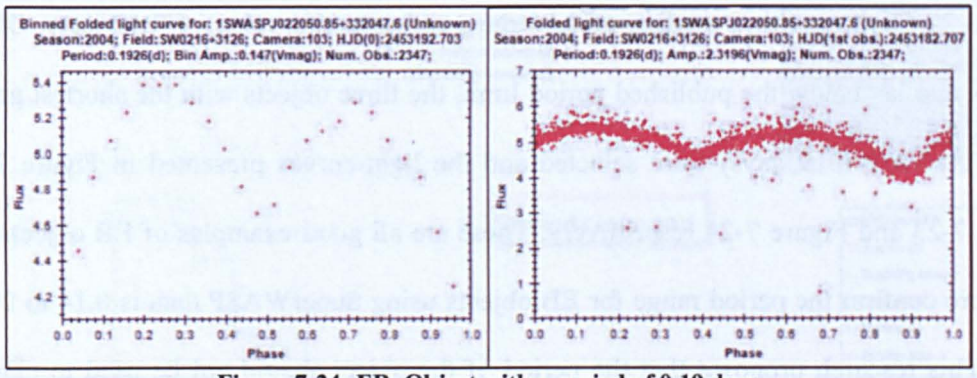

Figure 7-24: EB: Object with a period of 0.19 days (1SWASP J022050.85+332047.6)

7.2.4 Amplitude

The binned amplitude values for all EB objects were plotted as a distribution graph in Figure 7-25 and as a histogram in Figure 7-26 and the calculated amplitude range tabulated in Table 7-11. The 'expected' amplitude limit (<2Vmag) was obtained from the GCVS and also plotted on the distribution graph.

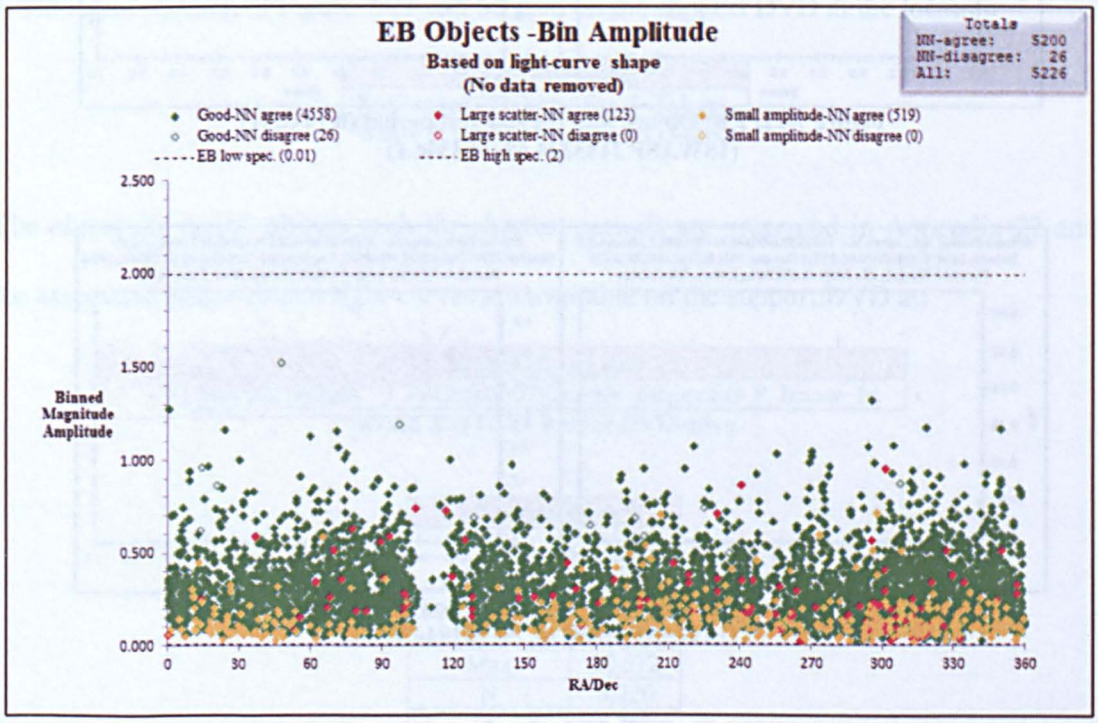

Figure 7-25: EB: Binned amplitudes

Figure 7-25 shows no significant difference between the amplitude populations and all the objects lay within the published amplitude limit. The histogram in Figure 7-26 and the data

in Table 7-11 show that the amplitude range was 0.02 to 1.52Vmag, with a median of 0.25 and a modal value of 0.15Vmag. This agrees well with the published limit of <2Vmag, but provides a more definitive range.

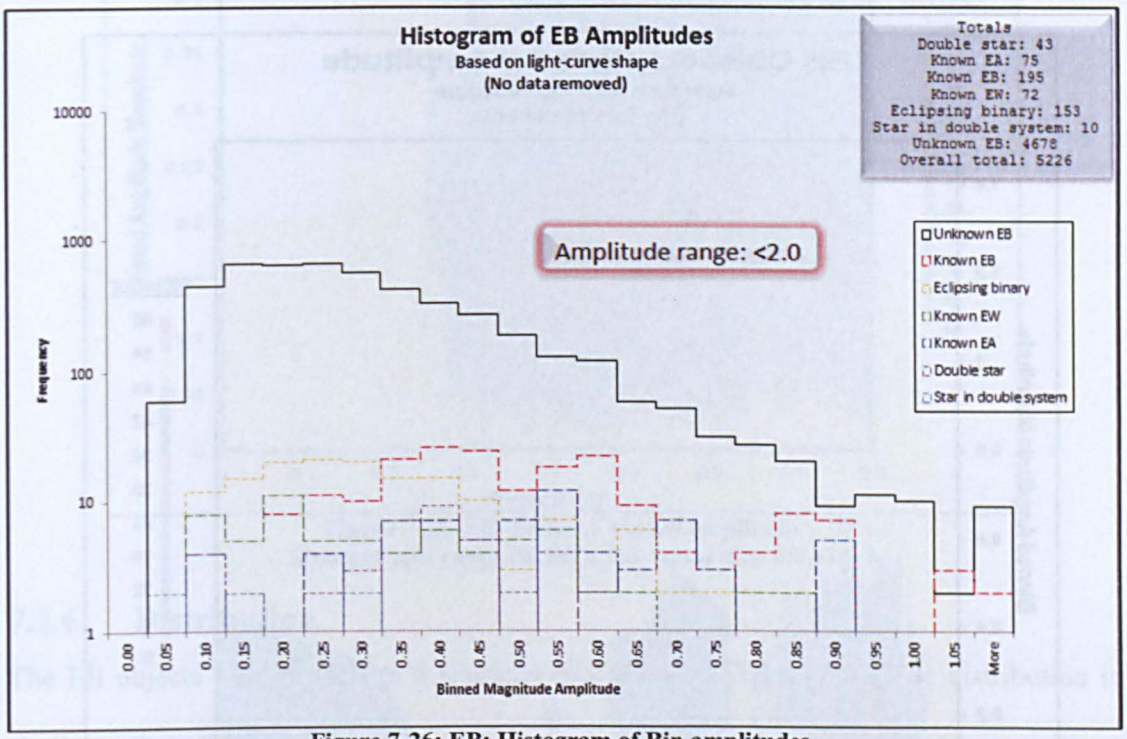

Figure 7-26: EB: Histogram of Bin amplitudes

A 3D representation of Figure 7-26 can be seen on the support DVD at the location:

Light-curve output
X:\Chapter07\3D-hist\Fig_7-25.bmp

EB amplitude (Vmag)	
Mean	0.290
Median	0.252
Mode	0.154
Min	0.020
Max	1.522
N	5,226
N > 2.0 Vmag	0

Table 7-11: EB: Amplitude statistics

7.2.5 Period v Amplitude

The period v amplitude graphs for EBs in Figure 7-27 and Figure 7-28 do not show any particular trend apart from the majority of 'Small amplitude' objects that have a period of less than 4.0 days.

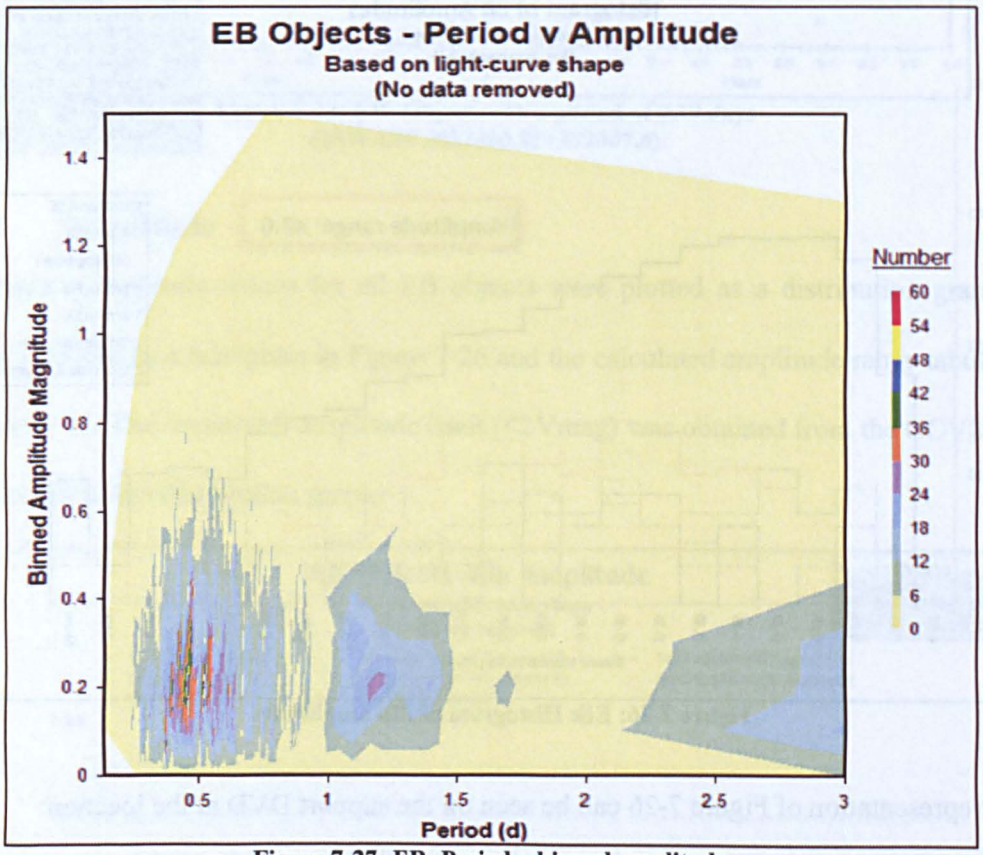

Figure 7-27: EB: Period v binned amplitude

A scatter plot of Figure 7-27 can be seen on the support DVD at the location:

Light-curve output
X:\Chapter07\Contour\Fig_7-26.bmp

Where X is DVD-1 in the DVD-drive

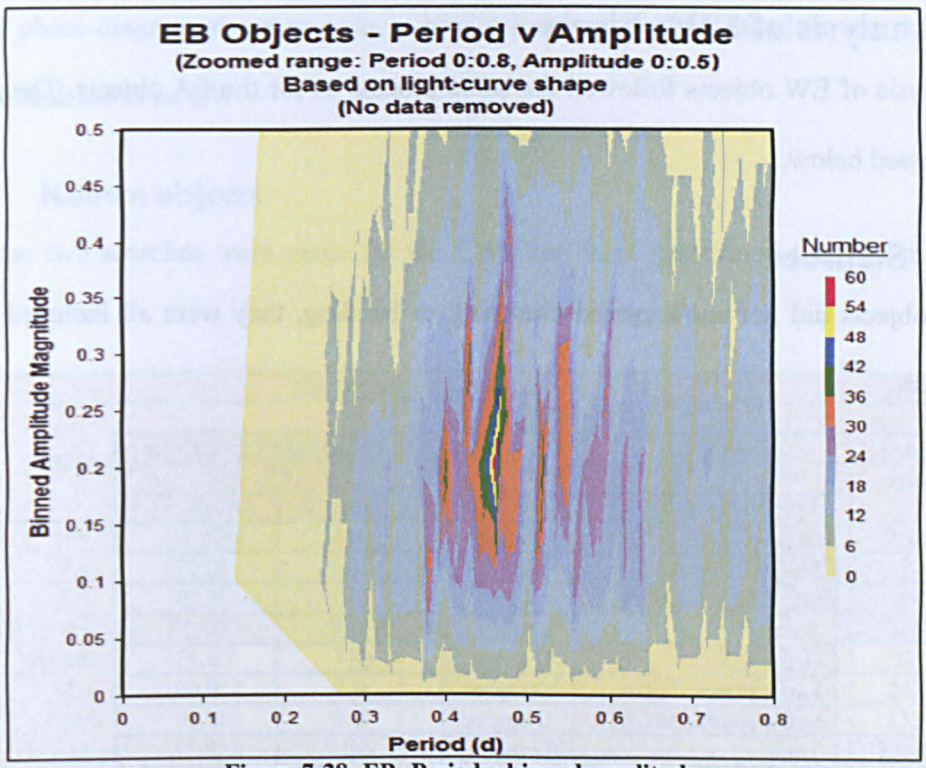

Figure 7-28: EB: Period v binned amplitude
(Zoomed into range Period 0:0.8, Amplitude 0:0.5)

7.2.6 Distribution

The EB objects were plotted as a Hammer projection in Figure 7-29. The distribution is similar to that of EA objects.

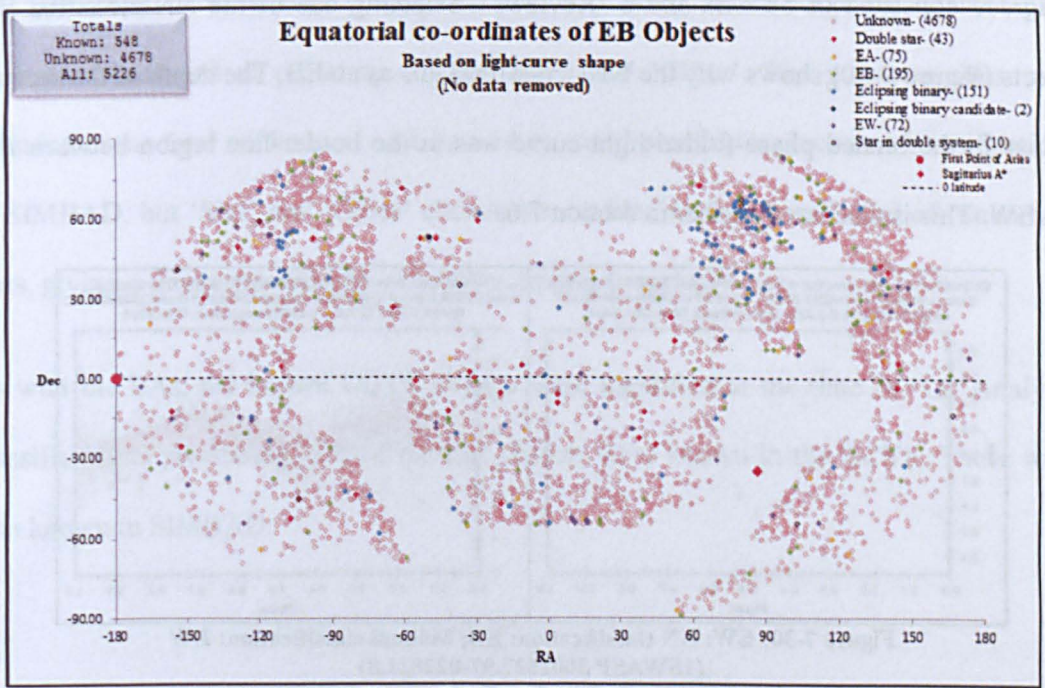

Figure 7-29: EB: Distribution

7.3. Analysis of EW objects

The analysis of EW objects followed the same process as for the EA objects. The results are discussed below.

7.3.1 Statistics

As EW objects did not show period-clumping or banding, they were all included in the assessment.

EW Objects		Based on light-curve shape	
		All	
Light-curve quality	NN	No.	%
Good (G)	Agree	2,746	95.51
Large scatter (LS)	Agree	28	0.97
Small amplitude (SA)	Agree	37	1.29
Total	Agree	2,811	97.77
Good (G)	Disagree	64	2.23
Large scatter (LS)	Disagree	0	0.00
Small amplitude (SA)	Disagree	0	0.00
Total	Disagree	64	2.23
Overall total	All	2,875	

Table 7-12: EW: Statistics for identified objects

Table 7-12 shows that 97.8% of EW objects classified by the NNs were confirmed by manual review. This was an excellent result for the NNs. The 2.2% of objects that disagreed consisted of 58 EBs and 6 'Reviews'. Selecting one of the NN-classified EB objects (Figure 7-30) shows why the NNs classified this as an EB. The depth of the second eclipse in the binned phase-folded light-curve was in the border-line region between EB and EW. This is discussed further in section 7.6.

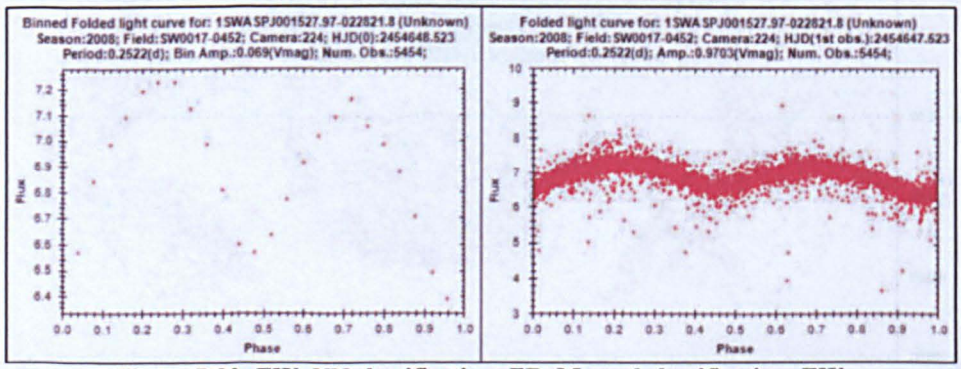

Figure 7-30: EW: NN classification: EB; Manual classification: EW (1SWASP J001527.97-022821.8)

The full phase-diagram above was also a border-line case in the manual review, but it was finally classified as an EW.

7.3.2 Known objects

The same two searches were made for the EWs that were performed for EAs in section 7.1.2.

EW objects (Overall total = 2,875)							
SIMBAD	Based on light-curve shape						
	Good		Large scatter		Small amplitude		Total
	NN agree	NN disagree	NN agree	NN disagree	NN agree	NN disagree	All
EW	200	3	3	0	0	0	206
EA	3	0	0	0	0	0	3
EB	9	0	0	0	0	0	9
Other eclipsing	358	10	5	0	2	0	375
Pulsating	29	1	1	0	0	0	31
Star	232	2	1	0	8	0	243
Other	126	5	1	0	1	0	133
Total known	957	21	11	0	11	0	1,000
Total unknowns							1,875
Total unknowns (including Star and Other categories)							2,251

Table 7-13: EW: Objects known in SIMBAD

Of the 2,875 EW objects, 1,000 had a nearest neighbour within 1 arc-min. Appendix 23 shows the breakdown of these per class. Of the 1,000 known objects, 206 confirmed the NN EW class. 3 were EA, 9 were EB and 375 were 'other eclipsing' classes. The remainder consisted of pulsating objects; Stars; and 'Other'. The pulsating stars were included in the total of 'known' objects as they could possibly be incorrect classifications in SIMBAD, but 'Star' and 'Other' classes were added to the overall total of 'unknown' stars, giving a final total of 2,251 new EW eclipsing binaries.

As with the EAs, the known GCVS objects were identified at the time of 'LC Analyser classifier' data processing. 105 of the EW objects were known in the GCVS. These were also known in SIMBAD.

7.3.3 Period

The period values for all EW objects were plotted as a distribution graph in Figure 7-31 and as a histogram in Figure 7-32 and the calculated period range was tabulated in Table 7-14. The 'expected' period limit (<1 day) obtained from the GCVS was also plotted on the distribution graph. Figure 7-31 shows that no obvious differences were observed with regards to the distribution, but 25 objects had a variability period greater than the GCVS published period limit of '<1 day'. The object-ids of all objects with a longer than expected period are listed in Appendix 24 and the associated phase-folded light-curves are available on the support DVD at:

Supplementary data	
Longer periods	X:\Chapter07\Outside_ranges\EW_P_above_1d

Where X is DVD-1 in the DVD-drive

Figure 7-32 contains a total of 2,875 EWs where 2,286 of them were 'unknown' and the remainder known in SIMBAD. Table 7-14 shows that the period range for EW objects was 0.18 to 3.6 days with a median of 0.34 days and a modal value of 0.26 days.

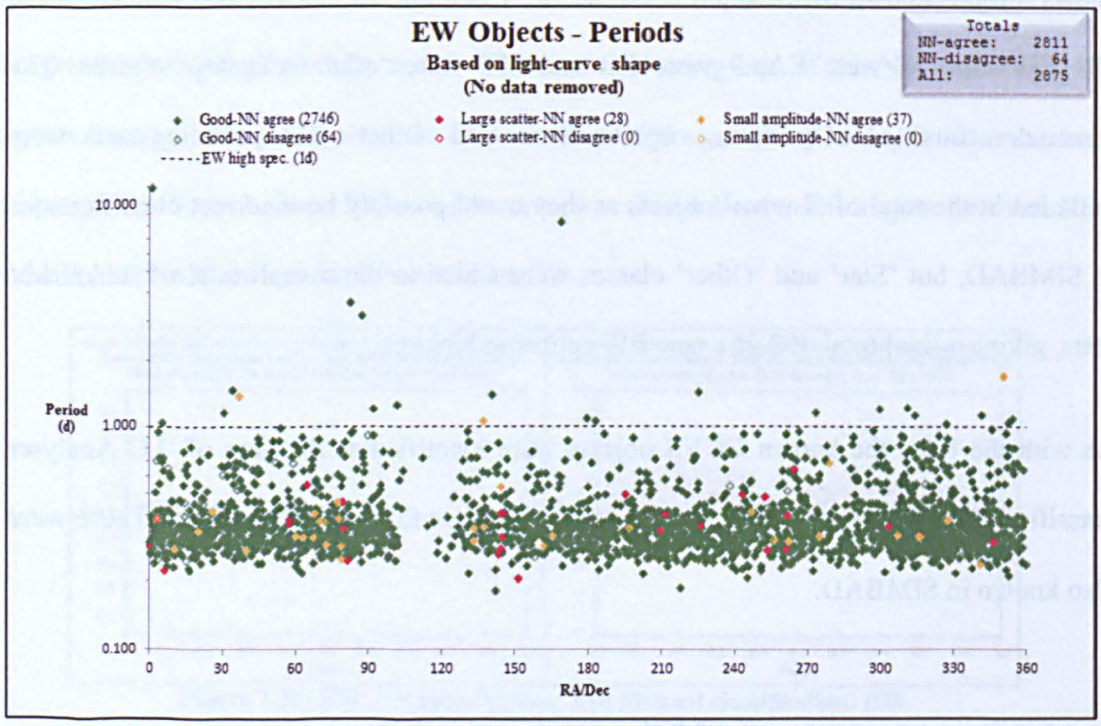

Figure 7-31: EW: Variability periods

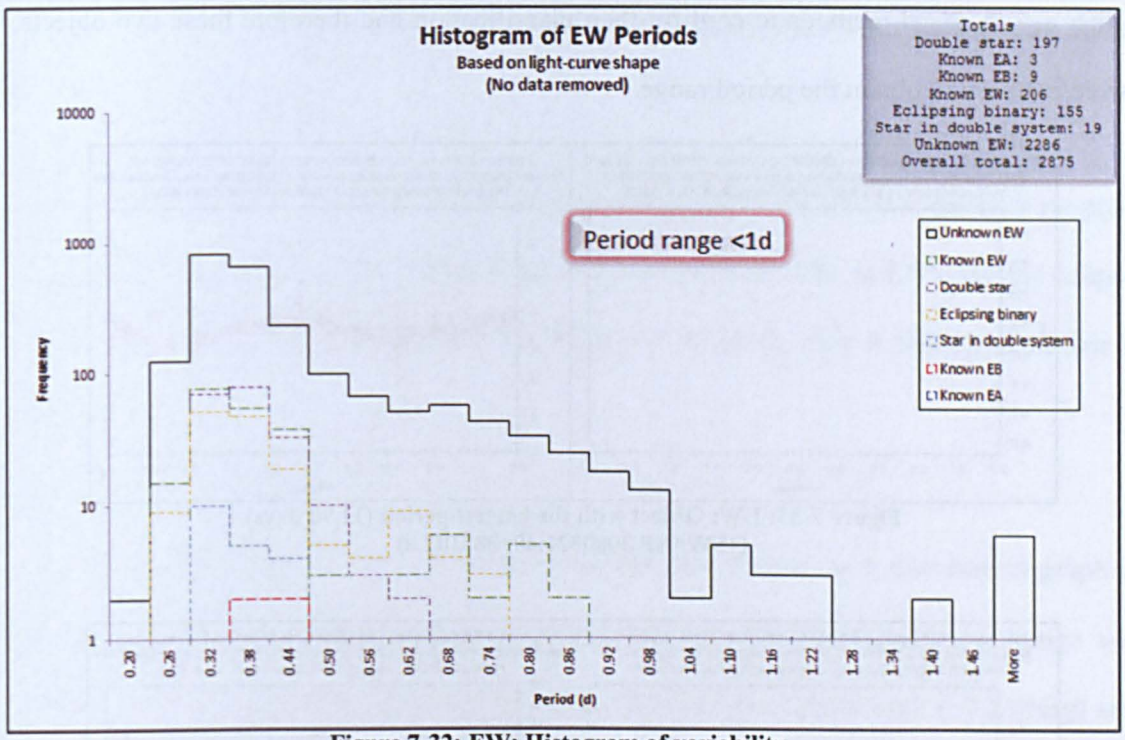

Figure 7-32: EW: Histogram of variability

A 3D representation of Figure 7-32 can be seen on the support DVD at the location:

Light-curve output
X:\Chapter07\3D-hist\Fig_7-30.bmp

EW period (days)	
Mean	0.389
Median	0.337
Mode	0.262
Min	0.184
Max	3.62 (11.904)
N	2,875
N > 1.0 days	25

Table 7-14: EW: Period statistics

Of the 25 objects that displayed periods above the published period limit, the three objects with the longest period (11.90, 8.32 and 3.62 days) were selected and the light curves for these objects are displayed in Figure 7-33, Figure 7-34 and Figure 7-35 respectively. These objects all showed binned phase-folded light-curves that have definite EW shape. The full phase-folded light-curve of the first two objects show a similar scatter on the light-curve to that observed in some semi-regular variables. These therefore need to be followed-up using

other astronomical methods to confirm their classification and therefore these two objects were not used to obtain the period range.

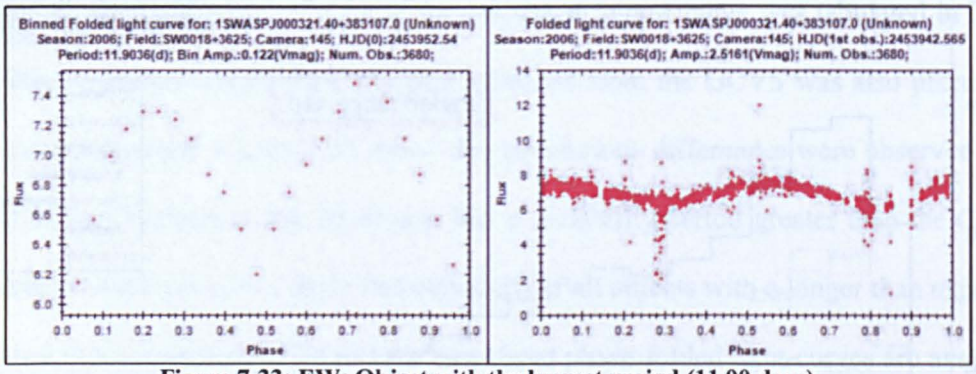

Figure 7-33: EW: Object with the longest period (11.90 days) (1SWASP J000321.40+383107.0)

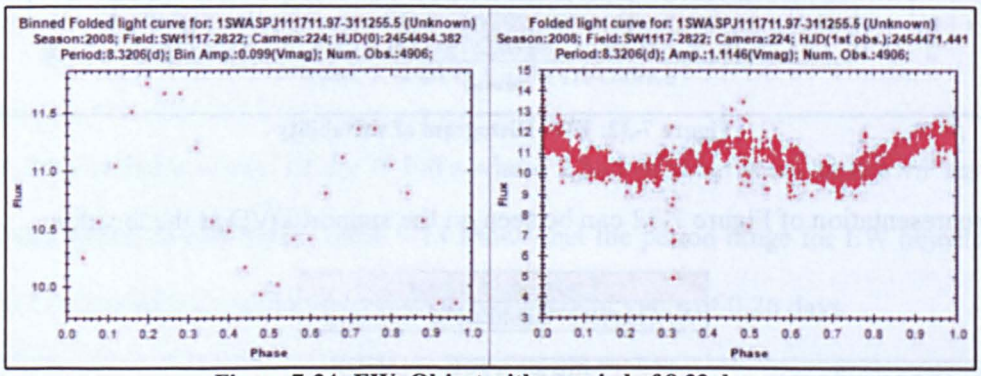

Figure 7-34: EW: Object with a period of 8.32 days (1SWASP J111711.97-311255.5)

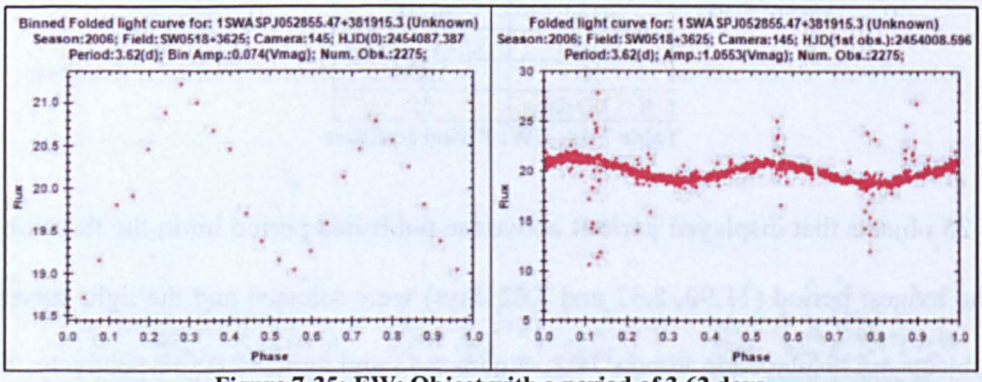

Figure 7-35: EW: Object with a period of 3.62 days (1SWASP J052855.47+381915.3)

The third object shows some scatter in the observations, but it was similar to many other EW light-curves and it has a definite EW shape. It was therefore included in the period

range. The period range for EW objects using SuperWASP data was therefore determined to be 0.18 to 3.62 days.

Due to the similarity in period values between EB and EW objects, this research proposes that the period of these objects should not be used to classify EBs or EWs, but the eclipse-depth ratio of the phase-folded light-curve should be used. This is discussed further in section 7.6.

7.3.4 Amplitude

The binned amplitude values for the EW objects were plotted as a distribution graph in Figure 7-36 and as a histogram in Figure 7-37. The calculated amplitude range was tabulated and is presented in Table 7-15. The 'expected' amplitude limit (<0.8Vmag) was obtained from the GCVS and also included on the distribution graph.

Figure 7-36 shows no significant difference between the amplitude populations, but 39 objects had amplitude values greater than the published limit of <0.8Vmag.

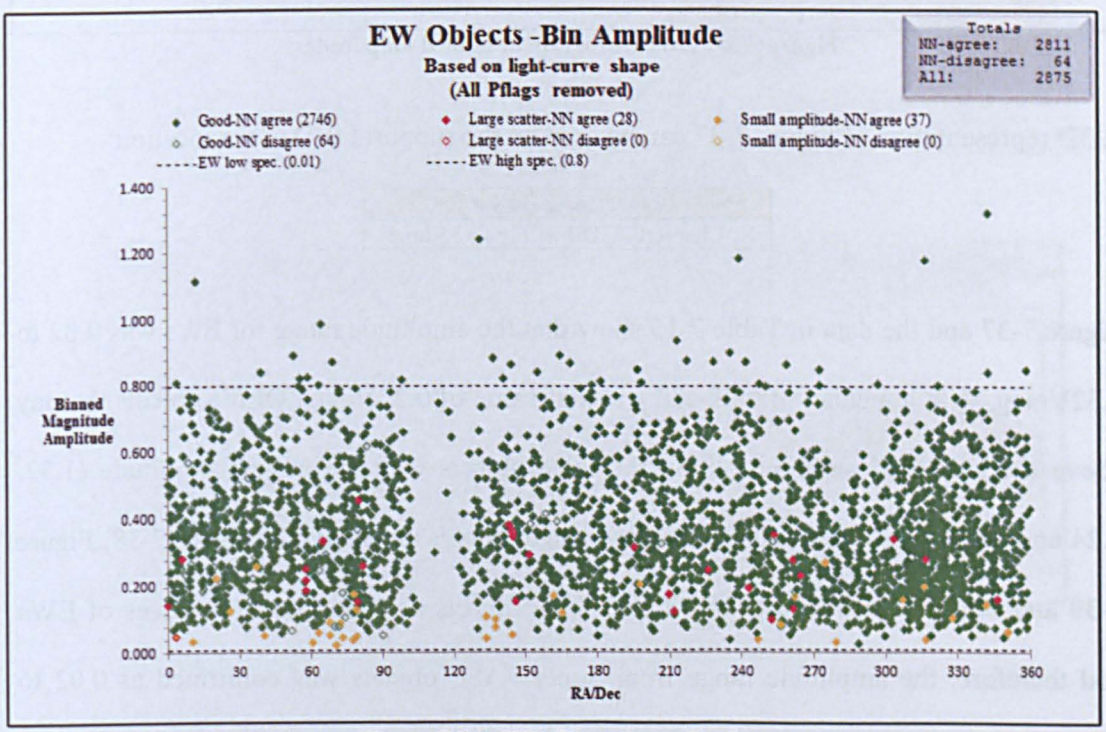

Figure 7-36: EW: Binned amplitudes

The object-ids are listed in Appendix 25 and the associated phase-folded light-curves are available on the support DVD at:

Supplementary data	
Higher amplitudes	X:\Chapter07\Outside_ranges\EW_A_above_0_8Vmag

Where X is DVD-1 in the DVD-drive

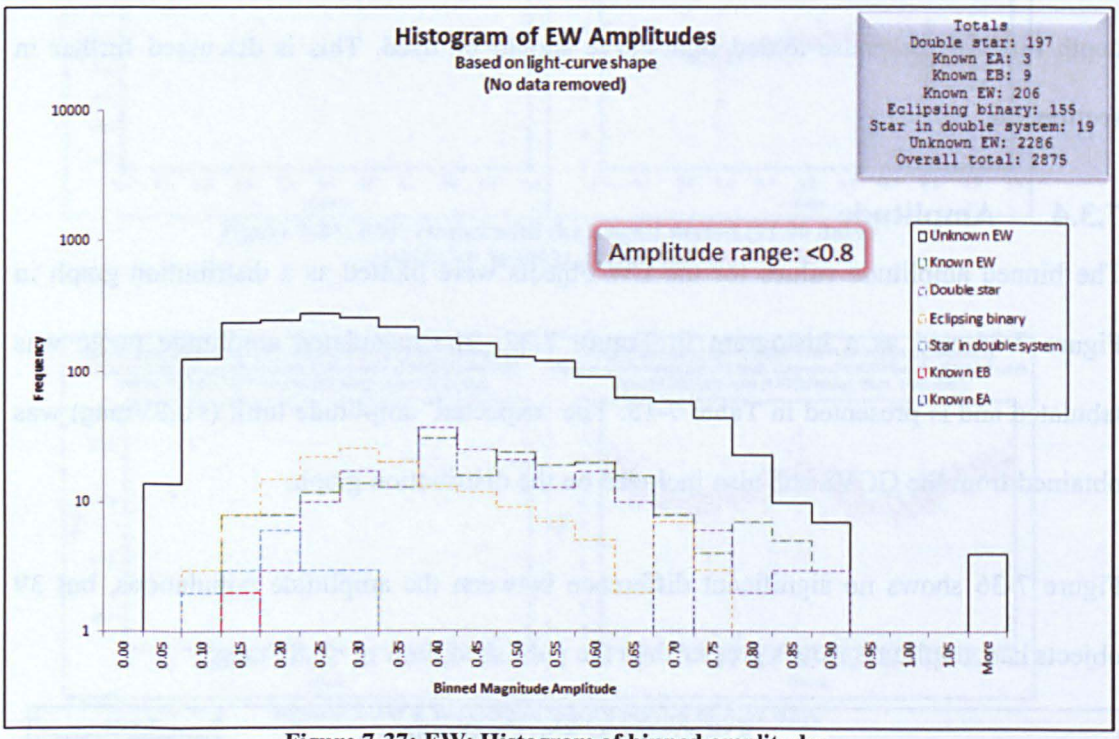

Figure 7-37: EW: Histogram of binned amplitudes

A 3D representation of Figure 7-37 can be seen on the support DVD at the location:

Light-curve output
X:\Chapter07\3D-hist\Fig_7-35.bmp

Figure 7-37 and the data in Table 7-15 show that the amplitude range for EWs was 0.02 to 1.32Vmag, with a median of 0.32 and a modal value of 0.27Vmag. Of the objects that lay above the published amplitude limit, the three objects with the largest amplitude (1.32, 1.24 and 1.18Vmag) were selected and their light curves are shown in Figure 7-38, Figure 7-39 and Figure 7-40 respectively. These three objects are good representatives of EWs and therefore, the amplitude range from SuperWASP objects was confirmed as 0.02 to 1.32Vmag.

EW amplitude (Vmag)	
Mean	0.349
Median	0.320
Mode	0.268
Min	0.022
Max	1.320
N	2,875
N > 0.8 Vmag	39

Table 7-15: EW: Amplitude statistics

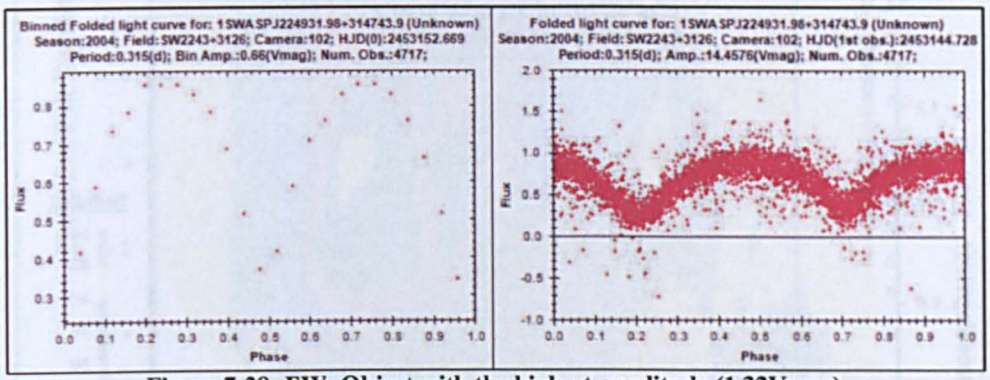

Figure 7-38: EW: Object with the highest amplitude (1.32Vmag) (1SWASP J224931.98+314743.9)

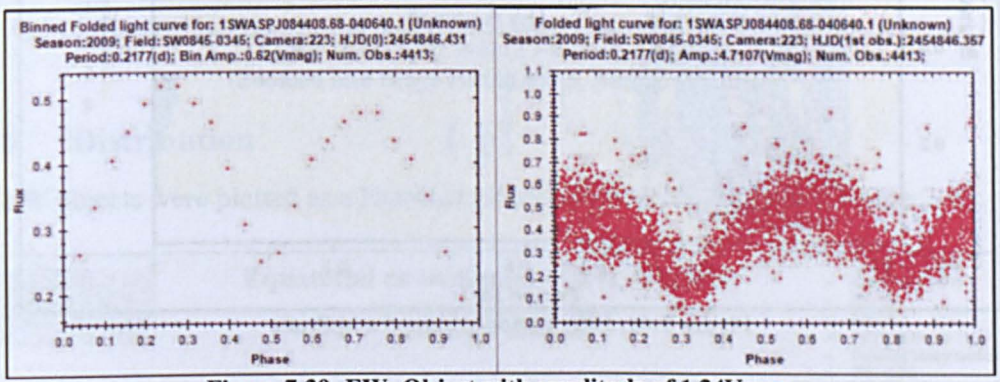

Figure 7-39: EW: Object with amplitude of 1.24Vmag (1SWASP J084408.68-040640.1)

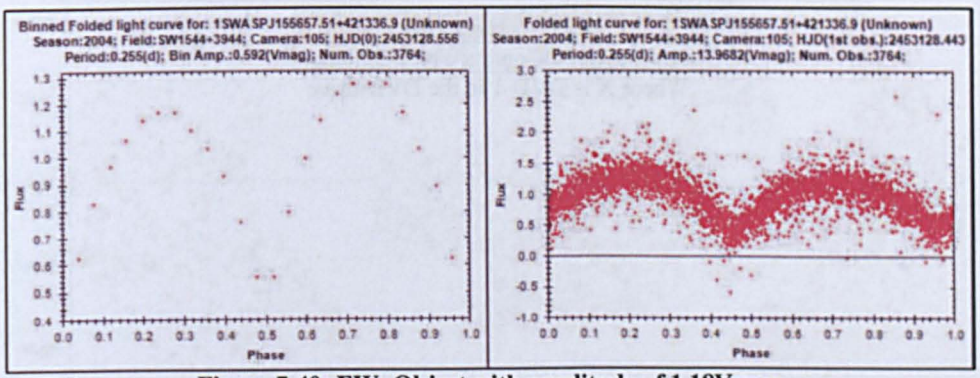

Figure 7-40: EW: Object with amplitude of 1.18Vmag (1SWASP J155657.51+421336.9)

7.3.5 Period v Amplitude

The period v amplitude graphs for EWs in Figure 7-41 and Figure 7-42 do not show any particular trend apart from confirming the fact that the majority of EW objects have a period of less than 4.0 days.

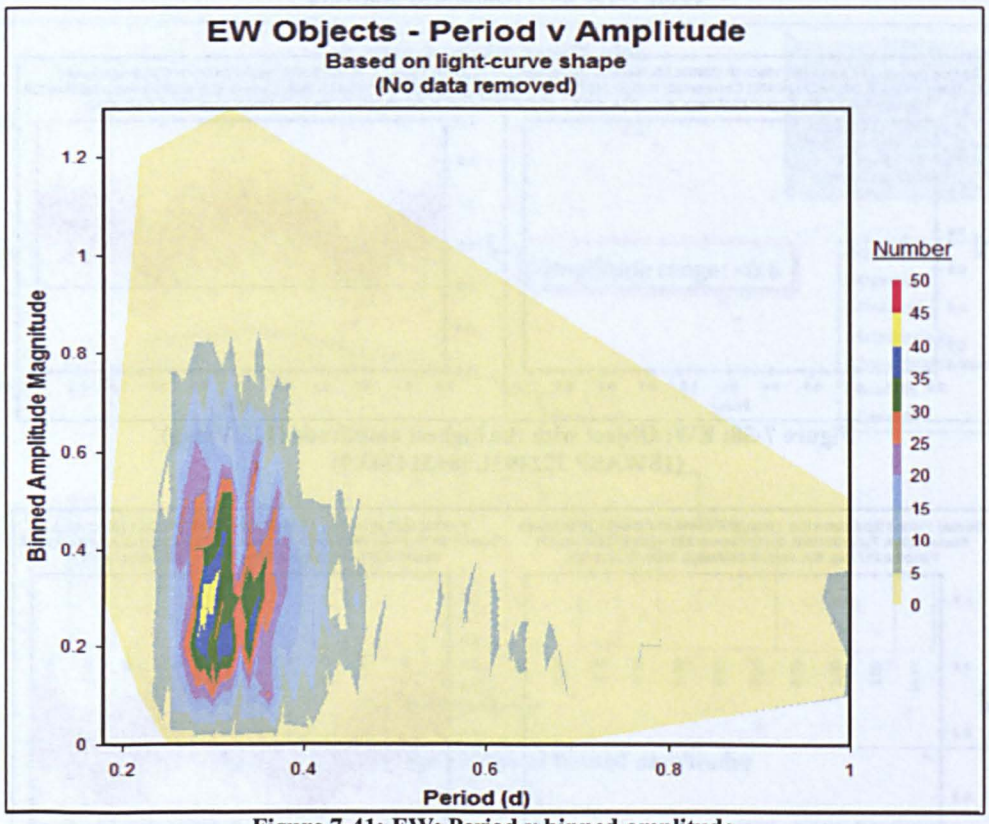

Figure 7-41: EW: Period v binned amplitude

A scatter plot of Figure 7-41 can be seen on the support DVD at the location:

Light-curve output
X:\Chapter07\Contour\Fig_7-39.bmp

Where X is DVD-1 in the DVD-drive

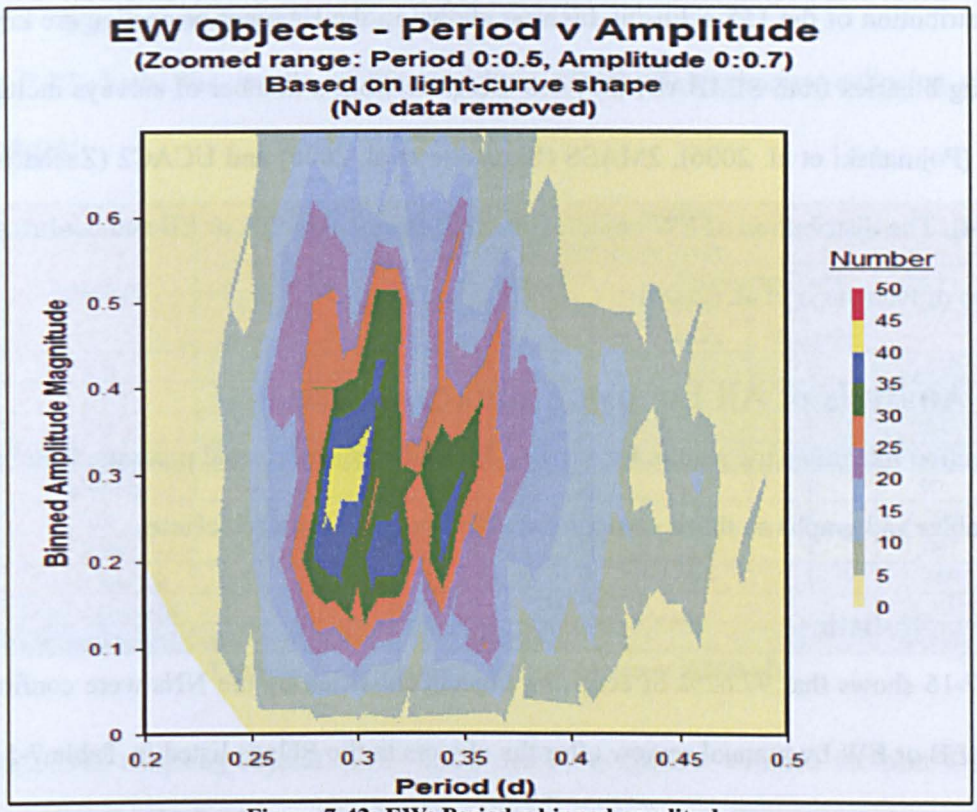

Figure 7-42: EW: Period v binned amplitude
(Zoomed into range Period 0:0.5, Amplitude 0:0.7)

7.3.6 Distribution

The EW objects were plotted as a Hammer projection which is shown in Figure 7-43.

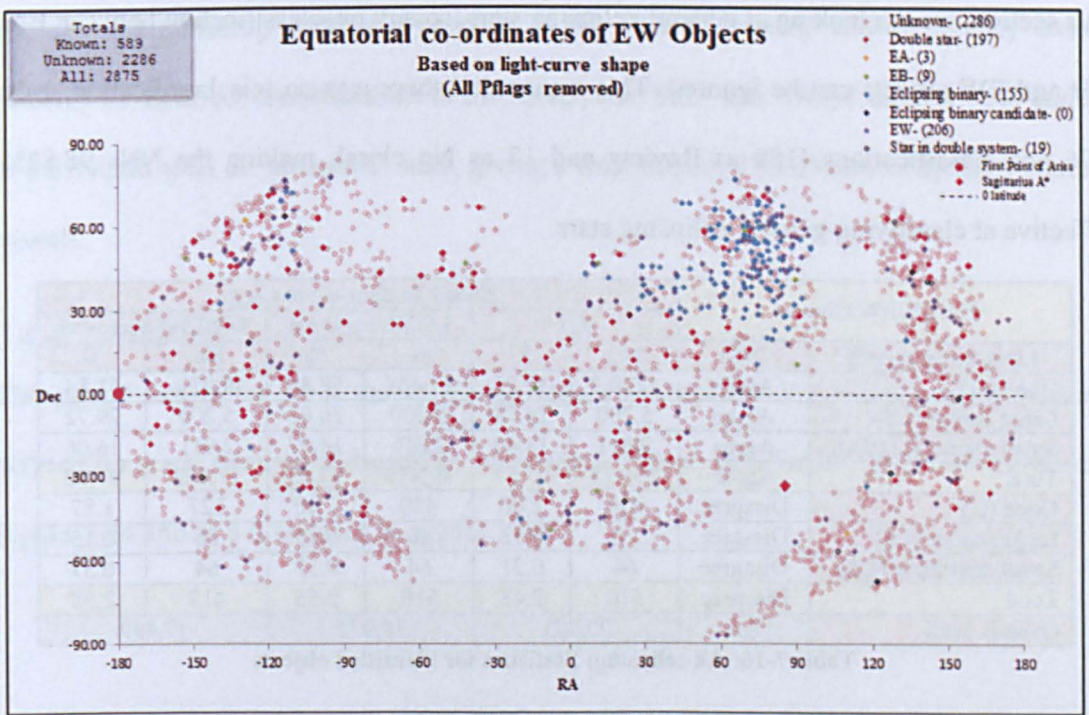

Figure 7-43: EW: Distribution

The distribution of the 155 eclipsing binaries shown in the Hammer projection are known eclipsing binaries from SIMBAD, they are therefore from a number of surveys including ASAS (Pojmański et al. 2006), 2MASS (Skrutskie et al. 2006) and UCAC2 (Zacharias et al. 2004). The distribution of EW objects is more isotropic than EA or EB and confirms the findings of Paczynski et al. (2006).

7.4. Analysis of All Eclipsing Binary objects

This section integrates the results for the EA, EB and EW objects and presents them in the same tables and graphs so that a comparison could be made between classes.

7.4.1 Statistics

Table 7-16 shows that 97.62% of eclipsing objects classified by the NNs were confirmed as EA, EB or EW by manual review after the objects in the PFlags listed in Table 7-5 that caused period-clumping and period-banding had been removed. The 2.38% that disagreed were mainly 'Review', 'No class' and as a result of misclassification between EB and EW due to the similarity in light-curve shape as discussed in the Chapter 5 (section 5.7.1). In this section, we are looking at general eclipsing stars, so any misclassification between EA, EB and EW objects can be ignored. This means that there was no misclassification, only 206 non-classifications (189 as Review and 17 as No class), making the NNs 98.82% effective at classifying general eclipsing stars.

EA/EB/EW Objects		Based on light-curve shape					
		All		LS/SA removed		G/LS/SA removed	
Light-curve quality	NN	No.	%	No.	%	No.	%
Good (G)	Agree	12,462	59.39	11,464	57.36	9,071	51.84
Large scatter (LS)	Agree	5.200	24.78	5,200	26.02	5,200	29.72
Small amplitude (SA)	Agree	2,811	13.40	2,811	14.07	2,811	16.06
Total	Agree	20,473	97.57	19,475	97.45	17,082	97.62
Good (G)	Disagree	420	2.00	420	2.10	327	1.87
Large scatter (LS)	Disagree	26	0.12	26	0.13	26	0.15
Small amplitude (SA)	Disagree	64	0.31	64	0.32	64	0.37
Total	Disagree	510	2.43	510	2.55	417	2.38
Overall total	All	20,983		19,985		17,499	

Table 7-16: All eclipsing: Statistics for identified objects

7.4.2 Known objects

Table 7-17 shows the results of the search in SIMBAD for known eclipsing objects EA/EB/EW.

EA/EB/EW objects (Overall total = 20,983)							
SIMBAD	Based on light-curve shape						
	Good		Large scatter		Small amplitude		Total
	NN agree	NN disagree	NN agree	NN disagree	NN agree	NN disagree	All
EA	1,071	37	12	0	18	0	1,138
EB	270	13	3	0	4	0	290
EW	273	4	6	0	1	0	284
Other eclipsing	888	34	30	0	29	0	981
Pulsating	79	2	5	0	4	0	90
Star	1,918	77	136	0	178	0	2,309
Other	920	48	57	0	72	0	1,097
Total known	5,419	215	249	0	306	0	6,189
Total unknowns							14,794
Total unknowns (including Star and Other categories)							18,200

Table 7-17: All eclipsing: Objects known in SIMBAD

Of the 20,983 eclipsing objects, 6,189 had a nearest neighbour within 1 arc-min. Of these known objects, 1,712 confirmed the NN EA/EB/EW class and 981 were 'other eclipsing' classes (i.e. Eclipsing binary, Eclipsing binary candidate, Double star, Star in double system and Spectroscopic binary). The remainder consisted of pulsating objects; Stars; and 'Other'. The pulsating stars were included in the total of 'known' objects as they could possibly be incorrect classifications in SIMBAD, but 'Star' and 'Other' classes were added to the overall total of 'unknown' stars, giving a final total of 18,200 new eclipsing binaries overall.

7.4.3 Period

The period values for ALL the eclipsing objects (except the EA objects that exhibited period-clumping and period-banding) were plotted as a distribution graph as shown in Figure 7-44 and as a histogram in Figure 7-45.

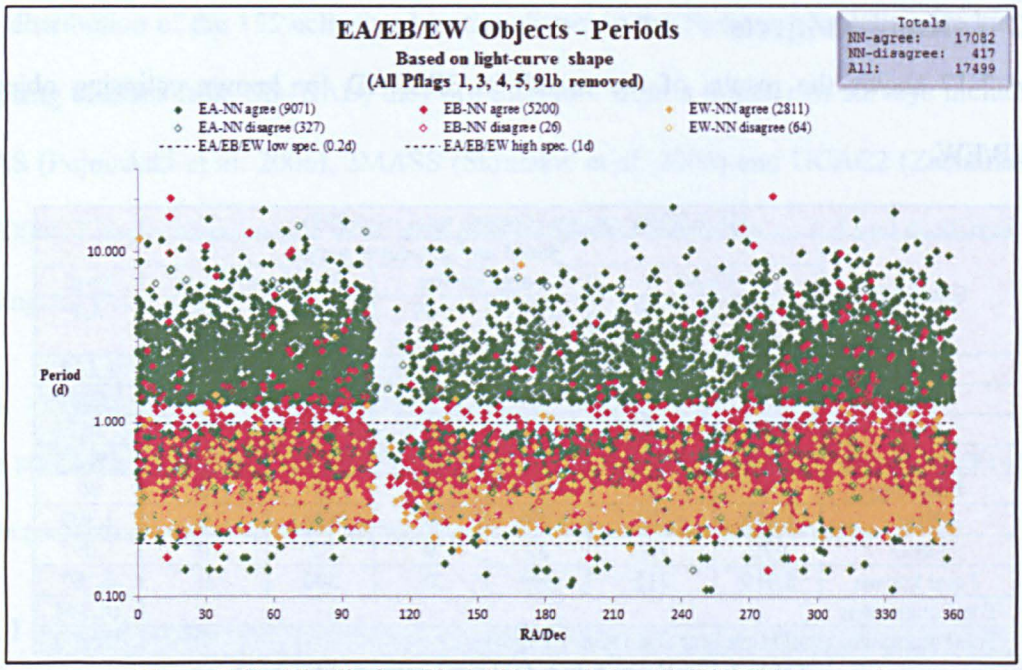

Figure 7-44: All eclipsing: Variability periods with G/LS/SA removed (i.e. where all objects in the PFlag range have been removed)

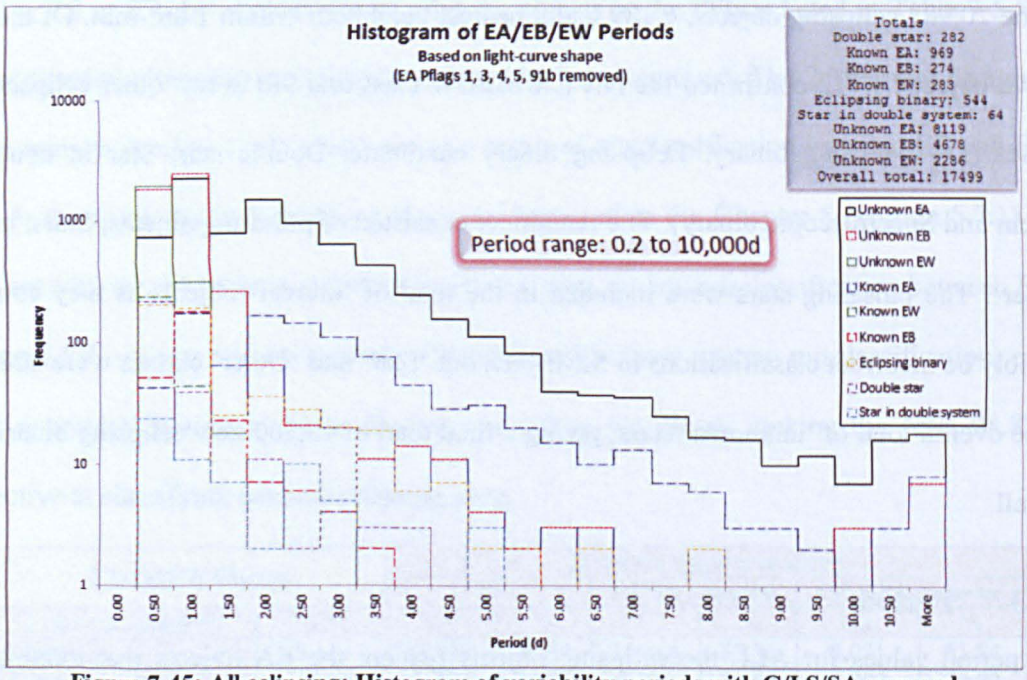

Figure 7-45: All eclipsing: Histogram of variability periods with G/LS/SA removed (i.e. where all objects in the PFlag range have been removed)

A 3D representation of Figure 7-45 can be seen on the support DVD at the location:

Light-curve output
X:\Chapter07\3D-hist\Fig_7-42.bmp

Figure 7-44 shows the expected separation into period ranges for EA, EB and EW objects,

but also showed that many EBs were intermixed at the top end of the EWs, way below the 1 day period cut-off. This was confirmed by the histogram in Figure 7-45.

7.4.4 Amplitude

The binned amplitude values for ALL the eclipsing objects were plotted on a distribution graph in Figure 7-46 and a histogram in Figure 7-47. The objects were plotted exactly like the individual classes, but all period-clumping and period-banding EA objects were removed.

The amplitude limits for EA, EB and EW were <3, <2, <0.8Vmag respectively according to the GCVS. This observation was supported in this research for EA and EB, but this research also shows 39 EW objects with amplitudes >0.8Vmag. This was discussed fully in section 7.3.4.

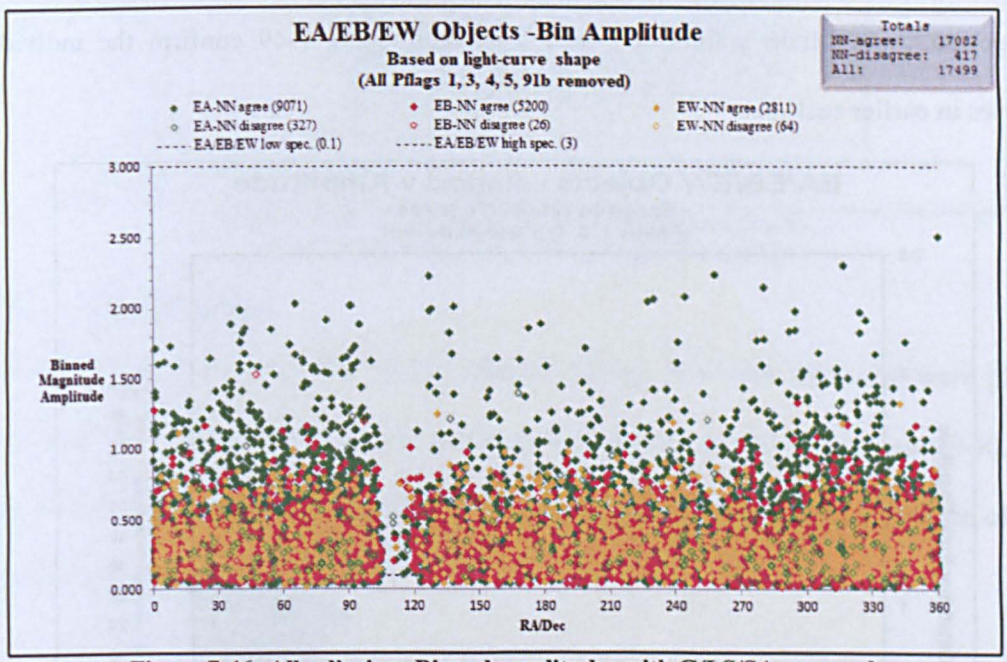

Figure 7-46: All eclipsing: Binned amplitudes with G/LS/SA removed (i.e. where all objects in the PFlag range have been removed)

A 3D representation of Figure 7-47 can be seen on the support DVD at the location:

Light-curve output
X:\Chapter07\3D-hist\Fig_7-44.bmp

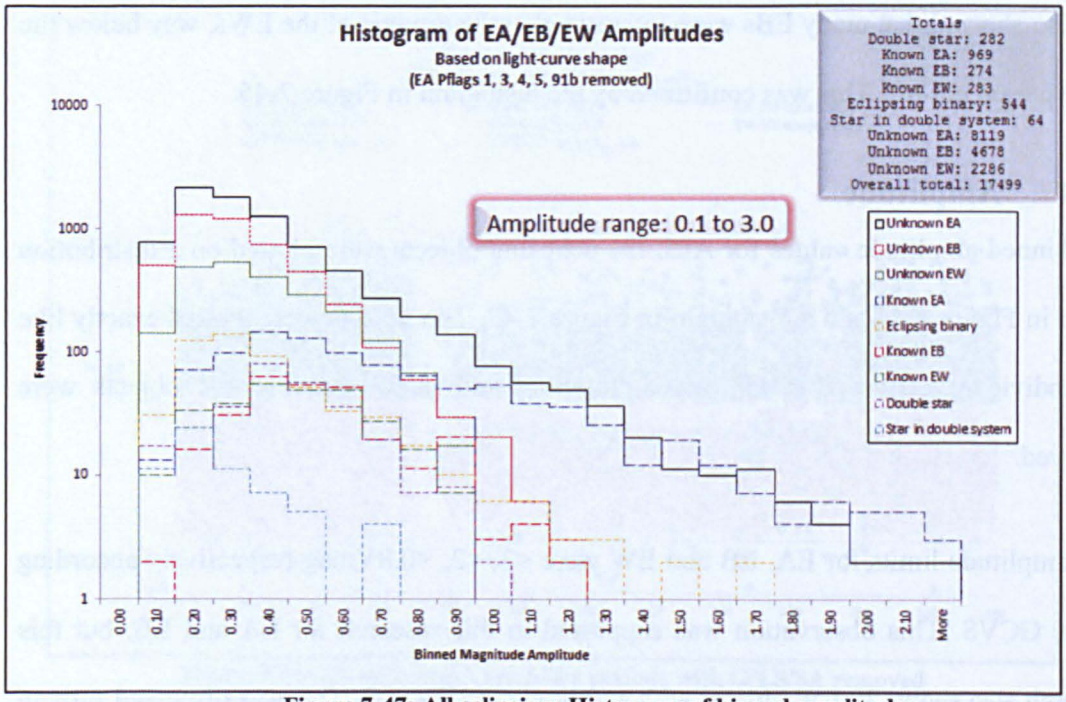

Figure 7-47: All eclipsing: Histogram of binned amplitudes

7.4.5 Period v Amplitude

The period v amplitude graphs in Figure 7-48 and Figure 7-49 confirm the individual analyses in earlier sections.

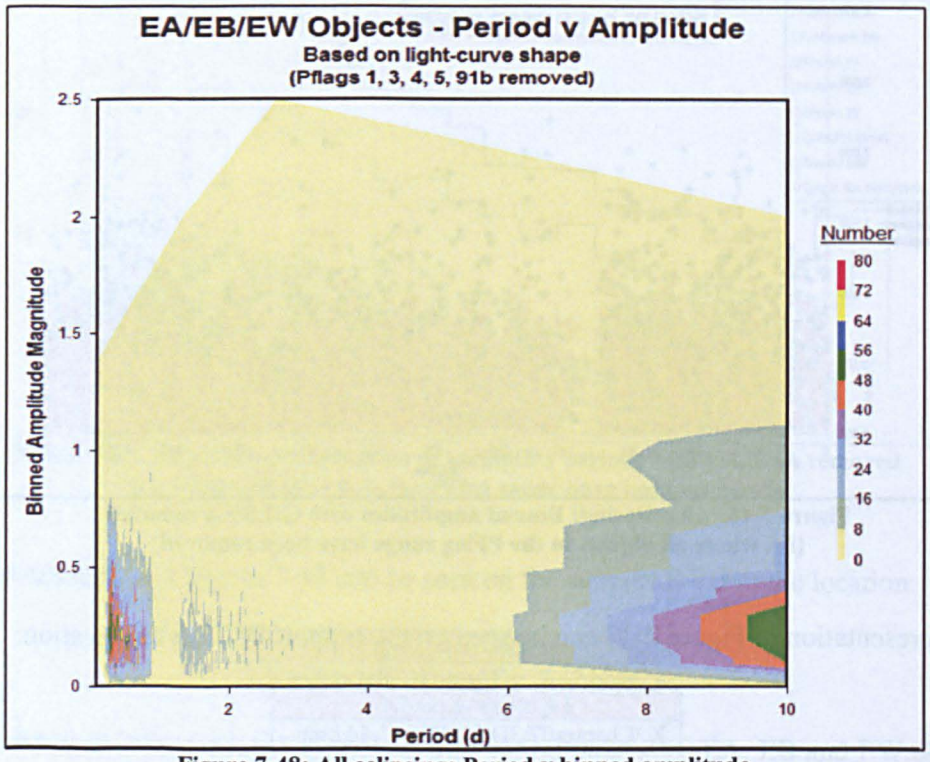

Figure 7-48: All eclipsing: Period v binned amplitude

A scatter plot of Figure 7-48 can be seen on the support DVD at the location:

Light-curve output
X:\Chapter07\Contour\Fig_7-45.bmp

Where X is DVD-1 in the DVD-drive

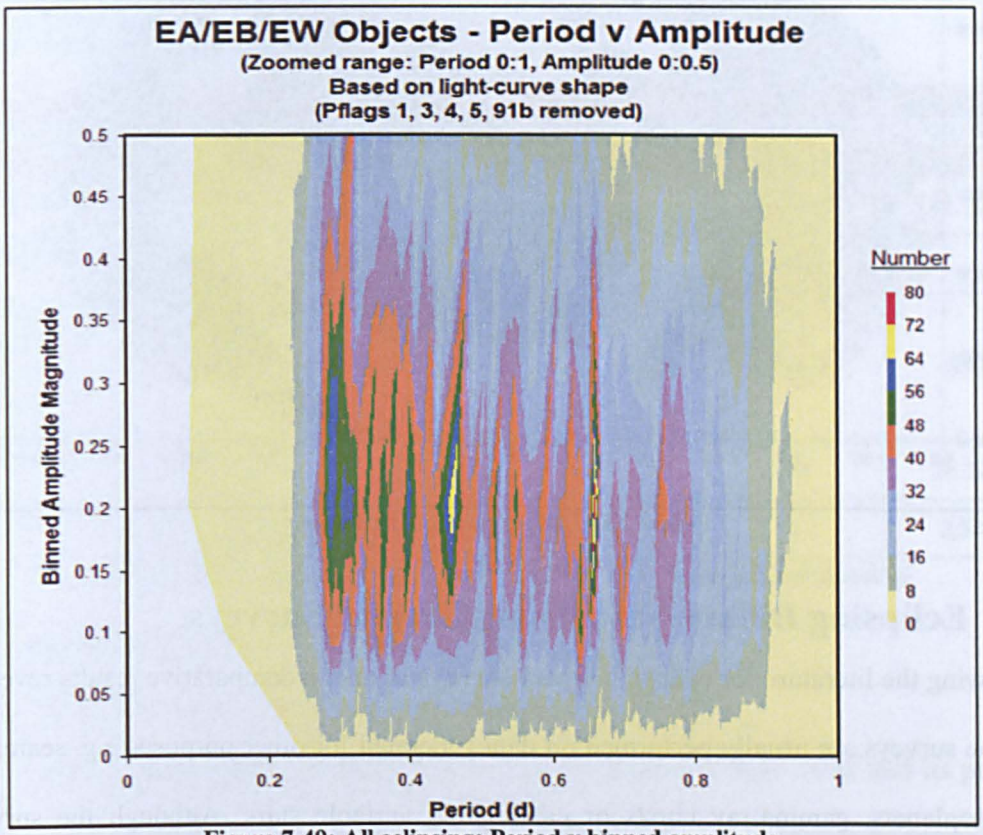

Figure 7-49: All eclipsing: Period v binned amplitude (Zoomed into range Period 0:1, Amplitude 0:0.5)

7.4.6 Distribution

The EA objects remaining after all the affected PFlags had been removed, were plotted along with the EB and EW objects as a Hammer projection as shown in Figure 7-50. This maps all the known eclipsing objects in SIMBAD as well as all the newly classified objects from this research.

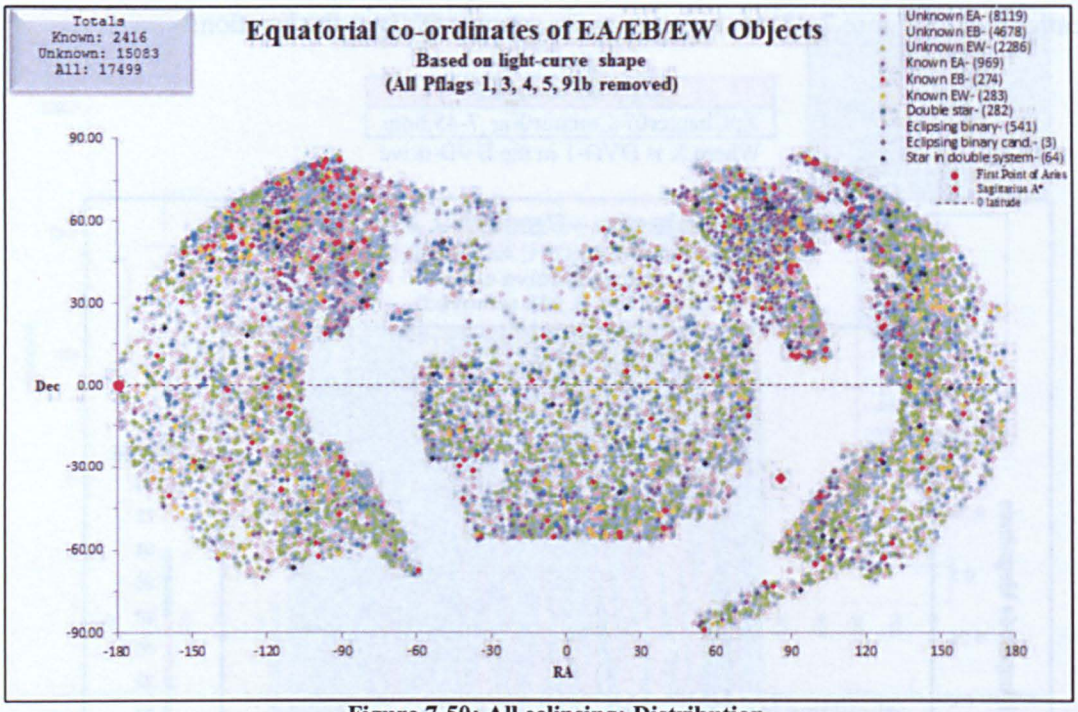

Figure 7-50: All eclipsing: Distribution

7.5. Eclipsing Binary Stars from General Surveys

Reviewing the literature for eclipsing binary surveys to obtain comparative results revealed that the surveys are usually performed on data generated for other purposes e.g. searching for Exoplanets, gamma-ray bursts or cataloguing variable stars. Although the surveys identified many eclipsing binaries, only a few surveys/papers published ranges for them and none of them discussed eclipse-depth ratio in terms of differentiating between EB and EW objects.

Table 7-18 shows a comparison of the percentage of eclipsing binaries from SuperWASP against those obtained from the literature. Unfortunately, the surveys are using the physical properties of the stellar system for the classification, not the shape of the light-curve used in this research. As such, the only comparison that can be made is that of EW stars in this research with the contact binaries in the published surveys (due to their strong association). So, assuming that EA and EB systems could be detached or semi-detached (i.e. grouping them together), the proportion of SuperWASP eclipsing binaries agrees well with the

results from the OGLE survey but indicates that SuperWASP located slightly more EWs. The high number of contact binaries in the ASAS and University of New South Wales surveys may be due to the fact that they used the period to class the systems rather than eclipse-depth ratio.

Survey	Source	EA (%)	EB (%)	EW (%)	Sample size
SuperWASP	N/A	61.4	24.9	13.7	20,983
Survey	**Source**	**Detached (%)**	**Semi-detached (%)**	**Contact (%)**	**Sample size**
ASAS	Pojmański et al. (2006)	24.8	26.6	48.6	11,099
Kepler	Prša et al. (2011)	52.3	7.5	25.4	
University of New South Wales Extrasolar Planet Search	Christiansen et al. (2008)	37.1		56.9	850
OGLE	Graczyk et al. (2011)	63	25	6	26,121
OGLE	Wyrzykowski et al. (2003)	70.0	25.9	6.1	2,580

Table 7-18: Comparing SuperWASP eclipsing binaries v published material

Some examples of general surveys are as follows:

- **MACHO**: (http://wwwmacho.anu.edu.au/ - June 2012)

  The 'Massive Compact Halo Objects' survey started in June 1992 and its primary aim was to test the hypothesis that a significant fraction of the dark matter in the halo of the Milky Way is made up of objects like brown dwarfs or planets. However preliminary analysis of the MACHO data has also been performed and approximately 39,000 variable stars were discovered in the LMC database (Cook et al. 1995). Derekas et al. (2007) reviewed 6,833 of these variables that were classified as 'eclipsing binary' and re-classified them on light-curve shape rather than period. They found that only 3,031 of them were correctly classified, the remainder being pulsating stars. This supports the observation in this research that EB and EW objects would be better separated using eclipse-depth ratio rather than period as this defines the shape of the light-curve. Other surveys have been

performed on the MACHO data e.g. Faccioli et al. (2007) where they discovered 4,634 eclipsing binaries, but did not state ranges to compare with SuperWASP data.

- **ASAS**: (Pojmański, 1997)

  The 'All Sky Automated Survey' started in 1997 and its ultimate goal was the detection and investigation of any kind of photometric variability. Paczynski et al. (2006) stated that they detected 2,743 detached binaries (24.8%), 2,949 semi-detached binaries (26.6%) and 5,384 contact binaries (48.6%) in the ASAS Catalogue of Variable Stars (ACVS) database. They also showed that detached binaries were most strongly concentrated in the Galactic plane while the short-period contact binaries had an almost isotropic distribution. As mentioned above, the distribution of eclipsing binary stars in this research cannot be compared directly with the ASAS results as the classification is based on the shape of the light-curve and not the physical properties of the stellar system (see Chapter 2). However, given the strong association of the EW class with contact binaries, SuperWASP data shows there to be far less EWs than ASAS discovered.

Paczynski et al. (2006) commented in their paper that their most surprising result was a very small number of detached eclipsing binaries with periods of less than one day as the systems are believed to be the progenitors of the W UMa stars. Looking back at Figure 7-7 and Figure 7-8 above, we can see that there are many EA objects that have a period less than one day, and many of these could be detached binaries. This result may offer support to Paczynski's qualitative confirmation of the 'decades old' idea of Flannery (1976) and Lucy (1976) that W UMa-type binaries evolve through a series of thermal relaxation oscillations, where the W UMa system spend time in semi-detached and contact states.

- **Hipparcos/Tycho Catalogues**: (ESA, 1997, The Hipparcos and Tycho Catalogues, ESA SP-1200)

  The 'High Precision Parallax Collecting Satellite' survey was operational between August 1989 and March 1993 and the catalogues were released between 1997 and 2000. The Hipparcos catalogue is a high-precision catalogue of more than 100,000 stars and combined with the lower precision Tycho I catalogue, it contains more than a million stars. The enhanced Tycho-2 (including the Hipparcos and Tycho I catalogue) contains about 2.5 million stars and was published in 2000. The catalogue summary on the Hipparcos web-site[16] states that it has 917 eclipsing binaries of classes EA, EB and EW. No period or amplitude ranges have appeared in the literature to-date.

- **Kepler**: (Borucki et al. 1997)

  Kepler was launched in March 2009 and is expected to complete its task by 2013. The project's main purpose is to identify Earth-like planets, but in doing so, (Prŝa et al. 2011) discovered 1,879 eclipsing binary stars. These were distributed as 52.3% detached, 7.5% semi-detached, 25.4% over-contact (strong correlation with EW in this research), 7.5% ellipsoidal variables, and 7.3% uncertain types. The contact binaries agree quite well with the EW distribution calculated in this research. At the present time (2012), the Kepler web-site currently boasts 2,165 binary stars, but no further literature is yet available.

- **COROT**: (Baglin et al. 2002)

  The 'Convection Rotation and Planetary Transits' survey started in December 2006 and had the main objective of discovering Exoplanets. Many papers have been written on eclipsing binaries using the COROT data e.g. Maciel et al. (2011), Da

[16] http://www.rssd.esa.int/index.php?project=HIPPARCOS &page=catalogue_summary (June 2012)

Silva & Silva-Valio (2011) and Maceroni et al. (2010), but the topics were not pursued in this research.

- **SDSS**: (http://www.sdss.org/ - June 2012)

  The 'Sloan Digital Sky Survey' collected data over the period 2000-2005 (SDSS-I) and 2005-2008 (SDSS-II) with an aim of obtaining deep, multi-colour images covering more than a quarter of the sky. The objective is to create three-dimensional maps containing more than 930,000 galaxies and 120,000 quasars. Over the years, it has supported fundamental work in all areas of astronomy, including the identification of 747 detached close binary systems in the fourth release (Silvestri et al. 2006).

- **HATNet**: (Bakos et al. 2002)

  The 'Hungarian-made Automated Telescope variability' survey started in 1999, with a scientific goal to detect and characterize Exoplanets using the transit method. While looking for the Exoplanets, eight eclipsing binaries were also identified (Latham et.al. 2009).

- **OGLE**: (Udalski, 2003)

  The 'Optical Gravitational Lensing Experiment' survey was started in April 1992 and is still running today, with the main goal of searching for dark matter with micro-lensing phenomena. Over the 20 years of the survey, Graczyk et al. (2011) has visually inspected 26,121 eclipsing binary stars identified in the Large Magellanic Cloud. They presented 68.0% detached, 25.9% semi-detached and 6.1% over-contact binaries. Their work was particularly useful in this research as they used an image recognition neural network to classify the eclipsing binaries into three classes (see Chapter 2). Wyrzykowski et al. (2003) also created a catalogue of eclipsing binaries using an automatic search algorithm. They discovered 2,580 eclipsing binaries consisting of 1882 EA (70%), 718 EB (25.9%) and 168 EW

(6.1%) and reported similar problems encountered in this research i.e. some periods were half/double the true period. They reported that the most difficult classification problem was the separation between EB and EW classes. To overcome this, when the orbital period was about one day or less they assigned an EW type, but as discovered in this research, it would have been more appropriate to use the eclipse-depth ratio as this feature determines if it is a contact binary. The period ranges quoted in the paper are: EA 1.5 to 2.5 days; EB 1 to 2 days; and EW about 1 day. These ranges agree with the current published ranges but do not agree with the SuperWASP ranges.

- **ROTSE**: (http://www.rotse.net)

  The 'Robotic Optical Transient Search Experiment' survey started in 2004 and is on-going today. Its primary goal is to achieve observations in optical light of the massive deep-space explosions called Gamma-Ray Bursts, but they have also created a catalogue of 1,022 contact binaries and observed a period range of 0.22 to 1.5 days, with most systems having periods between 0.25 and 0.5 days (Gettel et al. 2006). This is within the SuperWASP range for EWs of 0.18 to 3.62 days

- The University of New South Wales Extrasolar Planet Search[17]:

  As the name suggests, the main aim of this survey was to identify Exoplanets. The survey occurred between October 2004 and May 2007 and produced a catalogue of 850 variable stars containing 142 Algol-type, 23 Beta Lyrae-type and 218 contact binaries. The study lumped detached and semi-detached binaries together and reported a 37.1% frequency, while over-contact binaries (EW) constitute 56.9% of this sample and ellipsoidals constitute 6% (Christiansen et al. 2008). This was the highest proportion of contact binaries of all the surveys in the literature search.

[17] http://mcba11.phys.unsw.edu.au/~apt/index.html - June 2012

- **TrES**: (Alonso et al. 2004)

  The 'Trans-Atlantic Exoplanet Survey' started in 2004. Its main purpose was to locate Exoplanets, but binary stars were included in the dataset and 773 eclipsing binaries were assessed to obtain their absolute properties (Devor et al. 2008).

- **XO**: (McCullough et al. 2005)

  The 'XO Telescope' project was active from September 2003 to September 2005. Its main aim was also to look for Exoplanets, and during the survey, they discovered 69 'false positives' which were ultimately classified as eclipsing binaries (Poleski et al. 2010).

- **AAVSO**: (http://www.aavso.org)

  The 'American Association of Variable Star Observers' has been monitoring variable stars since 1911 and has data dating back to the 1800's. The AAVSO has about 1,400 members and observers from 52 countries contributing over a million observations per year. This is obviously a great repository of variability and will contain many eclipsing binaries.

Other upcoming surveys that will require very fast preliminary scans due to the large numbers of objects are mentioned below. These would be prime targets for use of the 'LC Analyser classifier' application:

- **Pan-STARRS**: (Kaiser et al. 2002)

  The 'Panoramic Survey Telescope & Rapid Response System' project started in May 2010 and the main aim is to discover and characterize Earth-approaching objects, both asteroids and comets that might pose a threat to Earth. There are already plans to search for eclipsing binaries amongst their data (Dupuy & Liu, 2009).

- **GAIA**: (Gilmore et al. 1998)

In August 2013, the 'Global Astrometric Interferometer for Astrophysics' survey is planned to start. The aim is to compile a catalogue of approximately 1 billion stars, i.e. roughly 1% of stars in the Milky Way. This provides an enormous opportunity to process objects from this survey with the 'LC Analyser classifier' application to obtain a preliminary classification for each star.

- **LSST**[18]

  The 'Large Synoptic Survey Telescope' project is due at the end of the decade and its three-billion pixel digital camera will take 'moving-pictures' of the night-sky. It has multiple aims, including investigation of dark energy and dark matter, looking at near-Earth objects and mapping the Milky Way. One of its functions will involve "detailed studies of variable star populations using 2% or better accurate multi-colour light curves for a sample of at least 50 million variable stars. (e.g. studies of cataclysmic variables, eclipsing binary systems, rare types of variables, etc.)".

Each of the above studies is suitable for analysis using the 'LC Analyser classifier' application, as the only inputs to the application are the visual observations of each object and the period. The method is fast and 98% accurate in providing a preliminary classification for eclipsing binaries.

7.6. Differentiate Eclipsing Binaries using Eclipse Depth Ratio

The Eclipse-depth ratio parameter has been used in a number of studies over the past 30 years for various purposes, such as calculating the ratio of surface brightness of stars (Nefs et al. 2012), investigating energy sources for the luminosity of the disk surrounding the secondary component of Beta Lyrae stars (Huang & Brown, 1976) and characterising eclipsing binary stars (Prŝa et al. 2011).

[18] http://www.lsst.org/lsst/

During the process of characterising eclipsing binaries, Prŝa et al. (2011) noted that the eclipse-depth ratio was strongly affected by eccentricity and star sizes. It was therefore thought that this parameter would be useful for differentiating between phase-folded light-curves of EB and EW classes in this research, as the method used was semi-quantitative in nature, i.e. the result is based on a predetermined cut-off value calculated for EB and EW classes in the SuperWASP archive.

Section 7.2.3 revealed that many EB objects were below the nominal 1 day cut-off period stated in the GCVS. It was possible that it reflected the difficulties in distinguishing EB from either EA or EW on the basis of just the photometry, but the majority of the light-curves were definitely EB-shape. With only the visible light-curve available, it was proposed that the eclipsing binaries could be more easily defined using an eclipse-depth ratio parameter in place of the period. The eclipse-depth ratio was calculated using the flux values of each object using Equation 7-1.

$$EDR = \frac{(F_0 - F_2)}{(F_0 - F_1)}$$

Equation 7-1: Eclipse-depth ratio
Where F_0=maximum flux; F_1=flux at first eclipse; F_2=flux at second eclipse

It should be noted that this calculation provides 'quantised' values for the eclipse depth ratios due to limits on the precision of the flux values. This is apparent in the banding effect shown in Figure 7-51 (EA), Figure 7-55 (EB), Figure 7-59 (EW) and Figure 7-63 (All eclipsing) below.

The following sections illustrate the analysis of eclipse-depth ratio for each of the classes EA, EB, EW. Each section contains tabulated values showing the ranges obtained and distribution graphs showing the scatter of ratios for each class within the range 0 to 1. They also describe 'Good', 'Large scatter' and 'Small amplitude' objects where the NN

classifications agreed and disagreed with the manual classification. Each section also contains histograms to show the spread of eclipse-depth ratio across the range indicating the proportion of objects in each bin.

7.6.1 EA Eclipse Depth Ratio

Figure 7-51 demonstrates that EA objects tend to cover the whole range, from a ratio of 0.02 for single-eclipse (e.g. Figure 7-52) to 1.0 for a double-eclipse with equal depth (e.g. Figure 7-53).

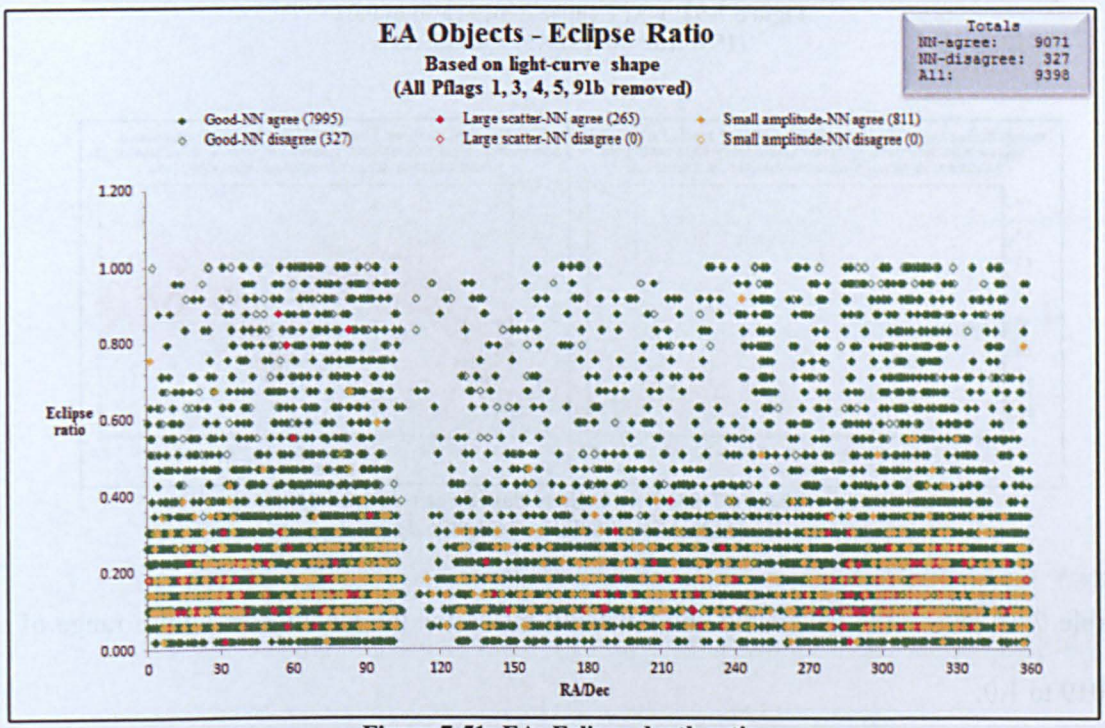

Figure 7-51: EA: Eclipse-depth ratio

Figure 7-51 also shows that the 'Good' objects spread from 0 to 1.0, but 'Large scatter and 'Small amplitude' objects tend to be below a ratio of 0.4. This was not due to the large scatter or small amplitudes themselves, as the method of calculating the eclipse-depth ratio involved normalising the primary and secondary eclipse by the maximum flux. This could cause difficulty in using the eclipse-depth ratio to separate the majority of large-scatter and small-amplitude EA objects from EB and EW. This was not the case though, as one of the

main features of the EA light-curve was the flat area before eclipse and this was detected very well in the NNs.

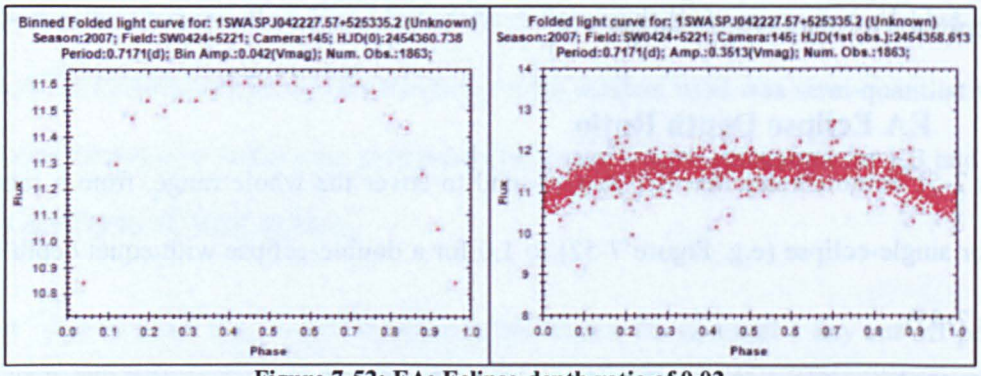

Figure 7-52: EA: Eclipse-depth ratio of 0.02 (1SWASP J042227.57+525335.2)

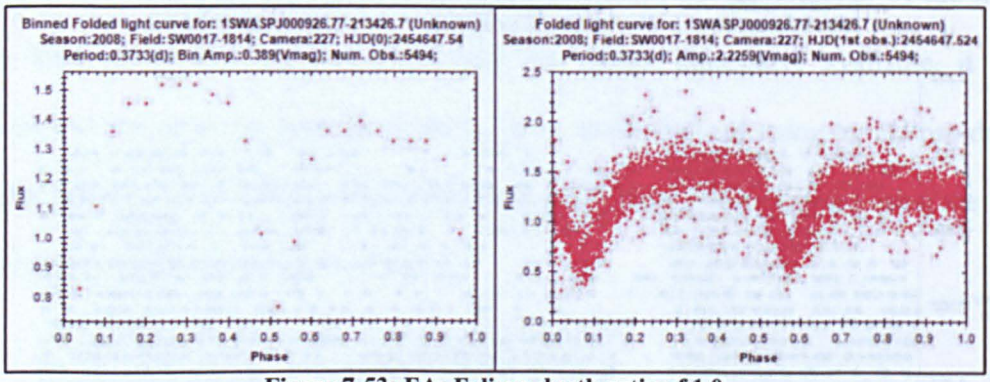

Figure 7-53: EA: Eclipse-depth ratio of 1.0 (1SWASP J000926.77-213426.7)

Table 7-19 shows the calculated eclipse-depth ratios for the EA objects with a range of 0.019 to 1.0.

EA eclipse-depth ratio	
Mean	0.258
Median	0.183
Mode	0.184
Min	0.019
Max	1.000
N	9,398

Table 7-19: EA: Eclipse-depth ratio statistics

The histogram in Figure 7-54 confirms that the majority of EAs have an eclipse-depth ratio around 0.18 with the majority of objects in the range 0.05 to 0.40. This area is separated well from the main areas of EB and EW as discussed in the following sections.

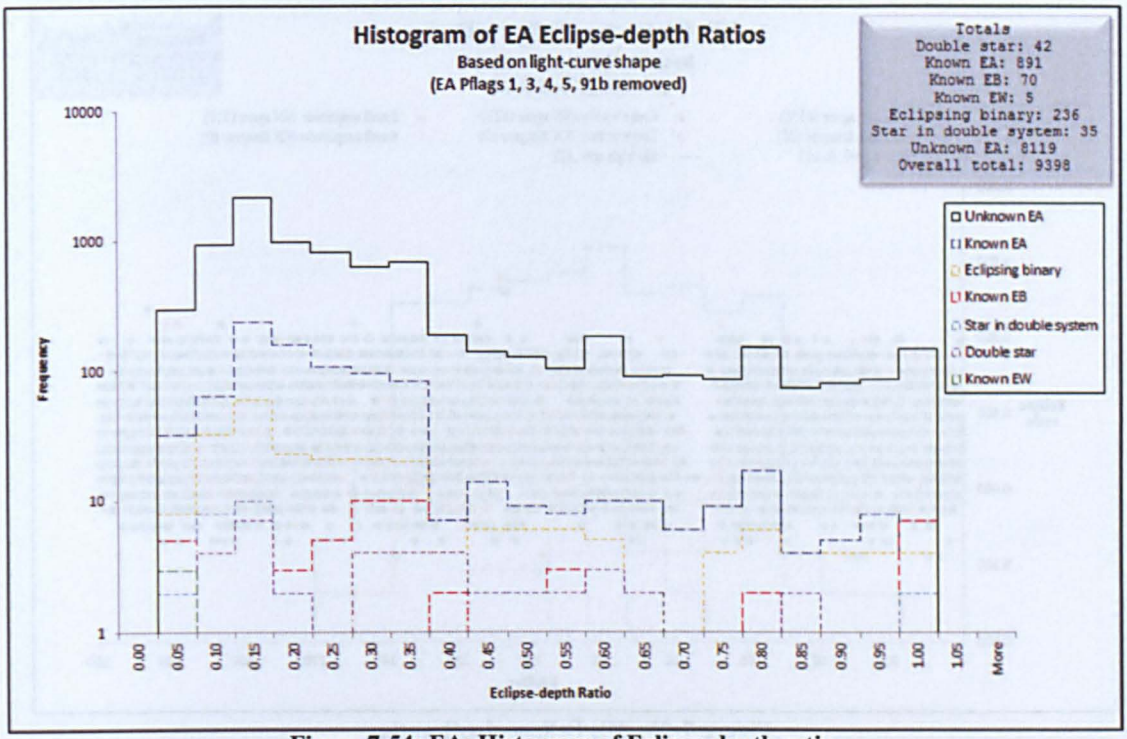

Figure 7-54: EA: Histogram of Eclipse-depth ratio

A 3D representation of Figure 7-54 can be seen on the support DVD at the location:

Light-curve output
X:\Chapter07\3D-hist\Fig_7-50.bmp

7.6.2 EB Eclipse Depth Ratio

Figure 7-55 indicates that EB objects occur in the eclipse-depth range 0.18 (e.g. Figure 7-56) to 0.96 (e.g. Figure 7-57). It also reveals that the 'Good' objects spread from 0.2 to 0.8 and 'Large scatter and 'Small amplitude' objects are evenly mixed.

Figure 7-58 clearly shows that the majority of EBs have an eclipse-depth ratio around 0.5, with the majority of them in the range 0.3 to 0.8. This area is separated well from the main area of EW as discussed in the following section 7.6.3.

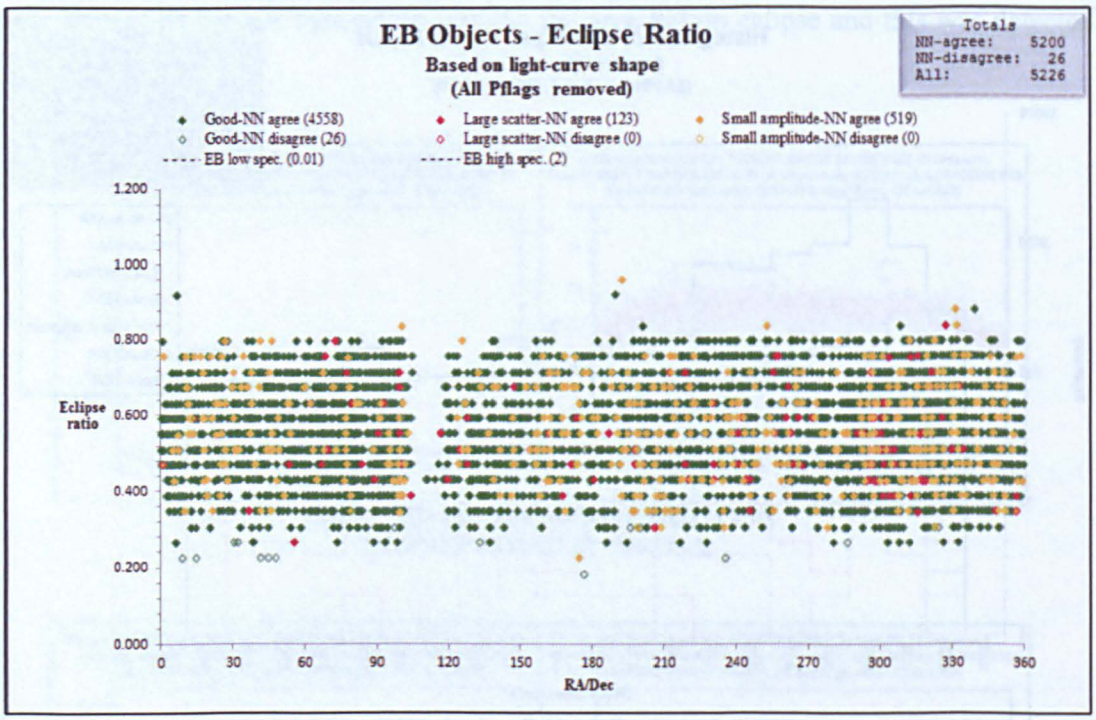

Figure 7-55: EB: Eclipse-depth ratio

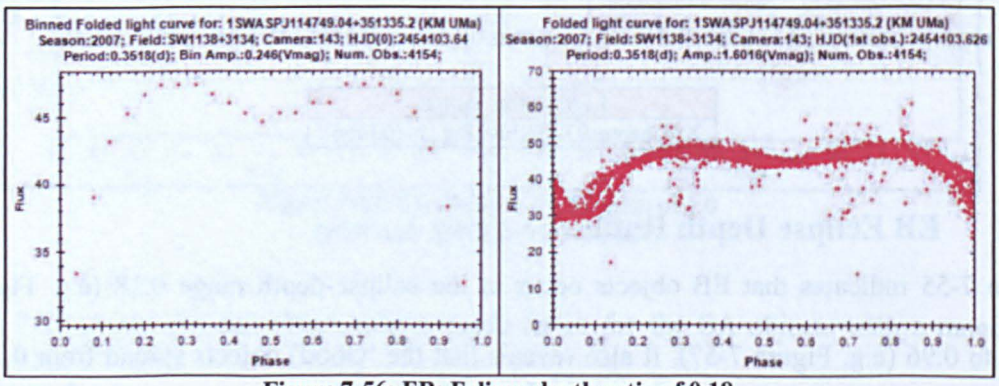

Figure 7-56: EB: Eclipse-depth ratio of 0.18
(1SWASP J114749.04+351335.2 → KM UMa)

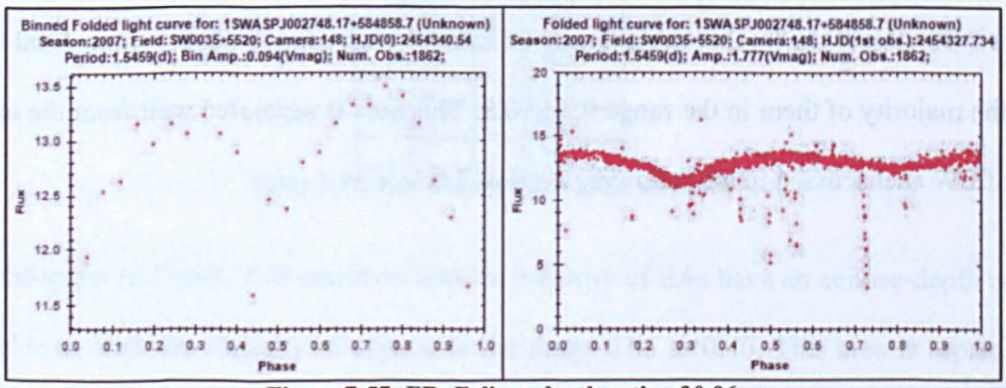

Figure 7-57: EB: Eclipse-depth ratio of 0.96
(1SWASP J002748.17+584858.7)

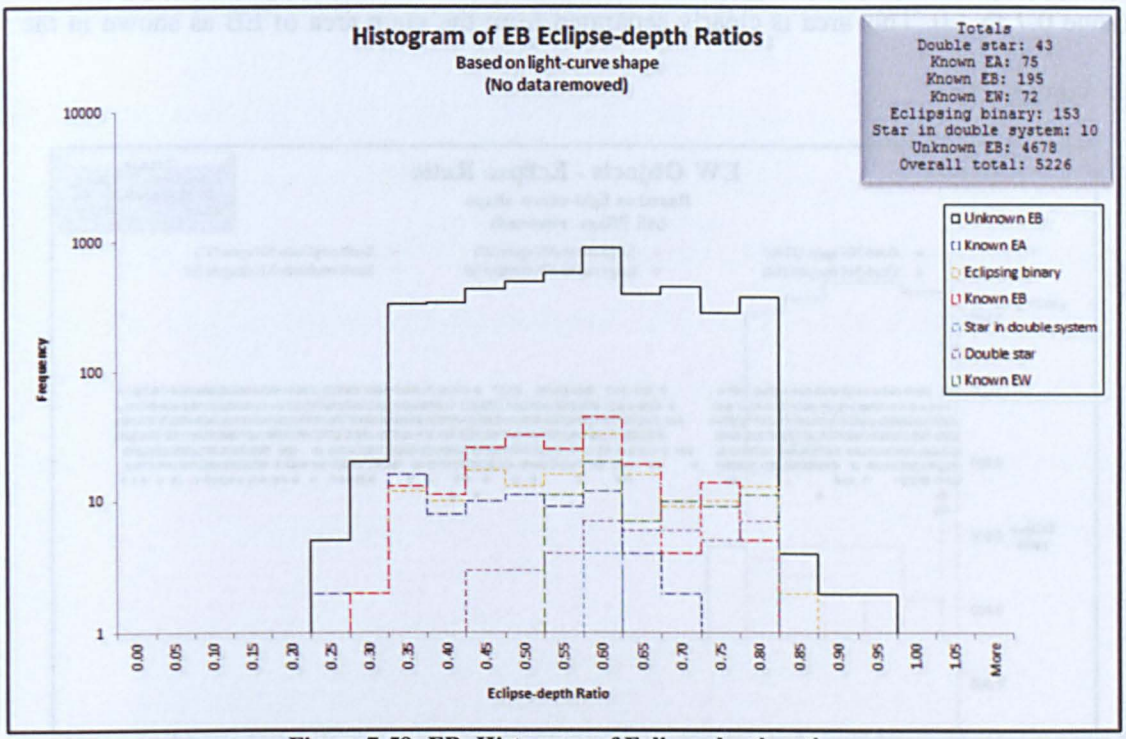

Figure 7-58: EB: Histogram of Eclipse-depth ratio

A 3D representation of Figure 7-58 can be seen on the support DVD at the location:

Light-curve output
X:\Chapter07\3D-hist\Fig_7-54.bmp

Table 7-20 describes the calculated eclipse-depth ratios for the EB objects with a range of 0.183 to 0.959.

EB eclipse-depth ratio	
Mean	0.547
Median	0.551
Mode	0.510
Min	0.183
Max	0.959
N	5,226

Table 7-20: EB: Eclipse-depth ratio statistics

7.6.3 EW Eclipse Depth Ratio

Figure 7-59 establishes that EW objects occur in the eclipse-depth range 0.67 (e.g. Figure 7-60) to 1.0 (e.g. Figure 7-61), with the 'Good' objects spread from 0.7 to 1.0 and the 'Large scatter and 'Small amplitude' objects evenly mixed. Figure 7-62 illustrates that the majority of EWs have an eclipse-depth ratio around 0.9, with the majority of them in the

range 0.7 to 1.0. This area is clearly separated from the main area of EB as shown in the previous section.

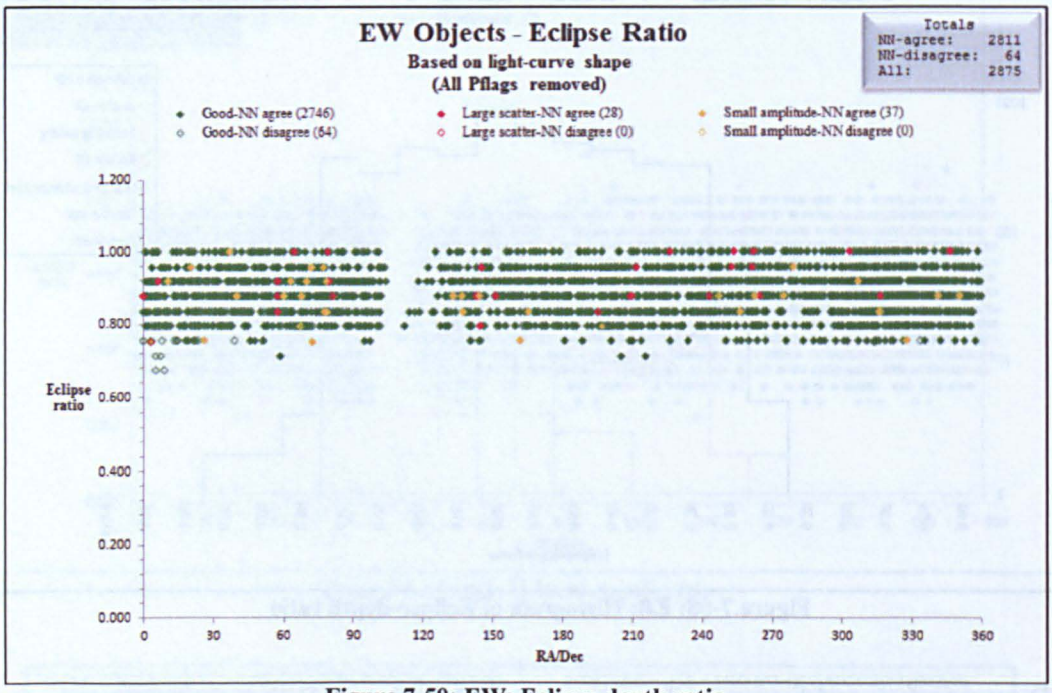

Figure 7-59: EW: Eclipse-depth ratio

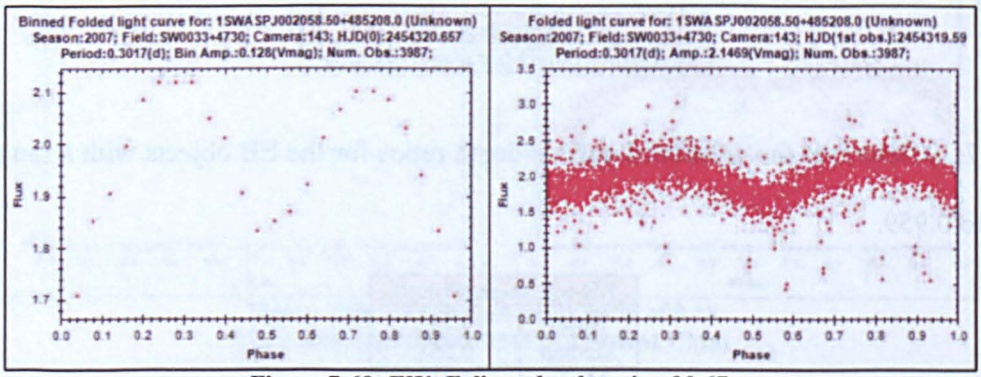

Figure 7-60: EW: Eclipse-depth ratio of 0.67 (1SWASP J002058.50+485208.0)

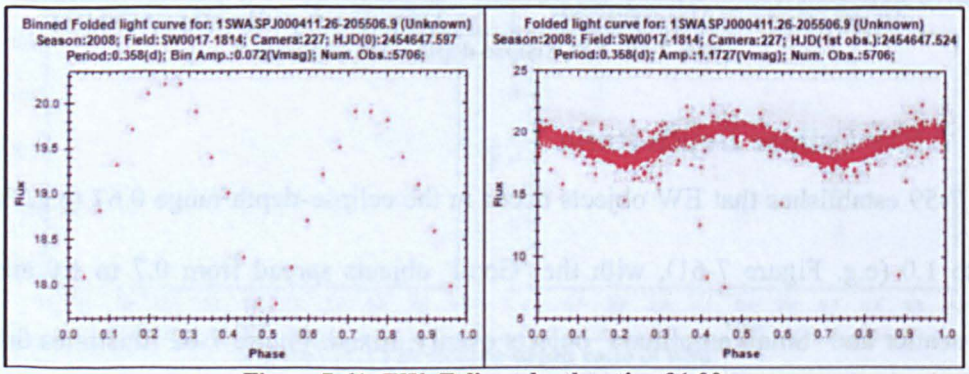

Figure 7-61: EW: Eclipse-depth ratio of 1.00 (1SWASP J000411.26-205506.9)

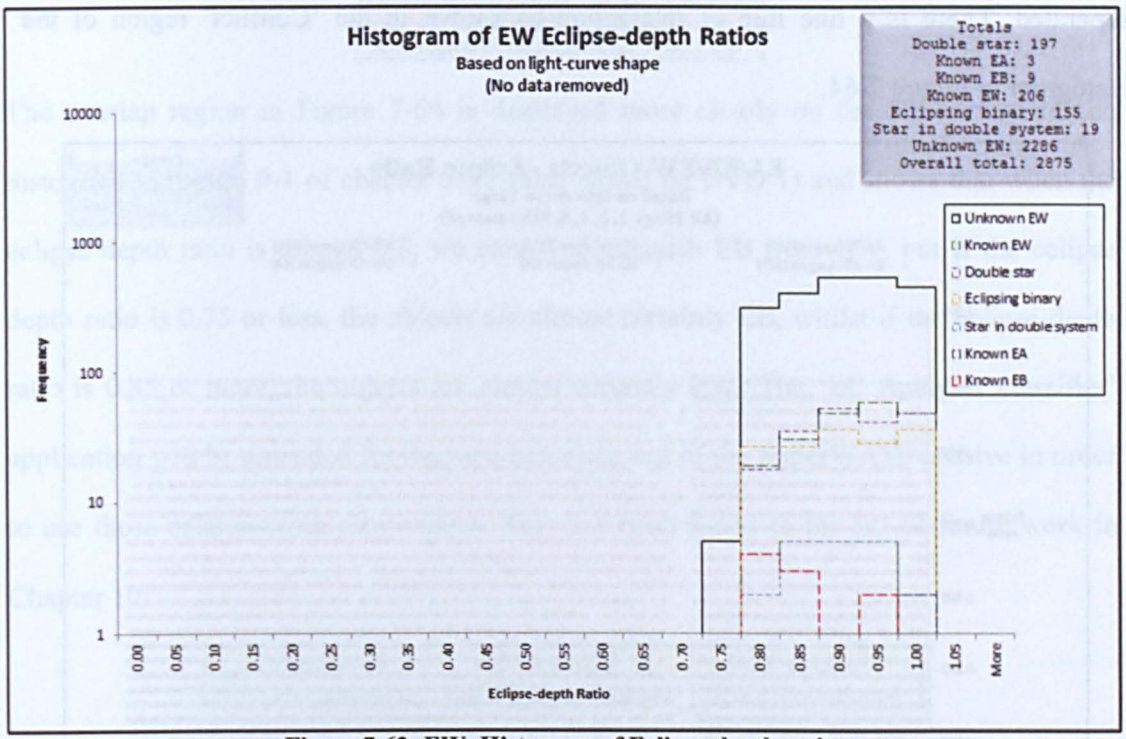

Figure 7-62: EW: Histogram of Eclipse-depth ratio

A 3D representation of Figure 7-62 can be seen on the support DVD at the location:

Light-curve output
X:\Chapter07\3D-hist\Fig_7-58.bmp

Table 7-21 confirms the calculated eclipse-depth ratios for the EW objects with a range of 0.673 to 1.000.

EW eclipse-depth ratio	
Mean	0.888
Median	0.878
Mode	0.918
Min	0.673
Max	1.000
N	2,875

Table 7-21: EW: Eclipse-depth ratio statistics

7.6.4 All Eclipsing Eclipse Depth Ratio

This section displays the eclipse-depth ratios of all the EA, EB and EW objects onto the same graphs so that their distribution and linear separation is revealed. Figure 7-63 shows that the EAs are distributed across the whole range, but EBs and EWs are clearly

separated. There is a fine line of interaction as shown in the 'Conflict' region of the histogram in Figure 7-64.

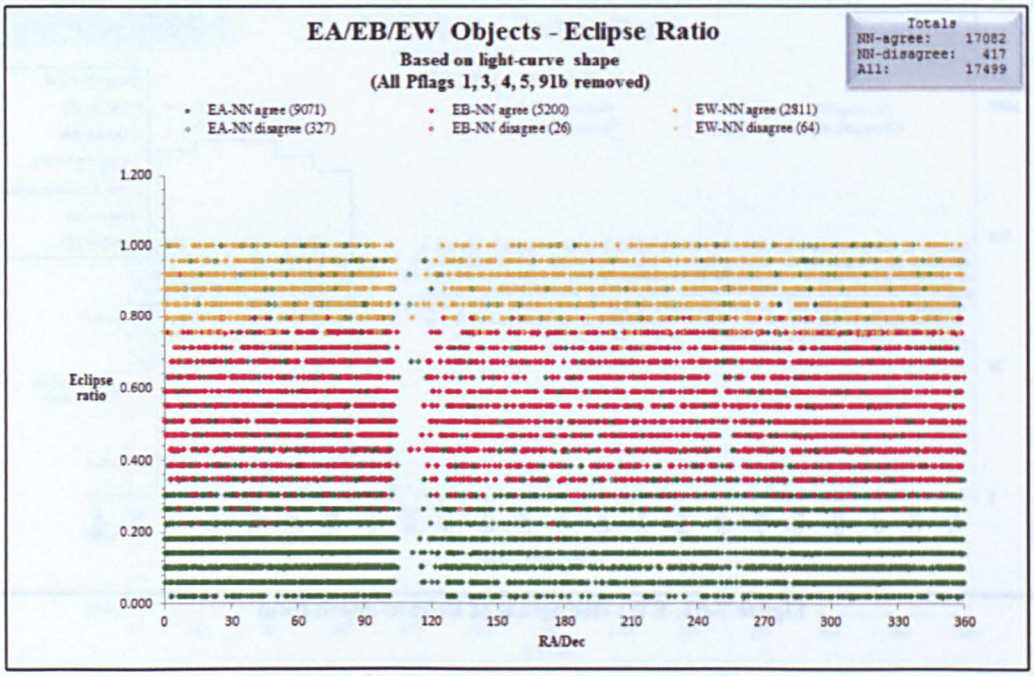

Figure 7-63: All eclipsing: Eclipse-depth ratio

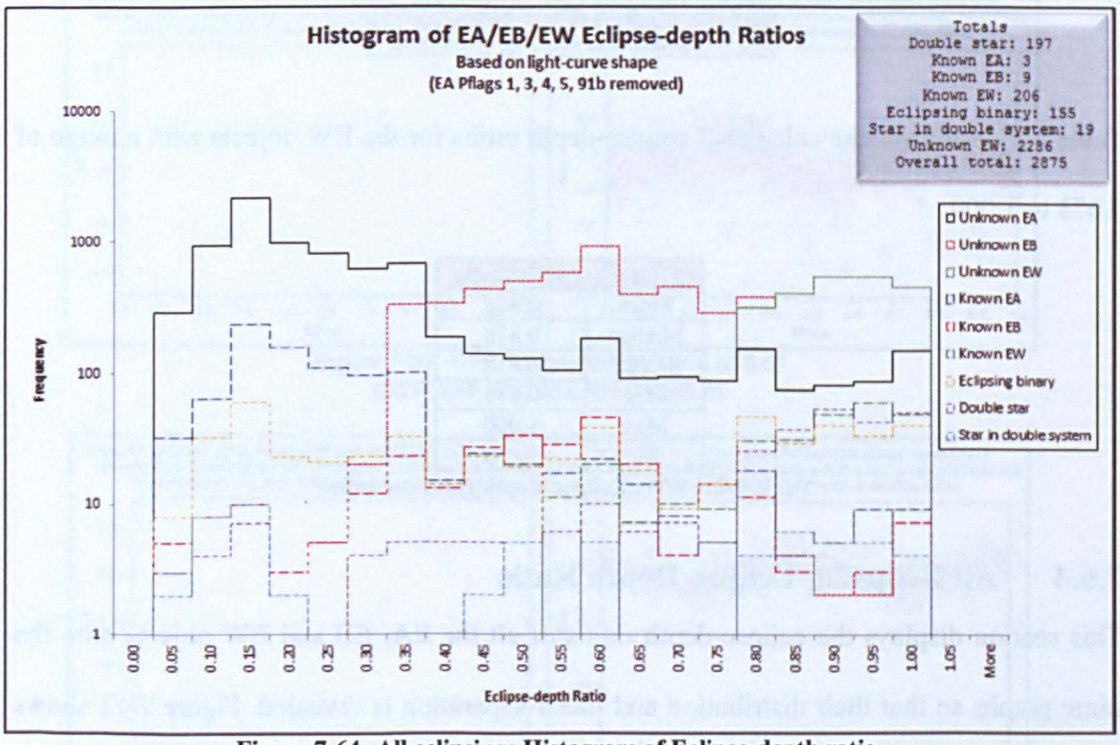

Figure 7-64: All eclipsing: Histogram of Eclipse-depth ratio

A 3D representation of Figure 7-64 can be seen on the support DVD at the location:

Light-curve output
X:\Chapter07\3D-hist\Fig_7-60.bmp

The overlap region in Figure 7-64 is displayed more clearly on the 3D version of the histogram in Figure 9-1 of chapter 9.4.2 (also stored on DVD 1) and shows that when the eclipse depth ratio is around 0.8, we cannot distinguish EB from EW, but if the eclipse depth ratio is 0.75 or less, the objects are almost certainly EB, whilst if the eclipse depth ratio is 0.85 or more, the objects are almost certainly EW. The 'LC Analyser classifier' application will be amended for the next complete run of the SuperWASP archive in order to use these eclipse-depth ratio values. This has been added to the list of future work in Chapter 10:

0.75 and below	0.76 to 0.84	0.85 and above
EB class assigned	EB/EW class assigned	EW class assigned

7.7. Chapter summary

From the analysis of the manually confirmed EA, EB and EW objects in this chapter, the following results were obtained.

7.7.1 Results for EA objects

- ✓ 12,882 EAs were assessed.
- ✓ 5,826 (45.2%) were double-eclipse and 7,056 (54.8%) were single-eclipse.
- ✓ 96.74% of the NN-provided EA classifications were manually confirmed.
- ✓ 1,060 of the EAs were known in SIMBAD and the GCVS.
- ✓ 11,308 new EAs were discovered (8,119 after removal of period-clumping and period-banding PFlag objects).
- ✓ EA period range was calculated as 0.12 to 18.0 days with a median of 1.63 days and a modal value of 0.67 days.
- ✓ 50 EAs had a period shorter than the lower published period limit of 0.2 days.
- ✓ EA amplitude range was 0.02 to 2.5Vmag, with a median of 0.27 and a modal value of 0.16Vmag.
- ✓ All EAs were within the published amplitude range of <3.0Vmag.
- ✓ A distribution map of EAs was created.
- ✓ EA eclipse-depth ratio was calculated as 0.019 to 1.0 with a median of 0.183 and a modal value of 0.184. These values have no value in this research as eclipse-depth ratio is more applicable for EB and EW classes. They have been included for completeness.

7.7.2 Results for EB objects

- ✓ 5,226 EBs were assessed.
- ✓ 99.5% of the NN-provided EB classifications were manually confirmed.
- ✓ 195 of the EBs were known in SIMBAD and the GCVS.
- ✓ 4,641 new EBs were discovered.
- ✓ EB period range was calculated as 0.14 to 20.57 days with a median of 0.56 days and a modal value of 0.48 days.
- ✓ Most EBs (4,751) had a period shorter than the published period limit of 1 day.
- ✓ EB amplitude range was 0.02 to 1.52Vmag, with a median of 0.25 and a modal value of 0.15Vmag.
- ✓ All EBs were within the published amplitude range of <2.0Vmag.
- ✓ A distribution map of EBs was created.
- ✓ EB eclipse-depth ratio was calculated as 0.183 to 0.959 with a median of 0.551 and a modal value of 0.510.

7.7.3 Results for EW objects

- ✓ 2,875 EWs were assessed.
- ✓ 97.8% of the NN-provided EW classifications were manually confirmed.
- ✓ 206 of the EWs were known in SIMBAD and the GCVS.
- ✓ 2,251 new EWs were discovered.
- ✓ EW period range was calculated as 0.18 to 3.62 days with a median of 0.34 days and a modal value of 0.26 days, but two objects with higher periods need to be assessed (see section 7.3.3).
- ✓ 25 EWs had a period longer than the published period limit of <1 day.
- ✓ EW amplitude range was 0.02 to 1.32Vmag, with a median of 0.32 and a modal value of 0.27Vmag.
- ✓ 39 EWs have amplitude values greater than the published range of <0.8Vmag.
- ✓ A distribution map of EWs was created.
- ✓ EW eclipse-depth ratio was calculated as 0.673 to 1.0 with a median of 0.878 and a modal value of 0.918.

- ✓ Eclipse-depth ratio separation range of: EB = 0.75 and below; EW = 0.85 and above; EB/EW = 0.76 to 0.84.

The next chapter performs a similar analysis as this chapter for the pulsating objects DSCT and RRAB objects and discusses the results obtained.

---------- o ----------

Chapter 8 SuperWASP Pulsating stars

In Chapter 5, all the periodic variables in the SuperWASP archive were processed with the ''LC Analyser classifier' application and preliminary classifications were given to 67,938 RRAB objects and 181,173 DSCT objects using a confidence index of 1, 2 or 4. In Chapter 6, the number of DSCT objects was reduced to include only those with confidence index 1 classifications and PFlag 0 classifications from confidence index 2 and 4. This was due to time constraints for the analysis of the objects. The phase-folded light-curves for the processed objects were reviewed to identify those where the NN classification was manually confirmed as RRAB or DSCT. This provided 8,556 RRAB objects and 1,979 DSCT objects for assessment in this current chapter. In this chapter, the distance to each of the RRAB stars was calculated in order to produce a three-dimensional map of their distribution in the Milky Way. Also, two topical areas of RRAB stars were reviewed with regard to the SuperWASP classified RRABs i.e. the Oosterhoff dichotomy and the Blazhko effect. The 10,535 objects reviewed were split into three categories based on the state of the light-curve (i.e. 'Good', 'Large scatter' and 'Small amplitude') using a similar process to the eclipsing binaries in Chapter 7. Examples of each state can be seen in Figure 8-1. The catalogues for each class and the supporting binned and full phase-folded light-curves are available on the supplementary DVD in the following location:

Supplementary data - Catalogues	
RRAB catalogue	X:\Chapter08\Catalogues\RRAB.xlsm
DSCT catalogue	X:\Chapter08\Catalogues\DSCT.xlsm
Pulsating catalogue	X:\Chapter08\Catalogues\Pulsating.xlsm

Where X is DVD-1 in the DVD-drive

Supplementary data – Light-curves	
RRAB Good	X:\Chapter08\Light_curves\RRAB\Good
RRAB Large scatter	X:\Chapter08\Light_curves\RRAB\LS
RRAB Small amplitude	X:\Chapter08\Light_curves\RRAB\SA
DSCT Good	X:\Chapter08\Light_curves\DSCT\Good
DSCT Large scatter	X:\Chapter08\Light_curves\DSCT\LS
DSCT Small amplitude	X:\Chapter08\Light_curves\DSCT\SA

Where X is the DVD-1 in the DVD-drive

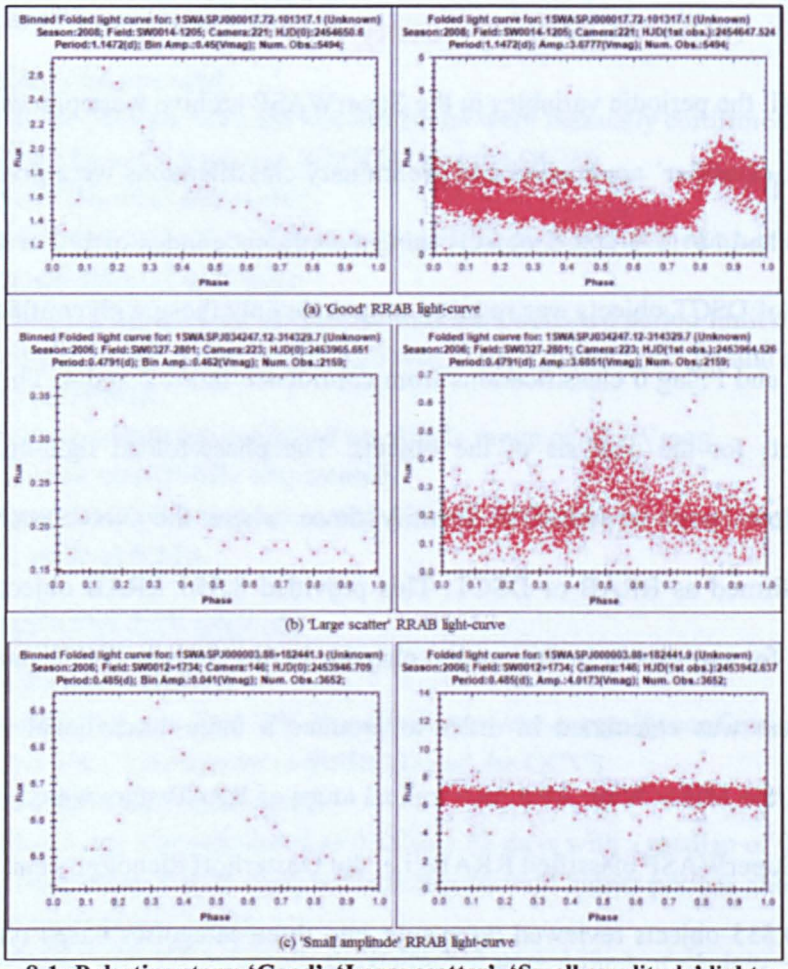

Figure 8-1: Pulsating stars: 'Good', 'Large scatter', 'Small amplitude' light-curves

In the analysis, each object was classified by manually reviewing the full phase-folded light-curve and the results compared against the classes obtained from the NNs to see how effective the NN classification was. A search was performed for each object in SIMBAD to identify the known objects. This was achieved in a similar way to the known eclipsing binaries in Chapter 7. Graphs were created for variability period and amplitude to obtain the SuperWASP limits for these parameters and also for galactic location to show the distribution of objects across the night sky. Finally, the distance to each RRAB star was calculated using a published absolute magnitude and three-dimensional graphs created to view their structure in the Galaxy.

8.1. Analysis of RRAB objects

The analysis was initially performed for 'All' 8,556 RRAB objects, but while plotting the period graph in section 8.1.3, it was noticed that period-clumping and period-banding were present as previously discussed in Chapter 6. The analysis was reworked twice after identifying the PFlags causing these anomalies. The first occasion removed both 'Large scatter' (LS) and 'Small amplitude' (SA) objects for the affected PFlags; and the second occasion removed ALL objects with the affected PFlags. The results of these analyses are discussed in the following sections.

8.1.1 Statistics

Table 8-1 shows that 78.86% of the RRAB objects that were classified by the NNs were subsequently confirmed by manual review. As shown in Table 8-2, the majority of the misclassified objects were DSCT class. This was expected as the shape of the DSCT light-curve is very much like that of RRAB. The major difference is the period, but as already mentioned in Chapter 6, the NN period-bin did not take into account the difference between these two object classes.

RRAB Objects		Based on light-curve shape					
		All		LS/SA removed		G/LS/SA removed	
Light-curve quality	NN	No.	%	No.	%	No.	%
Good (G)	Agree	5,897	68.92	5,897	71.02	5,834	71.87
Large scatter (LS)	Agree	253	2.96	223	2.69	223	2.75
Small amplitude (SA)	Agree	597	6.98	564	6.79	564	6.95
Total	Agree	6,747	78.86	6,684	80.50	6,621	81.57
Good (G)	Disagree	981	11.47	981	11.82	858	10.57
Large scatter (LS)	Disagree	364	4.25	261	3.14	261	3.22
Small amplitude (SA)	Disagree	464	5.42	377	4.54	377	4.64
Total	Disagree	1,809	21.14	1,619	19.50	1,496	18.43
Overall total	All	8,556		8,303		8,117	

Table 8-1: RRAB: Statistics for identified objects

Studying three of the misclassified objects (one CEP, one RM and one RRC) showed why the NNs classified them as RRAB. Figure 8-2 shows that the binned phase-folded light-curve on the left is quite rounded on the decline making it more CEP shape than RRAB. The full phase-folded light-curve on the right shows that this could possibly be a CEP

object and a possible manual misclassification. This shows how difficult it was to classify these objects using only the light-curve.

Class	Number
DSCT	1773
CEP	2
RM	2
RRC	3
Review	28
No class	1
Total	1809

Table 8-2: RRAB: NN class disagrees with manual class

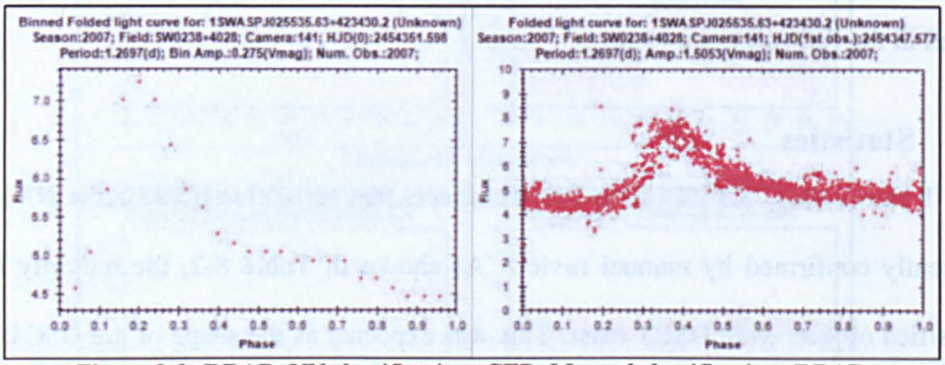

Figure 8-2: RRAB: NN classification: CEP; Manual classification: RRAB (1SWASP J025535.63+423430.2)

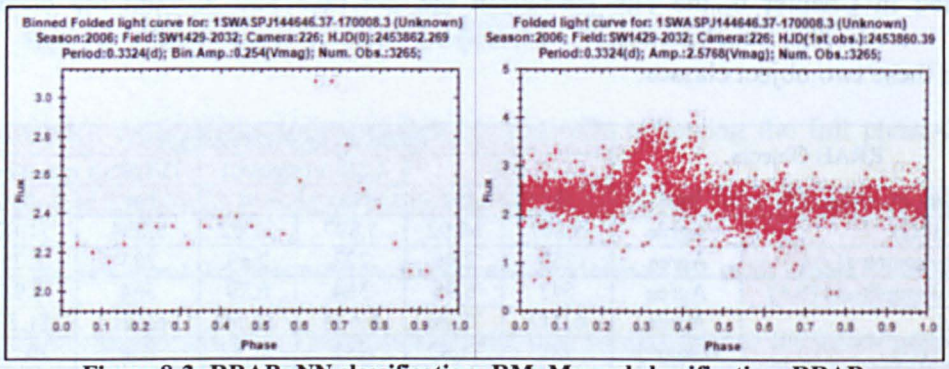

Figure 8-3: RRAB: NN classification: RM; Manual classification: RRAB (1SWASP J144646.37-170008.3)

In Figure 8-3, the NN classification was difficult to interpret, but it should be noted that the phase 0.0 point on the binned phase-folded light-curve is aligned to the lowest point on the full phase-folded light-curve, which is usually at the start of the incline. In the case of Figure 8-3 though, the lowest point in the full phase-folded light-curve was beyond the

pulsation around 0.65. This caused the incline in the binned phase-folded light-curve to start at around 0.6, thus giving a peculiar view to the NN and hence the misclassification.

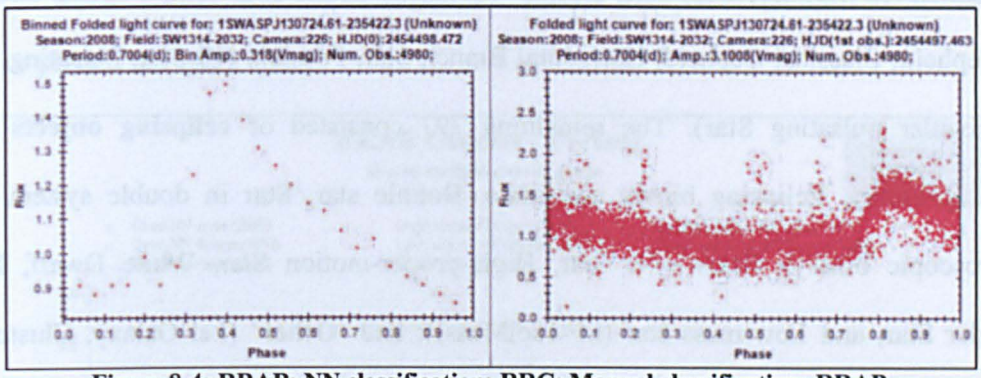

Figure 8-4: RRAB: NN classification: RRC; Manual classification: RRAB (1SWASP J130724.61-235422.3)

Figure 8-4 shows that there was an observation in the binned phase-folded light-curve around 0.2 that made the image lose the steep incline expected in an RRAB object and made it more RRC shape. The full phase-folded light-curve confirms that the object is RRAB. For the rest of this research, the manually obtained classes were used.

8.1.2 Known objects

Searches were made in SIMBAD and the GCVS for all 8,557 RRAB objects to see if they were known. Table 8-3 shows the results of the search in SIMBAD for known objects.

RRAB objects (Overall total = 8,556)							
SIMBAD	Based on light-curve shape						
	Good		Large scatter		Small amplitude		Total
	NN agree	NN disagree	NN agree	NN disagree	NN agree	NN disagree	All
RR	2,252	191	32	25	83	17	2,600
DSCT	1	1	0	0	0	0	2
W Vir	2	2	0	0	0	0	4
Other pulsating	140	23	2	19	7	13	204
Eclipsing	8	10	1	3	1	1	24
Star	160	44	27	38	20	43	332
Other	325	45	9	12	26	24	441
Total known	2,888	316	71	97	137	98	3,607
Total unknowns							4,949
Total unknowns (including Star and Other categories)							5,722

Table 8-3: RRAB: Objects known in SIMBAD

Of the 8,556 RRAB objects, 3,607 had a nearest neighbour within 1 arc-min. Appendix 26 shows the breakdown of these per class. Of the 3,607 known objects, 2,600 confirmed the NN **RRAB** class. 2 were **DSCT**, 4 were **W Vir** and 204 were '**other pulsating**' classes (i.e. Cepheid, Classical Cepheid, Horizontal Branch Star, Possible HB Star, Pulsating, and Semi-regular pulsating Star). The remaining 797 consisted of **eclipsing objects** (i.e. Eclipsing binary, Eclipsing binary candidate, Double star, Star in double system and Spectroscopic binary); **Stars** (i.e. Star, High proper-motion Star, White Dwarf, Blue Straggler Star, and Low-mass star (M<1solMass)); and '**Other**' (i.e. Galaxy, Cluster of Galaxies, Galaxy in Cluster of Galaxies, HII (ionized) region, Quasar, Possible Quasar, Radio - Source, Unknown nature, Variable, and X-ray source). The eclipsing stars were included in the total of 'known' objects as they could possibly be incorrect classifications in SIMBAD, but 'Star' and 'Other' classes were added to the overall total of 'unknown stars', giving a final total of 5,722 new RRABs.

As the SuperWASP archive is cross-matched with the GCVS, the known objects in the GCVS were identified at the time of 'LC Analyser classifier' data processing. 1,121 of the RRAB objects were known in the GCVS. These were also known in SIMBAD.

8.1.3 Period

The period values for ALL the RRAB objects were plotted in Figure 8-5 to obtain an overview and to determine the period range. The 'expected' period range (0.3 to 1.2 days) was obtained from the GCVS and also plotted.

The objects were plotted with 'Good', 'Large scatter' and 'Small amplitude' objects shown as different populations to see how they were distributed. These populations were also split by whether the NN-classifications agreed with the manual-classifications or not.

The results in Figure 8-5 showed period-clumping and period-banding as discussed in Chapter 6, so the PFlags containing the affected objects were identified as shown in Table 8-4. The 'Large scatter' and 'Small amplitude' objects were removed from the dataset and were re-plotted in Figure 8-6.

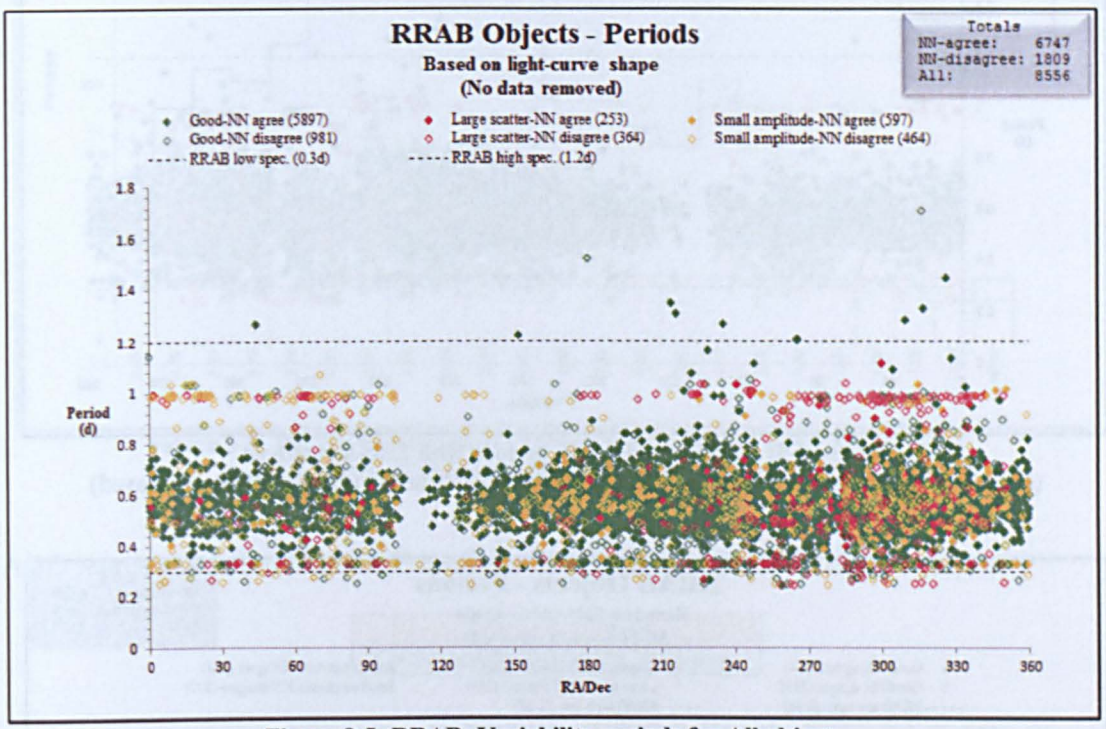

Figure 8-5: RRAB: Variability periods for All objects

Periods to remove		
PFlags	Low	High
1	0.332	0.335
3	0.97	0.990

Table 8-4: RRAB: PFlags containing clumped and banded periods

Figure 8-6 shows that all the period-clumping objects and a large number of the period-banding objects have been removed. However, as there was still some period-banding present, all objects with the PFlags in Table 8-4 were removed and the periods re-plotted as Figure 8-7. This removed the majority of clumped and banded periods and the remaining 8,117 objects became the dataset that was used to obtain the SuperWASP period and amplitude ranges. To obtain the period range, a histogram of periods was created in Figure 8-8.

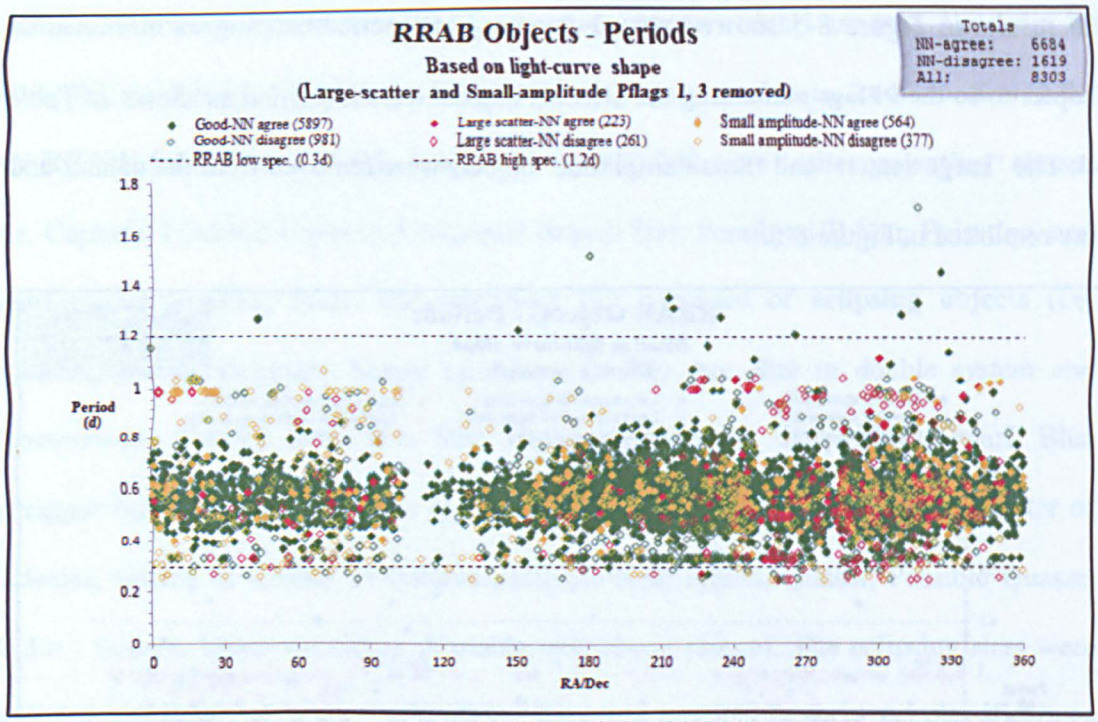

Figure 8-6: RRAB: Variability periods with LS/SA removed
(i.e. where 'Large scatter' and 'Small amplitude' objects in the affected PFlags removed)

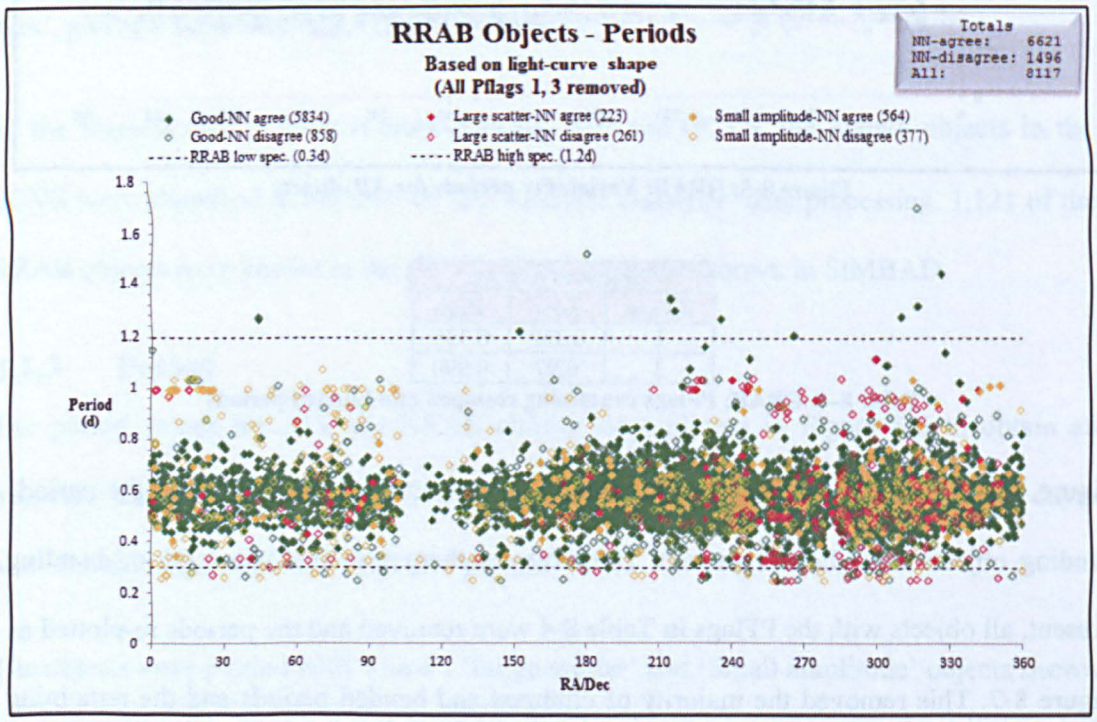

Figure 8-7: RRAB: Variability periods with G/LS/SA removed
(i.e. where all objects in the affected PFlags removed)

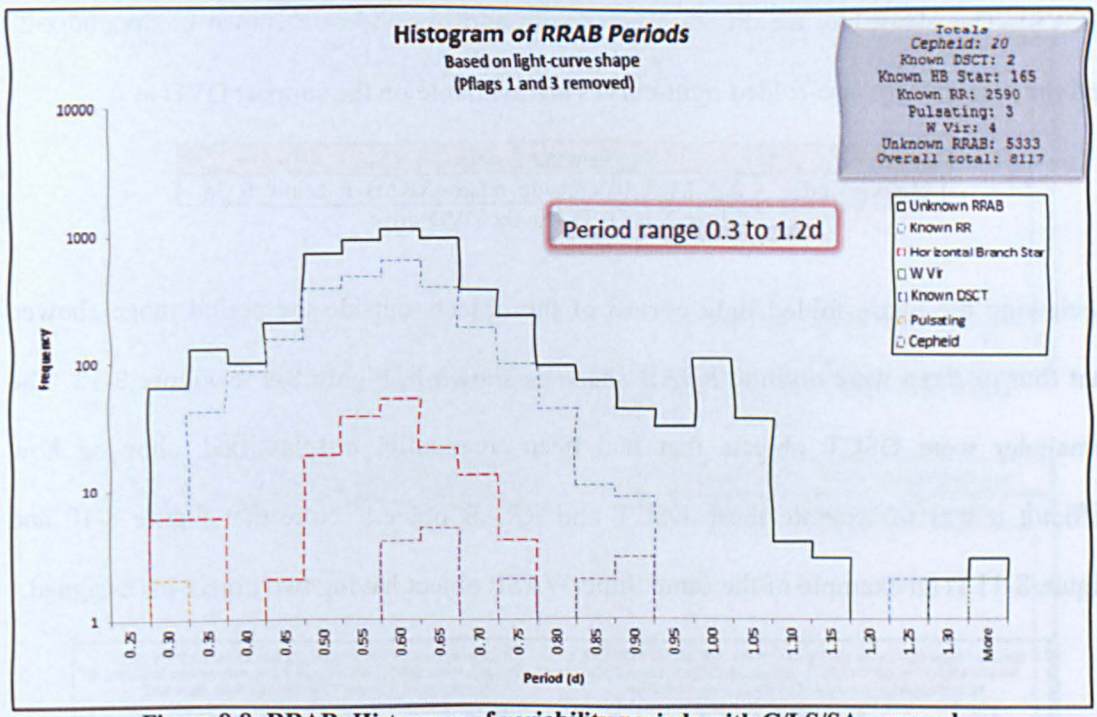

Figure 8-8: RRAB: Histogram of variability periods with G/LS/SA removed (i.e. where all objects in the affected PFlags removed)

A 3D representation of Figure 8-8 can be seen on the support DVD at the location:

Light-curve output
X:\Chapter08\3D-hist\Fig_8-08.bmp

RRAB period (days)	
Mean	0.574
Median	0.568
Mode	0.609
Min	0.250
Max	1.709
N	8,117
N < 0.3 days	79
N > 1.2 days	14

Table 8-5: RRAB: Period statistics

The histogram contains a total of 8,117 RRABs where 5,333 were 'unknown' and the rest were known in SIMBAD. The populations were displayed alongside one-another on the same axis in order to see the distribution of periods and Table 8-5 shows that the range was 0.25 to 1.71 days (median 0.57, mode 0.61). Figure 8-7 shows that 79 objects had a period lower than the published period range of 0.3 days and 14 above the period range 1.2 days

(GCVS). The identifiers for the 79 objects with short periods are shown in Appendix 27 and the associated phase-folded light-curves are available on the support DVD at:

Supplementary data	
Short periods	X:\Chapter08\Outside_ranges\RRAB_P_below_0_3d

Where X is DVD-1 in the DVD-drive

Reviewing the phase-folded light-curves of the objects outside the period range showed that four of them were definite RRAB shape as shown in Figure 8-9 to Figure 8-12. The remainder were DSCT objects that had been 'manually' misclassified, showing how difficult it was to separate these DSCT and RRAB objects. Note that Figure 8-10 and Figure 8-11 is an example of the same SuperWASP object having two object-ids assigned.

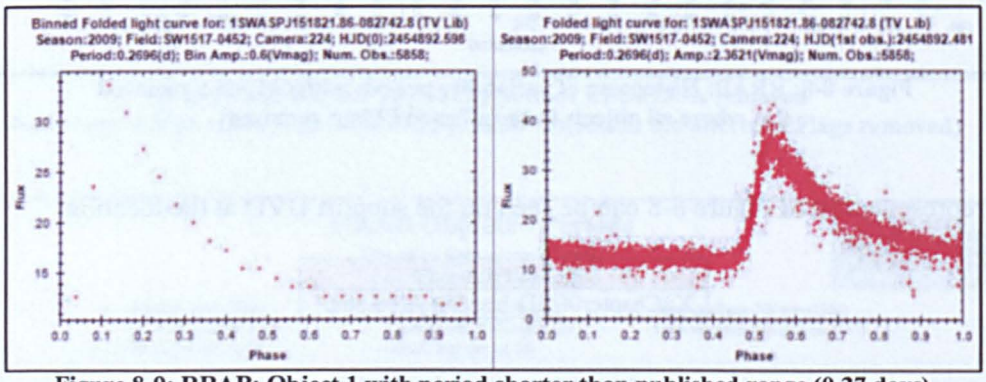

Figure 8-9: RRAB: Object 1 with period shorter than published range (0.27 days) (1SWASP J151821.86-082742.8 → TV Lib)

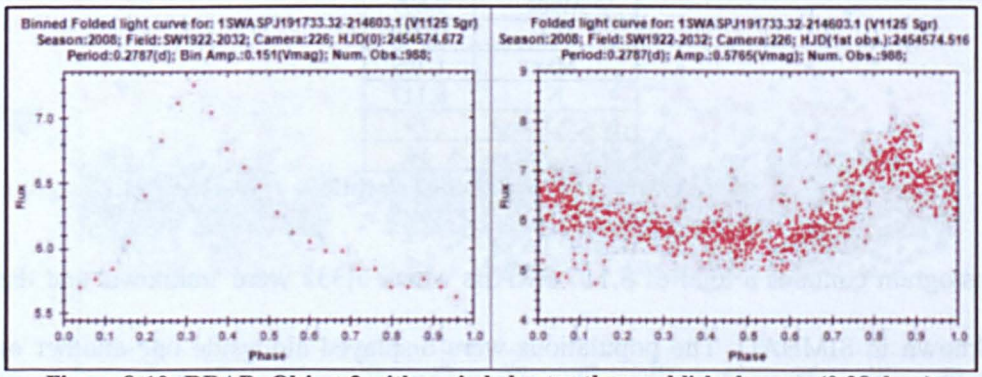

Figure 8-10: RRAB: Object 2 with period shorter than published range (0.28 days) (1SWASP J191733.32-214603.1 → V1125 Sgr)

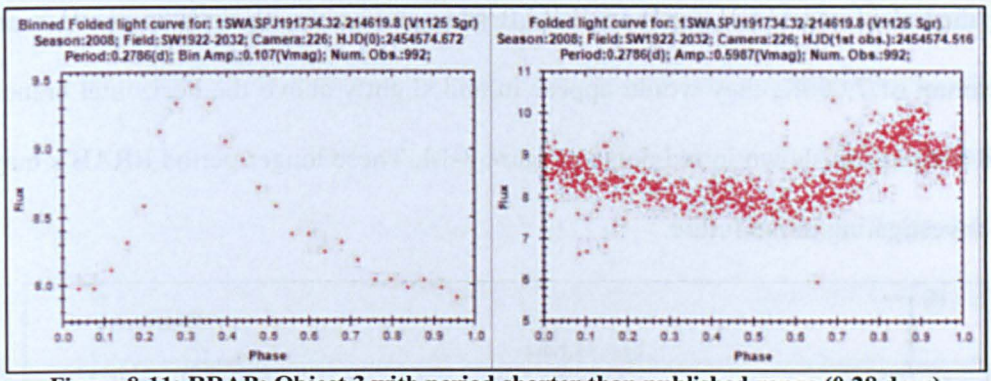

Figure 8-11: RRAB: Object 3 with period shorter than published range (0.28 days) (1SWASP J191734.32-214619.8 → V1125 Sgr)

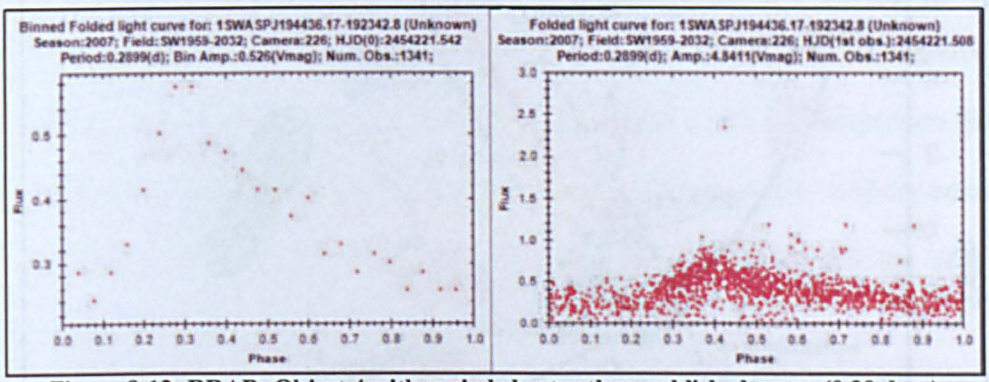

Figure 8-12: RRAB: Object 4 with period shorter than published range (0.29 days) (1SWASP J194436.17-192342.8)

Identifiers for the 14 long periods are shown in Appendix 28 along with their calculated Vmag. The associated phase-folded light-curves are available on the support DVD at:

Supplementary data	
Longer_periods	X:\Chapter08\Outside_ranges\RRAB_P_above_1_2d

Where X is DVD-1 in the DVD-drive

Reviewing the phase-folded light-curves showed that they were all definite RRAB shape, for example the highest period object is shown in Figure 8-13.

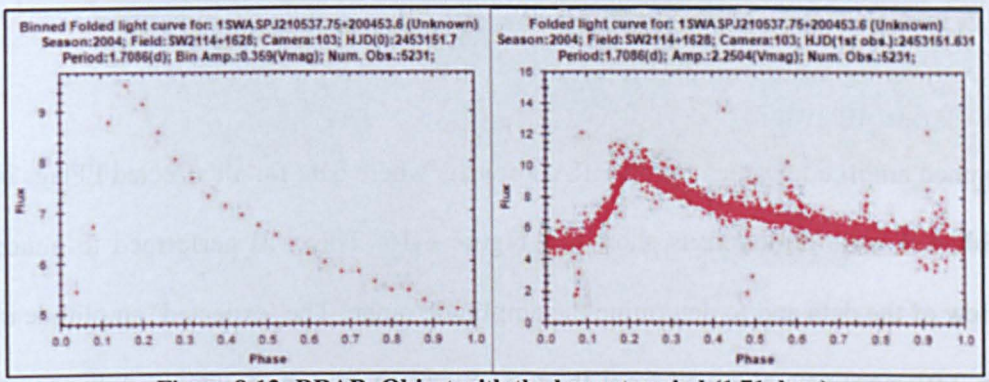

Figure 8-13: RRAB: Object with the longest period (1.71 days) (1SWASP J210537.75+200453.6)

Using the calculated Vmag for these RRAB stars and assuming that they have average temperature of 7,000K, they would appear in and slightly above the horizontal branch of the HR diagram as shown in red dots in Figure 8-14. These longer-period RRAB's may be worth investigating in the future.

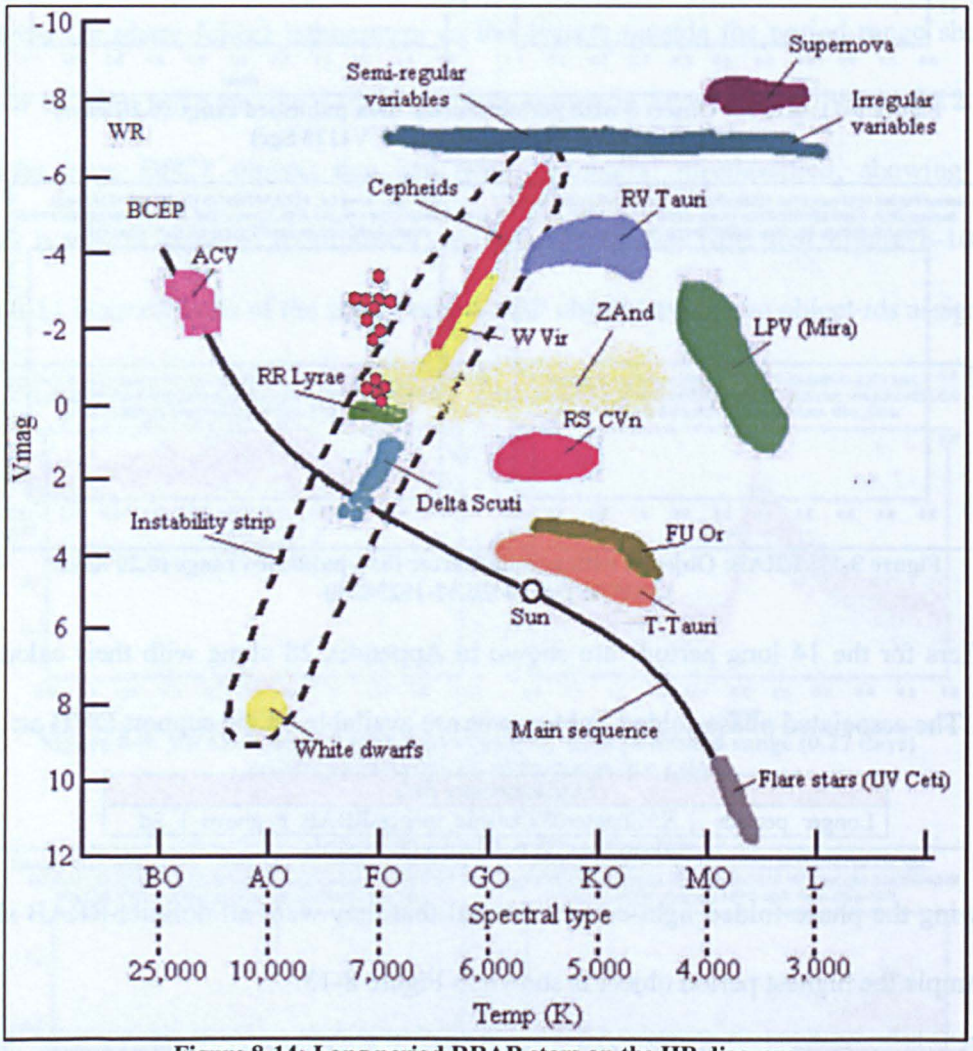

Figure 8-14: Long period RRAB stars on the HR diagram

8.1.4 Amplitude

The binned amplitude values for all RRAB objects where data for all affected PFlags listed in Table 8-4 were removed, is shown in Figure 8-15. This was performed to obtain an overview of the data and to determine the amplitude range. The 'expected' amplitude range (0.5 to 2.0Vmag) was obtained from the GCVS and shown on the graph. A histogram of

the amplitudes is presented in Figure 8-16. Again, the graphs show the distributions for 'Good', 'Large scatter' and 'Small amplitude' objects and whether the NN-classification agrees with the manual-classification. Figure 8-15 did not show any differences between the amplitude populations. The histogram in Figure 8-16 and the data in Table 8-6 show that the amplitude range was 0.02 to 2.43Vmag (median 0.41, mode 0.13). This is a far wider range than that published in the GCVS for RRABs (0.5 to 2.0Vmag), and although the GCVS describes a sub-class 'RR' that has a range of 0.2 to 2.0Vmag, the amplitudes were also outside this range. It should be noted that in Figure 8-16, the RRAB stars identified in this research have significantly more systems with low amplitude than the known sample, so the flat amplitude distribution in the known sample is likely an artefact (biased towards high amplitude objects). This analysis has shown that the underlying amplitude distribution is actually peaked to the lower values.

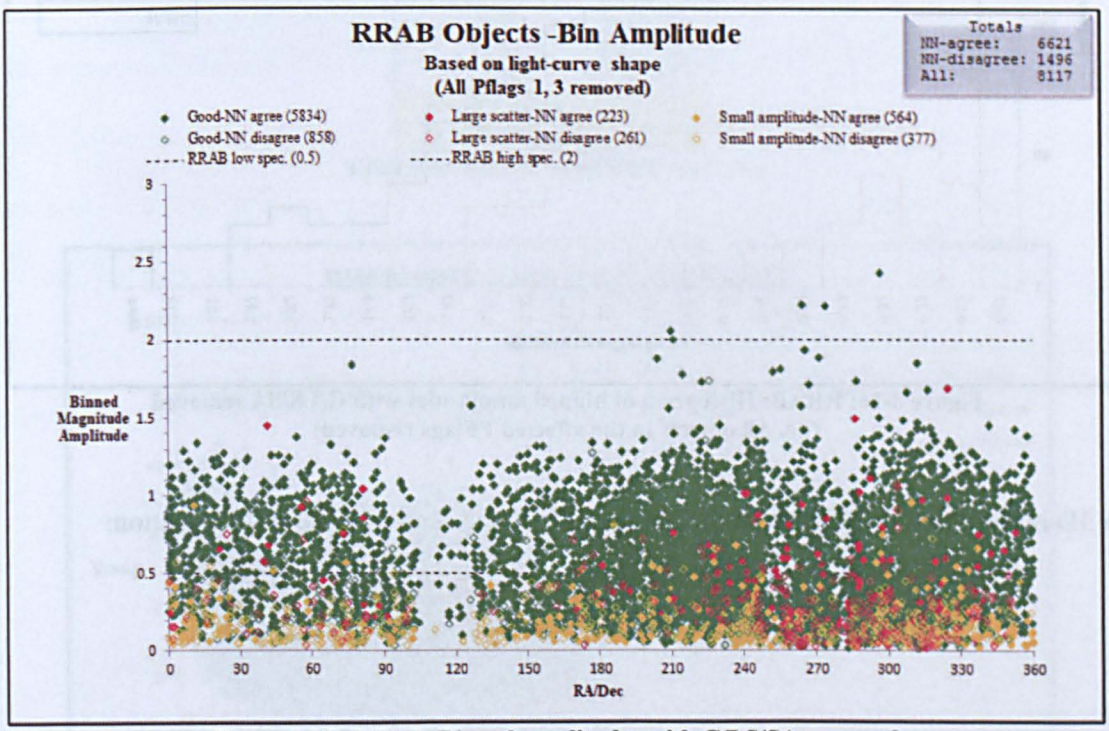

Figure 8-15: RRAB: Binned amplitudes with G/LS/SA removed (i.e. All objects in the affected PFlags removed)

Calculating the Vmag values for the 4,749 RRAB objects with low amplitudes gives a range of -7.87 to 1.23Vmag. Plotting these in a histogram (Figure 8-17) and assuming an average temperature of 7,000K shows that they would spread across the HR diagram from the Semi-regular variables down through the horizontal-branch to the Delta Scutis (see Figure 8-14 above), but looking at the plot in Figure 8-18 shows that the majority of the RRABs lie in the horizontal-branch between Vmag of 1.0 and -2.0 (dotted red lines), indicating that they are good representatives of the RRAB class.

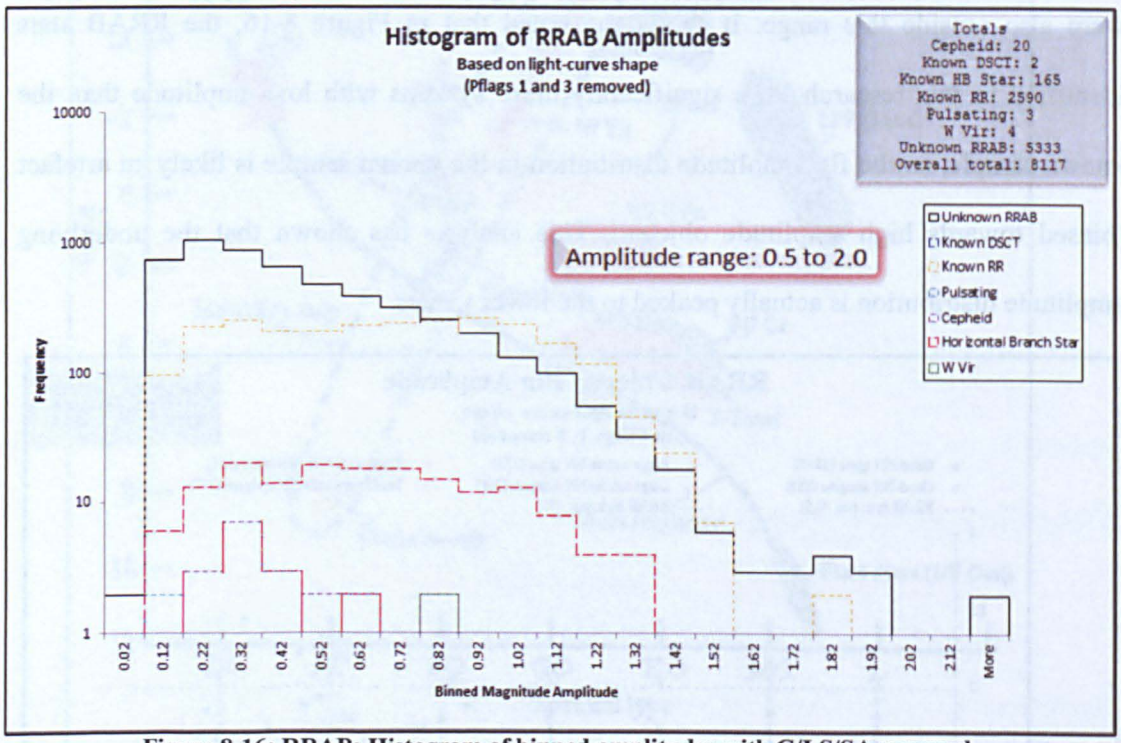

Figure 8-16: RRAB: Histogram of binned amplitudes with G/LS/SA removed (i.e. All objects in the affected PFlags removed)

A 3D representation of Figure 8-16 can be seen on the support DVD at the location:

Light-curve output
X:\Chapter08\3D-hist\Fig_8-16.bmp

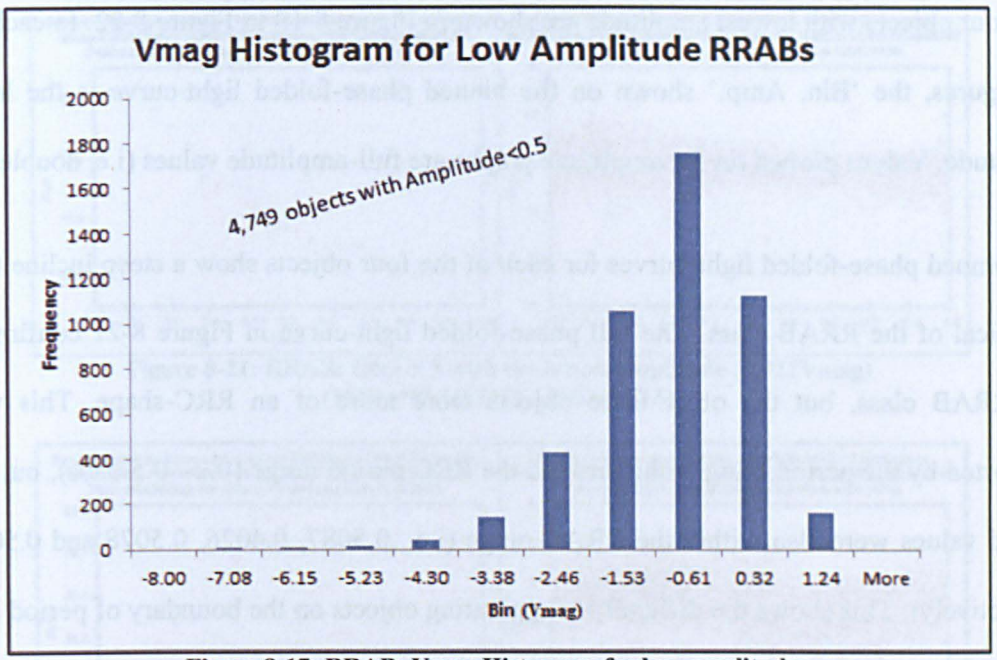

Figure 8-17: RRAB: Vmag Histogram for low-amplitudes

RRAB amplitude (Vmag)	
Mean	0.485
Median	0..406
Mode	0.126
Min	0.020
Max	2.432
N	8,117
N < 0.5 Vmag	4,749
N > 2.0 Vmag	4

Table 8-6: RRAB: Amplitude statistics

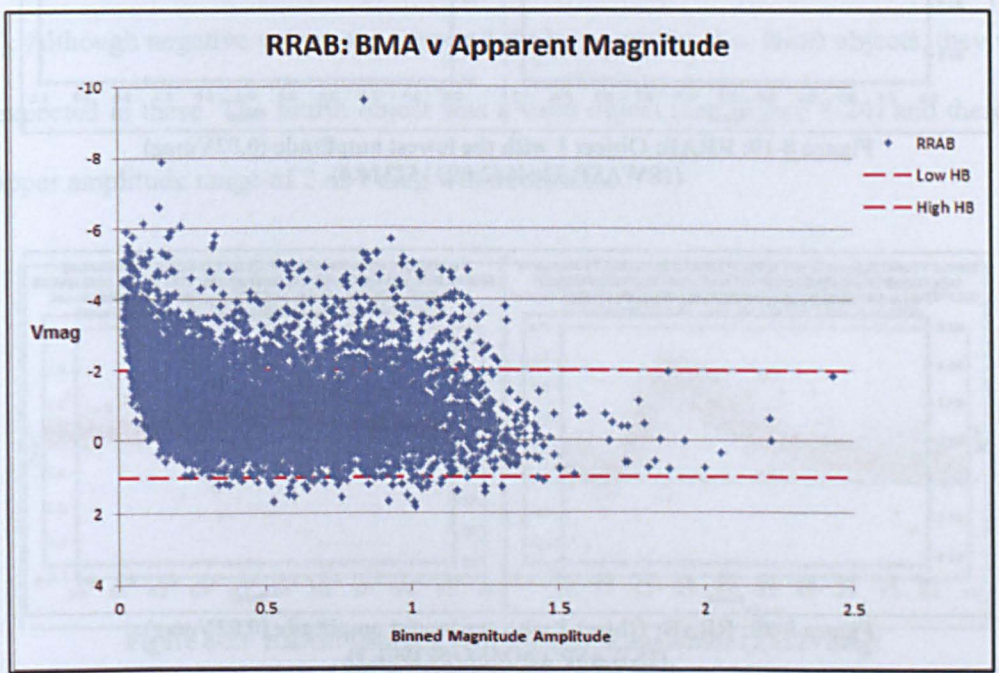

Figure 8-18: RRAB: Vmag against BMA for low-amplitudes

The four objects with lowest amplitude are shown in Figure 8-19 to Figure 8-22. In each of the figures, the 'Bin, Amp.' shown on the binned phase-folded light-curve is the half-amplitude. Values plotted on the amplitude graphs are full-amplitude values (i.e. double).

The binned phase-folded light-curves for each of the four objects show a steep incline that is typical of the RRAB class. The full phase-folded light-curve in Figure 8-21 confirmed the RRAB class, but the other three objects were more of an RRC-shape. This was supported by the period lying within/around the RRC period range (0.2 - 0.5 days), but the period values were also within the RRAB range (i.e. .0.5087, 0.4026, 0.5078 and 0.5087 respectively). This shows the difficulty in separating objects on the boundary of period and amplitude ranges. Therefore a catalogue was created for 'pulsating' objects that contains RRAB (RR, RRC) and DSCT objects (see section 8.3).

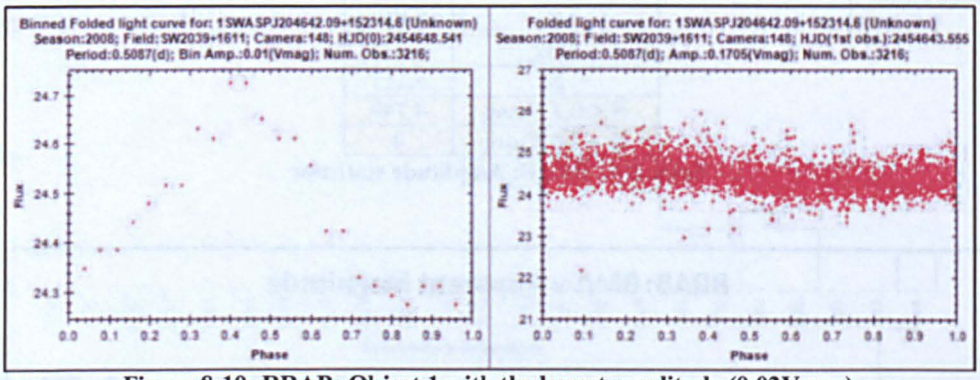

Figure 8-19: RRAB: Object 1 with the lowest amplitude (0.02Vmag) (1SWASP J204642.09+152314.6)

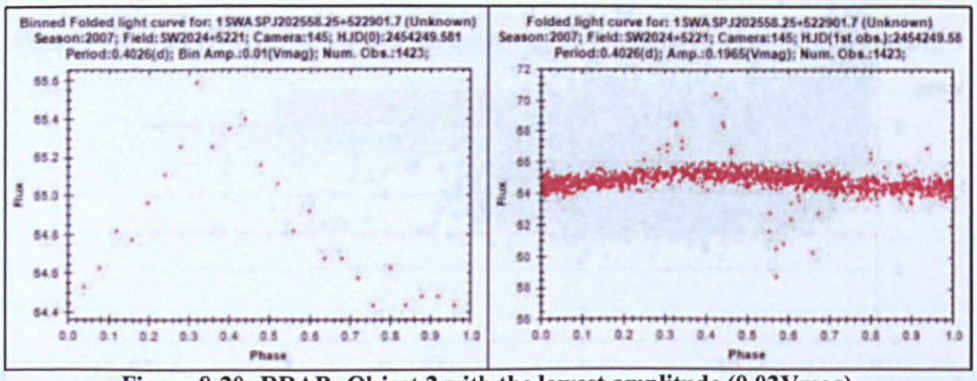

Figure 8-20: RRAB: Object 2 with the lowest amplitude (0.02Vmag) (1SWASP J202558+522901.7)

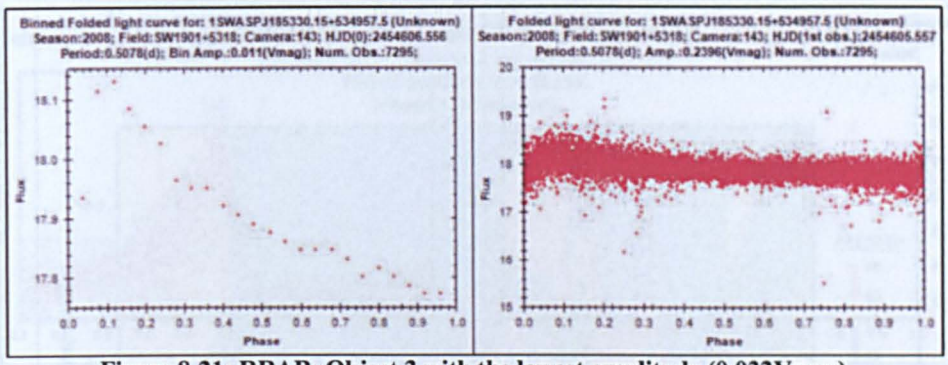

Figure 8-21: RRAB: Object 3 with the lowest amplitude (0.022Vmag) (1SWASP J185330.15+534957.5)

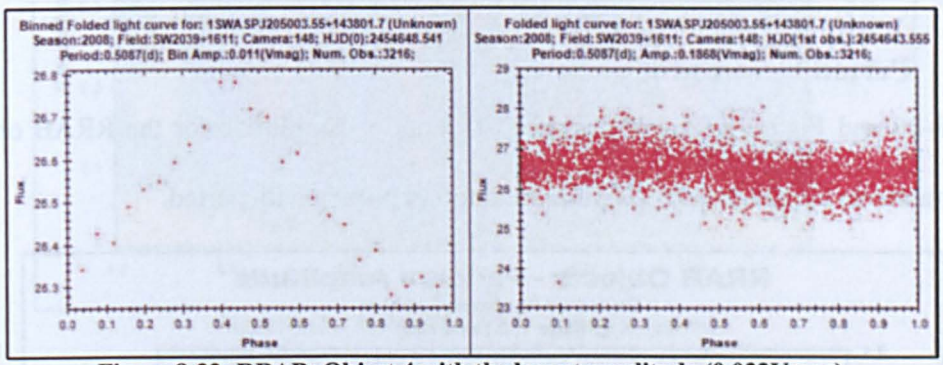

Figure 8-22: RRAB: Object 4 with the lowest amplitude (0.022Vmag) (1SWASP J205003.55+143801.7)

With regard to objects with high amplitude values, three of the four objects were definite RRAB objects (values 2.05, 2.22, 2.22 and 2.43Vmag) but their amplitude values were not included because there were a few negative-flux values in the observations (e.g. Figure 8-23). Although negative values are expected for large-scatter (i.e. faint) objects, they were not expected in these. The fourth object was a valid object (see Figure 8-24) and therefore the upper amplitude range of 2.43Vmag was acceptable.

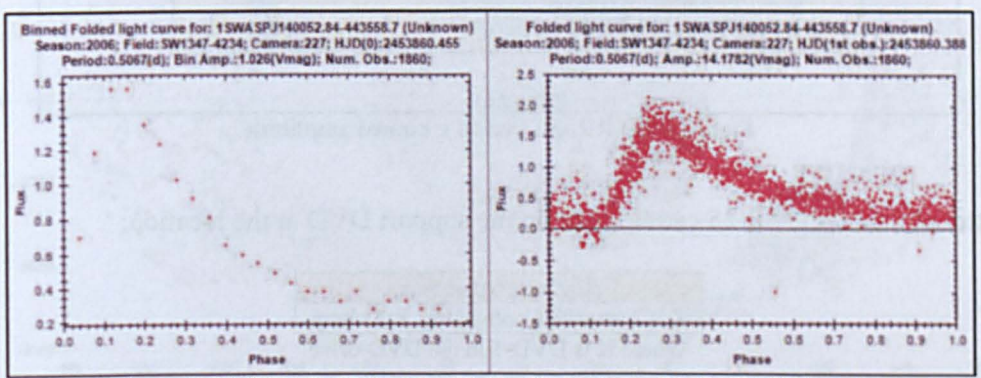

Figure 8-23: RRAB: Object 1 with the highest amplitude (2.052Vmag) (1SWASP J140052.84-443558.7)

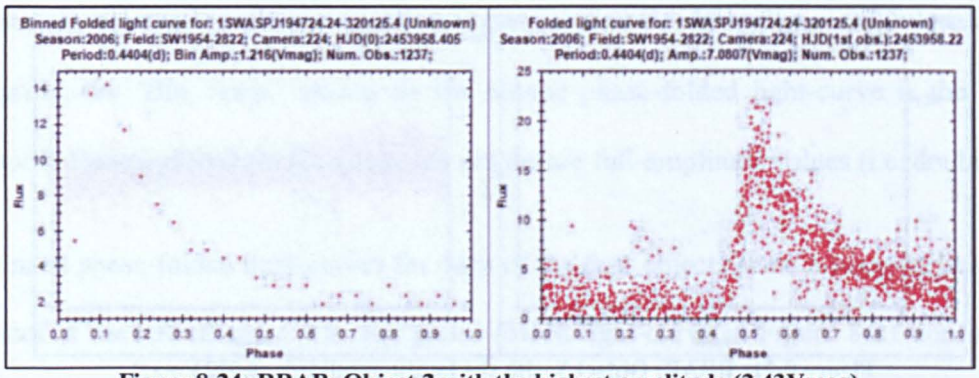

Figure 8-24: RRAB: Object 2 with the highest amplitude (2.43Vmag) (1SWASP J194724.24-320125.4X)

8.1.5 Period v Amplitude

Figure 8-25 and Figure 8-26 show graphs of Period v Amplitude for the RRAB objects.

These graphs do not show any particular trend of amplitude with period.

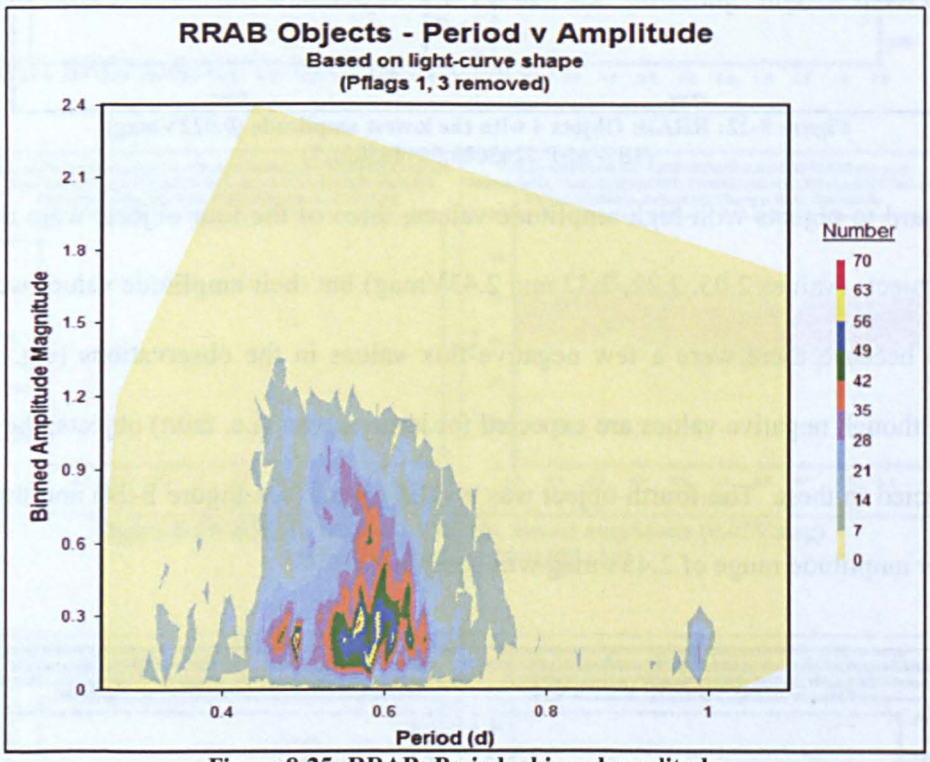

Figure 8-25: RRAB: Period v binned amplitude

A scatter plot of Figure 8-25 can be seen on the support DVD at the location:

Light-curve output
X:\Chapter08\Contour\Fig_8-25.bmp

Where X is DVD-1 in the DVD-drive

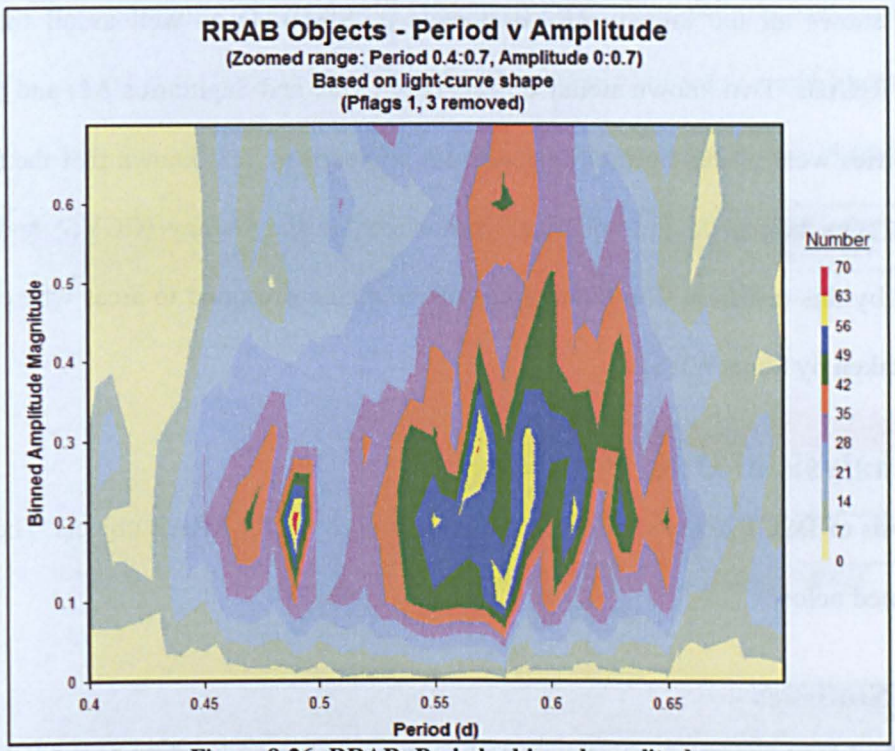

Figure 8-26: RRAB: Period v binned amplitude (Zoomed into range Period 0.4:0.7, Amplitude 0:0.7)

8.1.6 Distribution

The RRAB objects remaining after all the affected PFlags had been removed were plotted on a Hammer projection to view the distribution over the full sky (see Figure 8-27).

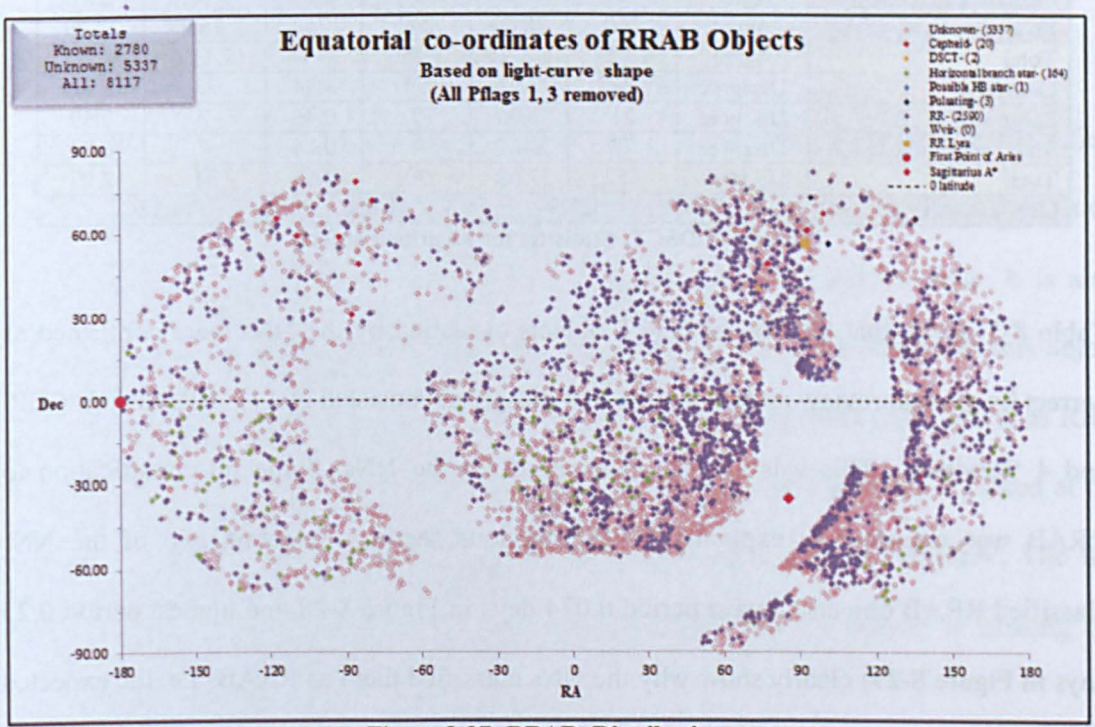

Figure 8-27: RRAB: Distribution

The map shows all the known RRAB objects in SIMBAD as well as all the newly classified RRABs. Two known stellar objects (RR Lyrae and Sagittarius A*) and the First Point of Aries were placed on the projection for comparison. It is known that the majority of RRAB stars belong to the spherical component of the Galaxy (GCVS) and this is supported by this research. The blank areas of the map correspond to areas where images were not taken by SuperWASP.

8.2. Analysis of DSCT objects

The analysis of DSCT objects followed the same process as for RRAB objects. The results are discussed below.

8.2.1 Statistics

The DSCT objects showed similar period-clumping and period-banding as the RRABs, so the same exclusion criteria were applied.

DSCT Objects		Based on light-curve shape					
		All		LS/SA removed		G/LS/SA removed	
Light-curve quality	NN	No.	%	No.	%	No.	%
Good (G)	Agree	1,170	59.12	1,170	76.17	856	72.18
Large scatter (LS)	Agree	97	4.90	34	2.21	34	2.87
Small amplitude (SA)	Agree	560	28.30	262	17.06	262	22.09
Total	Agree	1,827	92.32	1,466	95.44	1,152	97.13
Good (G)	Disagree	59	2.98	59	3.84	23	1.94
Large scatter (LS)	Disagree	21	1.06	7	0.46	7	0.59
Small amplitude (SA)	Disagree	72	3.64	4	0.26	4	0.34
Total	Disagree	152	7.68	70	4.56	34	2.87
Overall total	All	1,979		1,536		1,186	

Table 8-7: DSCT: Statistics for identified objects

Table 8-7 shows that 92.32% of DSCT objects classified by the NNs were confirmed as correct by manual review and the 7.68% that disagreed consisted of 147 'RRABs', 1 'CEP' and 4 'Reviews'. This was a very good result for the NNs. Some misclassification to RRAB was expected as explained in the previous section. Selecting two of the NN-classified RRAB objects (lowest period 0.074 days in Figure 8-28 and highest period 0.25 days in Figure 8-29) clearly show why the NNs classified them as RRABs i.e. the expected

incline is present on the binned phase-folded light-curve. The full phase-diagram shows that the first object is probably DSCT due to the low period, but it could be type RR as discussed earlier. The second object is likely to be RRAB due to the higher period.

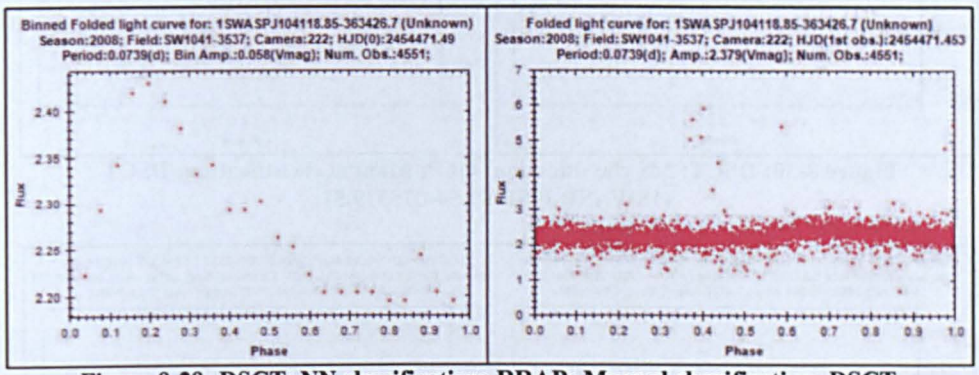

Figure 8-28: DSCT: NN classification: RRAB; Manual classification: DSCT (1SWASP J104118.85-363426.7)

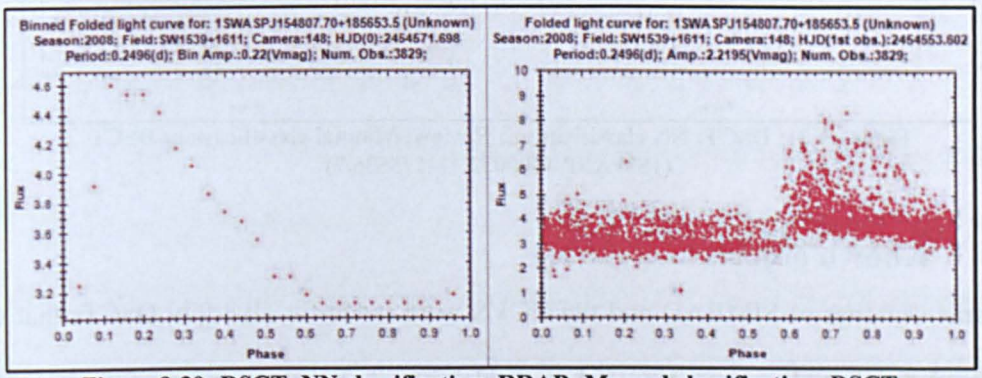

Figure 8-29: DSCT: NN classification: RRAB; Manual classification: DSCT (1SWASP J154807.70+185653.5)

Looking at the CEP and Review misclassifications, it is clear to see why the NNs classified Figure 8-30 as CEP. The rounded area at the top of the light-curve has a profound effect on the NNs. The full phase-folded light-curve is clearly typical of RRAB class. It is also apparent why the NNs classified Figure 8-31 as 'Review'. The data output for this object shows that NN1 classified it as EW (due to the middle eclipse), NN2 classified it as RRC (due to the rounded light-curve shape) and NN3 classified it as DSCT (as it looked at the overall light-curve shape). This generated an overall classification of 'Review'. The full phase-folded light-curve shows a definite RRAB shape, but the scatter is causing the classification problem.

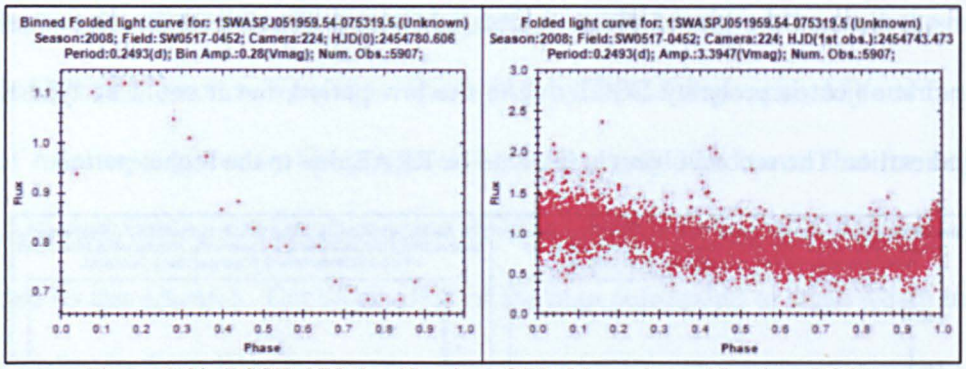

Figure 8-30: DSCT: NN classification: CEP; Manual classification: DSCT (1SWASP J051959.54-075319.5)

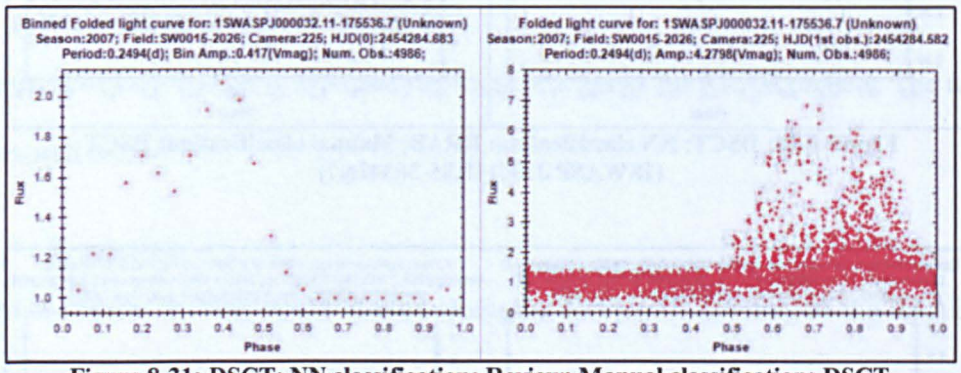

Figure 8-31: DSCT: NN classification: Review; Manual classification: DSCT (1SWASP J000032.11-175536.7)

8.2.2 Known objects

The same searches of SIMBAD and the GCVS were made for all 1,979 DSCTs that were performed for RRABs in section 8.1.2. Table 8-8 shows the results of the search in SIMBAD for known objects.

DSCT objects (Overall total = 1,979)							
SIMBAD	Based on light-curve shape						
	Good		Large scatter		Small amplitude		Total
	NN agree	NN disagree	NN agree	NN disagree	NN agree	NN disagree	All
DSCT	41	0	0	0	2	0	43
RR	16	3	0	0	1	0	20
W Vir	0	0	0	0	0	0	0
Other pulsating	14	2	2	0	2	0	20
Eclipsing	11	1	0	0	7	0	19
Star	138	3	5	1	51	6	204
Other	51	3	6	1	19	5	85
Total known	271	12	13	2	82	11	391
Total unknowns							1,588
Total unknowns (including Star and Other categories)							1,877

Table 8-8: DSCT: Objects known in SIMBAD

Of the 1,979 DSCT objects, 391 had a nearest neighbour within 1 arc-min. Appendix 29 shows the breakdown of these per class. Of the 391 known objects, 43 confirmed the NN DSCT class, 20 were RR and 20 were 'other pulsating' classes. The remainder consisted of eclipsing objects; Stars; and 'Other'. The pulsating stars were included in the total of 'known' objects as they were possibly incorrect classifications in SIMBAD, but 'Star' and 'Other' classes were added to the overall total of 'unknown' objects, giving a final total of 1,877 new DSCTs.

As with the RRABs, the known GCVS objects were identified at the time of 'LC Analyser classifier' data processing. 30 of the DSCT objects were known in the GCVS. These were also known in SIMBAD.

8.2.3 Period

Following a similar process to the RRAB analysis, the period values for all DSCT objects were plotted as a distribution graph in Figure 8-32. The 'Large scatter' and 'Small amplitude' objects in the affected PFlags shown in Table 8-9 were removed and re-plotted as Figure 8-33; then all objects with the affected PFlags were removed in Figure 8-34.

Periods to remove		
PFlags	Low	High
4	0.249	0.251
5	0.199	0.201
6	0.166	0.168
7	0.142	0.144
98	0.124	0.126

Table 8-9: DSCT: PFlags containing clumped and banded periods

The 'expected' period range (0.01 to 0.2 days) was obtained from the GCVS and plotted on the distribution graphs. A histogram was created and is shown in Figure 8-35 and the calculated period range is tabulated in Table 8-10.

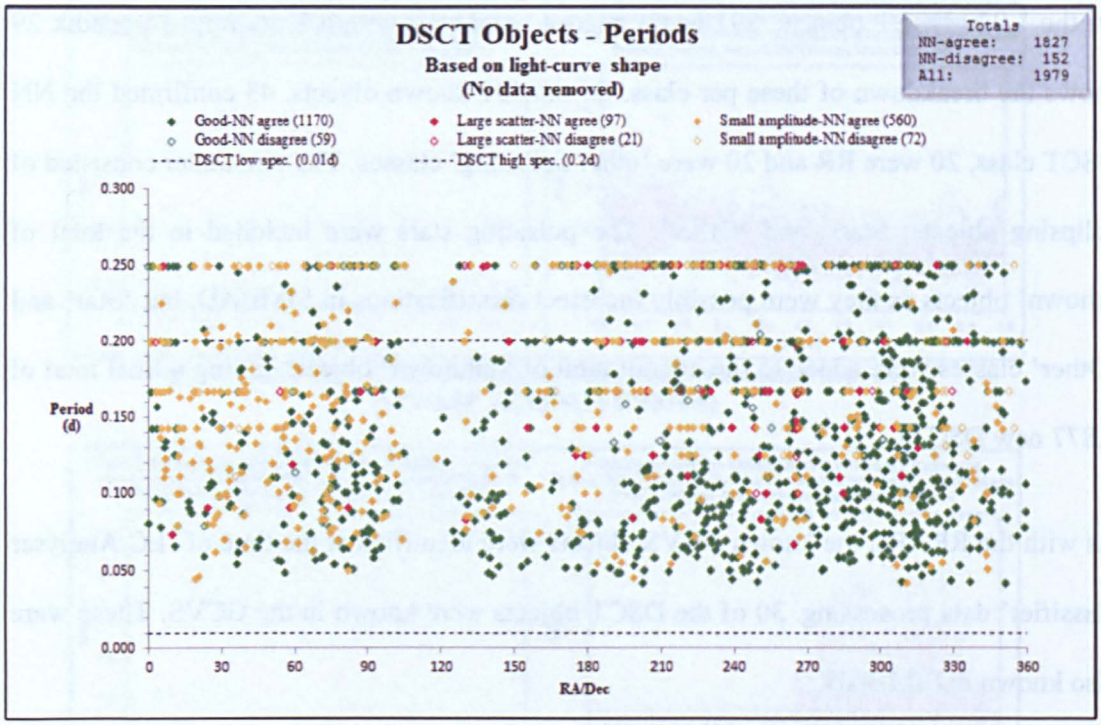

Figure 8-32: DSCT: Variability periods for All objects

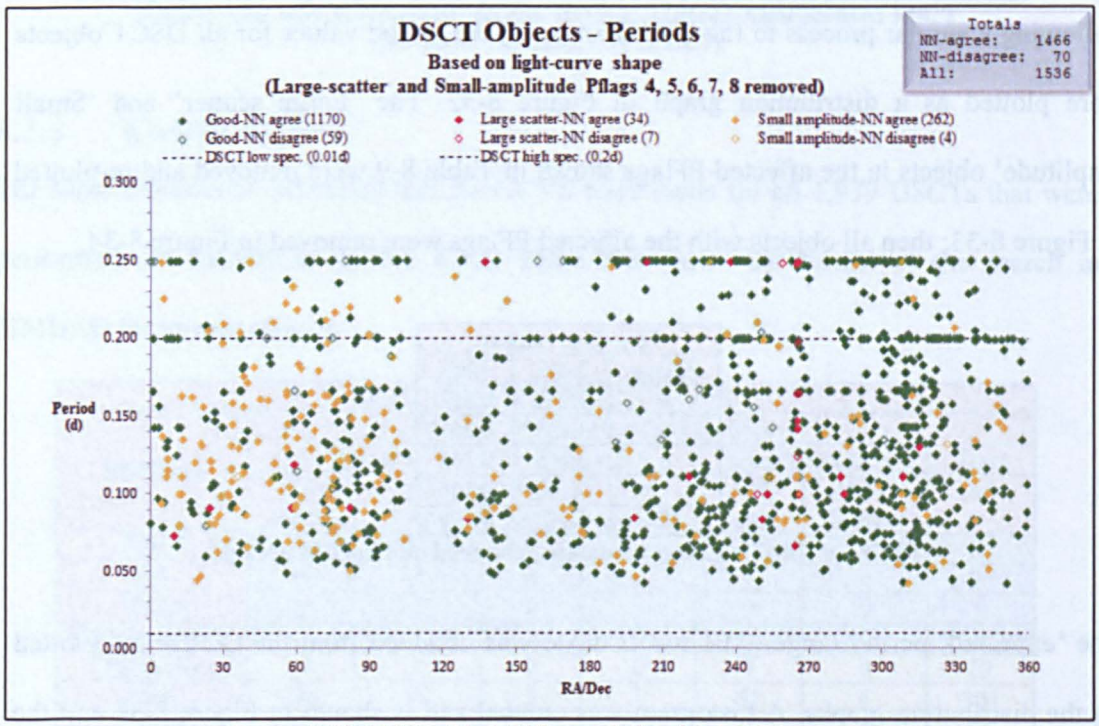

Figure 8-33: DSCT: Variability periods with LS/SA removed
(i.e. with Large-scatter and Small-amplitude in the affected PFlags removed)

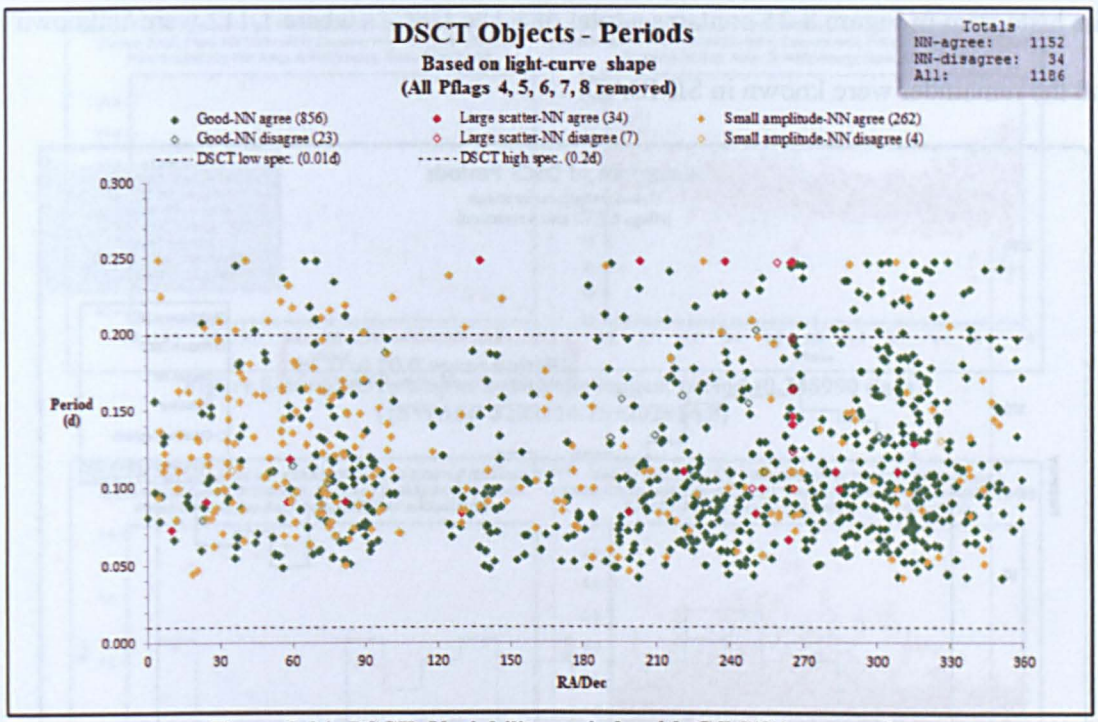

Figure 8-34: DSCT: Variability periods with G/LS/SA removed (i.e. with All objects in the affected PFlags removed)

DSCT period (days)	
Mean	0.119
Median	0.105
Mode	0.069
Min	0.042
Max	0.249
N	1,186
N < 0.01 days	0
N > 0.2 days	110

Table 8-10: DSCT: Period statistics

Figure 8-34 shows that no obvious differences were observed with regards to the distribution and the majority of objects had a period within the published period range of 0.01 to 0.2 days. Table 8-10 shows that the period range was 0.04 to 0.25 days (median 0.11, mode 0.07). The 110 objects that lay above the published period range are presented in Appendix 30 and the associated phase-folded light-curves are available on the support DVD at:

Supplementary data	
Longer_periods	X:\Chapter08\Outside_ranges\DSCT_P_above_0_2d

Where X is DVD-1 in the DVD-drive

The histogram in Figure 8-35 contains a total of 1,186 DSCTs where 1,112 were 'unknown' and the remainder were known in SIMBAD.

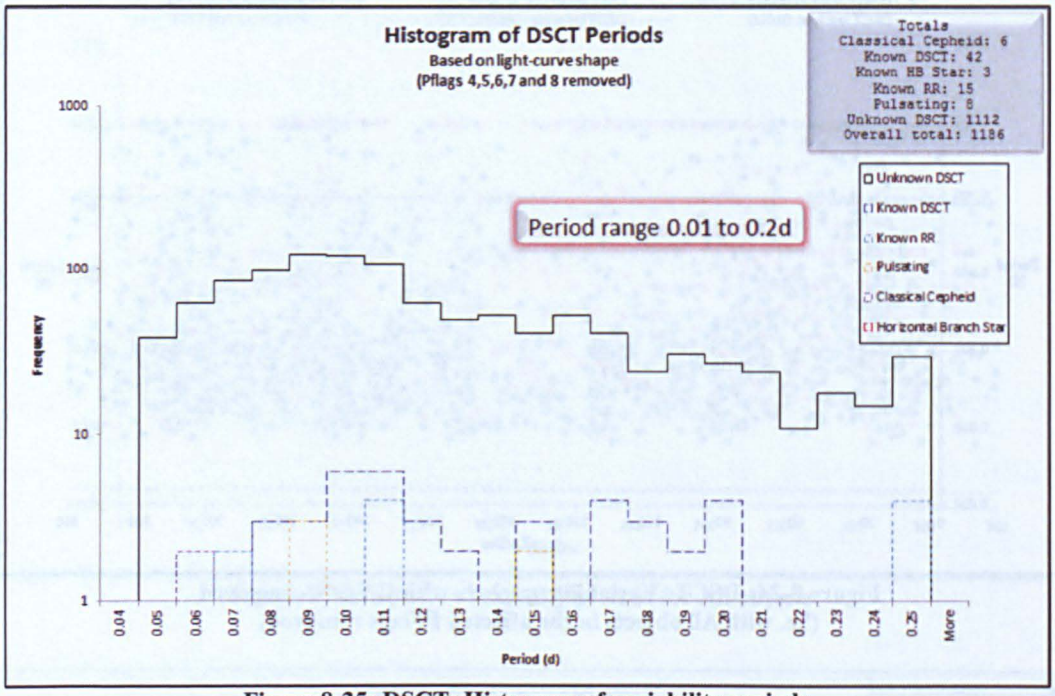

Figure 8-35: DSCT: Histogram of variability periods

A 3D representation of Figure 8-35 can be seen on the support DVD at the location:

Light-curve output
X:\Chapter08\3D-hist\Fig_8-34.bmp

The three objects with the largest period (0.248990, 0.248985 and 0.248957 days) were selected and the light-curves presented in Figure 8-36 to Figure 8-38 respectively. The objects confirm how difficult it was to differentiate between RRAB and DSCT classes. Figure 8-36 was almost certainly a RRAB object, but the other two objects could have been RRAB, RR or DSCT objects, in that they could not be differentiated using the period or amplitude values.

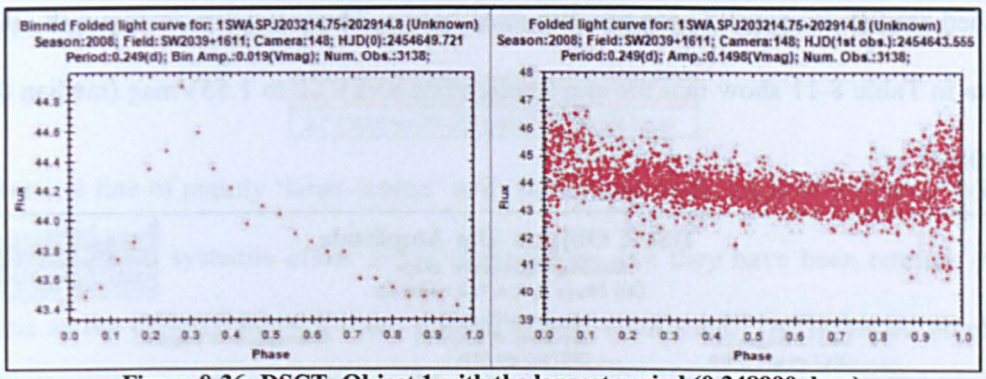

Figure 8-36: DSCT: Object 1 with the longest period (0.248990 days) (1SWASP J203214.75+202914.8)

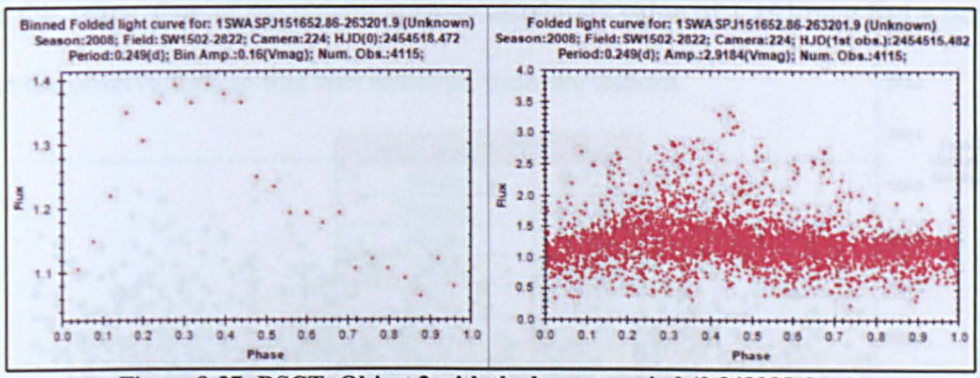

Figure 8-37: DSCT: Object 2 with the longest period (0.248985 days) (1SWASP J151652.86-263201.9)

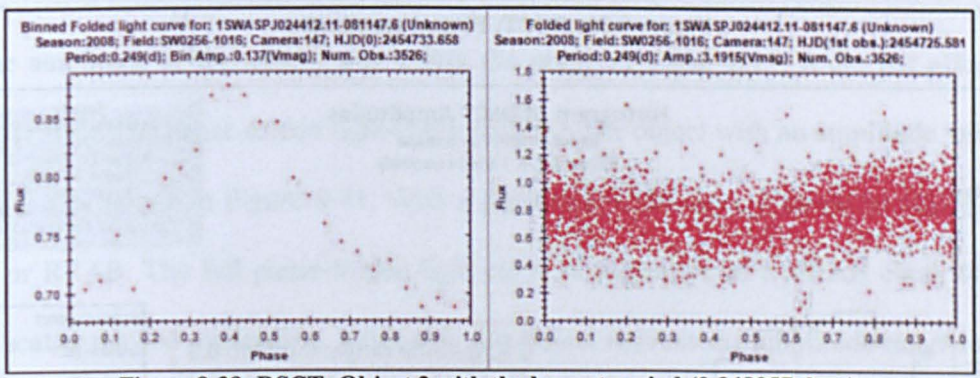

Figure 8-38: DSCT: Object 3 with the longest period (0.248957 days) (1SWASP J024412.11-081147.6)

8.2.4 Amplitude

The binned amplitude values for all DSCT objects were plotted on a distribution graph in Figure 8-39 and as a histogram in Figure 8-40 and the calculated amplitude range tabulated in Table 8-11. The 'expected' amplitude range (0.003 to 0.9Vmag) was obtained from the GCVS and was plotted on the distribution graph. Figure 8-39 shows no significant difference between the amplitude populations and all but two objects lay within the

published amplitude range. These are discussed below. The histogram in Figure 8-40 and the data in Table 8-11 show that the amplitude range was 0.02 to 1.55Vmag (median 0.18, mode 0.12).

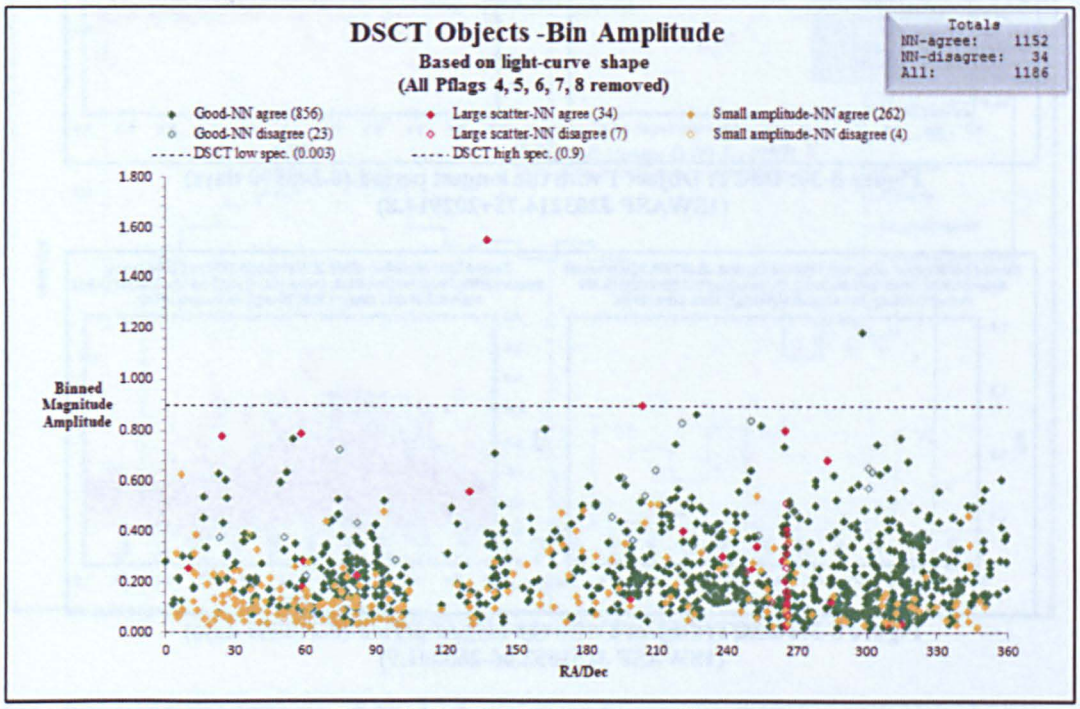

Figure 8-39: DSCT: Binned amplitudes

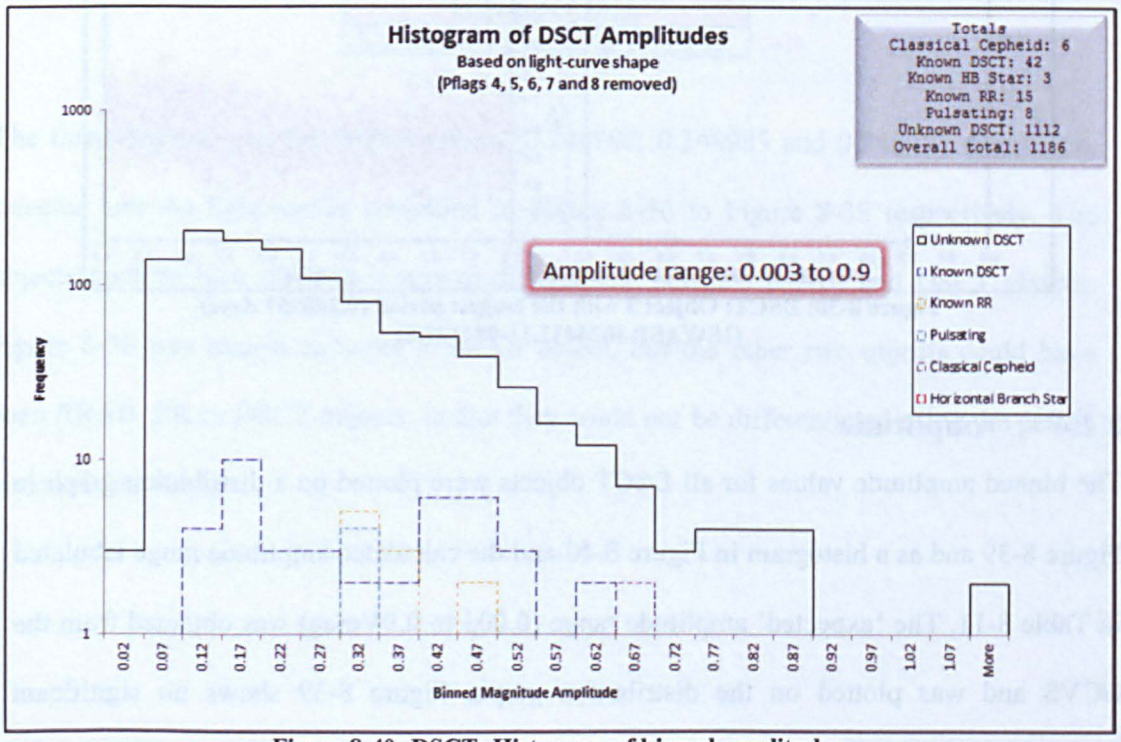

Figure 8-40: DSCT: Histogram of binned amplitudes

A 3D representation of Figure 8-40 can be seen on the support DVD at the location:

Light-curve output
X:\Chapter08\3D-hist\Fig_8-39.bmp

The vertical line of mainly 'large-scatter' and 'small-amplitude' objects in Figure 8-39 are probably due to a systemic effect in the observations, but they have been retained in the analysis as the period values of these objects appear unaffected. The observed amplitude range agreed well with the published range of 0.003 - 0.9Vmag, but two objects were above this range. One of the objects with an amplitude value of 1.19Vmag had a negative flux in the observations so this was removed from the dataset.

DSCT amplitude (Vmag)	
Mean	0.223
Median	0.184
Mode	1.124
Min	0.020
Max	1.552
N	1,186
N < 0.003 Vmag	0
N > 0.9 Vmag	2

Table 8-11: DSCT: Amplitude statistics

As the amplitude of this object was within the range in Table 8-11, it did not affect the overall result. The phase-folded light-curve for the other object with an amplitude value of 1.52Vmag is shown in Figure 8-41. With a period of 0.249 days, it could be DSCT, RR, RRC or RRAB. The full phase-folded light-curve is indicative of a RRAB class, but the large scatter may be misleading. Removing this object reduces the amplitude range to 0.02 to 0.90Vmag, which agrees with the published range.

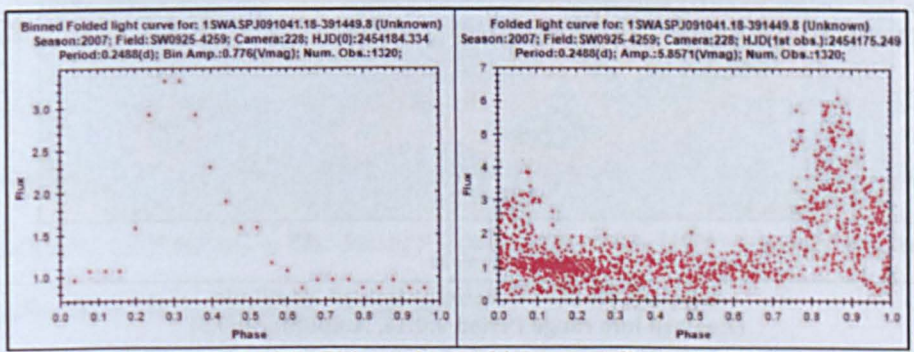

Figure 8-41: DSCT: Object with the highest amplitude (1.52Vmag) (1SWASP J091041.18-391449.8)

8.2.5 Period v Amplitude

The period v amplitude graphs for DSCTs are shown in Figure 8-42 and Figure 8-43, and do not show any particular trend.

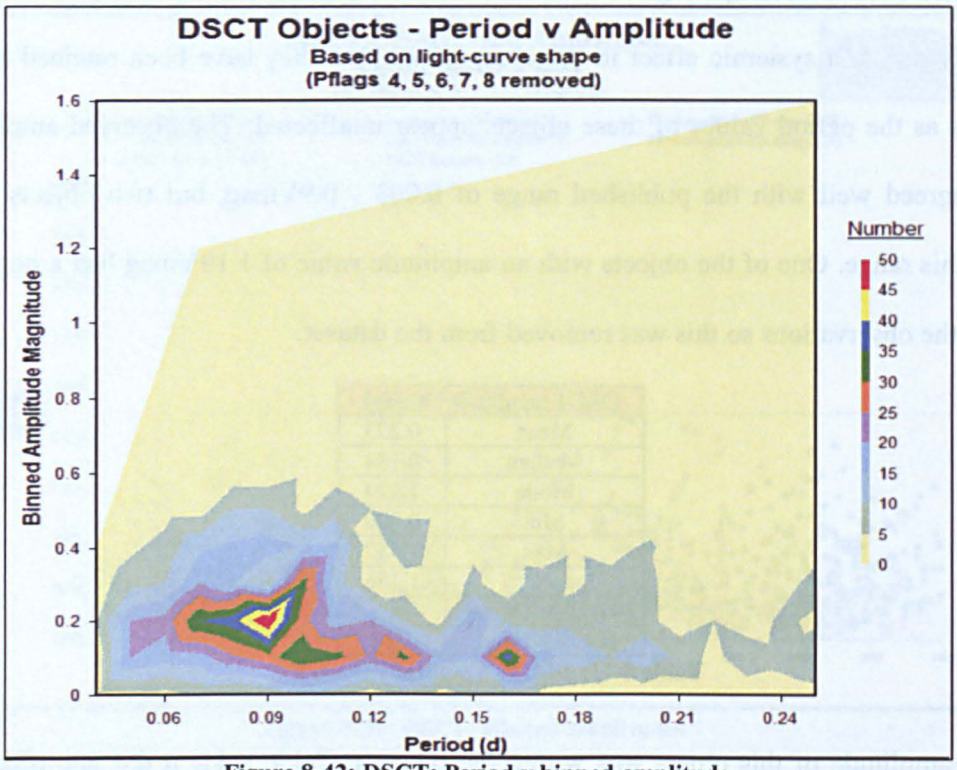

Figure 8-42: DSCT: Period v binned amplitude

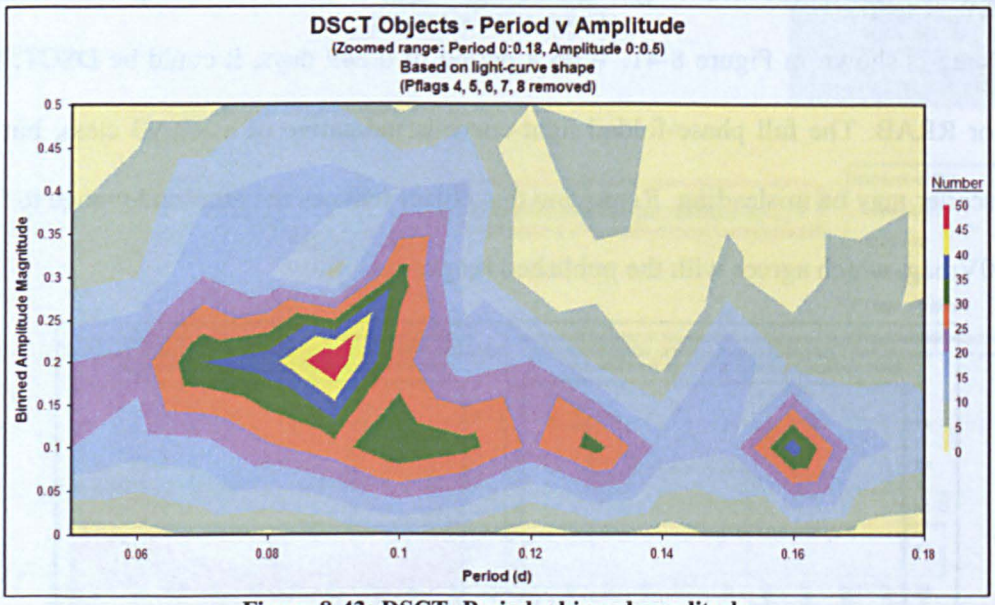

Figure 8-43: DSCT: Period v binned amplitude (Zoomed into range Period 0:0.18, Amplitude 0:0.5)

A scatter plot of Figure 8-42 can be seen on the support DVD at the location:

Light-curve output
X:\Chapter08\Contour\Fig_8-41.bmp

Where X is DVD-1 in the DVD-drive

8.2.6 Distribution

The DSCT objects were plotted as a Hammer projection as shown in Figure 8-44.

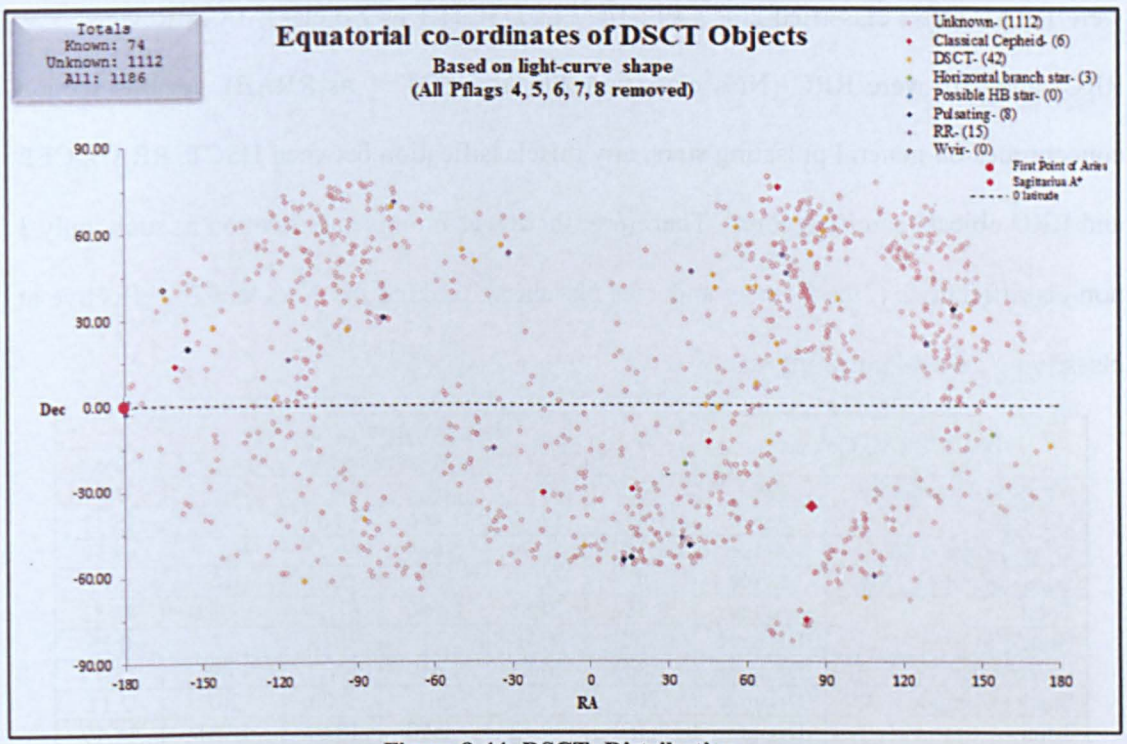

Figure 8-44: DSCT: Distribution

The distribution appears to be homogenous throughout the galaxy as expected and supports the observation by the GCVS that they are representatives of the galactic disk.

8.3. Analysis of All Pulsating objects

This section integrates the results for the DSCT and RRAB objects and presents them in the same tables and graphs so that comparisons can be made between classes. In addition, 211 manually confirmed RRC objects that were identified while analysing the DSCT and RRAB objects, were added to the dataset. These were included to identify any separation between the three classes of pulsating objects.

8.3.1 Statistics

Table 8-12 shows that 81.81% of pulsating objects classified by the NNs were confirmed as DSCT, RRAB or RRC by manual review, after the objects with the PFlags listed in Table 8-13 causing period-clumping and period-banding had been removed. Of the 18.19% that were not confirmed, 34 were DSCT (NNs classified 2 as Review; 32 as RRAB), 1,496 were RRAB (NNs classified 2 as CEP; 1472 as DSCT; 1 as No class; 18 as Review; 3 as RRC) and 201 were RRC (NNs classified 200 as DSCT; 1 as RRAB). As this section concentrates on general pulsating stars, any misclassification between DSCT, RRAB, CEP and RRC objects can be ignored. Therefore, there was no misclassification as such, only 3 non-classifications (2 as Review and 1 as No class), making the NNs 99.97% effective at classifying general pulsating stars.

DSCT/RRAB Objects		Based on light-curve shape					
		All		LS/SA removed		G/LS/SA removed	
Light-curve quality	NN	No.	%	No.	%	No.	%
Good (G)	Agree	1,827	17.00	1,466	14.59	1,152	12.11
Large scatter (LS)	Agree	6,747	62.79	6,684	66.51	6,621	69.59
Small amplitude (SA)	Agree	10	0.09	10	0.10	10	0.11
Total	Agree	8,584	79.88	8,160	81.19	7,783	81.81
Good (G)	Disagree	152	1.41	70	0.70	34	0.36
Large scatter (LS)	Disagree	1,809	16.83	1,619	16.11	1,496	15.72
Small amplitude (SA)	Disagree	201	1.87	201	2.00	201	2.11
Total	Disagree	2,162	20.12	1,890	18.81	1,731	18.19
Overall total	All	10,746		10,050		9,514	

Table 8-12: All pulsating: Statistics for identified objects

Periods to remove		
PFlags	Low	High
1	0.332	0.335
3	0.97	0.990
4	0.249	0.251
5	0.199	0.201
6	0.166	0.168
7	0.142	0.144
8	0.124	0.126

Table 8-13: All pulsating: PFlags containing clumped and banded periods

8.3.2 Known objects

Table 8-14 shows the results of the search in SIMBAD for known pulsating objects DSCT/RRAB.

Of the 10,746 pulsating objects, 4,071 had a nearest neighbour within 1 arc-min. Of these known objects, 2,634 confirmed the NN DSCT/RRAB class and 234 were 'other pulsating' classes (i.e. Cepheid, Classical Cepheid, Horizontal Branch Star, Possible HB Star, Pulsating, and Semi-regular pulsating Star). The remainder consisted of eclipsing objects; Stars; and 'Other'. The eclipsing stars were included in the total of 'known' objects as they could possibly be incorrect classifications in SIMBAD, but 'Star' and 'Other' classes were added to the overall total of 'unknown' stars, giving a final total of 7,782 new pulsating overall.

DSCT/RRAB objects (Overall total = 10,746)							
SIMBAD	Based on light-curve shape						
	Good		Large scatter		Small amplitude		Total
	NN agree	NN disagree	NN agree	NN disagree	NN agree	NN disagree	All
RR	2,269	207	32	25	84	17	2,634
DSCT	42	1	0	0	2	0	45
W Vir	2	2	0	0	0	0	4
Other pulsating	154	35	4	19	9	13	234
Eclipsing	20	14	1	3	8	1	47
Star	298	75	32	39	71	49	564
Other	377	64	15	13	45	29	543
Total known	3,162	398	84	99	219	109	4,071
Total unknowns							6,675
Total unknowns (including Star and Other categories)							7,782

Table 8-14: All pulsating: Objects known in SIMBAD

8.3.3 Period

The period values for ALL the pulsating objects (except those that exhibited period-clumping and period-banding) were plotted as a distribution graph as shown in Figure 8-45 and as a histogram in Figure 8-46.

Figure 8-45 shows the expected separation into period ranges for DSCT and RRAB objects, but also shows a range between 0.2 and 0.3 days where DSCT and RRAB objects are intermixed. This was confirmed by the histogram in Figure 8-46. This area is where there was difficulty in resolving DSCT and RRAB classes using just the light-curve shape and period.

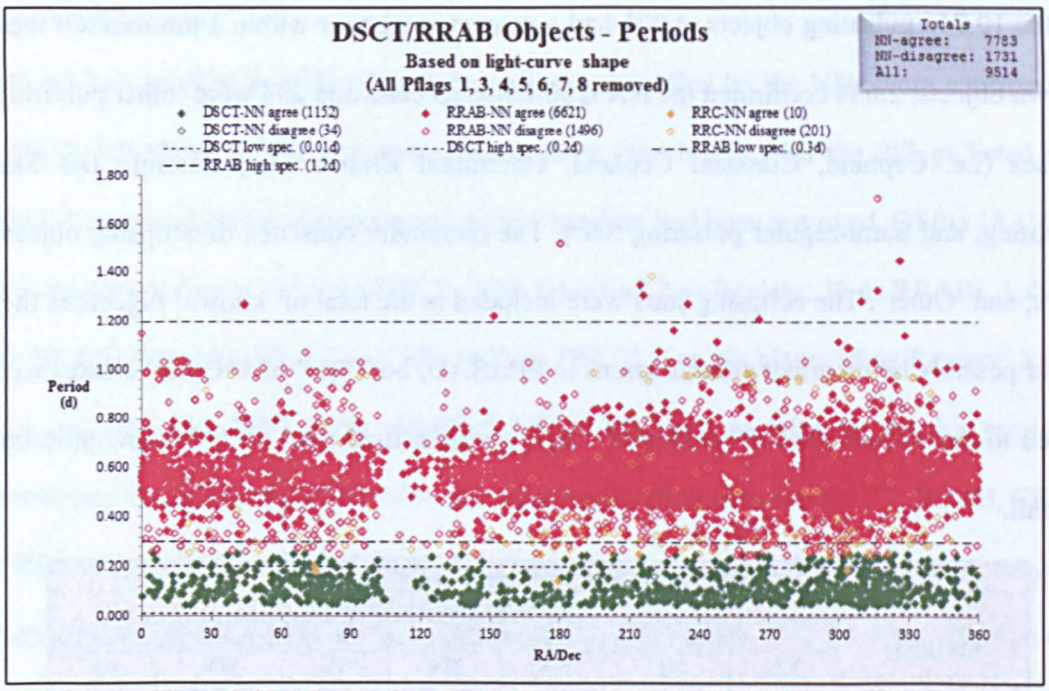

Figure 8-45: All pulsating: Variability periods with G/LS/SA removed (i.e. where All objects in the PFlag range have been removed)

The 14 objects above the 1.2 day range have already been discussed in section 8.1.3.

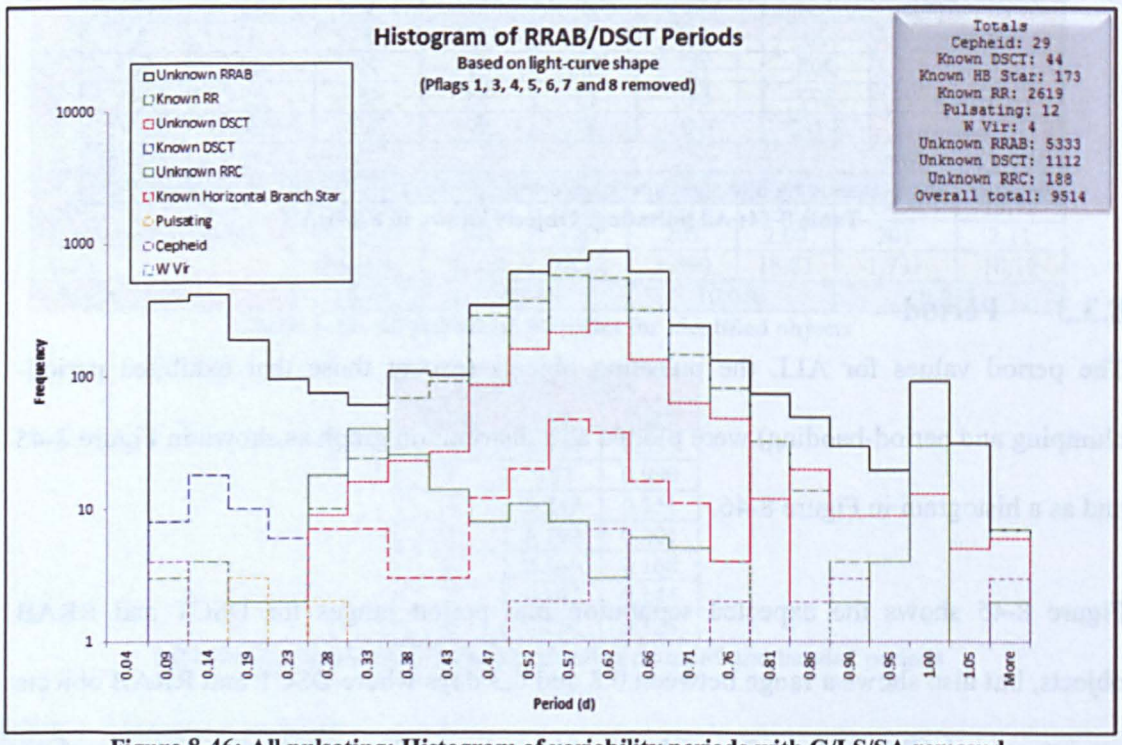

Figure 8-46: All pulsating: Histogram of variability periods with G/LS/SA removed (i.e. where all objects in the PFlag range have been removed)

A 3D representation of Figure 8-46 can be seen on the support DVD at the location:

Light-curve output
X:\Chapter08\3D-hist\Fig_8-44.bmp

An attempt was made to separate these objects using the colour of the stars and reduced proper-motion, but as not all stars in the SuperWASP archive had known colour information or proper-motion values, they could not be used directly in the NNs, but had to be used post-classification in the 'LC Analyser classifier' application. Neither colour nor proper-motion was effective at differentiating the classes therefore it was not pursued further in this research.

8.3.4 Amplitude

The binned amplitude values for ALL the pulsating objects were plotted on the distribution graph in Figure 8-47 and the histogram in Figure 8-48. The objects were plotted in the same manner as the individual classes, with all period-clumping and period-banding objects removed.

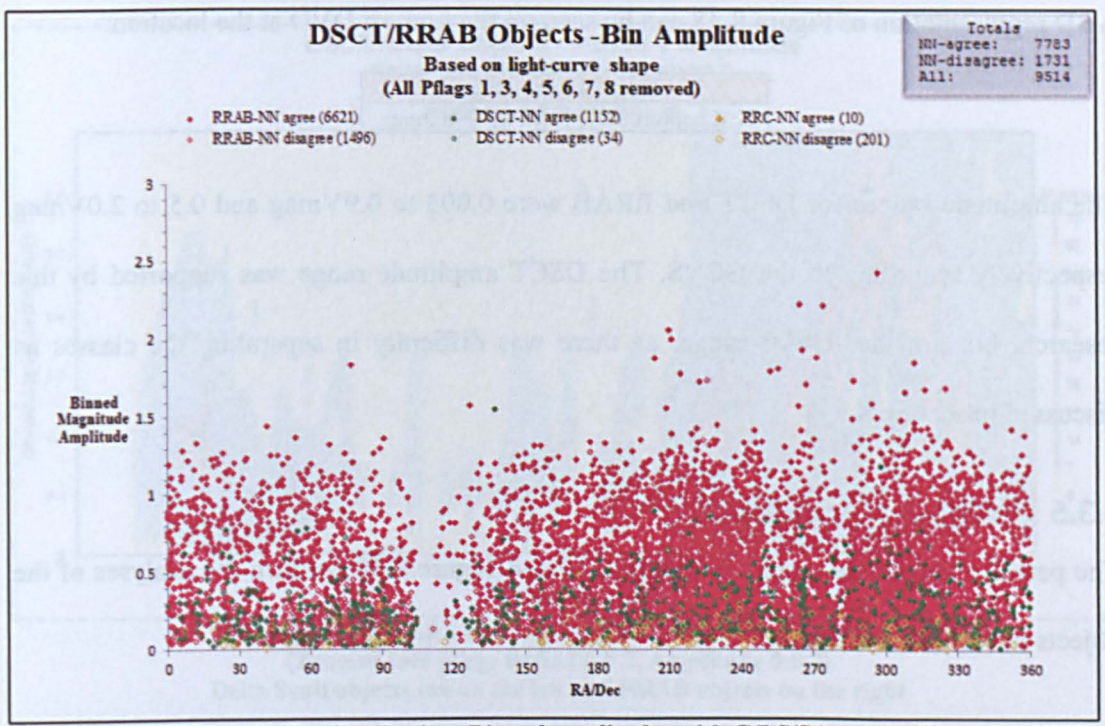

Figure 8-47: All pulsating: Binned amplitudes with G/LS/SA removed (i.e. where all objects in the PFlag range have been removed)

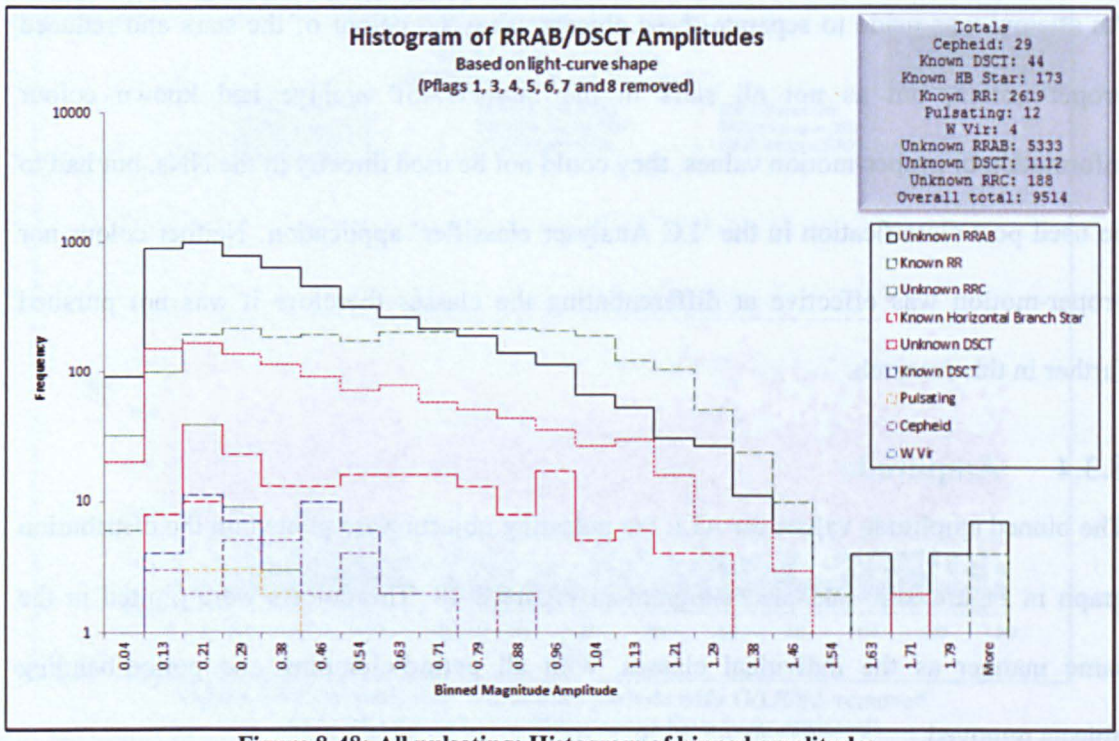

Figure 8-48: All pulsating: Histogram of binned amplitudes

A 3D representation of Figure 8-48 can be seen on the support DVD at the location:

Light-curve output
X:\Chapter08\3D-hist\Fig_8-46.bmp

The amplitude ranges for DSCT and RRAB were 0.003 to 0.9Vmag and 0.5 to 2.0Vmag respectively according to the GCVS. The DSCT amplitude range was supported by this research, but not the RRAB range, as there was difficulty in separating the classes as discussed in section 8.1.4.

8.3.5 Period v Amplitude

The period v amplitude graphs in Figure 8-49 and Figure 8-50 confirm the analyses of the objects in earlier sections.

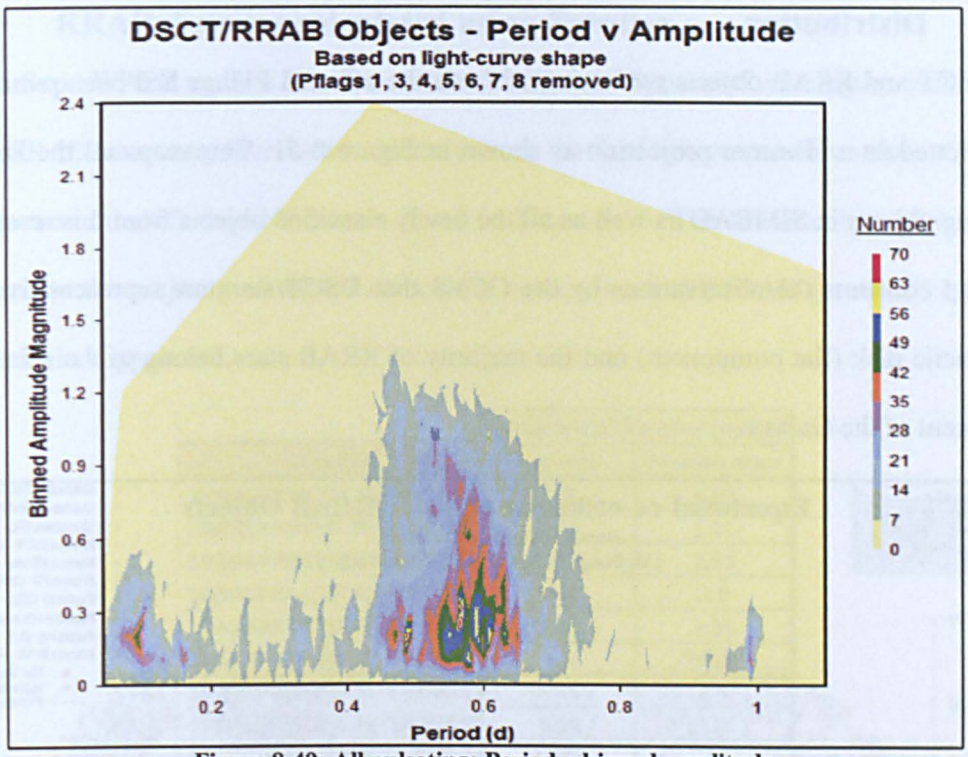

Figure 8-49: All pulsating: Period v binned amplitude

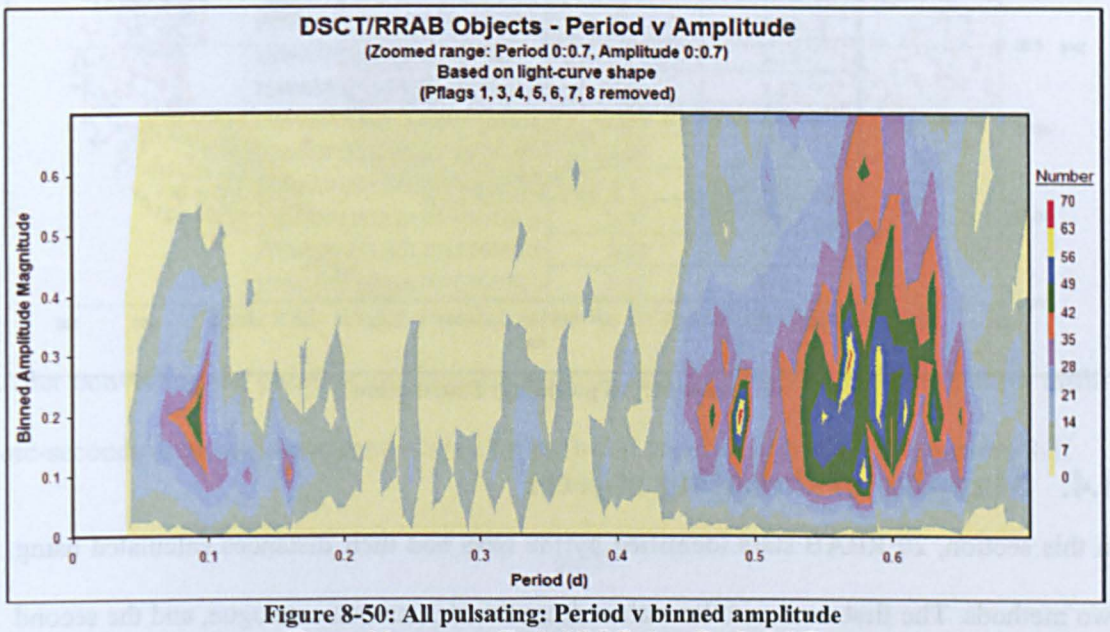

Figure 8-50: All pulsating: Period v binned amplitude
(Zoomed into range Period 0:0.7, Amplitude 0:0.7)
Delta Scuti objects are on the left and RRAB objects on the right

A scatter plot of Figure 8-49 can be seen on the support DVD at the location:

Light-curve output
X:\Chapter08\Contour\Fig_8-47.bmp

Where X is DVD-1 in the DVD-drive

8.3.6 Distribution

The DSCT and RRAB objects remaining after all the affected PFlags had been removed, were plotted as a Hammer projection as shown in Figure 8-51. This maps all the known pulsating objects in SIMBAD as well as all the newly classified objects from this research. The map confirms the observations by the GCVS that DSCT stars are representatives of the galactic disk (flat component) and the majority of RRAB stars belong to the spherical component of the Galaxy.

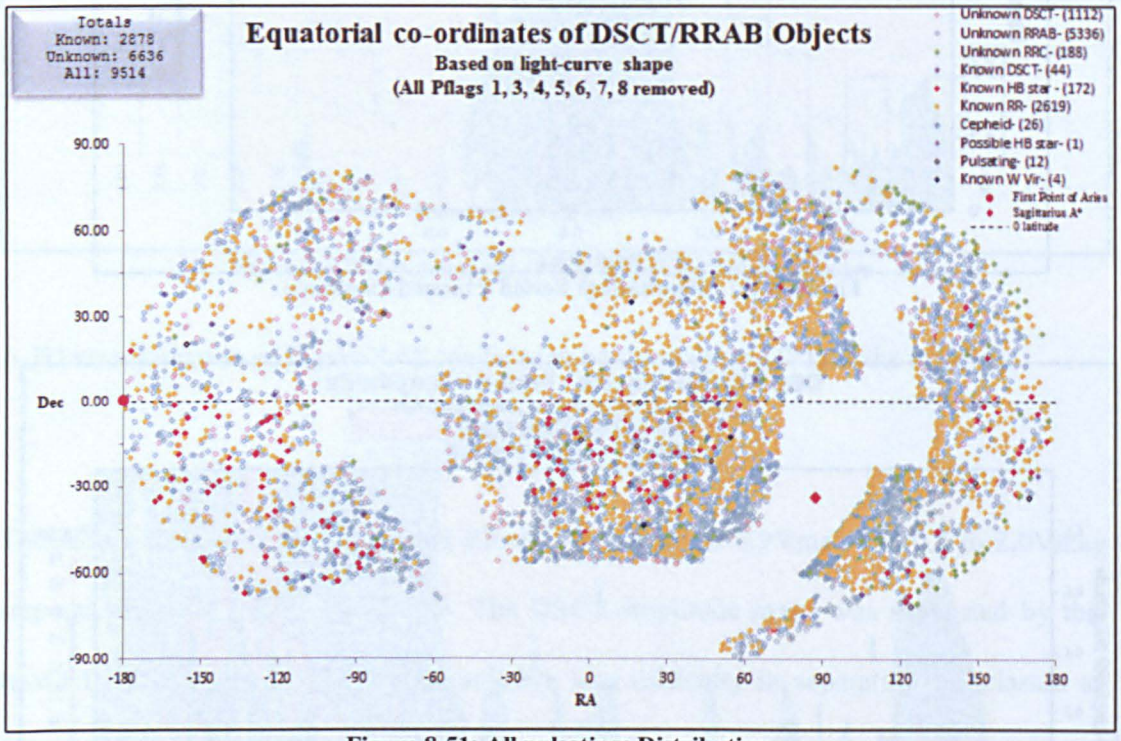

Figure 8-51: All pulsating: Distribution

8.4. Mapping of Pulsating objects

In this section, 20 RRAB stars identified by the NNs had their distances calculated using two methods. The first used parallax values from the Hipparcos2 catalogue, and the second used an absolute magnitude value obtained from the literature. The results were compared and a decision made on which method should be used to calculate the distances to all 8,117 RRAB stars. Additionally, the SuperWASP absolute magnitude was calculated and compared against the published absolute magnitude.

8.4.1 RRAB distance calculated using Parallax

As the SuperWASP archive is cross-matched with the Hipparcos2 catalogue, each of the 8,117 RRAB stars were reviewed to identify those that had known parallax values. Only 20 objects were identified and these are listed in Table 8-15. The low number of stars was expected as the majority of RRAB stars were not known in SIMBAD (section 8.1.2) and hence not in Hipparcos2.

	Hipparcos2 Parallax (mas)	
Object Id	Parallax	Parallax error
1SWASPJ000405.10-165951.5	5.3	4.06
1SWASPJ002343.08+292403.6	1.48	1.21
1SWASPJ003338.28-152914.7	7.2	2.83
1SWASPJ011727.41+385702.0	2.54	1.9
1SWASPJ020751.97-265157.7	2.96	1.51
1SWASPJ044944.29-154428.2	1.5	1.12
1SWASPJ045337.51-192601.1	4.35	2.8
1SWASPJ051204.26+335746.9	9.29	3.26
1SWASPJ094438.24-455237.2	11.27	3.6
1SWASPJ120447.27-274043.2	2.11	1.32
1SWASPJ123030.50-260251.1	4.49	1.76
1SWASPJ132011.56+091116.3	2.84	2.73
1SWASPJ152225.38-405536.2	1.57	1.18
1SWASPJ171303.98+355842.9	4.8	1.61
1SWASPJ190942.60+645132.1	2.26	0.88
1SWASPJ193229.30+562317.5	2.29	0.84
1SWASPJ203231.55+003507.0	2.8	2.59
1SWASPJ211129.90-450428.3	1.57	1.47
1SWASPJ215202.79+223429.3	2.28	1.72
1SWASPJ162946.70+074456.1	4.87	0.68

Table 8-15: RRAB: Parallax values for 20 stars from Hipparcos2

After converting the parallax and parallax error values for the 20 RRAB stars from milli-arc-seconds to arc-seconds, the distance for each star was calculated using Equation 8-1.

$$d_{Avg} = \frac{1}{pllx} pc$$

Where
d_{Avg} is the Average SuperWASP calculated distance (in parsecs),
pllx is the parallax value from the Hipparcos2 catalogue
Equation 8-1: Calculation of RRAB distance using parallax

The upper and lower distances (d_{High} and d_{Low}) were also calculated using the same equation with 'parallax + parallax error' and 'parallax – parallax error' respectively. The results are discussed in section 8.4.3.

8.4.2 RRAB distances calculated using Published Absolute Magnitude

To calculate the distance for each of the RRAB stars in this section, use was made of the observation that all RRAB stars have similar absolute values (For et al. 2011). The process involved identifying a known absolute magnitude for the RRAB class from the literature, then obtaining interstellar extinction values for each RRAB star. Using these values along with the SuperWASP apparent magnitude for each RRAB star, the distances were calculated. Table 8-16 lists a selection of RRAB absolute magnitude values obtained from the literature, ranging from years 1986 to 2011. The variability of the absolute magnitude over time shows the difficulty in obtaining the true value for this parameter, but with increasing numbers of large surveys being performed, each with better photometry, further knowledge is being obtained and better estimates are appearing in the literature. The row highlighted in green (0.45Vmag) was selected for use in this research as it was the most recent value obtained from the literature and had been corrected using the Lutz-Kelker-Hanson bias (Lutz & Kelker, 1973), which corrects a systematic bias where parallax measurements are systematically overestimated because they do not properly account for the larger volume of space that is sampled at smaller parallax values.

Average Mv	Mv Error (±)	Min. Mv	Max. Mv	[Fe/H]	Reference
0.68	0.14	0.54	0.82	Not stated	Barnes et al. (1986)
0.65	0.23	0.42	0.88	-1.51+/-0.06	Luri et al. (1998)
0.77	0.13	0.64	0.90	-1.60	Gould & Popowski (1998)
0.77	0.15	0.62	0.92	-1.53	Fernley et al. (1998)
0.72	0.10	0.62	0.82	-1.52	Fernley et al. (1998)
0.69	0.10	0.59	0.79	-1.41	Gratton (1998)
0.60	0.12	0.48	0.72	-1.51	Gratton (1998)
0.64	0.11	0.53	0.75	-1.39	Feast (2002)
0.55	0.12	0.43	0.67	-1.50	Cacciari & Clementini (2003)
0.65	-0.26, +0.20	0.39	0.85	-1.53	Van Leeuwen (2008)
0.46	0.03	0.43	0.49	-1.58	Benedict et al. (2011) – RP*
0.45	0.05	0.40	0.50	-1.50	Benedict et al. (2011) – LKH**

Table 8-16: RRAB: Absolute Magnitudes for stars obtained from literature
***RP = calculated by reduced parallaxes**
****LKH = calculated using Lutz-Kelker-Hanson bias in absolute magnitude**

Current work (For et al. 2011) indicated that the absolute magnitude of the RRAB stars may have a slight dependence on metallicity therefore this parameter was added to the

table. Unfortunately, it was not possible to obtain this value for the SuperWASP RRAB stars, so comparisons could not be made. Also, It is expected that the absolute magnitudes at other wavelengths would be different, but as SuperWASP only provides magnitudes in the visible domain, the similarity of absolute magnitudes of RRAB stars at other wavelengths were not investigated.

The extinction values for all 8,117 RRAB objects were obtained from the NASA/IPAC Infrared Science Archive web-site[19], by submitting a file containing 'Object Id, Right-ascension and Declination' for each observation. An example of the results obtained is shown in Table 8-17. The extinction values for the 20 selected RRAB stars in section 8.4.1 were extracted from this data. It should be noted that these are maximum values i.e. looking right through the galaxy in that direction. The true value along the line of sight to an object could be lower if some of the extinction is behind the object rather than in front.

Object Id	GCVS Name	RA	Dec	E(B-V)	Mean_E(B-V)	Std_Dev	Max_E(B-V)	A(V)
1SWASPJ154258.42-064922.9	Unknown	235.7434	-6.8231	0.186800	0.1842	0.0053	0.1923	0.5791
1SWASPJ151813.62-011907.9	Unknown	229.5568	-1.3189	0.099600	0.1022	0.0066	0.1147	0.3087
1SWASPJ151734.62-010608.8	Unknown	229.3943	-1.1025	0.090500	0.0872	0.0090	0.1033	0.2806
1SWASPJ160836.39-120628.1	V0783 Sco	242.1516	-12.1078	0.305900	0.3055	0.0053	0.3225	0.9484
1SWASPJ151734.98-010516.8	V0372 Ser	229.3958	-1.0880	0.086500	0.0847	0.0094	0.1008	0.2682
1SWASPJ224734.68-390333.0	XZ Gru	341.8945	-39.0592	0.012100	0.0119	0.0007	0.0130	0.0376
1SWASPJ155250.92-084400.6	Unknown	238.2122	-8.7335	0.211200	0.2091	0.0046	0.2167	0.6548
1SWASPJ202414.70-405210.6	V2273 Sgr	306.0613	-40.8696	0.054900	0.0544	0.0008	0.0556	0.1703
1SWASPJ200324.63-400855.7	V2227 Sgr	300.8527	-40.1488	0.084700	0.0857	0.0033	0.0926	0.2627

Table 8-17: RRAB: Example of Extinction values obtained

Using the published absolute magnitude from Table 8-16 along with the SuperWASP binned apparent magnitude for each RRAB star and its extinction value, the distance (d, in parsecs) was calculated using Equation 8-2. The results are discussed in section 8.4.3.

$$d = 10^{\frac{(m-M)+(5-A_v)}{5}} pc$$

Where
m is the SuperWASP binned apparent magnitude,
M is the published absolute magnitude from section 8.4.1 (i.e. 0.45) and
A_v is the extinction value for the star

Equation 8-2: Calculation of RRAB distance using published absolute magnitude

[19] http://irsa.ipac.caltech.edu/applications/DUST/

8.4.3 Comparison of calculated RRAB distances

The results of the RRAB distance calculations from sections 8.4.1 and 8.4.2 were tabulated and are presented in Table 8-18. The distances were also compared in Figure 8-52 by plotting the distance obtained using the parallax values against those calculated using the published absolute magnitude.

Table 8-18 shows the widespread variance between the two methods of calculating distances. Figure 8-52 shows that 11 of the 20 objects calculated using Parallax were within the lower/upper ranges calculated using absolute magnitude, with two other objects very close to this range. The remainder of the objects were well outside the range. The 'dotted' line in the figure is the expected 1:1 correspondence between the two different distances. Review of the data in Table 8-18 indicated that the seven objects outside the range all had high parallax error values (4.06, 2.83, 2.80, 3.26, 3.60, 1.76 and 1.61). The two objects close to the range had parallax errors of 1.51 and 0.88, with the remainder in the range of 0.68 and 2.73. As it was difficult to obtain accurate parallax values and the error values were quite large, it was decided to use the distance calculation method based on the published absolute magnitude for the rest of this section.

				Distance (pc) using Abs. Mag.			Distance (pc) using pllx		
Object Id	Min. Bin. Mag	Avg. Bin Mag	Max. Bin. Mag	Largest	Average	Smallest	Largest	Average	Smallest
1SWASPJ000405.10-165951.5	12.612	12.298	11.985	2320.57	2267.75	2216.13	806.45	188.68	106.84
1SWASPJ002343.08+292403.6	10.056	9.614	9.172	653.06	638.19	623.67	3703.70	675.68	371.75
1SWASPJ003338.28-152914.7	11.793	11.420	11.048	1535.74	1500.78	1466.62	228.83	138.89	99.70
1SWASPJ011727.41+385702.0	11.159	10.689	10.219	1069.04	1044.71	1020.92	1562.50	393.70	225.23
1SWASPJ020751.97-265157.7	10.585	10.029	9.474	824.74	805.97	787.62	689.66	337.84	223.71
1SWASPJ044944.29-154428.2	10.081	9.661	9.242	647.22	632.49	618.09	2631.58	666.67	381.68
1SWASPJ045337.51-192601.1	11.760	11.370	10.979	1456.19	1423.04	1390.65	645.16	229.89	139.86
1SWASPJ051204.26+335746.9	12.416	11.977	11.539	944.19	922.70	901.69	165.84	107.64	79.68
1SWASPJ094438.24-455237.2	12.553	12.190	11.827	1486.33	1452.49	1419.43	130.38	88.73	67.25
1SWASPJ120447.27-274043.2	10.360	10.007	9.654	757.30	740.06	723.21	1265.82	473.93	291.55
1SWASPJ123030.50-260251.1	10.577	10.129	9.681	779.87	762.12	744.77	366.30	222.72	160.00
1SWASPJ132011.56+091116.3	12.120	11.768	11.416	1793.55	1752.72	1712.83	9090.91	352.11	179.53
1SWASPJ152225.38-405536.2	9.330	9.163	8.996	436.30	426.37	416.67	2564.10	636.94	363.64
1SWASPJ171303.98+355842.9	11.930	11.354	10.778	1486.16	1452.34	1419.28	313.48	208.33	156.01
1SWASPJ190942.60+645132.1	10.626	10.235	9.843	830.75	811.84	793.36	724.64	442.48	318.47
1SWASPJ193229.30+562317.5	10.156	9.667	9.178	594.73	581.19	567.96	689.66	436.68	319.49
1SWASPJ203231.55+003507.0	11.333	10.758	10.184	1030.60	1007.14	984.21	4761.90	357.14	185.53
1SWASPJ211129.90-450428.3	10.419	9.915	9.411	745.37	728.40	711.82	10000.00	636.94	328.95
1SWASPJ215202.79+223429.3	10.898	10.417	9.937	909.76	889.05	868.81	1785.71	438.60	250.00
1SWASPJ162946.70+074456.1	7.192	7.118	7.045	199.11	194.58	190.15	238.66	205.34	180.18

Table 8-18: RRAB: Comparison of distances

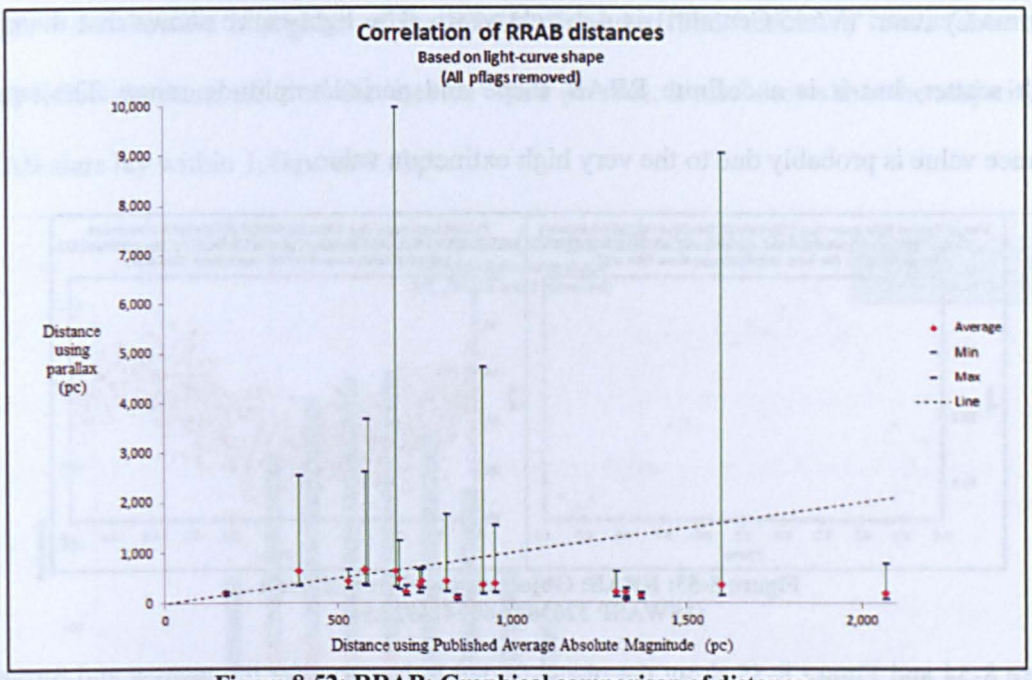

Figure 8-52: RRAB: Graphical comparison of distances

8.4.4 Calculation of RRAB distances

The distance to all 8,117 RRAB stars was calculated using the published absolute magnitude (0.45) and Equation 8-2. The results (and extinction values) are recorded on the supporting DVD at:

Supplementary data	
RRAB distances	X:\Chapter08\Catalogues\RRAB_distances.xlsx

Where X is DVD-1 in the DVD-drive

The results obtained showed a distance range of about 24pc to 17kpc or 78ly to 54kly however, as the extinction values used were upper limits (i.e. the total column density in the line of sight out of the galaxy), these distances are lower limits. If the true absorption is less, then the calculated distance would be greater. An upper limit to the distance of each RRAB star was calculated using a value of Av=0. This gave a maximum distance range of 96pc to 19kpc (314ly to 60kly).

One object (Figure 8-53) was removed from the data set because of low bin amplitude (0.032) and very high extinction value (17.509). This resulted in a distance of approximately 1ly (min 0.90, max 1.12). This could not be correct as the nearest star

Proxima Centauri (V645 Centauri) is 4.2 light-years. The light-curve shows that there is much scatter, but it is a definite RRAB shape and period/amplitude range. The small distance value is probably due to the very high extinction value.

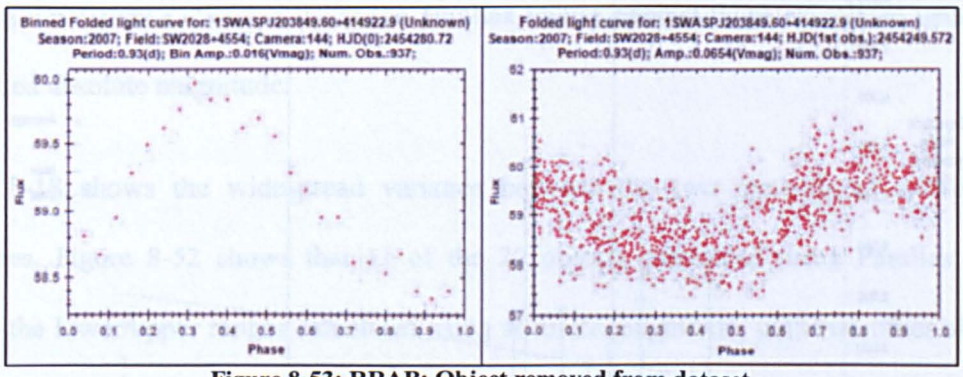

Figure 8-53: RRAB: Object removed from dataset (1SWASP J203849.60+414922.9)

Figure 8-54 and Figure 8-55 show the phase-folded light-curve for the nearest and furthest RRAB object respectively. These show good RRAB shape and have an appropriate period/amplitude.

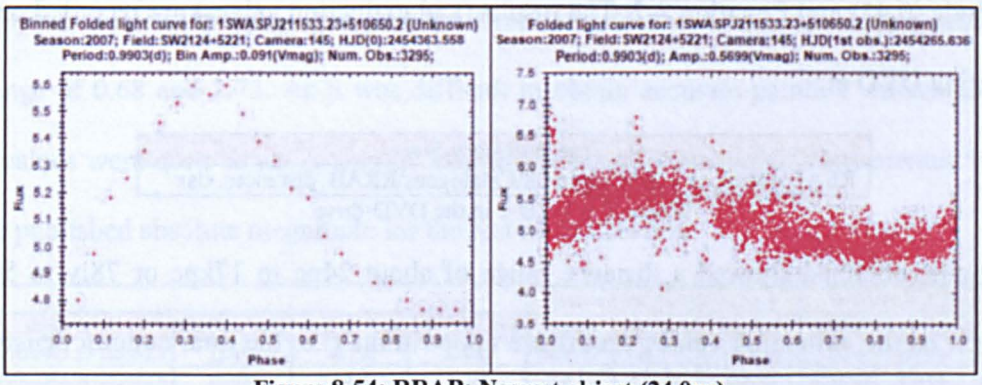

Figure 8-54: RRAB: Nearest object (24.0pc) (1SWASP J211533.23+510650.2)

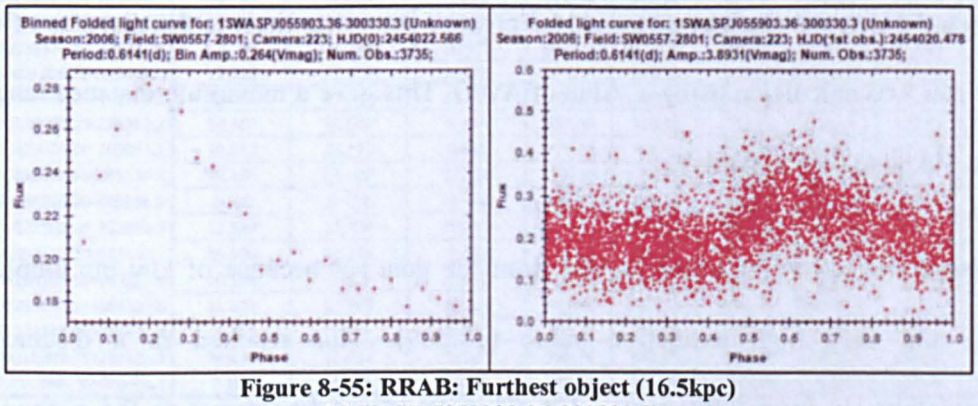

Figure 8-55: RRAB: Furthest object (16.5kpc) (1SWASP J055903.36-300330.3)

Figure 8-56 shows a histogram of the RRAB distances. The 'unknown' stars (shown in blue) follow the same trend as the 'known' stars (in red). It also shows that the majority of RRAB stars lay within 1.4kpc to 8.4kpc.

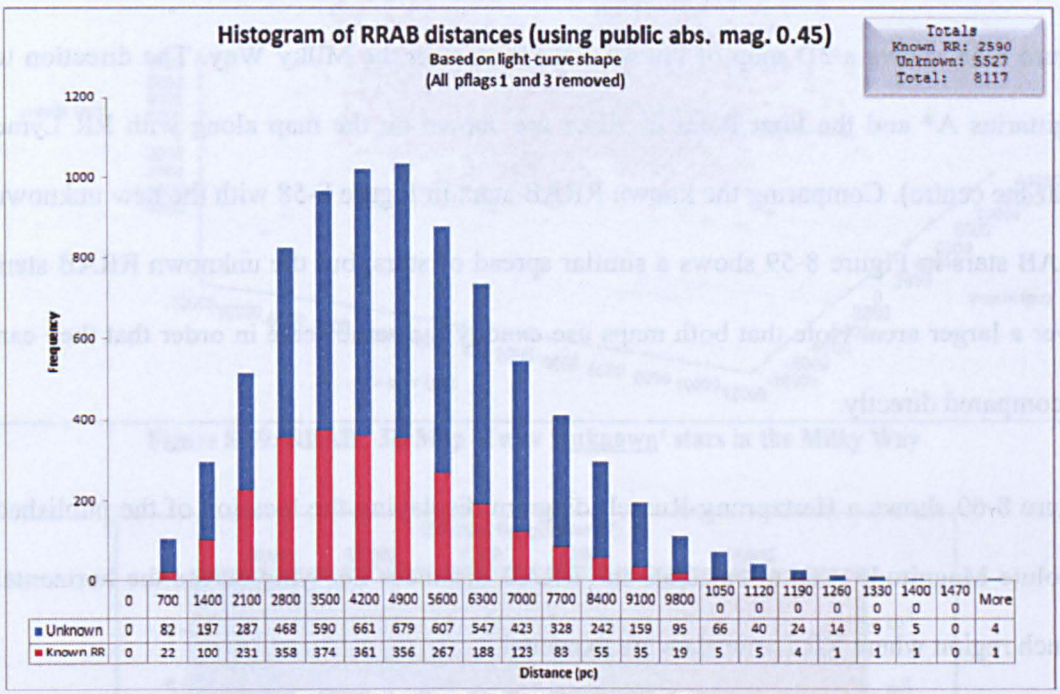

Distance (pc)	0	700	1400	2100	2800	3500	4200	4900	5600	6300	7000	7700	8400	9100	9800	10500	11200	11900	12600	13300	14000	14700	More
Unknown	0	82	197	287	468	590	661	679	607	547	423	328	242	159	95	66	40	24	14	9	5	0	4
Known RR	0	22	100	231	358	374	361	356	267	188	123	83	55	35	19	5	5	4	1	1	1	0	1

Figure 8-56: RRAB: Histogram of distances

Figure 8-57 shows a histogram of the RRAB distances below and above the galactic plane.

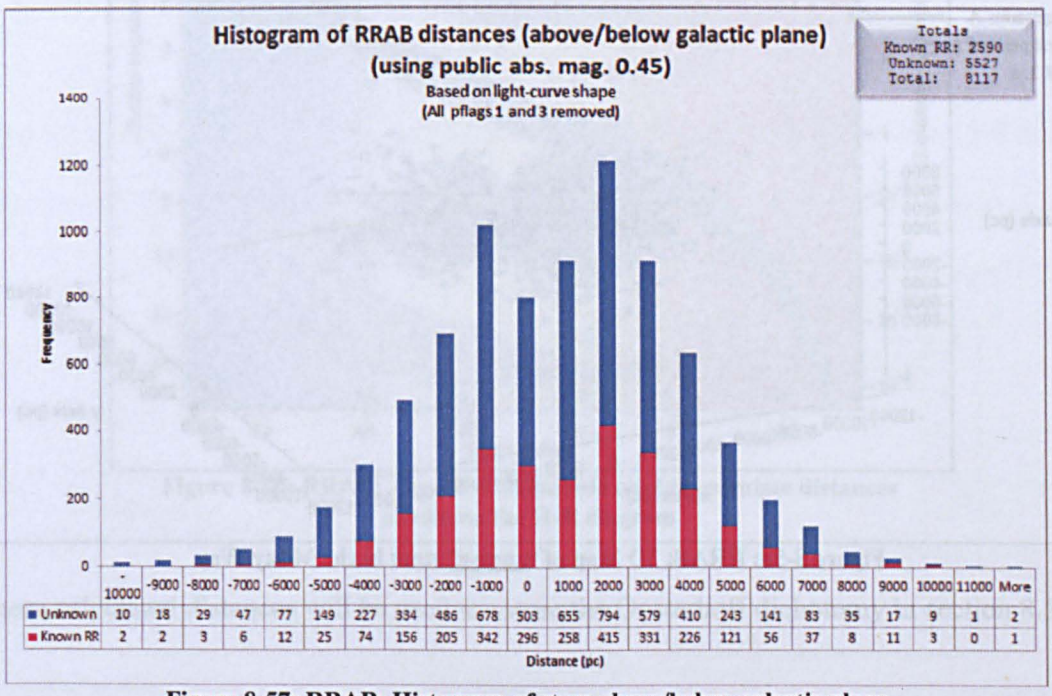

Distance (pc)	-10000	-9000	-8000	-7000	-6000	-5000	-4000	-3000	-2000	-1000	0	1000	2000	3000	4000	5000	6000	7000	8000	9000	10000	11000	More
Unknown	10	18	29	47	77	149	227	334	486	678	503	655	794	579	410	243	141	83	35	17	9	1	2
Known RR	2	2	3	6	12	25	74	156	205	342	296	258	415	331	226	121	56	37	8	11	3	0	1

Figure 8-57: RRAB: Histogram of stars above/below galactic plane

Again, the 'unknown' stars (shown in blue) follow the same trend as the 'known' stars (in red). It also shows that the majority of RRAB stars lay stars lay within -4kpc to +5kpc of the galactic plane.

Figure 8-58 shows a 3D map of known RRAB stars in the Milky Way. The direction to Sagittarius A* and the First Point of Aries are shown on the map along with RR Lyrae (near the centre). Comparing the known RRAB stars in Figure 8-58 with the new unknown RRAB stars in Figure 8-59 shows a similar spread of stars, but the unknown RRAB stars cover a larger area. Note that both maps use exactly the same scale in order that they can be compared directly.

Figure 8-60 shows a Hertzprung-Russell diagram displaying the location of the published absolute Magnitude used to calculate the RRAB distances i.e. lying across the horizontal branch region where RR Lyrae stars are expected.

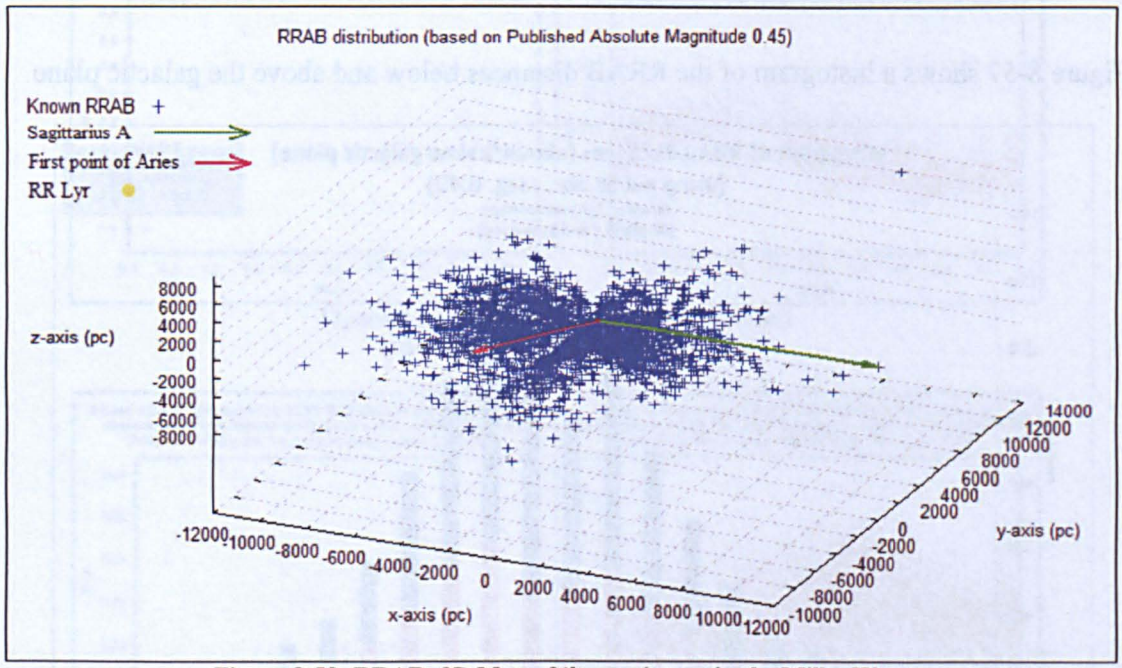

Figure 8-58: RRAB: 3D Map of '<u>known</u>' stars in the Milky Way

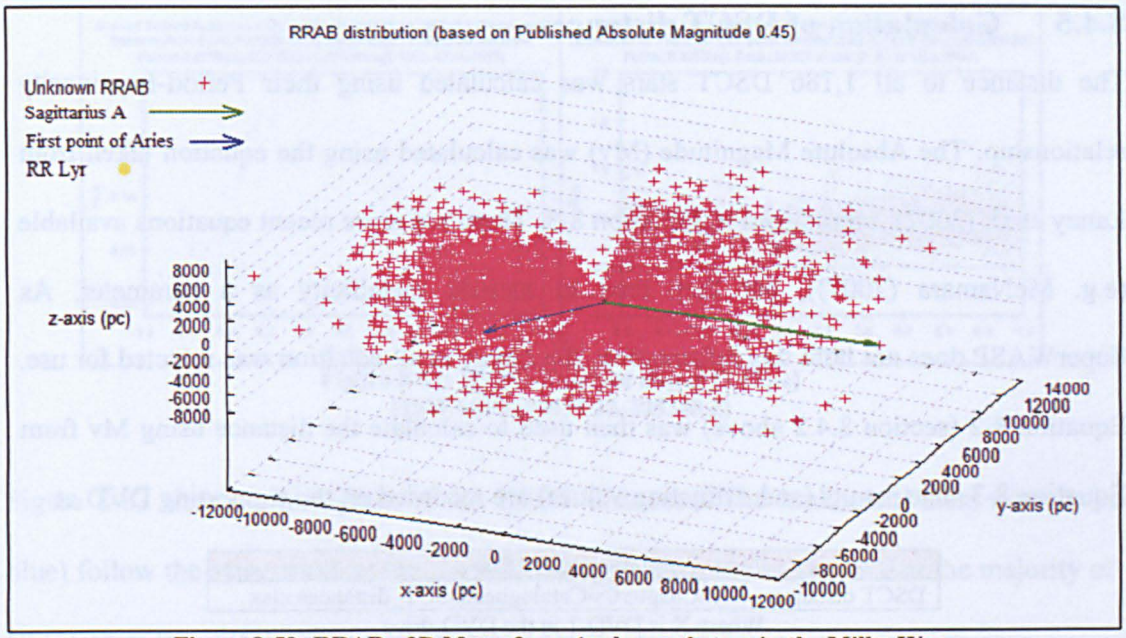

Figure 8-59: RRAB: 3D Map of new 'unknown' stars in the Milky Way

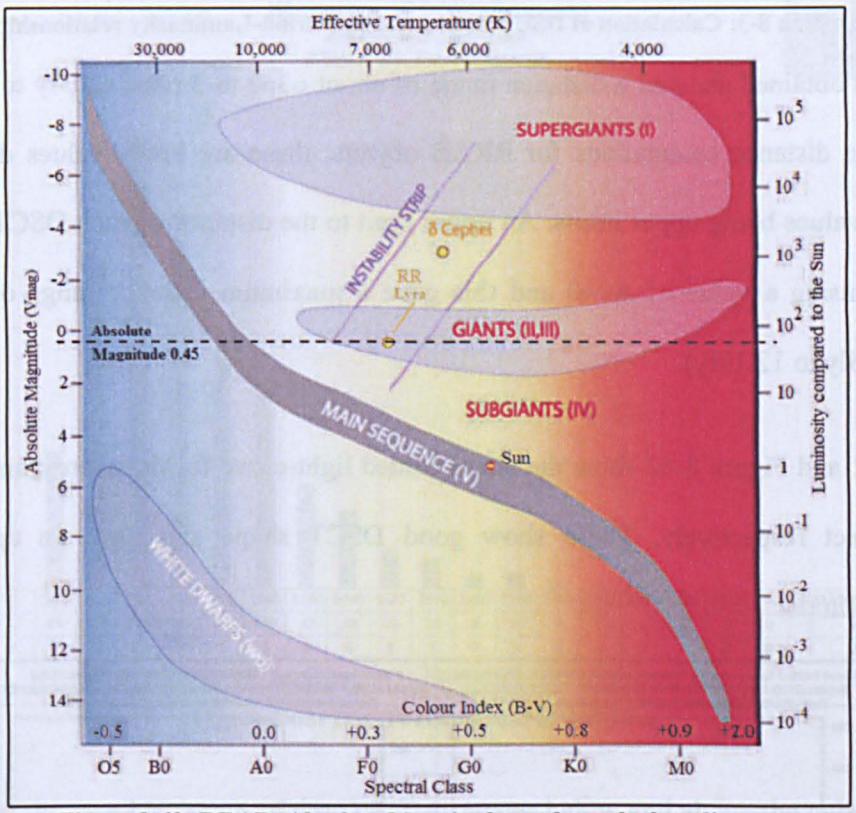

Figure 8-60: RRAB: Absolute Magnitude used to calculate distances shown on the H-R diagram

These calculated distances will be used to assess the Oosterhoff dichotomy in section 8.5.1

8.4.5 Calculation of DSCT distances

The distance to all 1,186 DSCT stars was calculated using their Period-Luminosity relationship. The Absolute Magnitude (Mv) was calculated using the equation taken from Laney et al. (2002), reproduced in Equation 8-3. There are more recent equations available (e.g. McNamara (2007)), but they tend to include metallicity as a parameter. As SuperWASP does not hold this information, the Laney et al. equation was selected for use. Equation 8-2 (section 8.4.2 above) was then used to calculate the distance using Mv from Equation 8-3. The results (and extinction values) are recorded on the supporting DVD at:

Supplementary data	
DSCT distances	X:\Chapter08\Catalogues\DSCT_distances.xlsx

Where X is DVD-1 in the DVD-drive

$$M_v = -2.92(\pm 0.04)\, Log(P/days) - 1.29(\pm 0.04)$$

Equation 8-3: Calculation of DSCT distance using Period-Luminosity relationship

The results obtained showed a distance range of about 63pc to 3.6kpc (205ly to 11.8kly), but like the distance calculations for RRAB objects, these are lower values due to the extinction values being upper limits. An upper limit to the distance of each DSCT star was calculated using a value of Av=0 and this gave a maximum distance range of 65pc to 3.7kpc (213ly to 12.1kly).

Figure 8-61 and Figure 8-62 show the phase-folded light-curve for the nearest and furthest DSCT object respectively. These show good DSCT shape and have an appropriate period/amplitude.

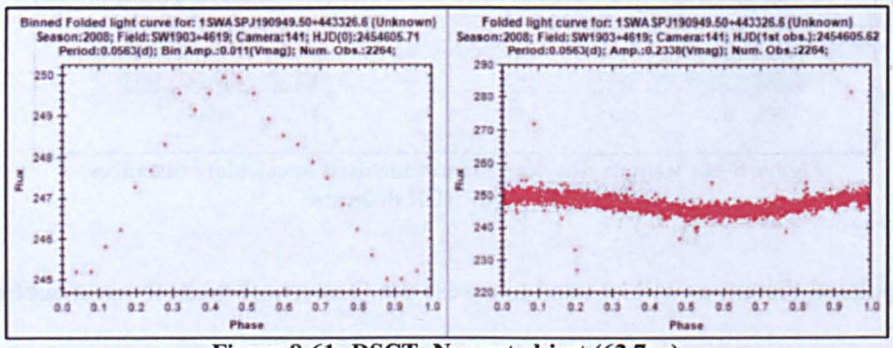

Figure 8-61: DSCT: Nearest object (62.7pc) (1SWASPJ190949.50+443326.6)

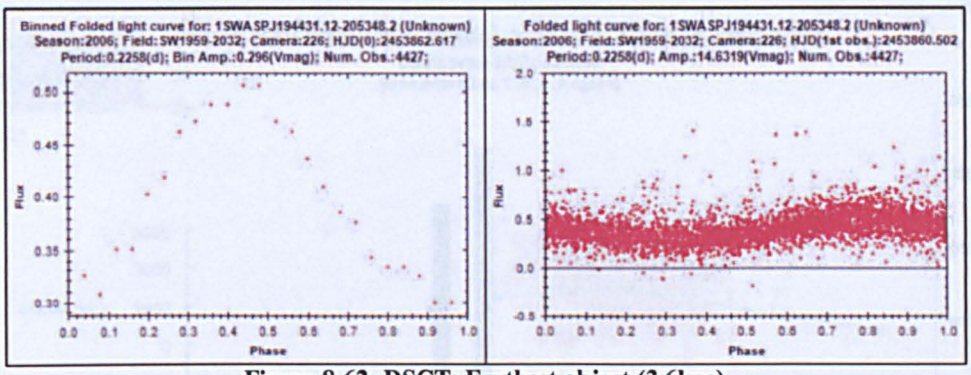

Figure 8-62: DSCT: Furthest object (3.6kpc) (1SWASPJ194431.12-205348.2)

Figure 8-63 shows a histogram of the DSCT distances. The 'unknown' stars (shown in blue) follow the same trend as the 'known' stars (in red). It also shows that the majority of DSCT stars lay within 180pc to 2.5kpc.

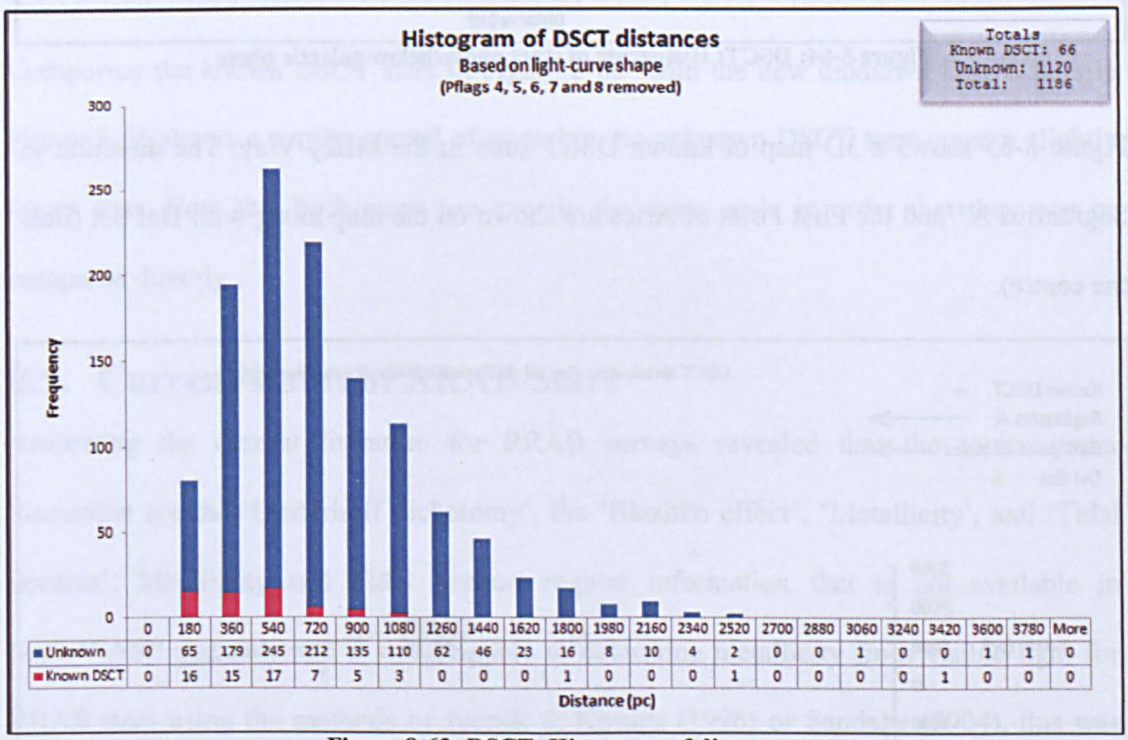

	0	180	360	540	720	900	1080	1260	1440	1620	1800	1980	2160	2340	2520	2700	2880	3060	3240	3420	3600	3780	More
Unknown	0	65	179	245	212	135	110	62	46	23	16	8	10	4	2	0	0	1	0	0	1	1	0
Known DSCT	0	16	15	17	7	5	3	0	0	0	1	0	0	0	1	0	0	0	0	1	0	0	0

Figure 8-63: DSCT: Histogram of distances

Figure 8-64 shows a histogram of the DSCT distances below and above the galactic plane. Again, the 'unknown' stars (shown in blue) follow the same trend as the 'known' stars (in red). It also shows that the majority of DSCT stars lay stars lay within -600pc to +800pc of the galactic plane.

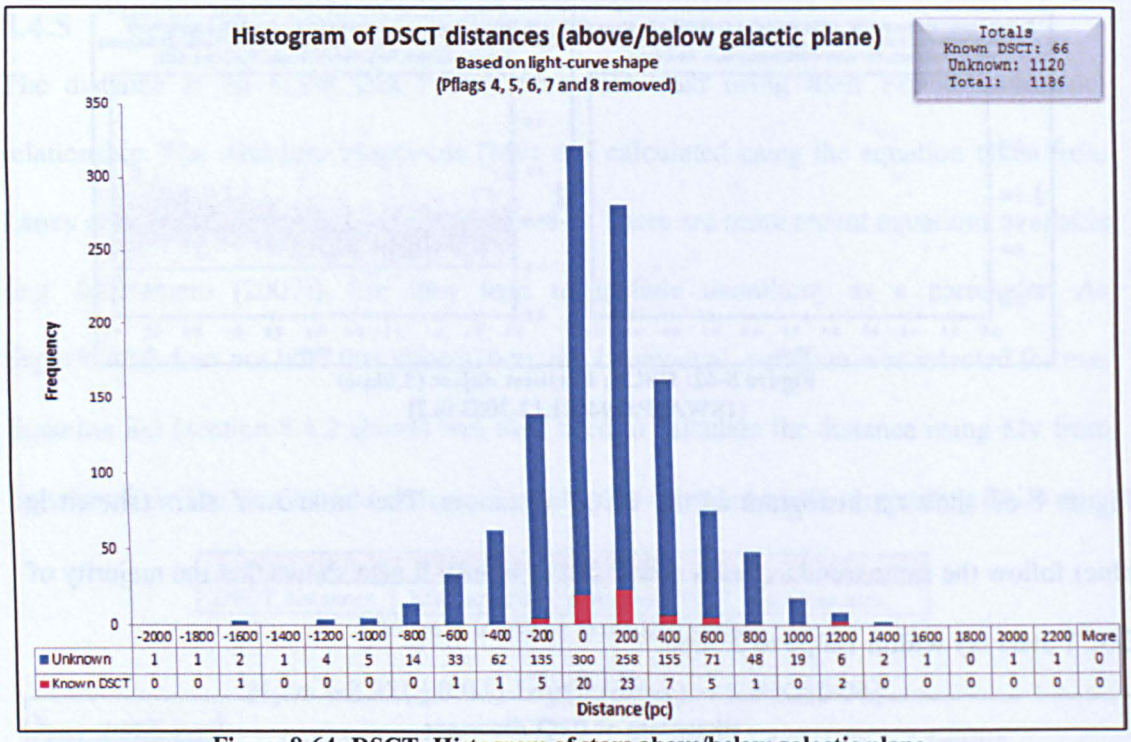

Figure 8-64: DSCT: Histogram of stars above/below galactic plane

Figure 8-65 shows a 3D map of known DSCT stars in the Milky Way. The direction to Sagittarius A* and the First Point of Aries are shown on the map along with Del Sct (near the centre).

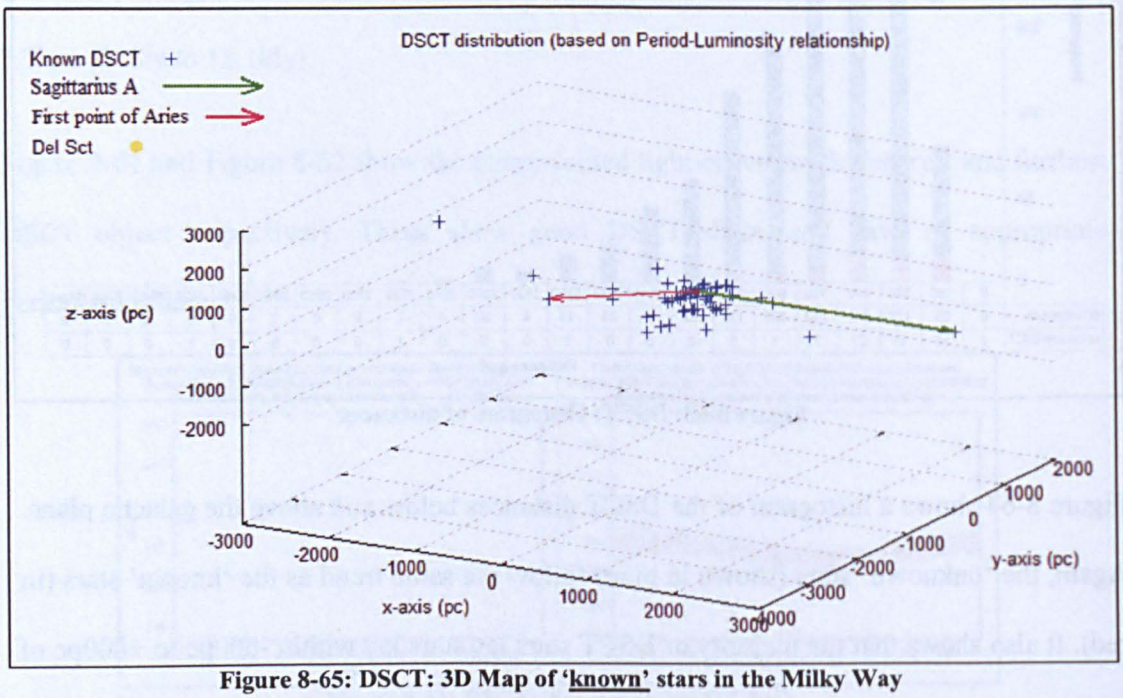

Figure 8-65: DSCT: 3D Map of 'known' stars in the Milky Way

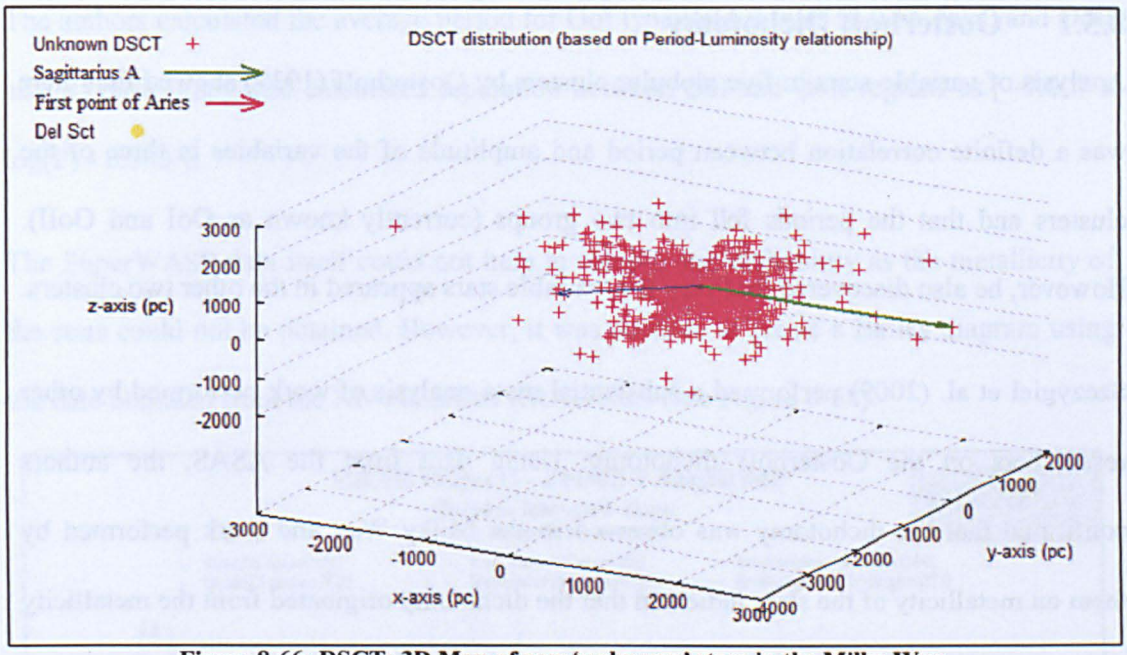

Figure 8-66: DSCT: 3D Map of new 'unknown' stars in the Milky Way

Comparing the known DSCT stars in Figure 8-65 with the new unknown DSCT stars in Figure 8-66 shows a similar spread of stars, but the unknown DSCT stars cover a slightly larger area. Note that both maps use exactly the same scale in order that they can be compared directly.

8.5. Current status of RRAB Stars

Reviewing the current literature for RRAB surveys revealed that the topics under discussion are the 'Oosterhoff dichotomy', the 'Blazhko effect', 'Metallicity', and 'Tidal streams'. Metallicity and Tidal streams require information that is not available in SuperWASP and although it was possible to determine metallicity from visible light for RRAB stars using the methods of Jurcsik & Kovács (1996) or Sandage (2004), this was outside the scope of this research. Therefore, this section discusses how the NN-classified RRAB stars from the SuperWASP archive fit into the Oosterhoff dichotomy and Blazhko effect.

8.5.1 Oosterhoff Dichotomy

Analysis of variable stars in five globular clusters by Oosterhoff (1939) showed that there was a definite correlation between period and amplitude of the variables in three of the clusters and that the periods fell into two groups (currently known as OoI and OoII). However, he also discovered that very few variable stars appeared in the other two clusters.

Szczygiel et al. (2009) performed a substantial meta-analysis of work performed by other researchers on the Oosterhoff dichotomy. Using data from the ASAS, the authors confirmed that the dichotomy was observed in the Milky Way and work performed by them on metallicity of the stars indicated that the dichotomy originated from the metallicity and age of the different areas of the galaxy. However, the final explanation still has not been constructed.

One aspect of the work performed by Szczygiel et al. (2009) was the creation of a Bailey graph using data from the ASAS. The graph (reproduced as Figure 8-67) shows two distinct regions of clumped stars labelled OoI and OoII, separated by the blue and green lines respectively. The authors placed dotted green lines on the graph to show the correlation between their work and the original M3 data from Oosterhoff, which agreed very well.

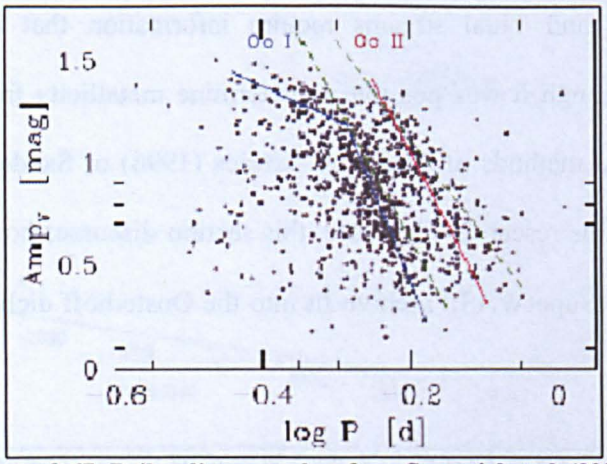

Figure 8-67: Bailey diagram taken from Szczygiel et al. (2009) Zoomed-in to show OoI and OoII regions

The authors calculated the average period for OoI type RRAB stars as 0.55 days, and OoII as 0.64 days. They also calculated separation between OoI and OoII regions as [-7.007 x log(P) - 0.343].

The SuperWASP data itself could not help to resolve this dichotomy as the metallicity of the stars could not be obtained. However, it was possible to create a Bailey diagram using the data obtained from the NN-classified RRAB stars (see Figure 8-68).

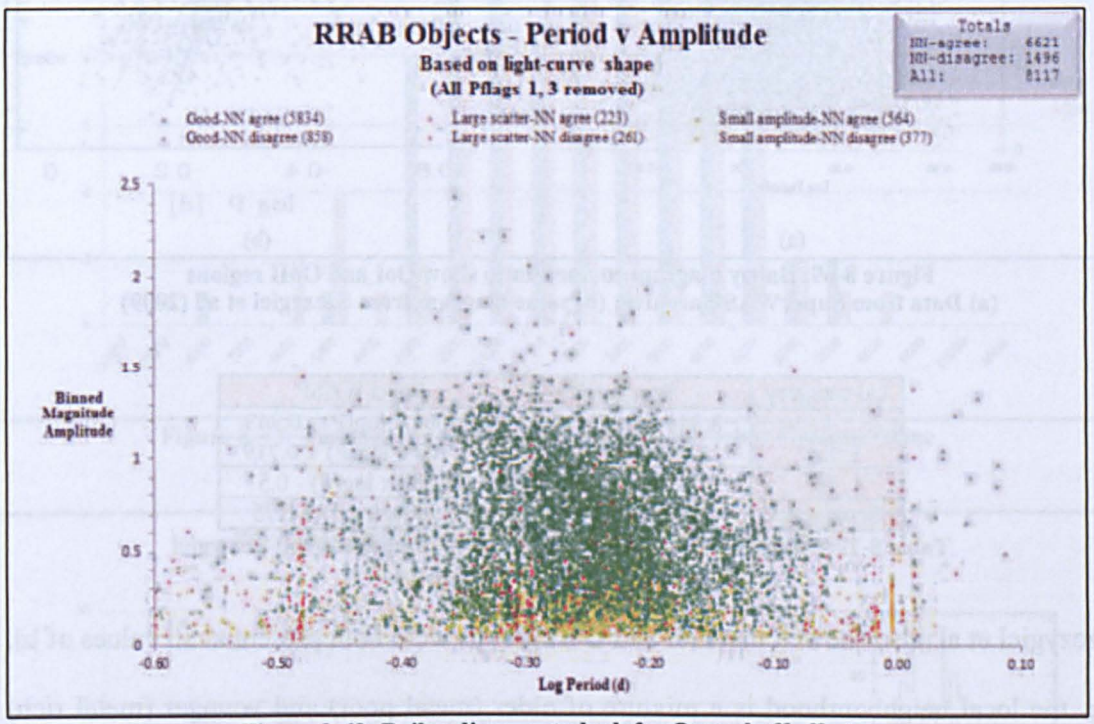

Figure 8-68: Bailey diagram to look for Oosterhoff effect

Although the data in the graph appeared evenly spread, there were two definite regions observed, similar to those seen by Szczygiel. The appropriate region of Figure 8-68 was therefore extracted and placed alongside the results from Szczygiel et al. to allow comparison (see Figure 8-69). To assess the similarities between the SuperWASP and Szczygiel datasets, lines of fit were calculated using Szczygiel's equations (Table 8-19) and the lines overlaid on Figure 8-69(a) using the amplitude and period values of all the SuperWASP RRAB stars. The OoI, 'Flat' and 'Separator' lines gave very good agreement,

while the OoII line was quite similar but with slightly longer periods, as shown by the dotted red line being offset to the right from the OoII region. Moving the lines (by eye) to the optimum position over the clumped regions provides the SuperWASP equations shown in Table 8-19.

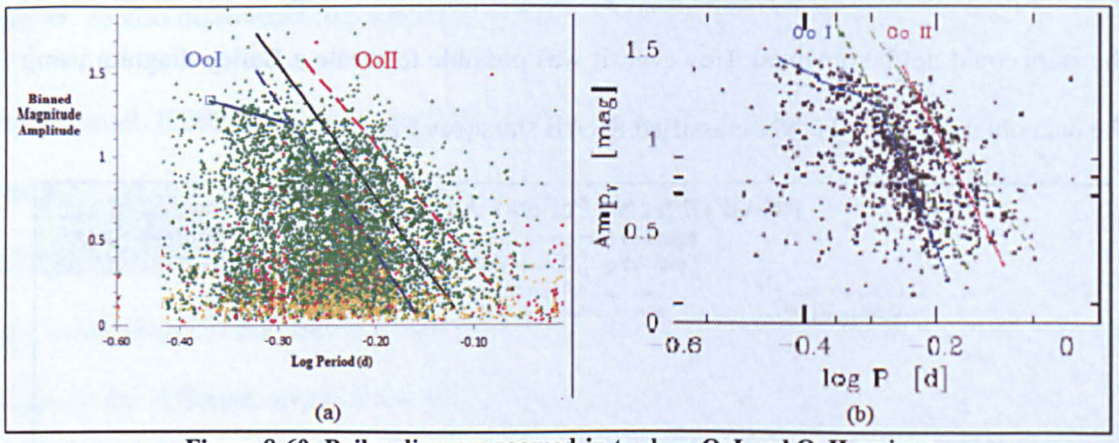

Figure 8-69: Bailey diagram zoomed-in to show OoI and OoII regions
(a) Data from SuperWASP archive; (b) same diagram from Szczygiel et al. (2009)

Oo category	Szczygiel	SuperWASP
I	−8.844×log(P)−1.343	-7.307 x log(P) - 0.943
I 'flat'	−1.654×log(P)+0.719	-1.700 x log(P) + 0.719
II	−7.007×log(P)−0.343	-7.300 x log(P) - 0.5
Separation	−8.0×log(P)−0.85	-7.500 x log(P) - 0.75

Table 8-19: SuperWASP OoI and OoII regions compared with Szczygiel

Szczygiel et al. also showed that OoI and OoII groups were both present at all values of |z|, i.e. the local neighbourhood is a mixture of older (metal poor) and younger (metal rich) stars, whereas the youngest stars were found only at low values of |z|, i.e. the thick disk region. To confirm this, 100 stars were identified in each of the OoI and OoII clumped regions in Figure 8-68 (see Appendix 31) and their distances plotted. Figure 8-70 shows that similar distances below/above the galactic plane were obtained for OoI and OoII stars. To perform a direct comparison with data from Szczygiel, the distance modulus was obtained and plotted as Figure 8-71. The inset in the figure shows the results obtained by Szczygiel where the plain area corresponds to OoIa, the red area to OoII and the darker

area to OoIb. The difference between OoIa and OoIb is simply the area where the data lay on the graph, OoIa is within the clumped area and OoIb is below this.

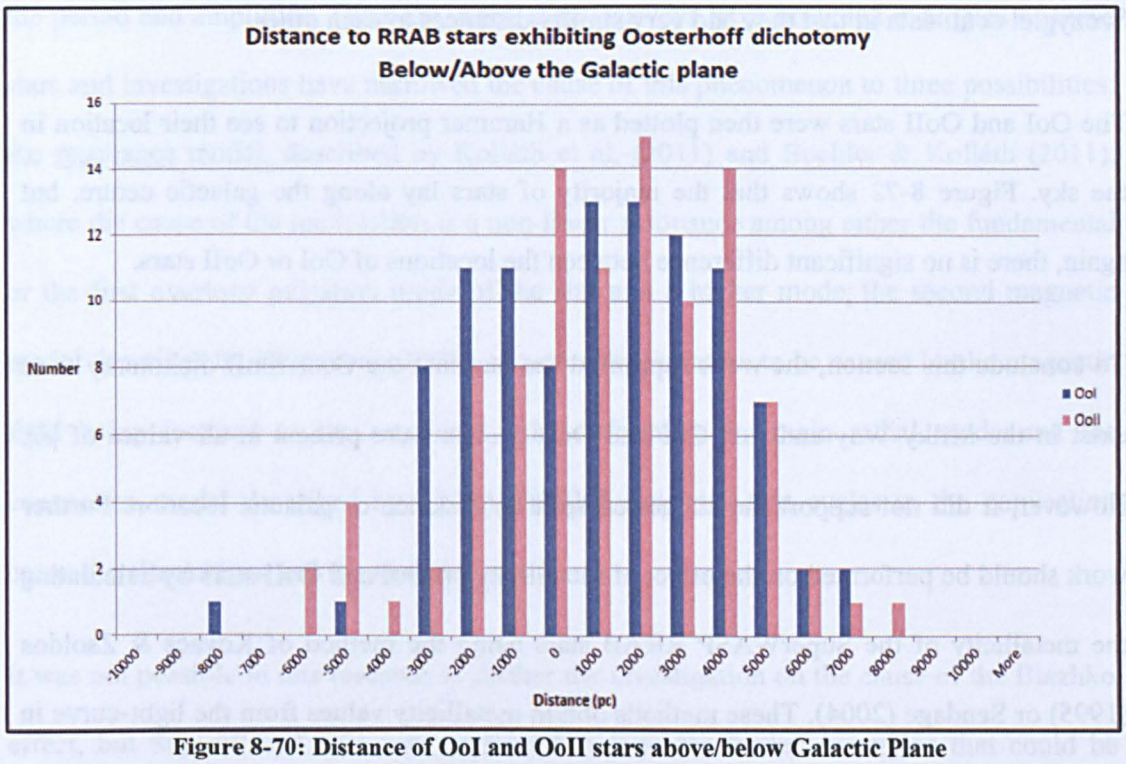

Figure 8-70: Distance of OoI and OoII stars above/below Galactic Plane

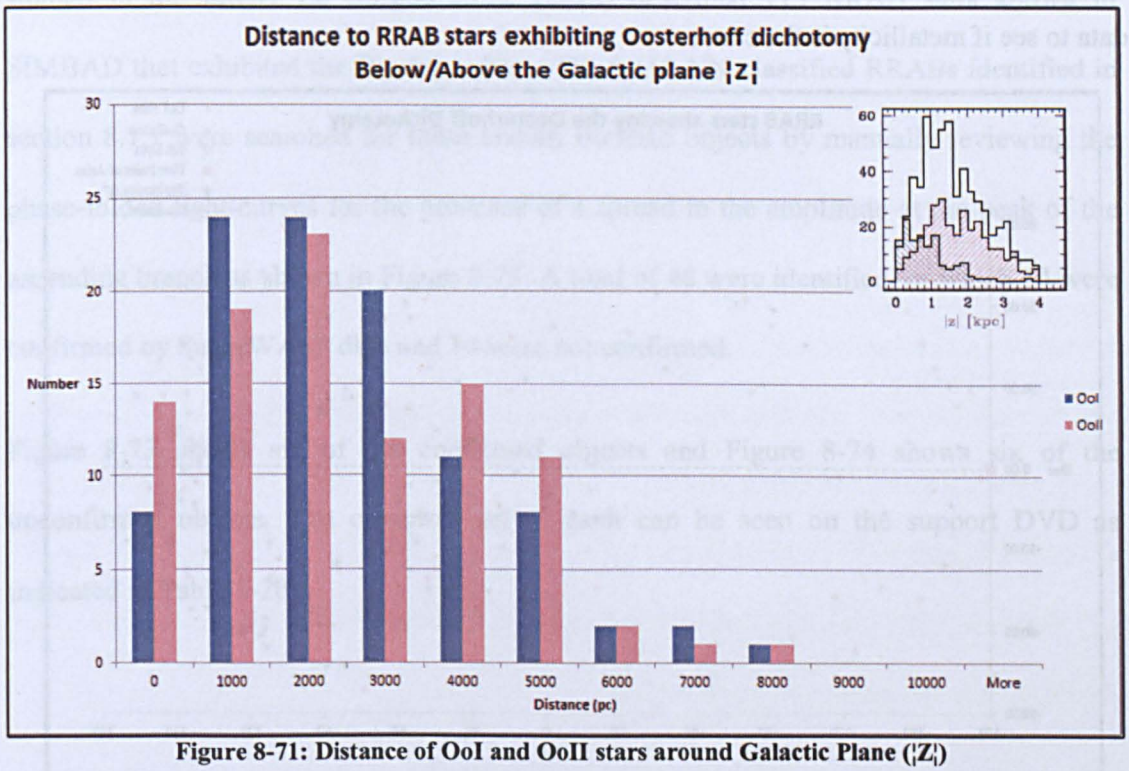

Figure 8-71: Distance of OoI and OoII stars around Galactic Plane (¦Z¦)

The SuperWASP data confirmed that both OoI and OoII stars were present in all values of |z|, but the split between OoI and OoII in the SuperWASP data did not support the Szczygiel et al. data in that they had very similar distances to each other.

The OoI and OoII stars were then plotted as a Hammer projection to see their location in the sky. Figure 8-72 shows that the majority of stars lay along the galactic centre, but again, there is no significant difference between the locations of OoI or OoII stars.

To conclude this section, the work supported the fact that the Oosterhoff dichotomy does exist in the Milky Way and that OoI and OoII groups were present at all values of |Z|. However, it did not support the suggested split by distance or galactic location. Further work should be performed on the effect of metallicity on OoI and OoII stars by calculating the metallicity of the SuperWASP RRAB stars using the method of Kovacs & Zsoldos (1995) or Sandage (2004). These methods obtain metallicity values from the light-curve in V-band and would then allow an analysis of the Oosterhoff dichotomy using SuperWASP data to see if metallicity is the cause.

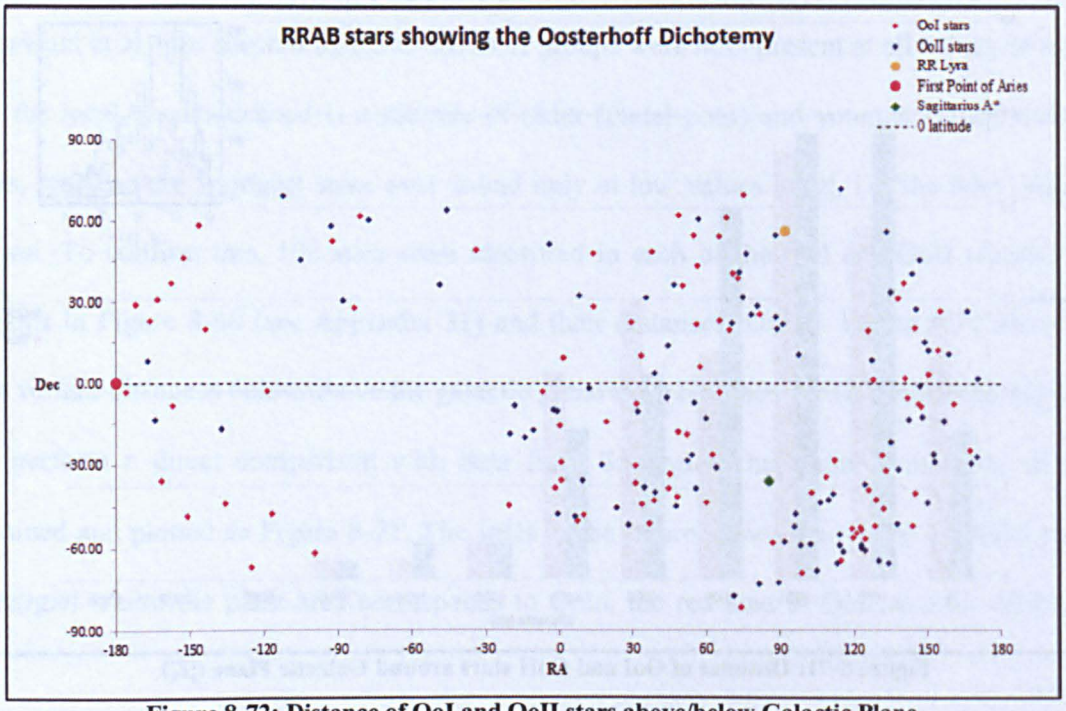

Figure 8-72: Distance of OoI and OoII stars above/below Galactic Plane

8.5.2 Blazhko effect

Blazko (1907) discovered long-period modulation in the star RW Dra due to a variation in the period and amplitude. Over the years, many surveys have provided examples of these stars and investigations have narrowed the cause of this phenomenon to three possibilities: the resonance model, described by Kolláth et al. (2011) and Buchler & Kolláth (2011), where the cause of the modulation is a non-linear resonance among either the fundamental or the first overtone pulsation mode of the star and a higher mode; the second magnetic model described by Kolenberg (2002), assumes the variation to be caused by the magnetic field being inclined to the rotational axis, deforming the main radial mode; and the convection model described by Stothers (2010), assumes that cycles in the convection cause the alternations and the modulations.

It was not possible in this research to further the investigation on the cause of the Blazhko effect, but SuperWASP data was examined to look for further examples that could be studied in the future. Le Borgne et al. (2012) described 113 RRAB stars known in SIMBAD that exhibited the Blazhko effect. The 8,117 NN-classified RRABs identified in section 8.1.1 were searched for these known Blazhko objects by manually reviewing the phase-folded light-curves for the presence of a spread in the amplitude at the peak of the ascending branch as shown in Figure 8-73. A total of 48 were identified, of which 34 were confirmed by SuperWASP data and 14 were not confirmed.

Figure 8-73 shows six of the confirmed objects and Figure 8-74 shows six of the unconfirmed objects. The complete set of each can be seen on the support DVD as indicated in Table 8-20.

Blazhko effect	Objects known in...	Confirmed by WASP	Number of objects	Object Id's Appendix	Location of Light-curves
Known	SIMBAD and GCVS	Yes	34	8-6 (a)	X:\Research\Thesis\DVD-support\Chapter08\Blazhko\Known_confirmed
Known	SIMBAD and GCVS	No	14	8-6 (e)	'X:\Research\Thesis\DVD-support\Chapter08\Blazhko\Known_unconfirmed
Query	SIMBAD and GCVS	Yes	20	8-6 (b)	X:\Research\Thesis\DVD-support\Chapter08\Blazhko\Possible_SIMBAD_GCVS
Query	SIMBAD only	Yes	38	8-6 (c)	X:\Research\Thesis\DVD-support\Chapter08\Blazhko\Possible_SIMBAD_only
Query	WASP only	Yes	28	8-6 (d)	X:\Research\Thesis\DVD-support\Chapter08\Blazhko\Possible_Unknown

Table 8-20: Location of support data for Blazhko stars

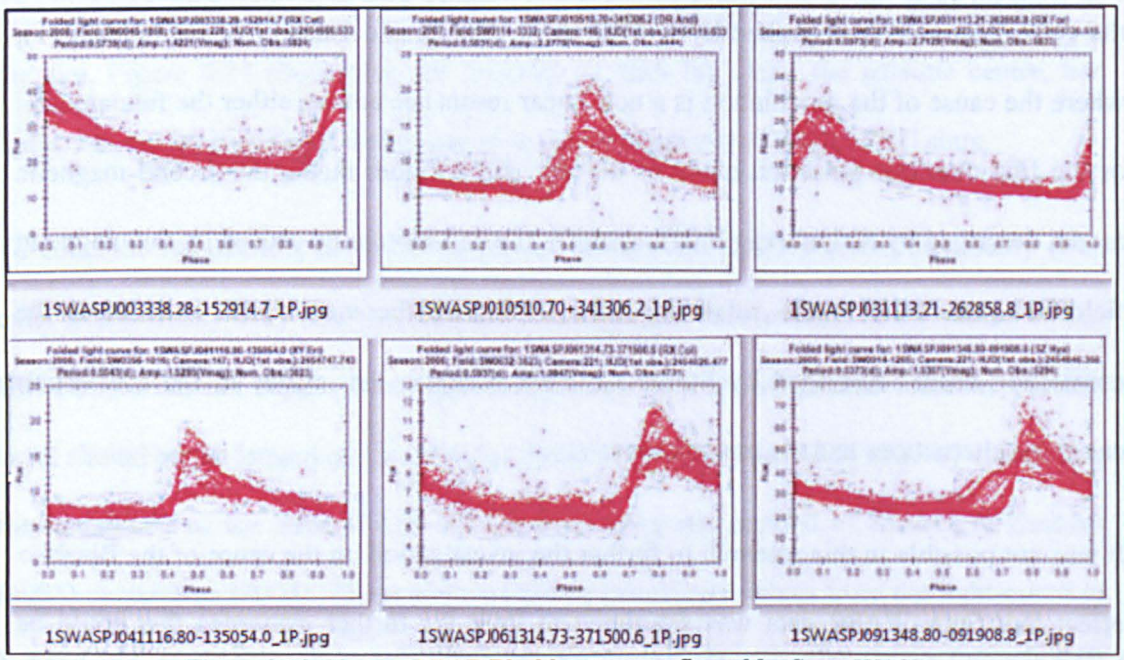

Figure 8-73: Known RRAB Blazhko stars confirmed by SuperWASP

As well as obtaining known Blazhko stars from the literature, the phase-folded light-curves of all 8,117 NN-classified RRABs were reviewed again for the Blazhko effect and 86 further examples were identified (see Table 8-20). 20 of the RRAB stars were known in SIMBAD and GCVS and 38 were only known in SIMBAD. The SuperWASP data clearly showed these as Blazhko stars, but there was no evidence in SIMBAD or GCVS to support this. As such, they are noted in the table as 'Query'. 28 other RRAB stars were identified which were not known in either SIMBAD or the GCVS. Six examples of each of these can be seen in Figure 8-75 (SIMBAD and GCVS), Figure 8-76 (SIMBAD only) and Figure 8-77 (SuperWASP only). The SuperWASP object Id's for all the RRAB stars showing the Blazhko effect can be seen in Appendix 32.

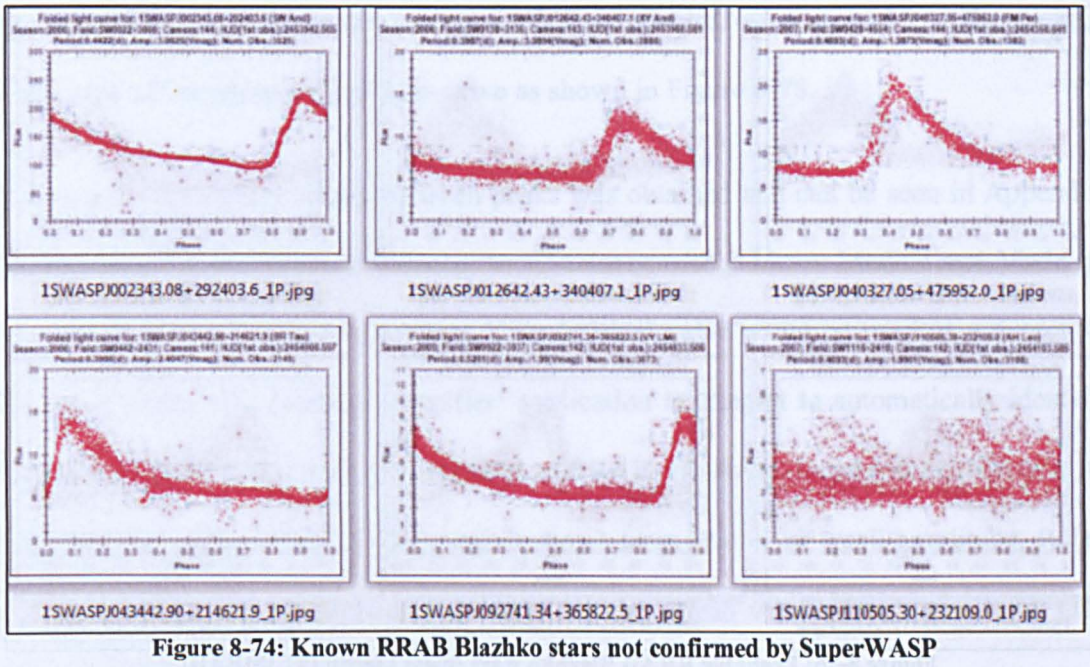

Figure 8-74: Known RRAB Blazhko stars not confirmed by SuperWASP

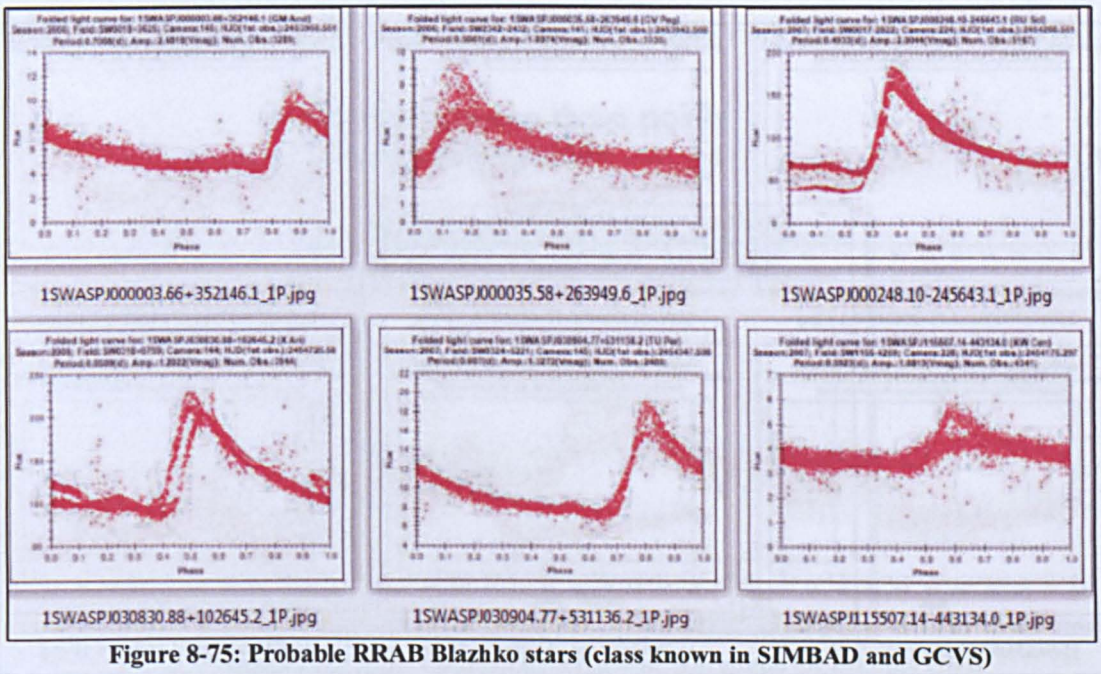

Figure 8-75: Probable RRAB Blazhko stars (class known in SIMBAD and GCVS)

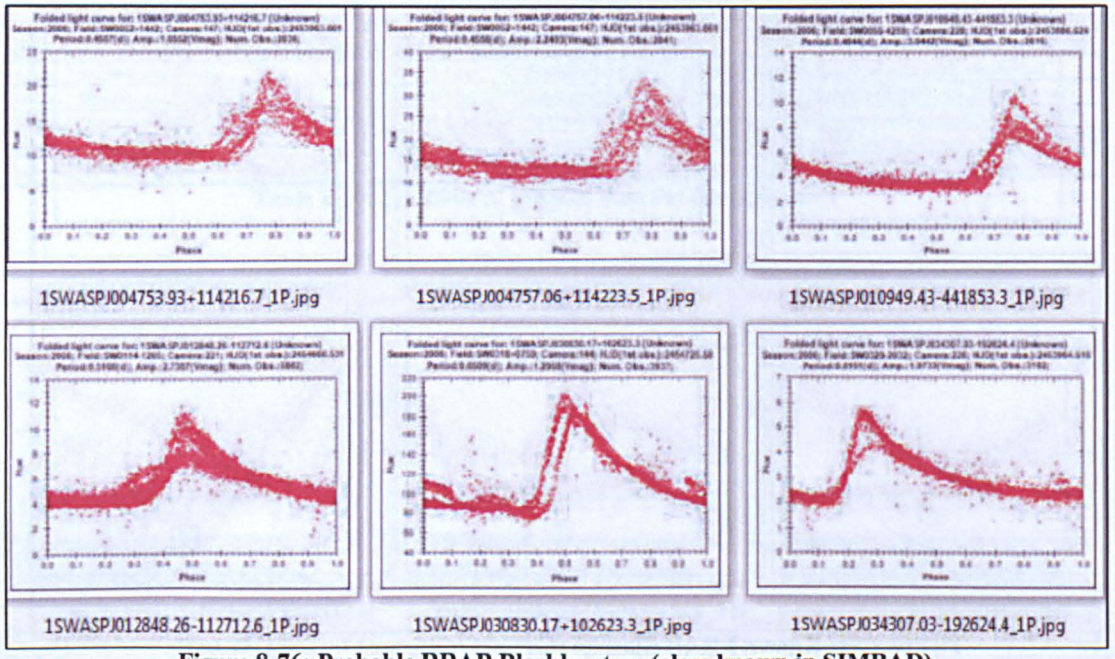

Figure 8-76: Probable RRAB Blazhko stars (class known in SIMBAD)

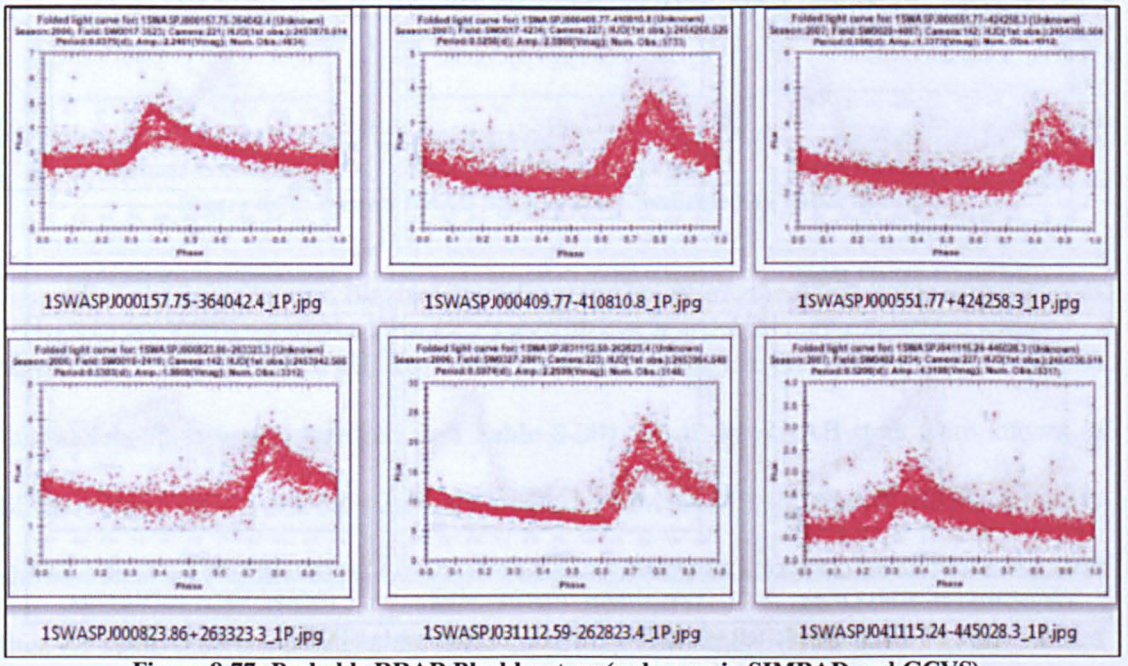

Figure 8-77: Probable RRAB Blazhko stars (unknown in SIMBAD and GCVS)

Based on the phase-folded light-curves of the 120 Blazhko stars manually reviewed above the spread of the peaks were calculated for each of the stars in order to find the minimum limit that SuperWASP data could support for identification of Blazhko stars. The spread

was calculated as the difference in magnitude between the lowest and highest flux values of the peak of the phase-folded light-curve as shown in Figure 8-78.

The range of difference values between peaks was obtained and can be seen in Appendix 33. The range obtained was 0.06Vmag to 1.51Vmag with a Mean, Median and Mode of 0.49, 0.51 and 0.47Vmag respectively. This 'spread' value could be used as a detection parameter in the 'LC Analyser classifier' application to attempt to automatically identify the Blazhko effect when stars are classified as RRAB. However, there will be difficulty in using this parameter when the light-curve shows large-scatter or small-amplitude. Rules could be included in the application to only use the spread value when the reduced chi-square and amplitude values gave a suitable indication that there was low scatter and suitable amplitude. This has been added to the list of future work in Chapter 10.

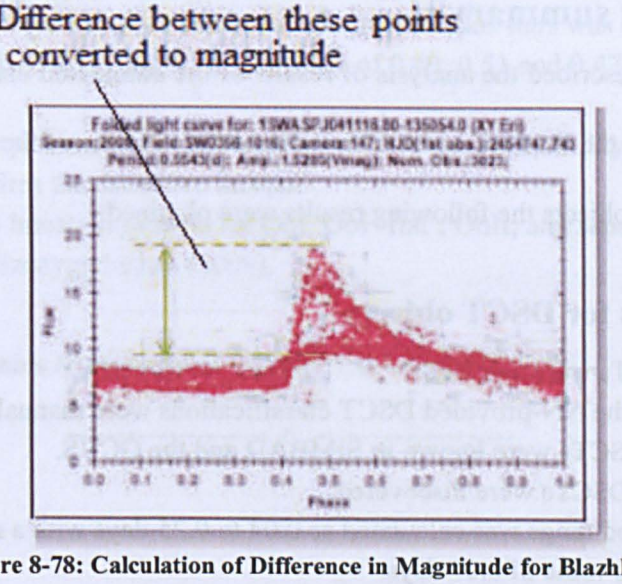

Figure 8-78: Calculation of Difference in Magnitude for Blazhko effect

Figure 8-79 shows a Hammer projection on the location of all 8,117 RRAB stars and all the Blazhko stars are highlighted. The star RR Lyr, First Point of Aries and Sagittarius A* are also placed on the map as a comparison. The Blazhko stars appear to be spread across the night sky.

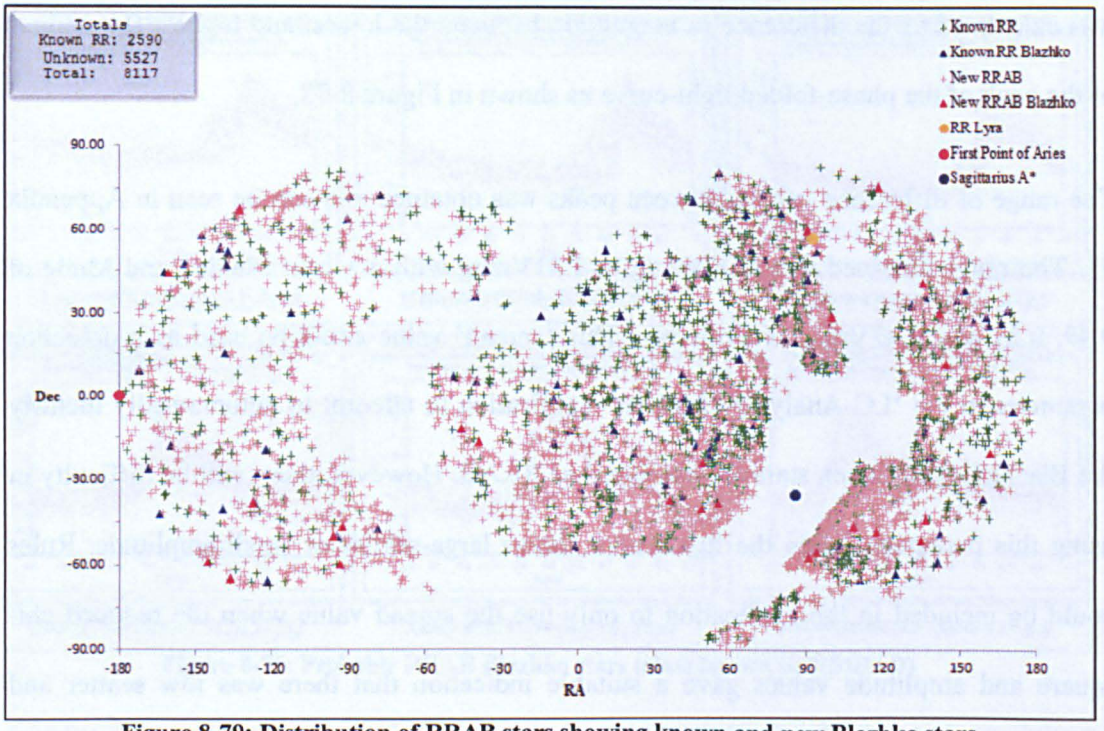

Figure 8-79: Distribution of RRAB stars showing known and new Blazhko stars

8.6. Chapter summary

This chapter has described the analysis of results of the automated classification of RRAB and DSCT stars in the SuperWASP archive. From the analysis of the manually confirmed DSCT and RRAB objects the following results were obtained.

8.6.1 Results for DSCT objects

- ✓ 1,979 DSCTs were assessed.
- ✓ 92.32% of the NN-provided DSCT classifications were manually confirmed.
- ✓ 43 of the DSCTs were known in SIMBAD and the GCVS.
- ✓ 1,877 new DSCTs were discovered.
- ✓ DSCT period range was calculated as 0.04 to 0.25 days with a median of 0.11 days and a modal value of 0.07 days.
- ✓ 110 DSCTs had a period longer than the upper published period limit of 0.2 days.
- ✓ DSCT amplitude range was 0.02 to 1.55Vmag, with a median of 0.18Vmag and a modal value of 0.12Vmag.
- ✓ 2 DSCTs were above the published amplitude range of <0.9Vmag.
- ✓ A 2D distribution map of DSCTs was created.
- ✓ DSCT distance range was calculated as 63pc to 4kpc, with a |z| range of -600pc to +800pc.
- ✓ A 3D distribution map of DSCTs was created.

8.6.2 Results for RRAB objects

- ✓ 8,556 RRABs were assessed.
- ✓ 78.86% of the NN-provided RRAB classifications were manually confirmed.
- ✓ 2,600 of the RRABs were known in SIMBAD and the GCVS.
- ✓ 5,722 new RRABs were discovered.
- ✓ RRAB period range was calculated as 0.25 to 1.71 days with a median of 0.57 days and a modal value of 0.61 days.
- ✓ 79 RRABs had a period shorter than the published period limit of >0.3 days.
- ✓ 14 RRABs had a period longer than the published period limit of <1.2 days.
- ✓ RRAB amplitude range was 0.02 to 2.43Vmag, with a median of 0.41Vmag and a modal value of 0.13Vmag.
- ✓ 4,749 RRABs were below the published amplitude range of >0.5Vmag.
- ✓ 4 RRABs were above the published amplitude range of <2.0Vmag.
- ✓ A 2D distribution map of RRABs was created.
- ✓ RRAB distance range was calculated as 24pc to 17kpc, with a |z| range of -4pc to +5pc.
- ✓ A 3D distribution map of RRABs was created.
- ✓ 48 known Blazhko stars were investigated and 34 were confirmed and 14 were not confirmed.
- ✓ 86 New Blazhko stars were discovered.
- ✓ The range of magnitudes between peaks in the Blazhko stars was 0.06Vmag to 1.51Vmag with a Mean, Median and Mode of 0.49, 0.51 and 0.47Vmag respectively.
- ✓ Confirmed the presence of the Oosterhoff dichotomy in the Milky Way galaxy, but could not confirm the causative factors.
- ✓ Confirmed the linear-fit models for OoI, OoI 'flat', OoII, and separation regions calculated by Szczygiel et al. (2009).

The next chapter contains a summary of Chapter 1 to Chapter 8.

---------- o ----------

Chapter 9 Summary of results

A total of 4,280,740 objects were processed in Chapter 5 by the 'LC Analyser classifier' application and results were obtained for 3,913,807 of these. The remainder had insufficient observations after pre-processing to assign a classification. Of the 3,913,807 tested objects, 3,214,104 were unique, the remainder being duplicates, probably due to multiple periods, seasons, fields and/or cameras. From the 3,214,104 unique objects, 1,136,566 were classified as follows: 274,808 had a classification that agreed in all three NNs (confidence index 1). 344,323 had a classification that agreed in two of the three NNs (confidence index 2) and 517,435 had a classification in one NN only (confidence index 4).

9.1. Effectiveness of the automated classification system

To test the effectiveness of the 'LC Analyser classifier' application, 342,974 unique objects of the following classifications were extracted from the above dataset and the phase-folded light-curves manually reviewed to confirm the classes: Algol-like (EA); Beta Lyrae-like (EB); W UMa-like (EW); RR Lyrae-like (RRAB); and Delta Scuti-like (DSCT). As shown in Chapter 6, only 31,728 (9.25%) of these had a confirmed 'Good' classification. This unsatisfactory result was investigated and the 'Poor' classifications were found to be due to a number of reasons:

- Harmonic periods of the 'real' period (i.e. PFlag > 0 as defined in the SuperWASP archive);
- Objects with a large scatter of observations;
- Objects with very small amplitudes;
- Systemic effects during collection of the observations by SuperWASP (shown as clumping and banding of periods);

Methods were examined in Chapter 6 for identifying these situations while processing the objects in the 'LC Analyser classifier' so that they could be removed prior to classification by the NN module (i.e. using the reduced chi-square). The chi-square method proved very

effective at reducing the 'poor' objects, so this and other enhancements discussed in Chapter 10 will be implemented in the 'LC Analyser classifier' in the near future and the periodic objects in the SuperWASP archive re-run to obtain the full catalogues. These will be stored in the SuperWASP archive and become available to the public.

9.2. Comparison of SuperWASP period and classification against GCVS

The observations for 2,621 objects in the SuperWASP archive that were also known in the GCVS were obtained from the SuperWASP archive. From these 2,621 objects, 1,683 had both a SuperWASP-calculated period and a GCVS-stored period, 649 objects had a SuperWASP-calculated period only and 289 objects had a GCVS-stored period only.

Analysis of the 1,683 objects that had both a SuperWASP and GCVS period, showed that 1,472 (87.5%) of the periods agreed within +/-1% and only 211 (12.5%) periods disagreed. Of the 211 objects where the period disagreed, phase-folded light-curves were created using the periods from SuperWASP and the GCVS. These were reviewed to identify the better period and it was found that the SuperWASP period identified a better period for 194 of the objects. The result is therefore to inform the GCVS of: confirmation of the periods for 1,472 stars; improvement in the period of 194 stars; and the addition of 649 new periodic stars. The assessment is described in Chapter 4.

The 2,621 objects in the SuperWASP archive with a known classification in the GCVS, had phase-folded light-curves created for their SuperWASP period and these were reviewed to confirm the GCVS class. The results of this review showed that 2,050 (78%) of the light-curves agreed with the GCVS classification. This also confirms the classifications of 333 objects that had unconfirmed classes in the GCVS (e.g. CEP: EA:

and RR etc.), and also suggested re-classification of 198 GCVS objects with suspected incorrect classes.

9.3. Creation of the stellar catalogues

As mentioned previously, two types of catalogues were created from this research. Table 9-1 shows the number of unique objects available in the catalogues from the work completed in Chapter 6 (personal catalogues), while the main catalogue available to the public will be completed when the enhancements in Chapter 10 have been implemented, shortly after this research has been submitted.

Catalogue	All	LS/SA removed	G/LS/SA removed
EA	12,882	11,884	9,398
EB	5,226	N/A	N/A
EW	2,875	N/A	N/A
All eclipsing	20,983	19,985	17,499
DSCT	1,979	1,536	1,186
RRAB	8,556	8,303	8,117
All Pulsating	10,746	10,050	9,514
Total	31,729	30,035	27,013

Table 9-1: Stellar catalogues available from this research

The terms G, LS and SA in the table means 'clumped' and 'banded' period objects within the affected PFlags were removed: LS/SA denotes large-scatter and small-amplitude objects only were removed, whereas, G/LS/SA indicates good, large-scatter and small-amplitude objects were removed (i.e. all objects for that PFlag). In comparison to the original number of objects, there may appear to be only a small number of classified objects obtained, but these objects were manually reviewed and the classifications confirmed. When the complete public catalogue is obtained (after the enhancements in Chapter 10 have been implemented), over one million objects are expected. Additionally, the automated method can be run repeatedly over a period of time, thereby updating the catalogues without further manual intervention and giving the opportunity to create O-C diagrams over time (i.e. seasons).

9.4. Investigation of Eclipsing Binary stars

9.4.1 Statistics

The period and amplitude ranges of the eclipsing binary stars Algol-like (EA double-eclipse and single-eclipse), Beta Lyrae-like (EB), and W UMa-like (EW) were obtained and compared against published ranges (shown as 'specification') and presented in Table 9-2 and Table 9-3.

	Period (days)						
	Range				Specification		Outside the range
Class	Min	Max	Median	Mode	Low	High	
EA	0.12	18.00	1.63	0.67	0.20	10,000	50 objects below
EB	0.14	20.57	0.56	0.48	1.00	N/A	4,751 objects below
EW	0.18	3.62*	0.34	0.26	N/A	1.00	25 objects above
*2 high outliers were removed							

Table 9-2: Period ranges calculated from SuperWASP data for EA, EB and EW stars

	Amplitude (Vmag)						
	Range				Specification		Outside the range
Class	Min	Max	Median	Mode	Low	High	
EA	0.02	2.50	0.27	0.16	N/A	Several	All within
EB	0.02	1.52	0.25	0.15	N/A	2.00	All within
EW	0.02	1.32	0.32	0.27	N/A	0.80	39 objects above

Table 9-3: Amplitude ranges calculated from SuperWASP data for EA, EB and EW stars

The 'Outside the range' column in Table 9-2 and Table 9-3 indicates how many objects were outside the published ranges and these were discussed in Chapter 7.

EA objects

After manual removal of the 'bad' objects identified by the 'LC Analyser classifier', 96.74% of the EA objects were manually confirmed. This was an excellent result providing the 'bad' objects can be removed from the final analysis as described in the improvements in Chapter 10. The results indicated that 5,826 (45.2%) of EA objects were Double-eclipse, while 7,056 (54.8%) were Single-eclipse. Of the 12,882 EA objects classified, 1,060 were known in SIMBAD and GCVS and 11,308 were newly discovered EA objects. The remainder disagreed with the GCVS classification and were discussed in Chapter 7. From

Table 9-2, 50 of the 12,882 EA objects (0.39%) had a period below the published period range, and from Table 9-3, all of the EA objects were within the published amplitude range.

EB objects

After manual removal of the 'bad' objects identified by the 'LC Analyser classifier', 99.50% of the EB objects were manually confirmed. Again, this was an excellent result. Of the 5,226 EB objects classified, 195 were known in SIMBAD and GCVS and 4,641 were newly discovered EB objects. The remainder disagreed with the GCVS classification and were discussed in Chapter 7. From Table 9-2, 4,751 of the 5,226 EB objects (90.19%) had a period below the published period range, and from Table 9-3, all of the EB objects were within the published amplitude range.

EW objects

After manual removal of the 'bad' objects identified by the 'LC Analyser classifier', 97.80% of the EW objects were manually confirmed. Again, this was an excellent result. Of the 2,875 EW objects classified, 206 were known in SIMBAD and GCVS and 2,251 were newly discovered EW objects. The remainder disagreed with the GCVS classification and were discussed in Chapter 7. From Table 9-2, 25 of the 2,875 EW objects (0.87%) had a period above the published period range, and from Table 9-3, 39 of the EW objects (1.36%) were above the published amplitude range.

9.4.2 Eclipse-depth Ratio

The eclipse-depth ratio values were investigated for the EB and EW classes to see if they could be differentiated using this parameter. Table 9-4 shows the results obtained for EA, EB and EW objects. The EB and EW eclipse-depth ratios are the most interesting, as these allow separation between the EB and EW classes as shown in Figure 9-1.

	Eclipse-depth ratio				
Class	Mean	Median	Mode	Min	Max
EA	0.258	0.183	0.184	0.019	1.000
EB	0.547	0.551	0.510	0.183	0.959
EW	0.888	0.878	0.918	0.673	1.000

Table 9-4: Depth ratio values calculated from SuperWASP data for EB and EW stars

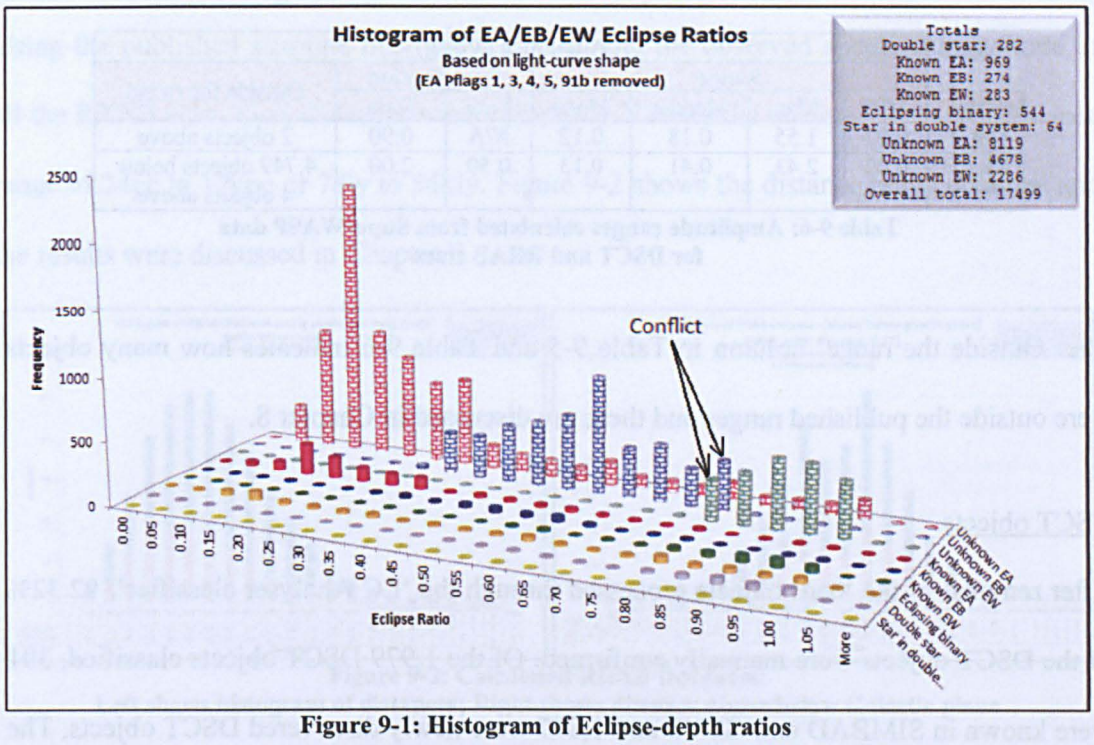

Figure 9-1: Histogram of Eclipse-depth ratios

The eclipse-depth ratio was resolved further in Chapter 7 providing the range for separation of EB and EW objects as:

EB = 0.75 and below; EW = 0.85 and above; EB/EW = 0.76 to 0.84.

9.5. Investigation of Pulsating stars

9.5.1 Statistics

The period and amplitude ranges of the pulsating stars RR Lyrae-like (RRAB) and Delta Scuti-like (DSCT) were obtained and compared against published ranges (shown as 'specification') as presented in Table 9-5 and Table 9-6.

	Period (days)						
	Range				Specification		Outside the range
Class	Min	Max	Median	Mode	Low	High	
DSCT	0.04	0.25	0.11	0.07	0.01	0.20	110 objects above
RRAB	0.25	1.71	0.57	0.61	0.30	1.20	79 objects below 14 objects above

Table 9-5: Period and Amplitude ranges calculated from SuperWASP data for DSCT and RRAB stars

	Amplitude (Vmag)						
	Range				Specification		Outside the range
Class	Min	Max	Median	Mode	Low	High	
DSCT	0.02	1.55	0.18	0.12	N/A	0.90	2 objects above
RRAB	0.02	2.43	0.41	0.13	0.50	2.00	4,749 objects below 4 objects above

Table 9-6: Amplitude ranges calculated from SuperWASP data for DSCT and RRAB stars

The 'Outside the range' column in Table 9-5 and Table 9-6 indicates how many objects were outside the published ranges and these are discussed in Chapter 8.

DSCT objects

After removal of the 'bad' objects processed through the 'LC Analyser classifier', 92.32% of the DSCT objects were manually confirmed. Of the 1,979 DSCT objects classified, 391 were known in SIMBAD and GCVS and 1,877 were newly discovered DSCT objects. The remainder disagreed with the GCVS classification and are discussed in Chapter 8. From Table 9-5, 110 of the 1,979 DSCT objects (5.56%) had a period above the published period range, and from Table 9-6, 2 of the DSCT objects (0.10%) were above the published amplitude range.

RRAB objects

After removal of the 'bad' objects processed through the 'LC Analyser classifier', 78.86% of the RRAB objects were manually confirmed. Of the 8,556 RRAB objects classified, 2,600 were known in SIMBAD and GCVS and 5,722 were newly discovered RRAB objects. The remainder disagreed with the GCVS classification and are discussed in Chapter 8. From Table 9-5, 79 of the 8,556 RRAB objects (0.92%) had a period below the

published period range and 14 (0.16%) above the published period range. From Table 9-6, 4,749 of the DSCT objects (55.50%) were below the published amplitude range and 4 (0.05%) above the published amplitude range.

9.5.2 Calculating distances for the RR Lyrae stars

Using the published absolute magnitude of 0.45 and the observed apparent magnitude of all the RRAB stars, their distances were calculated. The results obtained showed a distance range of 24pc to 17kpc or 78ly to 54kly. Figure 9-2 shows the distance range obtained and the results were discussed in Chapter 8.

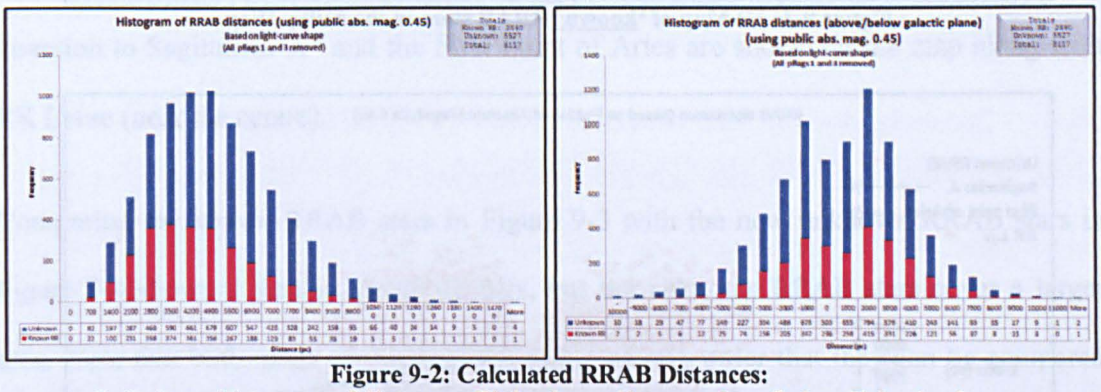

Figure 9-2: Calculated RRAB Distances:
Left shows histogram of distances; Right shows distance above/below Galactic plane

9.5.3 Creation of a 3D map of the galaxy using RR Lyrae stars

Figure 9-3 shows the 3D map created for the known RRAB stars in the Milky Way. The direction to Sagittarius A* and the First Point of Aries are shown on the map along with RR Lyrae (near the centre).

Comparing the known RRAB stars in Figure 9-3 with the new unknown RRAB stars in Figure 9-4 shows a similar spread of stars, but the unknown RRAB stars cover a larger area. Note that both maps use exactly the same scale in order that they can be compared directly.

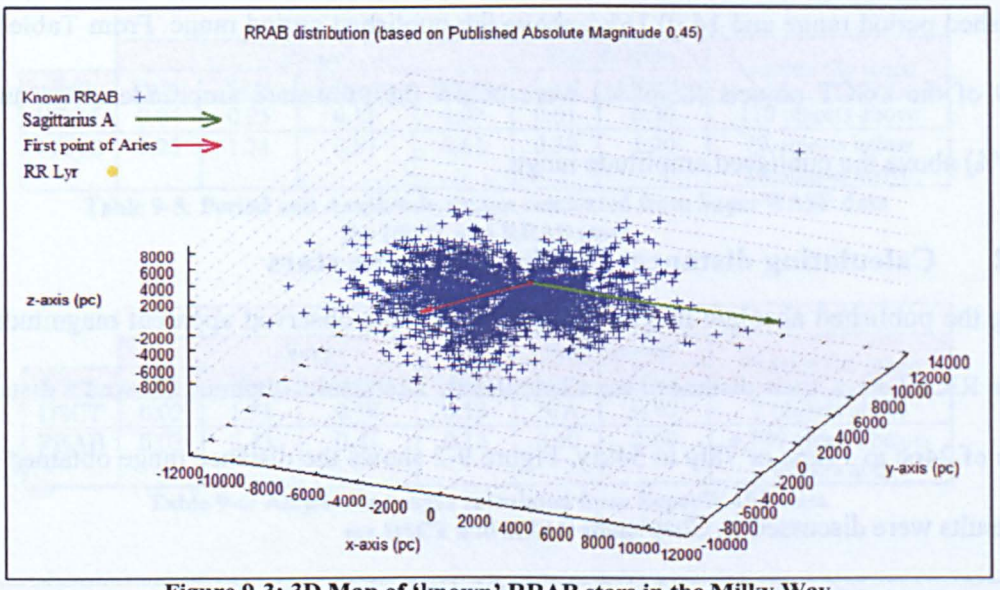

Figure 9-3: 3D Map of '<u>known</u>' RRAB stars in the Milky Way

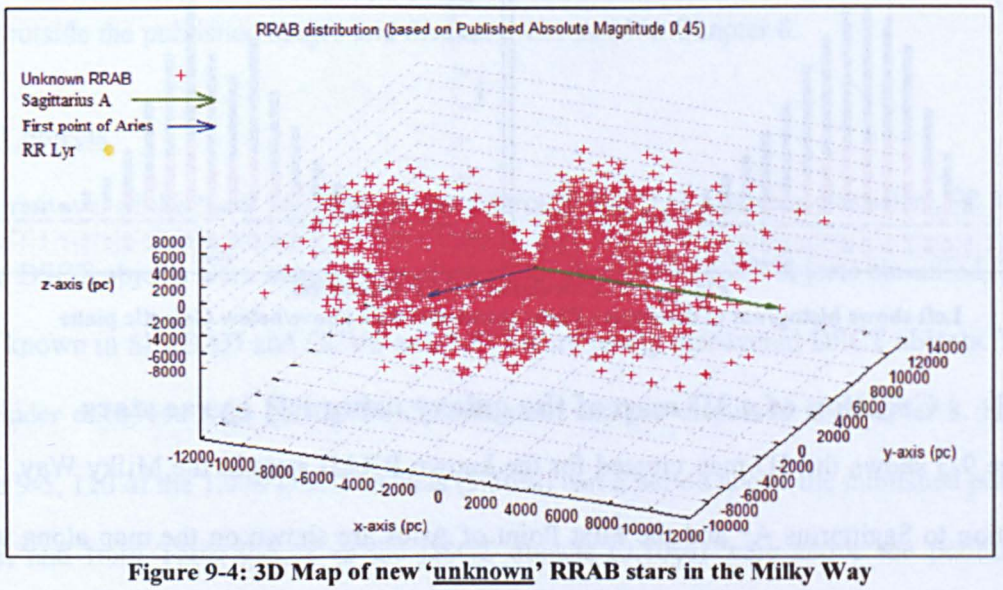

Figure 9-4: 3D Map of new '<u>unknown</u>' RRAB stars in the Milky Way

9.5.4 Calculating distances for the DSCT stars

Using the Period-Luminosity relationship of Delta-Scuti stars, the Absolute Magnitude for each star was calculated and together with the observed apparent magnitude, the distance to each Delta-Scuti stars was calculated. The results obtained showed a distance range of 63pc to 4kpc or 205ly to 12kly. Figure 9-5 shows the distance range obtained and the results were discussed in Chapter 8.

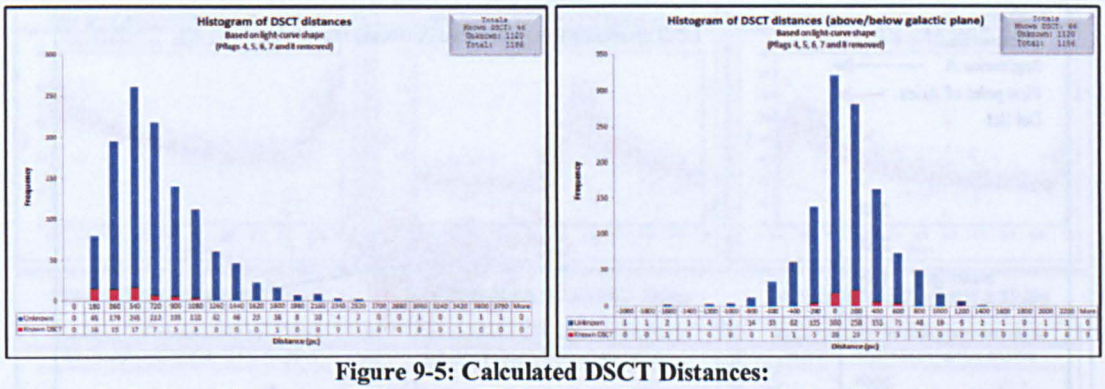

Figure 9-5: Calculated DSCT Distances:
Left shows histogram of distances; Right shows distance above/below Galactic plane

9.5.5 Creation of a 3D map of the galaxy using DSCT stars

Figure 9-3 shows the 3D map created for the known RRAB stars in the Milky Way. The direction to Sagittarius A* and the First Point of Aries are shown on the map along with RR Lyrae (near the centre).

Comparing the known RRAB stars in Figure 9-3 with the new unknown RRAB stars in Figure 9-4 shows a similar spread of stars, but the unknown RRAB stars cover a larger area. Note that both maps use exactly the same scale in order that they can be compared directly.

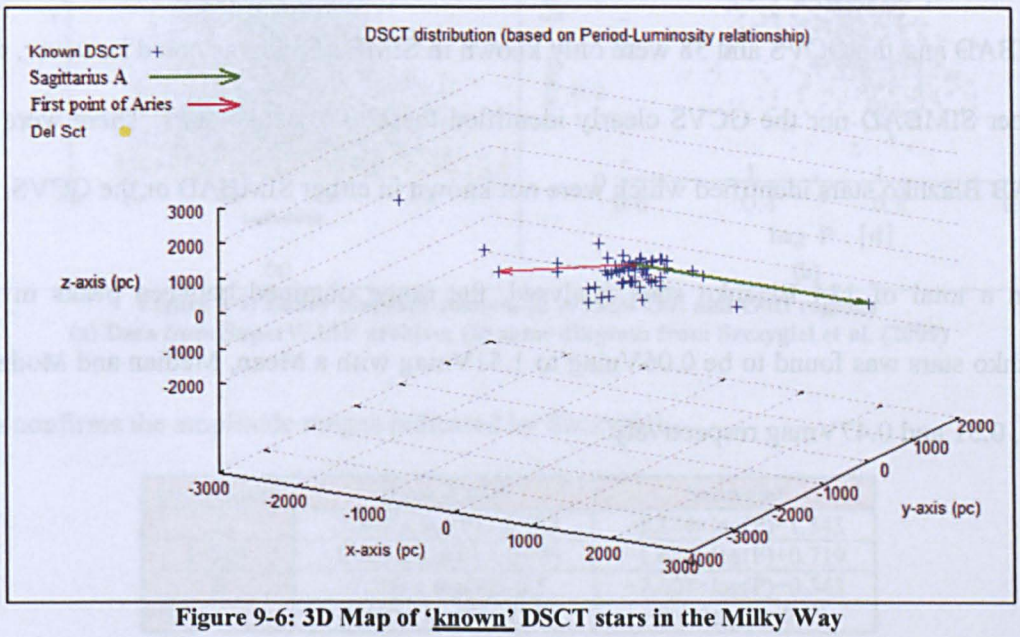

Figure 9-6: 3D Map of '<u>known</u>' DSCT stars in the Milky Way

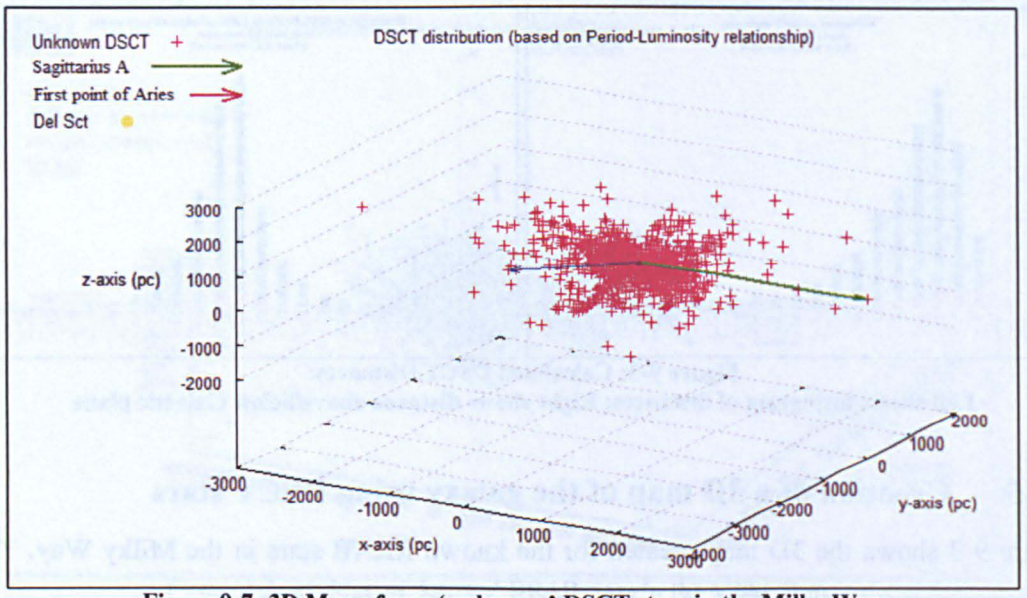

Figure 9-7: 3D Map of new '<u>unknown</u>' DSCT stars in the Milky Way

9.5.6 Investigation of the Blazhko effect using RR Lyrae stars

As the SuperWASP archive only provided observational data in the visible spectrum, it was not possible to further the investigation on the cause of the Blazhko effect, but the data was examined to look for further examples that could be studied in the future. Figure 9-8 confirmed six of the known objects to exhibit the Blazhko effect. A further 86 examples of the Blazhko effect were identified by this research, 20 of these were known in both SIMBAD and the GCVS and 38 were only known in SIMBAD. It was noted however, that neither SIMBAD nor the GCVS clearly identified these as Blazhko stars. There were 28 RRAB Blazhko stars identified which were not known in either SIMBAD or the GCVS.

From a total of 134 Blazhko stars analysed, the range obtained between peaks in the Blazhko stars was found to be 0.06Vmag to 1.51Vmag with a Mean, Median and Mode of 0.49, 0.51 and 0.47Vmag respectively

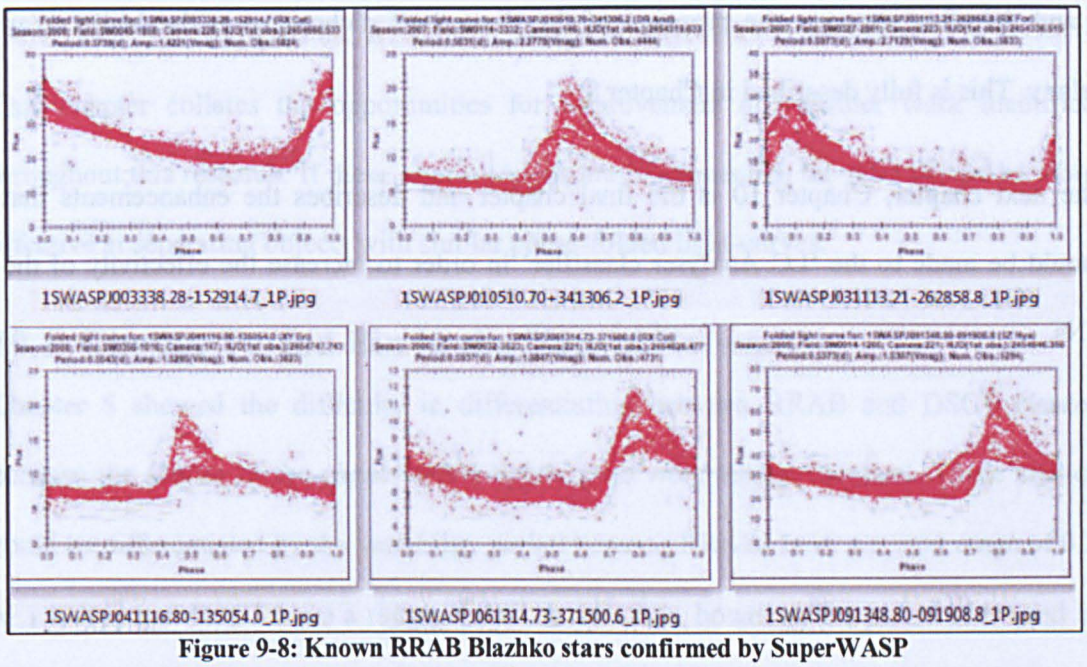

Figure 9-8: Known RRAB Blazhko stars confirmed by SuperWASP

9.5.7 Investigation of the Oosterhoff Dichotomy using RR Lyrae stars

Figure 9-9 shows the SuperWASP equivalent Bailey diagram to that produced by Szczygiel et al. (2009).

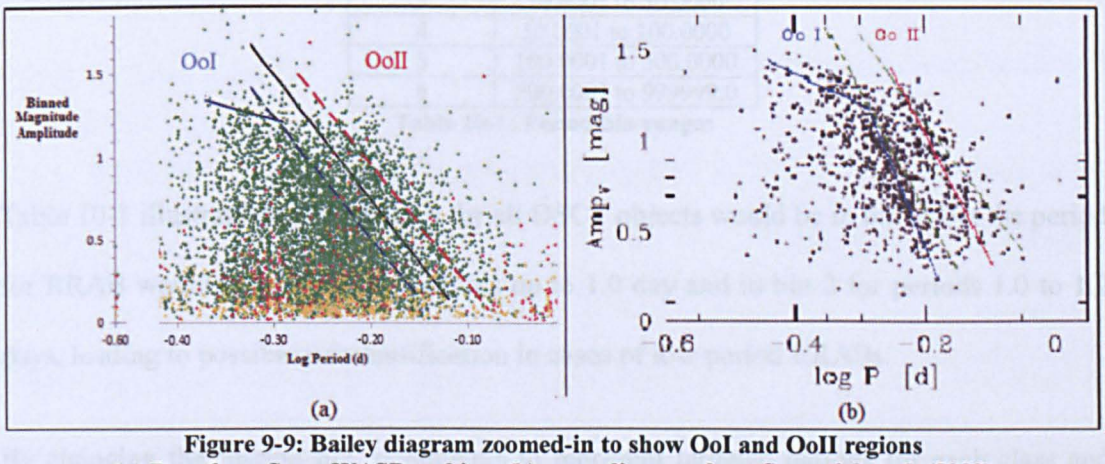

Figure 9-9: Bailey diagram zoomed-in to show OoI and OoII regions
(a) Data from SuperWASP archive; (b) same diagram from Szczygiel et al. (2009)

This confirms the amplitude ranges indicated by Szczygiel…

Oo category	SuperWASP	Szczygiel
I	-7.307 x log(P) - 0.943	−8.844×log(P)−1.343
I 'flat'	-1.700 x log(P) + 0.719	−1.654×log(P)+0.719
II	-7.300 x log(P) - 0.5	−7.007×log(P)−0.343
Separation	-7.500 x log(P) - 0.75	−8.0×log(P)−0.85

…and therefore supports the presence of the Oosterhoff dichotomy in the Milky Way galaxy. This is fully described in Chapter 8.

The next chapter, Chapter 10 is the final chapter and describes the enhancements that should be made to the 'LC Analyser classifier' in order to increase the effectivity of the NNs.

---------- o ----------

Chapter 10 Opportunities for improvement

This chapter collates the opportunities for improvement and further work identified throughout this research. If these improvements are implemented, the NNs should be more effective at separating objects with similar phase-folded light-curves.

10.1. Change Period Bin in the Neural Network

Chapter 5 showed the difficulty in differentiating between RRAB and DSCT classes because the shapes of the phase-folded light-curves were almost identical. These classes could be differentiated by the variability period because RRABs have a period range of 0.3 to 1.2 days and DSCT have a range of 0.01 to 0.2 days, however, the period bins used in the original classification were not specifically targeted for these object classes, they were evenly distributed as shown in Table 10-1 instead.

Period bin	Period range (days)
1	0.0000 to 1.0000
2	1.0001 to 10.0000
3	10.0001 to 50.0000
4	50.0001 to 100.0000
5	100.0001 to 500.0000
6	500.0001 to 999999.0

Table 10-1: Period bin ranges

Table 10-1 illustrates that the period for all DSCT objects would be in bin 1, but the period for RRAB would be in bin 1 for periods up to 1.0 day and in bin 2 for periods 1.0 to 1.2 days, leading to possible misclassification in cases of low period RRABs.

By changing the 'period bin' parameters to represent targeted periods for each class and then re-training the neural networks on the manually confirmed objects and the period ranges obtained in Chapter 7 and Chapter 8, much better results should be obtained from the NNs.

10.2. Use of eclipse-depth ratio

In Chapter 7, the following eclipse-depth ratio range was determined to allow the 'LC Analyser classifier' application to differentiate between EB and EW. The 'LC Analyser classifier' application should be amended to include this check after the classification has been confirmed as EB or EW:

0.75 and below	0.76 to 0.84	0.85 and above
EB class assigned	EB/EW class assigned	EW class assigned

10.3. Use Fourier components of the phase-folded light-curve

In Chapter 2 (section 2.4), a literature review of neural networks used in classification of stellar objects showed that Prŝa et al. (2008) trained a neural network to determine principal parameters and Blomme et al. (2010) identified three independent frequencies for every star. The neural networks they created were very effective at classifying stellar objects in large surveys, so introducing Fourier components into the LC Analyser NNs should improve the effectiveness of the LC Analyser classification. However, it is likely to slow the application considerably.

10.4. Retrain the neural networks using manually confirmed objects

The initial NNs in this research were trained and tested with objects obtained from the GCVS. The objects were processed through the 'LC Analyser classifier' application to obtain the phase-folded light-curve and these were manually confirmed. In Chapter 6, after a run of all the periodic objects in the SuperWASP archive, a similar manual check was performed and the catalogues for DSCT, EA, EB, EW and RRAB created. On completion of the improvements outlined in this chapter, the NNs should be re-trained and re-tested with the objects from the catalogues created in Chapter 6.

10.5. Removal of inappropriate light-curves

In Chapter 6 (section 6.2.3), an attempt was made to remove objects with poor light-curves by looking for a high reduced chi-squared value (χ^2_{red}) in any of the 25 x-axis bins of the binned phase-folded light-curve. The work showed that this method was not suitable, as high values were also observed for good curves. It was noticed at the time, that poor objects could be identified if the $\boldsymbol{\chi^2_{red}}$ test was implemented by comparing the $\boldsymbol{\chi^2_{red}}$ value for each x-axis bin against the largest $\boldsymbol{\chi^2_{red}}$ value from the bins in the 'good' objects. This 'target' value can be identified by calculating the RMS of the full-curve $\boldsymbol{\chi^2_{red}}$ values of a large number of known 'good' objects, and it can be placed into the 'LC Analyser classifier' application to automatically remove poor objects. Note the $\boldsymbol{\chi^2_{red}}$ values are already calculated in the application.

As well as including the $\boldsymbol{\chi^2_{red}}$ test to remove inappropriate light-curves, the Skewness, Kurtosis and Mean-Median tests from chapters 6.2.4, 6.2.5, and 6.2.6 respectively will also be implemented in the LC Analyser application.

10.6. Identify Blazhko effect RRAB stars

In Chapter 8, the spread values were calculated for each RRAB showing the Blazhko effect. The spread was calculated as the difference in magnitude between lowest and highest flux value of the peak of the phase-folded light-curve. This 'spread' value could be used as a detection parameter in the 'LC Analyser classifier' application to attempt to automatically identify the Blazhko effect when stars are classified as RRAB. However, there will be difficulty in using this parameter when the light-curve shows large-scatter or small-amplitude. Rules could be included in the application to only use the spread value when the reduced chi-square and amplitude values gave a suitable indication that there was low scatter and suitable amplitude.

10.7. Calculate the metallicity of RRAB stars

In Chapter 8 (section 8.5.1), the Oosterhoff dichotomy was investigated using SuperWASP-identified RRAB stars. The work was limited because SuperWASP does not contain metallicity values for stars. Further investigation showed that there are three methods available for calculating metallicity from observations in the visible spectrum as described by Sandage (2004).

Sandage (2004) using information from Simon & Lee (1981) and Kovacs & Zsoldos (1995), demonstrated that the combination of the first and third phase terms in a Fourier decomposition of RRAB light curves, called $\emptyset_{31}$varies monotonically across the RR Lyrae instability strip in the same way that amplitude, colour, and rise time vary with period within the strip. The author provides three equations calibrated on their data which can be used to calculate metallicity in RRAB stars. The author does mention two systems that do not follow this trend, but does discuss reasons why this may occur. This method should be used to calculate metallicity in SuperWASP identified RRAB stars to compare with Sandage (2004) results and if suitable, use the results to see if metallicity is the causative factor in the Oosterhoff dichotomy.

$$[Fe/H] = 1.411\phi_{31} - 7.012\ \log(P) - 6.025$$

Equation 10-1: Calculate Metallicity using Period
Limit on each parameter are (+/- 0.014), (+/- 0:071), (+/- 0:018) respectively

$$[Fe/H] = -1.453A_v - 7.990\ \log(P) - 2.145$$

Equation 10-2: Calculate Metallicity using Amplitude
Limit on each parameter are (+/- 0.027), (+/- 0.091), (+/- 0.025) respectively

$$[Fe/H] = 6.33RT - 9.11\ \log(P) - 4.60$$

Equation 10-3: Calculate Metallicity using Rise-time

---------- o ----------

References

Akerlof, C. et al. (2000): The Astronomical Journal, 119, Issue 4, 1901-1013, "ROTSE All-Sky Surveys for Variable Stars. I. Test Fields"

Alonso, R. et al. (2004): The Astrophysical Journal, 613, Number 2, "TrES-1: The Transiting Planet of a Bright K0 V Star"

Arentoft, T. et al. (2008): The Astrophysical Journal, 687, 1180 to 1190, "A Multisite Campaign To Measure Solar-like Oscillations in Procyon. I. Observations, Data Reduction and Slow Variations"

Baglin, A. et al. (2002): Proceedings of the First Eddington Workshop on Stellar Structure and Habitable Planet Finding, ISBN 92-9092-781-X, 2002, p. 17 - 24, "COROT: Asteroseismology and Planet Finding"

Bakos, G. Á. et al. (2002): Publications of the Astronomical Society of the Pacific, 114, 799, pp. 974-987, "System description and First Light Curves of the Hungarian Automated Telescope, an Autonomous Observatory for Variability Search"

Bansal, K. et al. (1998): Data Mining and Knowledge Discovery", Vol. 2, 1998, 97 to 102, "Brief application description: Neural networks based forecasting techniques for inventory control application"

Barnes, T. G. et al. (1986): The Astrophysical Journal, 307, L9-L13, "On the Absolute Magnitudes of RR Lyrae Stars"

Benedict, G. F. et al. (2011): The Astronomical Journal, 142, 187, "Distance Scale Zero-Points from Galactic RR Lyrae Star Parallaxes"

Bernard, E. J. et al. (2008): The Astrophysical Journal, 678: L21 to L24, "The ACS LCID Project: RR Lyrae stars as tracers of old population gradients in the isolated dwarf spheroidal galaxy Tucana"

Berry, M.J.A. & Linoff, G. (1997): Data Mining Techniques, p. 323, NY: John Wiley & Sons

Biazzo, K. et al. (2009a): Mem. S.A.It. Vol. 80, 75, "Magnetic activity in the young star SAO 51891"

Biazzo, K. et al. (2009b): Proceedings of the 15th Cambridge Workshop on Cool Stars, Stellar Systems and the Sun. AIP Conference Proceedings, Volume 1094, pp. 636-639, "Photometric/spectroscopic analyses and magnetic activity in young late-type stars"

Bilir, S. et al. (2008): Astronomische Nachrichten, 329, Issue 8, "New absolute magnitude calibrations for detached binaries"

Bird, J. C. et al. (2009): The Astrophysical Journal, 695, 874 to 882, "Using Ultra Long Period Cepheids to Extend the Cosmic Distance Ladder to 100 Mpc and Beyond"

Blazko, S. (1907): Astronomische Nachrichten, volume 175, p.325, "Mitteilung über veränderliche Sterne" (translated: Communication on variable stars)

Blomme, J. et al. (2010): The Astrophysical Journal Letters 713, L204, "Automated Classification of variable stars in the Asteroseismology Program of the Kepler Space Mission"

Blonda, P. et al. (1993): Proceedings of 1993 International Joint Conference on Neural Networks, Vol. 2, 25-29 Oct 1993, 1231 to 1234, "Comparison of Back Propagation, Cascade-Correlation and Kohonen Algorithms for Cloud Retrieval"

Blum, A. (1992): Neural Networks in C++, "An Object-Oriented Framework for Building Connectionist Systems", p60, NY: Wiley.

Boger, Z. & Guterman, H. (1997): IEEE Systems, Man, and Cybernetics Conference, Orlando, FL., "Knowledge extraction from Artificial Neural Network Models"

Boggess, N. W. et al. (1992): The Astrophysical Journal, 397, 420-429, "The COBE Mission: Its Design and Performance Two Years After Launch"

Bono, G. et al. (2008): The Astrophysical Journal, 686, Issue 2, pp. L87-L90, "On the Relative Distances of ω Centauri and 47 Tucanae"

Bono, G. et al. (2011): Carnegie Observatories Astrophysics Series, Vol. 5: RR Lyrae Stars, Metal-Poor Stars, and the Galaxy, "RR Lyrae the Stellar Beacons of the Galactic Structure"

Borucki, W. J. et al. (1997): Planets Beyond the Solar System and the Next Generation of Space Missions, ASP Conference Series, Vol. 119, 153-174, "The Kepler Mission: A Mission to Determine the Frequency of Inner Planets Near the Habitability Zone for a Wide Range of Stars"

Bowsher, D. (1988): "Introduction to the Anatomy and Physiology of the Nervous System", Chapter 4, Fifth Edition, Blackwell Scientific Publications, London, ISBN: 0-632-01928-X

Buchler, J. R. & Kolláth, Z. (2011): The Astrophysical Journal, 731, Issue 1, article id. 24, "On the Blazhko Effect in RR Lyrae Stars"

Burgess, J. et al. (2006): 25th IEEE International Conference on Computer Communications. Proceedings, Page 1-11, "MaxProp: Routing for Vehicle-Based Disruption-Tolerant Networks"

Butters O. W. et al. (2010): Astronomy and Astrophysics, 520, id.L10, "The first WASP public data release"

Byung-Su, J. et al. (2001): Sensors and Actuators, B77, 2001, 209 to 214, "Pattern recognition of gas sensor array using characteristics of impedance"

Cacciari C. & Clementini G. (2003): Stellar Candles for the Extragalactic Distance Scale, vol. 635 of Lecture Notes in Physics, Berlin Springer Verlag, 105–122, "Globular Cluster Distances from RR Lyrae Stars"

Cáceres, C. & Catelan, M. (2008): The Astrophysical Journal Supplement Series, 179, Issue 1, pp. 242-248, "The Period-Luminosity Relation of RR Lyrae Stars in the SDSS Photometric System"

Catelan, M. & Cortés, C. (2008): The Astrophysical Journal, 676, Issue 2, pp. L135-L138, "Evidence for an Overluminosity of the Variable Star RR Lyrae, and a Revised Distance to the LMC"

Chester, D.L. (1990): IJCNN-90-WASH-DC, Lawrence Erlbaum, 1990, volume 1, 265-268, "Why Two Hidden Layers are better than one"

Christiansen, J. L. et al. (2007): Transiting Extrasolar Planets Workshop, ASP Conference Series, Vol. 366, "Byproducts of the University of New South Wales Extrasolar Planet Search"

Christiansen, J. L. et al. (2008): MNRAS, 385, Issue 4, pp. 1749-1763, "The University of New South Wales Extrasolar Planet Search: a catalogue of variable stars from fields observed between 2004 and 2007"

Cook, K. H. et al. (1995): Astrophysical Applications of Stellar Pulsation, ASP Conference Series, 83, IAU Colloquium 155, Page 221, "Variable Stars in the Macho Collaboration Database"

Cooper, W. A. & Walker, E. N., (1989): "Getting the Measure of the Stars", Page 184, IOP Publishing Ltd., ISBN 0-85274-830-2

Cortés, C.& Catelan, M. (2008): The Astrophysical Journal Supplement Series, 177, 362-372, "The RR Lyrae Period-Luminosity-(Pseudo-) Color and Period-Color-(Pseudo-) Color Relations in the Strömgren Photometric System: Theoretical Calibration"

Craig, N. et al. (1997): The Astrophysical Journal Supplement Series, 113, 131-193, "The Extreme Ultraviolet Explorer Stellar Spectral Atlas"

Cybenko, G. (1989): Math. Control Signals Systems, 2, 303-314, "Approximation by Superpositions of a Sigmoidal Function*"

Da Silva, R. & Silva-Valio, A. (2011): Publications of the Astronomical Society of the Pacific, Volume 123, issue 903, pp.536-546, "A Method to Identify and Characterize Binary Candidates-A Study of CoRoT Data"

Debosscher, J. et al. (2011): Astronomy & Astrophysics, 529, id.A89, "Global stellar variability study in the field-of-view of the Kepler satellite"

Derekas, A. et al. (2007): The Astrophysical Journal, 663:249 to 257, "Eclipsing Binaries in the MACHO Database: New Periods and Classifications for 3031 Systems in the Large Magellanic Cloud"

Devor, J. et al. (2008): The Astronomical Journal, 135, Issue 3, pp. 850-877, "Identification, Classifications, and Absolute Properties of 773 Eclipsing Binaries found in the Trans-Atlantic Exoplanet Survey"

Donati, J. F. et al. (2008): MNRAS, 386, Issue 3, pp. 1234-1251, "Magnetospheric accretion on the T Tauri star BP Tauri"

Dupuy, Trent, J. & Liu, Michael (2009): The Astrophysical Journal, 704, 1519-1537, "Detectability of Transiting Jupiters and Low-Mass Eclipsing Binaries in Sparsely Sampled Pan-Starrs-1 Survey Data"

Dworetsky, M. M. (1983): MNRAS, 203, 917-924, "A period-finding method for sparse randomly spaced observations or 'How long is a piece of string?"

Eker, Z. et al. (2009): Astron. Nachr., 330, Issue 1, p68-76, "New absolute magnitude calibrations for W Ursa Majoris type binaries"

Elizondo, D. (2006): IEEE Transactions on Neural Networks, Vol. 17, No. 2, 330-344, "The Linear Separability Problem: Some Testing Methods"

Faccioli, L. et al. (2007): The Astronomical Journal, 134, 1963-1993, "Eclipsing binary stars in the Large and Small Magellanic Clouds from the MACHO project: The Sample"

Fahlman, S.E. (1988): Technical report CMU-CS-88- 162, Carnegie-Mellon University, Computer Science Dept., Pittsburgh, PA, "An Empirical Study of Learning Speed in Back-Propagation Networks"

Feast, M. (2002): MNRAS, 337, Issue 3, pp. 1035-1037, "Bias in absolute magnitude determination from parallaxes"

Feast, M. W. (2008): arXiv:0806.3019v1 [astro-ph], "Galactic and Extragalactic Distance Scales: The Variable Star Project". Note that the NASA-ADS link is broken, so unable to find published paper.

Feast, M. W. et al. (2008): MNRAS, 386, 2115 to 2134, "The luminosities and distance scales of type II Cepheid and RR Lyrae variables"

Fernley, J. et al. (1998): Astronomy and Astrophysics, 330, p.515-520, "The absolute magnitudes of RR Lyraes from HIPPARCOS parallaxes and proper motions"

Flannery, B. P. (1976): The Astrophysical Journal, 205, pp. 217-225, "A Cyclic Thermal Instability in Contact Binary Stars"

For, B. et al. (2011): The Astrophysical Journal Supplement Series, 197, Issue 2, 29, "The Chemical Compositions of Variable Field Horizontal-Branch Stars: RR Lyrae Stars"

Fukui, A. et al. (2007): The Astrophysical Journal, 670, 423 to 427, Observation of the First Gravitational Microlensing Event in a Sparse Stellar Field: The Tago Event

GAMP® 5 (2008): ISPE Corporate-Author, ISBN-13: 978-1931879613, "A Risk-Based Approach to Compliant GxP Computerized Systems"

Gazeas, K. & Stepien, K. (2008): MNRAS, 390, Issue 4, pp. 1577-1586, "Angular momentum and mass evolution of contact binaries"

GCVS (Samus+ 2004): General Catalogue of Variable Stars, http://cdsarc.u-strasbg.fr/viz-bin/Cat?II/250 (27-Oct-2007). This is still present, but marked as 'obsolete'. For current, refer to 'http://www.sai.msu.su/gcvs/gcvs/'

Gettel, S. J. et al. (2006): The Astronomical Journal, 131, Issue 1, pp. 621-632, "A Catalog of 1022 Bright Contact Binary Stars"

Gilmore, G. et al. (1998): SPIE, 3350, 541, "GAIA: Origin and Evolution of the Milky Way"

Gould, A. & Popowski, P. (1998): The Astrophysical Journal, 508, Number 2, "Systematics of RR Lyrae Statistical Parallax. III. Apparent Magnitudes and Extinctions"

Graczyk, D. et al. (2011): Acta Astronomica, Vol. 61, pp. 103-122, "The Optical Gravitational Lensing Experiment. The OGLE-III Catalog of Variable Stars. XII. Eclipsing Binary Stars in the Large Magellanic Cloud"

Gratton, R. G. (1998): MNRAS, 296, Issue 3, 739 to 745, "The absolute magnitude of field metal-poor horizontal branch stars"

Groenewegen, M.A.T. et al. (2008): Astronomy and Astrophysics, 481, Issue 2, pp.441-448, "The distance to the Galactic centre based on Population II Cepheids and RR Lyrae stars"

Grundahl, F. et al. (2008): Astronomy and Astrophysics, 492, Issue 1, 171-184, "A new standard: age and distance for the open cluster NGC 6791 from the eclipsing binary member V20"

Hebb, D. O. (1949), "The Organisation of Behaviour", Wiley, New York, ISBN: 0-80-584300-0

Hecht-Nielsen, R. (1989): Neural Networks, 1989. International Joint Conference, Vol. I, 593-605, "Theory of the Backpropagation neural network"

Hertz, J. et al. (1991): "Introduction to the theory of neural computation", Addison-Wesley Publishing Company, ISBN: 0-201-50395-6

Hopfield, J. J. (1982): Proceedings of the National Academy of Science, USA, Biophysics, 79, 2554-2558, "Neural networks and physical systems with emergent collective computational abilities"

Hornik, K. et al, (1989): Neural Networks, 2(5), 359-366, "Multilayer Feedforward Networks are Universal Approximators"

Hu, Haili et al. (2007): Astronomy and Astrophysics, 473, Issue 2, pp.569-577, "An evolutionary study of the pulsating subdwarf B eclipsing binary PG 1336-018 (NY Virginis)".

Huang, S. & Brown, D. A. (1976): The Astrophysical Journal, 204:151-159, "An elementary theory of eclipsing depths of the light-curve and its application to Beta Lyrae"

Hurta, Zs. (2008): Astron. Nachr., 328, Issue 8, p.841-844, "The Blazhko behavior of RV UMa"

Jacobs, R.A. (1988): Neural Networks, Vol. 1, 295-307, "Increased Rates of Convergence Through Learning Rate Adaptation"

Janson, M. et al. (2012): The Astrophysical Journal, 745 Number 4, "How do most planets form? - Constraints on Disk Instability from Direct Imaging"

Jardine, M. M. et al. (2008): MNRAS, 386, Issue 2, pp. 688-696, "Coronal structure of the classical T Tauri star V2129 Oph"

Johnson, J. & Picton, P. (1995): "Concepts in Artificial Intelligence", Butterworth-Heinmann Ltd., Great Britain, ISBN: 0-7506-2403-5, 111 to 113

Jurcsik, J. & Kovács, G. (1996): Astronomy and Astrophysics, 312, p.111-120, "Determination of [Fe/H] from the light curves of RR Lyrae stars"

Kaiser, N. et al. (2002): Proc. SPIE 4836, 154, "Pan-STARRS: A Large Synoptic Survey Telescope Array"

Khaw, J. F. C. et al. (1995): Neurocomputing, 7, Issue 3, Apr. 1995, 225 to 245, "Optimal design of neural networks using the Taguchi method"

Kniffen, D. A. et al. (1991): Nuclear Science Symposium and Medical Imaging Conference, 1, 24-31, "The Compton Gamma Ray Observatory"

Kohonen, T. (1990): Proceedings of the IEEE, Vol. 78, Issue 9, 1464 to 1480, "The self-organisation map"

Kolenberg, K. (2002): PhD Thesis, "A Spectroscopy Study of the Blazhko Effect in RR Lyrae"

Kolláth, Z. et al. (2011): MNRAS, Volume 414, Issue 2, pp. 1111-1118, "Period-doubling bifurcation and high-order resonances in RR Lyrae hydrodynamical models"

Kovács, G. (2009): Stellar Pulsation: Challenges for Theory and Observation: Proceedings of the International Conference. AIP Conference Proceedings, Volume 1170, pp. 261-272, "The Blazhko Effect"

Kovacs, G. & Zsoldos, E. (1995): Astronomy and Astrophysics, 293, L57-L60, "A new method for the determination of [Fe/H] in RR Lyrae stars"

Kovárová-Kovar et al. (2000): Journal of Biotechnology, 79, Issue 1, 39 to 52, "Application of model-predictive control based on artificial neural networks to optimise the fed-batch process for riboflavin production"

Kunder, A. & Chaboyer, B. (2008): The Astronomical Journal, 136, Issue 6, pp. 2441-2452, "Metallicity Analysis of MACHO Galactic Bulge RR0 Lyrae stars from their Light-curves"

Kyung-Hoon, K. et al. (1994): Proceedings of the seventh annual conference on Computational learning theory, New Brunswick, New Jersey, United States, 356 to 361, " "Generalization in partially connected layered neural networks"

Laney, C. D. et al. (2002): ASP Conf. Ser. 259, "Radial and Nonradial Pulsations as Probes of Stellar Physics"

Latham, D. W. et al. (2009): Astrophysical Journal, 704, Issue: 2, 1107-1119, "Discovery of a Transiting Planet and Eight Eclipsing Binaries In HATNet Field G205"

Le Borgne, J. F. et al. (2012): The Astronomical Journal, Volume 144, Issue 2, 39, "The all-sky GEOS RR Lyr survey with the TAROT telescopes. Analysis of the Blazhko effect"

Li, L. et al. (2008): MNRAS, 387, 97-104, "The evolutionary status of W Ursae Majoris-type systems"

Li, L. & Zhang. F. (2006): MNRAS, 369, 2001–2004, "The dynamical stability of W Ursae Majoris-type systems"

Lobel, A. (2008): Comm. in Asteroseismology, Contribution to the Proceedings of the 38th Liege International Astrophysical Colloquium: Evolution and Pulsation of Massive Stars on the Main Sequence and close to it, Liege, "3-D Radiative Transfer Modelling of Massive-Star UV Wind Line Variability"

Lucy, L. B. (1976): The Astrophysical Journal, 205, pp. 208-216, "W Ursae Majoris systems with marginal contact"

Luri, X. et al. (1998): Astron. Astrophys., 335, L81-L84, "The LMC distance modulus from Hipparcos RR Lyrae and classical Cepheid data"

Lutz, T. E. & Kelker, D. H. (1973): PASP, 85, 573-578, " On the Use of Trigonometric Parallaxes for the Calibration of Luminosity Systems : Theory"

Maceroni, C. et al. (2010): Astron. Nachr. 789-792, (arXiv:1004.1525 [astro-ph]), "Eclipsing binaries with pulsating components: CoRoT 102918586"

Maciel, S. C. et al. (2011): New Astronomy, 16, Issue 2, 68-71, "Ten CoRoT eclipsing binaries: Photometric solutions"

Maciel, W. J. et al. (2008): Formation and Evolution of Galaxy Bulges, Proceedings IAU Symposium, No. 245, 365-366, "The evolution of the Galactic bulge from planetary nebulae"

Maciel, W. J. & Costa, R. D. D. (2008): The Galaxy Disk in Cosmological Context, Proceedings IAU Symposium, No. 254, "Abundance gradients in the galactic disk: space and time variations"

Mahapatra, S. et al. (1999): Measurement, 26, Issue 4, 221-227, "An intelligent instrument for tracking and adaptive filtering of oscillatory signals using Hebbian learning rules"

Mathieu, R. D. (2007): Star-Disk Interaction in Young Stars, Proceedings IAU Symposium, No. 243, 315-324, "The implications of close binary stars for star-disk interactions"

McCulloch, W. S. & Pitts, W. (1943): Bulletin of Mathematical Biophysics, Vol. 5, 115-133, "A logical calculus of the ideas imminent in nervous activity"

McCullough, P. R. et al. (2005): Publications of the Astronomical Society of the Pacific, 117, 783-795, "The XO Project: Searching for Transiting Extra-solar Planet Candidates"

Mennickent, R. E. et al. (2008): MNRAS, 389, Issue 4, pp. 1605-1618, "The eclipsing LMC star OGLE 05155332–6925581: a clue for Double Periodic Variables"

Minai, A. & Williams, R. D. (1990): Proceedings of the 1990 IEEE/INNS International Joint Conference on Neural Networks, San Diego, CA, Vol. 1, pp 595-600, "Back-propagation Heuristics: A Study of the Extended Delta-Bar-Delta Algorithm"

Minsky, M. & Papert, S. (1989): "Perceptrons", MIT Press, 2nd Edition, ISBN: 0-2626-3111-3

Molnár, L. et al. (2012): MNRAS, 424, Issue 1, pp. 31-37, "Can turbulent convective variations drive the Blazhko cycle? Dynamical investigation of the Stothers idea"

Monet, D. G. et al. (2003): The Astronomical Journal, 125, pp. 984-993, "The USNO-B Catalog"

Morrison, H. L. et al. (2009): The Astrophysical Journal, 694, Issue 1, pp. 130-143, "Fashionably Late? Building up the Milky Way's Inner Halo"

Moskalik, P. & Kolaczkowski, Z. (2008): Comm. in Asteroseismology, Wroclaw HELAS Workshop 2008, Vol.157, p. 343-344, "Nonradial Modes in Classical Cepheids"

Moskalik, P. & Kolaczkowski, Z. (2009): EAS Publications Series, 38, 2009, pp.83-90, "Blazhko Effect in Double Mode Cepheids"

Moskalik, P. & Olech, A. (2008): Comm. in Asteroseismology, Vol.157, p. 345-346, "Multi-periodic RR Lyrae Stars in ω Centauri"

Nef, Pascal D. & Rucinski, S. M. (2008): MNRAS, 385, Issue 4, pp. 2239-2242, "Luminosity function of contact binaries at high galactic latitudes towards the LMC and the SMC"

Nefs, S. V. et al. (2012): MNRAS, 425, 950-968, "Four ultra-short period eclipsing M-dwarf binaries in the WFCAM Transit Survey"

Norton, A. J. et al. (2007): Astronomy and Astrophysics, 467, Issue 2, pp.785-905, "New periodic variable stars coincident with ROSAT sources discovered using SuperWASP"

Norton, A. J. & Payne, S. G. et al. (2011): Astronomy & Astrophysics, 528, id.A90, "Short period eclipsing binary candidates identified using SuperWASP"

O'Connell, D. J. K. (1951): Riverview College Observatory publications, v2, 6, p. 85-100, "The so-called periastron effect in close eclipsing binaries; New variable stars (fifth list)"

O'Donovan, F. T. & Charbonneau, D. (2007): Transiting Extrasolar Planets Workshop, ASP Conference Series, Vol. 366, "TrES Exoplanets and False Positives: Finding the Needle in the Haystack"

Oosterhoff, P. T, (1939): The Observatory, Vol. 62, p. 104-109, "Some Remarks on the Variable Stars in Globular Clusters"

Paczynski, B. (1997): Proceedings of 12th IAP Colloquium, 357, "The Future of Massive Variability Searches"

Paczynski, B. et al. (2006): MNRAS, 368, 1311-1318, "Eclipsing binaries in the All Sky Automated Survey catalogue"

Perlmutter, S. et al. (1997): The Astrophysical Journal, 483, 565-581, "Measurements of the Cosmological Parameters Ω and Λ from the First Seven Supernovae at z >= 0.35"

Picton, P. D. (1994): MacMillan Press, Great Britain, ISBN: 0-333-61832-7, "Introduction to neural networks"

Pietrzynski, G. et al. (2008): The Astronomical Journal, 135, Issue 6, pp. 1993-1997, "The Araucaria Project. The Distance to the Sculptor dwarf spheroidal galaxy from infrared photometry of RR Lyrae stars"

Pietrzynski, G. et al. (2012): Nature 484, 75-77, "RR-Lyrae-type pulsations from a 0.26-solar-mass star in a binary system"

Pietrzynski, G. & Udalski, A. (1999): Acta Astronomica, Vol. 49, pp. 157-164, "The Optical Gravitational Lensing Experiment. Age of Star Clusters from the SMC"

Pojmański, G. (1997): Acta Astronomica, Vol..47, pp.467-481, "The All Sky Automated Survey"

Pojmański, G. et al. (2006): VizieR On-line Data Catalog: II/264. Originally published in: 2002AcA....52..397P, "ASAS Variable Stars in Southern hemisphere (2002-2005)"

Poleski, R. et al. (2010): The Astrophysical Journal Supplement Series, 189, Issue 1, pp. 134-141, "The XO planetary survey project - Astrophysical false positives"

Pollacco, D. L. et al. (2006): Publications of the Astronomical Society of the Pacific, 118, Issue 848, pp. 1407-1418, "The WASP Project and the SuperWASP Cameras"

Pribulla, T. et al. (2008): MNRAS, 390, Issue 2, pp. 798-806, "VW LMi: tightest quadruple system known. Light-time effect and possible secular changes of orbits"

Pribulla, Theodor et al. (2009): The Astronomical Journal, 137, Issue 3, pp. 3646-3654, "Radial Velocity Studies of Close Binary Stars. XIV"

Prior, S. L. et al. (2009): The Astrophysical Journal, 691, Issue 1, pp. 306-319, "Extending the Virgo Stellar Stream with SEKBO Survey RR Lyrae Stars"

Prŝa, A. et al. (2008): The Astrophysical Journal, 687, 542-565, "Artificial Intelligence approach to the determination of physical properties of Eclipsing Binaries. I. The EBAI Project"

Prŝa, A. et al. (2011): The Astronomical Journal, 141, 83 (16pp), "Kepler Eclipsing Binary Stars. I. Catalog and Principal Characterization of 1879 Eclipsing Binaries in the First Data Release"

Ramsay, Gavin et al. (2006): MNRAS, 371, 957-962, "RApid Temporal Survey (RATS) - II. Followup observations of four newly discovered short-period variables"

Ramsay, G. et al. (2012): MNRAS, 425, 1479-1485, "Kepler observations of V447 Lyr: an eclipsing U Gem Cataclysmic Variable"

Ramsay, Gavin & Hakala, Pasi (2005): MNRAS, 360, 314-321, "RApid Temporal Survey (RATS) - I. Overview and first results"

Richmond, M. W. et al. (2000): Publications of the Astronomical Society of the Pacific, 112, 397-408, "TASS Mark III Photometric Survey of the Celestial Equator"

Romaniello, M. et al. (2008): Astronomy and Astrophysics, 488, Issue 2, pp.731-747, "The influence of chemical composition on the properties of Cepheid stars. II – The iron content"

Rosenplatt, F. (1958): Psychological Review, Vol. 65, 386 to 408, "The perceptron: a probabilistic model of information storage and organisation in the brain"

Rucinski, Slavek M. & Pribulla, Theodor (2008): MNRAS, 388, Issue 4, pp. 1831-1835, "The shortest period field contact binary"

Ryan, M. & Silver, D. L. (2003): http://www.wardsystems.com/page15.asp, Sep. 2012, "Web-based User Profiling Using Artificial Neural Networks"

Sanchez, M. S. et al. (1996), Chemometrics and Intelligent Laboratory Systems, 33, 101-119, "Performance of multi-layer feedforward and radial base function neural networks in classification and modelling"

Sandage, A. (2004): The Astronomical Journal, 128, Issue 2, pp. 858-868, "The Metallicity Dependence of the Fourier Components of RR Lyrae Light Curves is the Oosterhoff-Arp-Preston Period Ratio Effect in Disguise"

Silva Aguirre, V. et al. (2008): Astronomy and Astrophysics, 489, Issue 3, pp.1201-1208, "Stellar evolution and variability in the pre-ZAHB Phase"

Silvestri, N. M. et al. (2006): The Astronomical Journal, 131, 1674–1686, "A Catalog of Spectroscopically Selected Close Binary Systems from the Sloan Digital Sky Survey Data Release Four"

SIMBAD web-site: http://simbad.u-strasbg.fr/simbad/

Simon, N. R. & Lee, A. S. (1981): The Astrophysical Journal, 248, 291-297, "The Structural Properties of Cepheid Light Curves"

Skrutskie, M. F. et al. (2006): The Astronomical Journal, 131, 1163-1183, "The Two Micron All Sky Survey (2MASS)"

Stothers, R. B. (2010): Publications of the Astronomical Society of the Pacific 122, pp.536-540, "Observational Evidence of Convective Cycles as the Cause of the Blazhko Effect in RR Lyrae Stars"

Subramanian, S. & Subramanian, A. (2009): Astronomy and Astrophysics, 496, Issue 2, pp.399-412, "Depth Estimation of the Large and Small Magellanic Clouds"

Swingler, K. (1996): Applying Neural Networks: A Practical Guide, p. 53, London: Academic Press.

Szczygiel, D. M. et al. (2009): Acta Astronomica, Vol 59, no 2, pp. 137-167, "Galactic Fundamental Mode RR Lyrae Stars. Period-Amplitude Diagram, Metallicities and Distribution"

Szewczyk, O. et al. (2008): The Astronomical Journal, 136, Issue 1, pp. 272-279, "The Araucaria Project. The Distance of the Large Magellanic Cloud from Near-Infrared Photometry of RR Lyrae Variables"

Tajine, M. & Elizondo, D. (2002): Neurocomputing, 47, 161-188, "New methods for testing linear separability"

Thompson, I.M. (1994): PhD. Thesis, G4, Newcastle upon Tyne, Section 3.5, "Artificial neural networks in medicine: theory and application in biomedical systems (BL)"

Torres, G. et al. (2008): The Astronomical Journal, 136, Issue 5, pp. 2158-2171, "Absolute Properties of the Spotted Eclipsing Binary Star CV BOOTIS"

Turner, P. (1997): "Neural networks & associated technologies for control of chemical processes (BL)", PhD. Thesis, L4b, Newcastle upon Tyne, 47-2543

Udalski, A. (2003): Acta Astronomica, 53, 291-305, "The Optical Gravitational Lensing Experiment. Real Time Data Analysis Systems in the OGLE-III Survey"

Vandenberghe, L. & Vandewalle, J. (1989): International Joint Conference on Neural Networks, Vol. 1, 18-22, 627-630, "Brain-state-in-a-box neural networks with asymmetric coefficients"

Van Leeuwen, F. (2008): ISBN: 978-1-4020-6341-1, "Hipparcos, the New Reduction of the Raw Data"

Van Rensbergen, W. et al. (2008): Astronomy and Astrophysics, 487, Issue 3, pp.1129-1138, "Spin-up and hot spots can drive mass out of a binary"

Vivas, A. K. et al. (2008): The Astronomical Journal, 136, Issue 4, pp. 1645-1657, "Spectroscopy of Bright QUEST RR Lyrae Stars: Velocity Substructures toward Virgo"

Weisskopf, Martin C. et al. (2000): In X-Ray Optics, Instruments, and Missions III, J, "Chandra X-ray Observatory (CXO): overview"

Werbos, P. J. (1990): Proceedings of the IEEE, Vol. 78, Issue 10, 1550 to 1560, "Backpropagtion Through Time: What it Does and How to Do it"

Werner, M. W. et al. (2004): The Astrophysical Journal Supplement Series, 154, 1-9, "The Spitzer Space Telescope Mission"

Widrow, B. & Hoff, M. E. (1960): IRE WESCON Convention Record, New York:IRE, 96 to 104, "Adaptive Switching circuits"

Williamson, J. R. (1996): Neural Networks, Vol. 9, No. 5, pp. 881-897, "Gaussian ARTMAP: A Neural Network for Fast Incremental Learning of Noisy Multidimensional Maps"

Willoughby et al. (1996): Int. J. Radiation Oncology Biol. Phys., Vol. 34, No. 4, 923-930, "Evaluation and scoring of radiotherapy treatment plans using an artificial neural network"

Wils, P. et al. (2008): MNRAS, 387, Issue 2, pp. 783-787, "The unique frequency spectrum of the Blazhko RRc Star LS Her"

Wyrzykowski, L. et al. (2003): Acta Astronomica, Vol. 53, pp. 1-25, "The Optical Gravitational Lensing Experiment. Eclipsing Binary Stars in the Large Magellanic Cloud"

Zacharias N. et al. (2004): The Astronomical Journal, 127, 3043-3059, "The Second US Naval Observatory CCD Astrograph Catalog (UCAC2)"

Zasche, P. (2008): New Astronomy, 13, Issue 7, p. 481-484, "The first light-curve analysis of eclipsing binaries observed by the INTEGRAL/OMC"

Zasche, P. et al. (2008): New Astronomy, Volume 13, Issue 6, p. 405-413, "Period changes in six semi-detached Algol-type binaries"

Zasche, P. et al. (2009): New Astronomy, 14, Issue 2, p. 121-128, "Period changes in six contact binaries: WZ And, V803 Aql, DF Hya, PY Lyr, FZ Ori, AND AH Tau"

Zhao, W. et al. (2000): Signal Processing: Image Communication, 16, 123-136, "A reliable descriptor for face objects in visual content"

Zirilli, J. S. (1996): First edition, International Thompson Computer Press, Boston, MA, USA. ISBN: 1-85032-234-1, "Financial Prediction using Neural Networks"

---------- o ----------

Appendix 1 – Known Variability Class Objects for NN Analysis

CEP

Reason	Class	WASP Object Id	X-pattern	Y-pattern	P-bin	Mode-mean	BMA
Train	CEP	1SWASPJ001509.81+582527.4	0,4,11,16,21,24,20,17,18,15,11,11,9,7,6,3.5,3,3,0,0,0,1,0,1	5,2,0,3,1,1,1,1,0,1,0,3,0,0,0,0,1,1,1,1,0,1,1,0,0,1	2	-0.336	0.620
Train	CEP	1SWASPJ013714.02+574533.2	0,3,3,8,8,7,15,23,24,20,18,17,13,18,14,11,12,9,8,7,5,3,3,1,0	2,1,0,4,0,1,0,2,3,1,0,1,1,1,1,1,0,1,2,0,1,0,0,1,1	3	-0.854	0.958
Train	CEP	1SWASPJ014702.67+593623.0	0,2,6,-1,-1,23,21,19,24,15,14,13,12,13,15,7,10,4,6,7,-1,0,1,2,1	2,2,2,0,1,0,2,2,0,0,1,0,1,2,1,2,0,0,0,1,0,1,0,1,1	2	-0.828	0.430
Train	CEP	1SWASPJ021307.50+580447.7	0,1,3,7,14,21,24,22,22,18,16,15,10,11,8,9,8,6,5,6,4,5,5,1,3	1,2,0,2,1,3,2,1,2,1,1,1,0,0,1,1,1,0,1,0,0,1,2,0,1	2	-0.647	0.226
Train	CEP	1SWASPJ022735.43+585501.9	0,1,4,9,12,20,24,24,21,17,16,16,12,12,11,9,8,7,-1,5,3,1,1,0,0	3,3,0,1,1,1,0,1,1,2,0,1,3,0,0,0,2,1,0,0,1,1,0,0,2	2	-1.277	0.740
Train	CEP	1SWASPJ023352.56+570139.1	0,1,1,4,8,15,21,24,24,23,21,16,15,13,9,10,10,4,4,4,3,2,2,0,0	3,2,2,1,4,0,0,0,1,1,2,0,0,1,0,2,1,0,0,0,0,2,0,1,2	2	-0.995	0.198
Train	CEP	1SWASPJ023431.28+584954.0	0,2,7,11,18,23,24,22,20,19,16,15,12,12,10,8,7,6,5,4,3,1,0,0,0	4,1,1,1,1,1,1,2,1,0,1,1,2,0,0,1,1,0,1,1,1,0,1,1,1	2	-1.435	0.750
Train	CEP	1SWASPJ032347.84+592120.7	0,8,12,20,23,20,22,24,24,20,19,12,12,13,11,10,8,4,4,7,5,3,2,1,1	1,2,1,1,2,1,0,1,2,0,1,1,3,1,0,0,0,0,0,1,3,0,1,1,2	2	-0.057	0.476
Train	CEP	1SWASPJ034523.35+480500.5	0,3,4,11,14,20,23,24,18,15,15,12,12,10,9,9,7,5,5,2,3,3,2,1,0	2,1,2,3,1,2,0,1,0,2,1,1,2,0,1,2,0,0,1,0,1,0,0,1,1	2	-1.080	0.656
Train	CEP	1SWASPJ041706.06+414354.6	0,3,2,4,10,19,24,24,23,21,19,16,14,12,11,11,11,7,6,4,4,4,3,2,1	1,1,2,2,4,0,1,1,0,0,1,3,1,0,1,0,1,0,0,2,0,1,0,1,2	2	-1.070	0.680
Train	CEP	1SWASPJ051521.97+400440.9	0,3,5,5,5,7,17,22,24,23,20,18,16,15,15,-1,10,8,8,5,5,3,1,1,0	2,2,0,2,0,5,0,1,2,0,1,0,0,0,0,2,1,1,1,0,1,0,1,1,1	3	-0.529	0.802
Train	CEP	1SWASPJ051527.17+372221.0	0,6,12,20,24,24,21,20,16,17,19,15,13,11,10,10,8,7,6,6,4,5,3,1,1	1,2,0,1,1,1,3,1,1,0,2,1,1,1,0,1,1,1,0,1,2,1,0,0,2	2	-0.099	0.308
Train	CEP	1SWASPJ053436.59+261208.4	0,3,8,15,21,24,22,20,17,16,15,12,11,9,9,6,5,4,2,1,2,1,0,0,0	4,2,2,1,1,1,1,0,1,2,0,1,1,0,0,2,1,1,0,0,1,1,1,0,1	2	-0.974	0.532
Train	CEP	1SWASPJ053626.75+443527.9	0,2,2,12,18,24,24,22,20,15,12,13,10,8,10,-1,-1,5,3,2,2,1,1,0,0	3,2,4,1,0,1,0,0,1,0,2,0,2,1,0,1,0,0,1,0,1,0,1,0,2	2	-0.766	0.852
Train	CEP	1SWASPJ054414.00+373512.9	0,1,1,1,3,8,13,20,24,24,20,19,16,15,15,13,10,9,8,8,7,5,4,4,3	1,3,0,2,2,1,0,1,3,1,1,0,0,2,0,2,1,0,0,1,2,0,0,0,2	2	-0.683	0.782
Train	CEP	1SWASPJ054650.79+313552.5	0,2,6,12,19,24,24,23,20,17,14,13,11,8,7,6,5,4,3,2,1,-1,0,0,0	4,1,2,1,1,2,1,1,0,0,1,1,1,1,0,0,1,0,1,1,0,0,1,2	2	-1.227	0.328
Train	CEP	1SWASPJ054745.05+320052.7	0,1,5,12,19,24,24,23,20,18,20,14,12,-1,10,9,9,7,4,3,3,2,1,0,0	3,2,1,2,1,1,0,1,0,2,1,0,2,0,1,0,0,0,1,1,2,0,0,1,2	2	0.013	0.810
Train	CEP	1SWASPJ055734.38+194911.7	0,1,9,17,23,24,21,18,15,14,12,16,9,7,6,5,2,4,4,3,1,0,2,0,0	4,2,2,1,2,1,1,1,0,2,0,0,1,0,1,1,1,1,1,0,0,1,0,1,1	2	-0.760	0.460
Train	CEP	1SWASPJ060236.58+221402.9	0,5,8,24,21,23,22,19,14,13,10,10,9,10,9,6,5,4,4,3,1,0,1,1,0	3,3,0,1,2,2,1,0,1,2,3,0,0,1,1,0,0,0,0,1,0,1,1,1,1	2	-0.614	0.840
Train	CEP	1SWASPJ064307.51+205620.7	0,1,1,1,1,2,2,7,13,19,24,23,21,19,16,16,11,11,9,6,5,6,6,4,2	1,4,3,0,1,1,3,1,0,1,0,2,0,1,0,0,2,0,0,2,0,1,0,1,1	2	1.349	0.574
Train	CEP	1SWASPJ201043.82+045449.2	0,2,6,9,13,17,22,24,24,24,22,20,18,16,14,13,12,11,10,9,7,5,2,0,0	3,0,2,0,0,1,1,1,0,2,1,1,2,1,0,1,1,1,0,1,0,2,0,3	3	-0.403	0.476
Train	CEP	1SWASPJ202419.35+403339.9	0,1,2,2,2,7,21,24,22,19,17,15,15,12,12,11,8,7,5,4,2,2,0,0,0	4,1,5,0,1,1,0,2,1,0,0,1,2,0,0,2,0,1,0,1,0,1,1,0,1	3	-0.881	0.960
Train	CEP	1SWASPJ203254.29+463604.5	0,1,1,5,-1,4,10,9,24,22,23,18,18,15,12,11,11,10,9,7,3,3,3,0,-1	2,2,0,3,1,1,0,1,0,2,2,2,1,0,0,1,0,0,2,0,0,0,1,1,1	3	-0.725	0.756
Train	CEP	1SWASPJ204237.19+382725.5	0,9,8,9,8,13,18,24,24,24,20,18,16,14,12,10,10,7,5,5,3,1,1,0,1	2,3,0,1,0,2,0,1,2,2,2,0,1,1,1,0,1,0,2,0,1,0,0,0,3	3	-0.178	0.468
Train	CEP	1SWASPJ205720.82+401038.9	0,1,3,3,4,11,22,24,22,23,22,18,16,16,14,12,10,8,6,4,4,2,0,0,0	4,1,1,2,3,0,1,0,1,0,1,1,1,0,1,0,2,0,1,0,0,0,3,1,1	3	-1.202	0.840
Train	CEP	1SWASPJ211054.37+490831.4	0,2,7,12,15,21,24,24,23,21,17,15,16,17,16,14,11,8,7,6,4,3,2,0,0	3,0,2,1,1,0,1,2,1,0,0,1,1,0,1,2,2,2,0,0,0,2,0,1,2	2	0.662	0.584
Train	CEP	1SWASPJ212328.80+095554.9	0,2,4,8,11,13,16,19,21,23,24,24,24,22,21,19,18,15,12,8,6,3,0,0,0	4,0,1,1,1,0,1,0,2,0,0,1,1,1,0,1,1,0,1,2,0,2,1,1,3	1	-0.977	0.064
Train	CEP	1SWASPJ212938.93+485808.6	0,2,4,7,9,14,14,19,22,24,24,21,21,22,19,15,12,8,6,6,3,1,0,0,0	4,1,1,1,1,0,2,1,1,1,0,0,1,0,2,1,0,0,0,2,0,2,2,0,2	2	-0.931	0.162
Train	CEP	1SWASPJ215141.44+430802.5	0,3,9,13,18,22,24,24,20,18,17,15,14,10,9,9,7,7,5,3,4,2,2,0,0	3,0,2,2,1,1,0,2,0,3,1,0,0,1,1,1,0,1,2,0,1,0,1,0,2	2	-0.774	0.670
Train	CEP	1SWASPJ233459.62+592129.6	0,1,2,7,12,18,22,24,22,20,20,16,15,11,14,9,6,5,4,4,3,2,0,0,0	4,1,2,1,2,1,1,1,0,1,0,1,1,0,1,1,1,0,1,0,2,0,2,0,1	2	-0.850	0.752
Test	CEP	1SWASPJ001428.24+561510.5	0,4,2,3,6,16,14,-1,24,-1,24,22,17,18,14,16,14,13,10,7,8,6,4,3,2	1,0,2,2,2,0,2,1,1,0,1,0,0,1,3,0,2,1,1,0,0,0,1,0,2	2	-0.186	0.478
Test	CEP	1SWASPJ004023.21+583706.6	0,2,4,3,4,8,6,10,14,16,18,22,21,24,23,21,17,14,13,10,7,7,5,4,2	1,0,2,1,3,1,1,2,1,0,2,0,0,1,2,0,1,1,1,0,0,2,1,1,1	2	0.272	0.200
Test	CEP	1SWASPJ013026.95+084134.2	0,2,4,7,15,19,24,23,20,17,14,12,8,6,5,3,2,2,2,1,1,1,1,0,1	2,5,4,1,1,1,1,1,1,0,0,0,1,0,1,1,0,1,0,1,1,0,0,1,1	1	-0.836	0.632
Test	CEP	1SWASPJ021307.32+580421.0	0,3,2,9,21,19,24,24,24,20,18,14,13,9,7,7,5,4,3,2,1,0,0,0,0	5,1,2,2,1,1,0,2,0,2,0,0,0,1,1,0,0,0,1,1,1,1,0,0,3	1	-0.335	0.162
Test	CEP	1SWASPJ025530.76+423448.4	0,2,8,17,24,24,19,16,11,9,7,6,5,4,6,5,5,4,4,3,2,3,1,0,0	3,1,2,2,3,3,2,1,1,1,0,1,0,0,0,0,1,1,0,1,0,0,0,0,2	2	-0.546	0.576
Test	CEP	1SWASPJ031107.33+553029.7	0,5,11,17,22,24,22,20,18,16,15,12,11,9,7,6,6,5,3,3,1,1,0,0,0	4,2,0,2,0,2,2,1,0,1,0,2,1,0,0,1,1,1,1,0,1,0,2,0,1	2	-1.214	0.652
Test	CEP	1SWASPJ034608.20+584703.2	0,2,6,11,19,24,21,19,17,17,13,12,11,10,9,8,6,7,4,3,1,2,1,0,0	3,2,2,1,1,0,2,1,1,1,1,2,1,1,0,0,0,2,0,2,0,1,0,0,1	2	-1.303	0.966
Test	CEP	1SWASPJ035421.77+583912.0	0,1,3,7,6,7,13,21,24,21,24,20,15,16,15,14,13,7,-1,5,6,3,3,0,2	2,1,1,3,0,1,2,3,0,0,0,0,0,2,1,2,1,0,0,0,1,2,0,0,2	3	-1.112	0.728
Test	CEP	1SWASPJ040131.01+550243.5	0,1,3,5,5,8,15,24,23,24,24,21,20,16,15,12,11,10,6,5,5,3,3,0,0	3,1,0,3,0,4,1,0,1,0,1,1,1,0,0,2,1,0,0,0,1,1,0,1,3	1	-1.124	0.408
Test	CEP	1SWASPJ040134.22+550253.4	0,2,3,4,5,5,14,21,24,24,24,24,21,19,17,15,13,11,11,8,6,5,5,3,1,0	2,1,1,2,1,4,1,0,1,0,0,2,0,1,1,1,0,1,0,1,0,2,0,0,3	1	-0.978	0.314
Test	CEP	1SWASPJ041946.86+485711.7	0,-1,-1,14,17,24,-1,-1,21,18,16,-1,-1,14,10,6,-1,-1,6,4,2,-1,-1,1,0	2,1,1,0,1,0,2,0,0,0,1,0,0,0,2,0,1,1,1,0,0,1,0,0,1	2	-1.166	0.762
Test	CEP	1SWASPJ042319.15+441412.9	0,1,2,8,14,22,24,22,18,14,10,8,7,6,6,5,4,4,3,2,2,1,0,0,0	4,2,3,1,2,1,2,1,2,0,1,0,0,0,2,0,0,0,1,0,0,0,2,0,1	1	-0.580	0.796
Test	CEP	1SWASPJ042537.26+453713.4	0,1,4,6,7,7,7,9,19,22,24,22,-1,18,17,-1,-1,13,14,8,6,5,5,2,1	1,2,1,0,1,2,2,3,1,1,0,0,0,1,1,0,0,1,1,1,0,0,2,0,1	3	-1.000	0.714
Test	CEP	1SWASPJ042939.38+482519.0	0,8,24,-1,-1,24,23,20,18,16,15,13,11,9,8,6,5,4,3,1,1,0,0,0,1	4,3,0,1,1,1,1,0,2,1,0,1,0,1,0,1,1,0,1,0,1,0,1,0,1,2	3	-0.928	0.914
Test	CEP	1SWASPJ045941.53+405009.6	0,3,6,10,14,14,18,18,17,19,23,24,20,17,16,7,12,10,9,6,4,2,1,0,0	3,1,1,1,1,0,2,1,0,1,2,0,1,0,2,0,1,2,2,1,1,0,0,1,1	3	-1.220	0.634
Test	CEP	1SWASPJ051847.96+135911.9	0,-1,2,6,12,17,21,24,24,20,18,17,13,13,12,11,8,6,6,5,5,2,1,2,0	2,1,3,0,0,2,3,0,1,0,0,1,2,2,0,0,0,2,1,0,1,1,0,0,2	2	-1.088	0.650
Test	CEP	1SWASPJ052839.23+422615.8	0,1,3,7,11,18,24,24,23,23,22,18,13,14,11,8,9,7,6,3,1,3,2,3,1	1,3,1,4,0,0,1,2,1,1,0,2,0,1,1,0,0,0,2,0,0,0,1,2,2	2	-0.835	0.684
Test	CEP	1SWASPJ054410.16+373509.1	0,1,2,4,6,11,21,24,24,24,22,18,17,16,13,12,10,10,7,7,8,5,4,2,0	2,1,2,0,2,1,1,2,1,0,2,1,1,1,0,0,1,1,1,0,0,1,1,0,3	1	-1.028	0.526
Test	CEP	1SWASPJ054544.90+270404.7	0,1,4,11,21,24,24,21,18,15,13,11,10,9,9,6,5,11,2,1,4,2,0,2,2	2,2,4,0,2,1,1,0,0,2,1,3,0,1,0,1,0,0,1,0,0,2,0,0,2	2	-1.111	0.668
Test	CEP	1SWASPJ060524.41+284722.8	0,3,7,16,23,24,23,21,16,11,12,11,10,7,6,6,4,3,3,1,1,1,0,0,0	4,3,0,3,1,0,2,2,0,0,1,2,1,0,0,0,2,0,0,0,0,1,0,2,1	2	-1.002	0.600
Test	CEP	1SWASPJ060634.93+261945.2	0,6,5,9,5,7,11,12,19,24,22,23,23,21,19,17,13,9,8,5,5,1,2,-1,1	1,2,1,0,0,4,1,1,1,2,0,1,1,1,0,0,0,1,0,2,0,1,1,2,1	3	-0.371	0.518
Test	CEP	1SWASPJ061558.62+234511.4	0,3,8,12,13,17,21,24,24,22,18,16,13,10,11,9,6,4,3,3,2,2,1,0,0	3,1,2,3,1,0,1,0,1,1,1,1,1,2,0,0,1,1,1,0,0,1,1,0,2	1	-0.673	0.376
Test	CEP	1SWASPJ061559.88+234451.0	0,3,8,18,24,22,20,18,14,13,10,9,7,6,9,7,3,2,2,1,1,2,0,0,0	4,2,3,2,0,0,1,2,1,2,1,0,0,1,1,0,0,0,2,0,1,0,1,0,1	2	-0.928	0.602
Test	CEP	1SWASPJ105054.07-252114.7	0,1,2,6,16,24,24,21,17,13,10,7,6,4,3,2,1,0,0,0,0,0,0,0,0	9,2,2,1,1,0,2,1,0,0,1,0,0,1,0,0,1,1,0,0,0,1,0,0,2	1	-0.862	0.808
Test	CEP	1SWASPJ130245.47-235813.2	0,2,5,10,18,24,24,23,19,17,15,13,11,9,8,6,5,3,3,2,2,1,0,0,0	4,1,3,2,0,2,1,0,1,1,1,1,0,1,0,1,0,1,1,1,0,0,0,1,2	1	-1.073	0.616
Test	CEP	1SWASPJ143018.40+290429.4	0,1,3,4,6,10,15,17,20,22,24,24,22,19,18,16,15,12,10,6,7,5,3,1,1	1,3,0,2,1,1,2,1,0,0,2,0,1,0,0,2,1,1,1,1,0,2,0,0,2	1	0.246	0.108
Test	CEP	1SWASPJ144600.84-101315.9	0,1,3,7,15,21,24,24,22,19,16,14,11,9,6,5,3,3,2,1,1,0,0,0,0	5,3,1,3,0,1,1,1,0,1,0,1,0,0,1,1,1,0,0,1,0,1,1,0,2	1	-0.602	0.508
Test	CEP	1SWASPJ200315.62+585716.6	0,2,6,16,24,24,21,18,15,12,10,8,7,6,5,4,3,2,1,1,0,0,0,0,0	6,2,2,1,1,1,2,1,1,0,1,0,1,0,0,1,1,0,1,0,0,1,0,0,2	1	-0.938	0.658
Test	CEP	1SWASPJ205533.66-564431.1	0,1,3,5,9,12,16,20,23,24,24,23,21,18,15,13,10,8,6,4,3,1,0,0,0	4,2,0,2,1,1,1,0,1,1,1,0,1,1,0,1,0,1,1,0,2,2	1	-0.762	0.240
Test	CEP	1SWASPJ211055.23+490802.4	0,2,4,9,12,16,20,22,24,23,23,22,19,19,17,16,14,12,10,7,5,3,2,0,0	3,0,2,1,1,1,0,1,0,1,1,0,2,0,1,0,2,1,0,2,1,0,2,2,1	1	0.491	0.478

Appendix 1 continued...

DSCT

Reason	Class	WASP Object Id	X-pattern	Y-pattern	P-bin	Mode-mean	BMA
Train	DSCT	1SWASPJ021507.43+180348.3	0,1,2,3,5,10,16,20,24,24,23,20,18,16,13,11,9,6,5,4,3,1,1,0,0	3,3,1,2,1,2,1,0,0,1,1,1,0,1,0,0,2,0,1,0,2,0,0,1,2	1	-0.528	0.362
Train	DSCT	1SWASPJ021507.49+180428.0	0,1,2,3,5,9,15,20,24,24,23,21,18,15,13,10,9,6,5,4,3,1,1,0,0	3,3,1,2,1,2,1,0,0,2,1,0,0,1,0,2,0,0,1,0,1,1,0,1,2	1	-0.731	0.390
Train	DSCT	1SWASPJ042605.89+012626.2	0,1,3,5,8,14,19,22,24,24,23,22,19,17,14,11,9,6,4,3,1,1,0,0,0	4,3,0,2,1,1,1,0,1,1,0,1,0,0,2,0,0,1,0,2,0,0,2,1,2	1	-0.873	0.254
Train	DSCT	1SWASPJ044055.03+533753.4	0,1,2,4,6,10,14,18,22,24,24,23,21,18,14,10,7,5,3,1,0,0,0,0,0	6,2,1,1,1,1,1,1,0,0,2,0,0,0,2,0,0,0,2,0,0,1,1,1,2	1	-1.100	0.220
Train	DSCT	1SWASPJ044055.18+533806.5	0,1,2,4,6,10,14,18,22,24,24,23,21,18,14,10,7,5,3,1,0,0,0,0,0	6,2,1,1,1,1,1,1,0,0,2,0,0,0,2,0,0,0,2,0,0,1,1,1,2	1	-1.029	0.220
Train	DSCT	1SWASPJ055918.36+200117.9	0,1,3,6,12,18,24,24,24,22,19,17,14,13,10,9,6,6,3,4,3,2,1,1,0	2,3,1,3,1,0,3,0,0,1,1,0,1,1,1,0,0,1,1,1,0,0,1,0,3	1	-0.620	0.282
Train	DSCT	1SWASPJ055920.57+200207.5	0,1,3,6,11,18,23,24,24,21,19,17,14,12,10,8,6,5,4,3,3,2,0,0,0	4,1,1,3,1,1,2,0,1,0,1,1,1,0,1,0,0,1,1,1,0,1,0,1,2	1	-1.105	0.428
Train	DSCT	1SWASPJ055921.47+200235.2	0,1,3,6,11,17,22,24,24,21,19,17,14,12,10,8,7,5,5,4,3,2,1,0,0	3,2,1,2,1,2,1,1,1,0,1,1,1,0,1,0,0,2,0,1,0,1,1,0,2	1	-0.899	0.430
Train	DSCT	1SWASPJ055939.06-304018.6	0,1,2,5,9,12,17,21,23,24,24,24,22,19,17,14,12,9,6,5,3,2,1,0,0	3,2,2,1,0,2,1,0,0,2,0,0,2,0,1,0,0,2,0,1,0,1,1,1,3	1	-0.368	0.142
Train	DSCT	1SWASPJ055941.40-303953.6	0,2,6,9,13,17,21,23,24,24,23,20,18,15,13,11,9,7,4,3,1,1,0,0,0	4,2,1,1,1,0,1,1,0,2,0,1,0,2,0,1,0,1,1,0,1,1,0,2,2	1	-1.096	0.154
Train	DSCT	1SWASPJ055942.79-303950.0	0,2,4,8,12,17,20,23,24,24,23,20,18,15,14,11,10,8,5,4,1,1,0,0,0	4,2,1,0,2,1,0,0,2,0,1,1,1,0,1,1,0,1,1,0,2,0,0,2,2	1	-0.891	0.152
Train	DSCT	1SWASPJ080935.74+442817.6	0,1,3,6,12,19,24,24,23,20,18,15,13,11,9,7,6,5,4,3,2,1,0,0,0	4,2,1,2,1,1,2,1,0,1,0,1,1,1,0,1,0,0,1,1,1,0,0,1,2	1	-0.995	0.496
Train	DSCT	1SWASPJ084305.73+405941.3	0,1,2,4,7,10,14,19,20,21,24,21,21,19,15,14,11,9,7,6,4,3,1,0,0	3,2,1,1,2,0,1,2,0,1,1,1,0,0,2,1,0,0,0,2,1,3,0,0,1	1	-0.562	0.164
Train	DSCT	1SWASPJ091817.18+460911.2	0,1,3,5,10,15,22,24,24,22,20,17,15,13,11,9,8,6,5,4,3,2,1,1,0	2,3,1,2,1,2,1,0,1,1,1,1,0,1,0,2,0,1,0,0,1,0,2,0,2	1	-0.986	0.388
Train	DSCT	1SWASPJ115151.80-411709.3	0,1,5,9,15,22,24,24,21,19,17,14,12,9,7,6,4,4,3,2,1,0,0,0,0	5,2,1,1,2,1,1,1,0,2,0,0,1,0,1,1,0,1,0,1,0,1,1,0,2	1	-0.820	0.462
Train	DSCT	1SWASPJ144006.99+000145.0	0,5,6,7,12,14,16,19,22,24,23,24,20,19,16,14,11,8,7,4,4,2,3,2,2	1,0,3,1,2,1,1,2,1,0,0,1,1,0,2,0,2,0,0,2,1,0,1,1,2	1	-0.399	0.096
Train	DSCT	1SWASPJ145855.92-005653.0	0,1,3,7,14,21,24,23,21,18,15,13,11,9,7,6,5,4,3,2,1,0,0,0,0	5,2,1,2,1,1,1,2,0,1,0,1,0,1,1,1,0,0,1,0,0,2,0,1,1	1	-1.015	0.538
Train	DSCT	1SWASPJ145856.45-005737.5	0,1,3,7,13,22,24,23,20,18,15,13,11,9,7,6,5,4,3,2,1,1,0,0,0	4,3,1,2,1,1,1,2,0,1,0,2,0,1,0,0,1,0,1,0,1,1,1,1,1	1	-0.831	0.500
Train	DSCT	1SWASPJ152221.52+325845.2	0,2,4,9,17,24,24,22,19,16,13,12,9,8,6,6,4,3,3,1,1,0,0,0,0	5,2,1,2,2,0,2,0,1,2,0,0,1,1,0,0,1,1,0,1,0,0,1,0,2	1	-0.916	0.424
Train	DSCT	1SWASPJ152407.00+365200.5	0,1,3,7,12,18,23,24,23,21,18,16,14,11,9,8,6,5,3,2,1,0,0,0,0	5,2,1,2,0,1,1,1,1,1,0,1,1,0,1,0,1,0,2,0,0,1,0,2,1	1	-1.073	0.406
Train	DSCT	1SWASPJ155309.78+060525.8	0,1,3,7,12,18,23,24,23,21,19,16,14,12,10,8,7,6,5,4,3,2,1,0,0	3,2,1,2,1,1,1,2,1,0,1,0,2,0,1,0,1,0,1,1,0,1,0,2,1	1	-1.125	0.402
Train	DSCT	1SWASPJ161315.68-095323.4	0,1,2,5,8,14,19,23,24,24,21,18,15,14,11,10,7,6,5,3,3,3,1,0,0,0	4,2,1,2,0,2,1,1,1,0,1,1,0,0,2,1,0,0,1,1,0,1,0,1,2	1	-0.601	0.472
Train	DSCT	1SWASPJ161331.70+323442.6	0,1,4,7,9,14,18,21,24,24,22,21,19,16,13,10,8,6,4,3,1,0,0,0,0	5,2,0,1,2,0,1,1,1,1,1,0,0,1,1,0,1,0,1,1,0,2,1,0,2	1	-0.815	0.160
Train	DSCT	1SWASPJ162815.38+330107.7	0,4,5,8,10,12,17,19,22,23,24,24,23,23,21,19,15,12,9,6,4,1,0,0,0	4,1,0,0,2,1,1,0,1,1,1,0,2,0,0,1,0,1,0,2,0,1,1,3,2	1	0.227	0.134
Train	DSCT	1SWASPJ163016.39+165506.0	0,1,3,6,9,12,16,20,23,24,24,23,21,19,16,14,11,9,7,5,3,2,0,0,0	4,1,1,2,0,1,1,1,0,2,0,1,1,0,1,0,2,0,0,1,1,1,0,2,2	1	-1.153	0.246
Train	DSCT	1SWASPJ163117.95+115952.4	0,1,4,8,15,21,24,23,20,17,14,12,11,9,8,7,6,4,3,3,2,1,1,0,0	3,3,1,2,2,0,1,1,2,1,0,1,1,0,1,1,0,1,0,0,1,1,0,1,1	1	-1.003	0.470
Train	DSCT	1SWASPJ164839.26+302745.6	0,1,2,4,8,13,19,23,24,24,23,20,18,15,13,10,9,6,5,3,2,1,0,0,0	4,2,2,1,1,1,1,0,1,1,1,0,0,2,0,1,0,0,1,1,1,0,0,2,2	1	-0.903	0.384
Train	DSCT	1SWASPJ165617.99+500735.8	0,1,2,4,7,10,13,18,20,20,24,24,24,22,20,17,14,12,9,6,4,3,1,0,0	3,2,1,1,2,0,1,1,0,1,1,0,1,1,1,0,0,1,1,0,3,0,1,0,3	1	-0.860	0.100
Train	DSCT	1SWASPJ182945.62+281043.6	0,1,2,5,6,12,16,20,23,24,23,24,20,19,16,14,10,11,8,6,5,2,2,0,0	3,1,3,0,0,2,2,0,1,0,1,1,1,0,1,0,2,0,0,1,2,0,0,2,2	1	-0.005	0.152
Train	DSCT	1SWASPJ183206.43+403556.6	0,1,3,7,14,21,24,24,22,18,16,13,11,9,7,6,4,3,2,2,1,0,0,0,0	5,2,2,2,1,0,1,2,0,1,0,1,0,1,1,0,1,0,1,0,0,1,1,0,2	1	-0.941	0.590
Test	DSCT	1SWASPJ000012.42+242608.8	0,1,7,8,13,21,20,24,24,19,18,17,13,9,12,8,6,4,2,3,1,2,3,3,2	1,2,3,3,1,0,1,1,2,1,0,0,1,2,0,0,0,1,1,1,1,1,0,0,2	1	-0.084	0.286
Test	DSCT	1SWASPJ001346.45+200312.6	0,3,4,7,10,13,15,19,21,23,24,24,22,19,16,12,9,6,3,2,0,0,0,1,1	4,2,1,2,1,0,1,1,0,1,1,0,1,1,0,1,1,0,0,2,0,1,1,1,2	1	-0.459	0.132
Test	DSCT	1SWASPJ001855.86+223940.1	0,1,3,4,5,7,12,16,19,18,22,24,22,21,17,17,14,10,11,7,6,3,4,1,1	1,3,0,2,2,1,1,2,0,0,1,1,1,0,1,0,1,2,1,1,0,1,2,0,1	1	-0.580	0.074
Test	DSCT	1SWASPJ002338.85+283745.3	0,3,6,8,12,19,21,24,24,22,20,18,15,12,10,9,6,5,4,2,1,0,0,0,0	5,1,1,1,1,2,0,1,1,1,0,2,0,0,1,0,0,1,1,1,1,1,0,2	1	-0.666	0.210
Test	DSCT	1SWASPJ002338.90+283729.4	0,1,2,4,8,13,19,22,24,24,23,21,19,16,13,12,9,6,5,4,3,1,0,0,0	4,2,1,1,2,1,1,0,1,1,0,0,1,2,0,0,1,0,0,2,0,1,1,1,2	1	-0.516	0.218
Test	DSCT	1SWASPJ002838.22+323817.3	0,3,6,6,8,9,13,13,18,21,21,21,24,21,17,17,18,15,13,10,11,5,8,2,1	1,1,1,1,0,1,2,0,2,1,1,1,0,3,0,1,0,2,2,0,0,4,0,0,1	1	-0.096	0.306
Test	DSCT	1SWASPJ004423.07+281313.8	0,1,1,2,5,9,14,19,23,24,22,19,17,14,13,9,9,7,5,3,3,2,0,1,0	3,3,2,2,0,2,0,1,0,3,0,0,0,1,2,0,0,1,0,2,0,0,1,1,1	1	-0.484	0.304
Test	DSCT	1SWASPJ004810.36+473747.7	0,5,6,9,13,17,24,24,24,20,18,16,12,12,9,7,6,5,4,4,2,2,1,1,2	1,2,3,0,2,2,2,1,0,2,0,0,2,1,0,0,1,1,1,0,1,0,0,0,3	1	-0.132	0.184
Test	DSCT	1SWASPJ004811.15+473719.1	0,4,6,8,13,18,24,24,24,22,19,16,13,12,9,7,6,5,4,3,1,1,1,0,2	2,3,1,1,2,1,2,1,1,1,0,0,1,2,0,0,1,0,1,1,0,0,1,0,3	1	-0.022	0.176
Test	DSCT	1SWASPJ010535.61-090234.0	0,1,3,6,8,16,19,20,22,24,21,21,15,14,9,6,4,5,4,2,3,2,0,0,1	3,2,2,2,2,1,2,0,1,1,0,0,0,0,1,1,1,0,0,1,1,2,1,0,1	1	-0.075	0.538
Test	DSCT	1SWASPJ010547.15+443503.7	0,1,2,5,8,12,17,22,24,24,22,19,16,14,12,10,9,7,5,4,3,1,1,0,0	3,3,1,1,1,2,0,1,1,1,1,0,2,0,1,0,1,1,0,1,0,0,2,0,2	1	-1.065	0.456
Test	DSCT	1SWASPJ011024.13+271915.3	0,1,4,8,13,19,23,24,24,21,19,16,14,12,9,8,5,4,2,2,1,1,0,0,0	4,3,2,0,2,1,0,0,2,1,0,0,1,1,1,0,1,0,0,2,0,1,0,1,2	1	-0.860	0.340
Test	DSCT	1SWASPJ013104.98+163643.6	0,3,6,8,10,10,16,19,22,22,22,21,22,24,22,17,13,10,9,7,4,4,0,1,2	2,1,1,1,2,0,1,1,1,1,3,0,0,1,0,0,1,1,0,1,0,1,5,0,1	1	0.224	0.078
Test	DSCT	1SWASPJ013407.91-134957.1	0,1,2,5,8,12,15,19,21,24,24,23,21,18,15,14,12,10,8,6,6,4,2,0,0	3,1,2,0,1,1,2,0,2,0,1,0,2,0,1,2,0,0,1,1,0,2,0,1,2	1	-1.034	0.200
Test	DSCT	1SWASPJ013920.86+473154.1	0,1,1,3,6,15,23,24,22,20,17,14,12,10,7,8,6,5,4,2,3,1,1,1,0	2,5,1,2,1,1,2,1,1,0,1,0,1,0,1,1,0,1,0,0,1,0,1,1,1	1	-0.623	0.438
Test	DSCT	1SWASPJ014427.95+375853.8	0,1,4,9,19,24,24,21,19,16,13,11,9,7,6,5,4,3,2,1,1,1,0,0,0	4,4,1,1,2,1,1,1,0,2,0,1,0,1,0,0,1,0,0,2,0,1,0,0,2	1	-0.845	0.608
Test	DSCT	1SWASPJ014624.11+491311.7	0,1,2,6,13,22,24,22,18,16,13,10,8,7,6,5,4,3,2,1,1,0,0,0,0	5,3,2,1,1,1,2,1,1,0,1,0,0,2,0,0,1,0,1,0,0,0,2,0,1	1	-0.781	0.536
Test	DSCT	1SWASPJ015612.69+522723.8	0,1,3,6,13,21,24,24,23,20,17,14,11,10,8,7,5,4,3,2,1,0,0,0,0	5,2,1,2,1,1,1,1,0,1,1,0,1,1,0,0,1,0,0,1,1,0,1,2	1	-0.955	0.172
Test	DSCT	1SWASPJ015615.55+522654.9	0,2,2,7,13,20,24,22,21,19,16,13,11,9,8,6,5,4,3,3,1,1,0,1,0	3,3,2,2,1,1,1,1,1,1,0,1,0,2,0,0,1,0,0,1,1,1,1,0,1	1	-0.696	0.256
Test	DSCT	1SWASPJ023917.03-434805.9	0,3,2,1,3,7,12,14,20,24,24,20,19,16,20,15,12,11,10,9,7,4,2,2,0	2,1,3,2,1,0,0,2,0,1,1,2,0,1,1,1,0,0,1,3,0,0,0,2	1	0.195	0.090
Test	DSCT	1SWASPJ183208.23+403559.7	0,1,3,7,15,22,24,24,21,18,16,13,10,9,7,6,5,3,3,2,1,0,0,0,0	5,2,1,3,0,1,1,2,0,1,1,0,0,1,0,1,1,0,0,1,1,0,1,0,2	1	-0.957	0.608
Test	DSCT	1SWASPJ190815.94+495715.8	0,1,2,4,7,10,13,18,22,23,24,24,22,19,17,14,10,8,6,4,3,1,0,0,0	4,2,1,1,2,0,1,1,1,0,2,0,0,1,1,0,0,1,1,1,0,0,2,1,2	1	-0.913	0.146
Test	DSCT	1SWASPJ193445.57+455416.3	0,2,4,8,13,20,24,24,23,21,19,17,15,12,10,8,7,5,4,3,2,1,0,0,0	4,1,2,1,2,1,0,1,2,0,1,0,1,1,0,1,0,1,0,1,1,1,0,1,2	1	-1.024	0.346
Test	DSCT	1SWASPJ193449.05+455333.4	0,1,1,3,6,14,20,23,24,23,21,19,17,15,13,10,9,7,5,4,3,3,1,0,0	3,3,0,3,1,1,1,0,1,1,0,0,1,1,1,0,1,0,1,1,1,0,2,1	1	-0.453	0.164
Test	DSCT	1SWASPJ200850.32+485349.3	0,2,3,6,9,13,17,21,24,24,24,23,21,20,17,14,12,10,7,6,3,1,1,0,0	3,2,1,2,0,0,2,1,0,1,1,0,1,1,1,0,0,2,0,0,1,2,0,1,3	1	-0.842	0.160
Test	DSCT	1SWASPJ214304.21-481122.2	0,2,5,10,17,23,24,23,21,19,16,14,12,10,8,7,5,4,3,2,2,1,0,0,0	4,1,3,1,1,2,0,1,1,0,2,0,1,0,1,0,1,1,0,1,0,1,0,2,1	1	-0.984	0.454
Test	DSCT	1SWASPJ215152.32+174443.7	0,2,6,13,19,24,24,23,21,18,16,13,11,9,7,5,5,3,2,1,1,0,0,0,0	5,2,2,1,0,2,1,1,0,1,0,1,0,2,0,0,1,0,1,1,0,1,0,1,2	1	-0.843	0.288
Test	DSCT	1SWASPJ215155.04+174437.0	0,1,2,6,11,19,23,24,22,20,18,15,12,10,9,7,6,4,3,2,2,1,1,0,0	3,3,3,1,1,0,2,1,0,1,1,1,1,0,0,1,0,0,1,1,1,0,1,1,1	1	-0.604	0.244
Test	DSCT	1SWASPJ215832.72+214924.7	0,3,5,8,12,16,19,22,24,24,24,21,19,16,13,10,8,6,4,3,2,1,0,0,0	4,1,1,2,1,1,1,0,2,0,1,0,1,1,0,0,2,0,0,2,0,1,1,0,3	1	-0.826	0.180
Test	DSCT	1SWASPJ234846.01-080844.5	0,1,4,8,14,20,24,24,23,21,18,16,14,12,10,8,7,6,6,5,3,2,1,0,0	3,2,1,1,1,1,2,1,2,0,1,0,1,0,2,0,1,0,1,1,0,1,2	1	-1.230	0.420

Appendix 1 continued...

EA Double eclipse

Reason	Class	WASP Object Id	X-pattern	Y-pattern	P-bin	Mode-mean	BMA
Train	EA double	1SWASP J000007.28+184417.1	0,12,22,24,24,24,24,24,24,24,24,22,18,19,23,24,24,24,24,24,24,24,23,9	1,0,0,0,0,0,0,0,0,1,0,0,1,0,0,0,0,0,1,1,0,0,2,2,16	2	0.395	0.658
Train	EA double	1SWASP J000030.01-393729.1	0,14,23,23,23,23,24,24,23,23,23,23,21,20,22,23,23,23,24,24,23,24,24,23,15	1,0,0,0,0,0,0,0,0,0,0,0,0,0,0,1,1,0,0,0,0,1,1,1,13,6	2	0.384	1.002
Train	EA double	1SWASP J000318.22+325045.0	0,8,22,22,23,24,24,24,24,23,22,21,21,20,22,22,23,23,24,24,24,23,22,20,17	1,0,0,0,0,0,0,0,1,0,0,0,0,0,0,0,0,0,1,0,0,2,2,6,5,7	2	0.495	1.376
Train	EA double	1SWASP J000507.48+482705.2	0,13,22,22,23,24,24,24,24,23,23,23,21,21,22,23,23,24,23,24,23,23,23,22,16	1,0,0,0,0,0,0,0,0,0,0,0,0,0,0,1,0,0,1,0,0,0,0,2,4,10,6	2	0.393	1.144
Train	EA double	1SWASP J001625.00+562046.7	0,11,21,22,22,22,23,23,24,24,24,22,19,20,21,23,23,24,24,24,23,22,21,18,6	1,0,0,0,0,0,1,0,0,0,0,1,0,0,0,0,0,0,0,1,1,3,5,5,6	2	0.452	0.828
Train	EA double	1SWASP J003011.22+560748.0	0,10,23,23,24,23,24,24,24,24,23,23,24,22,22,22,23,22,23,22,24,24,24,23,23,17	1,0,0,0,0,0,0,0,0,0,1,0,0,0,0,0,0,0,1,0,0,0,0,5,9,8	2	0.214	0.840
Train	EA double	1SWASP J003016.31-462758.6	0,11,22,23,23,23,23,23,23,23,22,21,19,18,22,22,22,23,24,24,23,23,24,24,14	1,0,0,0,0,0,0,0,0,0,0,0,1,0,0,1,0,0,0,1,1,0,1,5,10,4	2	0.348	1.092
Train	EA double	1SWASP J003433.82+412006.0	0,8,22,24,24,24,24,24,24,24,24,23,22,21,23,24,24,24,24,24,24,24,24,23,15	1,0,0,0,0,0,0,0,1,0,0,0,0,0,0,0,1,0,0,0,0,0,1,2,3,16	2	0.401	0.984
Train	EA double	1SWASP J003509.39+414003.5	0,11,22,23,24,24,24,24,24,24,24,22,22,23,24,24,23,24,24,23,23,24,24,23,14	1,0,0,0,0,0,0,0,0,0,0,1,0,0,1,0,0,0,0,0,0,0,3,6,13	2	0.131	1.260
Train	EA double	1SWASP J003636.40+551332.0	0,17,22,23,22,23,23,24,24,23,23,23,19,20,22,22,24,24,23,24,22,24,22,21,9	1,0,0,0,0,0,0,0,0,1,0,0,0,0,0,0,0,1,0,1,1,1,6,7,6	2	0.148	1.118
Train	EA double	1SWASP J004345.09+305619.6	0,12,21,22,22,24,24,24,24,23,21,19,17,19,21,23,24,24,23,23,23,22,21,13,0	2,0,0,0,0,0,0,0,0,0,0,0,0,1,1,0,0,0,1,0,2,0,4,3,5,6	2	0.531	1.226
Train	EA double	1SWASP J004613.55+394608.6	0,11,21,23,22,23,23,24,24,23,23,22,21,21,22,23,23,24,24,24,24,22,22,20,6	1,0,0,0,0,0,1,0,0,0,0,1,0,0,0,0,0,0,0,0,0,1,3,5,7,6	1	0.194	1.208
Train	EA double	1SWASP J004917.94+503902.9	0,19,24,23,24,24,24,24,24,23,24,24,22,23,24,24,24,24,24,23,23,23,22,6	1,0,0,0,0,0,1,0,0,0,0,0,0,0,0,0,0,0,0,0,1,0,0,2,6,14	2	0.248	0.888
Train	EA double	1SWASP J005402.15+543101.1	0,19,21,21,23,24,24,22,21,23,22,16,19,18,21,23,23,24,24,24,22,19,17,14,6	1,0,0,0,0,0,1,0,0,0,0,0,0,0,1,0,1,1,1,3,0,4,3,4,5	2	0.379	0.758
Train	EA double	1SWASP J010031.81+584146.3	0,6,18,22,22,22,23,23,24,24,23,22,20,20,22,23,23,23,24,23,24,24,24,21,14	1,0,0,0,0,0,1,0,0,0,0,0,0,0,1,0,0,0,1,0,2,1,5,7,6	2	0.303	0.368
Train	EA double	1SWASP J013342.29-434922.9	0,23,24,22,23,24,23,22,22,22,23,23,13,19,23,23,23,24,24,23,24,24,24,23,20	1,0,0,0,0,0,0,0,0,0,0,0,0,1,0,0,0,0,0,1,1,0,4,10,7	2	0.316	0.392
Train	EA double	1SWASP J230119.08-062615.3	0,23,24,24,24,24,24,24,24,24,24,23,10,21,24,24,24,23,24,24,24,24,23,23,23,13	1,0,0,0,0,0,0,0,0,0,0,1,0,0,1,0,0,0,0,0,0,0,0,1,0,6,15	2	0.268	0.308
Train	EA double	1SWASP J230742.74-301359.9	0,23,23,23,24,23,24,24,24,24,24,24,23,5,17,20,24,21,24,24,23,23,24,24,24,16	1,0,0,0,0,1,0,0,0,0,0,0,0,0,0,0,0,0,1,1,0,0,1,1,0,7,12	2	0.408	0.242
Train	EA double	1SWASP J230956.48+413503.2	0,7,20,23,23,24,24,24,24,24,24,24,23,22,21,23,24,24,24,24,24,24,24,23,22,11	1,0,0,0,0,0,0,1,0,0,0,1,0,0,0,0,0,0,0,0,0,1,1,2,5,13	2	0.362	0.444
Train	EA double	1SWASP J231002.57+591206.1	0,18,23,21,23,24,24,23,22,23,23,16,0,19,23,23,23,24,23,23,24,24,23,22,8	2,0,0,0,0,0,0,0,1,0,0,0,0,0,0,0,0,1,0,1,1,0,1,2,11,5	2	0.426	0.450
Train	EA double	1SWASP J231322.89+460851.0	0,14,23,24,24,24,24,24,24,24,24,23,23,23,24,24,24,24,24,23,23,23,23,21,4	1,0,0,0,1,0,0,0,0,0,0,0,0,0,0,0,1,0,0,0,0,0,0,1,0,8,13	2	0.412	0.818
Train	EA double	1SWASP J231925.57-401726.4	0,11,22,23,24,24,24,24,24,24,24,24,22,21,21,23,24,24,24,24,24,24,23,23,23,21,9	1,0,0,0,0,0,0,0,0,0,1,0,1,0,0,0,0,0,0,0,0,0,0,3,2,5,12	2	0.553	0.690
Train	EA double	1SWASP J232328.60+501557.8	0,12,20,23,24,23,24,23,24,23,23,17,12,16,21,24,23,24,23,24,24,23,23,18,4	1,0,0,0,1,0,0,0,0,0,0,0,0,2,0,0,0,1,1,1,0,1,1,0,9,7	2	0.164	0.520
Train	EA double	1SWASP J232706.28+564445.0	0,5,16,23,23,24,23,23,23,24,24,24,22,20,19,23,23,23,24,24,21,20,22,23,15	1,0,0,0,0,1,0,0,0,0,0,0,0,0,0,0,0,1,1,0,0,1,2,1,2,9,6	2	0.103	0.374
Train	EA double	1SWASP J232737.31+501716.4	0,8,21,24,24,24,24,24,24,24,24,24,22,22,23,23,23,24,24,24,24,24,23,23,15	1,0,0,0,0,0,0,0,1,0,0,0,0,0,0,0,1,0,0,0,0,0,1,2,5,14	2	0.323	0.742
Train	EA double	1SWASP J233214.66+145808.7	0,2,13,21,23,24,24,24,24,24,24,23,21,18,20,22,23,24,24,24,24,24,23,20,11	1,0,1,0,0,0,0,0,0,0,0,1,0,1,0,0,0,0,1,0,2,2,1,4,11	1	0.460	0.898
Train	EA double	1SWASP J233447.58+555416.4	0,13,20,21,21,21,18,23,24,23,22,20,19,18,19,22,23,23,23,22,21,19,18,19,7	1,0,0,0,0,0,0,1,0,0,0,0,0,1,0,0,0,0,0,3,4,2,4,3,5,1	2	0.456	0.614
Train	EA double	1SWASP J233608.93-162808.3	0,9,17,19,19,21,20,21,21,20,19,18,16,18,20,23,23,24,24,24,23,23,22,19,6	1,0,0,0,0,0,1,0,0,1,0,0,0,0,0,0,1,1,2,4,3,3,1,4,3	2	0.193	0.740
Train	EA double	1SWASP J233901.77+471448.7	0,12,20,22,24,23,22,23,22,23,21,18,18,21,22,19,23,23,24,24,22,22,22,14,0	2,0,0,0,0,0,0,0,0,0,0,0,0,1,0,1,0,0,0,2,1,1,2,7,5,3	2	0.186	0.222
Train	EA double	1SWASP J233951.89+474501.9	0,9,22,23,24,24,24,24,24,24,24,24,22,22,23,24,24,24,24,24,24,23,24,23,15	1,0,0,0,0,0,0,0,0,1,0,0,0,0,0,1,0,0,0,0,0,0,3,4,15	2	0.330	1.422
Test	EA double	1SWASP J000030.83-393755.5	0,8,22,24,24,24,24,24,24,24,23,23,22,20,23,23,24,24,24,24,24,24,24,23,18	1,0,0,0,0,0,0,0,1,0,0,0,0,0,0,0,0,0,0,1,0,1,0,2,5,14	2	0.273	0.926
Test	EA double	1SWASP J005828.47+314044.8	0,21,21,23,24,22,22,23,23,22,20,18,18,22,22,23,23,23,22,22,22,22,21,5,-1	1,0,0,0,0,1,0,0,0,0,0,0,0,0,0,0,0,0,0,2,0,1,3,9,6,1	2	0.280	0.410
Test	EA double	1SWASP J010450.16+540619.8	0,11,22,22,22,21,22,23,23,23,24,24,21,21,23,22,23,23,23,23,23,23,23,22,10	1,0,0,0,0,0,0,0,0,0,1,1,0,0,0,0,0,0,0,0,0,0,0,3,6,11,2	2	0.301	1.312
Test	EA double	1SWASP J010703.18+372904.9	0,4,20,20,22,23,23,23,23,24,24,24,22,21,21,23,24,22,22,23,24,23,23,22,16	1,0,0,0,1,0,0,0,0,0,0,0,0,0,0,0,0,1,0,0,0,2,2,5,8,5	2	0.504	0.356
Test	EA double	1SWASP J011417.24+485925.7	0,16,22,22,-1,23,24,24,24,-1,24,22,19,20,-1,24,24,24,24,-1,24,23,23,21,-1	1,0,0,0,0,0,0,0,0,0,0,0,0,0,0,0,0,0,0,1,0,0,1,1,1,3,3,9	2	0.534	0.528
Test	EA double	1SWASP J013535.91-115630.6	0,10,22,24,24,24,24,24,24,24,24,23,21,22,23,24,24,24,24,24,24,23,23,23,21,8	1,0,0,0,0,0,0,0,1,0,1,0,0,0,0,0,0,0,0,0,0,0,2,2,5,13	2	0.393	0.926
Test	EA double	1SWASP J014100.69-064334.2	0,9,22,23,23,23,24,24,24,24,24,24,22,23,24,24,24,24,24,24,24,23,23,22,22,18	1,0,0,0,0,0,0,0,0,1,0,0,0,0,0,0,0,0,0,1,0,0,4,6,12	2	0.352	0.546
Test	EA double	1SWASP J014903.36+561626.8	0,15,20,20,22,24,23,23,23,22,20,21,18,20,22,22,22,21,21,22,21,21,23,18,6	1,0,0,0,0,1,0,0,0,0,0,0,0,0,1,0,0,2,0,4,5,6,4,1	2	0.363	1.028
Test	EA double	1SWASP J015651.52+420602.1	0,12,21,23,22,23,24,24,24,24,23,21,19,21,23,23,24,24,24,24,24,23,23,22,13,1	1,1,0,0,0,0,0,0,0,0,0,0,0,1,1,0,0,0,0,0,1,0,3,2,7,8	2	0.406	1.414
Test	EA double	1SWASP J020518.17+450534.0	0,18,22,23,24,24,24,24,24,22,22,18,2,11,23,23,23,24,24,23,24,23,23,22,5	1,0,1,0,0,1,0,0,0,0,0,1,0,0,0,0,0,0,2,0,0,0,4,7,8	2	0.595	0.362
Test	EA double	1SWASP J021042.53+381832.0	0,18,23,23,24,24,24,24,24,24,23,22,21,22,23,24,24,24,24,24,24,23,23,15,2	1,0,1,0,0,0,0,0,0,0,0,0,0,0,0,0,0,1,0,0,1,0,0,1,2,6,12	2	0.292	1.294
Test	EA double	1SWASP J021251.24+453751.6	0,12,23,24,24,24,24,24,24,24,24,24,23,23,23,24,23,24,24,24,24,24,24,24,23,11	1,0,0,0,0,0,0,0,0,0,0,1,1,0,0,0,0,0,0,0,0,0,0,0,6,16	2	0.500	1.432
Test	EA double	1SWASP J021318.15+370101.4	0,7,18,22,23,24,24,24,24,24,24,23,22,20,20,21,23,23,24,24,24,24,23,22,19,8	1,0,0,0,0,0,0,1,1,0,0,0,0,0,0,0,0,0,0,1,1,2,1,3,5,9	1	0.511	1.000
Test	EA double	1SWASP J022136.48-371245.6	0,5,22,23,23,24,24,24,24,24,24,23,22,22,23,24,24,23,24,24,24,24,23,23,16	1,0,0,0,0,1,0,0,0,0,0,0,0,0,0,0,0,0,1,0,0,0,0,0,3,7,12	2	0.397	1.216
Test	EA double	1SWASP J022323.60+370137.6	0,17,22,23,23,24,24,24,24,23,22,22,20,19,22,23,24,24,24,24,24,23,23,22,14	1,0,0,0,0,0,0,0,0,0,0,0,0,0,0,0,1,0,0,1,0,1,1,0,5,6,9	2	0.306	0.514
Test	EA double	1SWASP J022353.68+395902.8	0,13,22,23,23,23,24,24,24,24,23,22,22,23,24,24,23,24,24,24,24,24,24,22,21,6	1,0,0,0,0,0,1,0,0,0,0,0,0,0,1,0,0,0,0,0,0,0,0,1,4,6,11	2	0.217	1.390
Test	EA double	1SWASP J023448.38+561751.5	0,16,23,20,21,22,20,23,23,21,23,21,21,20,21,22,23,22,23,24,21,21,23,23,12	1,0,0,0,0,0,0,0,0,0,0,0,1,0,0,0,1,0,0,0,3,7,3,8,1	2	0.127	0.834
Test	EA double	1SWASP J052847.16+160832.5	0,11,21,21,21,22,22,23,22,21,20,20,19,20,22,24,21,22,23,23,22,22,19,15,2	1,0,1,0,0,0,0,0,0,0,0,1,0,0,0,1,0,0,2,3,5,7,3,1	2	0.403	0.920
Test	EA double	1SWASP J055128.86+240330.7	0,5,13,20,23,24,24,24,24,23,23,19,18,17,16,19,21,23,23,24,22,24,20,16,10,0	2,0,0,0,0,1,0,0,0,0,1,0,0,1,0,0,2,1,1,2,2,1,1,5,5	1	0.567	0.506
Test	EA double	1SWASP J061839.70+210236.4	0,8,17,24,19,24,22,23,22,21,20,16,14,16,20,24,22,23,24,22,24,21,20,17,7	1,0,0,0,0,0,0,1,1,0,0,0,0,0,1,0,2,2,0,1,3,2,4,2,5	1	0.120	0.192
Test	EA double	1SWASP J103820.77+141603.6	0,3,13,19,20,22,23,24,24,22,23,18,7,4,13,21,22,24,22,21,21,21,20,18,11	1,0,0,1,1,0,0,1,0,0,0,1,0,2,0,0,0,0,2,1,2,4,4,2,3	1	0.775	0.538
Test	EA double	1SWASP J121356.11+020034.0	0,7,19,23,24,24,24,24,22,21,20,15,13,12,17,21,23,23,24,24,24,23,21,15,3	1,0,0,1,0,0,0,1,0,0,0,0,0,1,1,0,2,0,1,0,1,1,3,1,4,7	1	0.639	0.300
Test	EA double	1SWASP J152154.83+335609.2	0,4,12,18,21,22,23,22,23,23,24,21,9,5,12,19,23,24,24,24,23,23,22,20,13	1,0,0,0,1,1,0,0,0,1,0,0,2,1,0,0,0,0,1,1,1,2,3,6,4	1	0.540	0.400
Test	EA double	1SWASP J181132.84+235512.6	0,3,19,22,22,23,24,24,24,22,21,21,13,14,16,21,22,22,24,24,24,24,22,22,16	1,0,0,1,0,0,0,0,0,0,0,0,0,0,0,1,1,0,2,0,0,1,0,3,7,1,7	2	0.665	0.722
Test	EA double	1SWASP J191754.97-301659.4	0,14,18,18,19,19,19,20,18,19,19,17,6,1,20,24,22,23,17,16,20,20,20,21,20	1,1,0,0,0,0,1,0,0,0,0,0,0,0,0,1,0,1,2,3,5,6,1,1,1,1	2	0.348	0.436
Test	EA double	1SWASP J193403.28+394241.3	0,7,19,23,24,24,24,24,24,23,22,19,14,14,18,21,23,24,23,24,23,22,21,18,6	1,0,0,0,0,0,1,1,0,0,0,0,0,0,0,2,0,0,0,2,2,0,2,2,5,7	1	0.595	0.614
Test	EA double	1SWASP J195844.04+095711.9	0,12,22,22,23,21,24,23,24,23,21,17,17,19,20,23,20,19,19,20,19,20,18,10,2	1,0,1,0,0,0,0,0,0,1,0,1,0,0,0,0,2,1,4,4,2,2,4,2	2	0.348	0.314
Test	EA double	1SWASP J202633.64-581137.0	0,3,14,21,23,24,24,24,24,23,22,18,14,14,17,22,23,24,24,24,24,23,22,17,6	1,0,0,1,0,0,1,0,0,0,0,0,0,3,0,0,2,1,0,0,1,3,4,8	1	0.673	0.702
Test	EA double	1SWASP J214250.09+415931.1	0,4,20,21,23,24,24,24,24,23,24,22,23,21,18,23,24,22,22,22,22,21,20,20,20,18	1,0,0,0,1,0,0,0,0,0,0,0,0,0,0,0,0,0,0,0,2,0,4,3,5,4,5	2	0.292	0.752
Test	EA double	1SWASP J214914.51+410816.6	0,9,18,23,24,24,24,24,24,24,23,21,18,16,18,20,22,23,24,23,24,23,22,20,13,3	1,0,0,1,0,0,0,0,0,1,0,0,0,1,0,0,1,0,3,0,2,1,2,5,7	2	0.617	0.640

Appendix 1 continued...

EA Single eclipse

Reason	Class	WASP Object Id	X-pattern	Y-pattern	P-bin	Mode-mean	BMA
Train	EA single	1SWASPJ005243.01+502810.1	0,1,9,16,21,23,23,23,24,24,24,24,24,23,24,24,24,24,23,23,23,22,19,13,6	1,1,0,0,0,0,1,0,0,1,0,0,0,1,0,0,1,0,0,1,0,1,1,7,9	1	0.569	0.658
Train	EA single	1SWASPJ010707.85+543707.9	0,2,19,23,23,24,23,24,23,24,22,23,22,21,23,22,23,22,23,23,24,23,23,22,13	1,0,1,0,0,0,0,0,0,0,0,0,0,0,1,0,0,0,0,0,1,0,1,5,11,4	2	-0.068	1.344
Train	EA single	1SWASPJ011124.84+465749.3	0,13,23,24,24,24,24,24,24,24,24,24,24,24,24,24,24,24,24,24,24,23,11	1,0,0,0,0,0,0,0,0,0,0,1,0,1,0,0,0,0,0,0,0,0,2,20	2	0.270	0.486
Train	EA single	1SWASPJ011612.92+561942.7	0,7,20,20,22,23,24,24,23,22,23,22,23,21,22,22,22,21,23,23,21,21,20,20,16	1,0,0,0,0,0,0,1,0,0,0,0,0,0,0,0,0,1,0,0,0,4,4,6,6,2	2	0.226	0.278
Train	EA single	1SWASPJ012627.92+445613.2	0,2,20,22,21,23,24,23,23,23,22,22,21,20,21,21,21,22,21,21,21,20,20,19,18	1,0,1,0,0,0,0,0,0,0,0,0,0,0,0,0,0,0,0,1,1,4,8,4,4,1	2	0.313	0.302
Train	EA single	1SWASPJ013752.39+571958.6	0,5,17,22,22,22,23,22,24,22,21,23,22,24,23,23,24,24,23,22,22,20,21,21,12	1,0,0,0,0,1,0,0,0,0,0,0,1,0,0,0,1,0,0,1,3,8,5,4	2	0.161	0.596
Train	EA single	1SWASPJ021858.05+551712.0	0,11,21,23,24,22,23,24,22,21,22,22,20,21,21,21,21,23,22,23,21,22,22,22,13	1,0,0,0,0,0,0,0,0,0,0,1,0,1,0,0,0,0,0,0,1,7,8,4,2	2	-0.147	0.922
Train	EA single	1SWASPJ023608.77+380921.6	0,20,24,24,24,24,23,21,24,23,24,24,24,24,24,24,24,24,24,24,24,23,23,23,23,24,12	1,0,0,0,0,0,0,0,0,0,0,0,0,0,1,0,0,0,0,0,0,0,1,1,0,6,15	2	0.388	0.426
Train	EA single	1SWASPJ024116.51+485618.7	0,13,23,23,23,23,22,23,22,23,22,23,23,23,23,24,22,23,23,22,23,22,23,21,5	1,0,0,0,0,1,0,0,0,0,0,0,0,0,1,0,0,0,0,0,0,0,1,6,14,1	2	0.307	0.538
Train	EA single	1SWASPJ024250.53+515311.8	0,13,21,23,21,20,19,21,22,23,23,24,22,24,24,24,23,22,23,23,24,22,18,21,19,10	1,0,0,0,0,0,0,0,0,1,0,0,1,0,0,0,0,1,2,1,4,4,6,4	2	0.429	0.394
Train	EA single	1SWASPJ024605.62+431707.9	0,8,23,24,23,19,24,19,20,21,23,24,22,22,24,24,23,23,22,22,19,21,20,23,14	1,0,0,0,0,0,0,0,1,0,0,0,0,0,1,0,0,0,0,3,2,2,4,6,5	2	0.679	1.164
Train	EA single	1SWASPJ025933.53+033103.2	0,7,20,23,23,23,24,24,24,24,24,24,24,24,24,24,24,24,24,24,24,23,22,21,12	1,0,0,0,0,0,1,0,0,0,1,0,0,0,0,0,0,0,1,1,1,4,15	2	0.443	0.528
Train	EA single	1SWASPJ034504.89+374715.9	0,17,24,24,24,24,24,22,23,24,24,23,23,23,24,24,24,22,24,24,23,23,23,22,0	2,0,0,0,0,0,0,0,0,0,0,0,0,0,0,0,0,0,0,1,0,0,0,3,7,12	2	0.468	1.526
Train	EA single	1SWASPJ045444.68+265527.3	0,7,15,20,23,23,23,23,23,22,21,23,23,24,24,24,24,22,21,22,23,23,21,15,7,0	2,0,0,0,0,0,2,0,0,0,0,0,0,0,2,0,0,0,0,1,3,3,8,4	1	0.519	0.566
Train	EA single	1SWASPJ053853.97-333756.2	0,6,17,24,23,24,24,24,23,23,24,24,24,24,24,24,24,24,24,24,24,23,20,9	1,0,0,0,0,1,0,0,1,0,0,0,0,0,0,0,1,0,0,1,0,0,4,16	2	0.521	0.480
Train	EA single	1SWASPJ062130.18+415101.1	0,6,20,23,23,23,23,23,23,23,23,22,22,20,22,24,23,24,24,23,22,21,21,23,14	1,0,0,0,0,0,1,0,0,0,0,0,0,0,1,0,0,0,0,0,2,2,4,11,3	2	0.180	0.716
Train	EA single	1SWASPJ202110.38-433352.8	0,4,9,16,20,22,23,23,23,24,24,24,24,24,24,24,23,23,23,22,20,16,10,4,0	2,0,0,0,2,0,0,0,0,1,1,0,0,0,0,0,2,0,0,0,2,0,2,6,7	1	0.596	0.694
Train	EA single	1SWASPJ202302.83+431432.4	0,16,19,20,20,21,23,24,22,21,22,22,18,19,22,22,21,22,23,21,20,22,22,19,2	1,0,1,0,0,0,0,0,0,0,0,0,0,0,0,0,0,1,0,1,3,3,4,8,2,1	2	0.334	1.108
Train	EA single	1SWASPJ202817.25+183317.3	0,20,22,22,23,22,22,22,22,22,24,21,21,24,23,22,22,22,23,22,24,24,22,15,1	1,1,0,0,0,0,0,0,0,0,0,0,0,0,0,0,0,1,0,0,0,0,1,2,12,3,4	2	0.302	0.638
Train	EA single	1SWASPJ203307.50+245149.6	0,11,20,23,24,24,22,23,22,22,23,24,24,21,21,22,23,23,22,22,23,21,20,23,12	1,0,0,0,0,0,0,0,0,0,0,1,1,0,0,0,0,0,0,2,3,6,7,4	2	0.001	0.644
Train	EA single	1SWASPJ203310.49+412222.5	0,6,17,21,21,23,22,23,24,22,24,23,22,21,23,24,24,23,23,23,21,20,21,21,11	1,0,0,0,0,0,1,0,0,0,1,0,0,0,0,0,1,0,0,1,6,3,7,4	2	0.193	0.096
Train	EA single	1SWASPJ203745.32+551631.2	0,4,11,14,18,22,23,22,24,24,24,24,24,24,23,23,24,23,23,22,21,20,17,11,4	1,0,0,0,2,0,0,0,0,0,0,2,0,0,1,0,0,1,1,0,1,1,3,5,7	1	0.618	0.624
Train	EA single	1SWASPJ212907.29+404011.5	0,8,14,20,23,23,23,23,23,23,23,24,24,24,24,23,24,23,24,22,19,15,9,3	1,0,0,1,0,0,0,0,1,1,0,0,0,0,1,1,0,0,0,1,1,0,1,11,5	1	0.213	0.356
Train	EA single	1SWASPJ213040.30+405622.9	0,1,18,20,21,19,21,22,21,19,20,20,20,18,20,21,21,21,21,20,21,21,20,24,12	1,1,0,0,0,0,0,0,0,0,0,0,1,0,0,0,0,0,2,2,7,9,1,0,1	2	0.453	0.442
Train	EA single	1SWASPJ213902.80+545802.1	0,17,22,24,23,24,24,21,24,23,23,23,22,22,23,23,23,24,24,24,23,23,23,22,7	1,0,0,0,0,0,0,1,0,0,0,0,0,0,0,0,0,1,0,0,0,1,4,10,7	2	0.259	1.466
Train	EA single	1SWASPJ214137.70+143930.7	0,6,19,22,24,23,24,24,24,23,24,23,24,24,23,23,23,24,23,20,-1,22,24,22,13	1,0,0,0,0,0,1,0,0,0,0,0,0,0,1,0,0,0,0,0,1,1,0,3,7,9	2	0.501	0.314
Train	EA single	1SWASPJ214744.61+271524.6	0,14,21,20,21,23,24,24,22,22,22,22,24,22,22,21,20,20,22,23,23,21,19,20,14	1,0,0,0,0,0,0,0,0,0,0,0,0,0,0,2,0,0,0,0,1,4,4,7,3,3	2	-0.123	1.382
Train	EA single	1SWASPJ214827.59+280629.6	0,9,21,24,24,24,24,24,24,24,24,24,23,23,24,24,23,23,24,23,24,24,24,23,12	1,0,0,0,0,0,0,0,0,0,1,0,0,1,0,0,0,0,0,0,0,0,1,0,6,15	2	0.382	1.912
Train	EA single	1SWASPJ215259.11+441819.4	0,11,20,22,22,21,22,21,22,22,22,21,21,21,22,24,24,21,23,22,23,21,21,22,10	1,0,0,0,0,0,0,0,0,0,1,1,0,0,0,0,0,0,0,0,1,8,9,2,2	2	0.229	0.314
Train	EA single	1SWASPJ215552.20+413546.8	0,20,21,21,21,22,20,21,23,22,17,20,19,21,24,21,22,23,22,24,21,22,20,20,2	1,0,1,0,0,0,0,0,0,0,0,0,0,0,0,0,0,0,1,0,1,5,7,5,2,2	2	0.570	0.390
Test	EA single	1SWASPJ002434.64+571819.2	0,19,23,23,22,22,22,24,24,24,23,22,20,19,20,21,22,21,23,22,20,19,21,21,11	1,0,0,0,0,0,0,0,0,0,0,1,0,0,0,0,0,0,0,3,3,4,6,4,3	2	0.433	0.506
Test	EA single	1SWASPJ003012.16+560655.6	0,11,22,24,23,23,24,20,22,23,23,24,21,22,21,22,23,21,22,23,22,23,24,23,17	1,0,0,0,0,0,0,0,0,0,0,0,1,0,0,0,0,1,0,0,1,3,6,8,4	2	0.128	0.816
Test	EA single	1SWASPJ003013.56+560837.1	0,11,23,23,22,21,24,24,23,23,23,22,20,21,21,22,22,22,21,23,23,24,23,22,17	1,0,0,0,0,0,0,0,0,0,1,0,0,0,0,0,1,0,0,1,4,6,8,3	2	0.344	0.190
Test	EA single	1SWASPJ003133.51-361625.2	0,24,24,23,23,23,23,23,23,23,23,20,23,22,23,23,24,24,23,24,22,23,23,0	2,0,0,0,0,0,0,0,0,0,0,0,0,0,0,0,0,0,0,0,0,1,0,2,15,5	2	0.298	0.124
Test	EA single	1SWASPJ003539.48+545544.5	0,10,21,23,24,24,24,24,24,24,24,24,24,24,24,24,24,24,24,24,24,24,22,11	1,0,0,0,0,0,0,0,0,0,1,1,0,0,0,0,0,0,0,0,0,1,1,3,17	2	0.468	0.470
Test	EA single	1SWASPJ034556.90+464826.9	0,20,24,19,19,20,21,22,21,19,19,20,18,19,20,21,21,22,21,19,19,20,20,19,0	2,0,0,0,0,0,0,0,0,0,0,0,0,0,0,0,0,0,0,1,8,6,5,2,0,1	2	0.221	0.912
Test	EA single	1SWASPJ035858.12-171346.5	0,17,17,18,22,23,22,21,21,21,21,22,24,24,23,23,23,23,23,23,24,24,22,22,21,14	1,0,0,0,0,0,0,0,0,0,0,0,0,0,0,0,0,1,0,0,2,1,0,0,4,5,7,4	2	0.529	0.744
Test	EA single	1SWASPJ044617.96+385724.5	0,19,22,22,23,21,22,22,22,24,21,22,18,18,22,21,23,23,24,22,21,20,23,19,6	1,0,0,0,0,1,0,0,0,0,0,0,0,0,0,0,0,0,2,2,1,4,8,4,2	2	0.386	0.968
Test	EA single	1SWASPJ050905.33+294019.4	0,9,23,22,23,24,22,22,24,24,23,23,23,23,23,23,24,17,24,24,24,24,22,18,5	1,0,0,0,0,1,0,0,0,1,0,0,0,0,0,0,0,1,1,0,0,0,4,8,8	2	0.188	0.204
Test	EA single	1SWASPJ051428.45+274324.5	0,5,17,16,16,16,17,17,17,24,16,16,16,-1,17,15,16,17,18,19,16,18,16,16,15,14	1,0,0,0,0,1,0,0,0,0,0,0,0,0,0,1,2,10,6,1,1,0,0,0,0,1	2	0.296	0.784
Test	EA single	1SWASPJ054922.37+314208.7	0,8,21,23,24,23,24,24,24,24,24,23,23,24,23,24,24,24,24,23,23,22,19,12,0	2,0,0,0,0,0,0,0,1,0,0,0,1,0,0,0,0,0,0,1,0,1,1,7,11	2	0.394	1.536
Test	EA single	1SWASPJ054942.03+310707.1	0,12,20,20,20,20,20,19,21,24,21,20,21,20,19,20,19,19,21,22,21,19,21,19,20,6	1,0,0,0,0,0,1,0,0,0,0,0,1,0,0,0,0,0,0,0,6,8,6,1,0,1	2	0.210	0.220
Test	EA single	1SWASPJ055741.48+214717.5	0,9,22,23,23,22,24,24,24,24,24,24,23,23,22,23,23,23,24,24,23,23,23,23,21,12	1,0,0,0,0,0,0,0,0,1,0,0,1,0,0,0,0,0,0,0,0,1,3,11,7	2	0.248	1.654
Test	EA single	1SWASPJ060505.13+264053.4	0,10,21,23,20,21,19,21,24,21,19,19,19,19,20,20,19,20,21,21,20,20,20,19,9	1,0,0,0,0,0,0,0,0,1,1,0,0,0,0,0,0,0,0,0,7,7,6,0,1,1	2	0.288	0.864
Test	EA single	1SWASPJ060643.59+315919.5	0,15,21,19,20,21,21,22,23,22,21,23,21,21,21,20,22,23,22,24,21,19,20,20,12	1,0,0,0,0,0,0,0,0,0,0,0,0,0,0,1,0,0,1,0,0,0,2,4,8,4,3,1	2	0.316	0.410
Test	EA single	1SWASPJ061150.61+195714.3	0,3,13,22,22,23,23,21,23,22,21,22,23,23,23,24,22,22,22,22,22,24,19,10,2	1,0,1,1,0,0,0,0,0,0,1,0,0,1,0,0,0,0,0,1,0,2,9,6,2	1	0.261	0.354
Test	EA single	1SWASPJ062334.79+135640.7	0,6,16,23,22,20,24,21,21,20,20,20,18,20,19,19,20,20,19,20,19,19,19,19,17,8	1,0,0,0,0,0,1,0,1,0,0,0,0,0,0,0,1,1,1,6,8,2,1,1,1	2	0.326	0.902
Test	EA single	1SWASPJ221208.72+484344.3	0,16,23,23,22,24,24,24,24,24,24,23,23,24,23,24,24,24,24,23,24,23,23,19,3	1,0,0,1,0,0,0,0,0,0,0,0,0,0,0,0,0,0,1,0,0,1,0,0,1,8,12	2	0.519	1.228
Test	EA single	1SWASPJ222218.72-041222.6	0,4,21,24,22,23,23,23,23,22,23,23,24,24,23,23,23,23,22,22,23,23,22,23,16	1,0,0,0,1,0,0,0,0,0,0,0,0,0,0,0,0,1,0,0,0,0,1,5,13,3	2	0.350	0.342
Test	EA single	1SWASPJ222425.43+460850.7	0,2,15,16,20,20,22,22,21,22,24,24,23,23,23,22,22,22,21,22,23,22,20,14,6	1,0,1,0,0,0,1,0,0,0,0,0,0,0,0,1,1,1,0,0,0,3,2,8,4,2	1	0.332	0.244
Test	EA single	1SWASPJ223430.67+441635.3	0,13,21,20,21,22,21,23,22,22,22,20,18,21,21,24,22,24,24,21,23,21,13,1	1,1,0,0,0,0,0,0,0,0,0,0,0,0,2,0,0,0,0,1,0,2,7,5,2,4	2	0.244	0.338
Test	EA single	1SWASPJ224118.66-435028.5	0,13,21,22,22,23,23,23,24,24,24,24,24,24,24,23,24,23,23,24,24,23,22,14,1	1,1,0,0,0,0,0,0,0,0,0,0,0,0,1,1,0,0,0,0,0,0,1,3,7,10	2	0.599	0.510
Test	EA single	1SWASPJ230900.86+493651.5	0,2,13,22,24,24,24,23,22,22,24,20,18,23,20,22,21,21,22,22,22,19,22,17,8	1,0,1,0,0,0,0,0,1,0,0,0,0,1,0,0,0,1,1,1,2,2,8,2,4	2	0.570	0.140
Test	EA single	1SWASPJ231202.62+534031.2	0,14,21,21,21,21,20,20,20,20,21,22,24,21,21,21,21,21,21,20,20,20,19,22,8	1,0,0,0,0,0,0,0,1,0,0,0,0,0,1,0,0,0,0,0,1,7,11,2,0,1	2	0.266	1.434
Test	EA single	1SWASPJ232540.57-425359.3	0,1,18,22,23,23,24,23,23,23,22,23,23,23,23,23,23,23,23,23,23,24,23,18	1,1,0,0,0,0,0,0,0,0,0,0,0,0,0,0,0,0,0,2,0,0,0,2,17,2	2	0.420	0.228
Test	EA single	1SWASPJ233848.72+442445.3	0,3,18,23,22,24,24,23,23,24,24,23,20,24,23,24,23,23,23,22,22,16	1,0,0,1,0,0,0,0,0,0,0,0,0,0,0,0,0,1,0,1,0,1,0,3,10,7	2	0.366	0.292
Test	EA single	1SWASPJ234546.04+580642.9	0,15,22,22,23,23,22,21,23,24,22,22,22,22,24,23,23,22,23,23,22,22,22,21,6	1,0,0,0,0,0,1,0,0,0,0,0,0,0,0,0,1,0,0,0,0,0,2,11,7,2	2	0.210	0.600
Test	EA single	1SWASPJ234708.46+263359.9	0,11,24,24,22,24,24,24,24,24,24,24,24,23,24,23,24,24,24,24,23,24,24,24,18	1,0,0,0,0,0,0,0,0,0,0,1,0,0,0,0,0,0,1,0,0,0,1,3,18	2	0.420	0.428
Test	EA single	1SWASPJ234930.70+454721.2	0,12,22,24,24,24,24,24,24,24,24,24,24,24,24,24,24,24,24,24,24,24,20,7	1,0,0,0,0,0,1,0,0,0,1,0,0,0,0,0,0,0,1,0,1,0,20	1	0.413	0.642
Test	EA single	1SWASPJ235546.30+561013.8	0,9,20,20,22,22,22,22,23,24,23,23,21,23,23,21,22,22,22,23,23,22,24,22,18,9	1,0,0,0,0,0,0,0,0,2,0,0,0,0,0,0,0,0,0,1,0,2,2,9,6,2	2	-0.057	0.564

Appendix 1 continued...

EB

Reason	Class	WASP Object Id	X-pattern	Y-pattern	P-bin	Mode-mean	BMA
Train	EB	1SWASPJ002220.06+573003.4	0,1,12,18,21,22,23,24,24,23,20,16,13,13,15,18,20,21,23,24,24,22,18,13,5	1,1,0,0,0,1,0,0,0,0,0,0,1,3,0,1,1,0,3,0,2,2,2,3,4	1	0.674	0.578
Train	EB	1SWASPJ002256.95-203923.6	0,2,12,20,22,24,24,24,23,22,19,17,16,16,17,20,22,23,24,24,24,23,21,14,3	1,0,1,1,0,0,0,0,0,0,0,0,1,0,1,0,2,2,0,1,2,1,3,3,6	1	0.812	0.296
Train	EB	1SWASPJ003139.65+531300.2	0,4,11,18,21,23,24,23,22,20,17,14,13,13,15,18,20,22,22,23,23,20,17,11,2	1,0,1,0,1,0,0,0,0,0,0,0,2,0,2,1,1,0,2,2,0,3,1,3,4,1	1	0.813	0.364
Train	EB	1SWASPJ003225.22-245234.4	0,2,5,12,16,22,24,22,23,20,16,11,9,9,12,17,20,23,24,23,20,16,11,6,2	1,0,2,0,0,1,1,0,0,2,0,2,2,0,0,0,3,1,0,0,3,0,2,3,2	1	1.016	0.246
Train	EB	1SWASPJ010143.64+380546.5	0,8,14,19,22,24,24,24,21,19,16,10,7,10,15,19,22,23,24,22,21,18,15,7,0	2,0,0,0,0,0,0,2,1,0,2,0,0,0,1,2,1,0,1,3,0,2,3,1,4	1	0.719	0.790
Train	EB	1SWASPJ013147.09+302201.6	0,8,16,21,23,24,24,23,22,21,19,16,15,15,18,20,22,23,24,24,23,21,18,11,2	1,0,1,0,0,0,0,0,1,0,0,1,0,0,0,0,2,2,0,2,1,1,3,2,4,4	1	0.678	0.848
Train	EB	1SWASPJ020012.04-181228.1	0,6,15,20,22,24,24,24,23,21,19,16,14,14,17,19,21,23,24,24,24,22,19,14,5	1,0,0,0,0,1,1,0,0,0,0,0,0,0,0,3,1,1,1,0,3,1,2,2,2,6	1	0.815	1.002
Train	EB	1SWASPJ022251.11+415535.1	0,12,19,22,23,24,24,24,23,21,17,12,9,14,17,21,22,24,24,24,22,21,17,9,0	2,0,0,0,0,0,0,0,0,0,2,0,0,2,0,1,0,0,3,0,1,0,3,3,2,6	1	0.481	0.832
Train	EB	1SWASPJ023557.16+560846.4	0,2,9,17,19,23,24,24,23,22,17,15,11,9,12,16,18,20,23,23,23,21,19,14,7	1,0,1,0,0,0,1,0,2,0,1,1,0,1,1,1,2,1,2,1,1,1,5,2	1	1.091	0.434
Train	EB	1SWASPJ034910.59-423655.1	0,2,10,17,21,23,24,24,24,22,19,15,12,11,13,16,19,21,22,23,23,21,18,13,5	1,0,1,0,0,1,0,0,0,0,1,1,1,2,0,1,1,1,1,2,0,3,2,3,3	1	-0.722	0.626
Train	EB	1SWASPJ035443.77-145606.6	0,1,9,17,21,23,24,24,24,22,20,17,14,13,15,18,20,22,24,24,24,23,20,15,7	1,1,0,0,0,0,0,1,0,1,0,0,0,1,1,2,0,2,1,0,3,1,2,2,6	1	0.855	0.638
Train	EB	1SWASPJ035846.07+444405.7	0,5,13,19,21,23,24,23,22,19,17,15,13,14,16,18,21,23,24,24,23,21,17,11,2	1,0,1,0,0,1,0,0,0,0,0,1,0,2,1,1,1,2,1,2,0,3,1,4,3	1	0.949	0.826
Train	EB	1SWASPJ040636.74-274007.5	0,3,12,18,21,24,24,23,21,19,16,14,13,13,15,17,20,22,23,24,23,20,16,9,2	1,0,1,1,0,0,0,0,0,1,0,0,1,2,1,1,2,1,1,1,2,2,1,3,3	1	0.996	0.570
Train	EB	1SWASPJ042937.57+442540.8	0,6,14,19,22,23,24,24,23,22,19,16,15,13,15,15,19,20,22,23,23,23,21,18,13,5	1,0,0,0,0,1,1,0,0,0,0,0,0,0,2,1,2,1,0,1,3,1,1,3,5,2	1	0.820	0.432
Train	EB	1SWASPJ043009.46+253226.9	0,4,13,19,23,24,24,24,21,19,15,13,13,13,14,17,20,22,24,23,21,18,14,7,1	1,1,0,0,1,0,0,1,0,0,0,0,0,0,4,2,1,0,1,1,2,1,2,1,2,4	1	0.807	0.544
Train	EB	1SWASPJ182305.40+585412.7	0,8,16,21,23,24,24,24,22,21,18,15,14,15,17,20,22,23,24,24,23,21,17,10,1	1,1,0,0,0,0,0,0,1,0,1,0,0,0,1,2,1,2,1,0,1,3,2,3,5	1	0.924	0.738
Train	EB	1SWASPJ182324.39+331107.1	0,1,10,17,21,23,24,24,23,22,20,17,15,14,15,18,21,22,24,24,24,22,20,15,7	1,1,0,0,0,0,0,1,0,0,1,0,0,0,1,3,0,2,1,0,2,2,3,2,5	1	0.782	0.786
Train	EB	1SWASPJ182731.35+091227.1	0,8,15,19,22,24,24,24,22,20,17,10,8,10,16,18,19,22,23,23,20,18,15,7,0	2,0,0,0,0,0,0,1,2,0,2,0,0,0,0,2,1,1,2,2,2,0,3,2,3	1	0.607	0.240
Train	EB	1SWASPJ190713.52-300937.7	0,3,10,15,18,23,24,22,21,18,16,14,12,12,13,16,18,20,20,21,21,18,15,7,2	1,0,1,1,0,0,0,1,0,0,1,0,2,1,1,2,2,0,4,0,2,3,1,1,1	1	0.418	0.726
Train	EB	1SWASPJ191905.95+382200.4	0,8,17,22,23,24,24,24,23,21,18,14,10,12,17,20,22,24,24,24,23,22,20,13,2	1,0,1,0,0,0,0,0,1,0,1,0,1,1,1,0,0,2,1,0,2,1,3,3,6	1	0.651	0.612
Train	EB	1SWASPJ193207.72+523714.1	0,5,12,18,21,23,24,23,21,18,13,9,7,8,14,18,22,24,24,24,21,18,13,6,0	2,0,0,0,0,1,1,1,1,1,0,0,1,2,1,0,0,0,4,0,0,3,1,2,4	1	0.903	0.440
Train	EB	1SWASPJ201431.80+151635.4	0,8,16,20,23,24,24,24,22,18,17,14,15,15,16,19,21,23,24,23,21,19,14,6,0	2,0,0,0,0,0,1,0,1,0,0,0,0,0,2,2,2,1,1,2,1,2,1,3,4	1	0.470	0.508
Train	EB	1SWASPJ201828.56-191729.4	0,3,9,16,21,23,24,23,21,17,12,7,6,7,11,16,19,22,24,24,23,19,14,8,1	1,1,0,1,0,0,1,2,1,1,0,1,1,0,1,0,2,1,0,2,0,2,1,3,3	1	1.072	0.318
Train	EB	1SWASPJ202441.32+542959.6	0,6,15,21,23,22,23,21,22,20,17,15,14,16,18,20,22,23,24,24,22,19,12,3,0	2,0,0,1,0,0,1,0,0,0,0,0,0,1,0,1,2,1,1,1,1,2,2,4,3,2	2	0.898	0.380
Train	EB	1SWASPJ203354.62-552831.2	0,4,12,17,21,24,24,24,22,20,17,14,12,12,14,16,19,21,23,23,22,20,17,11,3	1,0,0,1,1,0,0,0,0,0,0,1,3,0,2,0,1,3,0,1,2,2,2,2,3	1	1.012	0.598
Train	EB	1SWASPJ204053.99-003550.7	0,5,15,19,21,23,24,24,24,22,20,17,13,13,16,20,21,22,23,23,22,21,20,17,7	1,0,0,0,0,1,0,1,0,0,0,0,0,2,0,1,1,2,0,1,3,3,3,3,3	1	0.548	0.376
Train	EB	1SWASPJ204519.98+070220.0	0,1,9,15,19,21,24,18,21,17,15,12,11,10,12,14,17,20,23,23,21,18,13,7,1	1,2,0,0,0,0,0,1,0,1,1,1,2,1,1,2,0,2,2,1,1,3,0,2,1	1	0.995	0.234
Train	EB	1SWASPJ205306.77+384940.7	0,3,12,18,21,23,24,24,23,22,19,16,14,13,15,18,21,22,24,24,23,22,20,15,7	1,0,0,1,0,0,0,1,0,0,0,0,1,1,1,2,1,0,2,1,1,2,3,3,4	1	1.005	0.854
Train	EB	1SWASPJ205802.10-460400.3	0,5,14,20,23,24,24,24,23,22,21,18,15,15,17,20,21,23,24,24,24,22,20,15,6	1,0,0,0,0,1,1,0,0,0,0,0,0,0,0,1,3,0,1,1,0,3,2,2,3,6	1	0.639	0.582
Train	EB	1SWASPJ211514.78+022844.9	0,5,13,19,22,24,24,24,23,21,19,16,16,15,17,20,21,24,24,24,23,21,17,9,1	1,1,0,0,0,1,0,0,0,1,0,0,0,1,0,1,2,2,0,2,1,3,1,2,6	1	0.834	0.552
Test	EB	1SWASPJ002206.01+403124.4	0,9,18,22,23,24,24,24,23,22,20,17,16,16,19,21,23,23,24,24,23,22,20,12,2	1,0,1,0,0,0,0,0,0,1,0,0,1,0,0,0,2,1,1,1,2,1,3,5,5	1	0.548	0.338
Test	EB	1SWASPJ045321.90-032254.6	0,3,10,16,21,24,24,24,21,17,14,9,7,7,9,13,17,19,21,21,20,16,11,6,1	1,1,0,1,0,0,1,2,0,2,1,1,0,1,1,0,2,2,0,1,1,4,0,0,3	1	0.852	0.356
Test	EB	1SWASPJ050504.74-073342.9	0,5,12,18,21,23,24,24,22,20,15,11,10,11,14,19,21,22,22,22,20,16,12,4,0	2,0,0,0,1,1,0,0,0,0,1,2,2,0,1,1,1,0,1,1,2,2,4,1,2	1	-0.511	0.494
Test	EB	1SWASPJ050759.69-055037.7	0,6,15,20,22,24,24,24,23,21,19,17,16,16,18,20,22,23,24,24,23,22,18,9,1	1,1,0,0,0,0,1,0,0,1,0,0,0,0,0,1,2,1,2,1,2,1,3,3,5	1	0.767	0.338
Test	EB	1SWASPJ051954.09-355406.4	0,3,12,18,22,24,24,24,22,19,17,14,13,13,15,18,20,23,24,24,23,21,16,8,1	1,1,0,1,0,0,0,0,1,0,0,0,1,2,1,1,1,1,2,1,1,1,2,2,5	1	1.125	0.576
Test	EB	1SWASPJ052812.28+352552.0	0,9,18,20,22,24,24,22,21,21,17,12,12,12,20,22,22,23,24,24,22,20,18,2,0	2,0,1,0,0,0,0,0,0,1,0,0,3,0,0,0,0,1,2,0,3,2,5,1,4	2	0.552	0.178
Test	EB	1SWASPJ053834.73+225444.8	0,2,11,15,21,21,22,24,23,22,20,18,16,16,17,20,21,22,24,23,22,18,14,5,0	2,0,1,0,0,1,0,0,0,0,0,1,0,0,1,1,2,1,2,0,2,3,4,2,2	1	0.609	0.388
Test	EB	1SWASPJ054542.15+410859.1	0,4,13,19,21,23,24,24,23,21,19,16,14,14,16,18,21,22,24,24,23,22,18,13,4	1,0,0,0,2,0,0,0,0,0,0,0,0,2,2,0,2,0,2,2,0,3,2,3,4	1	0.896	0.856
Test	EB	1SWASPJ055717.67+140615.9	0,6,11,17,20,22,24,24,23,21,18,13,9,10,15,19,22,23,24,24,22,20,16,9,3	1,0,0,1,0,0,1,0,0,2,1,1,0,1,0,1,1,1,1,1,2,1,3,2,4	1	0.956	0.528
Test	EB	1SWASPJ061058.65-201241.6	0,8,15,20,23,24,24,23,21,19,15,11,9,11,14,18,20,22,22,22,20,18,14,7,0	2,0,0,0,0,0,0,1,1,0,2,0,0,2,2,0,0,2,1,3,1,3,2,2	2	0.946	0.816
Test	EB	1SWASPJ062100.19-543256.8	0,4,12,17,21,23,24,24,23,21,17,13,10,9,12,16,19,21,22,23,22,19,16,11,4	1,0,0,0,2,0,0,0,0,1,1,1,2,1,0,0,2,2,0,2,0,3,2,3,2	1	0.841	0.856
Test	EB	1SWASPJ091710.15-453250.1	0,3,13,17,21,23,24,24,23,21,20,18,15,13,13,13,17,20,22,21,23,24,21,18,12,3	1,0,0,2,0,0,0,0,0,0,0,0,0,1,4,0,1,0,2,2,0,2,4,1,3,2	2	0.590	0.858
Test	EB	1SWASPJ092523.74-221015.6	0,2,9,18,21,21,22,24,24,23,21,21,16,17,16,20,20,23,23,24,23,23,21,18,11	1,0,1,0,0,0,0,0,0,1,0,1,0,0,0,0,2,1,2,0,2,5,1,5,3	1	0.523	0.822
Test	EB	1SWASPJ094452.96-205412.6	0,3,12,18,21,23,24,24,24,22,20,17,14,14,16,19,22,23,24,24,24,22,19,14,6	1,0,0,1,0,0,1,0,0,0,0,0,1,0,3,0,1,1,1,2,1,1,3,2,6	1	0.886	0.692
Test	EB	1SWASPJ112758.51+144955.4	0,3,5,14,19,22,23,22,19,16,14,11,10,10,12,15,18,21,23,24,23,20,13,7,3	1,0,0,2,0,1,0,1,0,0,2,1,1,2,1,1,0,1,2,1,1,2,3,1,1	1	-0.294	0.162
Test	EB	1SWASPJ125902.84+180244.4	0,1,6,11,16,19,22,23,24,23,21,17,11,9,13,17,20,21,21,20,18,15,13,9,4	1,1,0,0,1,0,1,0,0,2,0,2,0,2,0,1,1,2,1,1,2,3,1,2,1	1	0.059	0.670
Test	EB	1SWASPJ165044.16+302408.8	0,4,11,15,18,22,24,24,22,18,15,13,11,12,15,15,17,21,22,22,19,18,16,12,6	1,0,0,0,1,0,1,0,0,0,0,2,2,1,0,4,1,1,3,1,0,1,4,0,2	2	0.346	0.164
Test	EB	1SWASPJ213555.98+405048.4	0,8,16,21,23,24,24,24,23,20,15,12,10,13,18,21,23,24,24,24,21,21,16,8,0	2,0,0,0,0,0,0,0,2,0,1,0,1,1,0,1,2,0,1,0,1,4,0,3,6	1	0.834	0.532
Test	EB	1SWASPJ213649.74-702000.7	0,4,12,18,21,24,24,24,23,20,17,14,13,13,14,17,20,22,24,24,23,21,17,10,1	1,1,0,0,1,0,0,0,0,0,1,0,1,2,2,0,0,3,1,0,2,2,1,2,5	1	1.127	0.590
Test	EB	1SWASPJ213733.26+490455.5	0,9,17,22,23,24,24,24,24,22,21,19,17,17,20,22,23,24,24,24,24,23,20,15,3	1,0,0,1,0,0,0,0,0,1,0,0,0,0,0,1,0,3,0,1,2,1,3,3,8	2	0.479	0.406
Test	EB	1SWASPJ213926.37+230138.3	0,5,12,18,21,23,24,23,21,18,15,12,10,11,14,18,20,23,24,24,23,20,15,8,1	1,1,0,0,0,1,0,0,1,0,1,1,2,0,1,2,0,0,3,0,2,2,0,4,3	2	0.817	0.400
Test	EB	1SWASPJ220608.50+461835.4	0,5,13,19,22,23,24,24,22,21,17,14,12,13,15,17,20,22,23,23,22,20,17,11,2	1,0,1,0,0,1,0,0,0,0,0,0,1,1,2,1,1,0,3,0,1,2,1,4,3,2	1	0.720	0.512
Test	EB	1SWASPJ221518.98-245927.0	0,3,9,13,18,22,23,24,22,20,14,12,9,8,10,14,17,20,21,24,24,21,18,7,3	1,0,0,2,0,0,0,1,1,2,1,0,1,1,2,0,0,1,2,0,2,2,2,1,3	1	0.751	0.222
Test	EB	1SWASPJ221922.26-165333.4	0,7,16,21,23,24,24,24,22,20,17,15,14,15,17,20,22,23,24,24,23,21,16,7,0	2,0,0,0,0,0,0,2,0,0,0,0,0,0,1,2,2,2,0,0,2,2,2,3,5	1	0.929	0.388
Test	EB	1SWASPJ222101.89-065751.4	0,1,7,14,20,21,23,23,21,19,17,15,13,13,14,16,19,21,22,24,23,20,18,13,5	1,1,0,0,0,1,0,1,0,0,0,0,0,0,3,2,1,1,1,2,2,3,1,3,1	1	0.026	0.494
Test	EB	1SWASPJ224553.28+010258.8	0,7,16,21,23,24,24,24,23,23,22,20,17,17,17,19,21,23,24,24,24,23,21,19,13,3	1,0,0,1,0,0,0,1,0,0,0,0,0,0,1,0,0,1,3,0,2,1,3,1,5,5	1	0.823	0.604
Test	EB	1SWASPJ225854.49+145145.4	0,2,9,15,20,22,24,24,24,22,18,14,12,12,14,18,20,22,23,22,21,18,14,8,2	1,0,2,0,0,0,0,0,1,1,0,0,2,0,3,1,0,0,3,0,2,1,4,1,3	1	-0.182	0.624
Test	EB	1SWASPJ230757.13+501143.8	0,5,16,20,22,24,24,23,21,21,19,17,14,14,15,14,18,21,24,24,23,21,17,11,4	1,0,0,0,1,1,0,0,0,0,0,0,1,0,0,3,1,1,2,1,1,1,4,1,2,4	2	0.268	0.670
Test	EB	1SWASPJ231124.26+515231.3	0,1,9,17,21,24,24,24,22,20,18,15,12,12,13,16,18,21,23,23,23,19,16,11,3	1,1,0,1,0,0,0,0,0,1,0,1,2,1,0,1,2,1,2,1,1,2,1,3,3	1	0.880	0.588
Test	EB	1SWASPJ235258.91+572650.4	0,3,13,19,21,23,24,24,23,22,20,18,14,14,16,20,21,22,24,24,24,22,19,15,7	1,0,0,1,0,0,0,1,0,0,0,0,0,1,2,1,1,0,1,2,2,2,3,2,5	1	0.653	0.828

Appendix 1 continued...

EW

Reason	Class	WASP Object Id	X-pattern	Y-pattern	P-bin	Mode-mean	BMA
Train	EW	1SWASPJ001445.75-391435.5	0,2,9,15,19,22,24,24,23,21,17,10,5,2,6,11,16,20,22,22,21,19,15,9,3	1,0,2,1,0,1,1,0,0,2,1,1,0,0,0,2,1,1,0,2,1,2,3,1,2	1	0.780	0.810
Train	EW	1SWASPJ003627.94+213214.4	0,3,9,16,21,24,24,23,20,15,10,4,2,3,6,12,18,21,23,23,21,15,10,4,0	2,0,1,2,2,0,1,0,0,1,2,0,1,0,0,2,1,0,1,0,1,3,0,3,2	1	1.222	0.366
Train	EW	1SWASPJ004006.26+501415.5	0,4,12,18,21,24,24,24,23,21,16,10,5,5,11,16,20,23,24,24,23,20,17,10,3	1,0,0,1,1,2,0,0,0,0,2,1,1,0,0,0,2,1,1,0,2,2,0,3,5	1	1.084	0.722
Train	EW	1SWASPJ005851.93+030357.8	0,4,11,16,20,22,23,23,20,15,10,4,3,6,10,16,20,23,24,22,20,16,10,5,0	2,0,0,1,2,1,1,0,0,0,3,1,0,0,0,1,3,0,0,0,4,0,2,3,1	1	1.081	0.366
Train	EW	1SWASPJ010945.77-201259.5	0,3,9,15,18,19,20,21,19,17,13,8,3,3,8,14,18,21,23,24,22,21,17,11,4	1,0,0,3,1,0,0,0,2,1,0,1,0,1,1,1,0,2,2,2,1,3,1,1,1	1	0.875	0.218
Train	EW	1SWASPJ010945.90-201256.2	0,3,9,15,18,19,20,21,19,17,13,8,3,3,8,14,18,21,23,24,22,21,17,11,4	1,0,0,3,1,0,0,0,2,1,0,1,0,1,1,1,0,2,2,2,1,3,1,1,1	1	0.821	0.218
Train	EW	1SWASPJ011638.06-394231.3	0,4,10,17,20,23,24,23,21,16,10,3,0,2,7,13,17,20,22,22,20,18,13,5,1	2,1,1,1,1,1,0,1,0,0,2,0,0,2,0,0,1,2,1,0,3,1,2,2,1	1	0.985	0.414
Train	EW	1SWASPJ014933.69-193729.2	0,1,9,15,19,22,24,24,24,21,18,12,4,1,7,14,19,22,24,24,24,22,19,14,6	1,2,0,0,1,0,1,1,0,1,0,0,1,0,2,1,0,0,1,3,0,1,3,0,6	1	1.035	0.588
Train	EW	1SWASPJ020402.90+324933.5	0,2,9,16,20,22,24,24,23,21,17,11,4,3,7,14,19,21,23,24,23,20,18,12,4	1,0,1,1,2,0,0,1,0,1,0,1,1,0,1,0,1,1,1,1,2,2,1,3,3	1	0.780	0.274
Train	EW	1SWASPJ021214.06+443936.2	0,4,12,17,20,23,24,24,22,19,14,7,1,3,9,16,20,23,24,24,23,20,15,9,2	1,1,1,1,1,0,0,1,0,2,0,0,1,0,1,1,1,1,0,1,3,0,1,3,4	1	1.113	0.252
Train	EW	1SWASPJ022129.86+315846.2	0,1,8,15,19,22,24,23,21,18,14,7,0,0,3,11,17,21,23,24,24,22,17,11,5	3,1,0,1,0,1,0,1,1,0,0,2,0,0,1,1,0,2,1,1,0,2,2,2,3	1	1.092	0.524
Train	EW	1SWASPJ022152.51+383742.3	0,4,12,18,21,24,24,23,21,18,12,5,1,3,9,15,20,22,23,23,21,18,14,6,1	1,2,0,1,1,1,1,0,0,1,0,0,2,0,1,1,0,0,3,0,1,3,1,3,2	1	0.557	0.682
Train	EW	1SWASPJ023128.95+394119.4	0,6,14,19,22,24,24,24,22,19,15,9,5,6,12,16,20,22,23,22,21,18,15,8,2	1,0,1,0,0,1,2,0,1,1,0,0,1,0,1,2,1,0,1,2,1,1,4,1,3	1	0.492	0.626
Train	EW	1SWASPJ031010.79+425209.2	0,1,9,16,20,23,24,24,23,22,18,12,6,6,9,16,20,23,24,24,23,20,18,12,4	1,1,0,0,1,0,2,0,0,2,0,0,2,0,0,0,2,0,2,0,3,0,1,4,4	1	1.002	0.554
Train	EW	1SWASPJ034927.76+125443.8	0,4,12,17,21,23,24,24,23,20,16,10,3,3,9,15,20,22,24,24,23,20,17,10,3	1,0,0,3,1,0,0,0,0,1,2,0,1,0,0,1,1,2,0,0,3,1,1,3,4	1	0.984	0.484
Train	EW	1SWASPJ165551.90+245336.1	0,3,10,16,20,23,24,24,22,19,14,8,2,2,7,14,19,22,24,24,22,20,16,10,3	1,0,2,2,0,0,0,1,1,0,2,0,0,0,2,0,2,0,0,2,2,0,3,1,4	1	1.075	0.482
Train	EW	1SWASPJ165819.77+334021.5	0,5,11,16,19,21,22,21,19,16,11,5,1,4,10,15,20,23,24,24,23,20,15,8,1	1,2,0,0,1,2,0,0,1,0,1,2,0,0,0,2,2,0,0,2,2,2,1,2,2	1	0.958	0.520
Train	EW	1SWASPJ171239.43+330800.8	0,3,9,14,19,22,24,22,19,16,11,4,0,1,6,13,18,22,24,24,23,19,13,8,2	2,1,1,1,0,1,0,1,1,0,1,0,2,1,0,1,0,1,3,0,0,3,1,3,1	1	1.032	0.374
Train	EW	1SWASPJ171824.84+222851.3	0,8,13,18,21,23,23,22,20,16,11,5,4,9,14,18,21,24,24,24,21,19,14,5,0	2,0,0,0,1,2,0,0,1,1,0,1,0,1,2,0,1,0,2,1,1,3,1,2,3	1	1.195	0.456
Train	EW	1SWASPJ171839.93+355426.2	0,5,12,18,21,23,24,24,22,19,15,8,2,4,11,16,20,23,24,24,23,20,17,10,2	1,0,2,0,1,1,0,0,1,0,1,1,1,0,0,1,1,1,1,1,2,1,1,3,4	1	1.051	0.780
Train	EW	1SWASPJ172441.57+135358.0	0,5,12,18,22,23,24,24,23,20,15,7,4,5,11,18,20,22,23,22,21,18,14,8,0	2,0,0,0,1,2,0,1,1,0,0,1,1,0,1,1,0,0,3,0,2,1,3,3,2	1	1.151	0.502
Train	EW	1SWASPJ173454.27+441152.7	0,3,10,16,17,19,20,22,20,15,11,5,0,2,9,14,19,23,24,24,22,20,15,8,1	2,1,1,1,0,1,0,0,1,1,1,1,0,0,1,2,1,1,0,2,3,0,2,1,2	1	0.669	0.554
Train	EW	1SWASPJ173920.60+354210.5	0,6,13,18,22,23,24,24,21,17,13,5,2,5,11,16,20,22,23,22,21,18,14,7,0	2,0,1,0,0,2,1,1,0,0,0,1,0,2,1,0,1,1,2,0,1,2,3,2,2	1	0.855	0.232
Train	EW	1SWASPJ174310.98+432709.6	0,4,12,17,20,23,24,24,22,19,14,8,4,5,11,16,20,23,24,24,22,19,15,9,2	1,0,1,0,2,1,0,0,1,1,0,1,1,0,1,1,1,1,0,2,2,0,2,2,4	1	0.842	0.600
Train	EW	1SWASPJ180835.75+334204.9	0,1,7,14,20,23,24,24,23,20,15,9,3,2,5,12,17,21,23,23,23,21,17,11,4	1,1,1,1,1,1,0,1,0,1,0,1,1,0,1,1,0,2,0,0,2,2,0,5,2	1	0.995	0.530
Train	EW	1SWASPJ185052.36+434012.2	0,4,12,17,20,22,23,23,21,18,14,8,2,5,11,17,21,23,24,24,23,21,17,10,2	1,0,2,0,1,1,0,0,1,0,1,1,1,0,1,0,0,3,1,0,1,3,1,4,2	1	0.949	0.466
Train	EW	1SWASPJ185343.51+372336.1	0,3,10,13,17,19,20,18,16,13,9,5,2,3,7,12,17,20,23,24,23,20,14,8,4	1,0,1,2,1,1,0,1,1,1,1,0,1,2,1,0,1,2,1,1,3,0,0,2,1	1	0.737	0.352
Train	EW	1SWASPJ185538.18+405857.5	0,6,13,19,22,24,24,24,24,21,18,11,4,6,13,18,22,23,24,23,22,20,16,11,3	1,0,0,1,1,0,2,0,0,0,0,2,0,2,0,0,1,0,2,1,1,1,3,2,5	1	0.846	0.782
Train	EW	1SWASPJ191844.50-332459.3	0,4,10,17,19,22,24,24,22,20,14,7,3,2,9,16,21,23,24,24,23,20,16,9,3	1,0,1,2,1,0,0,1,0,2,1,0,0,0,1,0,2,1,0,1,2,1,2,2,4	1	0.823	0.364
Train	EW	1SWASPJ192954.98+485500.3	0,3,9,15,20,23,24,24,23,20,15,9,3,2,6,13,18,21,23,23,23,20,16,10,3	1,0,1,3,0,0,1,0,0,2,1,0,0,1,0,2,1,0,1,0,3,1,0,5,2	1	0.942	0.426
Test	EW	1SWASPJ041418.36-462657.1	0,5,12,18,21,23,24,24,22,20,16,9,4,5,11,16,20,22,23,23,22,20,17,10,3	1,0,0,1,1,2,0,0,0,1,1,1,1,0,0,0,2,1,1,0,3,1,3,3,2	1	0.969	0.804
Test	EW	1SWASPJ043424.83+082201.8	0,6,14,19,22,24,24,24,22,18,14,7,1,3,10,16,19,22,24,24,22,20,17,10,2	1,1,1,1,0,0,1,1,0,0,2,0,0,0,2,0,1,1,2,1,0,4,0,5	1	0.725	0.424
Test	EW	1SWASPJ050702.10-004732.6	0,4,10,18,22,24,24,22,17,11,6,3,2,4,8,14,20,22,24,23,19,12,6,2,0	2,0,2,1,2,0,2,0,1,0,1,1,1,0,1,0,0,1,1,1,1,0,3,1,3	1	1.097	0.170
Test	EW	1SWASPJ091303.58-445657.1	0,3,12,18,21,21,21,23,22,20,15,9,3,6,11,14,20,22,24,24,24,18,13,10,2	1,0,1,2,0,0,1,0,0,1,1,1,1,1,1,1,0,0,2,0,2,3,2,1,3	1	0.648	0.330
Test	EW	1SWASPJ114424.25+232123.0	0,1,7,14,18,21,22,23,22,20,16,11,6,5,8,14,18,22,24,24,24,22,19,13,2	1,1,1,0,0,1,1,1,1,0,0,1,0,1,2,0,1,0,2,1,1,1,4,1,3	1	1.004	0.766
Test	EW	1SWASPJ115757.23-360611.4	0,4,12,17,21,23,24,24,22,19,13,6,1,3,10,16,19,22,23,23,21,18,14,8,0	2,1,0,1,1,0,1,0,1,0,1,0,1,1,1,0,1,1,1,2,0,2,2,3,2	1	0.589	0.648
Test	EW	1SWASPJ120450.98-330922.1	0,4,12,18,21,24,24,24,23,19,15,9,3,5,11,17,20,23,24,24,23,20,16,8,1	1,1,0,1,1,1,0,0,1,1,0,1,1,0,0,1,1,1,1,1,2,1,0,3,5	1	0.858	0.672
Test	EW	1SWASPJ123204.91+262247.8	0,8,14,19,22,23,24,24,21,18,12,5,2,6,13,18,21,24,24,23,21,19,13,6,0	2,0,1,0,0,1,2,0,1,0,0,0,1,2,1,0,0,0,2,2,0,3,1,2,4	1	0.778	0.654
Test	EW	1SWASPJ123300.28+264258.3	0,2,9,14,18,21,22,22,21,19,15,10,5,4,8,14,19,22,23,24,23,21,18,12,4	1,0,1,0,2,1,0,0,1,1,1,0,1,0,2,1,0,0,2,2,0,3,3,2,1	1	0.916	0.588
Test	EW	1SWASPJ123305.52+270803.6	0,6,13,18,22,24,24,23,20,16,10,5,2,3,9,13,17,20,22,21,20,16,12,6,0	2,0,1,1,0,1,2,0,0,1,1,0,1,2,0,0,2,1,1,0,3,1,2,1,2	1	0.903	0.476
Test	EW	1SWASPJ124015.04-184800.9	0,3,9,14,18,22,24,24,20,15,8,3,0,1,6,12,17,20,22,21,18,14,10,5,0	3,1,0,2,0,1,1,0,1,1,1,0,1,0,2,1,0,1,2,0,2,1,2,0,2	1	0.917	0.194
Test	EW	1SWASPJ124337.23+384415.6	0,4,11,16,20,23,24,24,22,19,14,8,4,5,10,16,19,22,24,23,22,18,14,8,1	1,1,0,0,2,1,0,0,2,0,1,1,0,0,0,2,0,2,0,1,2,1,0,3,2,3	1	1.115	0.460
Test	EW	1SWASPJ125121.44+271346.8	0,4,11,16,19,21,22,22,19,16,11,5,2,5,12,17,21,23,24,24,21,18,13,4,0	2,0,1,0,2,2,0,0,0,0,0,2,1,1,0,0,2,1,1,2,0,3,2,1,2	1	0.793	0.604
Test	EW	1SWASPJ125849.71-365832.9	0,1,6,12,18,22,24,24,22,20,15,8,2,1,5,11,16,20,22,23,22,19,16,11,5	1,2,1,0,0,2,1,0,1,0,0,2,1,0,0,1,2,0,1,1,2,0,4,1,2	1	1.016	0.482
Test	EW	1SWASPJ134325.64+043656.9	0,4,12,17,21,24,24,24,21,16,11,5,1,3,8,14,19,22,24,24,21,17,13,6,0	2,1,0,1,1,1,1,0,1,0,0,1,1,1,1,0,1,2,0,1,0,3,1,0,5	1	1.211	0.474
Test	EW	1SWASPJ203105.27+384701.8	0,8,15,19,22,24,24,23,21,18,13,7,4,8,15,19,22,24,24,24,22,19,14,6,0	2,0,0,0,1,0,1,1,2,0,0,0,0,1,1,2,0,0,1,3,0,1,3,1,5	1	1.017	0.568
Test	EW	1SWASPJ204813.27-012925.7	0,6,13,18,21,23,24,23,21,17,12,5,2,5,11,16,20,23,24,24,22,19,14,7,0	2,0,1,0,0,2,1,1,0,0,0,1,1,1,0,1,1,1,1,1,2,1,3,3,1	1	1.136	0.524
Test	EW	1SWASPJ210316.60-184154.5	0,3,11,17,21,23,24,24,22,20,15,9,4,4,9,15,19,22,24,24,23,20,17,11,3	1,0,0,2,2,0,0,0,0,2,0,2,0,0,0,2,0,2,0,1,2,1,2,2,4	1	1.028	0.484
Test	EW	1SWASPJ211205.73+312307.9	0,1,7,14,19,22,24,24,21,18,14,10,5,4,4,8,13,16,18,19,18,18,13,9,3	1,1,0,1,2,1,0,1,1,1,1,0,0,2,2,0,1,0,4,2,0,1,1,0,2	1	0.621	0.546
Test	EW	1SWASPJ212317.48-151052.0	0,4,12,17,21,23,24,23,21,17,12,5,2,4,11,16,20,23,24,24,22,19,13,5,0	2,0,1,0,2,2,0,0,0,0,0,1,2,1,0,0,1,2,0,1,1,2,1,3,3	1	0.898	0.612
Test	EW	1SWASPJ213849.39+264134.2	0,4,12,17,20,22,23,22,20,17,12,6,3,6,12,18,21,24,24,24,22,19,14,6,0	2,0,0,1,1,0,3,0,0,0,0,0,0,3,0,1,0,0,2,1,1,2,1,3,1,3	1	0.946	0.646
Test	EW	1SWASPJ213852.12+280545.1	0,4,12,17,21,23,24,23,21,16,10,3,1,2,9,15,19,22,23,22,20,17,11,3,0	2,1,1,2,1,0,0,0,0,1,1,1,1,0,0,1,1,2,0,1,1,2,2,3,1	1	0.878	0.542
Test	EW	1SWASPJ221107.43-193133.2	0,1,7,14,19,22,24,24,23,21,16,9,3,2,5,10,16,21,23,24,23,21,17,13,6	1,1,1,1,0,1,1,1,0,1,1,0,0,1,1,0,2,1,0,1,0,3,1,3,3	1	0.810	0.494
Test	EW	1SWASPJ221539.71-254442.1	0,5,10,16,19,23,23,22,20,15,9,5,3,5,10,17,21,24,24,24,21,17,12,5,0	2,0,0,1,0,4,0,0,0,1,2,0,1,0,0,1,1,2,0,1,1,2,1,2,3	1	0.667	0.394
Test	EW	1SWASPJ221954.11-050150.2	0,3,11,18,21,23,24,24,23,20,16,10,4,5,10,15,19,22,23,23,22,20,16,9,2	1,0,1,1,1,1,0,0,0,1,2,1,0,0,0,1,2,0,1,1,2,1,2,4,2	1	0.880	0.368
Test	EW	1SWASPJ222017.84-200650.8	0,6,14,19,22,24,24,24,21,18,12,6,2,5,11,16,20,22,23,23,21,18,13,5,0	2,0,1,0,0,2,2,0,0,0,0,1,1,1,1,0,1,0,2,1,1,2,2,2,3	1	0.829	0.364
Test	EW	1SWASPJ222256.88+161927.8	0,5,13,18,21,23,24,23,21,17,12,4,1,4,10,16,20,22,23,22,20,17,12,4,0	2,1,0,0,3,1,0,0,0,0,1,0,2,1,0,0,1,2,1,0,2,2,2,3,1	1	1.020	0.640
Test	EW	1SWASPJ222652.14-192510.4	0,6,13,18,22,24,24,24,22,18,12,5,1,4,11,17,21,23,24,24,22,19,15,7,0	2,1,0,0,1,1,1,1,0,0,0,1,1,1,0,1,0,1,2,1,0,1,3,1,5	1	0.854	0.716
Test	EW	1SWASPJ233916.16-090905.2	0,5,12,18,22,24,24,23,19,15,10,5,3,4,8,13,17,20,21,22,20,17,12,5,0	2,0,0,1,1,3,0,0,1,0,1,0,2,1,0,1,0,2,1,1,2,1,2,1,2	1	1.035	0.378
Test	EW	1SWASPJ235758.47+155710.0	0,5,12,17,21,23,24,24,22,19,14,7,2,4,10,16,20,23,24,24,22,19,14,8,1	1,1,1,0,1,1,0,1,1,0,1,0,1,0,2,0,1,1,0,2,1,1,2,2,4	1	1.121	0.548

Appendix 1 continued...

RM

Reason	Class	WASP Object Id	X-pattern	Y-pattern	P-bin	Mode-mean	BMA
Train	RMS	1SWASPJ000315.18+483253.4	0,1,3,6,9,10,14,17,21,22,24,24,23,24,22,21,19,16,14,13,9,6,3,2,1	1,2,1,2,0,0,2,0,0,2,1,0,0,1,2,0,1,1,0,1,0,2,2,1,3	1	-0.747	0.150
Train	RMS	1SWASPJ000756.23+143504.3	0,4,5,9,9,14,16,18,22,21,24,21,21,19,17,15,12,10,7,4,3,0,0,1,1	3,2,0,1,2,1,0,1,0,2,1,0,1,0,1,1,1,1,1,0,3,1,0,1	1	0.145	0.146
Train	RMS	1SWASPJ001008.14+261723.1	0,3,6,9,12,14,17,20,21,23,24,24,24,23,22,21,19,16,14,11,8,4,2,0,0	3,0,1,1,1,0,1,0,1,1,0,1,1,0,2,0,1,1,0,1,1,2,1,2,3	1	0.685	0.232
Train	RMS	1SWASPJ003846.78+204447.5	0,1,2,6,10,14,17,19,21,24,24,23,23,24,23,21,18,17,13,9,5,2,1,0,0	3,2,2,0,0,1,1,0,0,1,1,0,0,1,1,0,0,2,1,1,0,2,0,3,3	1	0.685	0.324
Train	RMS	1SWASPJ004406.89+492120.6	0,2,4,6,9,14,14,17,24,21,24,24,22,24,21,19,15,14,12,10,7,8,3,1,1	1,2,1,1,1,0,1,1,1,1,1,0,1,0,3,1,0,1,0,2,1,0,4	1	0.217	0.146
Train	RMS	1SWASPJ005555.11+495015.3	0,2,3,6,9,12,15,16,19,20,22,24,24,22,21,19,18,15,12,10,6,3,2,2,1	1,1,3,2,0,0,2,0,0,1,1,0,2,0,0,2,1,0,1,2,1,1,2,0,2	1	0.787	0.204
Train	RMS	1SWASPJ005615.32+220011.5	0,2,4,7,12,12,16,19,22,23,24,24,24,20,18,16,13,14,3,8,5,3,2,0,1	2,1,2,2,1,1,0,1,1,0,0,0,2,1,1,0,2,0,1,1,1,0,1,1,3	1	-0.689	0.128
Train	RMS	1SWASPJ010029.85+360358.0	0,2,6,10,12,14,16,17,19,21,22,24,24,24,19,19,17,15,13,12,8,6,3,1,0	2,1,1,1,0,0,2,0,1,0,1,0,2,1,1,1,1,2,0,3,0,1,1,0,3	1	0.664	0.310
Train	RMS	1SWASPJ011331.07+263921.0	0,1,4,6,9,12,14,17,20,21,22,24,23,24,22,22,18,16,14,11,9,6,3,1,0	2,2,0,1,1,0,2,0,0,2,0,1,1,0,2,0,1,1,1,0,1,1,3,1,2	1	0.821	0.232
Train	RMS	1SWASPJ012158.12+451757.6	0,4,6,12,9,13,15,19,21,23,22,24,24,22,22,23,16,15,12,8,6,6,1,0,1	2,2,0,0,1,0,3,0,1,1,0,0,2,1,0,2,1,0,0,1,0,1,3,2,2	1	0.029	0.064
Train	RMS	1SWASPJ013551.17+301928.7	0,2,3,6,7,9,13,18,20,24,22,23,23,19,19,19,15,12,9,7,6,3,1,0,0	3,1,1,2,0,0,2,2,0,2,0,0,1,1,0,1,0,0,1,3,1,0,1,2,1	1	-0.737	0.140
Train	RMS	1SWASPJ015348.34+141411.9	0,1,1,7,7,10,14,15,18,20,22,24,24,24,19,18,21,13,15,10,8,6,3,2,2	1,2,2,1,0,0,1,2,1,0,2,0,0,1,1,2,0,0,2,1,1,1,1,0,3	1	0.211	0.066
Train	RMS	1SWASPJ022730.04+360524.9	0,3,4,6,9,12,15,13,17,22,20,24,24,23,21,19,18,16,13,9,7,6,2,2,0	2,0,2,1,1,0,2,1,0,2,0,0,1,2,0,1,1,1,1,1,1,1,1,1,2	1	0.344	0.084
Train	RMS	1SWASPJ023201.43+062054.7	0,1,3,6,8,11,15,17,20,20,24,24,24,23,22,21,19,18,15,12,9,6,4,2,1	1,2,1,1,1,0,2,0,1,1,0,1,1,0,0,2,0,1,1,1,2,1,1,1,3	1	-0.370	0.196
Train	RMS	1SWASPJ025926.81-122251.7	0,1,3,6,9,14,16,20,21,24,24,24,23,22,20,17,14,11,9,6,4,4,1,0,0	3,2,0,1,2,0,2,0,0,2,0,1,0,0,2,0,1,1,0,0,2,1,1,1,3	1	-0.647	0.164
Train	RMS	1SWASPJ030615.55+001252.8	0,3,4,5,9,10,13,17,19,22,22,22,24,24,20,20,16,14,14,8,7,3,3,0,0	3,0,0,3,1,1,0,1,1,1,1,1,0,0,1,2,0,1,1,0,1,2,0,3,0,2	1	0.676	0.070
Train	RMS	1SWASPJ030930.98-454021.2	0,3,4,8,10,14,16,19,20,22,23,24,24,24,23,22,20,17,16,13,10,6,4,1,0	2,1,0,1,2,0,1,0,1,0,2,0,0,1,1,0,2,1,0,1,2,0,2,2,3	1	0.867	0.312
Train	RMS	1SWASPJ031821.06+404556.0	0,4,5,4,9,13,12,19,21,21,24,24,23,22,18,16,12,11,7,8,6,4,5,1,1	1,2,0,0,3,2,1,1,1,1,0,1,2,1,0,0,1,0,1,1,0,2,1,1,2	1	0.235	0.042
Train	RMS	1SWASPJ032027.47-165027.2	0,1,4,8,11,14,16,18,20,22,23,24,24,24,23,21,20,18,15,13,10,7,3,1,0	2,2,0,1,1,0,0,1,1,0,1,1,0,1,1,1,1,0,2,0,2,1,1,2,3	1	0.921	0.294
Train	RMS	1SWASPJ032842.83+230010.9	0,1,1,4,6,9,15,14,18,20,23,23,24,24,24,21,21,19,17,14,9,6,3,4,1	1,3,0,1,2,0,2,0,0,2,0,0,0,0,2,1,0,1,1,1,2,0,2,3	1	0.023	0.228
Train	RMS	1SWASPJ033205.43+130250.7	0,3,5,6,7,9,16,16,19,20,22,24,22,22,18,20,16,15,13,12,4,6,2,0,0	3,0,1,1,1,1,2,1,0,1,0,0,1,1,0,1,3,0,1,1,2,0,3,0,1	1	0.173	0.146
Train	RMS	1SWASPJ035139.63+144748.0	0,1,3,7,9,12,14,16,18,20,22,24,23,20,18,15,12,10,8,6,4,2,1,0,0	3,2,1,1,1,0,1,1,1,1,1,0,2,0,1,1,1,0,2,0,2,0,1,1,1	1	-0.694	0.126
Train	RMS	1SWASPJ040139.45+471009.6	0,2,3,4,7,8,12,14,19,21,24,23,23,23,21,21,17,15,15,10,8,6,4,2,2	1,0,3,1,2,0,1,1,2,0,1,0,1,0,1,2,0,1,0,1,0,3,0,3,1	1	-0.198	0.100
Train	RMS	1SWASPJ040209.48+114823.6	0,1,4,6,9,12,14,17,20,21,23,24,24,23,22,20,18,15,12,10,8,5,2,1,0	2,2,1,0,1,1,0,1,1,1,0,2,0,1,1,0,1,1,0,2,1,1,2,2,2	1	0.903	0.202
Train	RMS	1SWASPJ040347.68-025150.7	0,3,2,6,9,11,14,16,18,22,23,23,24,22,20,19,16,14,9,6,4,3,0,0,0	4,0,1,2,1,0,2,0,0,2,0,1,0,0,2,0,2,0,1,1,1,0,2,2,1	1	0.712	0.126
Train	RMS	1SWASPJ040522.20-344947.5	0,1,4,6,7,10,14,13,19,21,24,23,24,21,19,15,13,11,6,3,4,3,2,0,0	3,1,1,2,2,0,2,1,0,0,1,1,0,2,1,1,0,0,0,2,0,2,0,1,2	1	-0.306	0.066
Train	RMS	1SWASPJ040723.08-120938.3	0,1,3,6,9,11,14,18,19,23,24,24,23,24,21,20,17,13,12,9,5,3,1,1,0	2,3,0,2,0,1,1,0,0,2,0,1,1,1,1,0,0,1,1,1,1,1,0,2,3	1	-0.859	0.094
Train	RMS	1SWASPJ050127.77-443419.6	0,5,8,12,16,19,20,21,22,23,24,23,23,22,21,21,18,14,13,8,4,1,0,0,0	4,1,0,0,1,1,0,0,2,0,0,0,1,1,1,0,1,0,1,1,1,3,2,3,1	1	0.459	0.254
Train	RMS	1SWASPJ091602.64-130444.7	0,1,3,6,8,12,14,17,19,22,23,24,24,24,23,22,20,17,15,13,10,7,4,1,0	2,2,0,1,1,0,1,1,1,0,1,0,1,1,1,1,0,2,0,1,1,0,2,2,3	1	1.123	0.126
Train	RMS	1SWASPJ192716.66-321643.1	0,2,4,7,10,11,15,17,20,23,21,24,24,23,23,21,20,18,13,11,7,4,3,1,0	2,1,1,1,2,0,0,2,0,0,1,2,0,1,0,1,0,1,1,0,2,2,0,3,2	1	0.079	0.066
Test	RMS	1SWASPJ044145.54-180943.5	0,1,3,6,9,11,14,17,20,22,24,24,24,24,22,20,18,14,12,9,6,3,1,0,0	3,2,0,2,0,0,2,0,0,2,0,1,1,0,2,0,0,1,1,0,2,0,2,0,4	1	1.195	0.108
Test	RMS	1SWASPJ180722.01+292903.5	0,2,4,6,9,13,14,16,19,21,23,23,24,24,22,20,20,15,14,12,9,6,4,2,0	2,0,2,0,2,0,2,0,0,2,0,0,1,1,2,1,1,0,0,1,2,1,1,2,2	1	0.013	0.138
Test	RMS	1SWASPJ192712.87-415420.9	0,2,1,4,6,9,12,15,18,21,22,24,24,24,23,21,19,17,14,11,8,6,3,3,1	1,2,1,2,1,0,2,0,1,1,0,1,1,0,1,1,1,0,2,1,1,3	1	0.919	0.140
Test	RMS	1SWASPJ192934.16-414629.4	0,1,4,7,10,12,17,20,22,22,24,22,22,20,18,14,13,9,8,4,3,3,1,0,1	2,3,0,2,2,0,0,1,1,1,1,0,1,1,1,0,0,1,1,0,2,0,4,0,1	1	-0.641	0.130
Test	RMS	1SWASPJ193037.16-422747.6	0,2,6,7,10,13,16,19,20,23,23,24,21,24,20,18,15,15,12,9,6,5,2,1,0	2,1,2,0,0,1,2,1,0,1,1,0,1,1,0,2,1,0,1,1,2,1,0,2,2	1	-0.093	0.094
Test	RMS	1SWASPJ193249.23+441434.1	0,2,3,8,10,14,16,19,20,22,23,24,22,21,19,18,16,14,11,8,5,3,1,0,0	3,1,1,2,0,1,0,0,2,0,1,1,0,0,2,0,2,0,1,2,1,1,2,1,1	1	0.249	0.090
Test	RMS	1SWASPJ194108.19-300830.7	0,1,2,4,7,8,13,14,18,20,22,22,24,24,24,22,18,19,17,15,13,9,7,3,3	1,1,1,2,1,0,0,2,1,1,0,0,0,2,1,1,0,1,2,1,1,0,3,0,3	1	0.542	0.164
Test	RMS	1SWASPJ194333.91+440619.6	0,1,2,4,8,10,14,17,20,22,23,24,24,23,21,18,16,14,10,6,5,2,1,0,0	3,2,2,0,1,1,1,0,1,0,2,0,0,0,2,0,1,1,1,0,1,1,1,2,2	1	-0.389	0.062
Test	RMS	1SWASPJ200250.82-365310.7	0,2,4,8,10,11,16,16,21,23,20,22,24,24,22,20,19,17,15,13,9,6,5,3,2	1,0,2,1,1,1,0,1,1,1,1,0,1,0,1,2,1,0,1,2,1,2,1,2,2	1	-0.090	0.104
Test	RMS	1SWASPJ200304.30+590654.6	0,1,1,5,6,10,14,17,20,22,24,24,23,22,20,16,14,12,9,6,5,3,1,0,0	3,3,0,1,0,2,2,0,0,1,1,0,1,0,2,0,1,1,0,0,2,0,2,1,2	1	-0.527	0.106
Test	RMS	1SWASPJ200338.23-203940.1	0,1,4,6,9,10,15,17,20,23,23,24,22,24,22,22,18,14,12,10,7,5,3,1,0	2,2,0,1,1,1,1,1,0,1,2,0,1,0,1,1,0,1,1,0,1,0,3,2,2	1	-0.585	0.170
Test	RMS	1SWASPJ200517.78+092715.7	0,2,3,7,10,12,13,15,19,23,24,24,24,23,20,20,15,14,11,7,6,1,3,2,0	2,1,2,2,0,0,1,2,0,0,1,1,1,1,1,2,0,0,0,1,2,0,0,2,3	1	0.058	0.126
Test	RMS	1SWASPJ200733.17+452318.4	0,3,4,7,9,12,15,16,19,22,24,24,24,24,24,22,20,17,15,12,10,6,6,4,1,0	2,1,0,1,2,0,2,1,0,1,1,0,2,0,0,2,1,1,0,1,1,0,2,0,4	1	0.042	0.100
Test	RMS	1SWASPJ200735.76-274009.3	0,2,2,4,6,10,10,14,18,19,23,24,24,23,23,23,20,18,13,12,8,5,6,2,0	2,0,3,0,1,1,2,0,1,0,2,0,1,1,1,0,0,0,2,1,1,0,0,4,2	1	0.810	0.108
Test	RMS	1SWASPJ203253.01+474425.8	0,4,3,6,10,11,15,17,21,21,23,24,23,24,19,17,15,15,10,8,5,3,2,1,1	1,2,1,2,1,1,1,0,1,0,2,1,0,0,0,3,0,2,0,1,0,2,0,2,2	1	-0.315	0.044
Test	RMS	1SWASPJ205033.90+131643.5	0,1,2,3,6,9,13,18,20,22,24,24,24,23,21,17,14,11,9,6,4,2,1,0,0	3,2,2,1,1,0,2,0,0,2,0,1,0,1,1,0,0,1,1,0,1,1,1,1,3	1	-0.992	0.212
Test	RMS	1SWASPJ211720.29-415141.5	0,1,2,6,9,12,16,19,20,22,21,22,23,24,23,22,20,17,15,14,12,9,5,2,1	1,2,2,0,0,1,1,0,0,2,0,0,2,0,1,1,1,1,0,1,2,1,3,2,1	1	0.673	0.216
Test	RMS	1SWASPJ211720.52-415119.4	0,3,7,10,14,16,19,22,22,23,23,24,24,23,21,19,18,14,11,10,7,2,0,0,0	4,0,1,1,0,0,0,2,0,0,2,1,0,0,2,0,1,0,1,2,0,1,2,3,2	1	0.071	0.198
Test	RMS	1SWASPJ214122.57-031342.8	0,2,4,6,10,12,15,18,20,23,23,24,22,23,21,18,16,13,10,7,4,3,1,0,0	3,1,1,1,2,0,1,1,0,0,2,0,1,1,0,1,1,0,2,0,1,1,1,3,1	1	-0.780	0.214
Test	RMS	1SWASPJ215123.19-415536.7	0,1,3,4,7,10,13,15,19,21,24,24,24,24,23,21,19,15,13,10,8,6,3,2,1	1,2,1,2,1,0,1,1,1,0,2,0,0,2,0,2,0,0,2,0,2,0,1,4	1	-0.681	0.118
Test	RMS	1SWASPJ215138.89+283709.6	0,2,2,6,8,10,14,17,19,23,24,23,23,24,21,21,18,16,11,10,6,3,4,1,1	1,2,2,1,1,0,2,0,1,0,2,1,0,0,1,0,1,1,1,1,0,2,0,3,2	1	0.688	0.200
Test	RMS	1SWASPJ215349.16-262322.5	0,1,1,3,7,9,13,14,18,20,22,23,24,24,24,22,21,18,15,13,11,8,6,3,2	1,2,1,2,0,0,1,1,1,1,0,1,0,2,1,1,0,0,2,0,1,1,2,1,3	1	0.609	0.174
Test	RMS	1SWASPJ215711.96+304349.0	0,2,3,7,9,12,14,17,19,20,22,24,24,23,20,19,18,14,12,9,7,2,2,1,0	2,1,3,1,0,0,0,2,0,2,0,0,2,0,2,0,0,1,1,2,2,0,1,1,2	1	0.600	0.120
Test	RMS	1SWASPJ221016.22+203327.3	0,1,2,5,8,10,15,19,22,22,23,24,23,21,20,17,15,12,9,7,6,3,1,1,0	2,3,1,1,0,1,1,1,1,1,1,0,1,0,0,2,0,1,0,1,1,1,2,2,1	1	0.096	0.058
Test	RMS	1SWASPJ221409.90+304002.2	0,2,4,6,9,12,15,19,21,23,24,24,24,23,22,19,15,12,9,6,4,2,0,0,0	4,0,2,0,2,0,2,0,0,2,0,0,2,0,0,2,0,0,0,2,0,1,1,2,3	1	-0.969	0.060
Test	RMS	1SWASPJ221505.51-261532.8	0,2,3,6,10,12,15,16,21,23,23,24,23,24,20,19,15,13,11,10,7,4,2,1,0	2,1,2,1,1,0,1,1,0,0,2,1,1,1,0,2,1,0,0,1,1,1,0,3,2	1	-0.080	0.124
Test	RMS	1SWASPJ222117.83+471928.8	0,2,4,7,10,10,15,17,21,22,23,24,24,24,22,17,17,14,10,8,6,3,2,2,0	2,0,3,1,1,0,1,1,1,0,3,0,0,0,1,1,0,3,0,0,0,1,2,1,3	1	-0.250	0.096
Test	RMS	1SWASPJ222236.11+221526.5	0,2,3,7,10,12,18,20,21,22,24,24,24,23,20,19,16,13,10,6,5,2,1,1,0	2,2,2,1,0,1,1,1,0,0,2,0,1,1,0,0,1,0,1,1,2,1,1,1,3	1	0.085	0.100
Test	RMS	1SWASPJ225638.52-221333.4	0,1,3,6,9,11,14,17,20,22,24,24,24,24,23,22,20,17,15,12,9,6,3,1,0	2,2,0,2,0,0,2,0,0,2,0,1,1,0,1,1,0,2,0,0,2,0,2,1,4	1	1.085	0.250
Test	RMS	1SWASPJ235608.41+380306.3	0,1,4,7,10,13,15,18,21,22,23,24,24,24,22,20,18,15,13,10,7,4,2,0,0	3,1,1,0,2,0,0,2,0,0,2,0,0,2,0,0,2,0,0,2,0,1,1,2,3	1	1.148	0.230

Appendix 1 continued...

RRAB

Reason	Class	WASP Object Id	X-pattern	Y-pattern	P-bin	Mode-mean	BMA
Train	RRAB	1SWASPJ000003.66+352146.1	0,2,14,24,24,21,17,15,12,10,8,8,6,5,4,2,1,0,0,0,0,0,1,2,0	7,2,3,0,1,1,1,0,2,0,1,0,1,0,1,1,0,1,0,0,0,1,0,0,2	1	-0.928	0.736
Train	RRAB	1SWASPJ000248.10-245643.1	0,5,15,24,22,19,15,13,11,9,8,6,6,5,4,3,3,3,2,2,2,1,1,0,0	3,2,3,3,1,2,2,0,1,1,0,1,0,1,0,2,0,0,0,1,0,0,1,0,1	1	-0.652	1.196
Train	RRAB	1SWASPJ000405.10-165951.5	0,1,8,16,22,24,22,19,16,14,13,11,9,8,7,6,5,4,3,3,3,3,2,1,0	2,2,1,4,1,1,1,1,2,1,0,1,0,1,1,0,2,0,0,1,0,0,2,0,1	1	-0.712	0.628
Train	RRAB	1SWASPJ000658.70-293624.7	0,7,20,24,20,16,13,11,9,8,6,5,4,3,2,2,2,0,0,0,1,1,0,1,0	6,3,3,1,1,1,1,1,1,1,0,1,0,1,0,0,1,0,0,0,2,0,0,0,1	1	-0.637	0.716
Train	RRAB	1SWASPJ001141.10-014455.2	0,1,5,13,22,24,20,17,14,11,9,7,5,4,3,2,1,1,1,0,0,0,0,0,0	7,4,1,1,1,2,0,1,0,1,0,1,0,1,1,0,0,1,0,0,1,0,1,0,1	1	-0.783	0.860
Train	RRAB	1SWASPJ002343.08+292403.6	0,7,16,24,23,20,18,15,13,11,9,8,6,6,5,4,4,3,3,3,2,2,1,0,0	3,1,2,3,2,1,2,1,1,1,0,1,0,1,0,1,1,0,1,0,1,0,0,1,1	1	-0.509	0.884
Train	RRAB	1SWASPJ003338.28-152914.7	0,2,7,17,24,23,19,17,14,12,10,9,7,5,4,3,2,2,1,1,0,0,0,0,0	6,2,3,1,1,1,0,2,0,1,1,0,1,0,1,0,0,2,0,1,0,0,0,1,1	1	-0.874	0.744
Train	RRAB	1SWASPJ004631.92+450546.7	0,2,10,20,24,22,18,16,13,11,9,8,7,7,6,4,3,3,3,3,3,2,2,1,0	2,1,3,5,1,0,1,2,1,1,1,1,0,1,0,0,1,0,1,0,1,0,1,0,1	1	-0.548	0.820
Train	RRAB	1SWASPJ004818.65+372216.0	0,7,16,20,24,24,22,18,16,14,13,11,9,8,7,5,4,4,3,3,3,2,1,0,0	3,1,1,3,2,1,0,2,1,1,0,1,0,1,1,0,2,0,1,0,1,0,1,0,2	1	-0.505	0.468
Train	RRAB	1SWASPJ004904.31+022515.7	0,2,13,24,24,21,17,14,11,9,8,6,4,3,2,1,4,1,0,0,0,0,0,1,0	7,3,2,1,2,0,1,0,1,1,0,1,0,1,1,0,0,1,0,0,0,1,0,0,2	1	-0.683	0.984
Train	RRAB	1SWASPJ004934.85+270119.8	0,2,12,22,24,21,18,15,13,11,10,8,7,6,4,4,3,3,3,2,2,2,2,1,0	2,1,5,3,2,0,1,1,1,0,1,1,1,1,0,1,0,0,1,0,0,1,1,0,1	1	-0.657	0.866
Train	RRAB	1SWASPJ004935.02+022254.5	0,5,17,24,23,19,15,12,9,9,7,7,5,4,3,2,1,3,3,2,4,3,3,1,0	2,2,2,5,2,2,0,2,0,2,0,0,1,0,0,1,0,1,0,1,0,0,0,1,1	1	-0.501	0.916
Train	RRAB	1SWASPJ005558.57-262259.2	0,1,7,16,23,24,22,18,15,13,11,9,7,6,5,4,3,2,2,1,1,1,1,1,0	2,6,2,1,1,1,2,0,1,0,1,0,1,0,1,1,0,1,0,0,0,1,1,1,1	1	-0.807	0.838
Train	RRAB	1SWASPJ005639.89+371548.3	0,6,19,24,23,19,15,12,10,8,7,6,5,4,3,3,2,1,1,1,1,1,1,0,0	3,6,1,2,1,1,2,1,1,0,1,0,1,0,0,1,0,0,0,2,0,0,0,1,1	1	-0.686	0.992
Train	RRAB	1SWASPJ010040.30-155727.6	0,5,13,20,24,24,19,14,13,10,9,7,6,5,5,3,3,2,2,1,2,1,1,0,0	3,3,3,2,0,3,1,1,0,1,1,0,0,2,1,0,0,0,0,1,1,0,0,0,2	1	-0.690	0.980
Train	RRAB	1SWASPJ010308.31-253017.0	0,2,13,23,24,22,19,17,13,12,10,9,7,7,6,5,4,3,3,2,3,3,2,1,0	2,1,3,4,1,1,1,2,0,1,1,0,1,2,0,0,0,1,0,1,0,0,1,1,1	1	-0.577	0.624
Train	RRAB	1SWASPJ010725.81-321835.0	0,7,21,24,21,18,15,12,10,8,7,5,4,3,2,2,1,0,0,0,0,0,0,0,0	9,1,2,1,1,1,0,2,1,0,1,0,1,0,0,1,0,1,0,0,2,0,0,1	1	-0.726	0.982
Train	RRAB	1SWASPJ011103.63+572045.9	0,2,11,23,24,22,18,15,12,9,8,7,6,5,5,3,3,2,2,2,1,1,0,0,0	4,2,4,2,0,2,1,1,1,1,0,1,1,0,0,1,0,0,1,0,0,0,1,1,1	1	-0.814	0.820
Train	RRAB	1SWASPJ011727.41+385702.0	0,7,16,24,24,21,18,15,13,11,10,8,7,6,6,5,4,3,3,3,2,2,1,0,0	3,1,2,3,1,1,2,2,1,0,1,1,0,1,0,1,1,0,1,0,1,0,0,2	1	-0.765	0.940
Train	RRAB	1SWASPJ011814.97-391244.8	0,3,15,24,22,18,15,12,10,8,7,5,4,3,3,2,2,2,2,1,1,1,1,0,0	3,4,4,3,1,1,0,1,1,0,1,0,1,0,0,2,0,0,1,0,0,0,1,0,1	1	-0.849	1.194
Train	RRAB	1SWASPJ012253.56-261733.2	0,1,11,24,24,20,16,12,10,8,8,5,4,3,3,2,1,0,0,0,1,1,1,1,0	5,6,1,2,1,1,0,0,2,0,1,1,1,0,0,0,1,0,0,0,1,0,0,0,2	1	-0.718	1.240
Train	RRAB	1SWASPJ012642.43+340407.1	0,1,6,17,24,24,21,17,14,11,8,7,5,4,3,3,2,2,1,1,1,0,0,0,0	4,5,2,2,1,1,1,1,1,0,0,1,0,0,1,0,0,2,0,0,0,1,0,0,2	1	-0.724	0.844
Train	RRAB	1SWASPJ123335.16-324736.3	0,5,11,18,23,24,24,23,21,20,17,14,13,12,11,9,10,8,7,6,7,5,3,2,0,0	3,0,1,1,0,2,1,2,1,1,1,2,1,1,1,0,0,1,1,0,1,1,0,2,1	1	0.091	0.180
Train	RRAB	1SWASPJ141609.91-421947.5	0,5,12,24,24,24,21,18,14,14,13,11,6,7,4,4,6,3,7,0,0,0,5,4,6	4,0,0,1,3,2,3,2,0,0,0,1,1,1,2,0,0,0,1,0,0,1,0,0,3	1	0.099	0.130
Train	RRAB	1SWASPJ154535.82-194812.7	0,2,10,16,24,21,19,16,14,12,10,9,8,6,5,4,4,3,3,4,3,2,1,0,0	3,1,2,3,3,1,1,0,1,1,2,0,1,0,1,0,2,0,0,1,0,1,0,0,1	1	-0.334	0.674
Train	RRAB	1SWASPJ171233.01+203223.9	0,6,16,24,20,19,16,14,14,10,10,8,7,7,4,6,4,5,3,3,3,3,1,3,0	2,1,0,5,2,1,2,2,1,0,2,0,0,0,2,0,2,0,0,1,1,0,0,0,1	1	0.243	0.074
Train	RRAB	1SWASPJ190201.59-345513.4	0,2,7,15,20,24,24,22,18,16,15,13,10,10,8,8,7,4,6,4,3,4,2,2,0	2,0,3,1,3,0,1,2,2,0,2,0,0,1,0,2,1,0,1,0,1,0,1,0,2	1	-0.586	0.290
Train	RRAB	1SWASPJ191403.93-210347.8	0,3,12,21,24,22,19,16,11,12,13,12,7,5,7,5,9,3,2,6,0,1,0,4,0	4,1,1,2,1,2,1,2,0,1,0,1,3,1,0,0,1,0,0,1,0,1,1,0,1	1	0.268	0.146
Train	RRAB	1SWASPJ191736.58-214554.9	0,1,4,13,16,21,24,24,21,17,11,12,14,13,9,8,5,6,7,4,3,7,5,3,2	1,1,1,2,2,2,1,2,1,1,0,1,1,2,1,0,1,1,0,0,0,2,0,0,2	1	-0.124	0.158
Train	RRAB	1SWASPJ194209.17-394553.7	0,2,15,24,23,18,11,13,10,10,7,7,4,3,2,3,2,1,1,2,1,0,2,1,0	3,4,5,2,1,0,0,2,0,0,2,1,0,1,0,1,0,1,0,0,0,0,0,1,1	1	-0.112	0.160
Test	RRAB	1SWASPJ000018.15+193255.3	0,1,10,24,22,20,15,13,11,9,7,7,6,4,3,3,2,2,0,2,2,1,2,1,1	2,4,5,2,1,0,1,2,0,1,1,1,0,1,0,1,0,0,0,0,1,0,1,0,1	1	-0.102	0.858
Test	RRAB	1SWASPJ000023.75+361942.7	0,3,12,23,24,22,18,15,13,13,10,9,8,7,7,6,5,4,4,2,3,3,2,2,0	2,0,3,3,2,1,1,2,1,1,1,0,1,2,0,1,0,0,1,0,0,0,1,1,1	1	-0.542	0.874
Test	RRAB	1SWASPJ000049.23-284900.4	0,1,3,11,21,24,21,19,17,15,12,12,8,9,9,5,3,3,2,2,3,2,1,2,1	1,3,4,4,0,1,0,0,1,2,0,1,2,0,0,1,0,1,0,1,0,2,0,0,1	1	-0.287	0.436
Test	RRAB	1SWASPJ000321.17+032352.4	0,1,11,20,24,22,19,15,13,11,10,9,6,5,4,3,2,4,2,1,1,2,2,2,0	2,3,5,1,2,1,1,0,0,1,1,2,0,1,0,1,0,0,0,1,1,0,1,0,1	1	-0.682	0.764
Test	RRAB	1SWASPJ000347.51-112835.0	0,7,19,24,22,18,15,13,11,9,7,6,5,4,3,2,1,0,0,0,0,1,2,2,1	5,3,3,1,1,1,2,0,1,0,1,0,1,0,0,1,1,0,0,1,0,1	1	-0.768	0.766
Test	RRAB	1SWASPJ000620.83-351712.3	0,2,17,24,21,17,14,13,11,9,7,6,5,4,3,3,2,2,2,1,1,1,1,0,0	3,4,4,2,1,1,1,1,0,1,0,1,0,1,1,0,0,2,0,0,0,1,0,0,1	1	-0.688	1.116
Test	RRAB	1SWASPJ000652.94+114114.0	0,9,21,24,19,16,13,10,7,8,6,1,1,2,2,2,3,1,0,0,0,0,0,0,3,0	7,3,3,2,0,0,1,1,1,1,1,0,0,1,0,0,1,0,0,1,0,1,0,0,1	1	-0.421	0.884
Test	RRAB	1SWASPJ000940.57-003335.3	0,1,10,18,24,21,17,16,13,11,10,9,7,6,5,5,3,3,2,3,3,3,4,3,0	2,1,1,6,1,2,1,1,0,1,2,1,0,1,0,0,1,1,1,0,0,1,0,0,1	1	-0.096	0.348
Test	RRAB	1SWASPJ000942.43-003346.3	0,2,12,22,24,21,16,14,12,10,8,7,6,5,4,4,1,0,1,0,1,2,2,1,0	4,4,3,0,2,1,1,1,1,0,1,0,2,0,1,0,1,0,0,0,0,1,1,0,1	1	-0.240	0.284
Test	RRAB	1SWASPJ004119.42+052046.8	0,2,7,14,20,21,24,20,19,15,11,9,7,5,3,3,2,2,1,1,0,0,0,0,0	6,2,3,2,0,1,0,2,0,1,0,1,0,0,1,1,0,0,0,1,2,1,0,0,1	1	-0.603	0.938
Test	RRAB	1SWASPJ010144.87+304814.1	0,2,12,23,24,21,19,14,12,11,8,6,5,6,3,3,2,0,0,0,1,0,0,0,0	8,1,2,2,0,1,2,0,1,0,0,1,2,0,1,0,0,0,0,1,0,1,0,1,1	1	-0.341	0.770
Test	RRAB	1SWASPJ010440.69-450828.0	0,1,11,22,24,20,17,15,13,10,8,7,5,5,3,1,2,0,0,0,0,0,2,0,0	8,2,2,1,0,2,0,1,1,0,1,1,0,1,0,1,0,1,0,0,1,0,1,0,1	1	-0.644	0.780
Test	RRAB	1SWASPJ010510.70+341306.2	0,4,11,23,24,22,18,15,12,10,8,7,6,4,4,3,3,2,2,1,1,1,1,0,0	3,4,2,2,3,0,1,1,1,0,1,1,1,0,0,1,0,0,0,1,0,0,0,1,1	1	-0.767	1.078
Test	RRAB	1SWASPJ010600.28-001833.8	0,1,7,14,20,24,24,23,20,18,15,12,9,8,6,4,3,2,1,1,2,0,1,0,0,0	5,4,2,1,1,0,1,1,1,1,0,0,1,0,1,1,0,0,1,0,2,0,0,1,1	1	-0.717	0.656
Test	RRAB	1SWASPJ010846.81+363724.1	0,5,15,24,24,21,18,15,13,11,9,8,7,6,4,3,3,2,1,2,1,1,2,0,0	3,3,3,2,1,1,1,1,1,1,0,1,0,1,0,2,0,0,1,0,0,1,0,0,2	1	-0.720	0.302
Test	RRAB	1SWASPJ011548.34+394505.6	0,1,9,19,24,22,19,16,14,12,10,8,7,6,5,5,4,4,3,3,3,2,2,1,0	2,2,2,3,2,2,1,1,1,1,1,0,1,0,1,0,1,0,2,0,0,1,0,1,1	1	-0.837	0.882
Test	RRAB	1SWASPJ012624.36-273000.1	0,2,9,21,24,22,19,16,10,10,7,7,5,4,4,3,2,3,1,1,1,0,2,1,0	3,4,3,2,2,1,0,2,0,1,2,0,0,0,0,0,1,0,0,1,0,1,1,0,1	1	-0.431	0.690
Test	RRAB	1SWASPJ013208.17+012030.2	0,4,14,24,24,21,17,15,13,11,9,8,7,6,5,4,3,3,2,2,2,2,2,1,0	2,1,5,2,2,1,1,1,1,1,0,1,0,1,1,1,0,1,0,0,0,1,0,0,2	1	-0.858	0.886
Test	RRAB	1SWASPJ084212.77+074837.3	0,3,5,8,17,23,24,21,15,16,14,9,8,9,5,6,6,1,3,0,1,2,2,0,0	4,2,2,2,0,2,2,0,2,2,0,0,0,0,1,1,1,1,0,0,0,1,0,1,1	1	0.077	0.358
Test	RRAB	1SWASPJ122327.63-024004.7	0,5,9,15,20,24,21,23,17,14,12,10,9,7,6,6,3,3,3,3,2,2,1,2,0	2,1,3,4,0,1,2,1,0,2,1,0,1,0,1,1,0,1,0,0,1,1,0,1,1	1	-0.320	0.808
Test	RRAB	1SWASPJ132532.75+164944.2	0,4,6,10,10,14,17,21,24,22,21,18,17,17,13,9,8,8,7,6,6,2,2,0,0	3,0,2,0,1,0,3,1,2,1,2,0,0,1,1,0,0,3,1,0,0,2,1,0,1	1	-0.168	0.548
Test	RRAB	1SWASPJ192034.79-313821.9	0,3,9,11,16,22,24,23,18,17,17,19,18,15,14,10,8,6,5,7,6,6,6,2,3	1,0,1,2,0,1,4,1,1,1,1,1,0,0,1,1,1,2,2,1,0,0,1,1,1	1	-0.043	0.180
Test	RRAB	1SWASPJ194817.63-385750.0	0,5,16,21,24,23,19,17,15,13,8,9,8,11,7,5,3,3,4,1,5,3,2,0,4	2,1,1,3,2,3,0,1,2,1,0,1,0,1,0,1,1,1,0,1,0,1,0,1,1	1	0.098	0.248
Test	RRAB	1SWASPJ195948.74-444546.9	0,4,7,16,24,24,20,19,18,15,10,10,9,5,5,5,6,4,3,1,3,6,3,4,4	1,1,0,3,4,3,2,1,0,1,2,0,0,0,0,1,1,0,1,1,1,0,0,0,2	1	0.060	0.112
Test	RRAB	1SWASPJ200739.90-411024.6	0,6,16,24,24,21,20,17,13,12,11,9,9,7,4,6,2,4,6,5,3,1,2,0,1	2,2,2,1,2,1,3,1,0,2,0,1,1,1,0,0,1,1,0,0,1,1,0,0,2	1	-0.156	0.160
Test	RRAB	1SWASPJ200840.18-355855.4	0,6,14,22,24,24,23,18,17,13,10,10,9,7,7,5,3,4,3,5,6,3,0,0,1	3,1,0,3,1,2,2,2,0,1,2,0,0,1,1,0,0,1,1,0,0,0,1,1,2	1	-0.051	0.270
Test	RRAB	1SWASPJ201820.52-385401.2	0,8,18,20,24,24,22,18,17,14,13,12,9,8,8,6,7,5,4,3,2,3,2,2,0	2,0,3,2,1,1,1,1,3,1,0,0,1,1,1,0,0,1,2,0,1,0,1,0,2	1	-0.119	0.294
Test	RRAB	1SWASPJ203342.83-461236.1	0,2,12,19,24,21,15,17,13,12,12,10,6,6,6,6,3,3,2,0,3,4,3,1,0	3,1,2,4,1,0,4,0,0,0,1,0,3,1,0,1,0,1,0,1,0,0,1,0,1	1	-0.404	0.108
Test	RRAB	1SWASPJ205635.94-591003.1	0,4,16,24,23,15,16,10,9,6,7,5,5,3,4,2,2,1,0,0,3,1,1,2,0	4,3,3,2,2,2,1,1,0,1,1,0,0,0,0,1,2,0,0,0,0,0,0,1,1	1	-0.153	0.126
Test	RRAB	1SWASPJ234821.78-140824.4	0,3,16,24,23,18,15,12,10,8,8,6,5,3,3,2,2,1,1,2,2,2,1,0,0	3,3,5,3,0,1,1,0,2,0,1,0,1,0,0,1,1,0,1,0,0,0,0,1,1	1	-0.074	0.194

Appendix 1 continued...

RRC

Reason	Class	WASP Object id	X-pattern	Y-pattern	P-bin	Mode-mean	BMA
Train	RRC	1SWASPJ002829.53+473326.1	0,1,3,4,6,11,13,15,19,20,20,24,24,24,22,20,18,16,17,14,12,6,6,2,0	2,1,1,1,1,0,3,0,0,0,0,1,1,1,1,1,1,1,3,0,1,0,3	1	0.128	0.258
Train	RRC	1SWASPJ011823.10+503952.6	0,1,1,4,7,12,18,21,23,24,23,22,20,17,16,13,12,9,7,6,3,2,0,1,0	3,3,1,1,1,0,1,2,0,1,0,0,2,1,0,0,1,1,1,0,1,1,1,2,1	1	-1.014	0.244
Train	RRC	1SWASPJ011826.65+504018.4	0,2,4,9,15,19,23,24,24,23,21,19,16,15,12,10,8,6,3,2,1,0,0,0,0	5,1,2,1,1,0,1,0,1,1,1,0,1,0,0,2,1,0,0,2,0,1,0,2,2	1	-1.052	0.430
Train	RRC	1SWASPJ012016.82+142503.5	0,1,3,6,9,14,16,19,24,24,22,23,22,20,17,14,10,8,3,2,1,0,0,1,1	3,4,1,2,0,0,1,0,1,1,1,0,0,0,2,0,1,1,0,1,1,0,2,1,2	1	-0.799	0.408
Train	RRC	1SWASPJ050110.84+343026.6	0,2,6,10,13,16,19,21,23,24,24,24,24,23,21,18,16,13,10,6,2,0,0,0,0	5,0,2,0,0,0,2,0,0,0,2,0,0,2,0,0,2,0,1,1,0,2,0,2,4	1	-1.173	0.288
Train	RRC	1SWASPJ055514.60-374405.8	0,1,3,8,14,21,23,22,24,24,23,22,20,18,16,13,11,8,5,3,2,1,0,0,0	4,2,1,2,0,1,0,0,2,0,0,1,0,1,1,0,1,0,1,0,1,1,2,2,2	1	-1.049	0.572
Train	RRC	1SWASPJ063455.46-451830.1	0,1,1,5,6,12,13,21,23,23,23,24,21,17,14,12,10,7,5,3,3,1,1,0,0	3,4,0,2,0,2,1,1,0,0,1,0,2,1,1,0,0,1,0,0,0,2,0,3,1	1	-0.647	0.146
Train	RRC	1SWASPJ112708.82-175133.3	0,1,4,6,13,18,22,24,24,24,24,22,20,16,14,12,11,6,5,3,3,3,2,1,0	2,2,1,3,1,1,2,0,0,0,0,1,1,1,1,0,1,0,1,0,1,0,2,0,4	1	-0.966	0.988
Train	RRC	1SWASPJ113616.22-380211.3	0,6,11,15,17,22,24,24,22,21,20,17,15,12,9,6,5,3,1,1,0,1,0,3,6	3,3,0,2,0,1,3,0,0,1,0,1,1,0,0,2,0,2,0,0,1,1,2,0,2	1	-0.664	0.090
Train	RRC	1SWASPJ115742.19+074821.7	0,1,1,2,4,8,12,13,17,19,21,22,24,24,23,23,21,20,17,15,12,9,4,2,0	2,2,2,0,2,0,0,0,1,1,0,0,2,1,0,1,0,2,0,1,1,2,1,2,2	1	0.779	0.298
Train	RRC	1SWASPJ125922.64+374903.6	0,1,3,6,9,11,14,16,17,20,22,23,24,22,17,13,8,6,3,4,4,4,2,1,0	2,2,1,2,3,0,2,0,1,1,0,1,0,1,1,0,1,2,0,0,1,0,2,1,1	1	-0.772	0.178
Train	RRC	1SWASPJ140540.50+282912.5	0,2,1,3,6,9,13,18,20,22,24,23,23,21,17,16,12,10,7,6,4,3,2,0,0	3,1,2,2,1,0,2,1,0,1,1,0,1,1,0,0,1,1,1,0,1,1,1,2,1	1	-0.199	0.242
Train	RRC	1SWASPJ141250.81-272837.5	0,2,3,9,12,15,18,22,24,22,22,23,21,18,16,15,12,9,6,4,3,1,0,1,1	2,3,1,2,1,0,1,0,0,2,0,0,2,0,0,2,1,0,2,0,0,1,3,1,1	1	0.561	0.438
Train	RRC	1SWASPJ141421.40-152121.9	0,1,6,9,15,20,23,24,23,20,16,11,5,3,3,2,3,4,5,5,2,2,0,0,0	4,1,3,3,1,3,1,0,0,1,0,1,0,0,0,1,1,0,0,0,2,0,0,2,1	1	-0.668	0.102
Train	RRC	1SWASPJ151849.64-095959.6	0,2,7,15,21,23,22,24,24,24,22,20,18,15,13,11,9,6,3,2,1,0,0,0,0	5,1,2,1,0,0,1,1,0,1,0,1,0,1,0,2,0,0,1,0,1,1,2,1,3	1	-1.033	0.436
Train	RRC	1SWASPJ161240.50-185928.2	0,2,2,5,9,9,16,18,21,22,24,24,21,19,18,15,11,9,6,6,5,6,4,2,1	1,1,3,0,1,2,3,0,0,3,0,1,0,0,0,1,1,0,2,1,0,2,1,0,2	1	-0.177	0.126
Train	RRC	1SWASPJ184404.60+604612.8	0,1,3,6,12,20,24,23,24,24,23,21,18,17,15,13,11,9,6,4,2,1,0,0,0	4,2,1,1,1,0,2,0,0,1,0,1,1,1,0,1,0,1,1,0,1,0,2,3	1	-1.113	0.468
Train	RRC	1SWASPJ194014.36-392158.7	0,1,2,5,6,10,14,18,20,22,24,23,21,20,19,16,13,9,6,4,2,0,1,0,1	3,3,2,0,1,1,2,0,0,1,1,0,0,1,1,0,1,0,1,1,2,1,1,1,1	1	0.150	0.392
Train	RRC	1SWASPJ194552.21-182927.8	0,1,2,2,2,3,5,9,15,20,21,24,23,24,22,17,7,2,0,0,0,0,0,0,0	8,1,4,1,0,1,0,1,0,1,0,0,0,0,0,1,0,1,0,0,1,1,1,1,2	1	-0.393	0.644
Train	RRC	1SWASPJ201147.09-383941.2	0,2,3,6,9,11,15,18,21,22,24,23,21,19,13,13,9,6,4,3,1,1,0,0,1	3,3,1,2,1,0,2,0,0,2,0,1,0,2,0,1,0,0,1,1,0,2,1,1,1	1	-0.694	0.462
Train	RRC	1SWASPJ201352.75-601003.7	0,3,8,12,15,18,20,22,23,24,24,24,24,23,22,20,17,15,11,7,2,0,0,0,0	5,0,1,1,0,0,0,1,1,0,0,1,1,0,0,2,0,1,1,0,2,0,2,2,4	1	1.023	0.318
Train	RRC	1SWASPJ212723.07+013351.8	0,1,3,7,9,12,16,18,22,24,24,23,22,20,20,15,12,9,7,4,3,3,0,0,0	4,1,0,3,1,0,0,2,0,2,0,0,2,0,0,1,1,0,1,0,2,0,2,1,2	1	-0.769	0.382
Train	RRC	1SWASPJ213629.01+361917.9	0,2,1,1,3,6,8,10,15,17,19,21,24,24,23,24,24,17,16,14,10,4,6,2,3	1,2,2,2,1,0,2,0,1,0,2,0,0,0,1,1,1,2,0,1,0,1,0,1,4	1	-0.144	0.088
Train	RRC	1SWASPJ213940.73+503720.7	0,1,4,3,7,10,14,15,22,22,23,22,24,23,20,18,20,12,14,12,7,5,8,4,2	1,1,1,1,2,1,0,2,1,0,1,0,2,0,2,1,0,0,1,0,2,0,3,2,1	1	-0.089	0.022
Train	RRC	1SWASPJ214048.46-460026.8	0,1,4,5,6,6,9,13,16,18,22,24,24,23,21,19,15,13,10,8,7,6,3,1,0	2,2,0,1,1,1,3,1,1,1,0,0,2,0,1,1,0,1,1,0,1,1,1,2	1	0.191	0.238
Train	RRC	1SWASPJ215309.98+284551.5	0,3,6,12,20,23,24,24,24,24,23,20,18,15,15,10,9,7,4,4,2,1,0,0,0	4,1,1,1,2,0,1,1,0,1,1,0,1,0,0,2,0,0,1,0,2,0,0,2,4	1	-0.178	0.086
Train	RRC	1SWASPJ220136.64+095858.2	0,1,3,5,6,7,12,13,22,21,21,23,24,22,21,17,15,13,11,9,7,5,2,1,0	2,2,1,1,0,2,1,2,0,1,0,1,1,2,0,1,0,1,0,0,0,3,2,1,1	1	-0.371	0.188
Train	RRC	1SWASPJ220203.50-182715.8	0,2,2,4,6,10,13,19,24,23,23,24,23,22,19,16,14,13,11,8,6,4,2,0,0	3,0,3,0,2,0,2,0,1,0,1,1,0,2,1,0,1,0,0,2,0,0,1,3,2	1	-0.161	0.142
Train	RRC	1SWASPJ220502.82+173842.4	0,1,6,6,2,4,9,14,17,22,23,24,19,15,15,12,9,7,5,3,3,2,1,0,0	3,2,2,2,1,1,2,1,0,2,0,0,1,0,1,2,0,1,0,1,0,0,1,1,1	1	-0.113	0.102
Train	RRC	1SWASPJ220800.70+082352.1	0,1,4,9,12,13,15,18,19,18,20,24,24,15,12,15,12,5,6,4,1,1,1,0,1	2,5,0,0,2,1,1,0,0,1,0,0,3,1,0,3,0,0,2,1,1,0,0,0,2	1	-0.556	0.202
Test	RRC	1SWASPJ013245.09+565244.9	0,4,10,17,22,23,23,22,24,22,21,19,20,17,15,12,8,7,3,3,3,3,0,1,0	3,1,0,4,1,0,0,1,1,0,1,0,1,0,0,1,0,2,0,1,1,1,3,2,1	1	0.272	0.066
Test	RRC	1SWASPJ013549.55+052143.7	0,1,3,4,6,13,14,17,19,20,20,24,19,17,15,12,9,6,5,3,2,1,0,0,0	4,2,1,2,1,1,2,0,0,1,0,0,1,1,1,1,0,2,0,2,2,0,0,0,1	1	-0.864	0.152
Test	RRC	1SWASPJ014929.59+525941.7	0,6,4,9,14,16,20,22,23,23,24,24,20,20,15,16,10,13,10,6,5,1,1,0,1	2,3,0,0,1,1,2,0,0,1,2,0,0,1,1,1,2,0,0,0,0,3,0,1,2,2	1	0.449	0.066
Test	RRC	1SWASPJ015558.07+504027.6	0,4,6,9,12,14,18,20,23,24,22,24,22,22,16,18,14,11,9,6,3,2,0,1,0	3,1,1,1,1,0,2,0,0,2,0,1,1,0,2,0,1,0,2,0,1,0,3,1,2	1	-0.230	0.082
Test	RRC	1SWASPJ023351.62+381554.5	0,2,4,4,6,9,13,14,16,17,24,19,16,15,11,12,2,1,4,4,4,1,0,0,0	4,2,2,0,5,0,1,0,0,1,0,1,1,1,1,1,2,1,0,1,0,0,0,0,1	1	-0.478	0.170
Test	RRC	1SWASPJ024437.82+385821.9	0,2,6,9,11,13,22,15,21,22,23,24,24,24,23,19,15,13,9,8,9,3,2,1,3	1,1,2,2,0,0,1,0,1,3,0,1,0,2,0,2,0,0,0,1,0,1,2,2,3	1	0.318	0.028
Test	RRC	1SWASPJ025236.01+293720.8	0,6,9,14,17,20,23,23,24,24,23,23,15,17,12,10,7,5,5,4,2,1,1,0,1	2,3,1,0,1,2,1,1,0,1,1,0,1,0,1,1,0,2,0,0,1,0,0,4,2	1	-0.148	0.312
Test	RRC	1SWASPJ031427.17+102747.5	0,4,5,9,12,14,18,21,24,24,24,23,24,24,22,22,19,17,17,13,9,6,3,0,0	3,0,0,1,1,1,1,0,0,2,0,0,1,1,1,0,0,2,1,1,0,1,2,1,5	1	0.759	0.310
Test	RRC	1SWASPJ032139.62+472718.7	0,1,1,3,5,9,11,16,19,22,24,24,24,22,18,15,9,10,7,3,3,0,0,0,0	5,2,0,3,0,1,0,1,0,2,1,1,0,0,0,1,1,0,1,1,0,0,2,0,3	1	-0.661	0.092
Test	RRC	1SWASPJ042426.57+410331.3	0,3,6,4,12,11,12,14,19,23,23,24,20,24,23,21,14,12,6,6,2,3,1,1,3	1,2,1,3,1,0,3,0,0,0,0,1,3,0,2,0,0,0,0,1,1,1,0,3,2	1	-0.160	0.042
Test	RRC	1SWASPJ043137.66-250415.7	0,1,6,7,10,12,15,17,21,21,22,24,23,24,22,16,14,12,9,6,5,3,1,0,0	3,2,0,1,0,1,2,1,0,1,1,0,2,0,1,1,1,1,0,0,0,2,2,1,2	1	-0.471	0.084
Test	RRC	1SWASPJ043917.02-325146.6	0,2,4,8,12,17,21,23,24,24,23,20,18,15,12,10,8,6,4,3,2,1,0,0,0	4,1,2,1,2,0,1,0,2,0,1,0,2,0,0,1,0,1,1,0,1,1,0,2,2	1	-1.036	0.380
Test	RRC	1SWASPJ045632.76-064150.5	0,1,2,2,2,2,2,6,20,22,19,20,24,21,12,10,8,2,4,3,2,2,1,0,0	3,2,8,1,1,0,1,0,1,0,1,0,1,0,0,0,0,0,0,0,1,2,1,1,0,1	1	-0.485	0.380
Test	RRC	1SWASPJ051654.52-012635.5	0,3,5,8,15,14,17,20,21,21,24,21,20,18,16,12,10,8,9,9,6,8,4,3,1	1,1,0,2,1,1,1,0,3,2,1,0,1,0,1,1,1,1,1,0,2,3,0,0,1	1	0.188	0.202
Test	RRC	1SWASPJ053641.37+273237.5	0,1,3,11,15,19,21,21,21,22,24,20,19,16,12,12,6,7,2,3,3,2,1,0,0	3,2,2,3,0,0,1,1,0,0,0,1,2,0,0,1,1,0,0,2,1,3,1,0,1	1	0.304	0.172
Test	RRC	1SWASPJ054150.67-403909.9	0,3,3,9,11,12,17,20,22,22,24,23,23,20,16,12,8,6,6,2,0,1,0,0,0	5,1,1,2,0,0,2,0,1,1,0,1,2,0,0,0,1,1,0,0,2,0,2,2,1	1	-0.527	0.044
Test	RRC	1SWASPJ141627.97-390831.9	0,2,5,9,16,24,24,24,22,24,24,24,20,18,12,11,8,6,1,0,1,1,1,1,0	3,5,1,0,0,1,1,0,1,1,0,1,1,0,0,0,1,0,1,0,1,0,1,0,6	1	-0.663	0.526
Test	RRC	1SWASPJ220839.64+460111.4	0,3,4,7,13,11,14,16,20,24,23,24,19,22,20,15,9,9,5,3,2,1,0,0,0	4,1,1,2,1,1,0,1,0,2,0,1,0,1,1,1,1,0,0,1,2,0,1,1,2	1	-0.211	0.140
Test	RRC	1SWASPJ220925.01+125228.3	0,5,5,8,13,16,20,20,23,24,24,21,19,18,13,12,7,9,4,4,3,0,0,0,0	5,0,0,1,2,2,0,1,1,0,0,1,2,0,0,1,0,1,1,2,1,0,1,2	1	-0.249	0.214
Test	RRC	1SWASPJ221636.93+203302.6	0,2,6,9,12,18,18,23,24,24,22,20,19,16,15,12,8,7,6,4,3,0,0,0,0	5,0,1,1,1,0,2,1,1,1,0,0,2,0,0,1,1,0,2,1,1,0,1,1,2	1	-0.278	0.156
Test	RRC	1SWASPJ222509.37+370305.4	0,2,3,4,7,10,13,14,18,20,22,24,24,24,22,20,19,15,15,12,6,4,3,0,0	3,0,1,2,2,0,1,1,0,0,1,0,1,1,1,2,0,0,1,1,2,0,2,0,3	1	0.438	0.106
Test	RRC	1SWASPJ222630.72+424646.3	0,3,5,8,12,14,18,19,22,23,24,24,24,23,21,21,16,15,15,10,8,6,2,1,0	2,1,1,1,0,1,1,0,2,0,1,0,1,0,1,2,1,0,1,1,0,2,1,2,3	1	0.565	0.162
Test	RRC	1SWASPJ222632.54+424611.5	0,5,4,7,11,12,16,18,20,22,22,22,24,23,18,20,15,14,14,8,8,6,3,1,0	2,1,0,1,1,1,1,2,0,0,1,1,0,2,1,1,0,2,0,2,0,3,1,1	1	0.188	0.116
Test	RRC	1SWASPJ223245.09-112513.5	0,2,4,7,11,14,19,22,24,24,24,21,18,14,12,9,6,5,3,1,2,0,1,0,0	4,2,2,1,1,1,1,0,1,0,1,1,0,2,0,0,0,1,1,0,1,1,0,3	1	-0.803	0.386
Test	RRC	1SWASPJ223452.66+424002.3	0,3,5,8,10,13,15,19,22,21,23,24,24,23,21,20,18,15,12,10,8,4,3,1,1	1,2,0,2,1,1,0,0,2,0,2,0,1,1,0,2,0,0,1,1,1,2,1,2,2	1	0.199	0.216
Test	RRC	1SWASPJ223718.95+371542.9	0,2,2,5,7,12,12,19,22,24,24,21,19,19,11,14,11,9,9,6,3,1,3,1,0	2,2,2,2,0,1,1,1,0,2,0,2,2,0,1,0,0,0,0,3,0,1,1,0,2	1	-0.299	0.108
Test	RRC	1SWASPJ224932.13-025530.8	0,1,3,4,9,12,14,18,21,24,24,24,24,23,21,20,15,13,12,7,6,3,2,0,0	3,1,1,2,1,0,1,1,0,1,0,0,2,1,1,1,0,0,1,0,1,2,0,1,4	1	-0.016	0.122
Test	RRC	1SWASPJ231209.15-185526.1	0,1,4,7,10,15,16,20,24,23,20,21,20,19,17,14,12,10,8,7,5,2,0,0,0	4,1,1,0,1,1,0,2,1,0,2,0,1,0,1,1,1,1,0,1,3,1,0,1,1	1	-0.641	0.148
Test	RRC	1SWASPJ232026.09-432106.5	0,1,4,6,10,14,18,22,23,24,24,23,21,18,15,14,11,10,7,6,4,3,1,0,0	3,2,0,1,2,0,2,1,0,0,2,1,0,0,2,1,0,0,2,0,0,1,1,2,2	1	-0.583	0.250
Test	RRC	1SWASPJ233143.40+392416.8	0,6,5,9,12,14,16,18,21,24,24,24,22,20,15,13,12,10,7,4,5,4,3,0,1	2,1,0,1,2,2,1,1,0,1,1,0,2,1,1,1,1,0,1,0,1,1,1,0,3	1	-0.199	0.082

Appendix 1 continued...

No class

Reason	Class	WASP Object Id	X-pattern	Y-pattern	P-bin	Mode-mean	BMA
Train	No class	1SWASPJ000239.31-192638.8	0,1,1,4,5,7,12,13,18,16,24,23,21,20,8,11,0,6,4,2,3,2,0,2,0	4,2,3,1,2,1,1,1,1,0,0,1,1,1,0,0,1,0,1,0,1,1,0,1,1	3	-0.807	0.342
Train	No class	1SWASPJ013708.77+505720.5	0,2,5,10,13,3,1,5,0,1,1,2,24,9,9,24,17,5,0,14,24,14,3,-1,8	3,3,2,2,0,3,0,0,1,2,1,0,0,1,2,0,0,1,0,0,0,0,0,0,3	3	-0.425	0.866
Train	No class	1SWASPJ014635.34+190504.5	0,2,7,7,11,15,20,23,24,-1,23,23,19,24,-1,-1,-1,21,22,23,-1,13,9,13,15	1,0,1,0,0,0,0,2,0,1,0,1,0,2,0,2,0,0,0,1,1,1,1,4,2	5	0.786	0.350
Train	No class	1SWASPJ030632.19+333730.9	0,24,23,21,23,24,24,23,23,24,19,23,24,24,24,24,24,24,24,23,24,24,24,19	1,0,0,0,0,0,0,0,0,0,0,0,0,0,0,0,0,0,0,0,2,0,1,0,6,15	2	0.289	0.936
Train	No class	1SWASPJ040310.85+380317.2	0,13,17,19,13,14,22,19,19,17,18,11,24,13,7,9,8,9,9,15,6,7,9,9,11	1,0,0,0,0,1,2,1,5,0,2,0,3,1,1,0,2,1,3,0,0,1,0,1	2	0.288	0.062
Train	No class	1SWASPJ041104.54-200305.1	0,11,24,-1,5,15,17,20,6,8,14,-1,-1,-1,-1,17,11,-1,-1,18,13,20,9,3,12,15	1,0,0,1,0,1,1,0,1,1,0,2,1,1,1,2,0,2,1,0,2,0,0,0,1	5	-0.476	0.120
Train	No class	1SWASPJ052925.39-324901.0	0,12,6,13,13,15,6,4,15,18,19,12,19,22,24,20,24,14,19,15,17,16,19,22,14	1,0,0,0,1,0,2,0,0,0,0,0,2,2,2,3,1,1,1,4,1,0,2,0,2	1	-0.427	0.164
Train	No class	1SWASPJ103707.64-235335.4	0,3,2,4,6,11,23,20,24,24,22,20,19,18,18,22,24,14,11,11,8,8,8,1,1	1,2,1,1,1,0,1,0,3,0,0,3,0,0,1,0,0,0,2,1,2,0,2,1,3	0	-0.576	0.198
Train	No class	1SWASPJ112620.65-254518.6	0,2,4,14,13,14,13,9,6,0,-1,-1,7,14,17,23,24,-1,12,12,4,4,1,2,1	2,2,2,0,3,0,1,1,0,1,0,0,2,2,3,0,0,1,0,0,0,0,0,1,1	4	-1.066	0.260
Train	No class	1SWASPJ115143.06-391226.9	0,6,15,24,-1,18,18,19,-1,21,14,8,6,14,9,12,4,7,23,6,7,22,24,18,1	1,1,0,0,1,0,3,2,1,1,0,0,1,0,2,1,0,0,3,1,0,1,1,1,2	5	0.990	0.306
Train	No class	1SWASPJ140936.83+384034.3	0,6,11,11,14,17,16,17,17,22,22,24,19,24,11,11,-1,-1,-1,-1,4,14,14,13,2	1,0,1,0,1,0,1,0,0,0,0,4,0,1,3,0,1,3,0,1,0,0,2,0,2	4	-0.410	0.642
Train	No class	1SWASPJ142125.22+062632.7	0,1,2,4,-1,4,4,5,9,24,11,12,9,7,7,8,18,14,11,-1,-1,-1,2,1,-1	1,2,2,0,3,1,0,2,1,2,0,2,1,0,1,0,0,0,1,0,0,0,0,0,1	4	-0.845	0.870
Train	No class	1SWASPJ153115.88-232136.2	0,4,8,12,17,24,18,14,19,19,14,1,12,1,8,8,1,-1,15,17,18,13,13,8,2	1,3,1,0,1,0,0,4,4,0,0,0,2,2,2,1,0,2,2,2,0,0,0,0,1	4	0.478	0.452
Train	No class	1SWASPJ153223.20-083200.9	0,4,9,10,15,18,21,19,18,18,18,21,21,22,22,24,24,24,24,23,18,15,9,5,5	1,0,0,0,1,2,0,0,0,2,1,0,0,0,0,2,0,0,5,1,0,3,2,1,4	2	0.597	0.124
Train	No class	1SWASPJ174820.38+244227.3	0,10,18,22,20,17,9,11,13,16,24,23,23,22,20,16,4,6,1,2,6,-1,-1,-1,-1	1,1,1,0,1,0,2,0,0,1,1,1,0,1,0,0,2,1,1,0,2,0,2,2,1	5	0.388	0.356
Train	No class	1SWASPJ180456.57+283246.5	0,3,8,14,18,17,12,15,15,9,9,1,0,6,4,3,3,11,13,17,24,20,14,3,3	2,1,0,5,1,0,1,0,1,2,0,1,1,1,2,2,0,2,1,0,1,0,0,0,1	5	0.477	0.274
Train	No class	1SWASPJ180538.59+310018.2	0,1,7,19,13,24,-1,-1,-1,9,6,10,7,3,0,0,3,9,8,6,4,9,7,3,0	4,1,0,3,1,0,2,3,1,3,1,0,0,1,0,0,0,0,0,1,0,0,0,0,1	5	-0.716	0.238
Train	No class	1SWASPJ180649.16+324407.9	0,5,7,11,19,22,20,21,17,14,14,10,10,8,10,12,15,20,24,24,22,19,16,12,8	1,0,0,0,0,1,0,1,2,0,3,1,2,0,2,1,1,1,0,2,2,1,2,0,2	4	-0.446	0.106
Train	No class	1SWASPJ183110.68+315317.5	0,1,4,8,11,15,15,12,10,10,10,12,15,20,23,21,24,20,17,15,10,4,3,1,1	1,3,0,1,2,0,0,0,1,0,4,1,2,0,0,4,0,1,0,0,2,1,0,1,1	4	0.687	0.412
Train	No class	1SWASPJ183355.77+514308.8	0,10,21,13,17,16,19,22,17,24,20,12,12,14,13,13,14,3,1,6,8,1,5,7,8	1,2,0,1,0,1,1,1,2,0,1,0,2,3,2,0,1,2,0,1,1,1,1,0,1	2	0.119	0.040
Train	No class	1SWASPJ191233.03-192627.6	0,-1,-1,7,12,-1,-1,10,20,24,19,16,14,12,10,9,5,-1,-1,-1,3,-1,-1,-1,0	2,0,0,1,0,1,0,1,0,1,2,0,2,0,1,0,1,0,0,1,1,0,0,0,1	4	-0.162	0.792
Train	No class	1SWASPJ193653.95-312204.5	0,7,8,9,7,-1,7,6,7,9,9,10,13,-1,-1,-1,-1,-1,4,24,9,0,0,-1,-1	3,0,0,0,1,0,1,4,1,4,1,0,0,1,0,0,0,0,0,0,0,0,0,0,1	5	0.029	0.840
Train	No class	1SWASPJ201921.71+405316.4	0,7,17,10,3,7,14,20,19,16,7,8,2,12,14,11,15,15,12,17,24,16,10,8,0	2,0,1,1,0,0,0,3,2,0,2,1,2,0,2,2,2,2,0,1,1,0,0,0,1	2	-0.606	0.100
Train	No class	1SWASPJ203241.01+122134.4	0,4,10,14,15,16,19,21,15,22,23,24,20,17,17,16,17,16,17,15,15,11,12,10,8	1,0,0,0,1,0,0,0,1,0,2,1,1,0,1,4,3,4,0,1,1,1,1,1,1	4	-0.014	0.116
Train	No class	1SWASPJ204254.90+174431.6	0,13,24,20,9,8,22,15,7,10,18,-1,-1,-1,-1,-1,-1,-1,-1,-1,-1,-1,10,23,11	1,0,0,0,0,0,0,1,1,1,2,1,0,1,0,1,0,0,1,0,1,0,1,1,1	5	-0.826	0.270
Train	No class	1SWASPJ204356.99+102401.7	0,20,20,14,10,7,4,2,9,15,21,12,15,16,19,20,24,24,22,19,15,15,14,16,12	1,0,1,0,1,0,0,1,0,1,1,0,2,0,2,4,2,0,2,3,1,1,0,2	4	0.602	0.120
Train	No class	1SWASPJ210209.23+442435.7	0,-1,2,-1,-1,13,24,19,15,21,24,20,16,-1,9,10,11,6,3,4,7,7,5,3,3	1,0,1,3,1,1,1,2,0,1,1,1,0,1,0,1,1,0,0,1,1,1,0,0,2	5	-0.608	0.354
Train	No class	1SWASPJ212103.25+403826.0	0,3,11,15,18,21,4,14,21,24,23,23,18,18,23,8,8,3,4,10,15,17,18,19,19	1,0,0,2,2,0,0,0,2,0,1,1,0,0,1,2,0,1,4,2,0,2,0,3,1	4	0.274	0.272
Train	No class	1SWASPJ224250.31-211044.6	0,4,-1,-1,-1,-1,-1,-1,21,-1,24,14,14,15,8,17,-1,13,11,10,9,9,0,5,2,5	2,0,1,0,1,2,0,0,1,2,1,1,0,1,2,1,0,1,0,0,0,1,0,0,1	5	0.492	0.736
Train	No class	1SWASPJ225153.53+314515.1	0,1,2,3,4,6,11,14,19,13,17,18,21,24,22,18,15,21,17,11,14,14,8,12,1	1,2,1,1,1,0,1,0,1,0,0,2,1,1,3,1,0,2,2,1,0,2,1,0,1	2	0.120	0.078
Test	No class	1SWASPJ030616.60-361240.5	0,5,17,17,20,22,22,21,21,22,24,24,24,22,20,24,21,22,23,21,19,20,17,13,3	1,0,0,1,0,1,0,0,0,0,0,0,0,1,0,0,0,3,0,1,3,4,5,1,4	1	0.138	0.138
Test	No class	1SWASPJ030955.94-112908.6	0,14,18,19,20,21,21,21,23,21,23,21,22,22,21,24,22,20,22,21,21,21,18,15,13	1,0,0,0,0,0,0,0,0,0,0,0,0,0,1,1,1,0,0,2,1,2,9,4,2,1	2	0.112	0.282
Test	No class	1SWASPJ034528.07-401604.3	0,16,20,20,21,21,-1,-1,-1,-1,-1,-1,-1,-1,-1,-1,-1,-1,-1,-1,24,20,20,17	1,0,0,0,0,0,0,0,0,0,0,0,0,0,0,0,0,1,1,0,0,4,2,0,0,1	1	0.219	0.100
Test	No class	1SWASPJ040502.18-431140.8	0,2,18,13,16,19,24,21,24,22,22,22,22,21,22,24,22,23,24,23,22,20,22,18,1	1,1,1,0,0,0,0,0,0,0,0,0,0,0,0,0,1,0,0,1,0,2,1,1,2,8,2,4	2	0.285	0.254
Test	No class	1SWASPJ041743.26-062358.5	0,2,12,19,20,20,18,19,23,24,24,20,19,24,22,24,22,20,20,22,23,20,22,18,10	1,0,1,0,0,0,0,0,0,0,1,0,1,0,0,0,0,0,2,3,6,0,4,2,4	2	0.225	0.178
Test	No class	1SWASPJ054705.16+281411.3	0,15,14,19,24,24,11,14,11,23,20,11,13,15,13,17,19,21,21,22,18,13,14,2,8	1,0,1,0,0,0,0,0,1,0,0,3,0,3,3,2,0,1,1,2,1,2,1,1,2	1	0.330	0.070
Test	No class	1SWASPJ060109.56+142431.4	0,9,19,22,23,22,24,22,22,24,22,21,21,21,22,23,18,20,24,23,23,22,23,16,0	2,0,0,0,0,0,0,0,0,1,0,0,0,0,0,0,0,1,0,1,1,1,3,7,5,3	1	0.375	0.096
Test	No class	1SWASPJ060617.50+214042.4	0,10,5,8,16,21,21,20,24,24,24,23,24,24,22,21,22,24,23,19,15,2,10,0,6	2,0,1,0,0,1,1,0,1,0,2,0,0,0,0,1,1,0,0,1,1,3,2,2,6	2	0.409	0.196
Test	No class	1SWASPJ083345.58+570553.7	0,4,16,17,17,19,23,22,6,12,20,11,7,4,8,13,16,19,15,15,14,21,24,21,14	1,0,0,0,2,0,1,1,1,0,0,1,1,1,2,2,2,2,0,2,1,2,1,1,1	2	0.107	0.248
Test	No class	1SWASPJ091036.83+561902.3	0,7,17,19,21,20,21,23,23,23,24,23,24,22,23,23,22,21,21,18,18,19,15,19,4	1,0,0,0,1,0,0,1,0,0,0,0,0,0,0,0,1,0,1,2,3,1,4,2,6,2	1	0.276	0.124
Test	No class	1SWASPJ121253.89-442815.9	0,2,2,3,8,2,3,4,3,2,12,10,0,0,6,4,4,8,8,8,24,19,3,9,5	3,0,4,4,3,1,1,0,4,1,1,0,1,0,0,0,0,0,0,1,0,0,0,0,1	3	-0.581	1.496
Test	No class	1SWASPJ121734.59-391804.6	0,11,14,22,24,23,24,24,24,24,23,23,23,23,23,23,22,24,24,24,23,17,16,12,6	1,0,0,0,0,1,0,0,0,0,1,1,0,1,0,1,1,0,0,0,0,2,8,8	1	0.341	0.550
Test	No class	1SWASPJ125740.26+351330.1	0,7,11,4,1,18,16,14,13,12,16,10,15,11,1,18,5,2,12,16,6,21,24,14,15	1,2,1,0,1,1,1,1,0,0,1,2,2,1,2,2,3,0,2,0,0,1,0,0,1	2	0.233	0.020
Test	No class	1SWASPJ142202.32-441745.7	0,13,8,10,11,-1,-1,-1,5,4,5,2,3,3,2,1,9,21,13,1,24,0,0,-1,12	3,2,2,2,1,2,0,0,1,1,1,1,1,2,0,0,0,0,0,0,0,1,0,0,1	4	-0.879	1.104
Test	No class	1SWASPJ143642.76-392756.3	0,-1,16,13,13,13,-1,16,18,4,11,14,-1,24,24,-1,20,13,11,-1,-1,-1,-1,-1,0	2,0,0,0,1,0,0,0,0,0,0,2,0,4,1,0,2,0,1,0,1,0,0,0,2	5	0.132	0.250
Test	No class	1SWASPJ144654.09-403220.4	0,4,20,20,22,23,22,22,22,23,22,23,23,23,23,23,22,23,23,23,23,24,23,24,14	1,0,0,0,1,0,0,0,0,0,0,0,0,0,0,1,0,0,0,0,0,2,0,6,12,2	1	0.332	0.356
Test	No class	1SWASPJ144703.66+045307.6	0,9,19,19,21,22,20,9,6,22,16,24,18,14,19,15,16,20,-1,18,17,15,9,7,4	1,0,0,0,1,0,1,0,3,0,0,0,0,1,2,2,1,2,3,2,1,2,0,1	0	0.069	0.270
Test	No class	1SWASPJ144805.46-414522.7	0,3,12,16,23,24,20,19,13,7,7,12,9,9,6,-1,-1,-1,9,13,5,3,1,0,0	3,1,0,2,0,1,1,2,0,3,0,0,2,2,0,0,1,0,0,1,1,0,0,1,1	4	-0.477	0.278
Test	No class	1SWASPJ151134.36+083101.4	0,16,21,20,24,24,8,19,16,9,13,0,0,17,18,14,15,17,14,17,20,20,23,13,15	3,0,0,0,0,0,0,1,1,0,0,2,2,2,2,3,1,1,3,1,0,1,2	2	0.690	0.108
Test	No class	1SWASPJ153158.42-210334.4	0,3,15,19,20,22,20,21,21,22,23,20,20,18,24,22,23,24,23,22,17,17,19,16,3	1,0,0,2,0,0,0,0,0,0,0,0,0,0,0,0,0,1,1,2,1,2,4,2,4,3,2	1	0.155	0.060
Test	No class	1SWASPJ153454.51-234316.1	0,1,-1,10,11,15,10,19,16,19,20,21,24,21,19,-1,11,7,4,-1,-1,-1,3,-1,0	2,1,0,1,1,0,0,1,0,0,2,2,0,0,0,1,1,0,0,3,1,2,0,0,1	5	-0.725	1.200
Test	No class	1SWASPJ154831.73+281654.5	0,8,3,3,3,8,11,15,24,17,21,16,22,22,20,21,15,13,12,10,6,4,3,3,2	1,0,1,5,1,0,1,0,2,0,1,1,1,0,2,1,1,0,0,1,2,2,0,1	4	-1.257	0.288
Test	No class	1SWASPJ162454.89+025957.5	0,1,3,1,4,6,6,6,13,11,9,11,14,20,23,14,17,22,24,-1,-1,18,8,3,5	1,2,0,2,1,1,3,0,1,1,0,2,0,1,2,0,0,1,1,0,1,0,1,1,1	4	-0.089	0.578
Test	No class	1SWASPJ164629.40+194514.2	0,9,24,23,17,15,18,16,11,13,14,13,15,15,20,16,17,16,13,15,19,19,19,4,0	2,0,0,0,1,0,0,0,0,1,0,1,0,3,1,4,3,2,1,3,1,0,0,1,1	2	0.263	0.028
Test	No class	1SWASPJ205745.08+253025.9	0,1,5,4,4,-1,11,5,2,15,6,2,3,10,14,13,14,2,0,4,5,1,6,24,18	2,2,3,1,3,3,2,0,0,0,1,1,0,1,2,1,0,0,1,0,0,0,0,0,1	3	-0.518	0.726
Test	No class	1SWASPJ214736.42-171741.0	0,6,3,9,5,15,16,9,6,8,9,3,10,16,21,21,21,24,19,12,0,8,3,5,5	2,0,0,3,0,3,2,0,2,3,1,0,1,0,0,1,2,0,0,1,0,3,0,0,1	2	-0.045	0.054
Test	No class	1SWASPJ220049.07+424539.4	0,2,11,21,24,17,15,10,5,4,-1,15,20,18,15,11,-1,9,13,18,18,15,9,5,0	2,0,1,0,1,2,0,0,0,2,1,2,0,1,0,4,0,1,3,0,1,1,0,0,1	5	0.676	0.806
Test	No class	1SWASPJ223845.57-203716.0	0,2,7,1,14,5,2,9,8,7,6,24,8,11,6,8,7,9,8,2,6,2,8,10,5	1,1,4,0,0,2,3,3,5,2,1,1,0,0,1,0,0,0,0,0,0,0,0,0,1	2	0.118	0.064
Test	No class	1SWASPJ230038.89-413052.4	0,12,14,14,14,19,18,18,21,22,24,22,19,15,12,19,22,18,14,13,12,10,10,12,13	1,0,0,0,0,0,0,0,0,0,2,0,4,2,4,1,0,0,3,3,0,1,3,0,1	3	0.278	0.214
Test	No class	1SWASPJ233601.04+523757.1	0,9,10,7,9,12,13,17,22,18,17,17,23,22,19,18,23,24,14,20,17,13,13,8,7	1,0,0,0,0,0,0,2,1,2,1,0,1,3,1,0,0,4,2,1,1,0,2,2,1	2	0.344	0.030

Appendix 2 – Linear separability graphs for each NN model

Graphs showing 20 objects for each of the classes CEP, DSCT, EA (Double eclipse), EA (Single eclipse), EB, EW, RM, RRAB, RRC and 'No class', each enclosed within a convex hull:

NN Model 1:

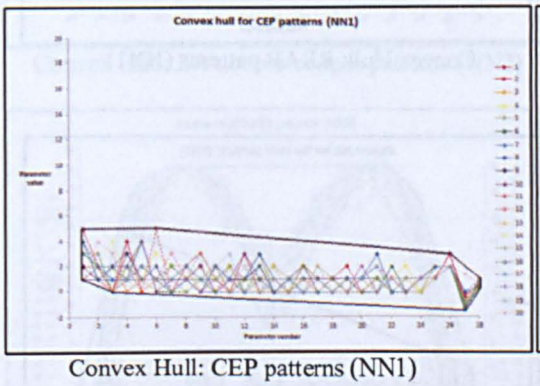

Convex Hull: CEP patterns (NN1)

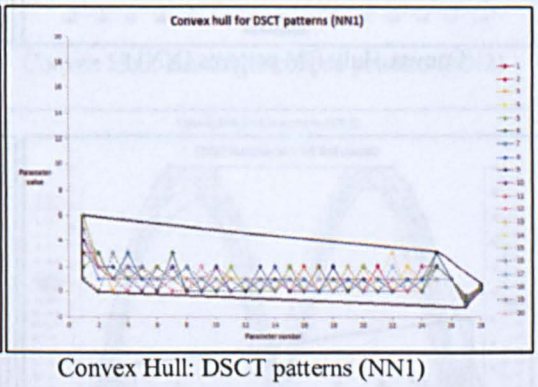

Convex Hull: DSCT patterns (NN1)

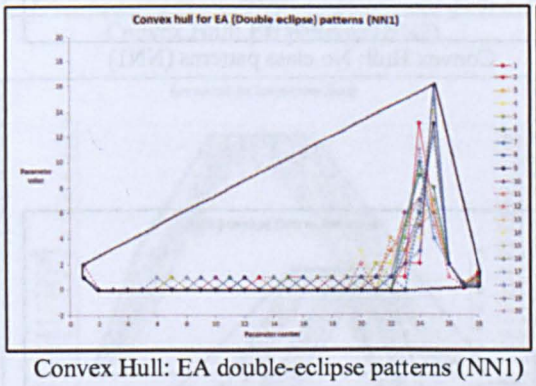

Convex Hull: EA double-eclipse patterns (NN1)

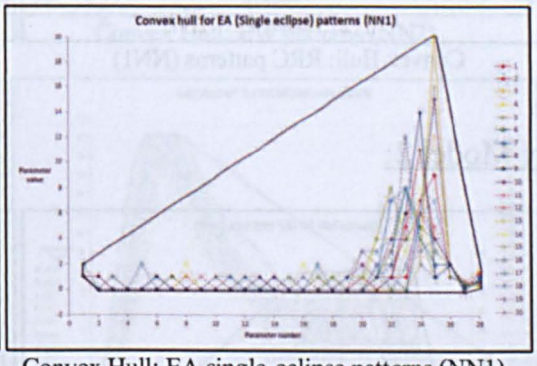

Convex Hull: EA single-eclipse patterns (NN1)

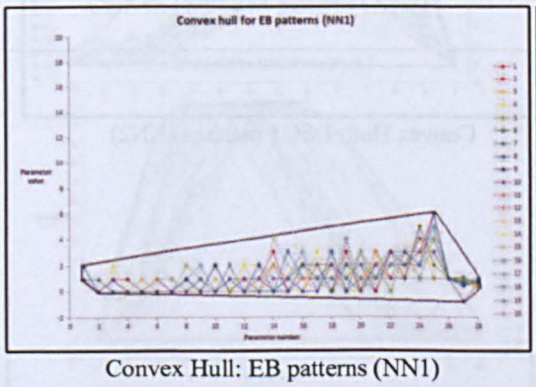

Convex Hull: EB patterns (NN1)

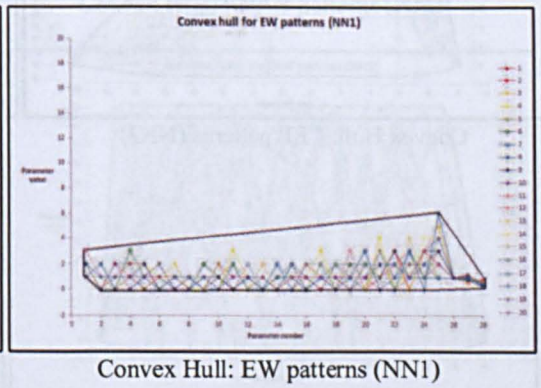

Convex Hull: EW patterns (NN1)

Appendix 2 continued…

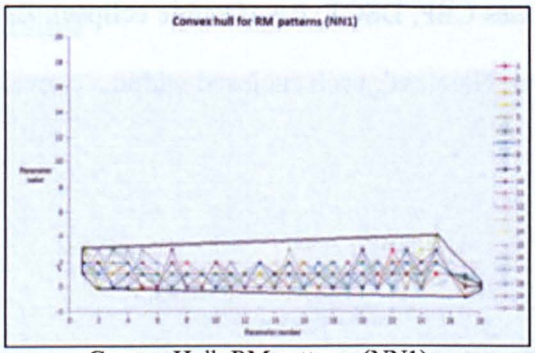

Convex Hull: RM patterns (NN1)

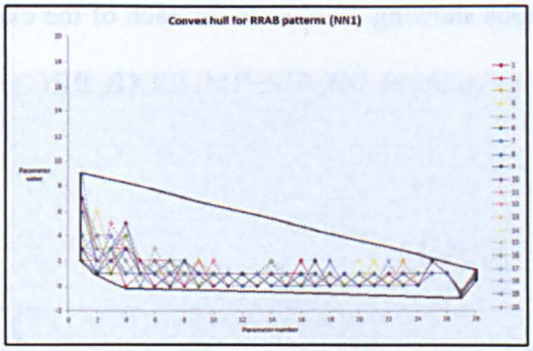

Convex Hull: RRAB patterns (NN1)

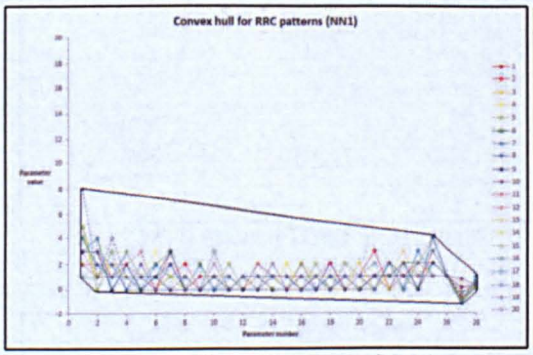

Convex Hull: RRC patterns (NN1)

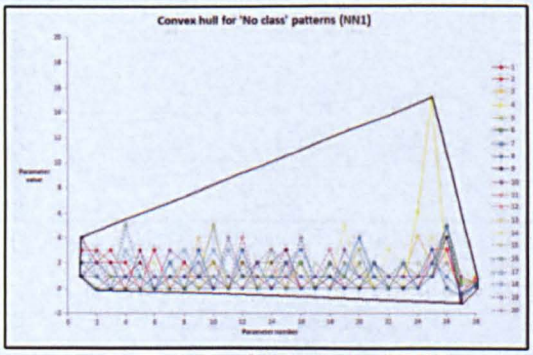

Convex Hull: No class patterns (NN1)

NN Model 2:

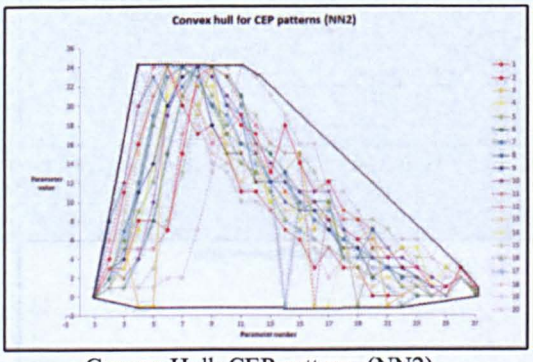

Convex Hull: CEP patterns (NN2)

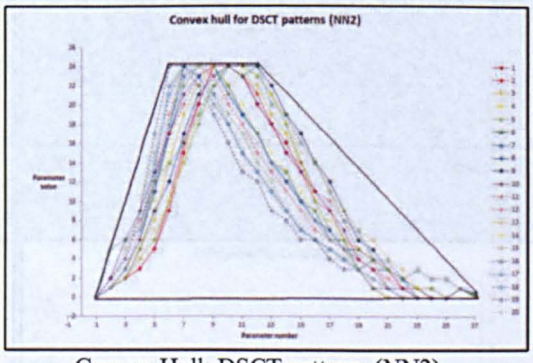

Convex Hull: DSCT patterns (NN2)

Appendix 2 continued...

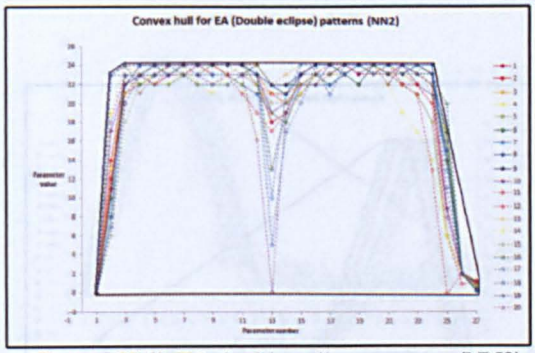

Convex Hull: EA double-eclipse patterns (NN2)

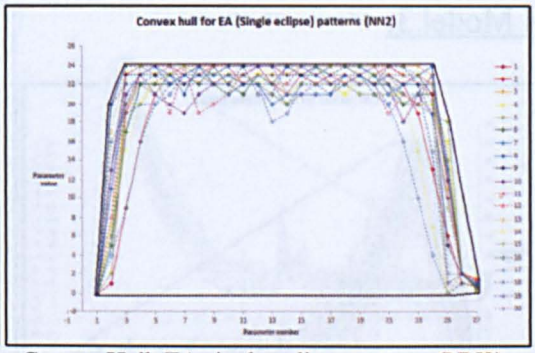

Convex Hull: EA single-eclipse patterns (NN2)

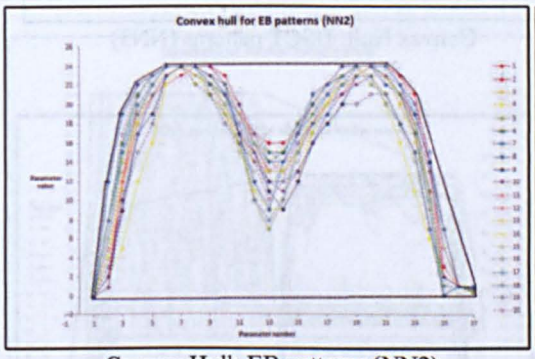

Convex Hull: EB patterns (NN2)

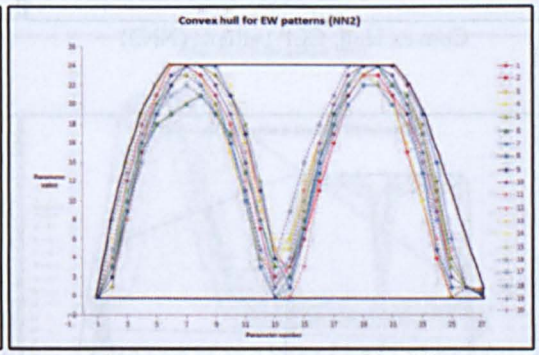

Convex Hull: EW patterns (NN2)

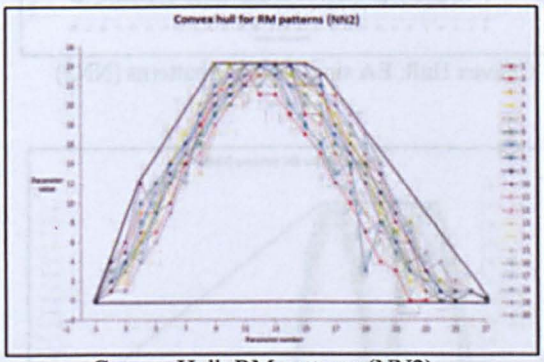

Convex Hull: RM patterns (NN2)

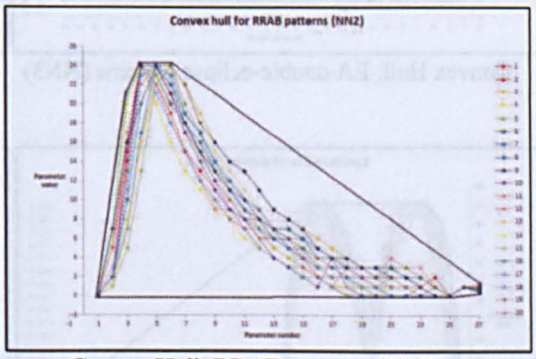

Convex Hull: RRAB patterns (NN2)

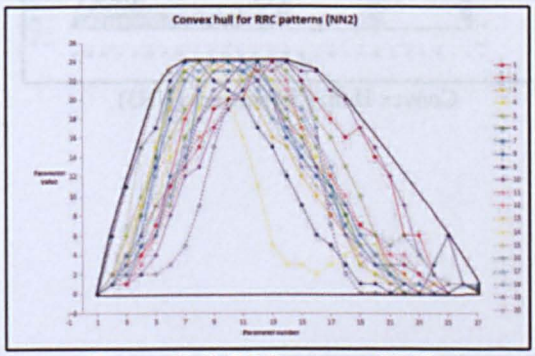

Convex Hull: RRC patterns (NN2)

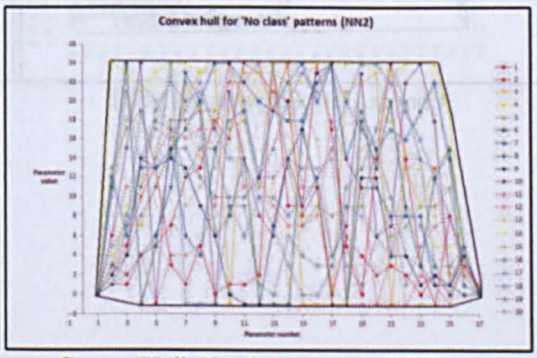

Convex Hull: No class patterns (NN2)

Appendix 2 continued…

NN Model 3:

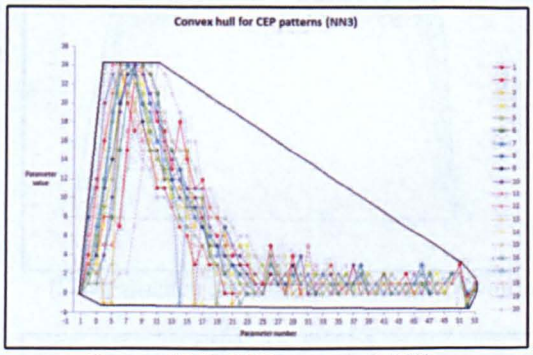

Convex Hull: CEP patterns (NN3)

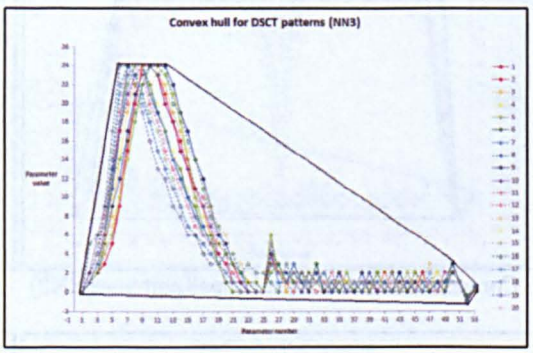

Convex Hull: DSCT patterns (NN3)

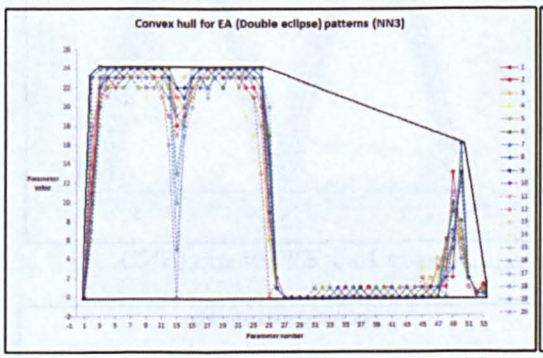

Convex Hull: EA double-eclipse patterns (NN3)

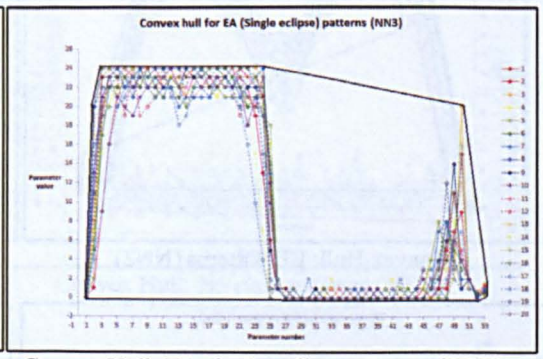

Convex Hull: EA single-eclipse patterns (NN3)

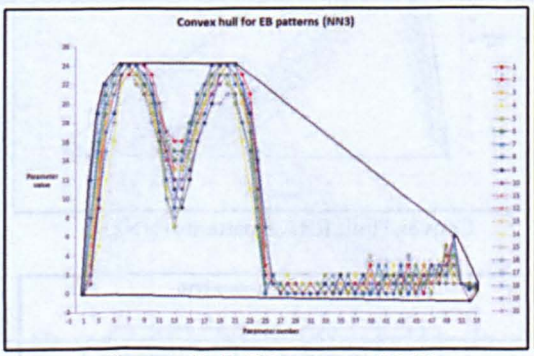

Convex Hull: EB patterns (NN3)

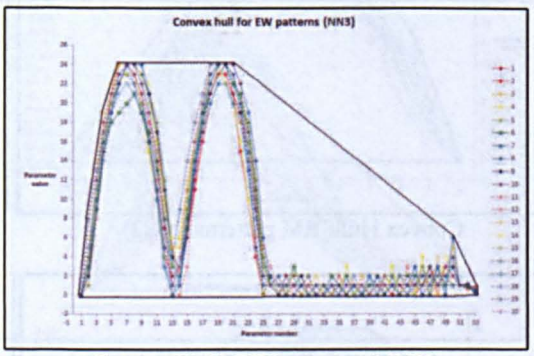

Convex Hull: EW patterns (NN3)

Appendix 2 continued…

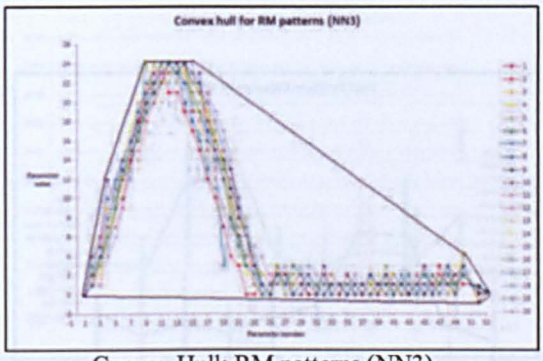

Convex Hull: RM patterns (NN3)

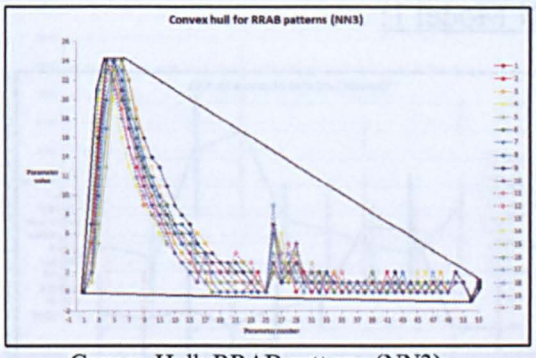

Convex Hull: RRAB patterns (NN3)

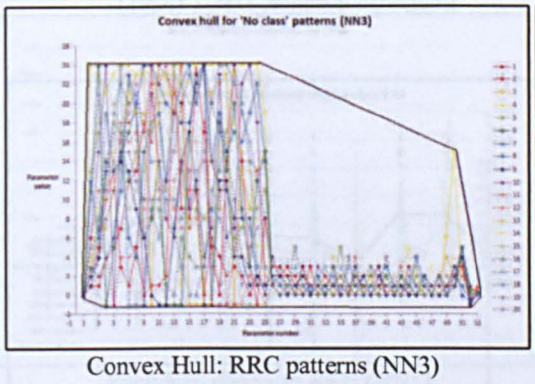

Convex Hull: RRC patterns (NN3)

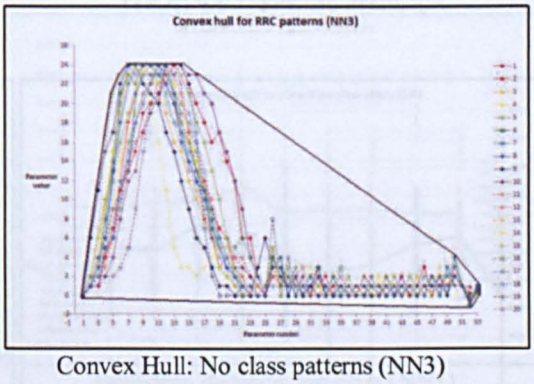

Convex Hull: No class patterns (NN3)

Appendix 3 – Euclidean Distances for each NN model

NN Model 1:

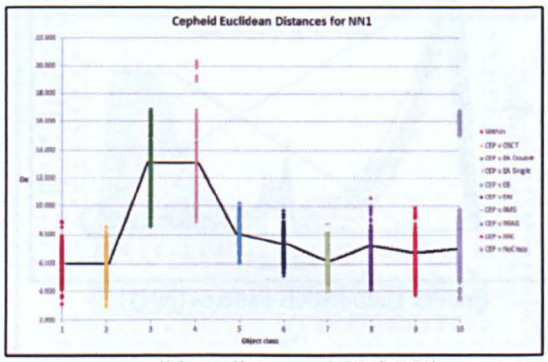

Euclidean distance: CEP (NN1)

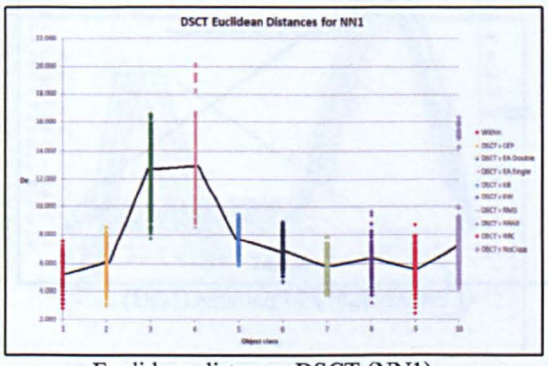

Euclidean distance: DSCT (NN1)

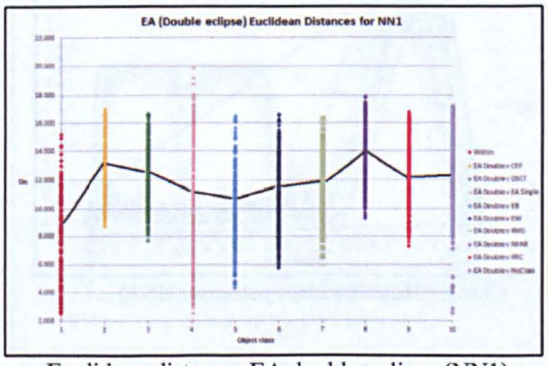

Euclidean distance: EA double-eclipse (NN1)

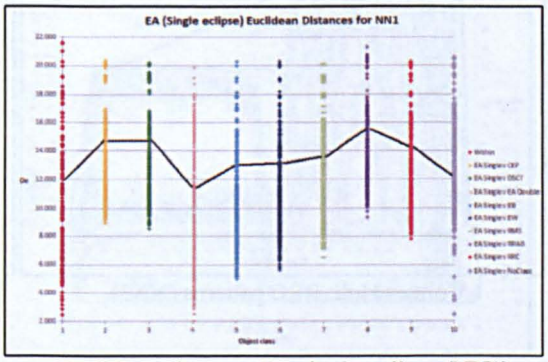

Euclidean distance: EA single-eclipse (NN1)

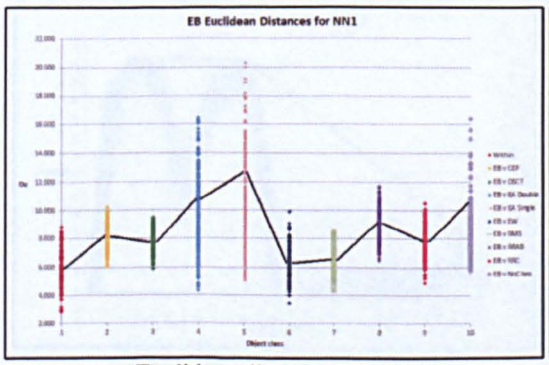

Euclidean distance: EB (NN1)

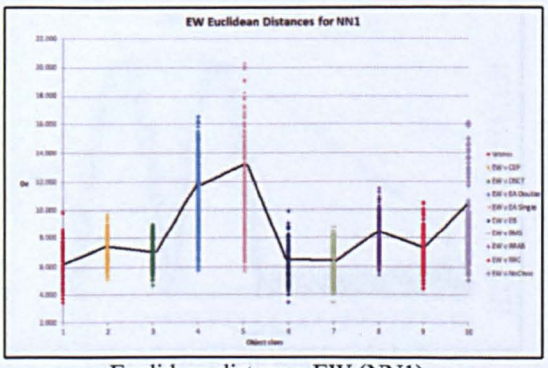

Euclidean distance: EW (NN1)

Appendix 3 continued…

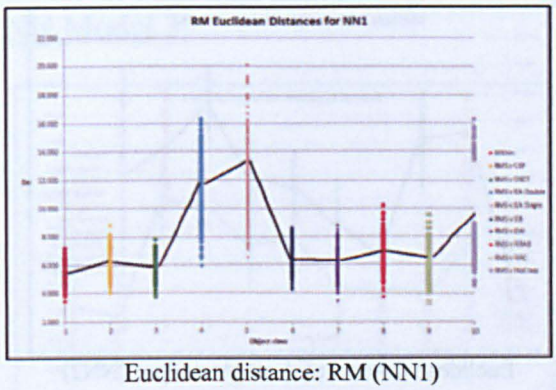

Euclidean distance: RM (NN1)

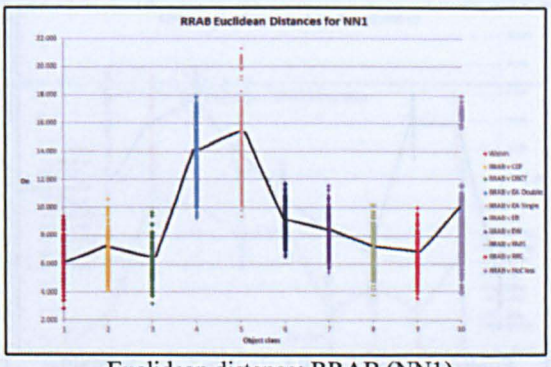

Euclidean distance: RRAB (NN1)

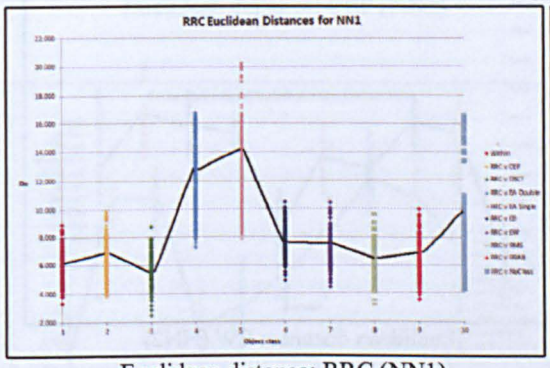

Euclidean distance: RRC (NN1)

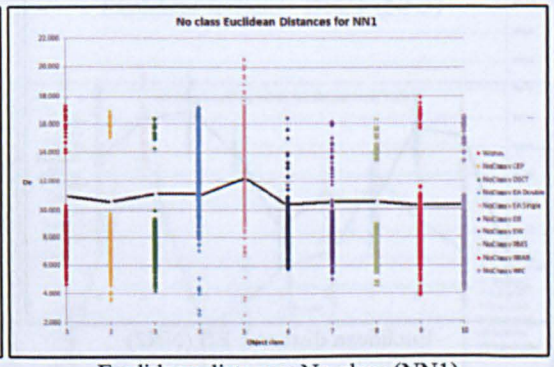

Euclidean distance: No class (NN1)

NN Model 2:

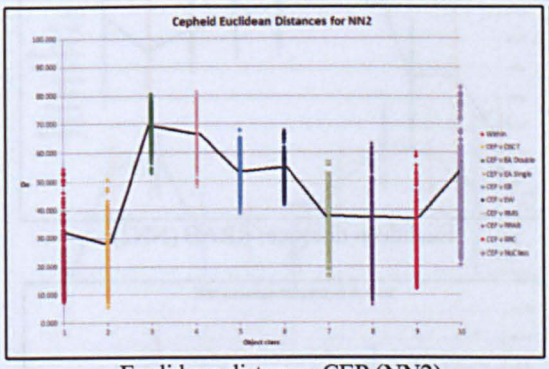

Euclidean distance: CEP (NN2)

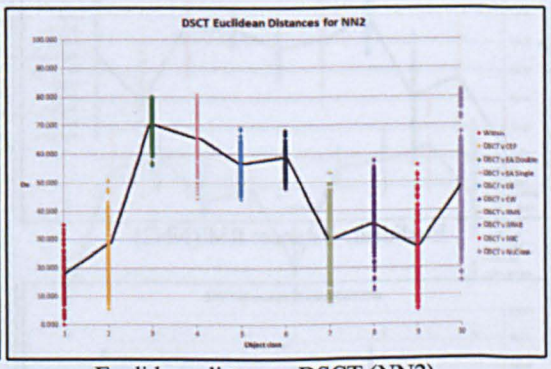

Euclidean distance: DSCT (NN2)

Appendix 3 continued…

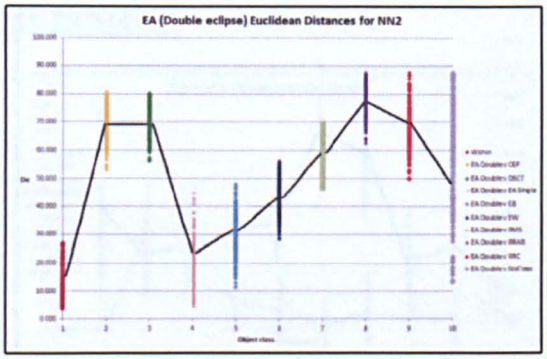

Euclidean distance: EA double-eclipse (NN2)

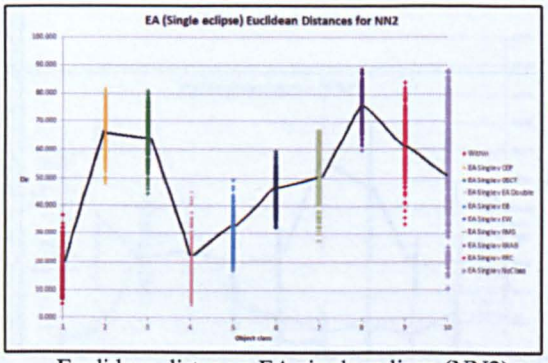

Euclidean distance: EA single-eclipse (NN2)

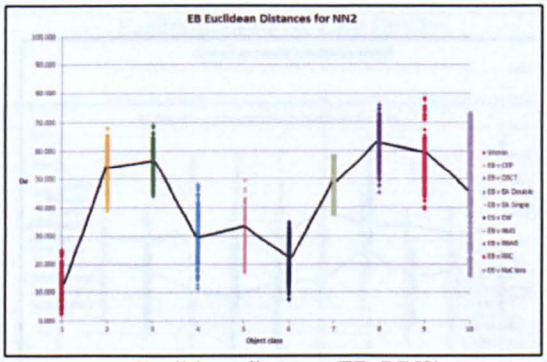

Euclidean distance: EB (NN2)

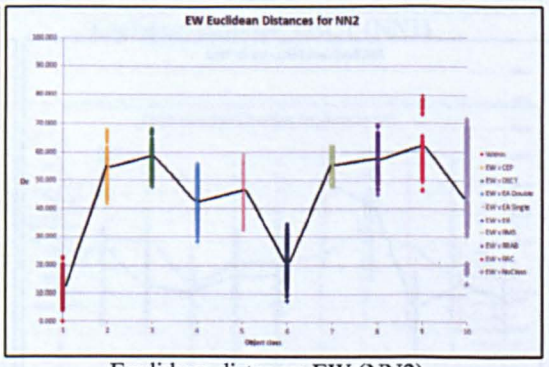

Euclidean distance: EW (NN2)

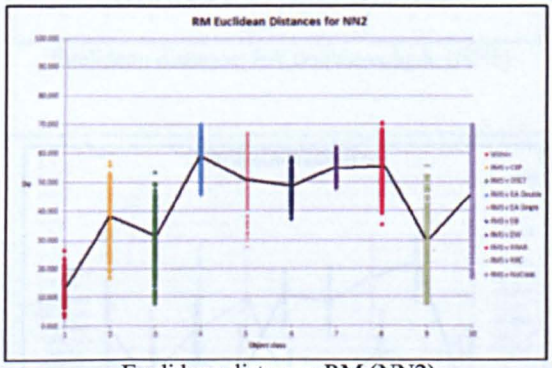

Euclidean distance: RM (NN2)

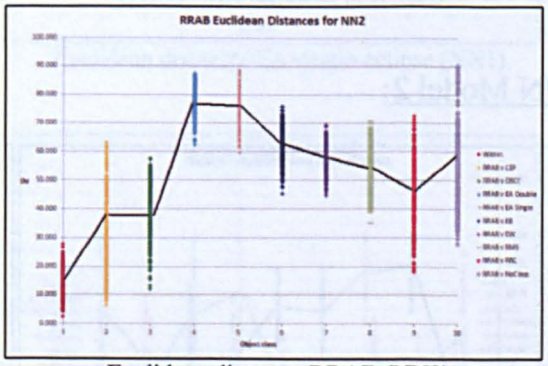

Euclidean distance: RRAB (NN2)

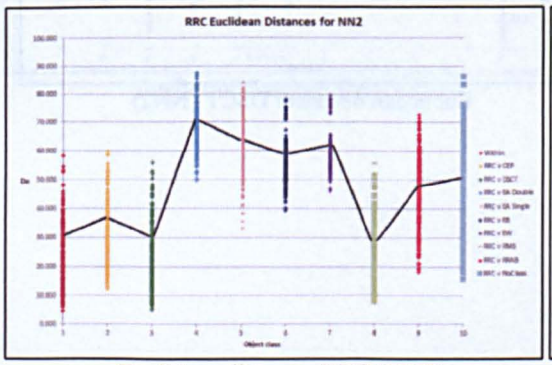

Euclidean distance: RRC (NN2)

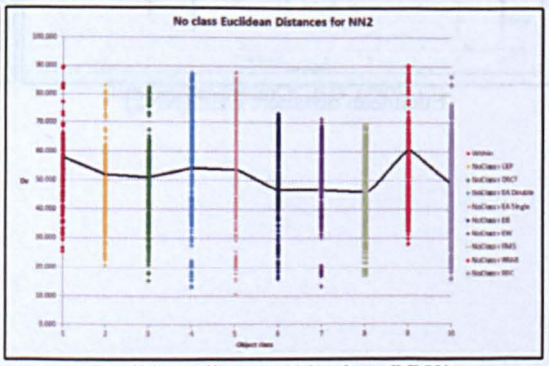

Euclidean distance: No class (NN2)

Appendix 3 continued…

NN Model 3:

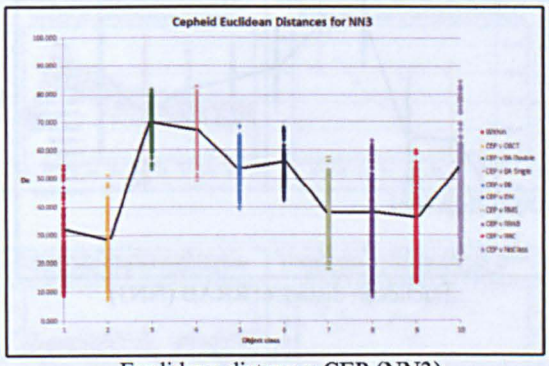

Euclidean distance: CEP (NN3)

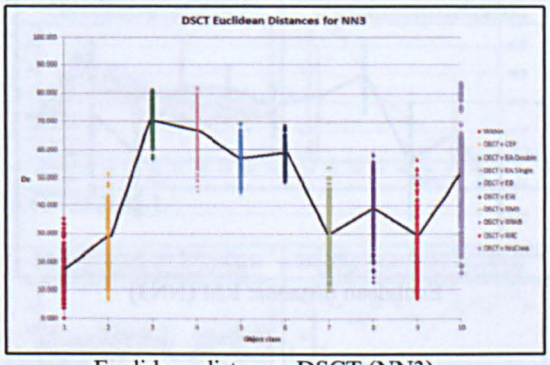

Euclidean distance: DSCT (NN3)

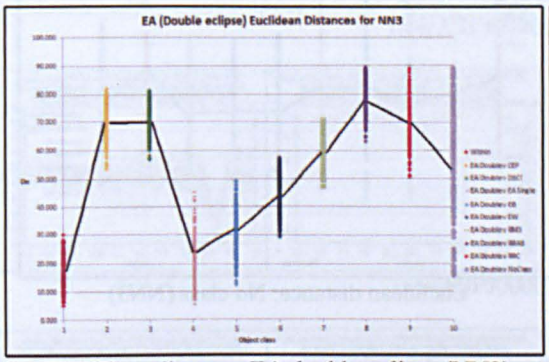

Euclidean distance: EA double-eclipse (NN3)

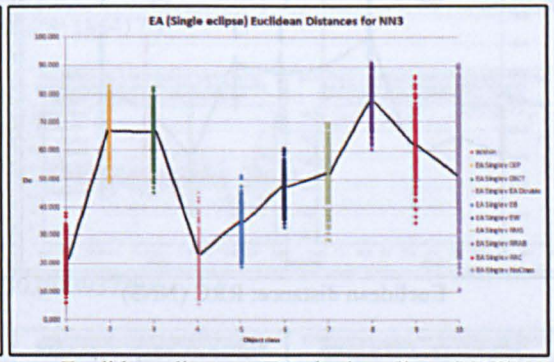

Euclidean distance: EA single-eclipse (NN3)

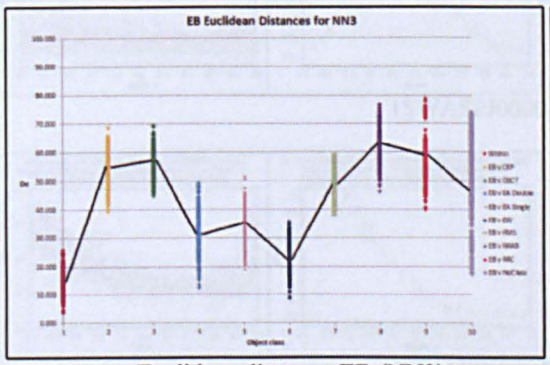

Euclidean distance: EB (NN3)

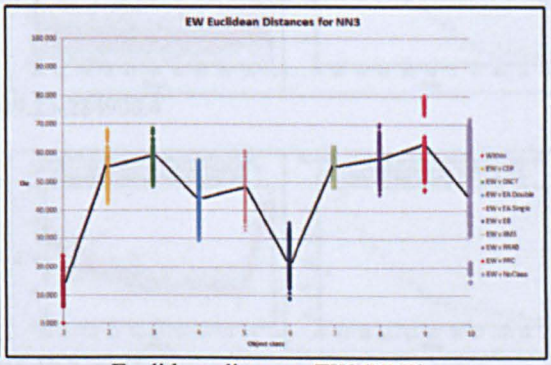

Euclidean distance: EW (NN3)

Appendix 3 continued…

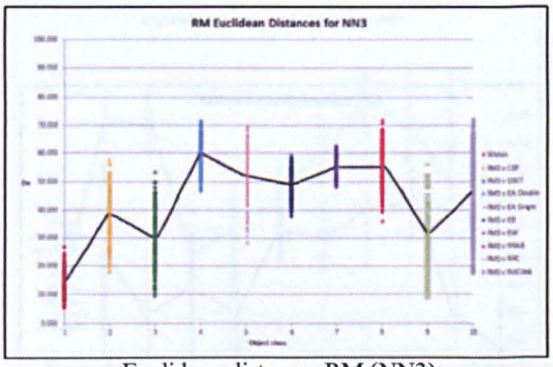

Euclidean distance: RM (NN3)

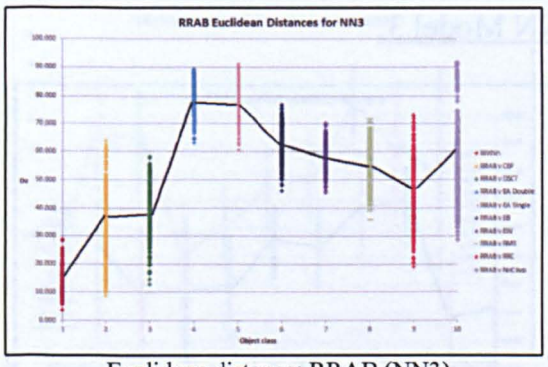

Euclidean distance: RRAB (NN3)

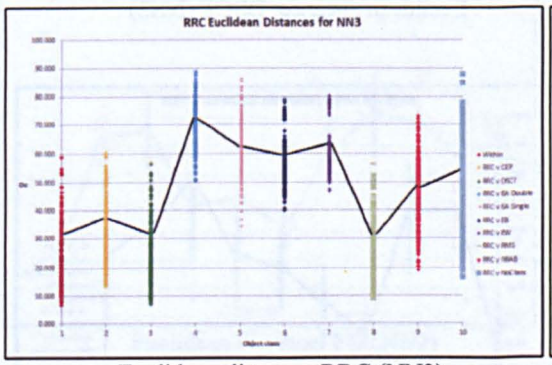

Euclidean distance: RRC (NN3)

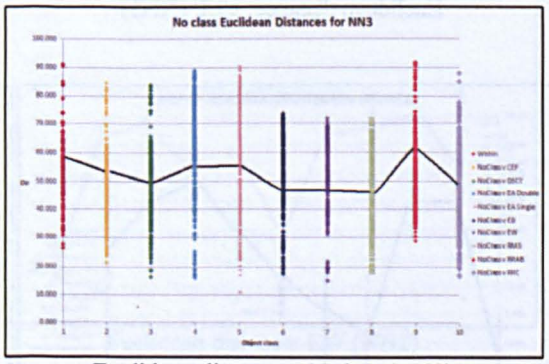

Euclidean distance: No class (NN3)

Appendix 4 – SuperWASP period within +/- 1% of GCVS period

GCVS period WASP period

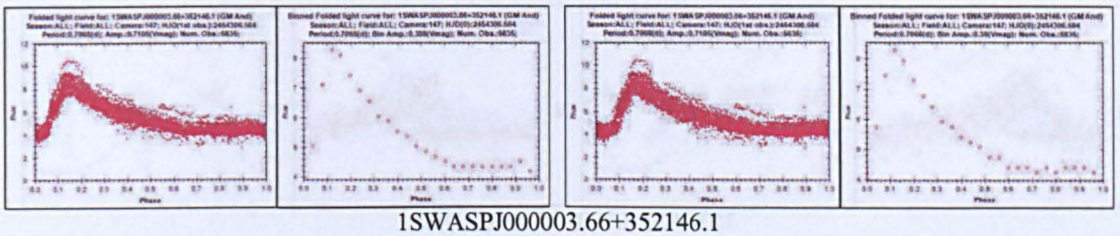

1SWASPJ000003.66+352146.1

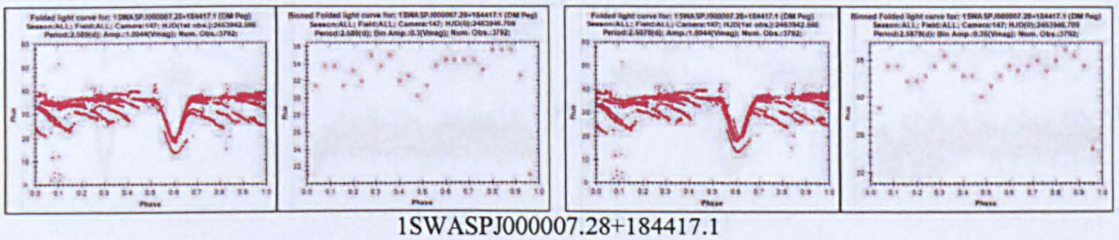

1SWASPJ000007.28+184417.1

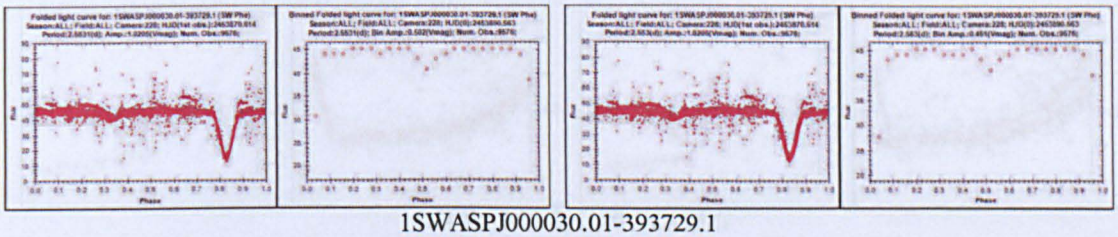

1SWASPJ000030.01-393729.1

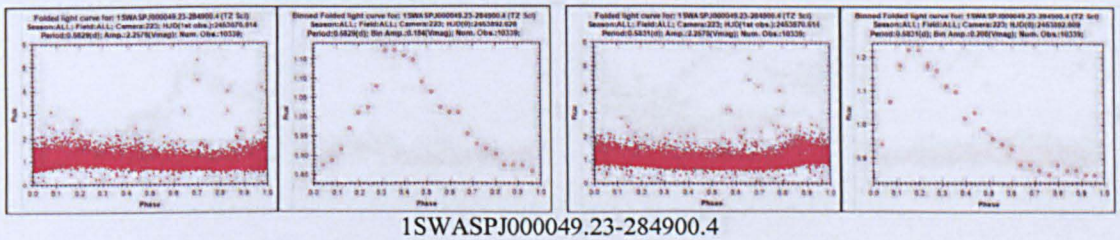

1SWASPJ000049.23-284900.4

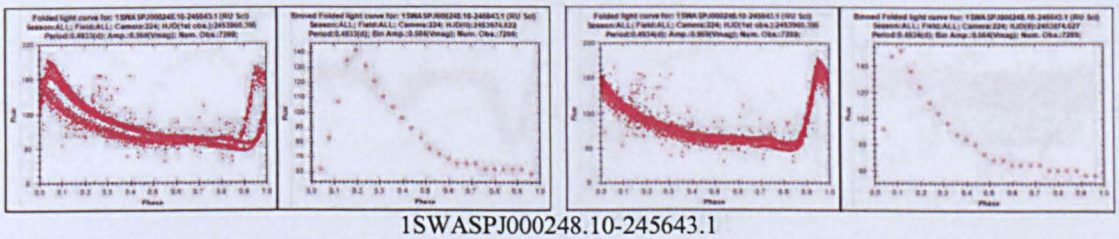

1SWASPJ000248.10-245643.1

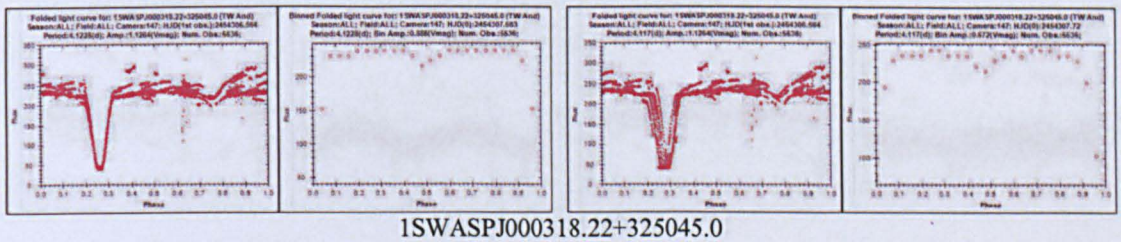

1SWASPJ000318.22+325045.0

Appendix 5 – SuperWASP has a more appropriate period than GCVS

GCVS period WASP period

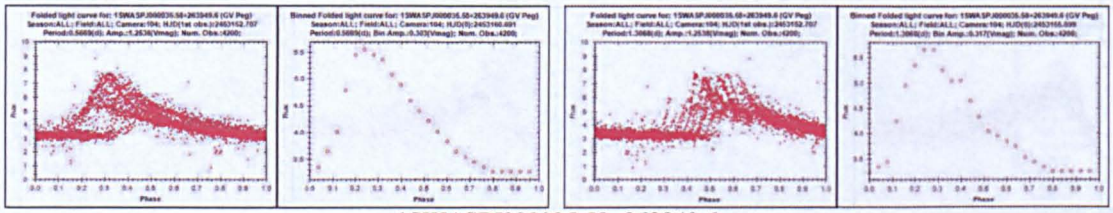

1SWASPJ000035.58+263949.6

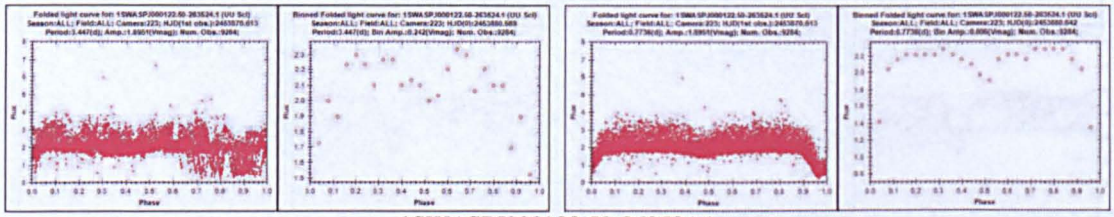

1SWASPJ000122.50-263524.1

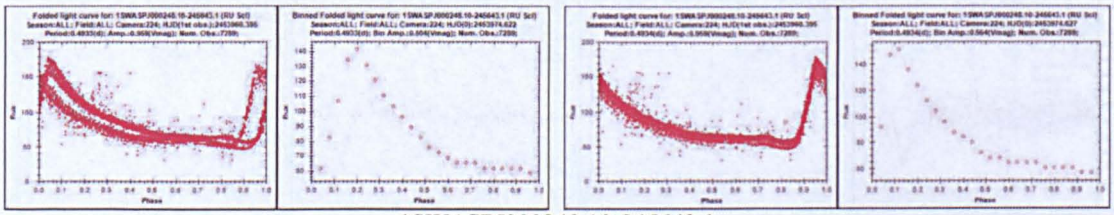

1SWASPJ000248.10-245643.1

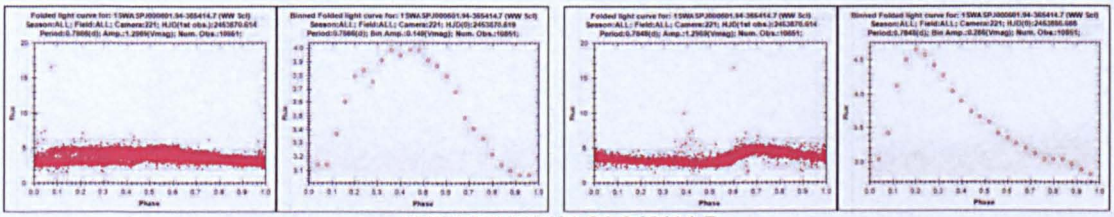

1SWASPJ000601.94-365414.7

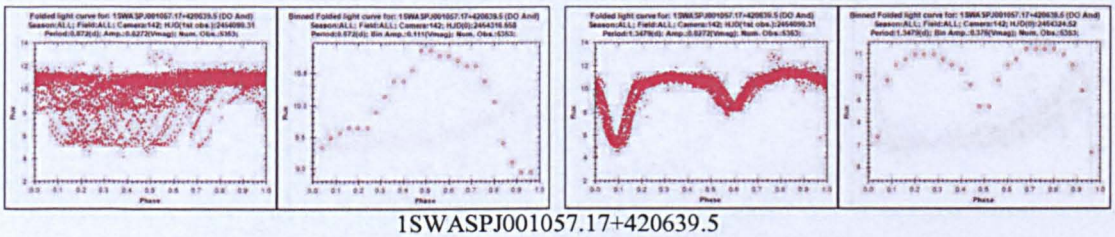

1SWASPJ001057.17+420639.5

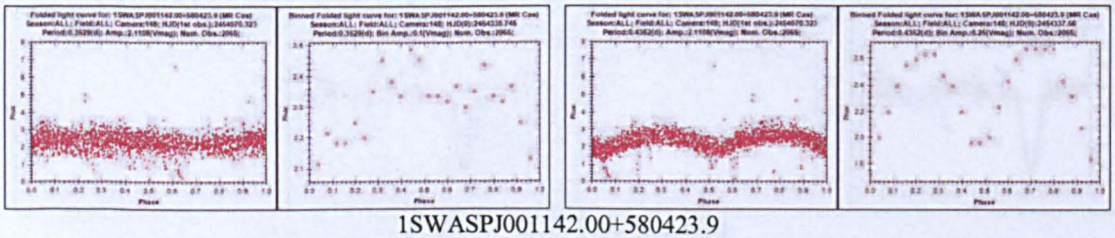

1SWASPJ001142.00+580423.9

Appendix 6 – GCVS has a more appropriate period than SuperWASP

GCVS period WASP period

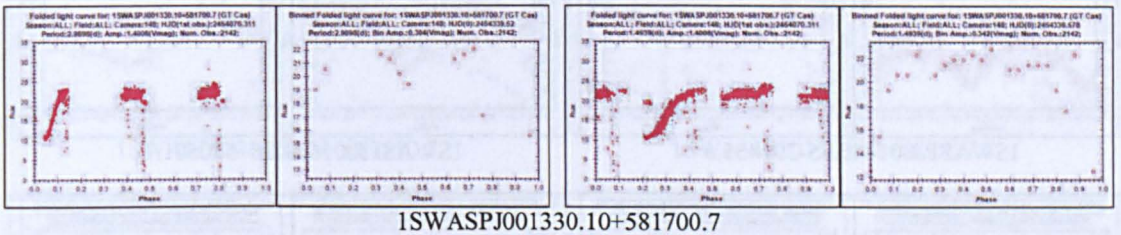

1SWASPJ001330.10+581700.7

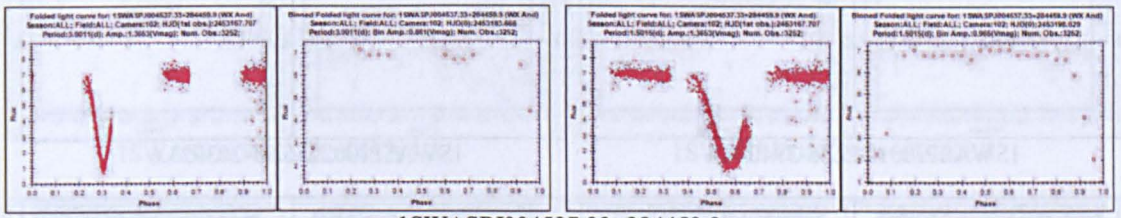

1SWASPJ004537.33+284459.9

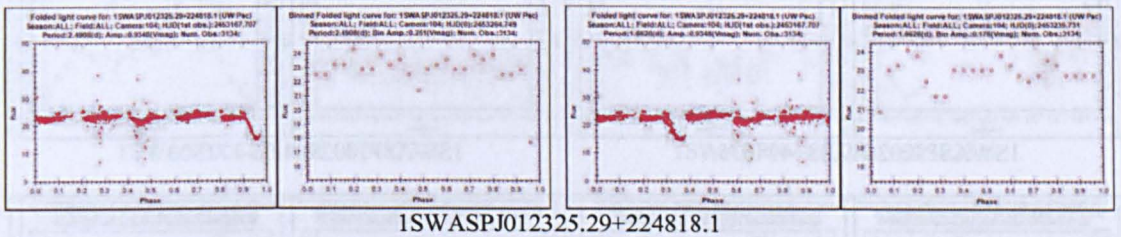

1SWASPJ012325.29+224818.1

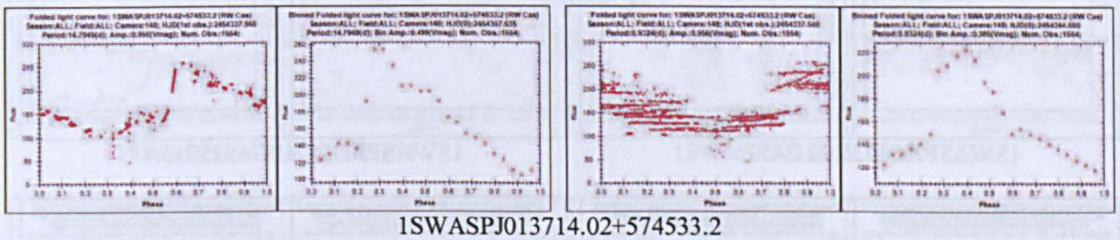

1SWASPJ013714.02+574533.2

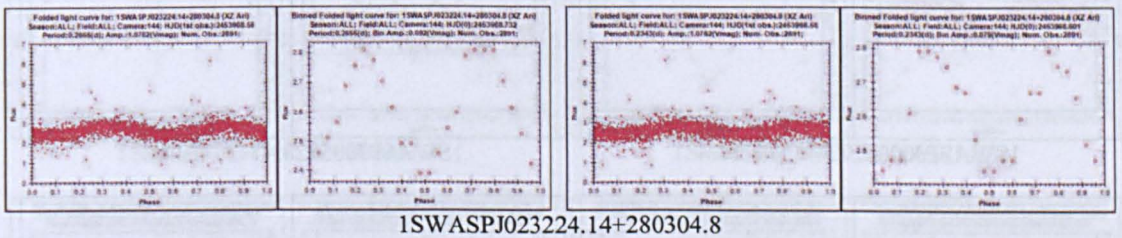

1SWASPJ023224.14+280304.8

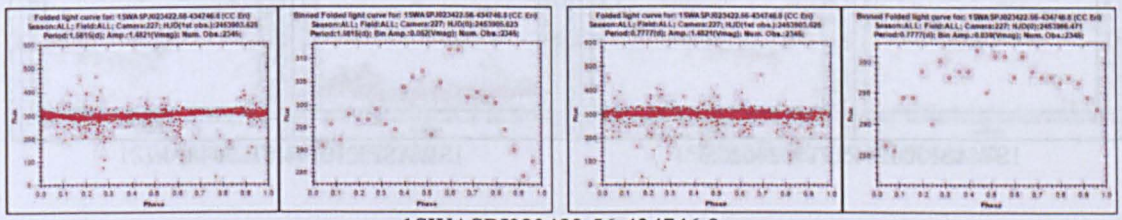

1SWASPJ023422.56-434746.8

Appendix 7 – SuperWASP objects that do not have GCVS periods

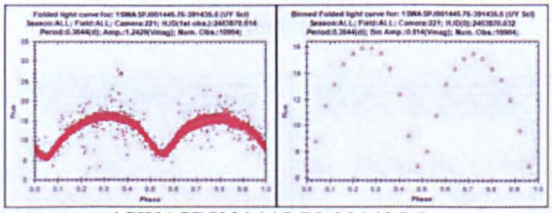

1SWASPJ001445.75-391435.5

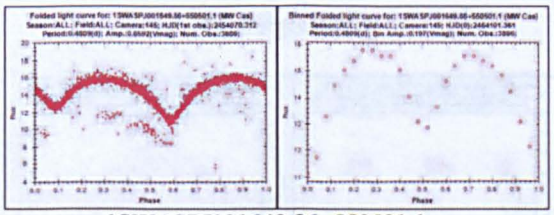

1SWASPJ001649.86+550501.1

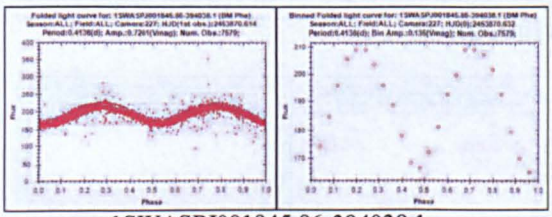

1SWASPJ001845.86-394038.1

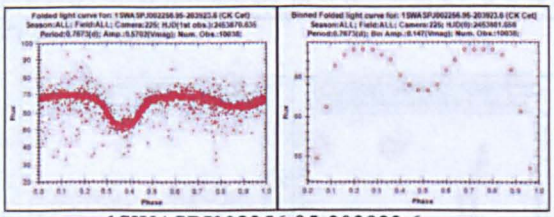

1SWASPJ002256.95-203923.6

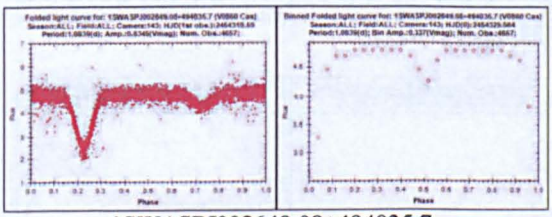

1SWASPJ002649.08+494035.7

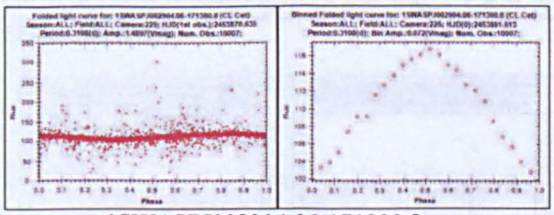

1SWASPJ002904.06-171300.8

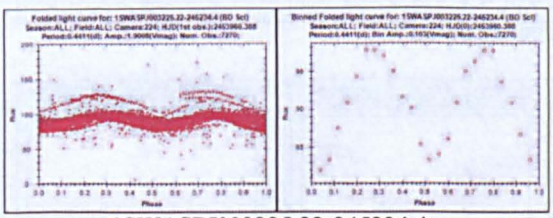

1SWASPJ003225.22-245234.4

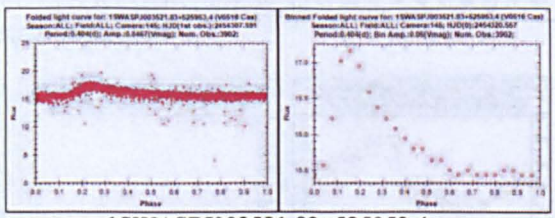

1SWASPJ003521.83+525953.4

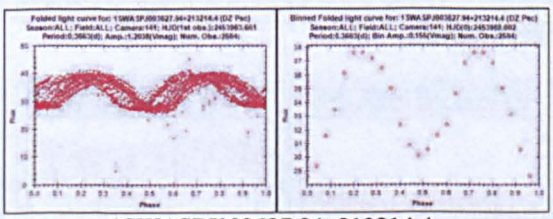

1SWASPJ003627.94+213214.4

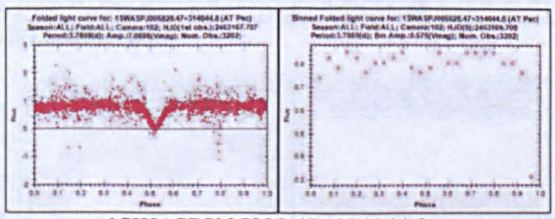

1SWASPJ005828.47+314044.8

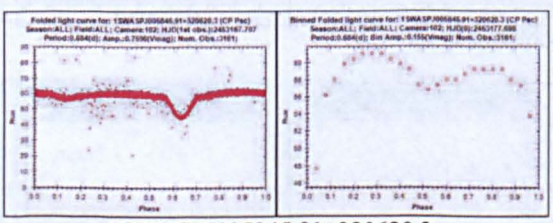

1SWASPJ005845.91+320620.3

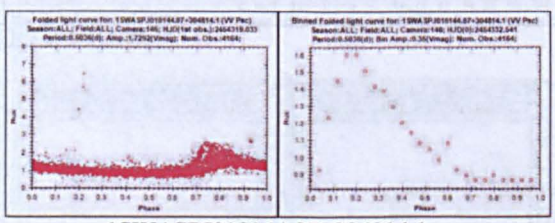

1SWASPJ010144.87+304814.1

Appendix 8a – SuperWASP CEP object class agree with the GCVS

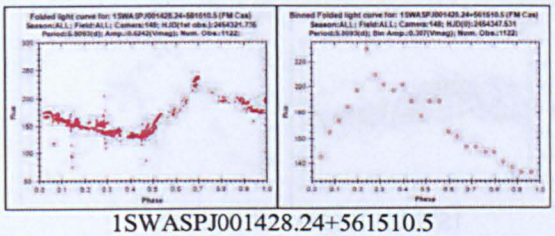

1SWASPJ001428.24+561510.5

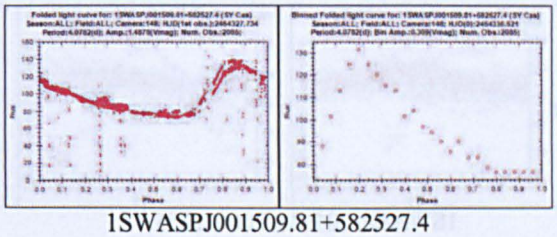

1SWASPJ001509.81+582527.4

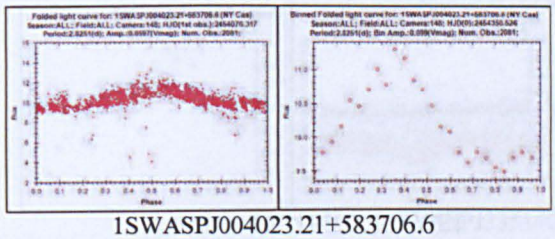

1SWASPJ004023.21+583706.6

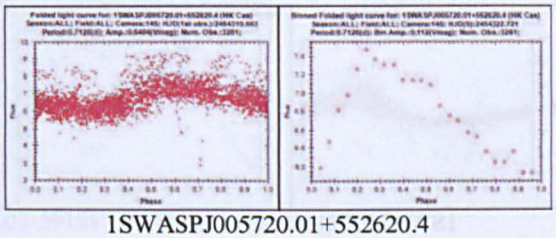

1SWASPJ005720.01+552620.4

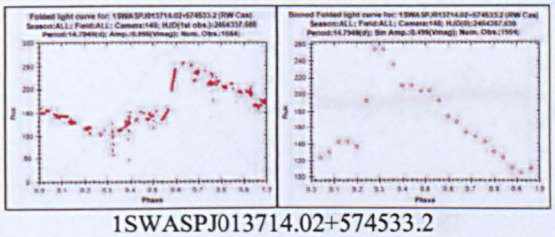

1SWASPJ013714.02+574533.2

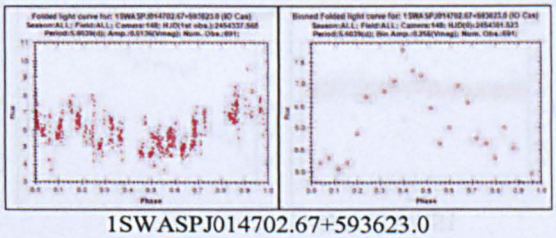

1SWASPJ014702.67+593623.0

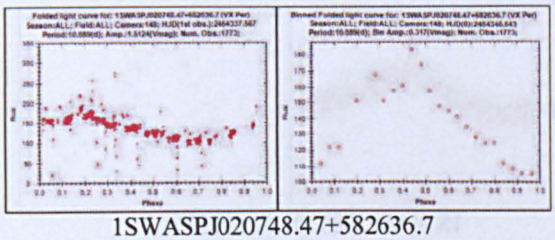

1SWASPJ020748.47+582636.7

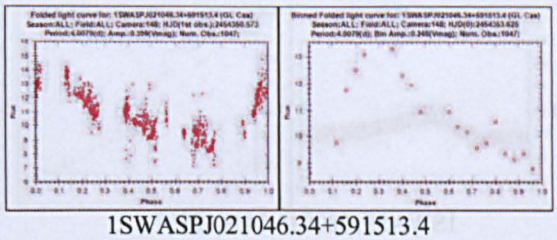

1SWASPJ021046.34+591513.4

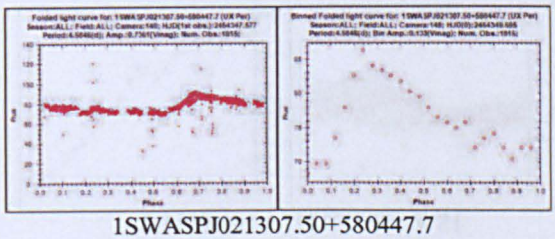

1SWASPJ021307.50+580447.7

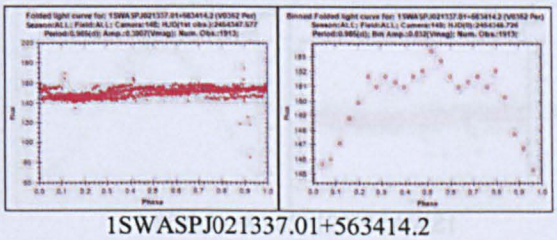

1SWASPJ021337.01+563414.2

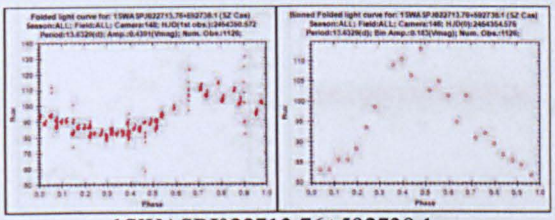

1SWASPJ022713.76+592738.1

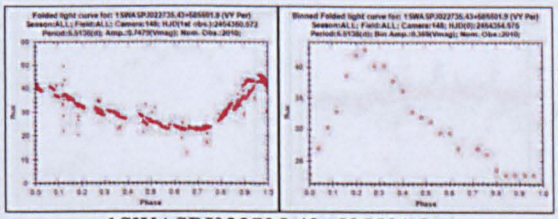

1SWASPJ022735.43+585501.9

Appendix 8b – SuperWASP DSCT object class agree with the GCVS

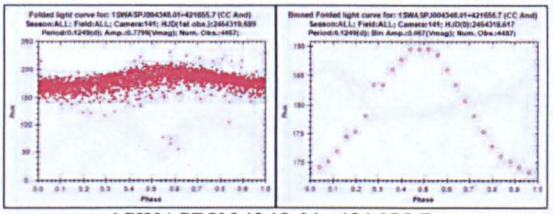

1SWASPJ004348.01+421655.7

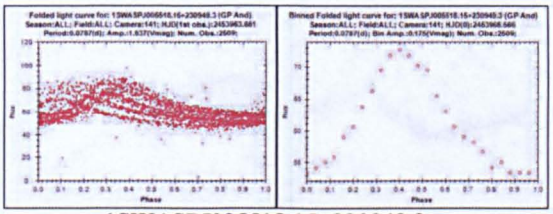

1SWASPJ005518.15+230949.3

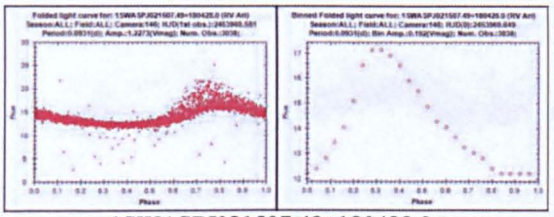

1SWASPJ021507.49+180428.0

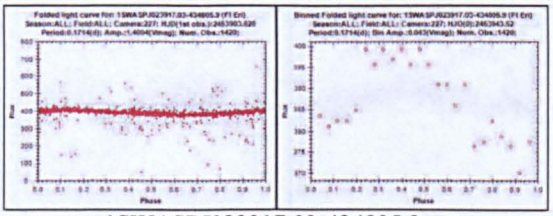

1SWASPJ023917.03-434805.9

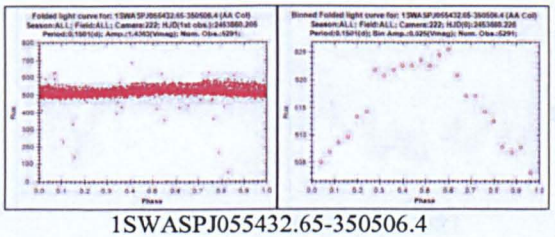

1SWASPJ055432.65-350506.4

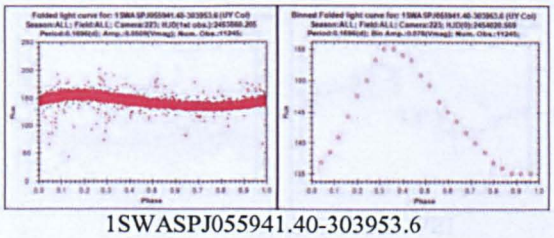

1SWASPJ055941.40-303953.6

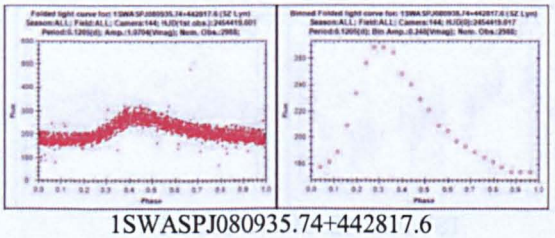

1SWASPJ080935.74+442817.6

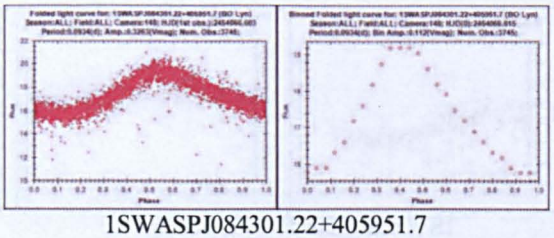

1SWASPJ084301.22+405951.7

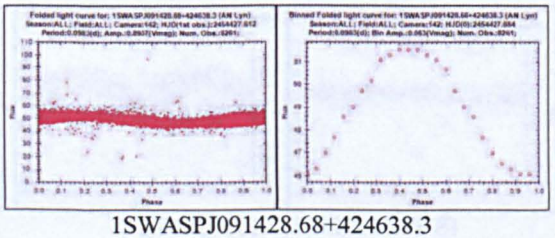

1SWASPJ091428.68+424638.3

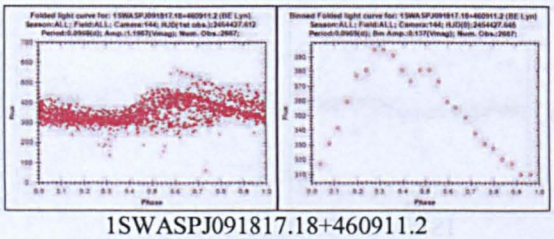

1SWASPJ091817.18+460911.2

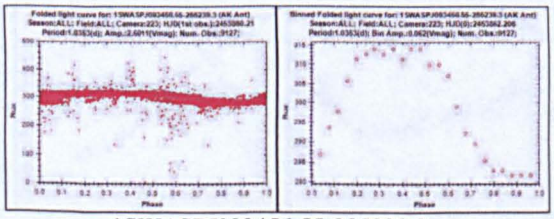

1SWASPJ093456.55-285239.3

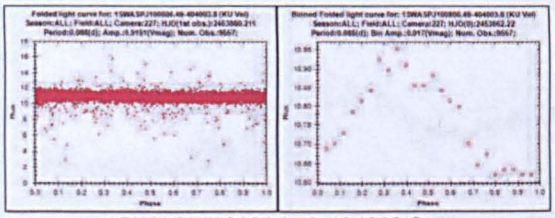

1SWASPJ100806.49-404003.8

Appendix 8c – SuperWASP E object class agree with the GCVS

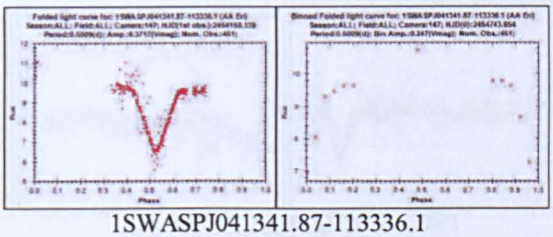

1SWASPJ041341.87-113336.1

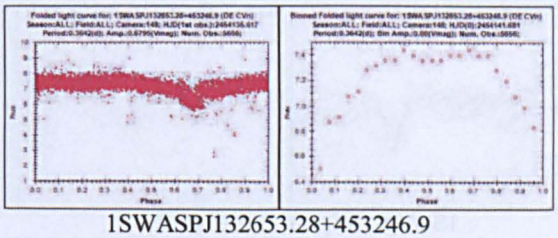

1SWASPJ132653.28+453246.9

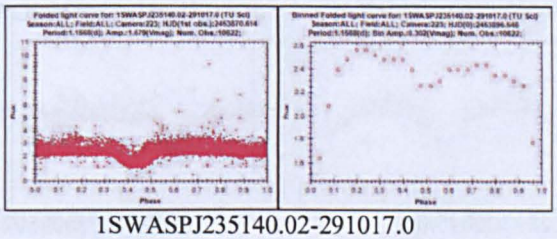

1SWASPJ235140.02-291017.0

Appendix 8d – SuperWASP EA object class agree with the GCVS

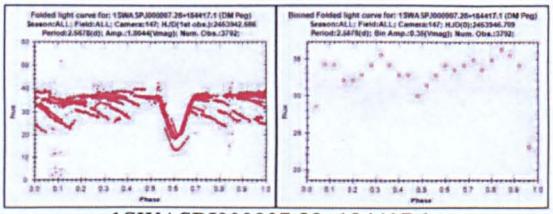

1SWASPJ000007.28+184417.1

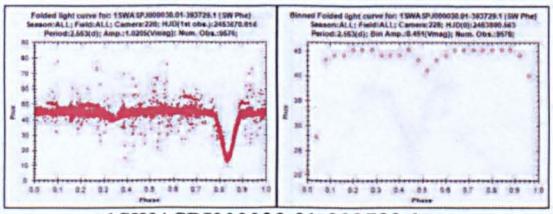

1SWASPJ000030.01-393729.1

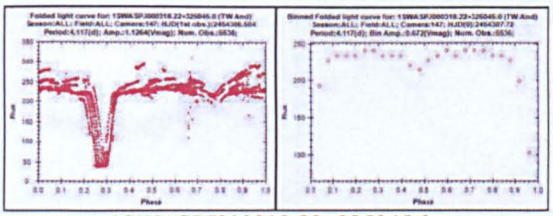

1SWASPJ000318.22+325045.0

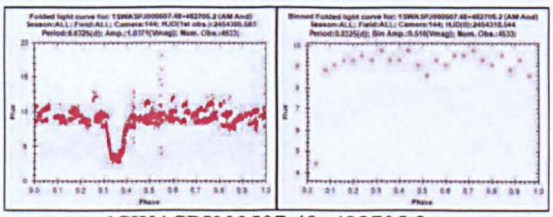

1SWASPJ000507.48+482705.2

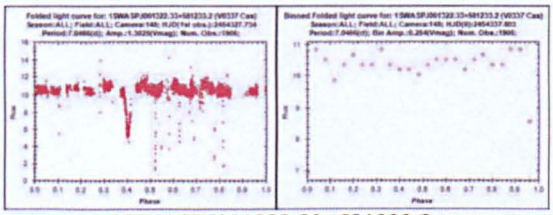

1SWASPJ001322.33+581233.2

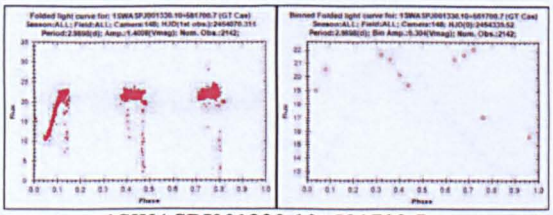

1SWASPJ001330.10+581700.7

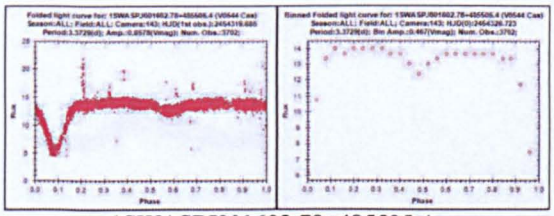

1SWASPJ001602.78+485505.4

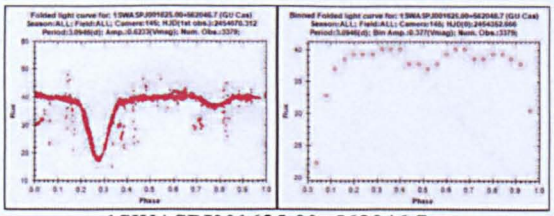

1SWASPJ001625.00+562046.7

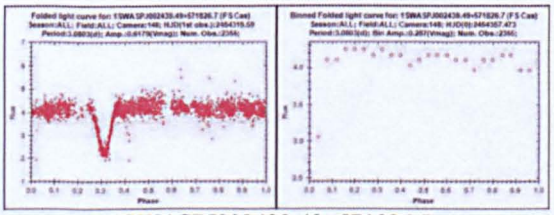

1SWASPJ002439.49+571826.7

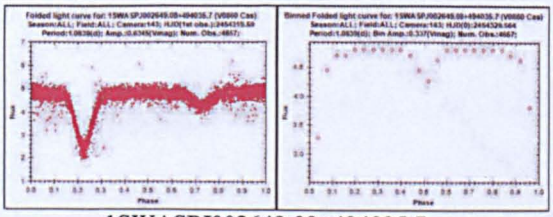

1SWASPJ002649.08+494035.7

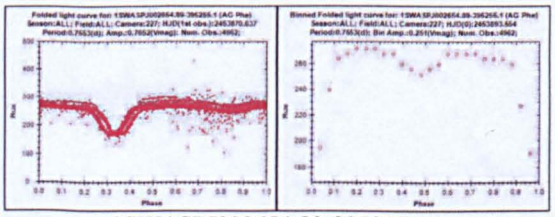

1SWASPJ002654.89-395255.1

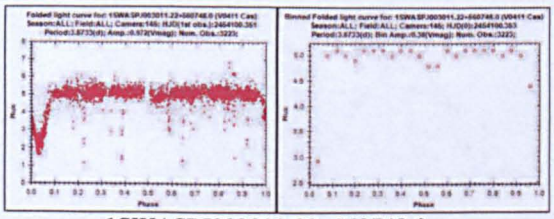

1SWASPJ003011.22+560748.0

Appendix 8e – SuperWASP EB object class agree with the GCVS

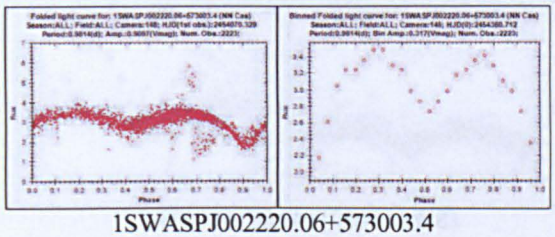
1SWASPJ002220.06+573003.4

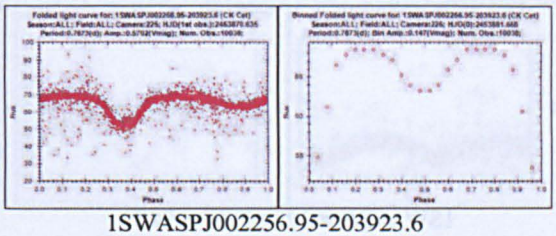
1SWASPJ002256.95-203923.6

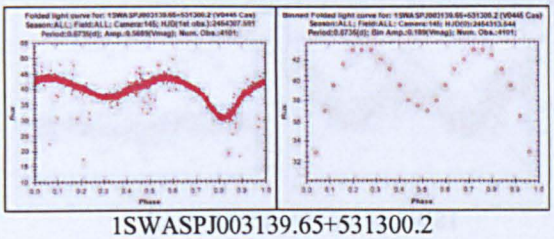
1SWASPJ003139.65+531300.2

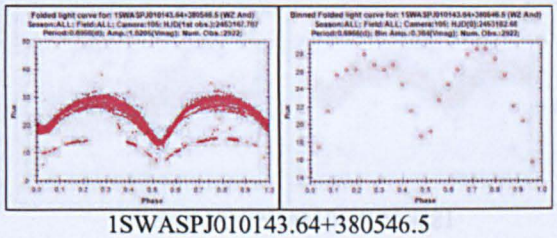
1SWASPJ010143.64+380546.5

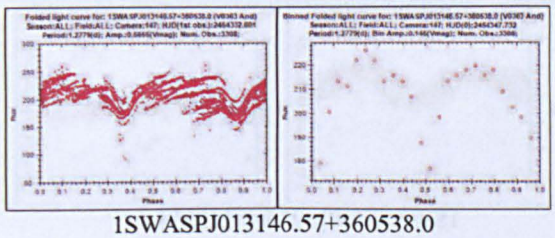
1SWASPJ013146.57+360538.0

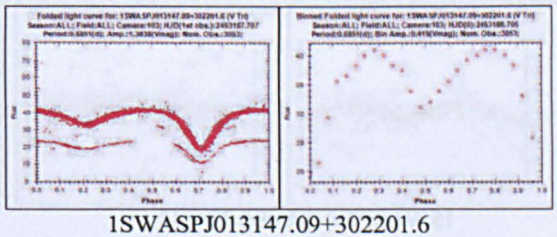
1SWASPJ013147.09+302201.6

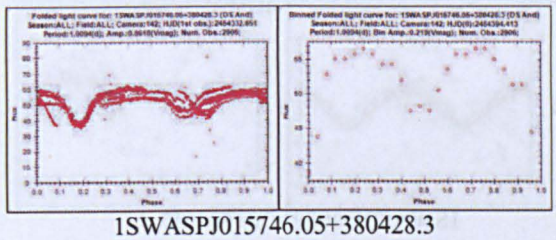
1SWASPJ015746.05+380428.3

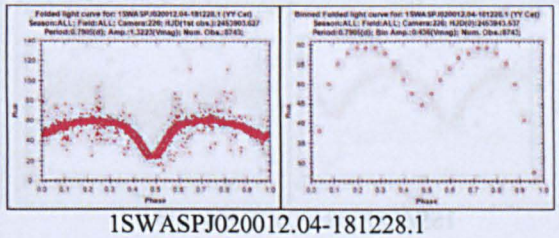
1SWASPJ020012.04-181228.1

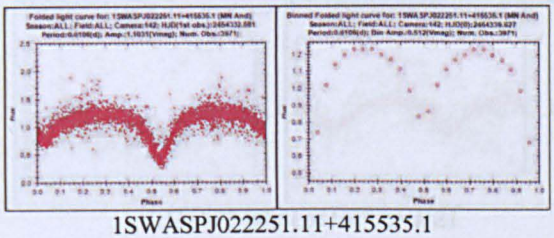
1SWASPJ022251.11+415535.1

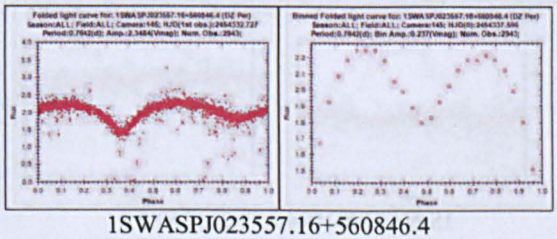
1SWASPJ023557.16+560846.4

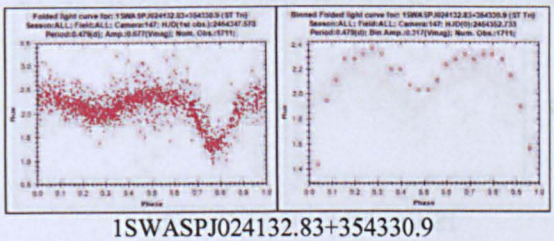
1SWASPJ024132.83+354330.9

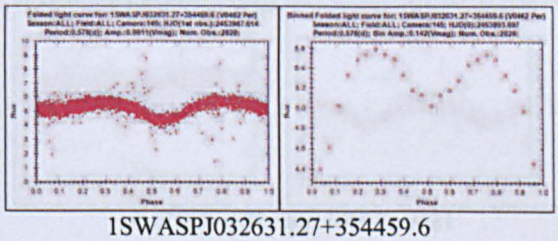
1SWASPJ032631.27+354459.6

Appendix 8f – SuperWASP EW object class agree with the GCVS

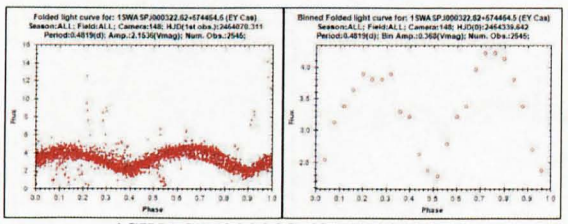

1SWASPJ000322.62+574454.5

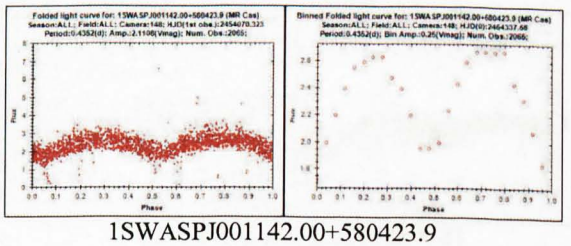

1SWASPJ001142.00+580423.9

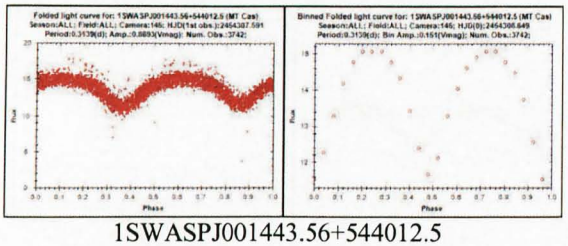

1SWASPJ001443.56+544012.5

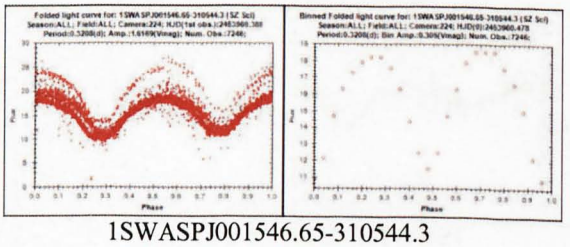

1SWASPJ001546.65-310544.3

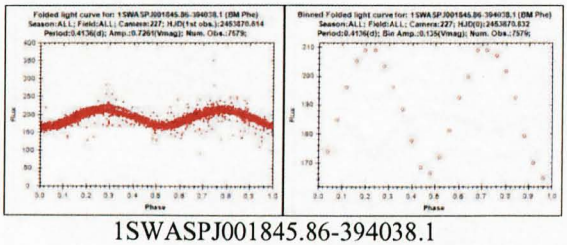

1SWASPJ001845.86-394038.1

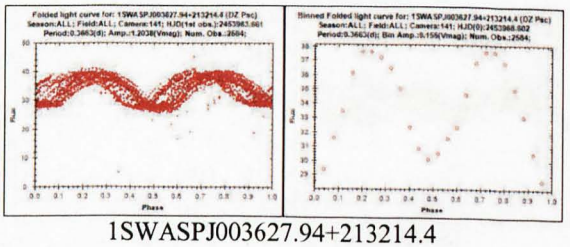

1SWASPJ003627.94+213214.4

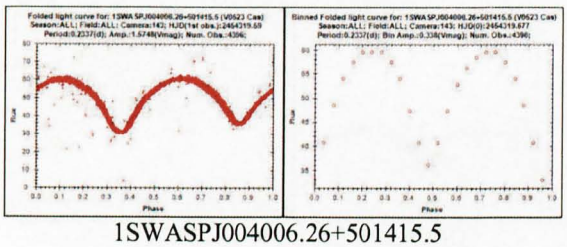

1SWASPJ004006.26+501415.5

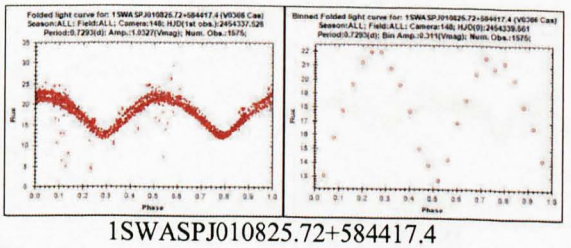

1SWASPJ010825.72+584417.4

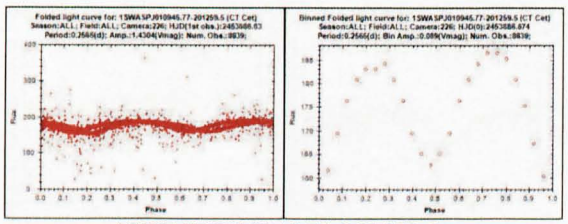

1SWASPJ010945.77-201259.5

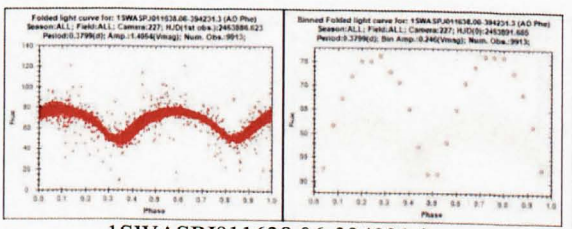

1SWASPJ011638.06-394231.3

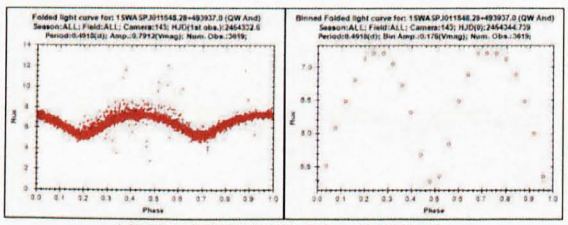

1SWASPJ011848.28+493937.0

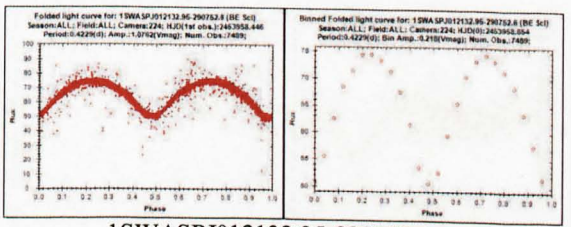

1SWASPJ012132.95-290752.6

Appendix 8g – SuperWASP RM object class agree with the GCVS

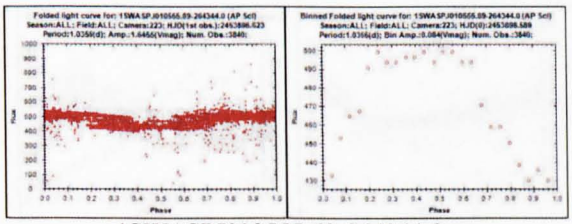

1SWASPJ010555.69-264344.0

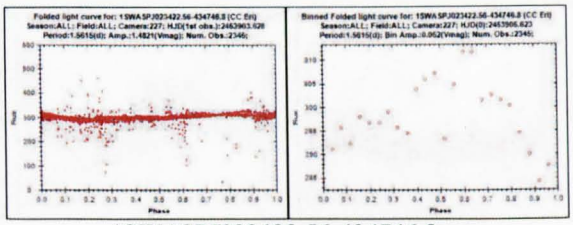

1SWASPJ023422.56-434746.8

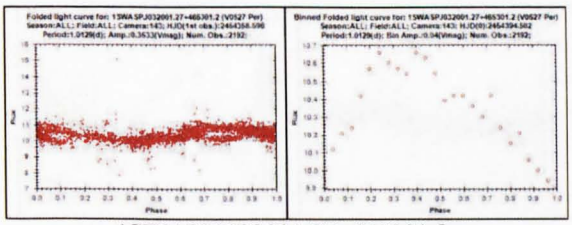

1SWASPJ032001.27+465301.2

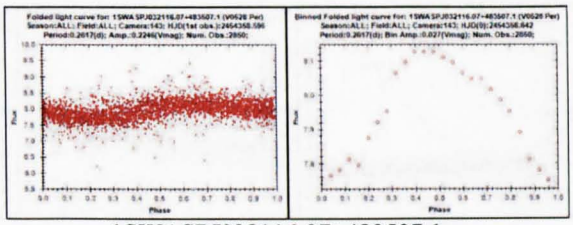

1SWASPJ032116.07+483507.1

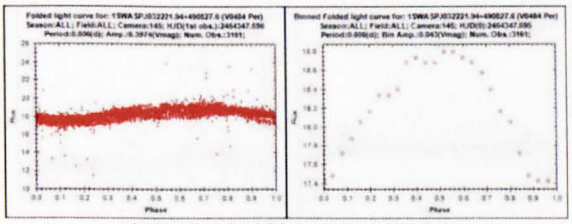

1SWASPJ032221.94+490827.6

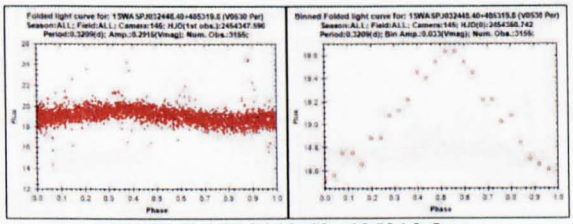

1SWASPJ032448.40+485319.8

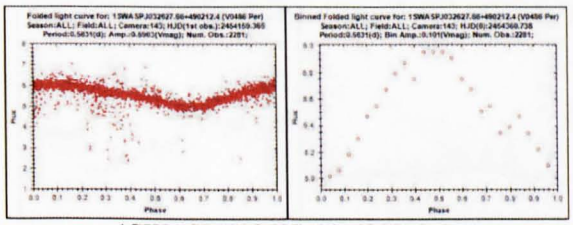

1SWASPJ032627.66+490212.4

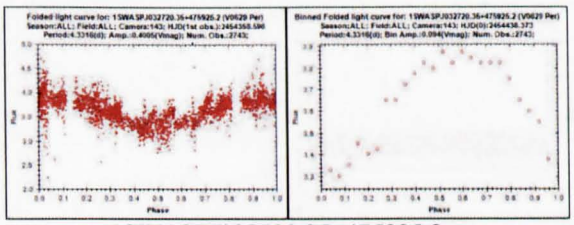

1SWASPJ032720.35+475925.2

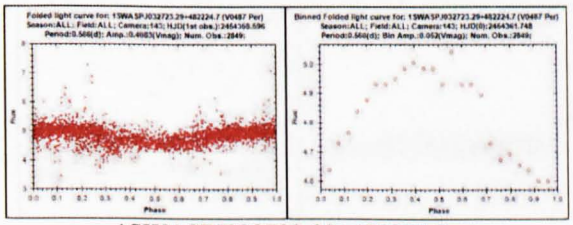

1SWASPJ032723.29+482224.7

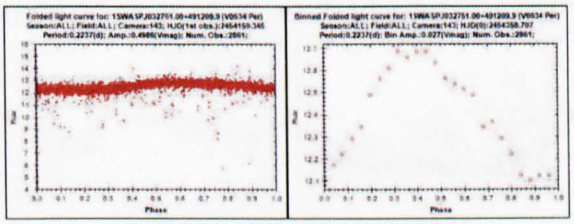

1SWASPJ032751.00+491209.9

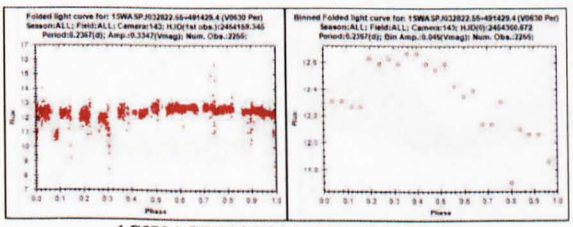

1SWASPJ032822.55+491429.4

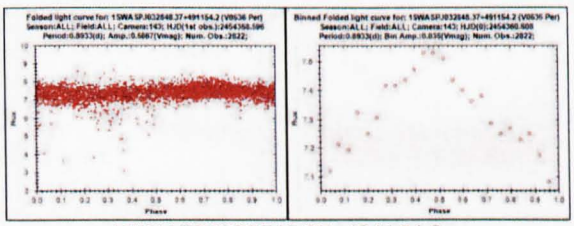

1SWASPJ032848.37+491154.2

Appendix 8h – SuperWASP RR object class agree with the GCVS

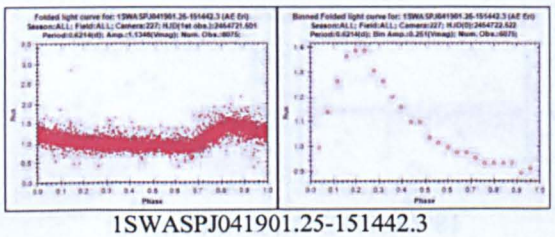
1SWASPJ041901.25-151442.3

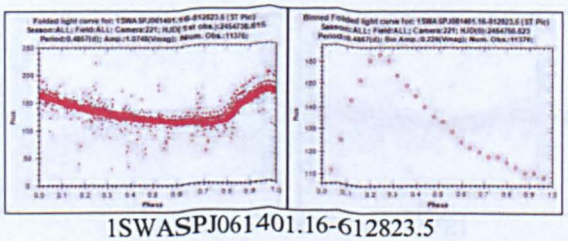
1SWASPJ061401.16-612823.5

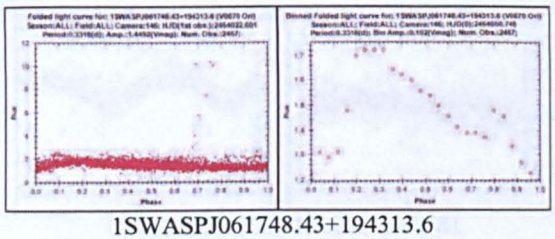
1SWASPJ061748.43+194313.6

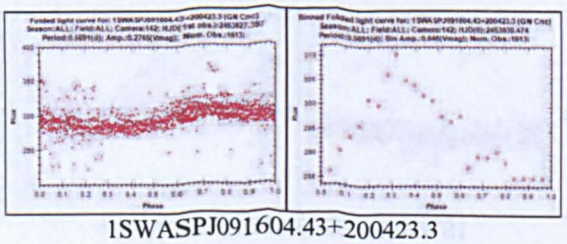
1SWASPJ091604.43+200423.3

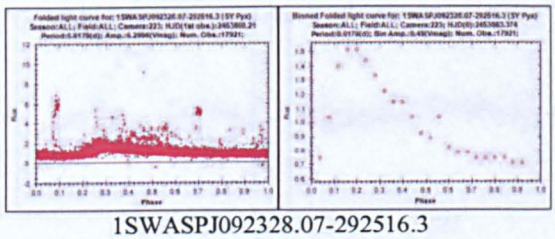
1SWASPJ092328.07-292516.3

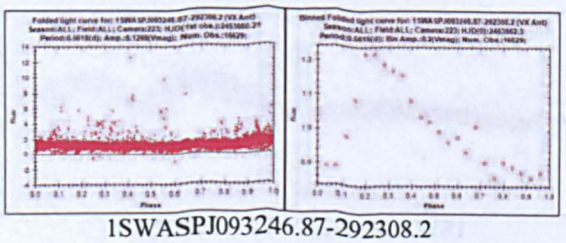
1SWASPJ093246.87-292308.2

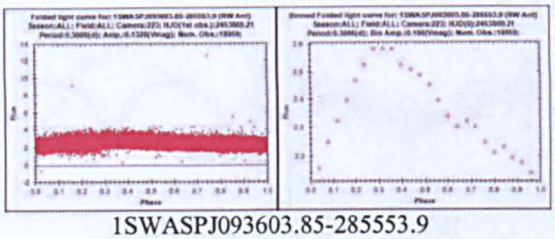
1SWASPJ093603.85-285553.9

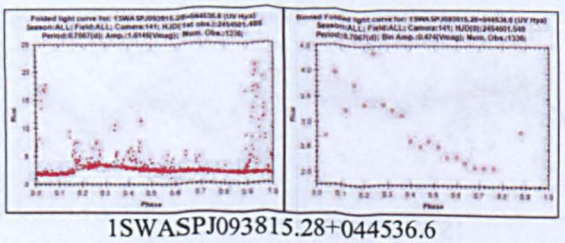
1SWASPJ093815.28+044536.6

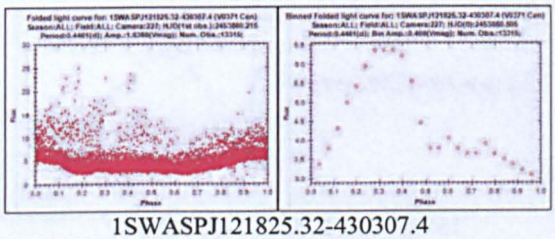
1SWASPJ121825.32-430307.4

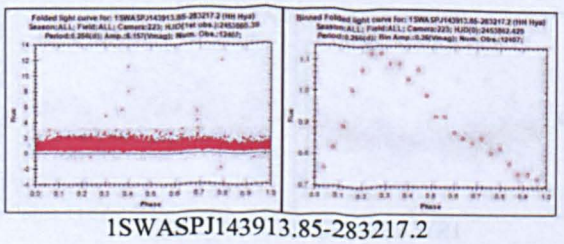
1SWASPJ143913.85-283217.2

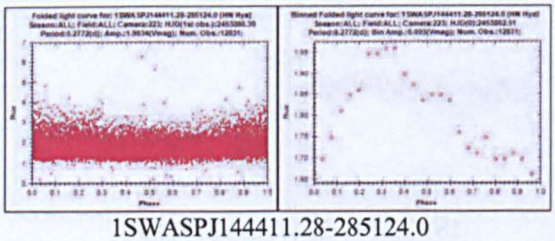
1SWASPJ144411.28-285124.0

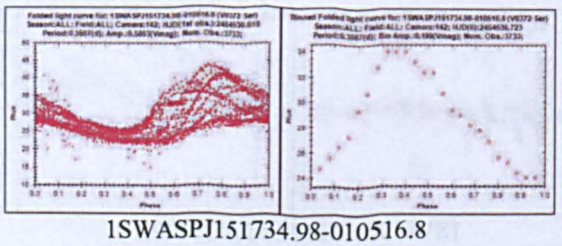
1SWASPJ151734.98-010516.8

Appendix 8i – SuperWASP RRAB object class agree with the GCVS

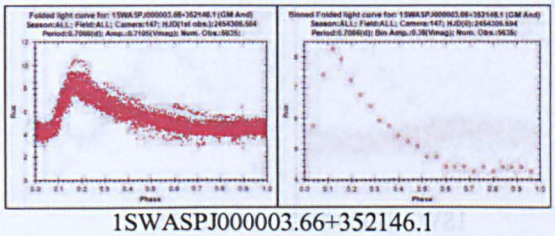

1SWASPJ000003.66+352146.1

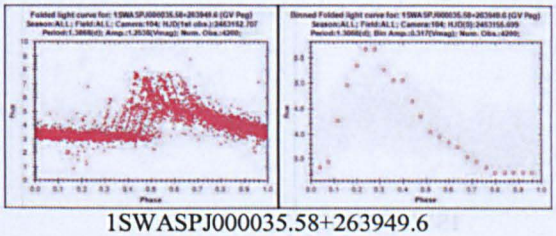

1SWASPJ000035.58+263949.6

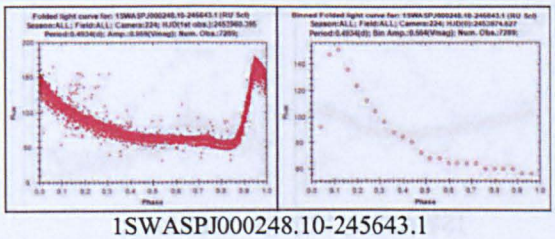

1SWASPJ000248.10-245643.1

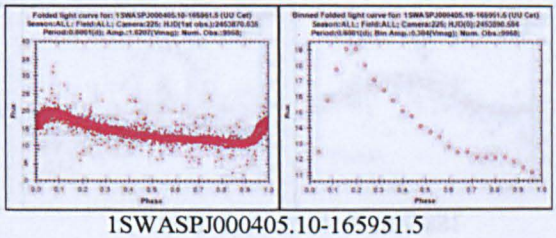

1SWASPJ000405.10-165951.5

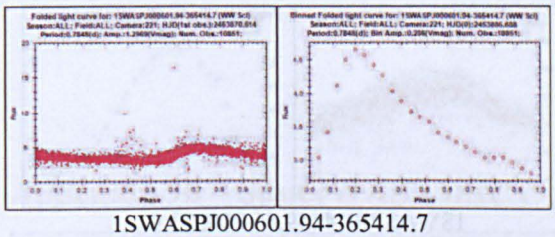

1SWASPJ000601.94-365414.7

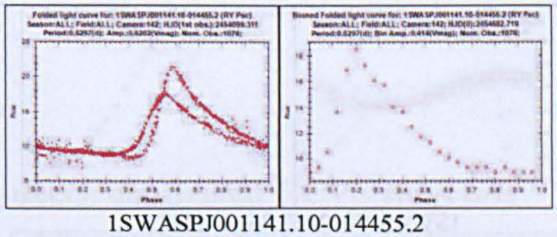

1SWASPJ001141.10-014455.2

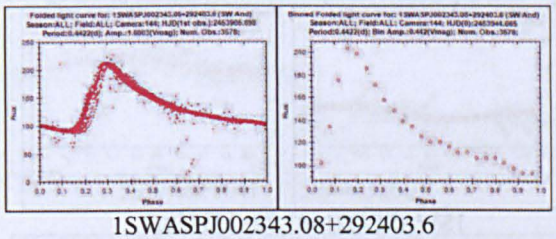

1SWASPJ002343.08+292403.6

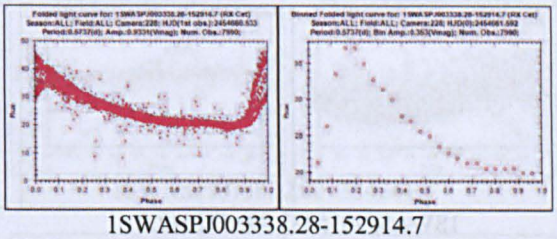

1SWASPJ003338.28-152914.7

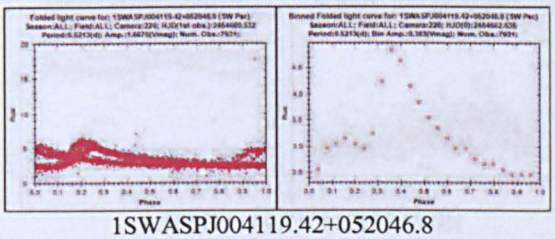

1SWASPJ004119.42+052046.8

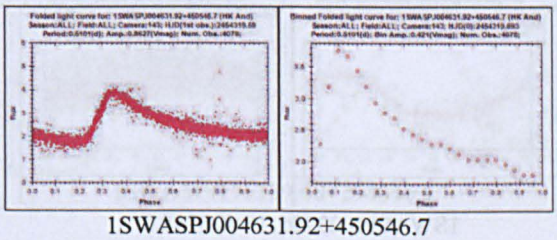

1SWASPJ004631.92+450546.7

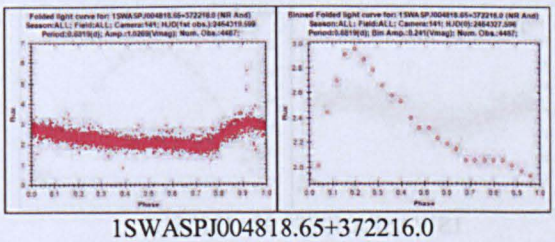

1SWASPJ004818.65+372216.0

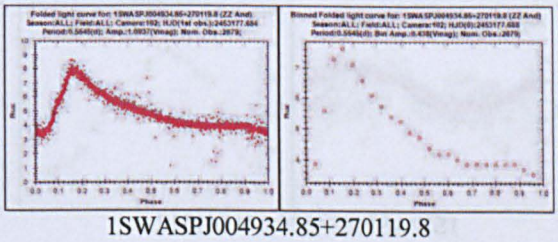

1SWASPJ004934.85+270119.8

Appendix 8j – SuperWASP RRC object class agree with the GCVS

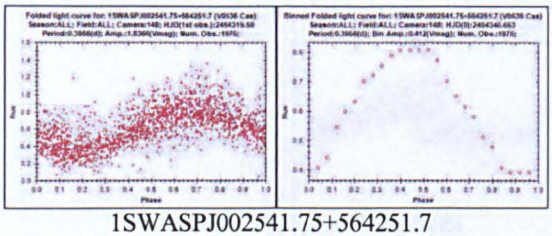
1SWASPJ002541.75+564251.7

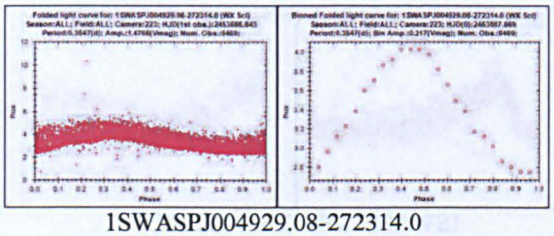
1SWASPJ004929.08-272314.0

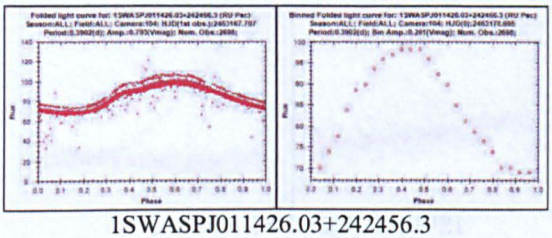
1SWASPJ011426.03+242456.3

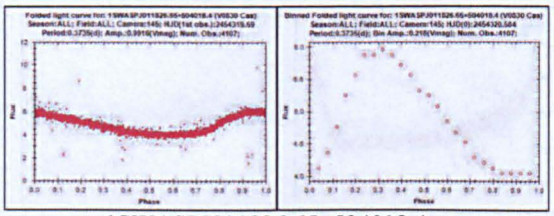
1SWASPJ011826.65+504018.4

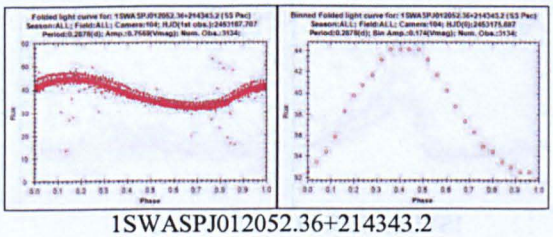
1SWASPJ012052.36+214343.2

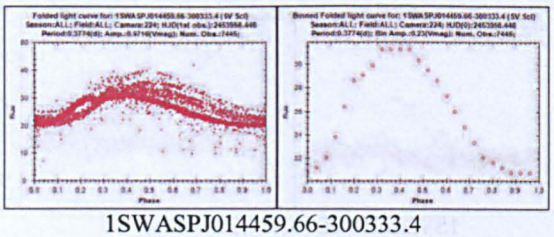
1SWASPJ014459.66-300333.4

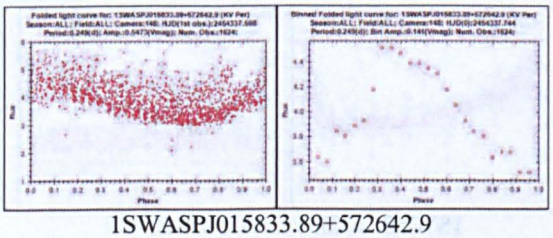
1SWASPJ015833.89+572642.9

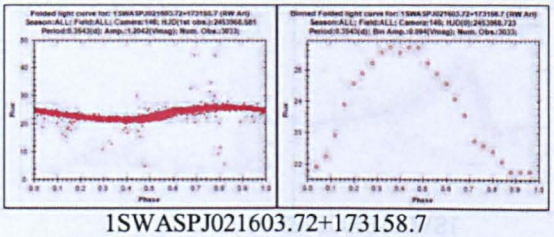
1SWASPJ021603.72+173158.7

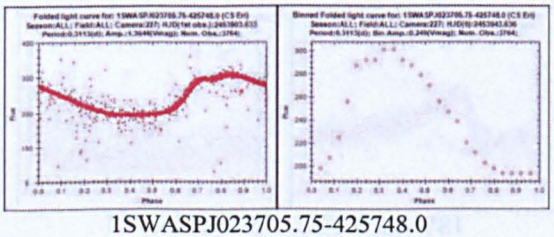
1SWASPJ023705.75-425748.0

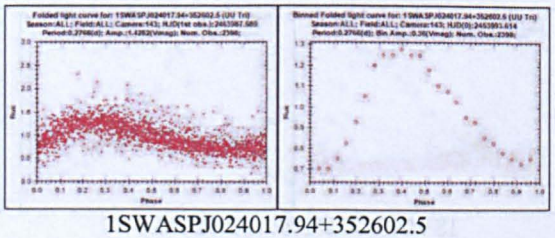
1SWASPJ024017.94+352602.5

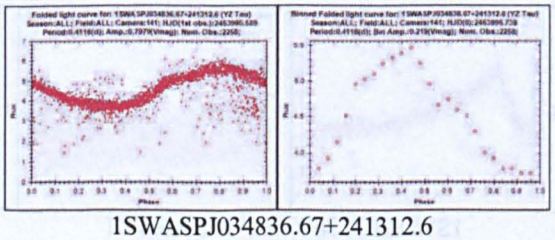
1SWASPJ034836.67+241312.6

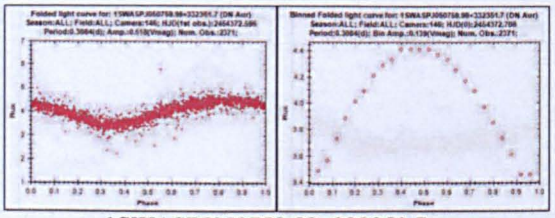
1SWASPJ050759.98+332351.7

Appendix 9a – SuperWASP CEP objects: confirmed GCVS sub-class

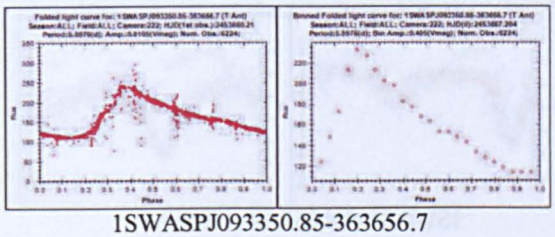

1SWASPJ093350.85-363656.7

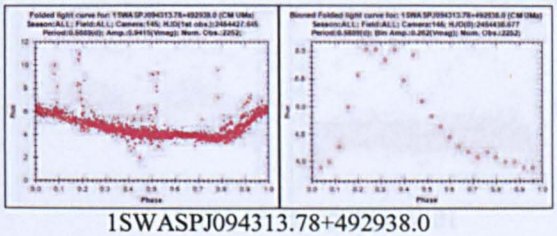

1SWASPJ094313.78+492938.0

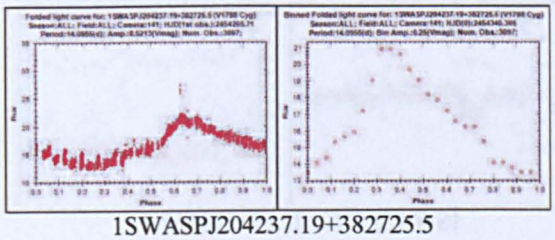

1SWASPJ204237.19+382725.5

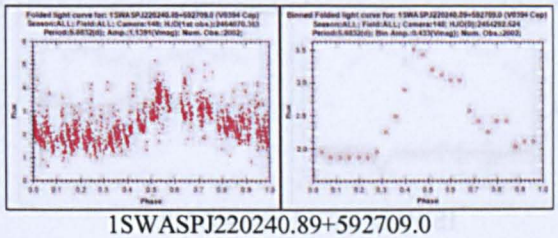

1SWASPJ220240.89+592709.0

Appendix 9b – SuperWASP DSCT objects: confirmed GCVS sub-class

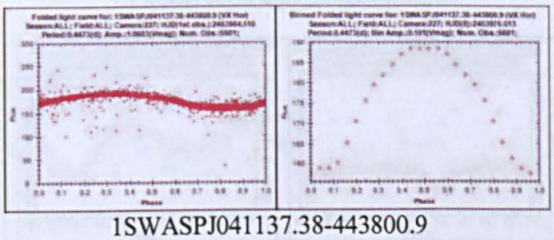

1SWASPJ041137.38-443800.9

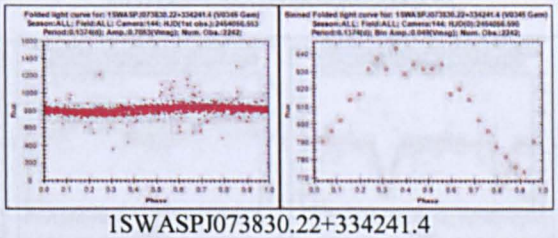

1SWASPJ073830.22+334241.4

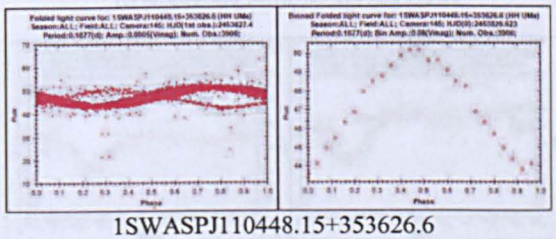

1SWASPJ110448.15+353626.6

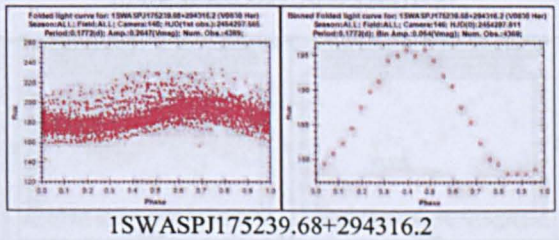

1SWASPJ175239.68+294316.2

Appendix 9c – SuperWASP EA objects: confirmed GCVS sub-class

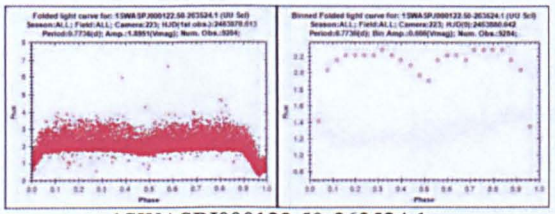
1SWASPJ000122.50-263524.1

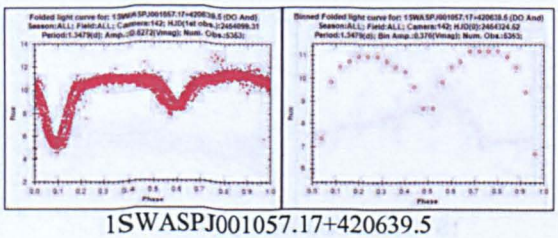
1SWASPJ001057.17+420639.5

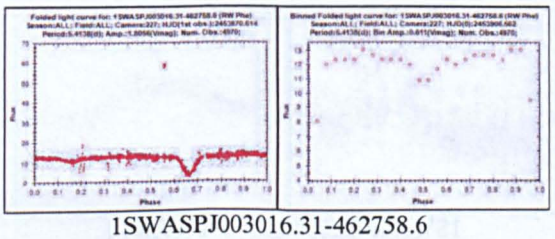
1SWASPJ003016.31-462758.6

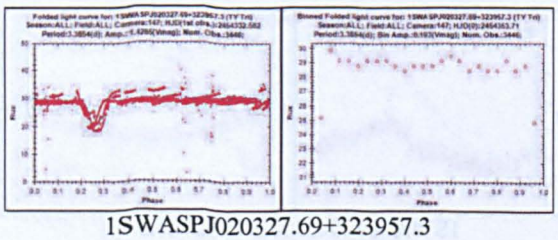
1SWASPJ020327.69+323957.3

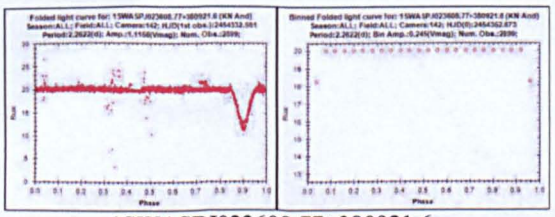
1SWASPJ023608.77+380921.6

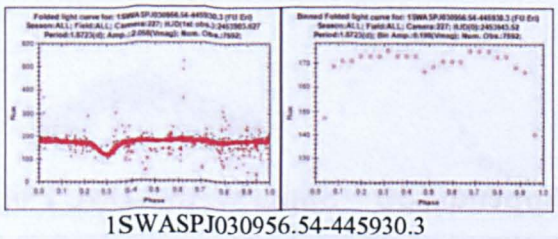
1SWASPJ030956.54-445930.3

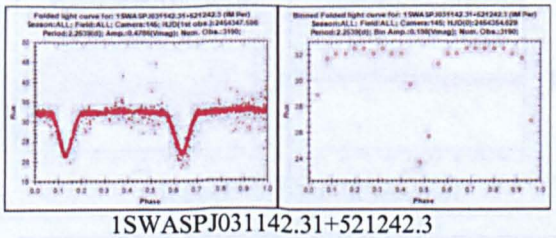
1SWASPJ031142.31+521242.3

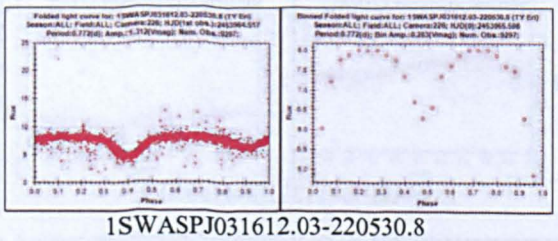
1SWASPJ031612.03-220530.8

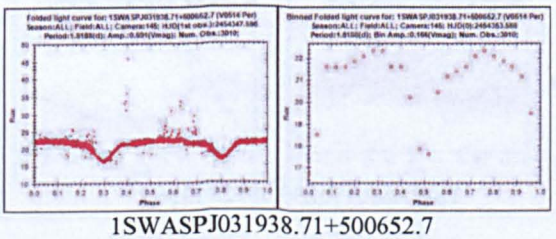
1SWASPJ031938.71+500652.7

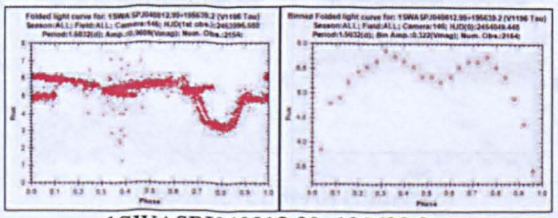
1SWASPJ040812.99+195639.2

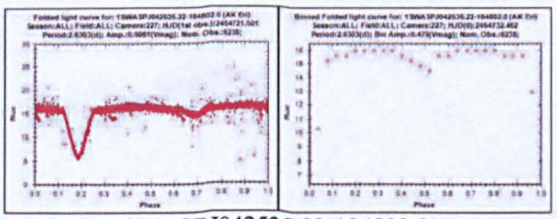
1SWASPJ042535.22-184802.0

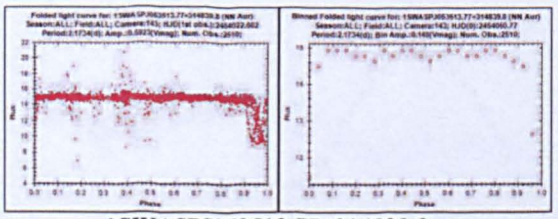
1SWASPJ053513.77+314839.8

Appendix 9d – SuperWASP EB objects: confirmed GCVS sub-class

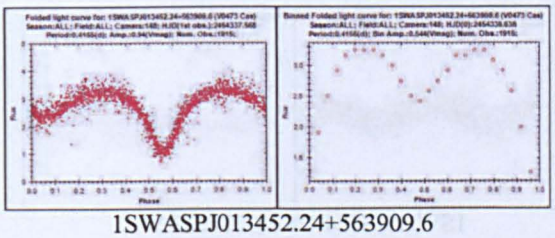

1SWASPJ013452.24+563909.6

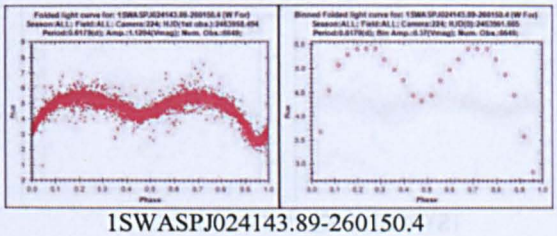

1SWASPJ024143.89-260150.4

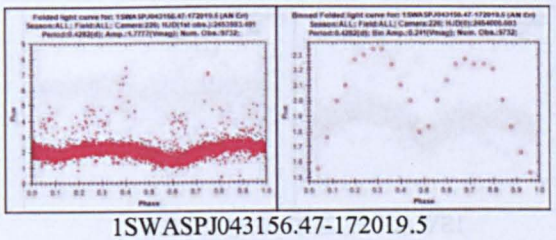

1SWASPJ043156.47-172019.5

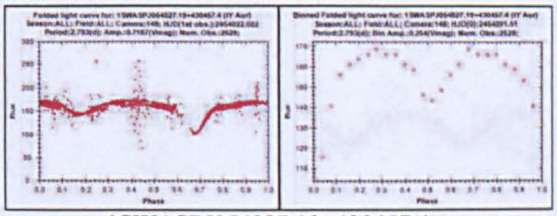

1SWASPJ054827.19+430457.4

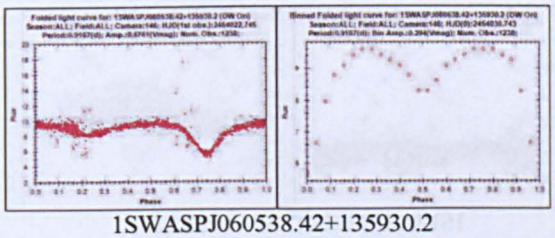

1SWASPJ060538.42+135930.2

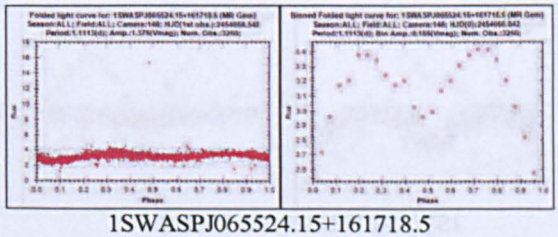

1SWASPJ065524.15+161718.5

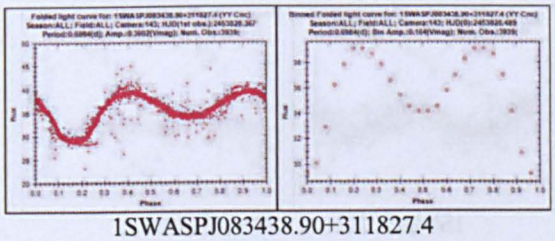

1SWASPJ083438.90+311827.4

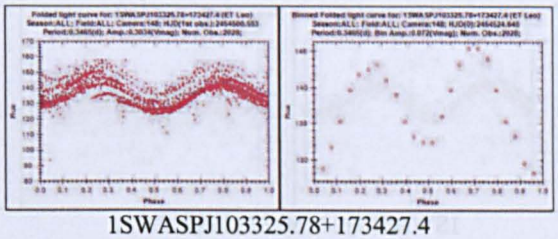

1SWASPJ103325.78+173427.4

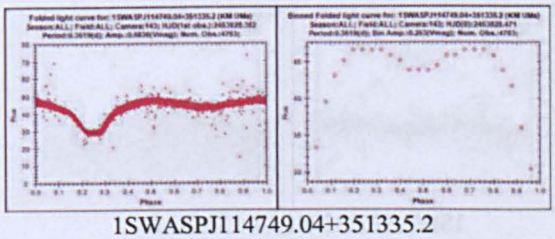

1SWASPJ114749.04+351335.2

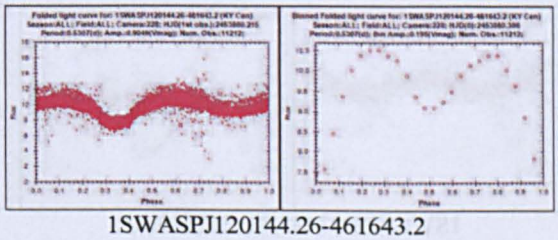

1SWASPJ120144.26-461643.2

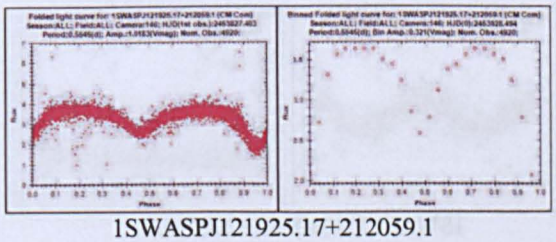

1SWASPJ121925.17+212059.1

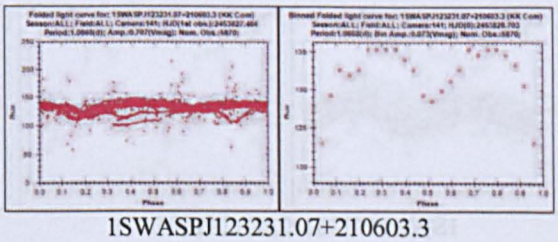

1SWASPJ123231.07+210603.3

Appendix 9e – SuperWASP EW objects: confirmed GCVS sub-class

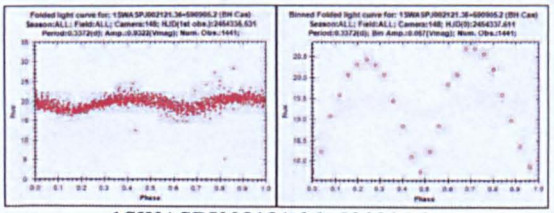
1SWASPJ002121.36+590905.2

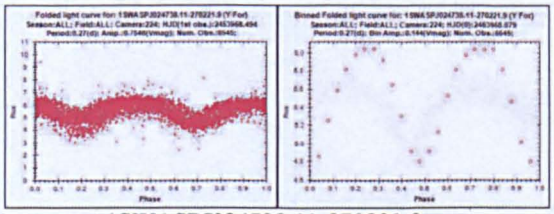
1SWASPJ024738.11-270221.9

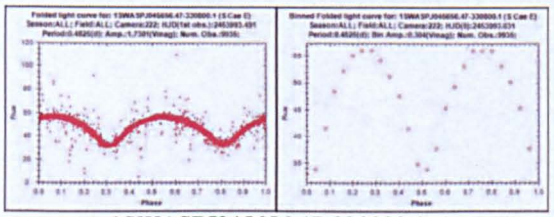
1SWASPJ045656.47-330800.1

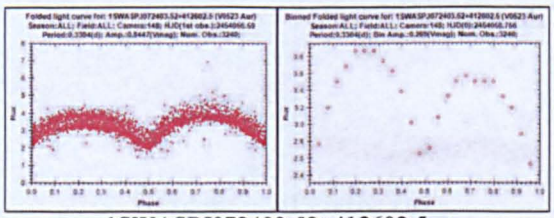
1SWASPJ072403.52+412602.5

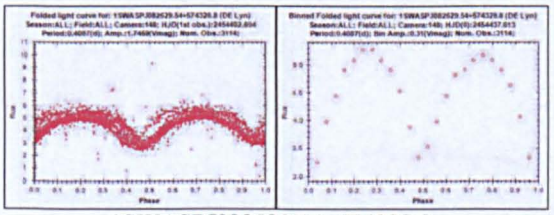
1SWASPJ082529.54+574328.8

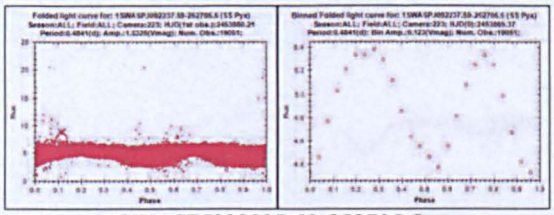
1SWASPJ092237.59-252705.5

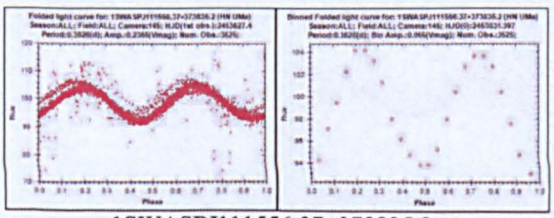
1SWASPJ111556.37+373835.2

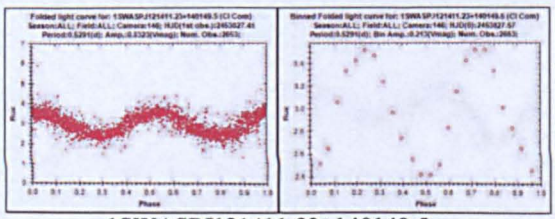
1SWASPJ121411.23+140149.5

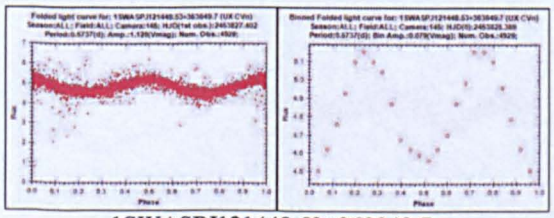
1SWASPJ121448.53+363849.7

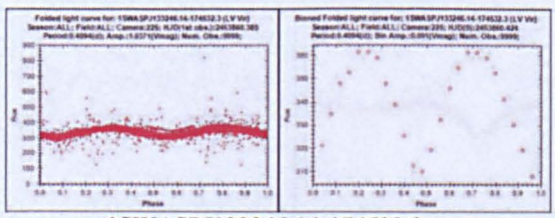
1SWASPJ133246.14-174532.3

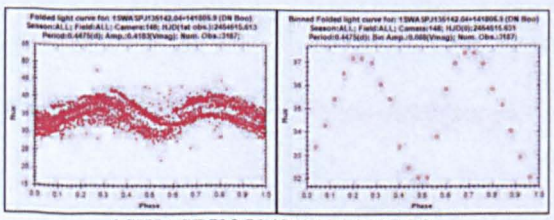
1SWASPJ135142.04+141805.9

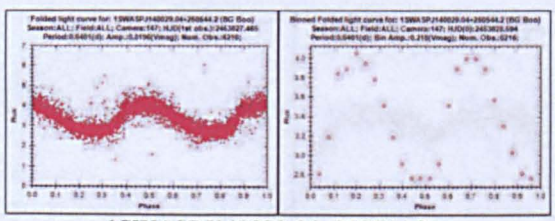
1SWASPJ140029.04+250544.2

Appendix 9f – SuperWASP RM objects: confirmed GCVS sub-class

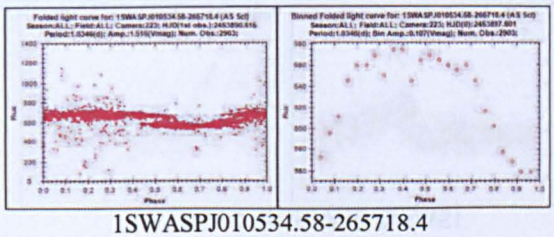

1SWASPJ010534.58-265718.4

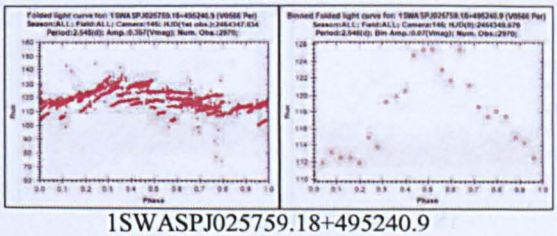

1SWASPJ025759.18+495240.9

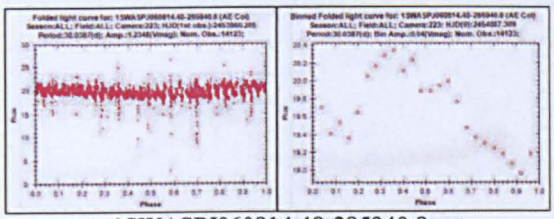

1SWASPJ060814.48-285940.8

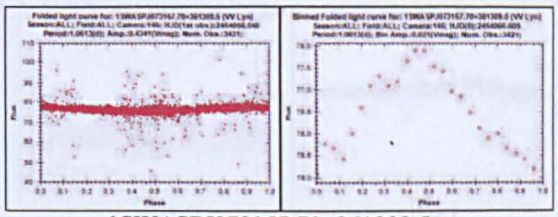

1SWASPJ073157.70+361309.5

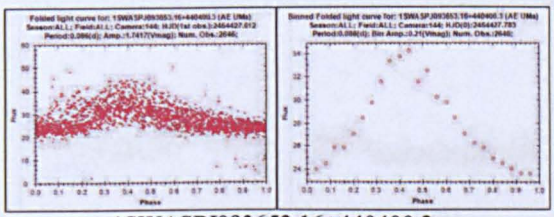

1SWASPJ093653.16+440400.3

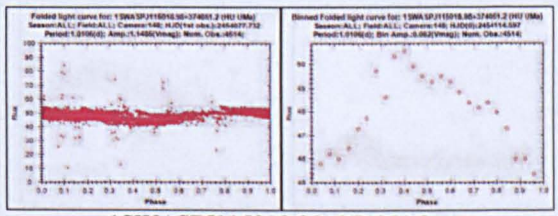

1SWASPJ115018.98+374051.2

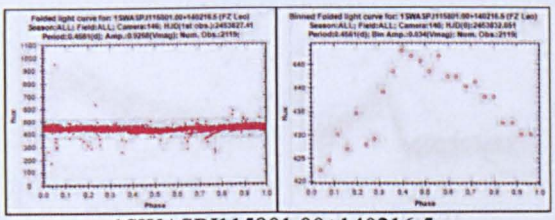

1SWASPJ115801.00+140216.5

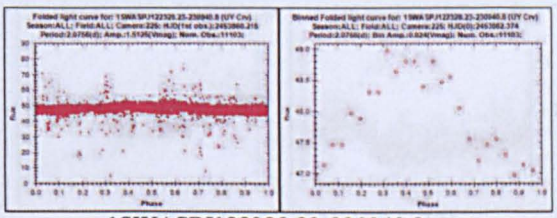

1SWASPJ122328.23-230940.8

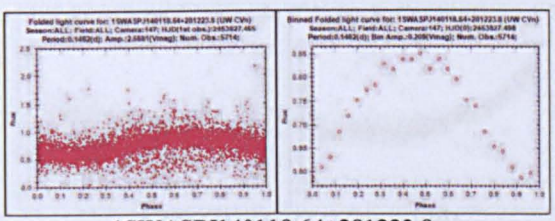

1SWASPJ140118.64+281223.8

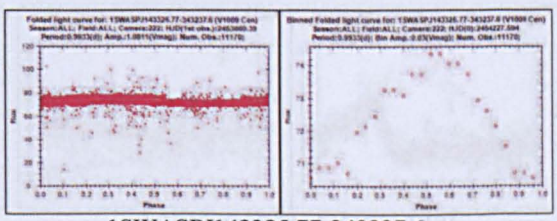

1SWASPJ143325.77-343237.6

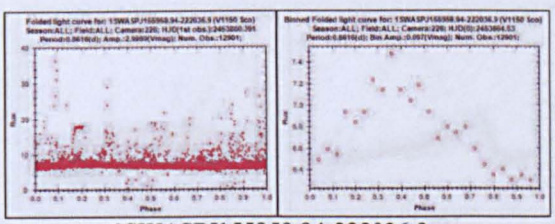

1SWASPJ155959.94-222036.9

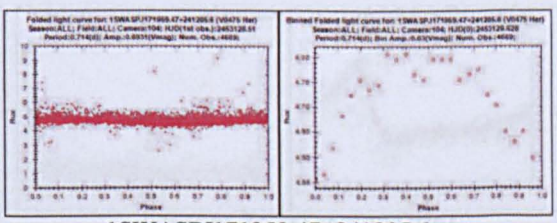

1SWASPJ171959.47+241205.6

Appendix 9g – SuperWASP RRAB objects: confirmed GCVS sub-class

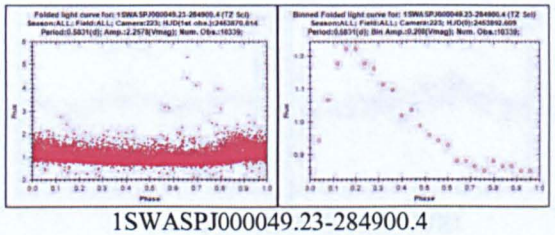

1SWASPJ000049.23-284900.4

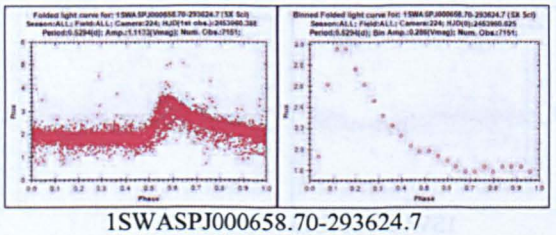

1SWASPJ000658.70-293624.7

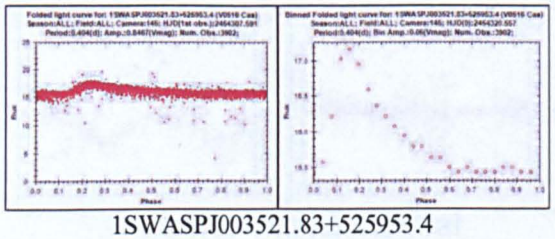

1SWASPJ003521.83+525953.4

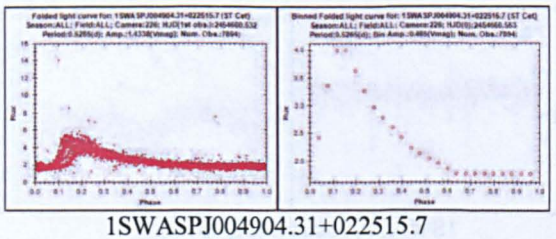

1SWASPJ004904.31+022515.7

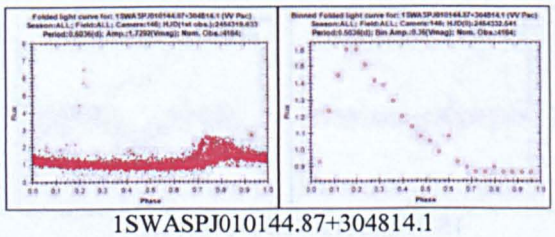

1SWASPJ010144.87+304814.1

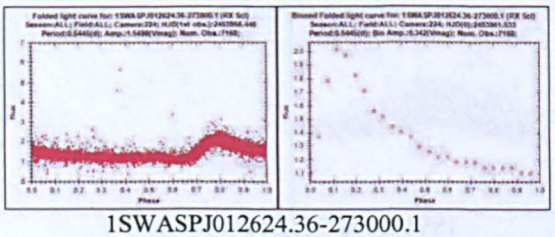

1SWASPJ012624.36-273000.1

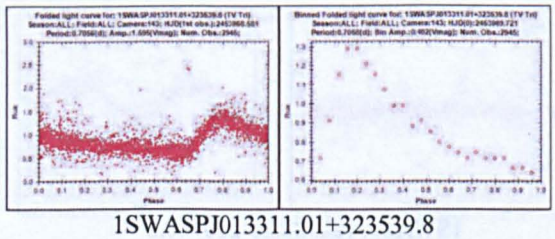

1SWASPJ013311.01+323539.8

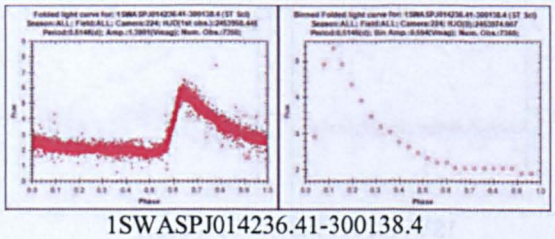

1SWASPJ014236.41-300138.4

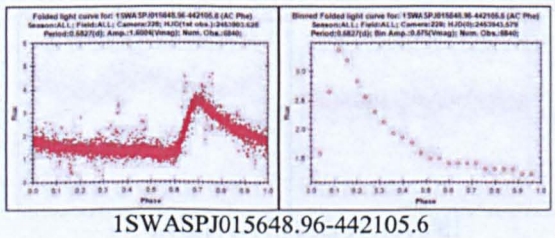

1SWASPJ015648.96-442105.6

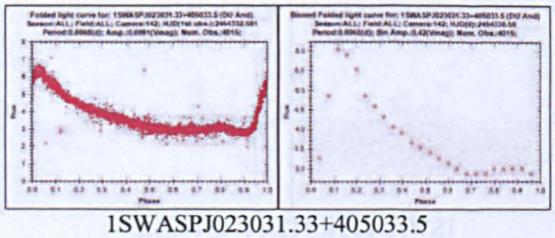

1SWASPJ023031.33+405033.5

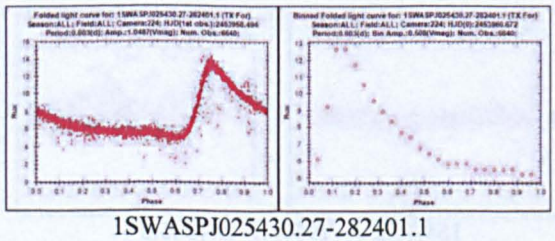

1SWASPJ025430.27-282401.1

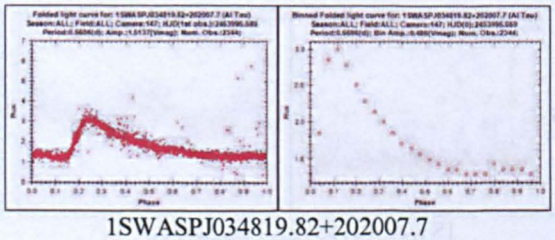

1SWASPJ034819.82+202007.7

Appendix 9h – SuperWASP RRC objects: confirmed GCVS sub-class

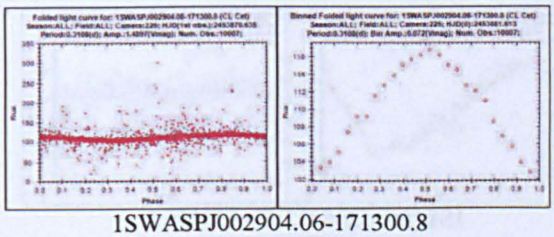
1SWASPJ002904.06-171300.8

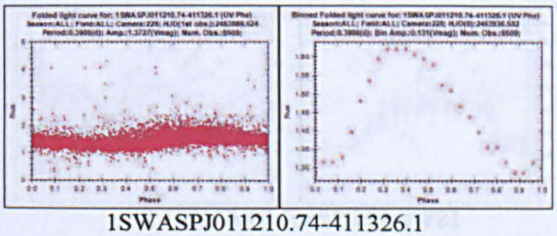
1SWASPJ011210.74-411326.1

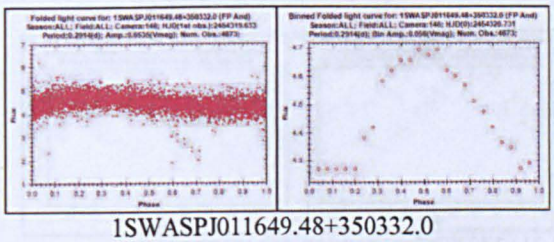
1SWASPJ011649.48+350332.0

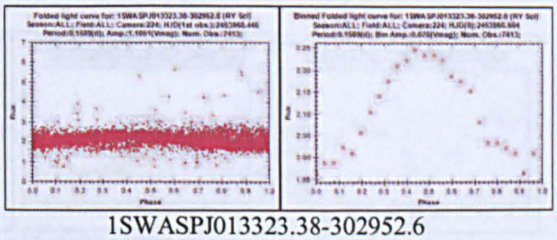
1SWASPJ013323.38-302952.6

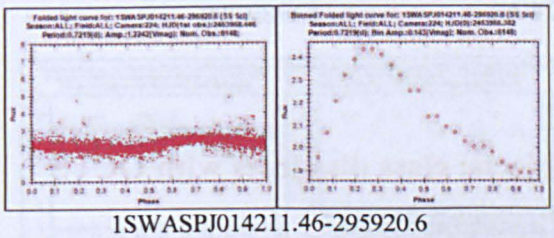
1SWASPJ014211.46-295920.6

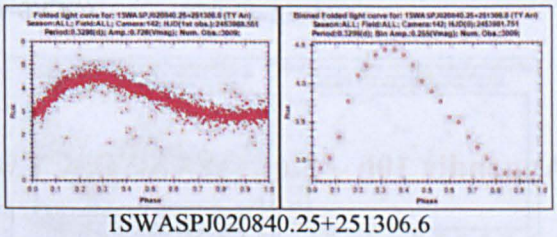
1SWASPJ020840.25+251306.6

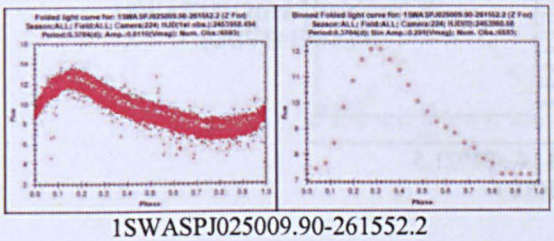
1SWASPJ025009.90-261552.2

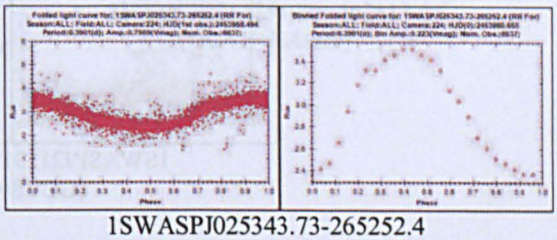
1SWASPJ025343.73-265252.4

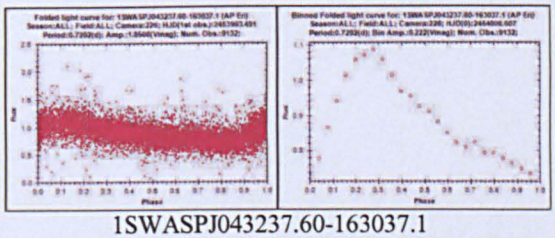
1SWASPJ043237.60-163037.1

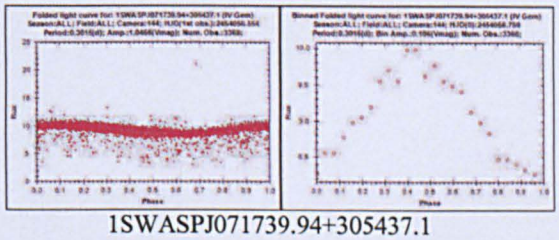
1SWASPJ071739.94+305437.1

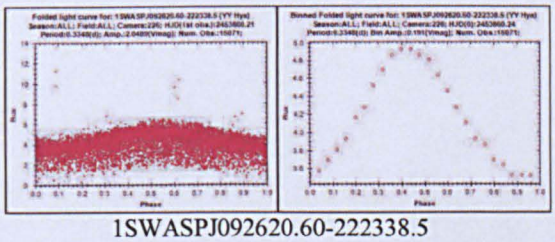
1SWASPJ092620.60-222338.5

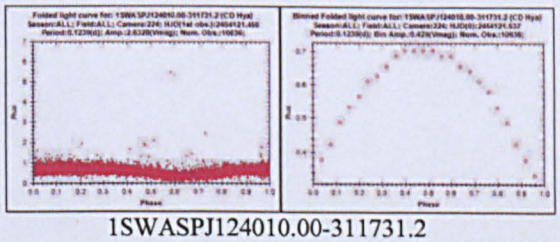
1SWASPJ124010.00-311731.2

Appendix 10a – SuperWASP CEP objects: class disagrees with GCVS

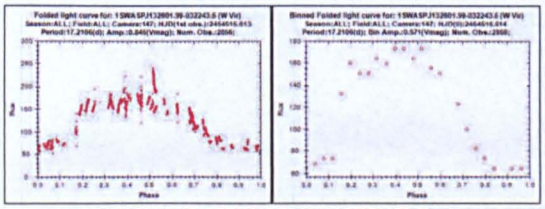

1SWASPJ132601.99-032243.5
(GCVS=CWA)

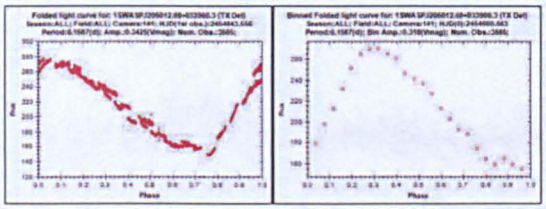

1SWASPJ205012.69+033908.3
(GCVS=CWB:)

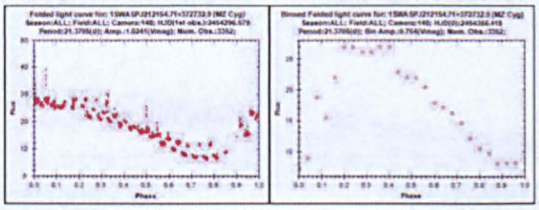

1SWASPJ212154.71+372732.9
(GCVS=CWA:)

Appendix 10b – SuperWASP DSCT objects: class disagrees with GCVS

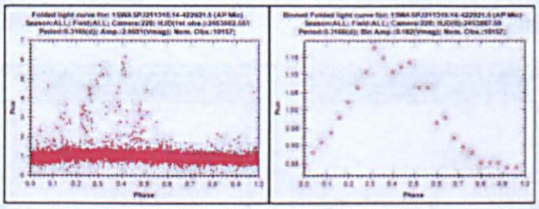

1SWASPJ211318.14-422921.5
(GCVS=RRC)

Appendix 10c – SuperWASP E objects: class disagrees with GCVS

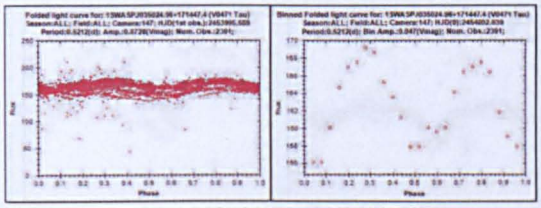

1SWASPJ035024.96+171447.4
(GCVS=EA/D/RS+X)

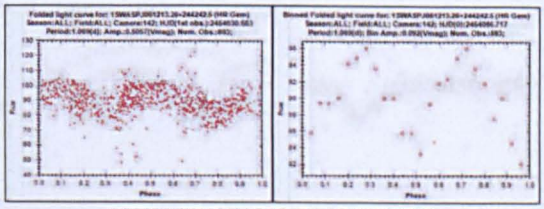

1SWASPJ061213.26+244242.5
(GCVS=EA/SD)

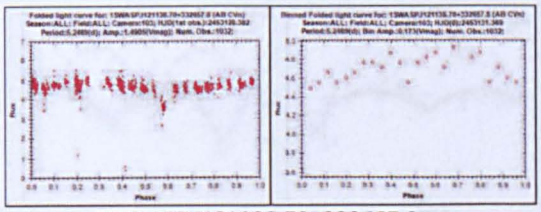

1SWASPJ121138.70+332657.8
(GCVS=EA)

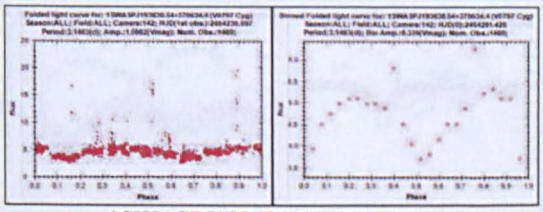

1SWASPJ193630.54+370634.4
(GCVS=EB/AR)

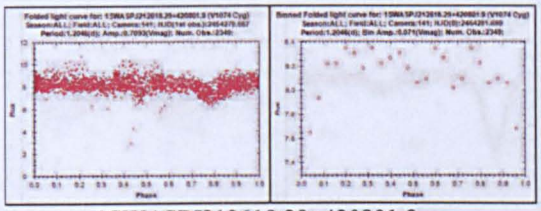

1SWASPJ212618.29+420801.9
(GCVS=EB/KE)

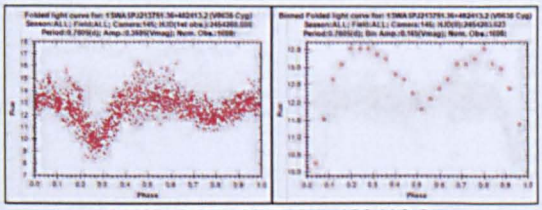

1SWASPJ213751.36+482413.2
(GCVS=EA/SD)

Appendix 10d – SuperWASP EA objects: class disagrees with GCVS

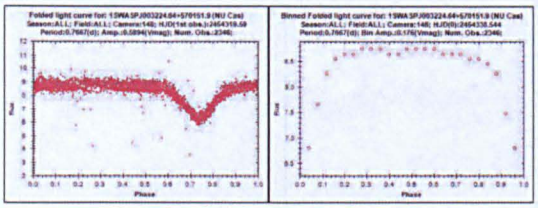

1SWASPJ003224.64+570151.9
(GCVS=EB/KE)

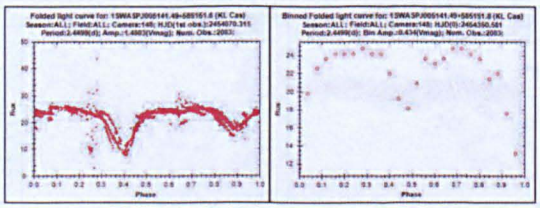

1SWASPJ005141.49+585151.8
(GCVS=EB/SD)

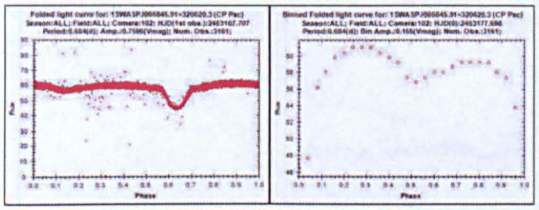

1SWASPJ005845.91+320620.3
(GCVS=EB:)

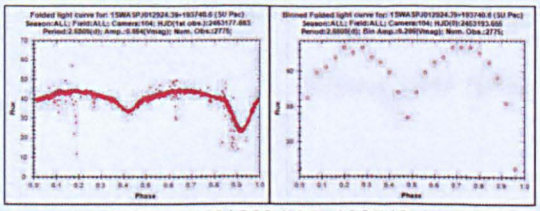

1SWASPJ012924.39+193740.6
(GCVS=EB/D:)

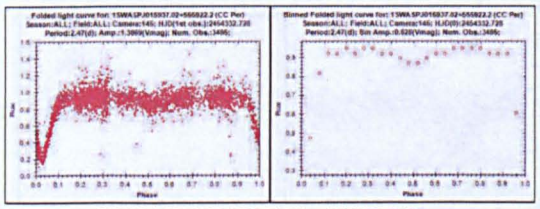

1SWASPJ015937.02+555922.2
(GCVS=EB/SD)

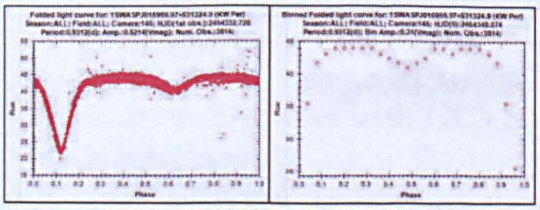

1SWASPJ015959.97+531324.9
(GCVS=EB/SD)

Appendix 10e – SuperWASP EB objects: class disagrees with GCVS

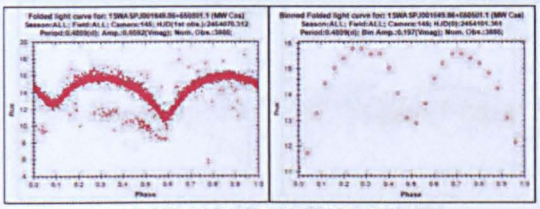

1SWASPJ001649.86+550501.1
(GCVS=EA)

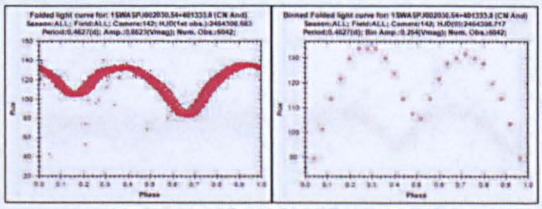

1SWASPJ002030.54+401333.8
(GCVS=EW/KW)

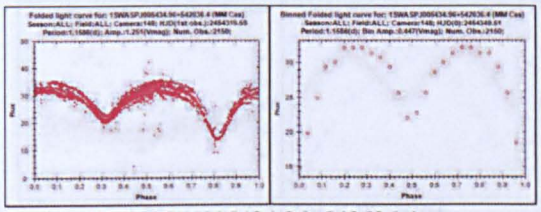

1SWASPJ005434.96+542636.4
(GCVS=EA/SD)

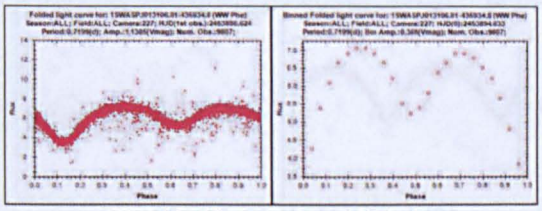

1SWASPJ013106.81-435934.8
(GCVS=EA)

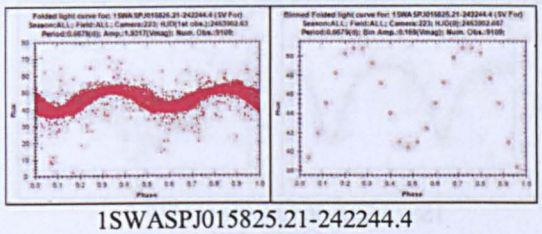

1SWASPJ015825.21-242244.4
(GCVS=SRD)

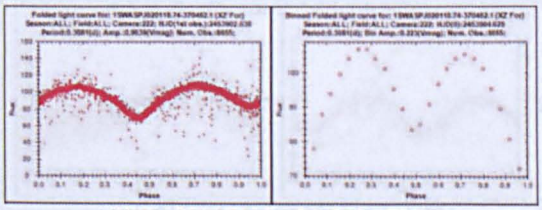

1SWASPJ020118.74-370452.1
(GCVS=EW)

Appendix 10f – SuperWASP EW objects: class disagrees with GCVS

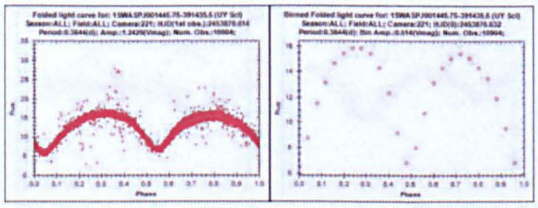

1SWASPJ001445.75-391435.5
(GCVS=RRC:)

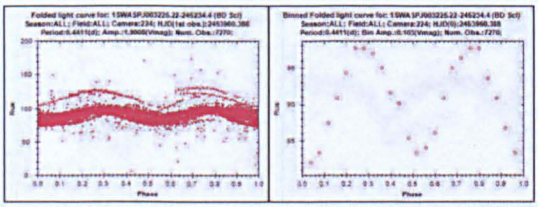

1SWASPJ003225.22-245234.4
(GCVS=EB)

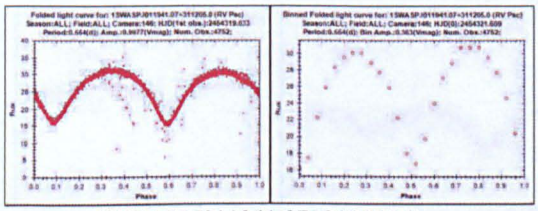

1SWASPJ011941.07+311205.0
(GCVS=EA/DW)

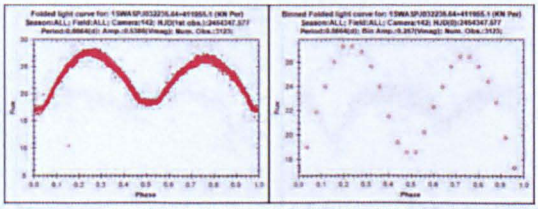

1SWASPJ032235.64+411955.1
(GCVS=RRC)

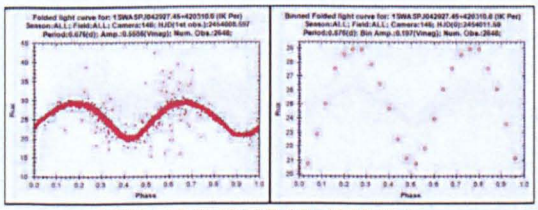

1SWASPJ042927.45+420310.6
(GCVS=EB/KE)

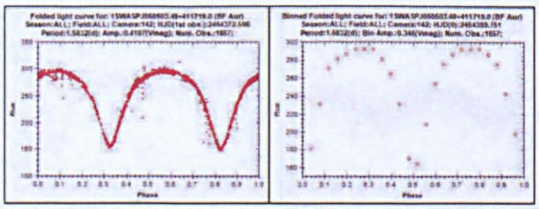

1SWASPJ050503.49+411719.0
(GCVS=EB)

Appendix 10g – SuperWASP RM objects: class disagrees with GCVS

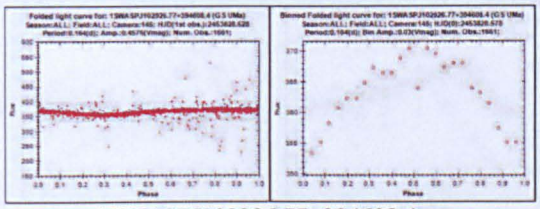

1SWASPJ102926.77+394608.4
(GCVS=DSCTC:)

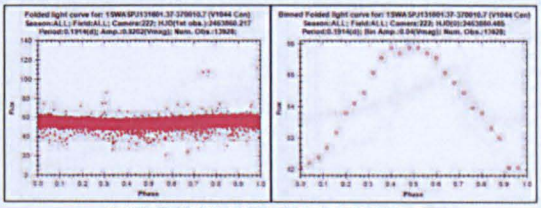

1SWASPJ131601.37-370010.7
(GCVS=ZAND)

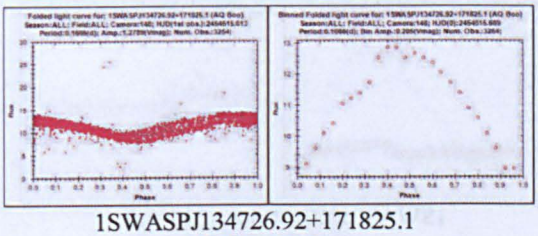

1SWASPJ134726.92+171825.1
(GCVS=CST)

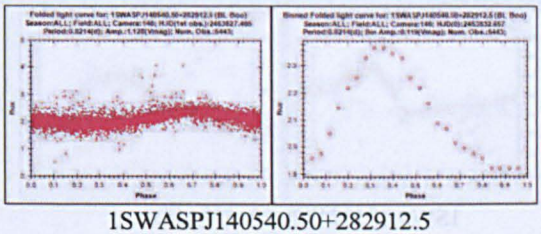

1SWASPJ140540.50+282912.5
(GCVS=CWB)

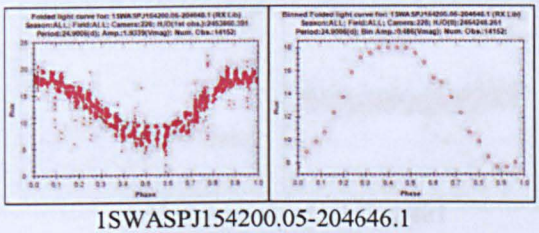

1SWASPJ154200.05-204646.1
(GCVS=CWA)

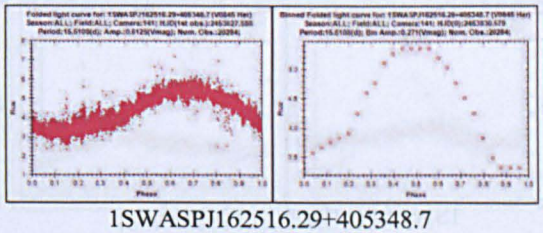

1SWASPJ162516.29+405348.7
(GCVS=CWA)

Appendix 10h – SuperWASP RR objects: class disagrees with GCVS

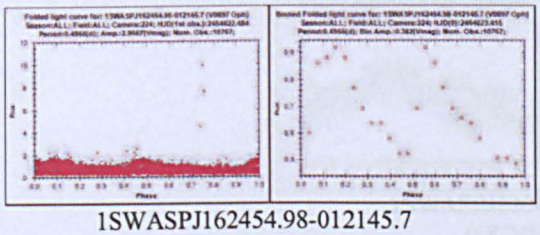

1SWASPJ162454.98-012145.7
(GCVS=RRAB)

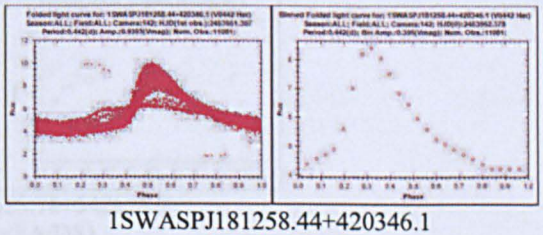

1SWASPJ181258.44+420346.1
(GCVS=RRAB)

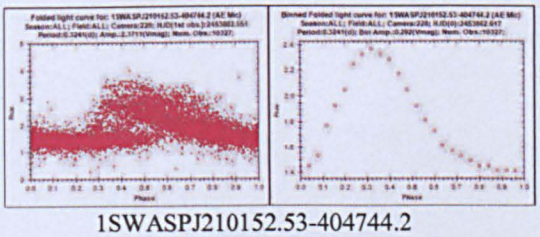

1SWASPJ210152.53-404744.2
(GCVS=RRAB)

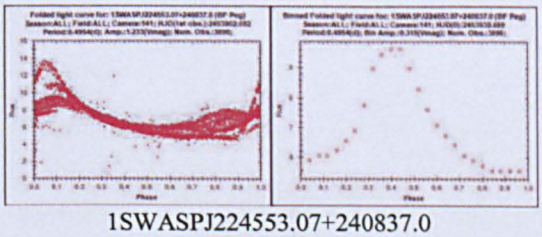

1SWASPJ224553.07+240837.0
(GCVS=RRAB)

Appendix 10i – SuperWASP RRAB objects: class disagrees with GCVS

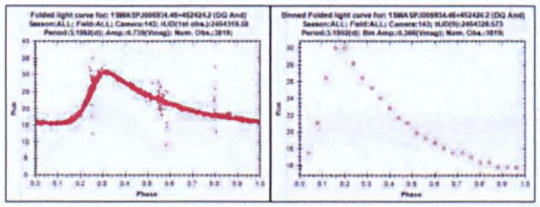

1SWASPJ005934.46+452424.2
(GCVS=CWB:)

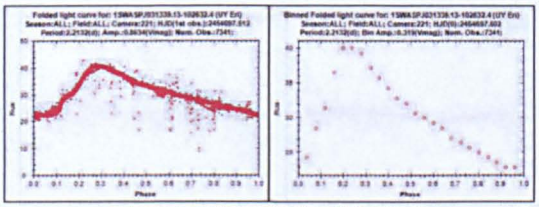

1SWASPJ031339.13-102632.4
(GCVS=CWB)

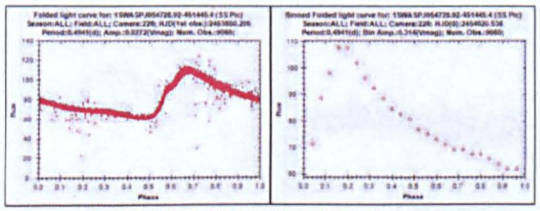

1SWASPJ054728.92-451445.4
(GCVS=SR:)

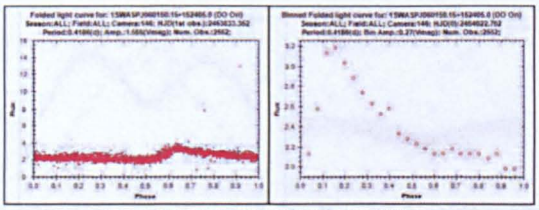

1SWASPJ060150.15+152405.0
(GCVS=CEP:)

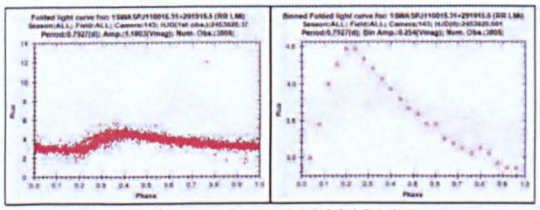

1SWASPJ110015.31+291915.5
(GCVS=E)

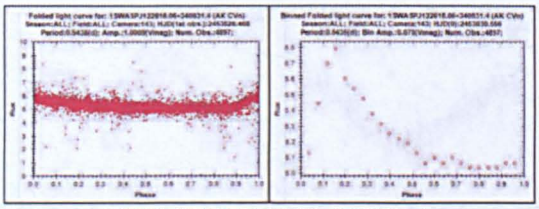

1SWASPJ122618.06+340831.4
(GCVS=RRC)

Appendix 10j – SuperWASP RRC objects: class disagrees with GCVS

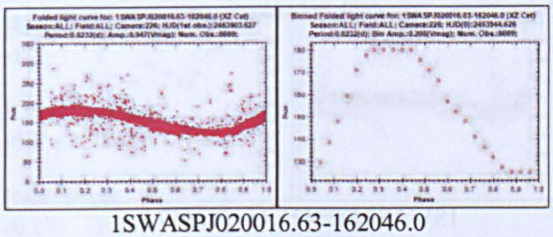

1SWASPJ020016.63-162046.0
(GCVS=RRAB)

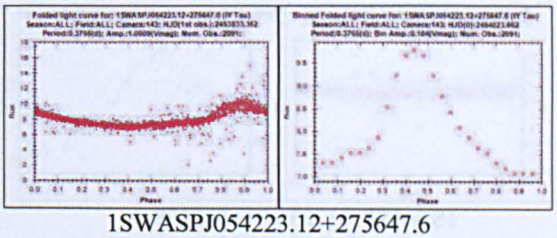

1SWASPJ054223.12+275647.6
(GCVS=RRAB)

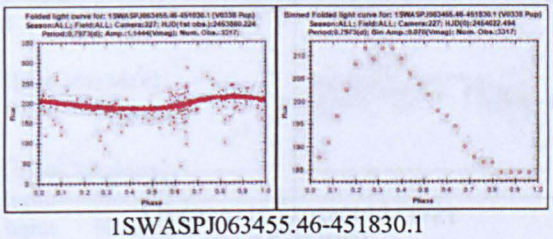

1SWASPJ063455.46-451830.1
(GCVS=RRAB)

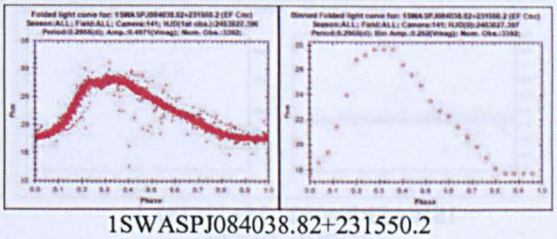

1SWASPJ084038.82+231550.2
(GCVS=EW)

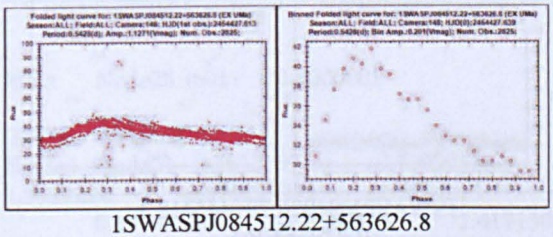

1SWASPJ084512.22+563626.8
(GCVS=RRAB)

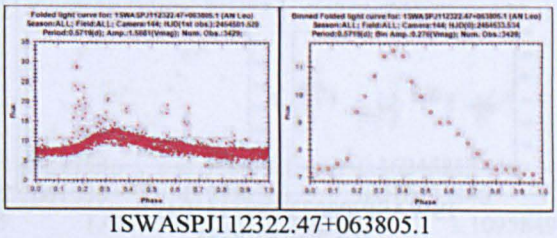

1SWASPJ112322.47+063805.1
(GCVS=RRAB)

Appendix 10k – SuperWASP ??? objects: class disagrees with GCVS

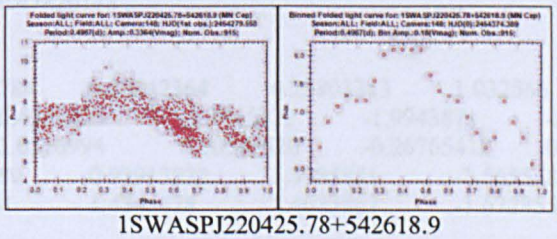

1SWASPJ220425.78+542618.9
(GCVS=EA/DS)

Appendix 11 – SuperWASP objects: unable to obtain a classification

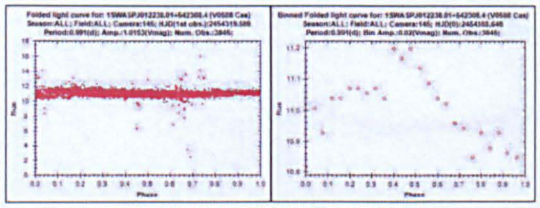

1SWASPJ012238.01+542308.4
(GCVS=DCEP:)

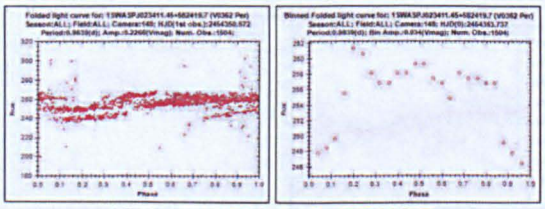

1SWASPJ023411.45+582419.7
(GCVS=BCEP:)

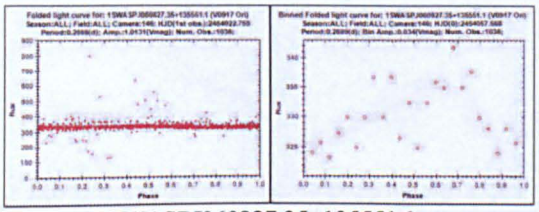

1SWASPJ060827.35+135551.1
(GCVS=BCEP)

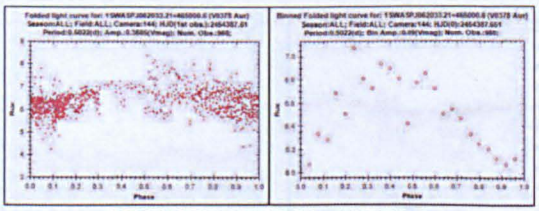

1SWASPJ062033.21+465000.6
(GCVS=RRAB)

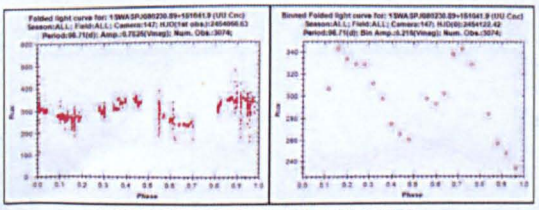

1SWASPJ080230.89+151041.9
(GCVS=EB/GS)

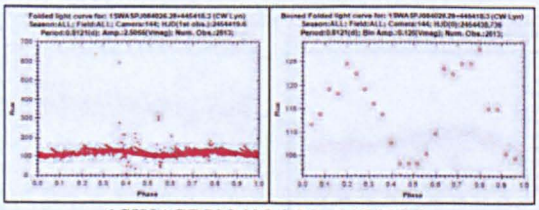

1SWASPJ084026.28+445418.3
(GCVS=EB:)

Appendix 12 – Neural Network parameters for NN Model 1

```
[Input range]
-1      1

[Output range]
-0.8    0.8

[NN range]
-0.13   1.13

[Nodes]
1       28      17      9

[Bias MinMax]
Bias    Bias    1       1

[Input MinMax]
Input   Node01 1       17
Input   Node02 0       10
Input   Node03 0       8
Input   Node04 0       7
:
:
Input   Node28 0.01    2.4000001

[Hidden Weights]
Hidden  Node01 -0.36321971      -0.77999538     -1.4885858      -1.4920248      0.16248217      -
1.0730222       0.071239211     -2.7804813      -2.1061635      -0.9820286      0.010435948
        0.19749688      -1.2564863      1.4171305       1.4871309       2.2802622       1.1095849
        1.5641618       0.96187127      1.065275        1.7890054       0.66552711      1.1803769
        0.74743855      0.040217854     -0.2476809      -2.7949901      2.6258104
        0.39161751
Hidden  Node02 0.3244226        -0.7175191      1.2874358       0.035814945     1.9963434       -
0.3575606       1.3972421       1.3789128       2.146363        0.3187938       1.1877239
        1.6906841       -0.69225496     1.620533        0.81504786      0.32358891
        0.80837816      1.090207        -0.42793065     -1.8321444      0.35827851      -
0.73517781      -1.5569304      -2.4216897      -1.4584519      -2.5824733      0.90799767
        0.34971538      0.47820148
:
:
Hidden  Node17 -0.41946784      0.88242364      0.25803313      1.032566        -0.058922909
        0.091726549     0.4256424       -1.1945772      -1.9943871      -2.3648674      1.4612937
        -2.0083377      1.0516994       0.20547526      -0.26765412     0.65330243      -
0.82417083      -1.2707989      0.92913532      1.3985851       -1.5655683      -0.6901539      -
1.4559066       2.4470761       1.4345478       2.4023867       -1.6728551      1.1550934       -
0.038360748

[Output Weights]
Output  Node01 0        1       -0.69797146     -0.15628842     0.28812733      0.3736513
        0.70542169      0.15918633      0.024707228     -0.15351942     -1.0065464      -
0.17322427      -0.028277783    -0.27085412     -0.75804454     -1.5606997      -1.7109754      -
1.106482        -0.3838881      0.5424059       -0.52491742     0.89342374      1.0787262       -
0.15054211      0.61984307      0.12430585      0.79820907      0.2332221       -0.33700386     -
2.9868803       2.0396912       -0.37060103     -0.016429203    -0.23104136     0.19775654
        0.08726529      -0.97610623     0.30150694      0.2281038       0.50256658      -
0.87823558      0.15819979      -0.37481448     -0.002349268    -0.49169433     -0.73645854
        0.32911137      0.16661149
```

Appendix 12 continued…

```
Output  Node02 0       1       -0.52273226     2.3152242       1.6805102       -0.080867447
        1.5084165       -0.078024887    0.12049725      0.042929891     -0.76498663     -
0.55972254      1.4303806       -0.024045035    0.27429751      0.5071497       0.84753191
        0.55965841      0.21080127      -0.66171539     -0.06689284     -1.0995061      -
0.41286707      -1.5084099      -0.077230848    1.6319066       1.2064196       1.6360683       -
0.86121565      -1.3246306      -6.5995007      0.29587144      -0.081509493    -0.51815313
        0.007708982     -0.51336271     0.30395493      -0.057231378    0.59957856
        0.97976017      0.96171826      0.46278873      -1.081174       0.82973647
        0.91688532      -0.57983637     -0.1759446      -0.34321088
:
:
Output  Node09 0       1       -0.31315768     -0.2798534      -0.75060213     -0.19558872     -
1.0207283       -0.057383083    -0.25149298     0.29470751      0.11657826      0.84685051      -
0.017074734     0.74031264      0.52087361      0.90279216      1.9058238       1.1561334
        0.74136442      -0.53574765     -0.15062375     -0.36559901     -1.0633585
        0.036821891     -0.68144488     -0.65976-0.68695551     -0.86925739     1.8539118
        0.33966219      -0.92233282     0.17216356      0.1580586       0.081905499     -
0.19283549      0.018779859     0.3556889       -0.037805598    0.14666368      -0.12532212
        0.52444106      -0.016180661    -0.02093173     -0.30633917     0.37565264
        0.44185081      -0.38978606     0.10606147

[Threshold]
0.6
```

Appendix 13 – Duplicate Object Analyser Application

With reference to the image below, the user selects an object to analyse in the left pane and then presses the <Select> button. This loads all images for that object into the grid. Each light-curve is then viewed and the one that has the best EA shape is selected by clicking the image. When the user selects the <Move objects> button, the selected object is moved to the 'Unique' folder, and the other images moved to the 'Duplicates' folder. The images are then removed from the list, ready for the next object.

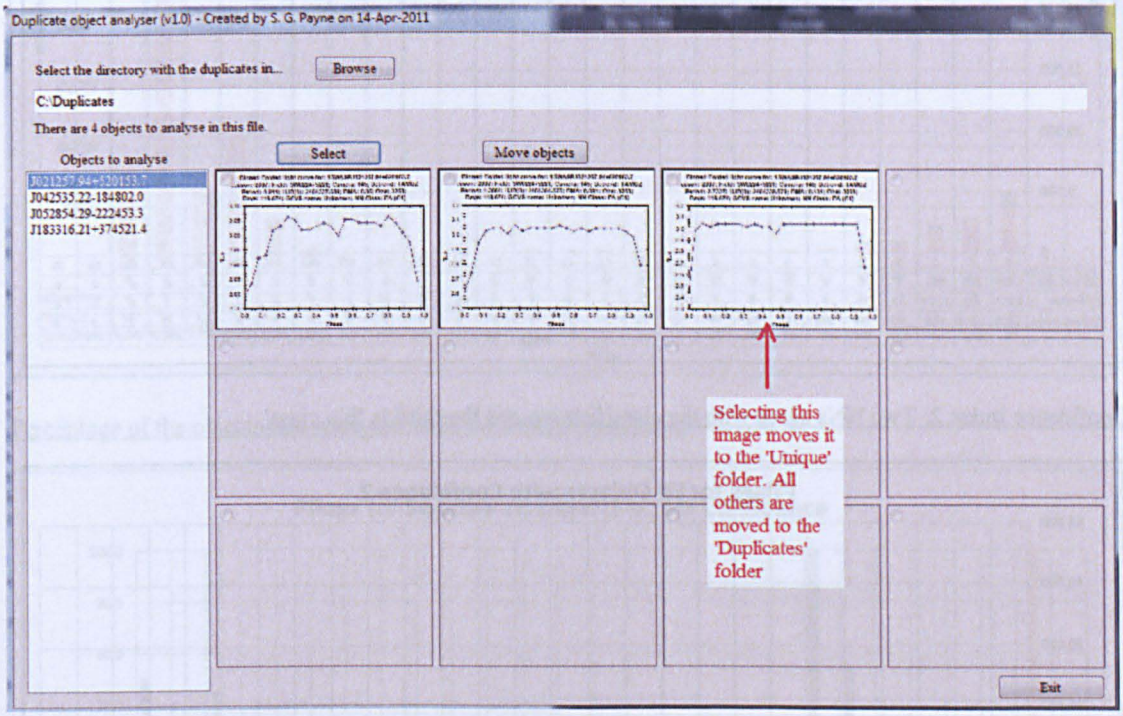

Appendix 14 – PFlags for EB Objects

Confidence Index 1: All three NNs agree with the classification

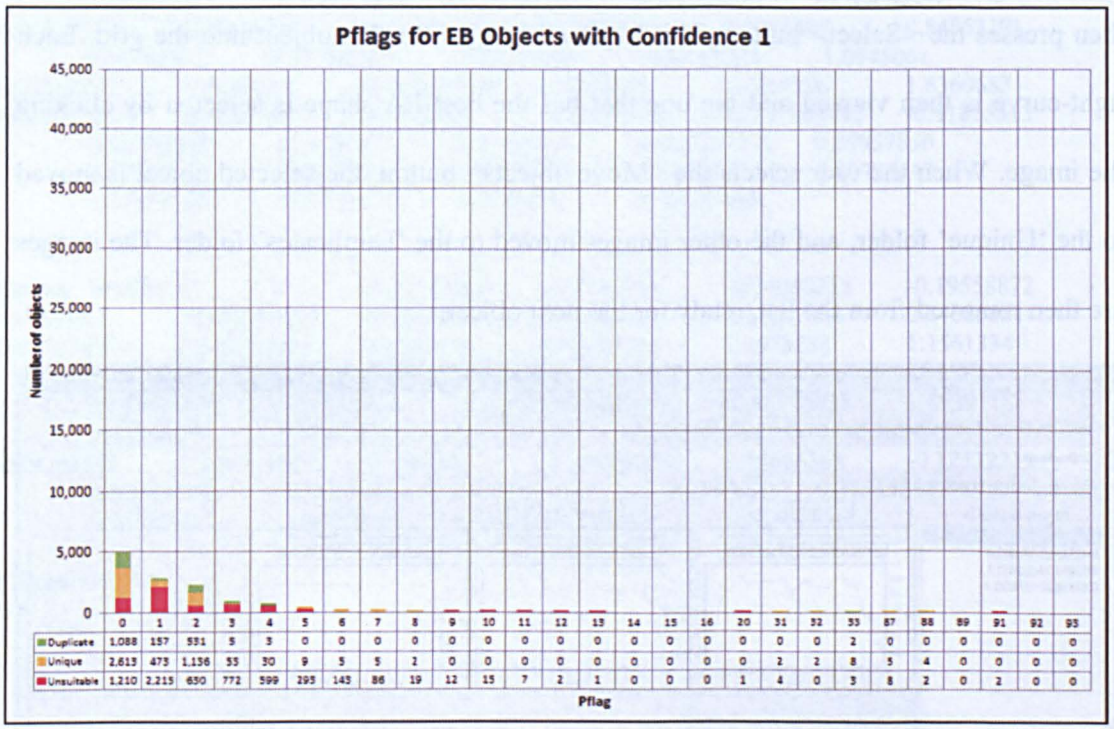

Confidence Index 2: Two NNs agree with the classification and the third is 'No class'

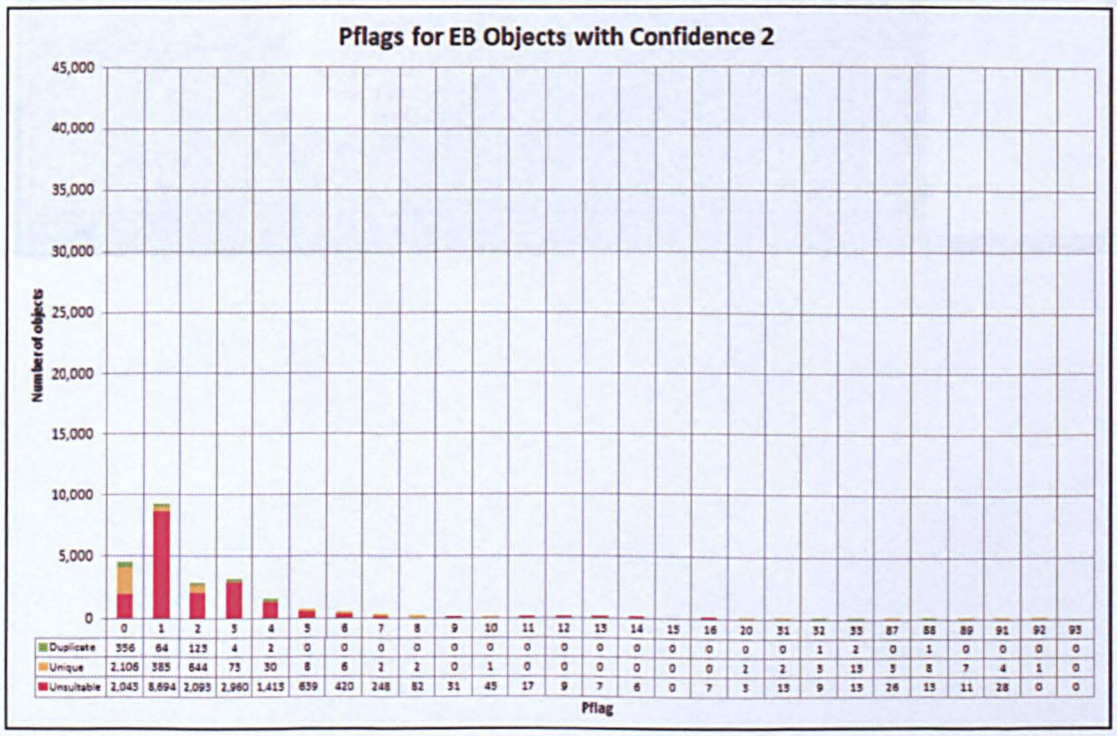

Appendix 14 continued...

Confidence Index 4: One NN provides the classification and the other two shows 'No class'

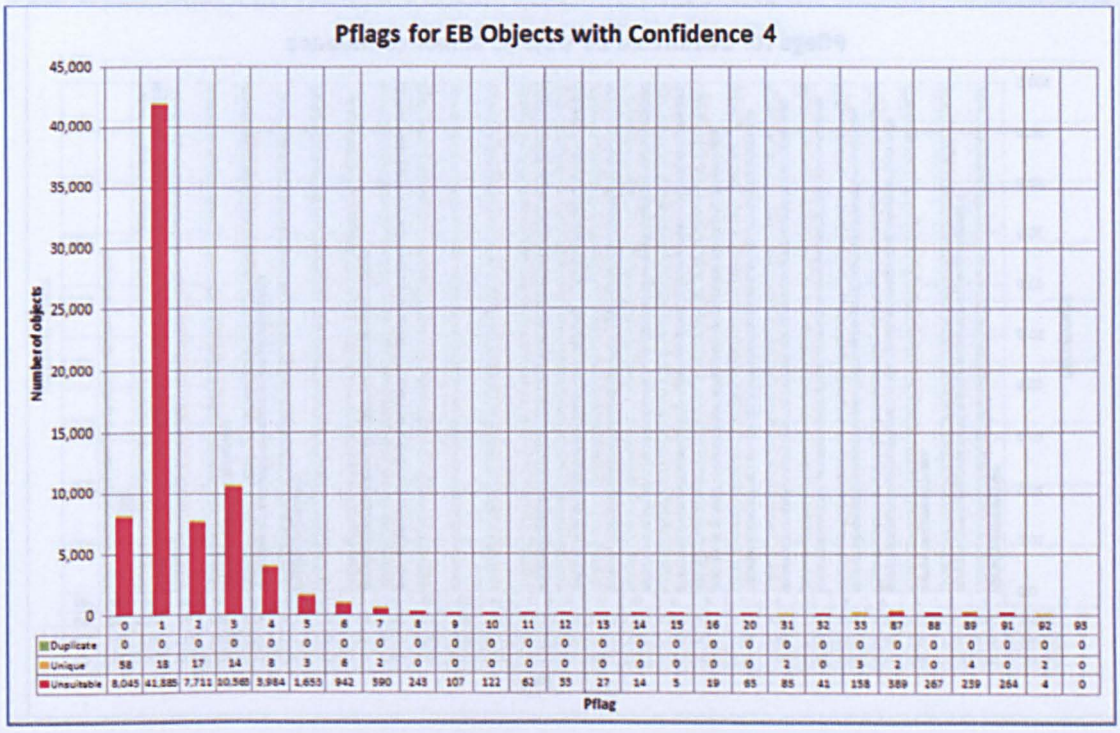

Percentage of the objects that were manually confirmed as suitable

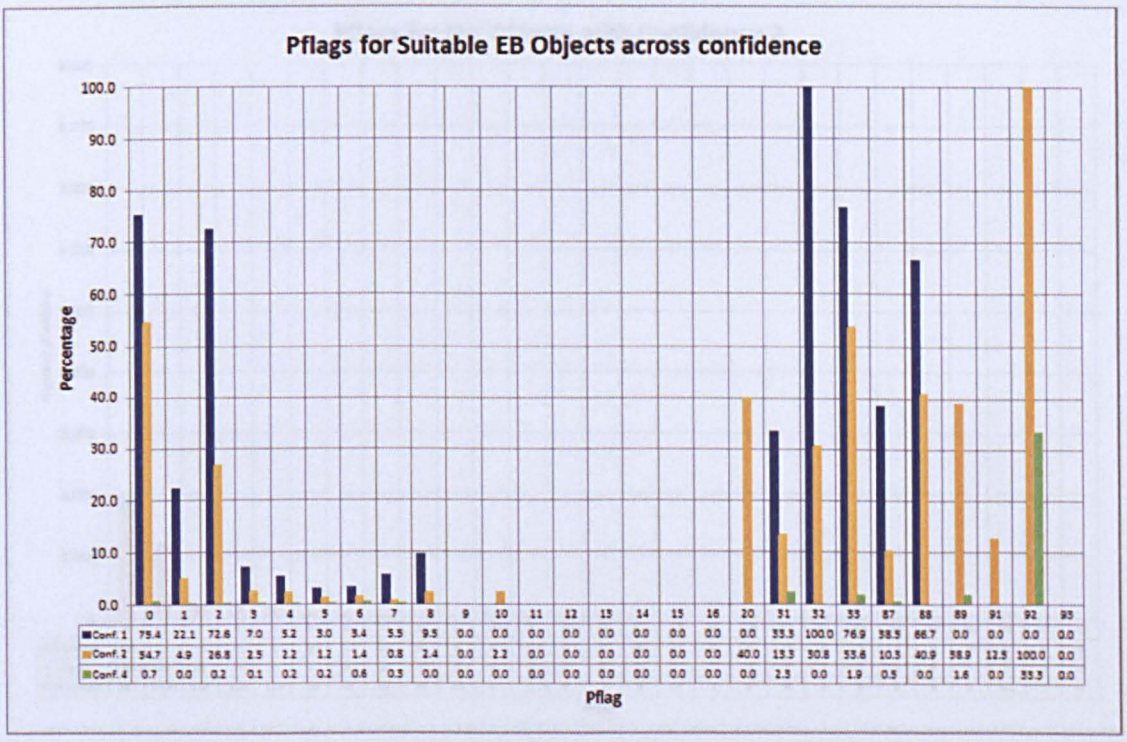

Appendix 14 continued…

Percentage of the objects that were manually confirmed as unsuitable

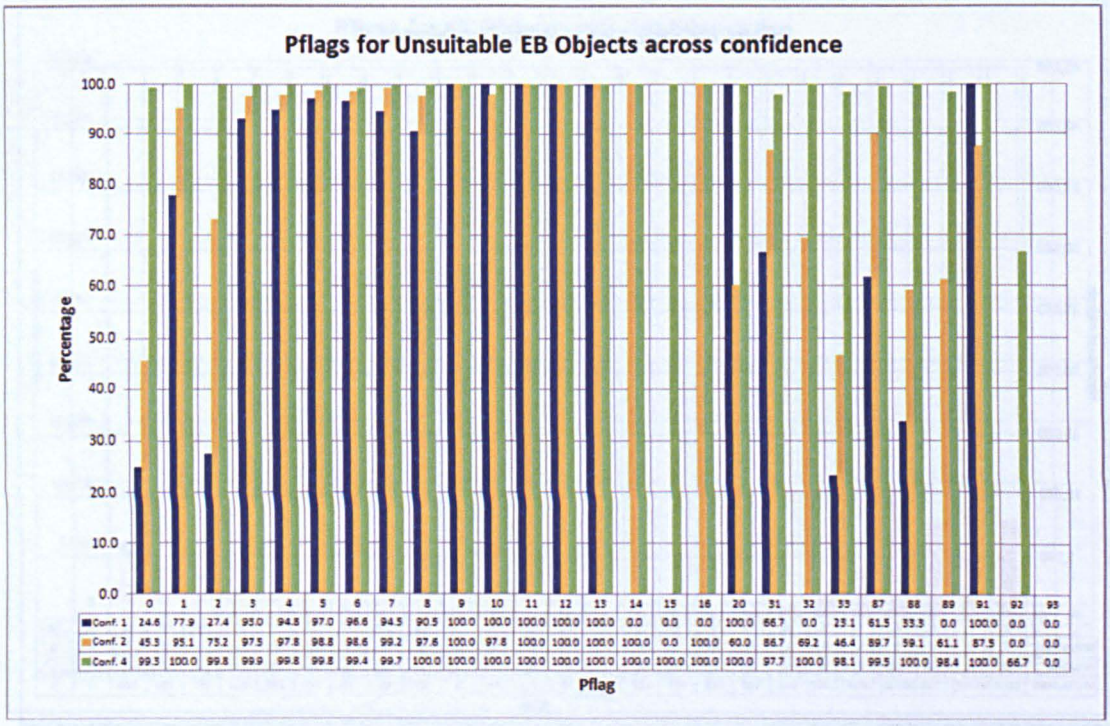

Pflag	0	1	2	3	4	5	6	7	8	9	10	11	12	13	14	15	16	20	31	32	33	87	88	89	91	92	93
Conf. 1	24.6	77.9	27.4	93.0	94.8	97.0	96.6	94.5	90.5	100.0	100.0	100.0	100.0	100.0	0.0	0.0	0.0	100.0	66.7	0.0	23.1	61.5	33.3	0.0	100.0	0.0	0.0
Conf. 2	45.3	95.1	73.2	97.5	97.8	98.8	98.6	99.2	97.6	100.0	97.8	100.0	100.0	100.0	100.0	0.0	100.0	60.0	86.7	69.2	46.4	89.7	59.1	61.1	87.5	0.0	0.0
Conf. 4	99.3	100.0	99.8	99.9	99.8	99.8	99.4	99.7	100.0	100.0	100.0	100.0	100.0	100.0	100.0	100.0	100.0	100.0	97.7	100.0	98.1	99.5	100.0	98.4	100.0	66.7	0.0

Appendix 15 – PFlags for EW Objects

Confidence Index 1: All three NNs agree with the classification

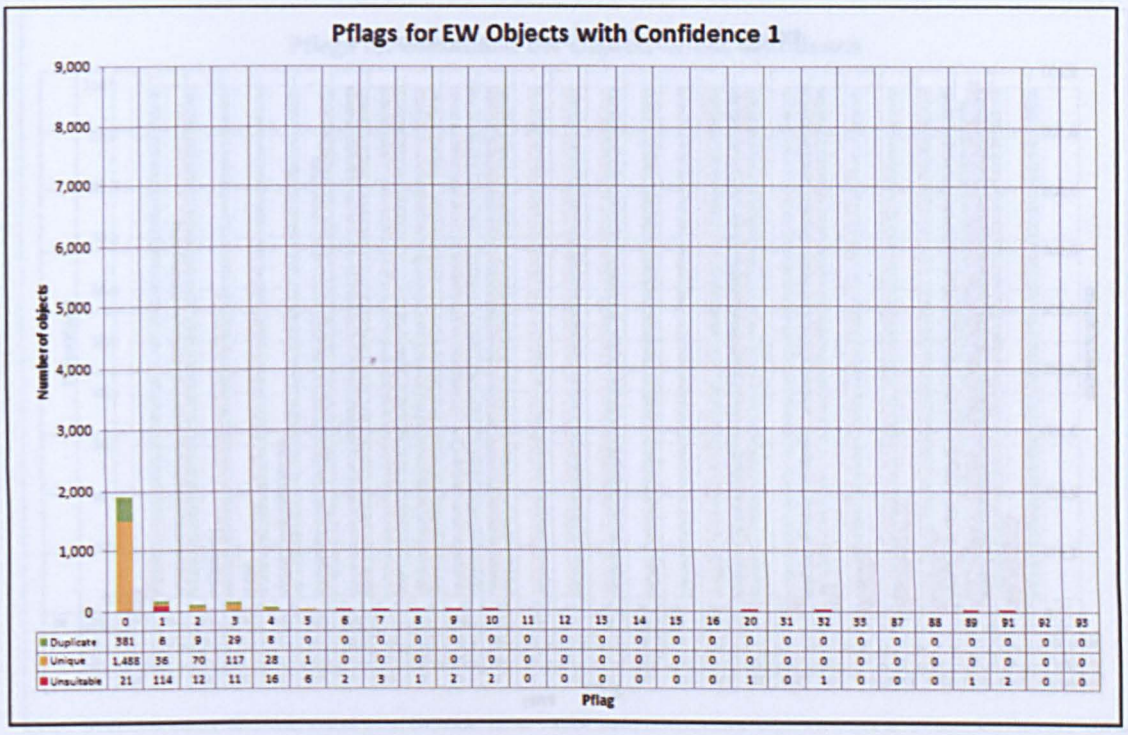

Pflag	0	1	2	3	4	5	6	7	8	9	10	11	12	13	14	15	16	20	31	32	33	87	88	89	91	92	93
Duplicate	381	8	9	29	8	0	0	0	0	0	0	0	0	0	0	0	0	0	0	0	0	0	0	0	0	0	0
Unique	1,488	36	70	117	28	1	0	0	0	0	0	0	0	0	0	0	0	0	0	0	0	0	0	0	0	0	0
Unsuitable	21	114	12	11	16	6	2	3	1	2	2	0	0	0	0	0	0	1	0	1	0	0	0	1	2	0	0

Confidence Index 2: Two NNs agree with the classification and the third is 'No class'

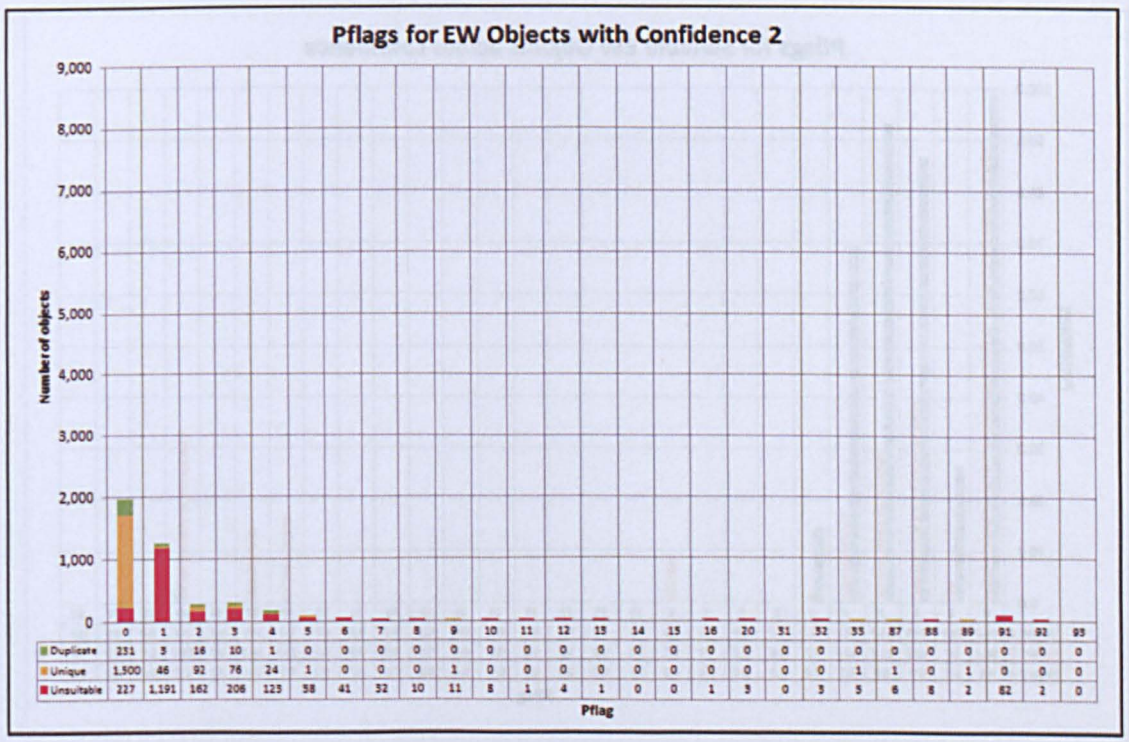

Pflag	0	1	2	3	4	5	6	7	8	9	10	11	12	13	14	15	16	20	31	32	33	87	88	89	91	92	93
Duplicate	231	3	16	10	1	0	0	0	0	0	0	0	0	0	0	0	0	0	0	0	0	0	0	0	0	0	0
Unique	1,500	46	92	76	24	1	0	0	0	1	0	0	0	0	0	0	0	0	0	0	1	1	0	1	0	0	0
Unsuitable	227	1,191	162	206	125	58	41	32	10	11	5	1	4	1	0	0	1	3	0	3	5	6	8	2	62	1	0

Appendix 15 continued…

Confidence Index 4: One NN provides the classification and the other two shows 'No class'

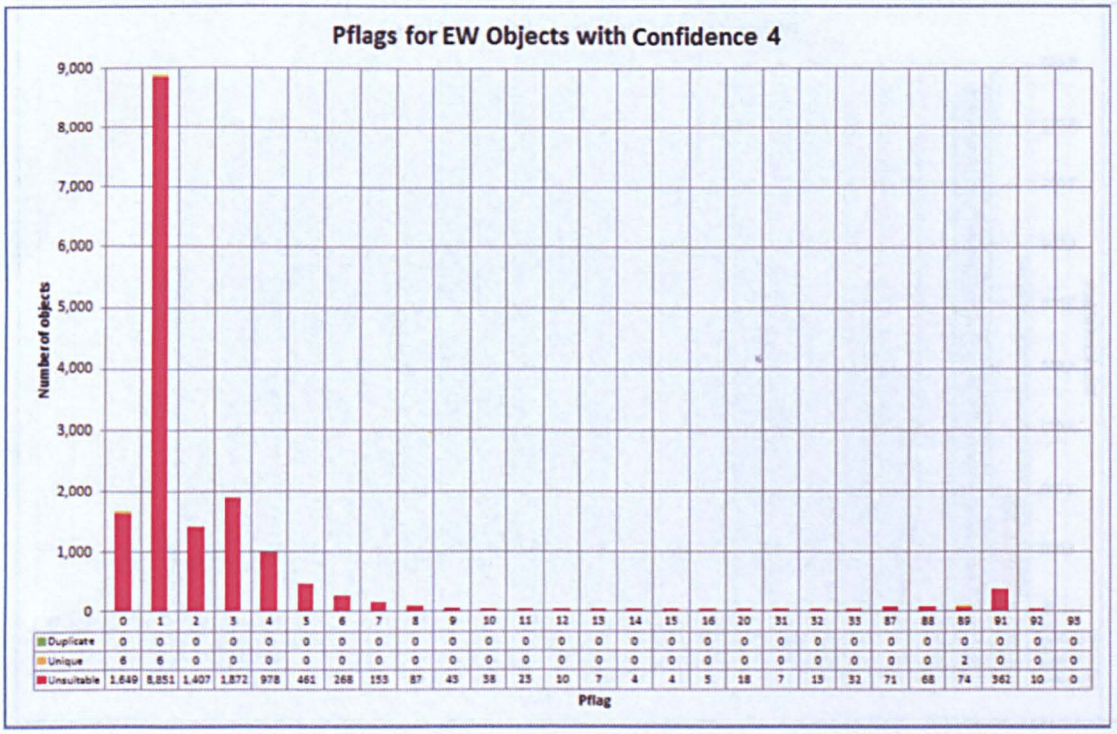

Percentage of the objects that were manually confirmed as suitable

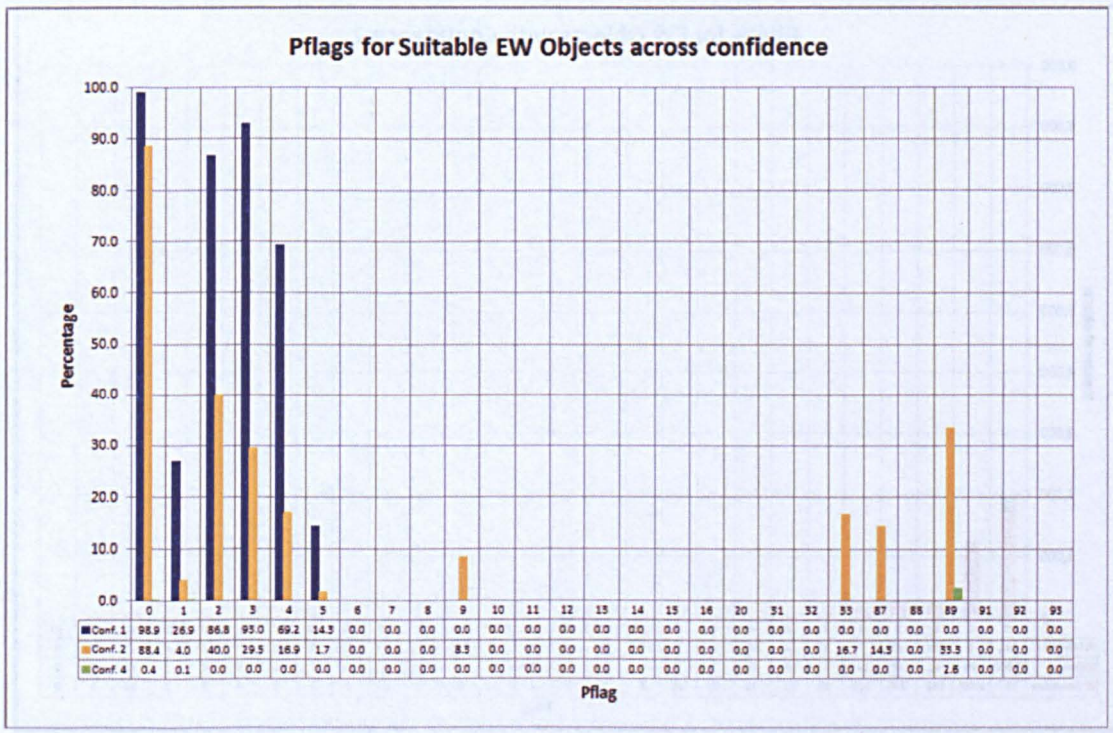

Appendix 15 continued…

Percentage of the objects that were manually confirmed as unsuitable

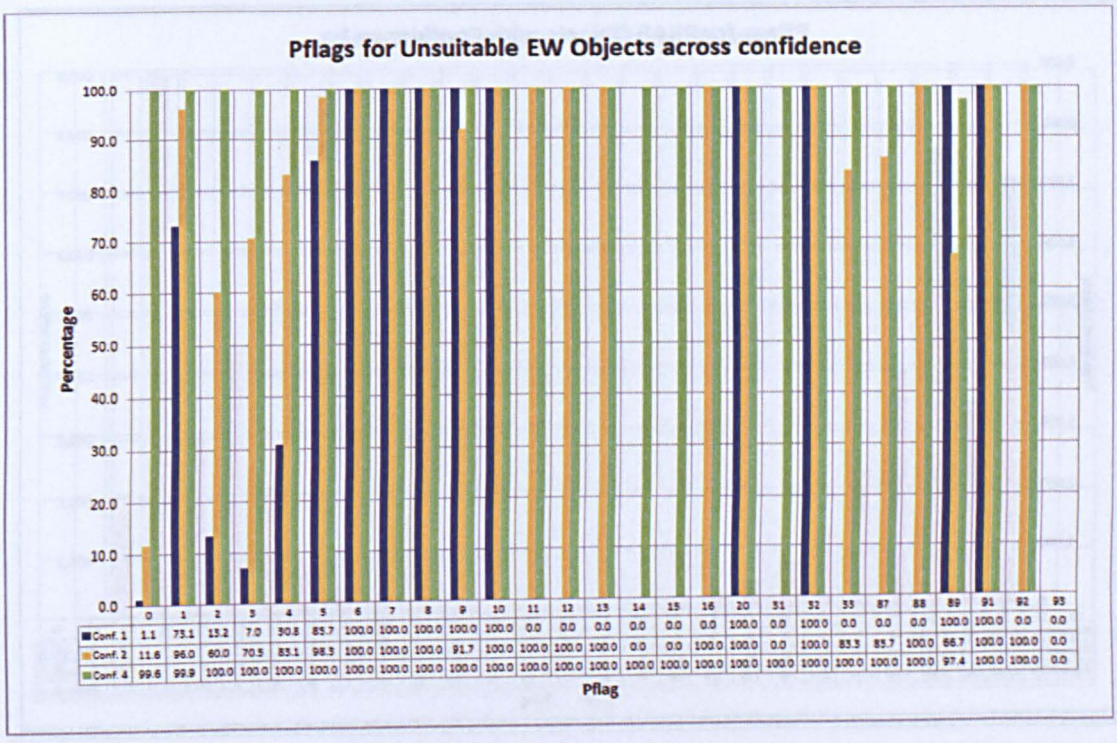

	0	1	2	3	4	5	6	7	8	9	10	11	12	13	14	15	16	20	31	32	33	87	88	89	91	92	93
Conf. 1	1.1	73.1	13.2	7.0	30.8	85.7	100.0	100.0	100.0	100.0	100.0	0.0	0.0	0.0	0.0	0.0	0.0	100.0	0.0	100.0	0.0	0.0	0.0	100.0	100.0	0.0	0.0
Conf. 2	11.6	96.0	60.0	70.5	83.1	98.3	100.0	100.0	100.0	91.7	100.0	100.0	100.0	100.0	0.0	0.0	100.0	100.0	0.0	100.0	83.3	85.7	100.0	66.7	100.0	100.0	0.0
Conf. 4	99.6	99.9	100.0	100.0	100.0	100.0	100.0	100.0	100.0	100.0	100.0	100.0	100.0	100.0	100.0	100.0	100.0	100.0	100.0	100.0	100.0	100.0	100.0	97.4	100.0	100.0	0.0

Appendix 16 – PFlags for RRAB Objects

Confidence Index 1: All three NNs agree with the classification

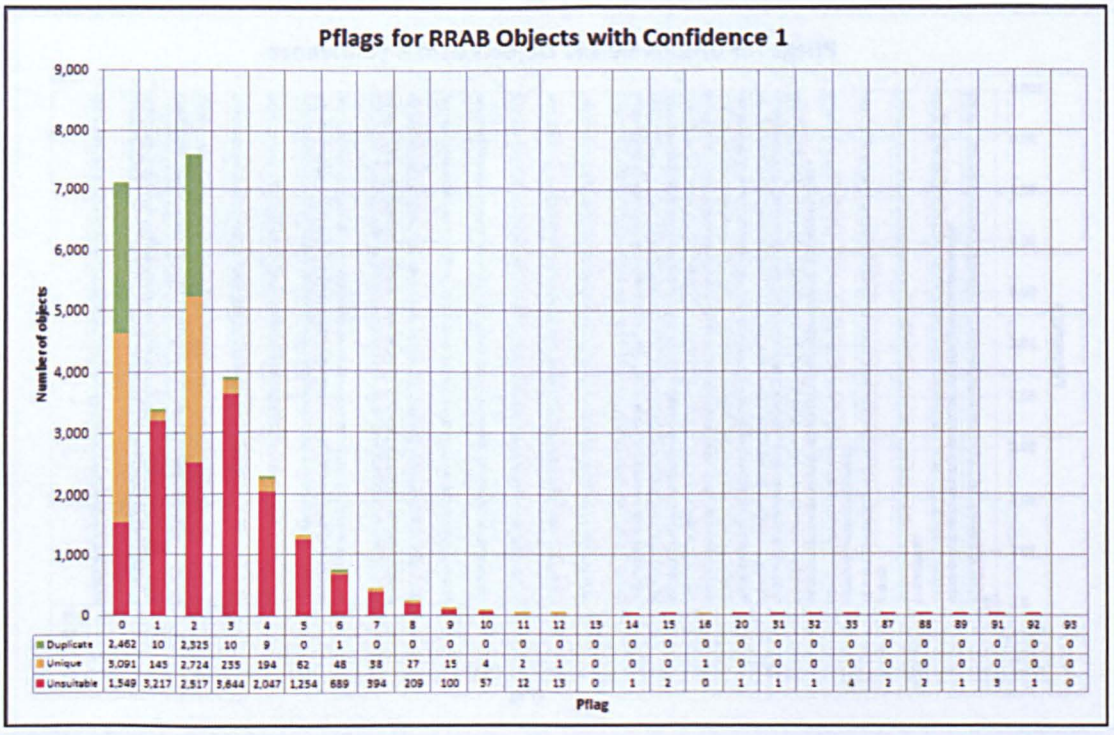

Pflag	0	1	2	3	4	5	6	7	8	9	10	11	12	13	14	15	16	20	31	32	33	87	88	89	91	92	93
Duplicate	2,462	10	2,325	10	9	0	1	0	0	0	0	0	0	0	0	0	0	0	0	0	0	0	0	0	0	0	0
Unique	3,091	145	2,724	235	194	62	48	38	27	15	4	2	1	0	0	0	1	0	0	0	0	0	0	0	0	0	0
Unsuitable	1,549	3,217	2,517	3,644	2,047	1,254	689	394	209	100	57	12	13	0	1	2	0	1	1	1	4	2	2	1	3	1	0

Confidence Index 2: Two NNs agree with the classification and the third is 'No class'

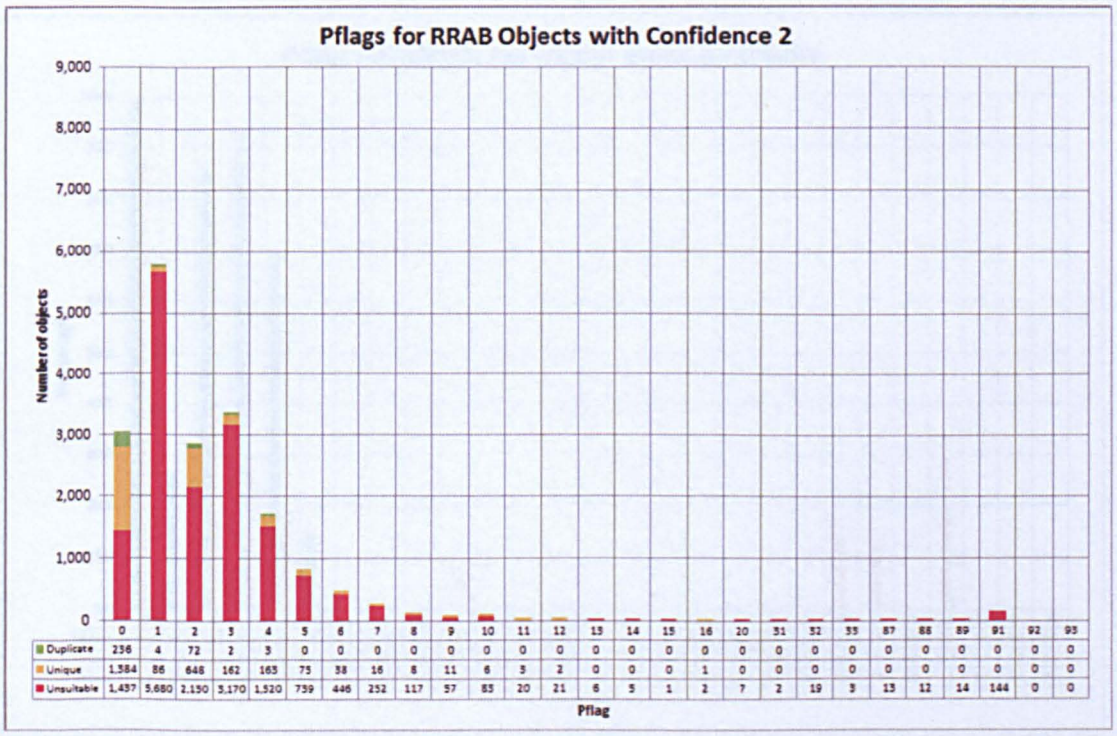

Pflag	0	1	2	3	4	5	6	7	8	9	10	11	12	13	14	15	16	20	31	32	33	87	88	89	91	92	93
Duplicate	256	4	72	2	3	0	0	0	0	0	0	0	0	0	0	0	0	0	0	0	0	0	0	0	0	0	0
Unique	1,384	86	648	162	163	75	38	16	8	11	6	3	2	0	0	0	1	0	0	0	0	0	0	0	0	0	0
Unsuitable	1,437	5,680	2,150	3,170	1,520	739	446	252	117	57	33	20	21	6	5	1	2	7	2	19	3	13	12	14	144	0	0

Appendix 16 continued…

Confidence Index 4: One NN provides the classification and the other two shows 'No class'

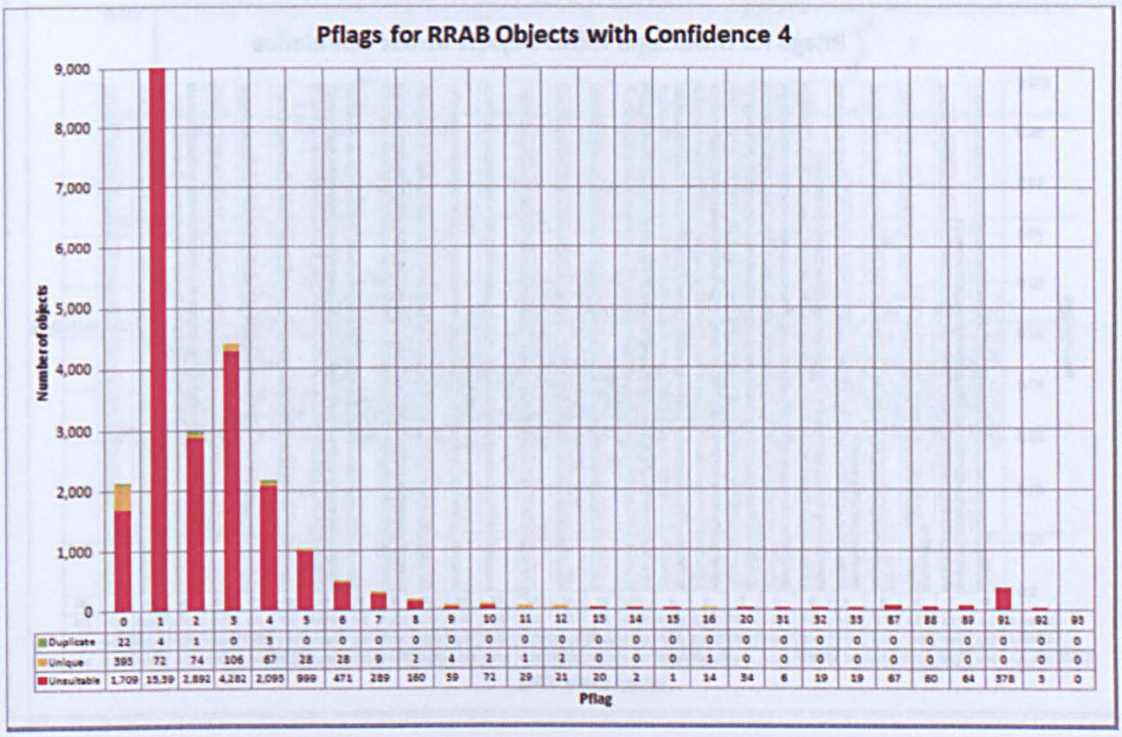

Pflag	0	1	2	3	4	5	6	7	8	9	10	11	12	13	14	15	16	20	31	32	33	87	88	89	91	92	93
Duplicate	22	4	1	0	3	0	0	0	0	0	0	0	0	0	0	0	0	0	0	0	0	0	0	0	0	0	0
Unique	395	72	74	106	67	28	28	9	2	4	2	1	2	0	0	0	1	0	0	0	0	0	0	0	0	0	0
Unsuitable	1,709	15,39	2,892	4,282	2,095	999	471	289	160	59	72	29	21	20	2	1	14	34	6	19	19	67	80	64	378	3	0

Percentage of the objects that were manually confirmed as suitable

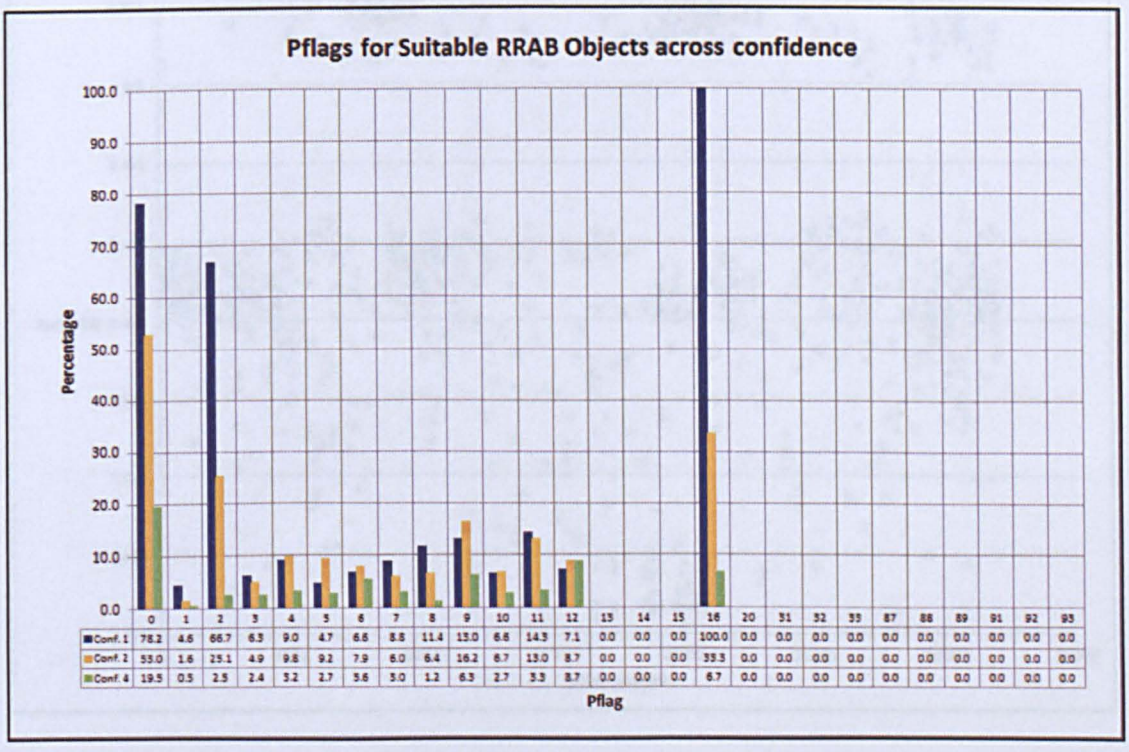

Pflag	0	1	2	3	4	5	6	7	8	9	10	11	12	13	14	15	16	20	31	32	33	87	88	89	91	92	93
Conf. 1	78.2	4.6	66.7	6.3	9.0	4.7	6.6	8.8	11.4	13.0	6.6	14.3	7.1	0.0	0.0	0.0	100.0	0.0	0.0	0.0	0.0	0.0	0.0	0.0	0.0	0.0	0.0
Conf. 2	53.0	1.6	25.1	4.9	9.8	9.2	7.9	6.0	6.4	16.2	6.7	13.0	8.7	0.0	0.0	0.0	33.3	0.0	0.0	0.0	0.0	0.0	0.0	0.0	0.0	0.0	0.0
Conf. 4	19.5	0.5	2.5	2.4	5.2	2.7	5.6	5.0	1.2	6.3	2.7	3.3	8.7	0.0	0.0	0.0	6.7	0.0	0.0	0.0	0.0	0.0	0.0	0.0	0.0	0.0	0.0

Appendix 16 continued…

Percentage of the objects that were manually confirmed as unsuitable

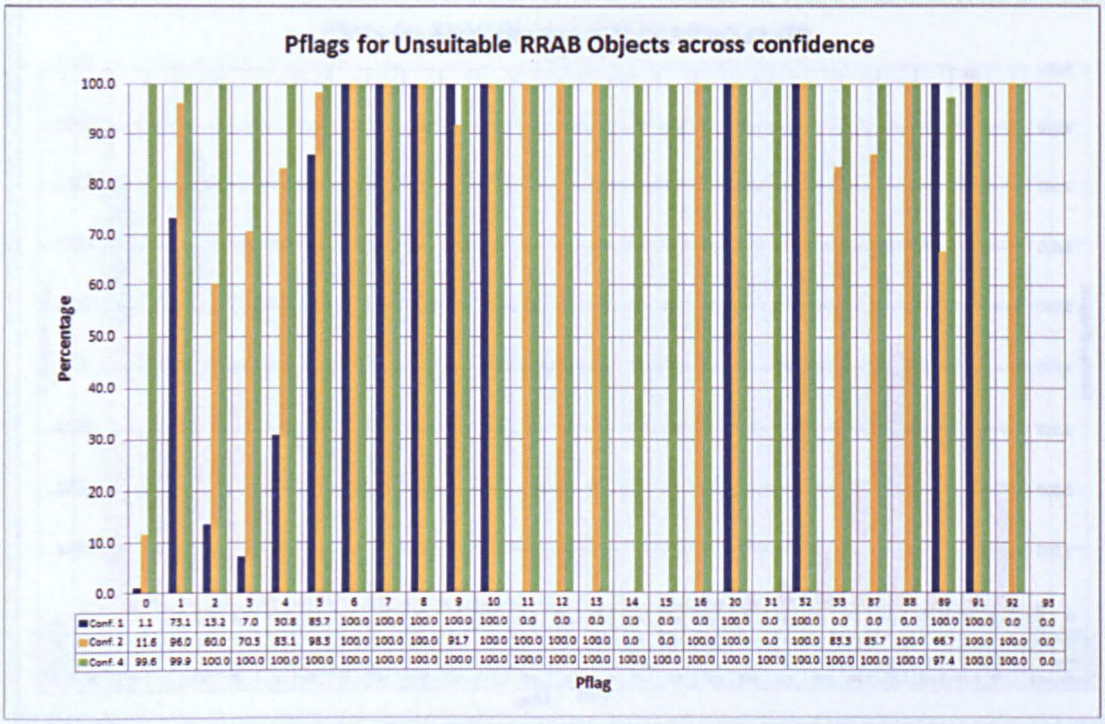

	0	1	2	3	4	5	6	7	8	9	10	11	12	13	14	15	16	20	31	32	33	87	88	89	91	92	95
Conf. 1	1.1	73.1	13.2	7.0	30.8	85.7	100.0	100.0	100.0	100.0	100.0	0.0	0.0	0.0	0.0	0.0	0.0	100.0	0.0	100.0	0.0	0.0	0.0	100.0	100.0	0.0	0.0
Conf. 2	11.6	96.0	60.0	70.5	83.1	98.3	100.0	100.0	100.0	91.7	100.0	100.0	100.0	100.0	0.0	0.0	100.0	100.0	0.0	100.0	83.3	85.7	100.0	66.7	100.0	100.0	0.0
Conf. 4	99.6	99.9	100.0	100.0	100.0	100.0	100.0	100.0	100.0	100.0	100.0	100.0	100.0	100.0	100.0	100.0	100.0	100.0	100.0	100.0	100.0	100.0	100.0	97.4	100.0	100.0	0.0

Appendix 17 – Clumped period ranges for RRAB Objects

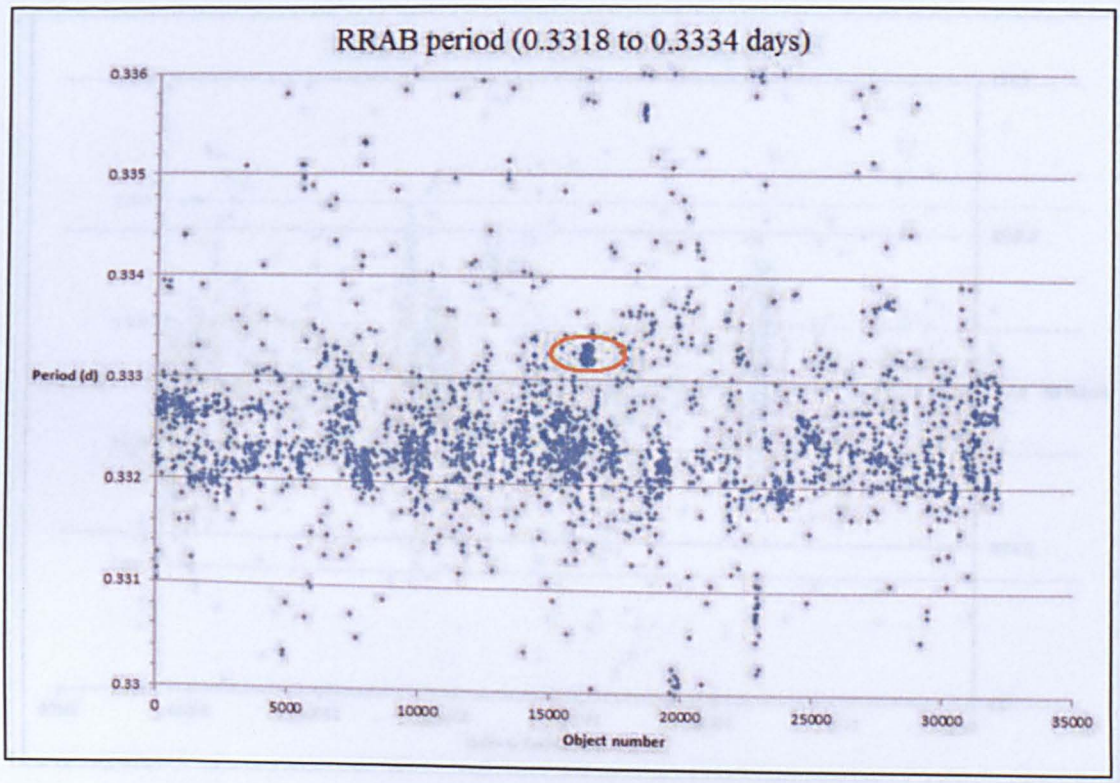

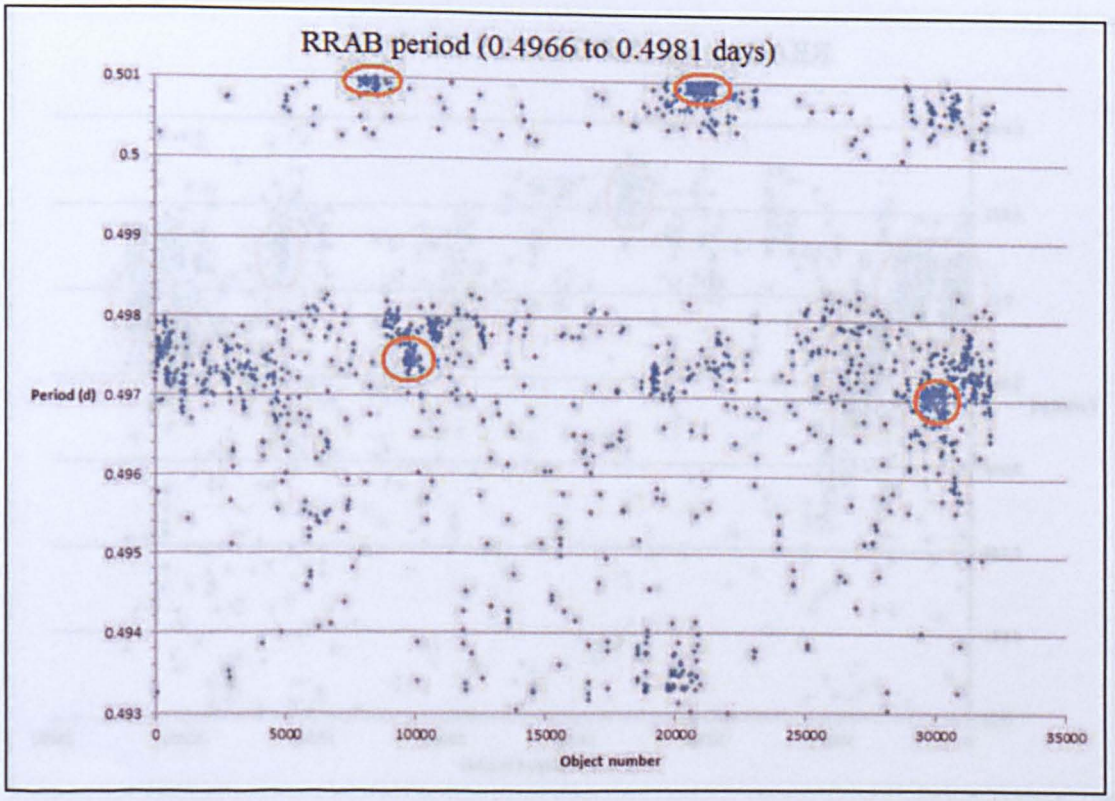

Appendix 17 continued…

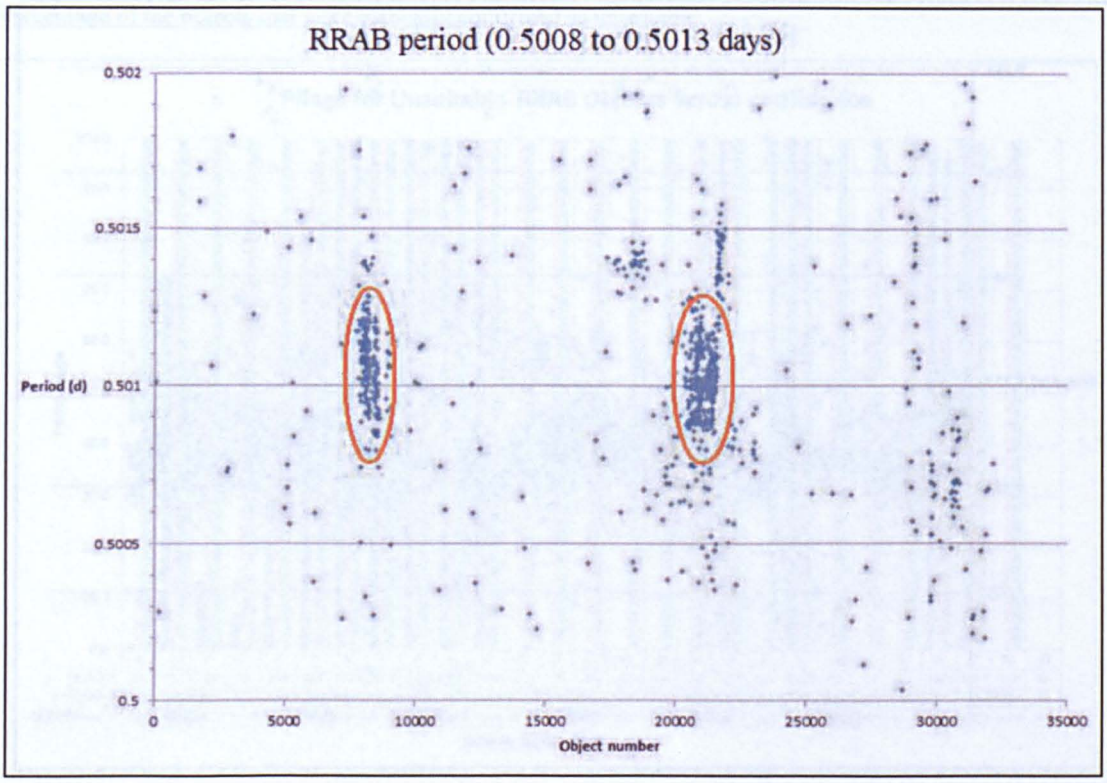

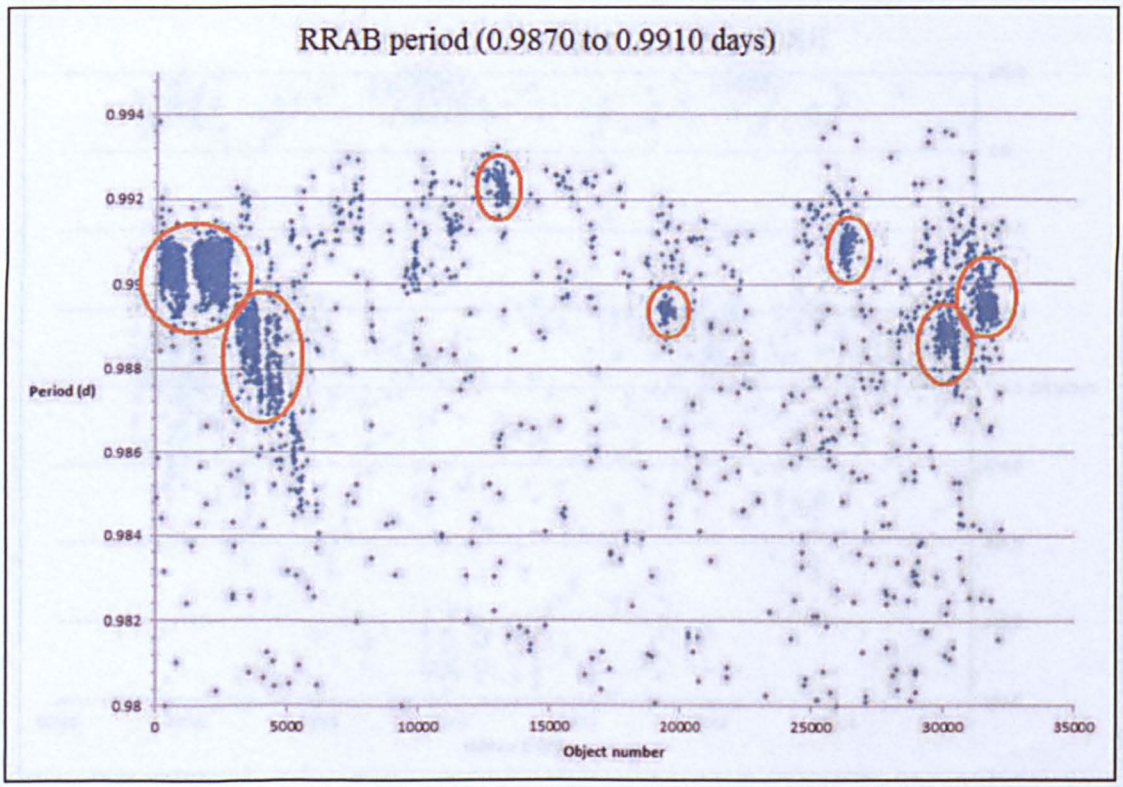

Appendix 17 continued…

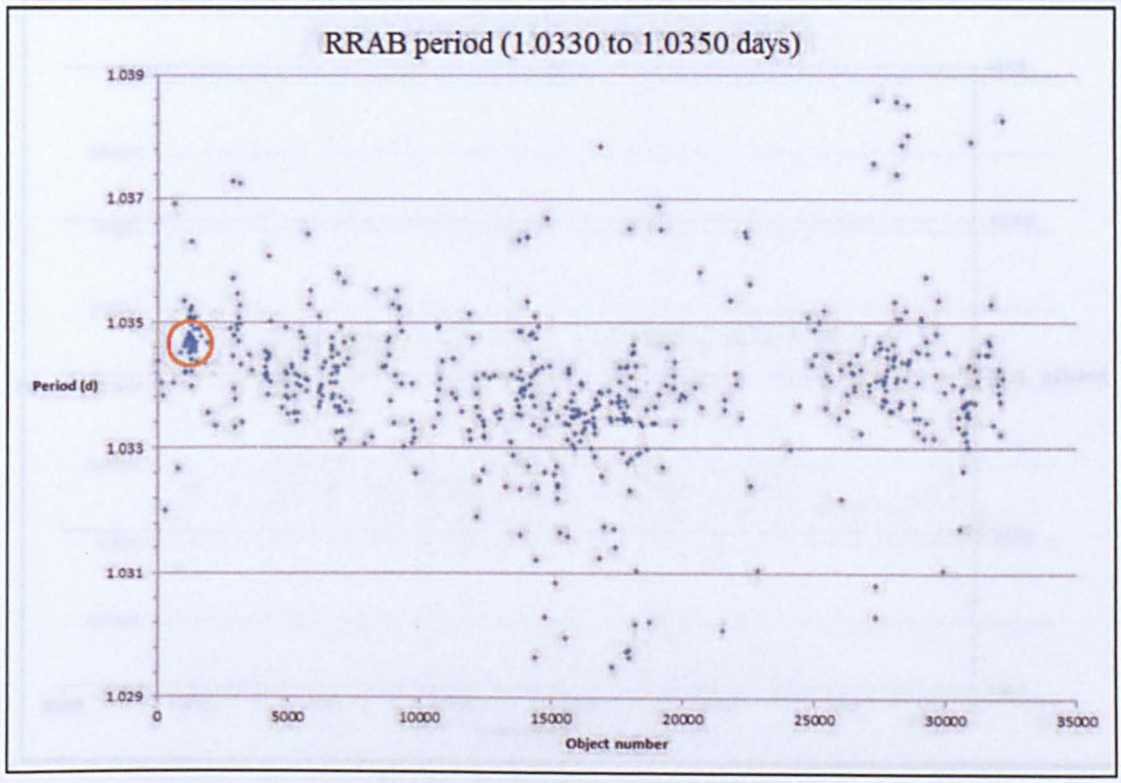

Appendix 18 – Clumped period ranges for DSCT Objects

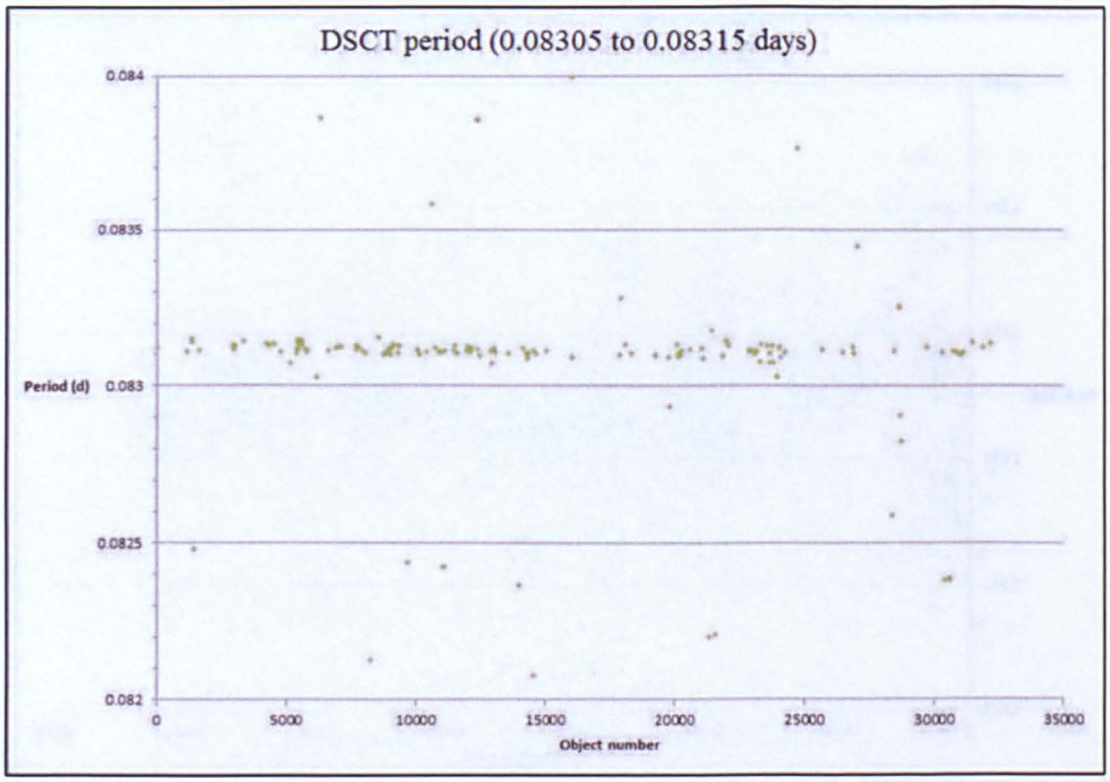

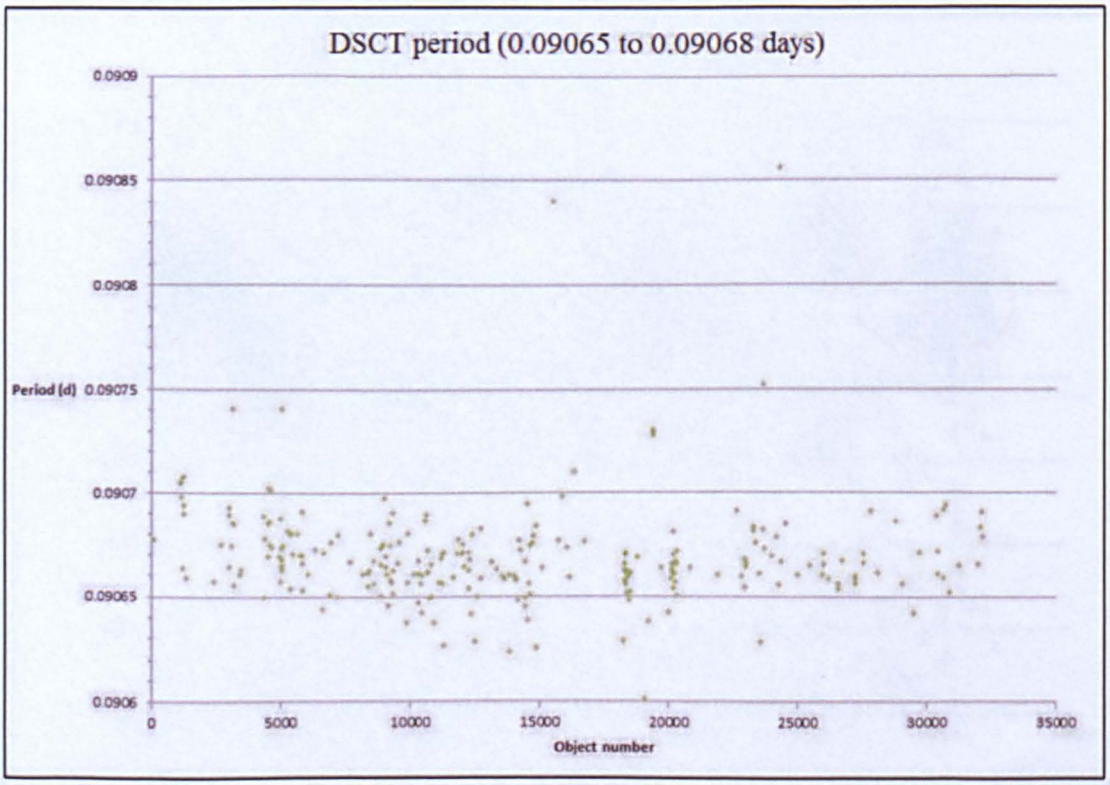

Appendix 18 continued...

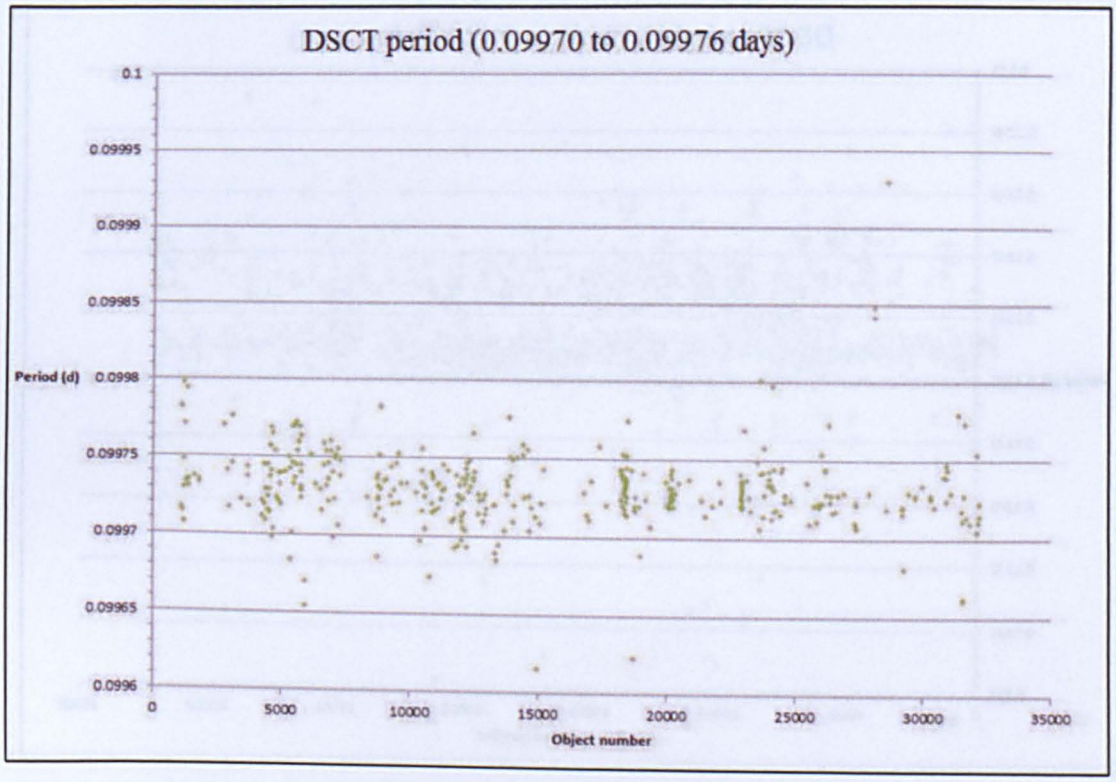

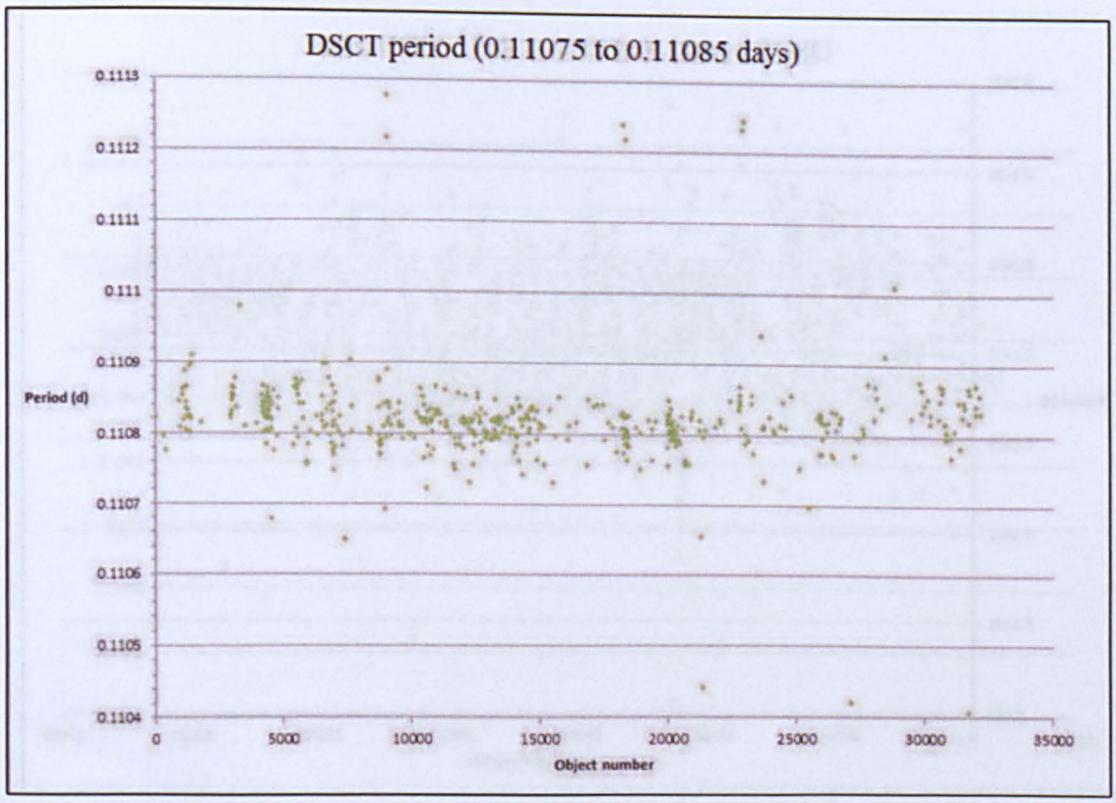

Appendix 18 continued…

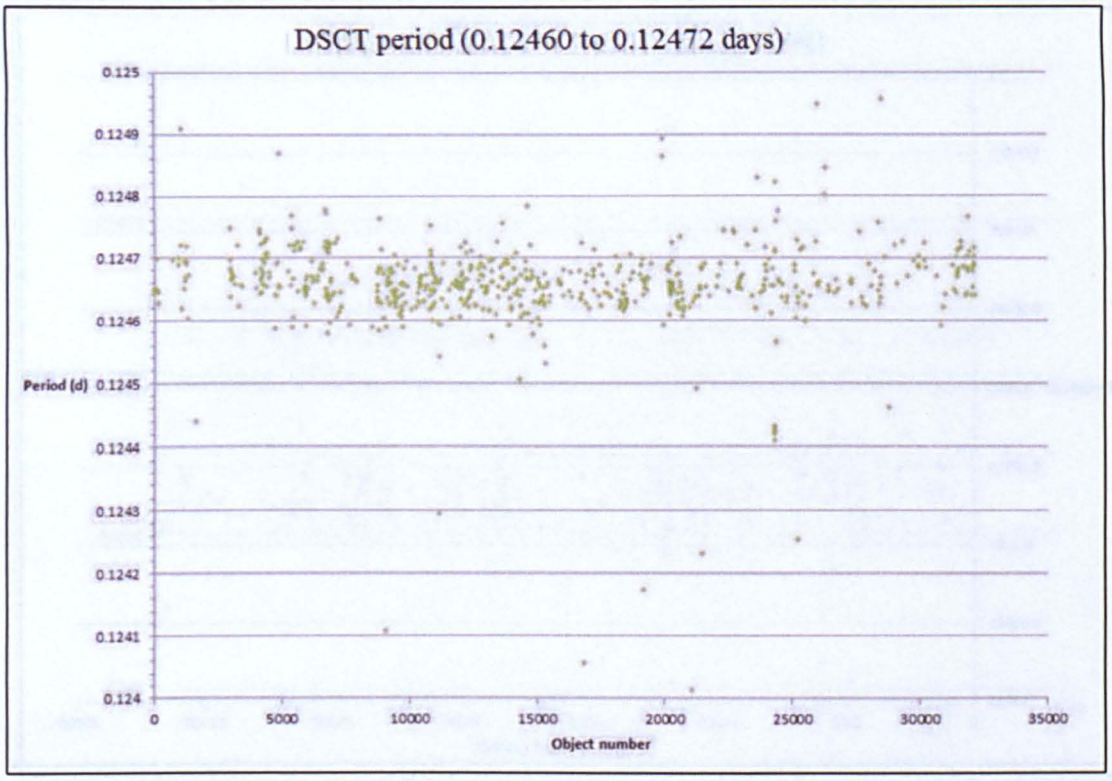

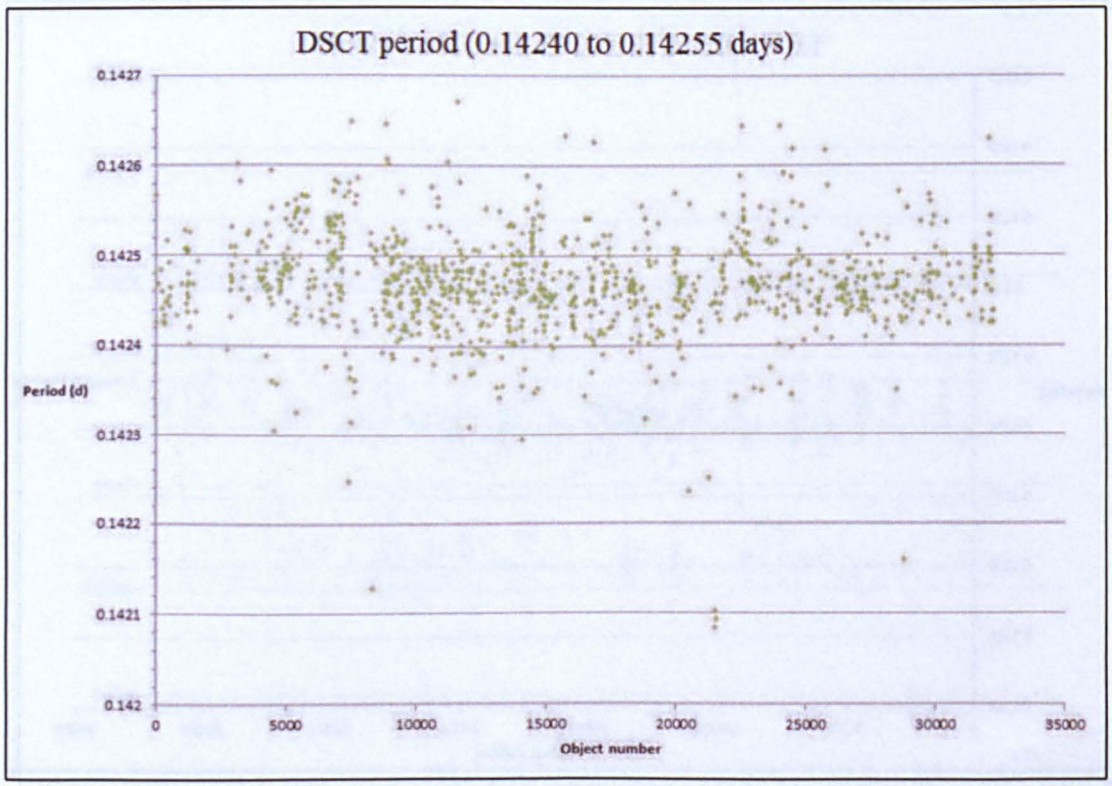

Appendix 18 continued...

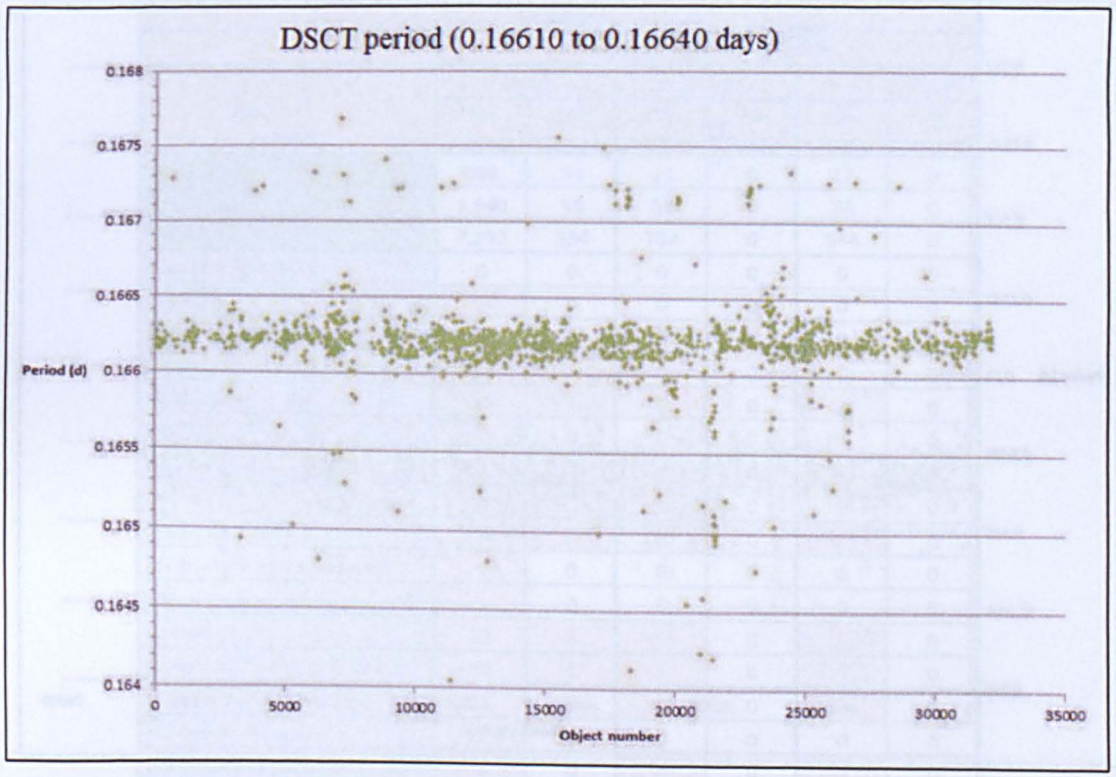

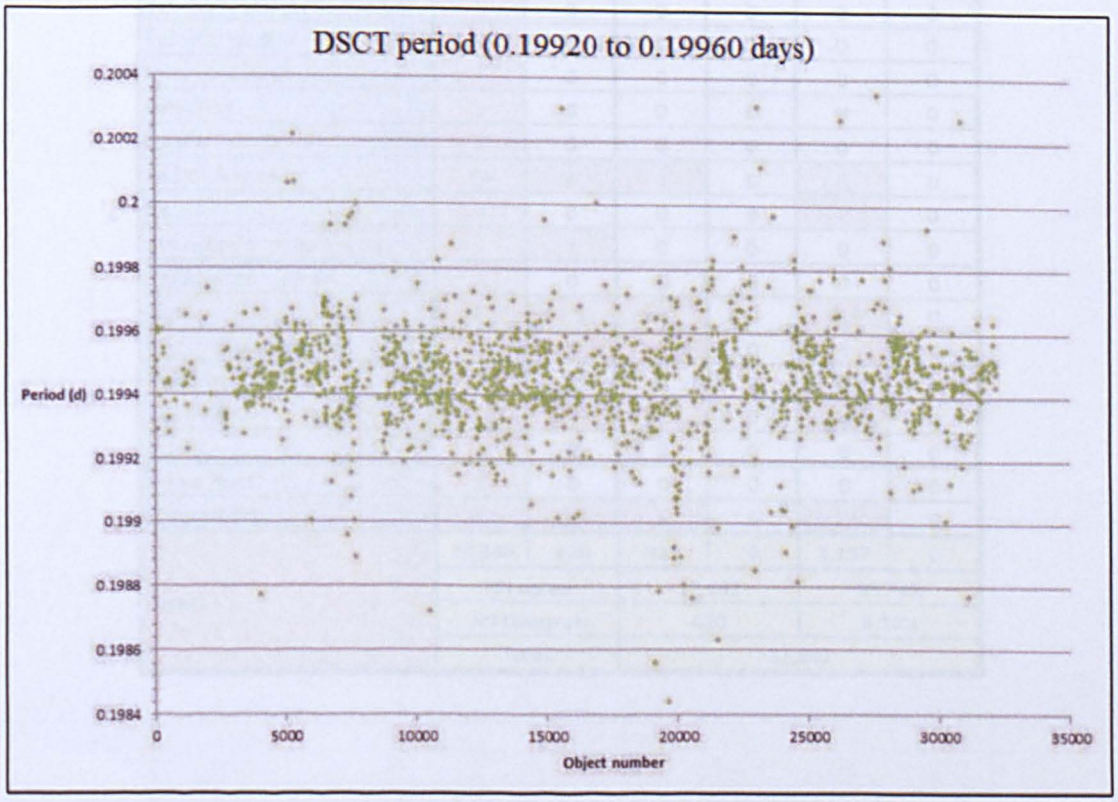

Appendix 18 continued...

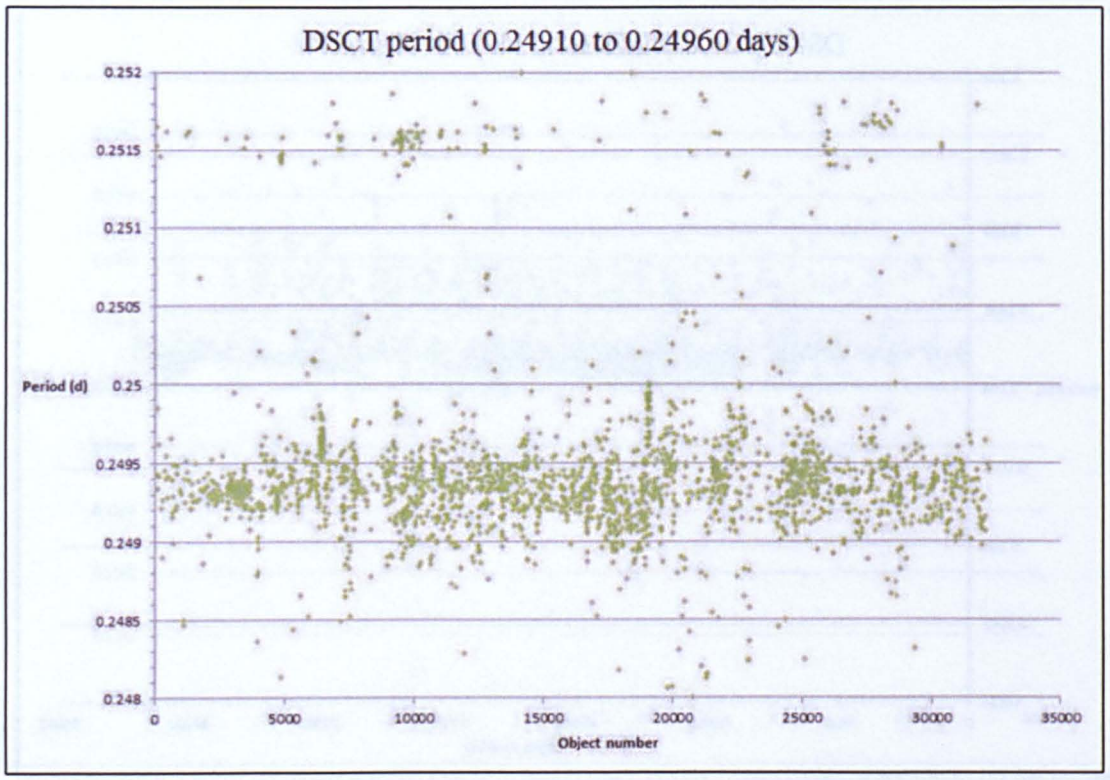

Appendix 19 – EA class objects in SIMBAD

EA objects						
	Based on light-curve shape					
	Good		Large Scatter		Small Amplitude	
SIMBAD	NN Agree	NN Disagree	NN Agree	NN Disagree	NN Agree	NN Disagree
Agree	998	34	11	0	17	0
Possible matches	1,340	58	30	0	34	0
Unknown	7,193	234	704	0	944	0
Blue Straggler Star	0	0	0	0	0	0
Cepheid	1	0	0	0	0	0
Classical Cepheid	0	0	0	0	0	0
Cluster of Galaxies	2	1	0	0	0	0
Double star	51	3	5	0	2	0
DSCT	1	0	0	0	0	0
EA	998	34	11	0	17	0
EB	73	12	1	0	0	0
Eclipsing binary	246	17	13	0	10	0
Eclipsing binary candidate	1	0	0	0	0	0
EW	6	0	0	0	0	0
Galaxy	87	8	30	0	22	0
Galaxy in Cluster of Galaxies	10	1	5	0	2	0
High proper-motion Star	26	0	6	0	8	0
HII (ionized) region	1	0	0	0	0	0
Horizontal Branch Star	5	0	2	0	1	0
Low-mass star (M<1solMass)	3	0	0	0	0	0
Possible HB Star	2	0	0	0	0	0
Possible Quasar	4	0	0	0	0	0
Pulsating	2	0	0	0	0	0
Quasar	5	0	0	0	0	0
Radio - Source	54	4	3	0	7	0
RR	4	0	0	0	1	0
Semi-regular pulsating Star	2	1	0	0	0	0
Spectroscopic binary	3	0	0	0	0	0
Star	1,185	75	121	0	113	0
Star in double system	38	4	1	0	5	0
Unknown nature	5	0	0	0	0	0
Variable	196	7	6	0	8	0
W Vir	1	0	0	0	0	0
White Dwarf	2	0	0	0	0	0
X-ray source	181	19	9	0	17	0
Totals	10,388	420	917	0	1,157	0
	NN Agree:		12,462		96.74%	
	NN Disagree:		420		3.26%	
	Total:		12,882			

Appendix 20 – EA: Period shorter than published period (0.2d)

Object Id	Period (d)	Overall class	Manual class	Confirmed state
1SWASPJ101903.31-404426.7	0.091	EA	EA	Small Amplitude
1SWASPJ165118.06+512206.5	0.111	EA	EA	Good
1SWASPJ164230.08+512110.1	0.111	EA	EA	Good
1SWASPJ221234.22-440300.2	0.111	EA	EA	Small Amplitude
1SWASPJ124420.23-084016.8	0.117	EA	EA	Good
1SWASPJ121733.81-444052.9	0.125	EA	EA	Good
1SWASPJ124905.35-404444.5	0.125	EA	EA	Large Scatter
1SWASPJ101509.59-030834.3	0.135	EA	EA	Good
1SWASPJ120214.27-454858.3	0.142	EA	EA	Small Amplitude
1SWASPJ162041.19+510558.9	0.142	EB	EA	Good
1SWASPJ022355.73-211734.8	0.142	EA	EA	Large Scatter
1SWASPJ193353.71-430806.7	0.142	EA	EA	Large Scatter
1SWASPJ120006.84-454724.5	0.142	EA	EA	Small Amplitude
1SWASPJ120006.94-454723.7	0.142	EA	EA	Small Amplitude
1SWASPJ031843.03+511333.9	0.142	EA	EA	Good
1SWASPJ205805.71-185041.9	0.142	EA	EA	Good
1SWASPJ133159.70-453436.2	0.142	EA	EA	Good
1SWASPJ012409.09+564207.0	0.142	EA	EA	Good
1SWASPJ114414.27-181135.7	0.142	EA	EA	Small Amplitude
1SWASPJ120038.89-454730.0	0.142	EA	EA	Small Amplitude
1SWASPJ020637.66-280137.1	0.142	EA	EA	Large Scatter
1SWASPJ201740.02-392915.8	0.142	EA	EA	Small Amplitude
1SWASPJ034921.73+512948.3	0.143	EA	EA	Good
1SWASPJ134952.07-131337.3	0.151	EA	EA	Good
1SWASPJ212130.18-540432.6	0.155	EA	EA	Good
1SWASPJ090258.02-075850.5	0.156	EA	EA	Good
1SWASPJ153349.46+375928.2	0.162	EA	EA	Good
1SWASPJ190100.23-341430.9	0.166	EA	EA	Large Scatter
1SWASPJ164251.86+513121.0	0.166	EA	EA	Good
1SWASPJ031307.75-194129.1	0.166	EA	EA	Small Amplitude
1SWASPJ175431.49+343951.2	0.166	EA	EA	Large Scatter
1SWASPJ164449.20+513219.1	0.166	EA	EA	Good
1SWASPJ234821.88-200021.1	0.166	EA	EA	Good
1SWASPJ193735.22-322810.2	0.166	EA	EA	Large Scatter
1SWASPJ054708.28-235402.0	0.166	EA	EA	Good
1SWASPJ133201.36-453440.0	0.166	EA	EA	Large Scatter
1SWASPJ023159.46-191924.0	0.166	EA	EA	Large Scatter
1SWASPJ190730.25-330204.7	0.166	EA	EA	Large Scatter
1SWASPJ163426.72+512733.6	0.166	EA	EA	Good
1SWASPJ030614.92-450350.9	0.166	EA	EA	Good
1SWASPJ035538.08-340844.6	0.171	EA	EA	Good
1SWASPJ201138.36+503917.8	0.181	EA	EA	Large Scatter
1SWASPJ150656.89+011530.5	0.182	EA	EA	Good
1SWASPJ091612.27+361533.6	0.183	EA	EA	Good
1SWASPJ091616.99+361549.4	0.183	EA	EA	Good
1SWASPJ200306.06-632806.0	0.187	EA	EA	Small Amplitude
1SWASPJ041237.09-310147.5	0.193	EA	EA	Good
1SWASPJ010744.41+484458.2	0.194	EA	EA	Good
1SWASPJ143003.54-072541.8	0.197	EA	EA	Good
1SWASPJ095759.37+030700.1	0.199	EA	EA	Good

Appendix 21 – EB class objects in SIMBAD

EB objects						
	Based on light-curve shape					
	Good		Large Scatter		Small Amplitude	
SIMBAD	NN Agree	NN Disagree	NN Agree	NN Disagree	NN Agree	NN Disagree
Agree	188	1	2	0	4	0
Possible matches	327	4	10	0	12	0
Unknown	3,291	18	98	0	437	0
Blue Straggler Star	0	0	0	0	0	0
Cepheid	3	0	0	0	0	0
Classical Cepheid	0	0	0	0	0	0
Cluster of Galaxies	0	0	0	0	0	0
Double star	42	0	1	0	0	0
DSCT	5	0	1	0	0	0
EA	70	3	1	0	1	0
EB	188	1	2	0	4	0
Eclipsing binary	136	0	5	0	10	0
Eclipsing binary candidate	2	0	0	0	0	0
EW	67	1	3	0	1	0
Galaxy	64	1	2	0	3	0
Galaxy in Cluster of Galaxies	3	0	0	0	0	0
High proper-motion Star	7	0	0	0	3	0
HII (ionized) region	0	0	0	0	0	0
Horizontal Branch Star	4	0	0	0	0	0
Low-mass star (M<1solMass)	0	0	0	0	0	0
Possible HB Star	0	0	0	0	0	0
Possible Quasar	1	0	0	0	0	0
Pulsating	0	0	1	0	1	0
Quasar	7	0	1	0	0	0
Radio - Source	26	0	0	0	6	0
RR	17	0	0	0	1	0
Semi-regular pulsating Star	3	0	0	0	0	0
Spectroscopic binary	1	0	0	0	0	0
Star	462	0	8	0	46	0
Star in double system	10	0	0	0	0	0
Unknown nature	0	0	0	0	0	0
Variable	80	1	0	0	0	0
W Vir	0	0	0	0	0	0
White Dwarf	1	0	0	0	0	0
X-ray source	68	1	0	0	6	0
Totals	4,558	26	123	0	519	0
	NN Agree:		5,200		99.50%	
	NN Disagree:		26		0.50%	
	Total:		5,226			

Appendix 22 – EB: Period shorter than published period (>1 day)

Object Id	Period (d)	Overall class	Manual class	Confirmed state
1SWASPJ183224.69+604344.1	0.142	EB	EB	Small Amplitude
1SWASPJ005228.75+251844.7	0.166	EB	EB	Small Amplitude
1SWASPJ131743.62-405020.0	0.166	EB	EB	Small Amplitude
1SWASPJ191540.22-372432.0	0.166	EB	EB	Small Amplitude
1SWASPJ022050.85+332047.6	0.193	EB	EB	Good
1SWASPJ165957.84+443532.6	0.221	EB	EB	Good
1SWASPJ211359.46+122712.4	0.222	EB	EB	Good
1SWASPJ093443.60+420831.9	0.222	EB	EB	Good
1SWASPJ215826.52+253437.4	0.223	EB	EB	Good
1SWASPJ043341.22+385132.0	0.223	EB	EB	Large Scatter
1SWASPJ011732.82+525201.3	0.224	EB	EB	Good
1SWASPJ011732.10+525204.9	0.224	EB	EB	Good
1SWASPJ014630.33-185710.7	0.235	EB	EB	Small Amplitude
1SWASPJ014527.13+245037.2	0.235	EB	EB	Good
1SWASPJ143909.28-105502.1	0.235	EB	EB	Good
1SWASPJ155656.43-111835.5	0.239	EB	EB	Good
1SWASPJ205149.21-374919.7	0.239	EB	EB	Good
1SWASPJ150433.06-413015.4	0.240	EB	EB	Good
1SWASPJ025324.03-135246.4	0.240	EB	EB	Good
1SWASPJ171332.59+300749.7	0.242	EB	EB	Good
1SWASPJ023008.08-450833.8	0.244	EB	EB	Good
1SWASPJ181543.59+134959.6	0.245	EB	EB	Good
1SWASPJ182939.50+460926.2	0.246	EB	EB	Good
1SWASPJ182940.74+460942.3	0.246	EB	EB	Good
1SWASPJ220918.66-090629.0	0.246	EB	EB	Small Amplitude
1SWASPJ023425.12+074911.9	0.247	EB	EB	Good
1SWASPJ163449.01+371642.5	0.247	EB	EB	Good
1SWASPJ011639.34-075832.1	0.247	EB	EB	Good
1SWASPJ031158.75+521437.8	0.248	EB	EB	Good
1SWASPJ031158.93+521432.2	0.248	EB	EB	Good
1SWASPJ171048.64+334600.9	0.249	EB	EB	Good
1SWASPJ135204.62-420443.4	0.249	EB	EB	Good
1SWASPJ212325.50-170251.1	0.249	EB	EB	Large Scatter
1SWASPJ061622.57-271127.2	0.249	EB	EB	Good
1SWASPJ160327.36-215949.3	0.249	EB	EB	Large Scatter
1SWASPJ054803.86+283047.6	0.251	EB	EB	Good
1SWASPJ054800.47+283024.8	0.251	EB	EB	Good
1SWASPJ173030.53+255415.0	0.251	EB	EB	Good
1SWASPJ115643.63-164056.5	0.252	EB	EB	Good
1SWASPJ040721.80-121003.3	0.254	EB	EB	Good
1SWASPJ063003.43-404905.6	0.255	EB	EB	Good
1SWASPJ024752.25+543843.7	0.255	EB	EB	Good
1SWASPJ043547.44-313851.4	0.255	EB	EB	Good
1SWASPJ130146.81+163146.1	0.256	EB	EB	Good
1SWASPJ045200.31-090956.0	0.257	EB	EB	Large Scatter
1SWASPJ192719.67-393604.8	0.258	EB	EB	Good
1SWASPJ192716.38-393526.4	0.258	EB	EB	Good
1SWASPJ143209.99-174257.1	0.260	EB	EB	Good
1SWASPJ153323.73+135638.3	0.260	EB	EB	Good
1SWASPJ124534.52-131209.8	0.260	EB	EB	Good

Appendix 23 – EW class objects in SIMBAD

EW objects						
	Based on light-curve shape					
	Good		Large Scatter		Small Amplitude	
SIMBAD	NN Agree	NN Disagree	NN Agree	NN Disagree	NN Agree	NN Disagree
Agree	200	3	3	0	0	0
Possible matches	557	13	8	0	2	0
Unknown	1,789	43	17	0	26	0
Blue Straggler Star	1	0	0	0	1	0
Cepheid	1	0	0	0	0	0
Classical Cepheid	1	0	0	0	0	0
Cluster of Galaxies	2	0	0	0	0	0
Double star	188	6	3	0	0	0
DSCT	14	0	1	0	0	0
EA	3	0	0	0	0	0
EB	9	0	0	0	0	0
Eclipsing binary	150	3	2	0	0	0
Eclipsing binary candidate	0	0	0	0	0	0
EW	200	3	3	0	0	0
Galaxy	32	2	0	0	0	0
Galaxy in Cluster of Galaxies	1	0	0	0	1	0
High proper-motion Star	11	0	0	0	0	0
HII (ionized) region	0	0	0	0	0	0
Horizontal Branch Star	0	0	0	0	0	0
Low-mass star (M<1solMass)	0	0	0	0	0	0
Possible HB Star	0	0	0	0	0	0
Possible Quasar	0	0	0	0	0	0
Pulsating	0	0	0	0	0	0
Quasar	2	0	0	0	0	0
Radio - Source	10	1	0	0	0	0
RR	12	1	0	0	0	0
Semi-regular pulsating Star	1	0	0	0	0	0
Spectroscopic binary	4	0	0	0	0	0
Star	220	2	1	0	7	0
Star in double system	16	1	0	0	2	0
Unknown nature	1	0	0	0	0	0
Variable	43	0	0	0	0	0
W Vir	0	0	0	0	0	0
White Dwarf	0	0	0	0	0	0
X-ray source	35	2	1	0	0	0
Totals	2,746	64	28	0	37	0
	NN Agree:		2,811		97.77%	
	NN Disagree:		64		2.23%	
	Total:		2,875			

Appendix 24 – EW: Period longer than published period (<1 day)

Object Id	Period (d)	Overall class	Manual class	Confirmed state
1SWASPJ000321.40+383107.0	11.904	EW	EW	Good
1SWASPJ111711.97-311255.5	8.321	EW	EW	Good
1SWASPJ052855.47+381915.3	3.620	EW	EW	Good
1SWASPJ054829.96+334818.5	3.162	EW	EW	Good
1SWASPJ232112.97+505258.0	1.676	EW	EW	Small Amplitude
1SWASPJ021745.58-081701.9	1.461	EW	EW	Good
1SWASPJ150012.69-012756.0	1.427	EW	EW	Good
1SWASPJ092116.20-095420.5	1.377	EW	EW	Good
1SWASPJ022805.20+332814.7	1.364	EW	EW	Small Amplitude
1SWASPJ064538.73+303952.1	1.254	EW	EW	Good
1SWASPJ204517.61+162756.3	1.213	EW	EW	Good
1SWASPJ195831.19-352958.5	1.200	EW	EW	Good
1SWASPJ060613.54+323510.5	1.196	EW	EW	Good
1SWASPJ181301.82+340224.0	1.154	EW	EW	Good
1SWASPJ020225.26+514430.4	1.146	EW	EW	Good
1SWASPJ224709.52-054347.1	1.127	EW	EW	Good
1SWASPJ205721.48+553005.0	1.123	EW	EW	Good
1SWASPJ115747.22-242327.8	1.085	EW	EW	Good
1SWASPJ115747.78-242350.8	1.084	EW	EW	Good
1SWASPJ233627.95+392214.2	1.081	EW	EW	Good
1SWASPJ121146.06-304001.5	1.052	EW	EW	Good
1SWASPJ090803.23-090300.6	1.051	EW	EW	Small Amplitude
1SWASPJ002127.00+301322.9	1.039	EW	EW	Good
1SWASPJ232949.12-310249.9	1.034	EW	EW	Good
1SWASPJ214818.48+274922.0	1.024	EW	EW	Good

Appendix 25 – EW: Amplitude greater than published (<0.8Vmag)

Object Id	BMA	Overall class	Manual class	Confirmed state
1SWASPJ224931.98+314743.9	1.320	EW	EW	Good
1SWASPJ084408.68-040640.1	1.240	EW	EW	Good
1SWASPJ155657.51+421336.9	1.184	EW	EW	Good
1SWASPJ210559.73-460647.8	1.180	EW	EW	Good
1SWASPJ004637.72+315117.4	1.114	EW	EW	Good
1SWASPJ041716.59-341509.8	0.984	EW	EW	Good
1SWASPJ104709.65-020617.4	0.972	EW	EW	Good
1SWASPJ124406.25-291544.4	0.970	EW	EW	Good
1SWASPJ141338.38-035146.7	0.934	EW	EW	Good
1SWASPJ154126.94-321043.3	0.896	EW	EW	Good
1SWASPJ033147.96-263141.3	0.890	EW	EW	Good
1SWASPJ105746.59+095840.6	0.890	EW	EW	Good
1SWASPJ090705.80-084320.4	0.884	EW	EW	Good
1SWASPJ143041.24+174151.0	0.876	EW	EW	Good
1SWASPJ151407.68-303301.1	0.872	EW	EW	Good
1SWASPJ160722.02+102940.1	0.872	EW	EW	Good
1SWASPJ043720.00-292802.5	0.870	EW	EW	Good
1SWASPJ111431.61-433214.0	0.866	EW	EW	Good
1SWASPJ093632.42+485242.3	0.862	EW	EW	Good
1SWASPJ171600.32+271615.1	0.862	EW	EW	Good
1SWASPJ130710.36-463535.1	0.848	EW	EW	Good
1SWASPJ181033.53+421623.2	0.848	EW	EW	Good
1SWASPJ235233.97+385919.2	0.848	EW	EW	Good
1SWASPJ023705.63+330845.0	0.842	EW	EW	Good
1SWASPJ102004.60+064930.1	0.842	EW	EW	Good
1SWASPJ224942.99+004601.5	0.840	EW	EW	Good
1SWASPJ035438.99-191923.2	0.826	EW	EW	Good
1SWASPJ034143.26-022235.9	0.820	EW	EW	Good
1SWASPJ092319.39-182714.7	0.820	EW	EW	Good
1SWASPJ063306.99-451609.5	0.818	EW	EW	Good
1SWASPJ120622.56-160429.8	0.816	EW	EW	Good
1SWASPJ131358.96-090235.9	0.812	EW	EW	Good
1SWASPJ001445.75-391435.5	0.810	EW	EW	Good
1SWASPJ163007.37+012513.2	0.806	EW	EW	Good
1SWASPJ194722.46+535234.7	0.806	EW	EW	Good
1SWASPJ041418.36-462657.1	0.804	EW	EW	Good
1SWASPJ115049.18-242303.1	0.804	EW	EW	Good
1SWASPJ180947.64+490255.0	0.804	EW	EW	Good
1SWASPJ212606.24+002242.7	0.802	EW	EW	Good

Appendix 26 – RRAB class objects in SIMBAD

RRAB objects						
	Based on light-curve shape					
	Good		Large Scatter		Small Amplitude	
SIMBAD	NN Agree	NN Disagree	NN Agree	NN Disagree	NN Agree	NN Disagree
Agree	2,252	191	32	25	83	17
Possible matches	7	10	1	2	1	0
Unknown	3,009	665	182	267	460	366
Blue Straggler Star	1	0	0	0	0	0
Cepheid	10	2	1	1	0	0
Classical Cepheid	0	1	0	3	0	2
Cluster of Galaxies	3	0	0	0	1	0
Double star	0	0	0	1	0	0
DSCT	1	1	0	0	0	0
EA	1	0	0	0	0	0
EB	1	0	0	0	0	0
Eclipsing binary	4	6	0	0	0	0
Eclipsing binary candidate	0	0	0	0	0	0
EW	2	0	0	0	1	0
Galaxy	79	18	2	6	8	2
Galaxy in Cluster of Galaxies	16	1	0	0	5	0
High proper-motion Star	10	3	1	2	0	1
HII (ionized) region	0	0	0	0	0	0
Horizontal Branch Star	126	17	1	6	7	7
Low-mass star (M<1solMass)	2	0	1	0	0	0
Possible HB Star	0	1	0	0	0	0
Possible Quasar	4	0	0	0	1	0
Pulsating	0	2	0	1	0	1
Quasar	7	1	0	1	0	0
Radio - Source	27	4	3	1	3	4
RR	2,252	191	32	25	83	17
Semi-regular pulsating Star	4	0	0	8	0	3
Spectroscopic binary	0	0	0	1	0	1
Star	147	39	25	36	19	39
Star in double system	0	4	1	1	0	0
Unknown nature	0	0	0	0	0	0
Variable	178	9	4	4	8	5
W Vir	2	2	0	0	0	0
White Dwarf	0	2	0	0	1	3
X-ray source	11	12	0	0	0	13
Totals	5,897	981	253	364	597	464
	NN Agree:		6,747		78.86%	
	NN Disagree:		1,809		21.14%	
	Total:		8,556			

Appendix 27 – RRAB: Period shorter than published period (0.3 days)

Object Id	Period (d)	Overall class	Manual class	Confirmed state
1SWASPJ001700.96+340313.4	0.255	DSCT	RRAB	Small Amplitude
1SWASPJ002526.63+421107.7	0.264	DSCT	RRAB	Small Amplitude
1SWASPJ002531.87+355406.3	0.269	DSCT	RRAB	Small Amplitude
1SWASPJ010721.91+343208.7	0.278	DSCT	RRAB	Small Amplitude
1SWASPJ010723.17+343135.1	0.278	DSCT	RRAB	Good
1SWASPJ014152.28-005327.4	0.269	DSCT	RRAB	Large Scatter
1SWASPJ020013.26-172843.8	0.258	DSCT	RRAB	Small Amplitude
1SWASPJ023534.12-013912.4	0.263	DSCT	RRAB	Good
1SWASPJ025842.70-133223.0	0.263	DSCT	RRAB	Small Amplitude
1SWASPJ030533.41+404500.1	0.299	DSCT	RRAB	Small Amplitude
1SWASPJ030535.42+404448.4	0.298	DSCT	RRAB	Small Amplitude
1SWASPJ031505.49+404357.5	0.299	DSCT	RRAB	Large Scatter
1SWASPJ032753.59+281257.8	0.285	DSCT	RRAB	Small Amplitude
1SWASPJ042951.68-392039.6	0.277	DSCT	RRAB	Small Amplitude
1SWASPJ042952.36-392004.6	0.277	DSCT	RRAB	Small Amplitude
1SWASPJ044554.64-120416.2	0.273	DSCT	RRAB	Good
1SWASPJ045450.62+320411.8	0.280	DSCT	RRAB	Small Amplitude
1SWASPJ052341.00+211849.8	0.277	DSCT	RRAB	Good
1SWASPJ053011.36-241051.4	0.291	DSCT	RRAB	Small Amplitude
1SWASPJ054046.15-245535.4	0.252	DSCT	RRAB	Good
1SWASPJ062241.66+183140.7	0.287	DSCT	RRAB	Good
1SWASPJ062244.33+183153.3	0.287	DSCT	RRAB	Good
1SWASPJ081112.03+465956.0	0.290	DSCT	RRAB	Small Amplitude
1SWASPJ084932.98+364945.5	0.250	DSCT	RRAB	Small Amplitude
1SWASPJ091816.99+315849.0	0.287	DSCT	RRAB	Good
1SWASPJ093232.31+422123.7	0.254	DSCT	RRAB	Small Amplitude
1SWASPJ093504.09-214033.6	0.252	DSCT	RRAB	Good
1SWASPJ111907.95-452252.7	0.254	DSCT	RRAB	Good
1SWASPJ113342.29+055814.7	0.299	DSCT	RRAB	Small Amplitude
1SWASPJ115037.49-254210.7	0.291	DSCT	RRAB	Large Scatter
1SWASPJ115333.88-281200.0	0.287	DSCT	RRAB	Good
1SWASPJ121434.51-344654.6	0.286	DSCT	RRAB	Large Scatter
1SWASPJ131820.92-442249.1	0.268	DSCT	RRAB	Small Amplitude
1SWASPJ132918.09+070335.3	0.270	DSCT	RRAB	Small Amplitude
1SWASPJ134903.00-192306.9	0.270	DSCT	RRAB	Large Scatter
1SWASPJ142031.07+283125.6	0.292	DSCT	RRAB	Good
1SWASPJ150740.70-142411.4	0.254	DSCT	RRAB	Good
1SWASPJ150849.11-412923.6	0.268	RRAB	RRAB	Large Scatter
1SWASPJ151635.28-162003.6	0.267	DSCT	RRAB	Good
1SWASPJ151821.86-082742.8	0.270	RRAB	RRAB	Good

Object Id	Period (d)	Overall class	Manual class	Confirmed state
1SWASPJ160742.67-244354.0	0.294	DSCT	RRAB	Small Amplitude
1SWASPJ162402.62-124409.7	0.286	DSCT	RRAB	Good
1SWASPJ162418.60-285447.5	0.275	DSCT	RRAB	Small Amplitude
1SWASPJ170509.55+551231.2	0.252	DSCT	RRAB	Small Amplitude
1SWASPJ170701.30+302710.0	0.271	DSCT	RRAB	Good
1SWASPJ171225.52+334338.5	0.250	DSCT	RRAB	Large Scatter
1SWASPJ171440.44+335037.0	0.250	RRAB	RRAB	Good
1SWASPJ172333.12+200233.3	0.253	DSCT	RRAB	Good
1SWASPJ172902.85+362440.7	0.250	DSCT	RRAB	Large Scatter
1SWASPJ173540.29+392205.1	0.250	DSCT	RRAB	Large Scatter
1SWASPJ174605.37+201651.6	0.255	DSCT	RRAB	Good
1SWASPJ175249.06+244515.8	0.291	DSCT	RRAB	Good
1SWASPJ175717.05+372805.9	0.289	DSCT	RRAB	Large Scatter
1SWASPJ182445.25+060531.4	0.285	DSCT	RRAB	Small Amplitude
1SWASPJ183026.21+401724.4	0.250	DSCT	RRAB	Small Amplitude
1SWASPJ190857.59-412620.2	0.271	DSCT	RRAB	Good
1SWASPJ190938.69-324411.4	0.260	DSCT	RRAB	Large Scatter
1SWASPJ191733.32-214603.1	0.279	DSCT	RRAB	Good
1SWASPJ191734.32-214619.8	0.279	DSCT	RRAB	Good
1SWASPJ192007.83+434317.4	0.275	DSCT	RRAB	Good
1SWASPJ192321.88-293249.2	0.287	DSCT	RRAB	Large Scatter
1SWASPJ192610.75-404347.5	0.277	DSCT	RRAB	Large Scatter
1SWASPJ194355.56-233740.1	0.266	DSCT	RRAB	Small Amplitude
1SWASPJ194436.17-192342.8	0.290	DSCT	RRAB	Good
1SWASPJ200222.07-425458.9	0.283	DSCT	RRAB	Good
1SWASPJ200222.23-425454.0	0.283	DSCT	RRAB	Good
1SWASPJ200225.13+220333.2	0.263	DSCT	RRAB	Large Scatter
1SWASPJ200748.80+413948.5	0.252	DSCT	RRAB	Small Amplitude
1SWASPJ200748.84+414021.4	0.252	DSCT	RRAB	Large Scatter
1SWASPJ201106.41+233908.9	0.298	DSCT	RRAB	Large Scatter
1SWASPJ201410.06-434916.6	0.272	DSCT	RRAB	Small Amplitude
1SWASPJ201745.72-271748.6	0.256	DSCT	RRAB	Good
1SWASPJ205333.49+364333.6	0.252	DSCT	RRAB	Large Scatter
1SWASPJ210353.69+390432.3	0.257	DSCT	RRAB	Large Scatter
1SWASPJ210510.24-355453.0	0.290	DSCT	RRAB	Small Amplitude
1SWASPJ212224.22+363720.6	0.252	DSCT	RRAB	Large Scatter
1SWASPJ231834.52+135126.2	0.258	DSCT	RRAB	Large Scatter
1SWASPJ234132.26+330906.2	0.269	DSCT	RRAB	Good
1SWASPJ235653.29+345516.0	0.288	DSCT	RRAB	Small Amplitude

Appendix 28 – RRAB: Period longer than published period (1.2 days)

Object Id	Period (d)	MeanVmag	Overall class	Manual class	Confirmed state
1SWASPJ025530.76+423448.4	1.269	-3.74	RRAB	RRAB	Good
1SWASPJ100809.71-153345.2	1.224	-0.61	RRAB	RRAB	Good
1SWASPJ141648.58-061714.9	1.348	-2.89	RRAB	RRAB	Good
1SWASPJ142357.88-010010.0	1.307	-1.88	RRAB	RRAB	Good
1SWASPJ154107.55+353316.5	1.271	-0.25	RRAB	RRAB	Good
1SWASPJ174156.61+150431.0	1.210	-2.84	RRAB	RRAB	Good
1SWASPJ174157.30+150510.8	1.207	-2.56	RRAB	RRAB	Good
1SWASPJ203823.65-232400.8	1.282	0.09	RRAB	RRAB	Good
1SWASPJ210622.50-184940.1	1.327	0.00	RRAB	RRAB	Good
1SWASPJ214504.11+024621.4	1.447	-0.79	RRAB	RRAB	Good
1SWASPJ025535.63+423430.2	1.270	-1.80	CEP	RRAB	Good
1SWASPJ120154.50-461624.0	1.520	-2.65	DSCT	RRAB	Good
1SWASPJ120155.18-461641.4	1.520	-2.66	DSCT	RRAB	Good
1SWASPJ210537.75+200453.6	1.709	-2.05	CEP	RRAB	Good

Appendix 29 – DSCT class objects in SIMBAD

DSCT objects						
	Based on light-curve shape					
	Good		Large Scatter		Small Amplitude	
SIMBAD	NN Agree	NN Disagree	NN Agree	NN Disagree	NN Agree	NN Disagree
Agree	41	0	0	0	2	0
Possible matches	11	1	0	0	6	0
Unknown	899	47	84	19	478	61
Blue Straggler Star	0	0	0	0	0	0
Cepheid	0	0	0	0	0	0
Classical Cepheid	4	2	0	0	0	0
Cluster of Galaxies	0	0	1	0	0	0
Double star	2	1	0	0	1	0
DSCT	41	0	0	0	2	0
EA	0	0	0	0	0	0
EB	0	0	0	0	0	0
Eclipsing binary	5	0	0	0	3	0
Eclipsing binary candidate	0	0	0	0	0	0
EW	2	0	0	0	1	0
Galaxy	14	2	2	1	7	3
Galaxy in Cluster of Galaxies	1	0	0	0	1	0
High proper-motion Star	1	0	0	0	4	1
HII (ionized) region	0	0	0	0	0	0
Horizontal Branch Star	3	0	1	0	2	0
Low-mass star (M<1solMass)	2	0	0	0	0	1
Possible HB Star	0	0	0	0	0	0
Possible Quasar	4	0	0	0	1	0
Pulsating	7	0	1	0	0	0
Quasar	3	0	1	0	2	1
Radio - Source	8	0	1	0	1	1
RR	16	3	0	0	1	0
Semi-regular pulsating Star	0	0	0	0	0	0
Spectroscopic binary	0	0	0	0	1	0
Star	135	3	5	1	47	4
Star in double system	2	0	0	0	1	0
Unknown nature	0	0	0	0	0	0
Variable	16	1	1	0	4	0
W Vir	0	0	0	0	0	0
White Dwarf	0	0	0	0	0	0
X-ray source	5	0	0	0	3	0
Totals	1,170	59	97	21	560	72
	NN Agree:		1,827		92.32%	
	NN Disagree:		152		7.68%	
	Total:		1,979			

Appendix 30 – DSCT: Period longer than published period (0.2 days)

Object Id	Period (d)	Overall class	Manual class	Confirmed state
1SWASPJ001834.63+045019.5	0.249	DSCT	DSCT	Small Amplitude
1SWASPJ002229.06+483216.0	0.225	DSCT	DSCT	Small Amplitude
1SWASPJ013058.29+170208.1	0.208	DSCT	DSCT	Good
1SWASPJ013623.20+480028.4	0.205	DSCT	DSCT	Small Amplitude
1SWASPJ015944.95+143309.6	0.209	DSCT	DSCT	Small Amplitude
1SWASPJ022644.44+335256.5	0.203	DSCT	DSCT	Small Amplitude
1SWASPJ022800.17+563843.1	0.245	DSCT	DSCT	Good
1SWASPJ024409.16-064626.7	0.249	DSCT	DSCT	Small Amplitude
1SWASPJ024412.11-081147.6	0.249	DSCT	DSCT	Good
1SWASPJ025743.57+353129.2	0.203	DSCT	DSCT	Good
1SWASPJ032135.72+472750.6	0.210	DSCT	DSCT	Small Amplitude
1SWASPJ034105.15-302506.8	0.222	DSCT	DSCT	Small Amplitude
1SWASPJ034508.10+482405.7	0.237	DSCT	DSCT	Good
1SWASPJ035451.77-133056.6	0.232	DSCT	DSCT	Small Amplitude
1SWASPJ035453.66-133043.1	0.232	DSCT	DSCT	Good
1SWASPJ040010.87+354435.6	0.218	DSCT	DSCT	Small Amplitude
1SWASPJ042159.71-040946.2	0.248	DSCT	DSCT	Good
1SWASPJ042846.23+551700.8	0.219	DSCT	DSCT	Good
1SWASPJ044009.87+114317.0	0.249	DSCT	DSCT	Good
1SWASPJ044028.61+422934.4	0.210	DSCT	DSCT	Good
1SWASPJ044833.30-114508.0	0.211	DSCT	DSCT	Small Amplitude
1SWASPJ050159.41+270012.9	0.216	DSCT	DSCT	Small Amplitude
1SWASPJ050845.33+335231.4	0.235	DSCT	DSCT	Good
1SWASPJ052807.14+342526.8	0.219	DSCT	DSCT	Small Amplitude
1SWASPJ052817.00+042129.5	0.212	RRAB	DSCT	Good
1SWASPJ052819.04+042200.6	0.212	DSCT	DSCT	Good
1SWASPJ055918.36+200117.9	0.201	DSCT	DSCT	Good
1SWASPJ055920.01+200059.8	0.201	DSCT	DSCT	Small Amplitude
1SWASPJ055920.57+200207.5	0.201	DSCT	DSCT	Good
1SWASPJ055921.47+200235.2	0.201	DSCT	DSCT	Good
1SWASPJ064649.23-355352.1	0.224	DSCT	DSCT	Small Amplitude
1SWASPJ081911.84+350101.5	0.239	DSCT	DSCT	Small Amplitude
1SWASPJ081914.33+350123.2	0.239	DSCT	DSCT	Good
1SWASPJ084526.07-053238.2	0.205	DSCT	DSCT	Small Amplitude
1SWASPJ091041.18-391449.8	0.249	DSCT	DSCT	Large Scatter
1SWASPJ094546.85-120014.4	0.223	DSCT	DSCT	Good
1SWASPJ094550.76-115942.7	0.223	DSCT	DSCT	Small Amplitude
1SWASPJ121006.02-405334.4	0.233	DSCT	DSCT	Good
1SWASPJ123700.69-331824.8	0.214	DSCT	DSCT	Good
1SWASPJ123804.93+344937.7	0.245	DSCT	DSCT	Small Amplitude
1SWASPJ124550.78-123321.0	0.247	DSCT	DSCT	Good
1SWASPJ130616.11+090333.9	0.212	DSCT	DSCT	Good
1SWASPJ133256.77+123949.4	0.231	DSCT	DSCT	Good
1SWASPJ133431.17-223508.7	0.249	DSCT	DSCT	Large Scatter
1SWASPJ141709.18-162057.7	0.210	DSCT	DSCT	Good
1SWASPJ142149.75-195058.8	0.242	DSCT	DSCT	Good
1SWASPJ150255.80-192213.8	0.219	DSCT	DSCT	Good
1SWASPJ151652.86-263201.9	0.249	DSCT	DSCT	Small Amplitude
1SWASPJ153727.96+254023.5	0.226	DSCT	DSCT	Good
1SWASPJ154605.53-384642.9	0.202	DSCT	DSCT	Good
1SWASPJ154605.57-384617.1	0.202	DSCT	DSCT	Small Amplitude
1SWASPJ154610.69-384630.2	0.202	DSCT	DSCT	Good
1SWASPJ154759.01+422745.4	0.227	DSCT	DSCT	Good
1SWASPJ155227.96+043413.3	0.249	DSCT	DSCT	Large Scatter
1SWASPJ162546.40+435503.5	0.227	DSCT	DSCT	Good

Object Id	Period (d)	Overall class	Manual class	Confirmed state
1SWASPJ163631.52-335251.1	0.210	DSCT	DSCT	Small Amplitude
1SWASPJ163635.36-335242.6	0.210	DSCT	DSCT	Good
1SWASPJ163637.30-335314.4	0.210	DSCT	DSCT	Good
1SWASPJ164146.37+172104.4	0.204	RRAB	DSCT	Good
1SWASPJ164946.35+420400.3	0.230	DSCT	DSCT	Good
1SWASPJ165209.49+262759.7	0.238	DSCT	DSCT	Good
1SWASPJ171659.17+323346.4	0.248	RRAB	DSCT	Large Scatter
1SWASPJ174001.99+370109.9	0.248	DSCT	DSCT	Large Scatter
1SWASPJ174105.39+375910.8	0.248	DSCT	DSCT	Large Scatter
1SWASPJ174106.93+375316.6	0.248	DSCT	DSCT	Large Scatter
1SWASPJ174134.60+411059.1	0.245	DSCT	DSCT	Good
1SWASPJ174336.84+310314.4	0.249	DSCT	DSCT	Large Scatter
1SWASPJ175134.66+194544.0	0.247	DSCT	DSCT	Good
1SWASPJ175727.24+390841.0	0.207	DSCT	DSCT	Good
1SWASPJ175924.66+120338.4	0.246	DSCT	DSCT	Good
1SWASPJ175956.99+111749.5	0.238	DSCT	DSCT	Good
1SWASPJ185012.68+453544.3	0.204	DSCT	DSCT	Good
1SWASPJ190826.32-321033.1	0.236	DSCT	DSCT	Good
1SWASPJ190830.84-423049.3	0.205	DSCT	DSCT	Good
1SWASPJ191227.54-213041.0	0.236	DSCT	DSCT	Good
1SWASPJ191640.74-433516.5	0.247	DSCT	DSCT	Small Amplitude
1SWASPJ192226.27-223442.5	0.218	DSCT	DSCT	Good
1SWASPJ192920.63+463724.9	0.229	DSCT	DSCT	Good
1SWASPJ194412.97+474144.8	0.248	DSCT	DSCT	Good
1SWASPJ194431.12-205348.2	0.226	DSCT	DSCT	Good
1SWASPJ200236.09-385850.0	0.203	DSCT	DSCT	Good
1SWASPJ200635.46+170920.2	0.228	DSCT	DSCT	Good
1SWASPJ200638.16+092921.3	0.248	DSCT	DSCT	Good
1SWASPJ200759.10+450249.8	0.237	DSCT	DSCT	Good
1SWASPJ202039.28+151431.4	0.249	DSCT	DSCT	Good
1SWASPJ202041.44+151515.1	0.249	DSCT	DSCT	Good
1SWASPJ202849.85+433647.3	0.222	DSCT	DSCT	Good
1SWASPJ203214.75+202914.8	0.249	DSCT	DSCT	Small Amplitude
1SWASPJ204152.15+193327.4	0.202	DSCT	DSCT	Good
1SWASPJ204204.52+104614.4	0.224	DSCT	DSCT	Good
1SWASPJ204443.05-621536.8	0.239	DSCT	DSCT	Good
1SWASPJ205143.90+114506.2	0.225	DSCT	DSCT	Small Amplitude
1SWASPJ205408.55+152807.8	0.221	DSCT	DSCT	Good
1SWASPJ210149.61+001006.0	0.248	DSCT	DSCT	Good
1SWASPJ210150.84+000923.0	0.248	DSCT	DSCT	Good
1SWASPJ210406.00+163325.1	0.236	DSCT	DSCT	Good
1SWASPJ210930.31+101444.4	0.236	DSCT	DSCT	Good
1SWASPJ211949.70+323634.8	0.243	DSCT	DSCT	Good
1SWASPJ212732.38+371940.0	0.227	DSCT	DSCT	Good
1SWASPJ212840.92+290955.1	0.242	DSCT	DSCT	Good
1SWASPJ213229.22+241054.2	0.214	DSCT	DSCT	Good
1SWASPJ213525.51+202832.1	0.249	DSCT	DSCT	Good
1SWASPJ215011.66+283417.3	0.214	DSCT	DSCT	Good
1SWASPJ215724.61-063603.8	0.248	DSCT	DSCT	Good
1SWASPJ215929.03+145817.0	0.206	DSCT	DSCT	Small Amplitude
1SWASPJ222118.51+472016.3	0.228	DSCT	DSCT	Good
1SWASPJ223205.83+394836.0	0.231	DSCT	DSCT	Good
1SWASPJ223307.06+244327.5	0.204	DSCT	DSCT	Good
1SWASPJ225755.39+432721.2	0.244	DSCT	DSCT	Good
1SWASPJ232234.72-092544.1	0.244	DSCT	DSCT	Good

Appendix 31 – RRAB stars selected for the Oosterhoff dichotomy

OoI					
No.	Log(P)	BMA	Object Id	Avg. Dist	Z Dist.
1	-0.25	0.874	1SWASPJ000023.75+361942.7	5610.44	-3323.70
2	-0.27	0.928	1SWASPJ000624.38+170443.3	7056.92	-2072.51
3	-0.31	1.288	1SWASPJ002444.06-014729.9	9670.55	302.36
4	-0.22	0.566	1SWASPJ003604.11+290337.3	4509.19	-2190.26
5	-0.19	0.508	1SWASPJ003604.34-301612.3	9109.46	4591.87
6	-0.25	0.804	1SWASPJ004024.61-213434.2	4434.72	1630.82
7	-0.26	0.942	1SWASPJ004540.89+185702.6	3298.60	-1071.24
8	-0.23	0.816	1SWASPJ004548.19-435509.3	4275.96	2966.00
9	-0.25	0.844	1SWASPJ004929.46+142111.6	8529.28	-2114.40
10	-0.18	0.382	1SWASPJ005009.90+231011.4	6506.74	-2560.13
11	-0.20	0.452	1SWASPJ015226.11-051246.6	5131.78	466.27
12	-0.30	1.220	1SWASPJ021213.38-292251.8	7750.09	3802.32
13	-0.23	0.572	1SWASPJ023835.08+133210.6	10030.32	-2347.71
14	-0.20	0.280	1SWASPJ032208.41-335205.8	3950.11	2201.34
15	-0.19	0.334	1SWASPJ033103.18-452402.8	3606.83	2568.19
16	-0.24	0.832	1SWASPJ043803.45-015943.5	2956.65	102.95
17	-0.17	0.328	1SWASPJ045522.23+395836.5	1492.73	-959.04
18	-0.18	0.262	1SWASPJ045907.96+482128.1	1393.10	-1041.08
19	-0.19	0.260	1SWASPJ063824.27+215711.2	2093.01	-782.47
20	-0.17	0.264	1SWASPJ093040.26+410607.4	6000.69	-3944.87
21	-0.21	0.382	1SWASPJ103311.32-362857.8	6255.01	3719.10
22	-0.24	0.654	1SWASPJ113619.83-023810.7	5332.91	245.29
23	-0.25	0.892	1SWASPJ115400.20-311539.9	3214.29	1668.02
24	-0.24	0.940	1SWASPJ120207.37-123124.7	6245.73	1354.32
25	-0.18	0.304	1SWASPJ120301.09-290316.5	4395.98	2134.88
26	-0.17	0.244	1SWASPJ120409.23-231258.0	11448.83	4513.13
27	-0.20	0.364	1SWASPJ120730.10+074858.4	8677.27	-1180.07
28	-0.24	0.668	1SWASPJ123404.82-413452.8	7490.41	4971.26
29	-0.20	0.640	1SWASPJ124403.23-393505.9	9369.38	5970.37
30	-0.27	1.088	1SWASPJ125455.50+231526.0	5016.23	-1980.71
31	-0.23	0.608	1SWASPJ130350.78+402148.0	4424.15	-2865.22
32	-0.18	0.332	1SWASPJ131045.69-112743.1	7605.07	1511.26
33	-0.19	0.430	1SWASPJ134023.46-372036.1	3276.40	1987.44
34	-0.19	0.488	1SWASPJ134025.55-371938.4	5327.68	3230.53
35	-0.23	0.754	1SWASPJ135203.47+183340.0	12127.16	-3860.27
36	-0.21	0.626	1SWASPJ135459.92-060104.0	2804.10	293.97
37	-0.28	1.024	1SWASPJ140130.13-241717.2	9824.99	4041.27
38	-0.24	0.760	1SWASPJ140155.35+082104.3	12394.87	-1800.24
39	-0.21	0.656	1SWASPJ140453.54-292248.8	7685.91	3770.73
40	-0.21	0.544	1SWASPJ142359.27-360253.5	4402.33	2590.62
41	-0.26	0.890	1SWASPJ144205.65-343804.2	4112.00	2337.01
42	-0.18	0.450	1SWASPJ144630.75-415334.7	3835.35	2561.02
43	-0.23	0.710	1SWASPJ144949.48+401336.9	5306.97	-3427.33
44	-0.23	0.766	1SWASPJ145702.10-264236.8	3452.76	1551.94
45	-0.30	1.254	1SWASPJ145956.57-303824.4	5496.31	2801.16
46	-0.17	0.368	1SWASPJ150018.72-141900.7	4067.97	1005.95
47	-0.21	0.404	1SWASPJ151316.95-144556.0	2033.78	518.34
48	-0.22	0.760	1SWASPJ151823.76-330429.8	6312.15	3444.77
49	-0.22	0.718	1SWASPJ152220.77+291058.5	5790.14	-2823.27
50	-0.27	1.028	1SWASPJ152839.21+050050.6	3568.48	-311.89
51	-0.19	0.372	1SWASPJ152922.80+172947.5	4633.83	-1393.15
52	-0.26	0.958	1SWASPJ155734.35-024006.9	5329.09	248.12

Appendix 31 continued…

OoI					
No.	Log(P)	BMA	Object Id	Avg. Dist	Z Dist.
53	-0.18	0.372	1SWASPJ155804.99-202244.8	5500.72	1915.52
54	-0.28	1.088	1SWASPJ160003.49+345820.8	5030.70	-2883.52
55	-0.23	0.726	1SWASPJ160632.45+181930.6	9082.16	-2855.52
56	-0.23	0.544	1SWASPJ161249.64-343321.8	3343.14	1896.27
57	-0.22	0.654	1SWASPJ161801.06+511152.4	4436.15	-3457.16
58	-0.19	0.276	1SWASPJ161926.32+152255.0	6794.00	-1802.13
59	-0.29	1.176	1SWASPJ162254.03+443941.3	5375.76	-3778.71
60	-0.29	1.162	1SWASPJ165603.46+321603.9	6853.82	-3659.10
61	-0.20	0.438	1SWASPJ165943.87+304935.5	5980.72	-3064.76
62	-0.20	0.620	1SWASPJ170929.44+434523.1	8015.06	-5543.17
63	-0.26	1.018	1SWASPJ171447.83+195701.0	8183.02	-2792.09
64	-0.23	0.586	1SWASPJ175239.91+483702.2	3119.92	-2340.91
65	-0.21	0.320	1SWASPJ190538.40-442154.2	6815.51	4765.59
66	-0.25	0.720	1SWASPJ190715.68-292954.0	7319.08	3603.91
67	-0.20	0.500	1SWASPJ191804.14-245253.2	6999.16	2944.85
68	-0.25	0.914	1SWASPJ192030.25-203254.0	2542.52	892.42
69	-0.21	0.542	1SWASPJ192555.07+542109.6	10281.52	-8354.96
70	-0.24	0.718	1SWASPJ195950.89+005314.2	6873.57	-106.44
71	-0.21	0.408	1SWASPJ200436.88+134316.9	3402.50	-807.08
72	-0.29	1.088	1SWASPJ204042.10-181249.1	5245.90	1639.67
73	-0.18	0.380	1SWASPJ204749.99-271644.6	6092.48	2792.34
74	-0.29	1.186	1SWASPJ205406.76+011537.5	6742.83	-148.32
75	-0.20	0.502	1SWASPJ210004.46-215320.5	3256.91	1214.21
76	-0.24	0.786	1SWASPJ210033.81-034535.3	1981.99	129.97
77	-0.26	0.856	1SWASPJ211204.06-370008.1	5567.35	3350.70
78	-0.27	0.990	1SWASPJ211428.60-291039.4	3524.33	1718.17
79	-0.29	1.120	1SWASPJ212031.55-495916.4	6960.06	5330.77
80	-0.22	0.468	1SWASPJ212033.31+211445.5	3744.10	-1356.76
81	-0.25	1.022	1SWASPJ212159.57-051026.1	4976.62	448.79
82	-0.26	0.762	1SWASPJ212250.94-620625.5	4280.57	3783.27
83	-0.26	1.022	1SWASPJ212544.55-054801.0	3440.85	347.74
84	-0.22	0.648	1SWASPJ212749.95+133039.7	5045.81	-1178.86
85	-0.29	1.132	1SWASPJ212839.96-362143.7	10332.51	6126.00
86	-0.27	0.992	1SWASPJ213212.69-374418.0	7148.61	4375.36
87	-0.24	0.704	1SWASPJ213530.97-390630.5	6885.17	4343.11
88	-0.21	0.586	1SWASPJ213555.79-365240.9	5244.37	3147.21
89	-0.22	0.604	1SWASPJ213653.21+015847.0	4064.82	-140.42
90	-0.25	0.784	1SWASPJ213943.36-305338.4	3547.88	1821.66
91	-0.25	0.958	1SWASPJ214652.64+244315.0	3143.26	-1314.51
92	-0.29	1.200	1SWASPJ215514.55-352203.0	6193.40	3584.85
93	-0.28	1.118	1SWASPJ220007.71+075053.0	8509.85	-1162.00
94	-0.28	0.960	1SWASPJ220048.76-383717.8	6062.14	3783.83
95	-0.28	1.142	1SWASPJ220703.97-444926.6	9051.32	6380.57
96	-0.29	1.120	1SWASPJ222024.36-260809.5	4755.96	2095.02
97	-0.28	1.018	1SWASPJ222502.50-045656.0	4277.67	369.02
98	-0.30	1.256	1SWASPJ222721.53+164816.8	2212.31	-639.60
99	-0.23	0.838	1SWASPJ230747.55-330219.7	3765.60	2053.03
100	-0.20	0.310	1SWASPJ232030.71-144757.0	2897.90	740.22

Appendix 31 continued...

OoII					
No.	Log(P)	BMA	Object Id	Avg. Dist	Z Dist.
101	-0.16	0.658	1SWASPJ010449.87+051721.8	9066.78	-835.83
102	-0.11	0.328	1SWASPJ011436.94-083106.7	7338.50	1087.04
103	-0.24	1.210	1SWASPJ012712.94+481330.5	7654.50	-5708.48
104	-0.15	0.620	1SWASPJ031149.91-112025.8	1379.75	271.31
105	-0.15	0.574	1SWASPJ031152.10-112114.0	719.07	141.56
106	-0.17	0.810	1SWASPJ042145.58+340411.4	3561.23	-1995.01
107	-0.17	0.796	1SWASPJ042319.15+441412.9	1345.09	-938.37
108	-0.22	1.036	1SWASPJ052619.78+474038.7	8390.27	-6203.48
109	-0.14	0.488	1SWASPJ061559.88+234451.0	677.82	-272.96
110	-0.18	0.820	1SWASPJ075357.89+531005.6	5906.93	-4727.90
111	-0.24	1.198	1SWASPJ084658.96+294928.3	4564.44	-2270.11
112	-0.12	0.338	1SWASPJ104643.79-150507.9	6853.31	1783.66
113	-0.20	0.898	1SWASPJ105456.88-064656.3	8705.79	1028.13
114	-0.16	0.718	1SWASPJ110823.07-162554.2	4150.34	1174.02
115	-0.13	0.488	1SWASPJ112154.05-135906.3	5762.72	1392.68
116	-0.12	0.338	1SWASPJ114414.73+432241.2	7313.10	-5022.71
117	-0.13	0.416	1SWASPJ115334.83-075606.8	2680.23	370.01
118	-0.19	0.862	1SWASPJ115706.89-393131.0	5777.16	3676.70
119	-0.11	0.372	1SWASPJ115838.48-080806.3	8444.82	1195.01
120	-0.20	0.934	1SWASPJ122821.44-401722.7	8397.78	5430.45
121	-0.23	1.176	1SWASPJ123245.62+270145.4	1525.14	-693.09
122	-0.15	0.656	1SWASPJ123754.99-284932.1	7031.82	3390.36
123	-0.13	0.494	1SWASPJ124351.22-012314.0	7604.66	184.10
124	-0.15	0.636	1SWASPJ130724.61-235422.3	6248.55	2532.17
125	-0.11	0.312	1SWASPJ134005.61-372611.6	2470.33	1501.67
126	-0.13	0.404	1SWASPJ135722.58-080409.6	9227.21	1295.25
127	-0.11	0.336	1SWASPJ140945.10-423358.1	4575.69	3095.18
128	-0.23	1.150	1SWASPJ141939.22+254724.3	6330.19	-2754.11
129	-0.25	1.306	1SWASPJ141942.13-302804.5	7659.36	3883.72
130	-0.22	1.044	1SWASPJ142148.43+030135.4	9326.37	-492.41
131	-0.17	0.600	1SWASPJ143947.53-040805.5	2797.43	201.71
132	-0.14	0.410	1SWASPJ144042.42-315915.8	3275.89	1735.36
133	-0.12	0.462	1SWASPJ144225.44+110150.3	4200.77	-803.75
134	-0.12	0.390	1SWASPJ151027.20+294300.1	6753.06	-3347.57
135	-0.18	0.658	1SWASPJ151922.46-051714.9	3914.42	360.73
136	-0.19	0.784	1SWASPJ152040.28-221808.6	2855.80	1083.76
137	-0.10	0.282	1SWASPJ152257.73-360508.9	4603.83	2711.64
138	-0.23	1.210	1SWASPJ152559.01-204022.1	9099.51	3212.41
139	-0.11	0.404	1SWASPJ154046.17-100814.5	6191.45	1089.75
140	-0.14	0.550	1SWASPJ154548.14-303113.6	8674.88	4405.51
141	-0.14	0.528	1SWASPJ161011.29-241053.9	5371.46	2200.31
142	-0.17	0.634	1SWASPJ162558.65+174252.1	5040.81	-1533.79
143	-0.18	0.754	1SWASPJ165324.14+491257.7	8145.15	-6167.33
144	-0.15	0.458	1SWASPJ165604.57+245933.5	4363.64	-1843.64
145	-0.20	0.992	1SWASPJ170050.39+194347.3	4114.11	-1388.86
146	-0.17	0.782	1SWASPJ170703.15+321635.1	9596.55	-5124.60
147	-0.17	0.686	1SWASPJ171435.35+222341.9	6428.07	-2449.03
148	-0.20	0.876	1SWASPJ173546.47+152936.2	9454.58	-2525.58
149	-0.25	1.278	1SWASPJ173709.06+374245.7	4584.96	-2804.63
150	-0.22	0.946	1SWASPJ173811.32+185317.2	4519.95	-1463.20
151	-0.26	1.330	1SWASPJ174731.59+164949.4	4717.91	-1366.02
152	-0.17	0.624	1SWASPJ180223.14+080139.8	5692.01	-794.90

Appendix 31 continued…

OoII					
No.	Log(P)	BMA	Object Id	Avg. Dist	Z Dist.
153	-0.23	1.112	1SWASPJ190145.28+421435.0	8900.56	-5983.65
154	-0.13	0.450	1SWASPJ190424.84-352914.0	4616.30	2679.86
155	-0.19	0.834	1SWASPJ192053.31-385706.2	7055.16	4435.33
156	-0.18	0.892	1SWASPJ192629.00-432356.0	5764.91	3960.92
157	-0.24	1.186	1SWASPJ193522.49-315835.7	3624.97	1919.69
158	-0.14	0.560	1SWASPJ194645.90-305617.1	5364.17	2757.78
159	-0.18	0.756	1SWASPJ194840.71-290307.9	5220.48	2535.10
160	-0.13	0.456	1SWASPJ200007.40+060632.2	4199.49	-446.91
161	-0.13	0.446	1SWASPJ200008.04+060641.4	3995.24	-425.35
162	-0.17	0.722	1SWASPJ200728.30-434950.2	4379.85	3033.17
163	-0.10	0.362	1SWASPJ201026.16-600814.2	4836.34	4194.18
164	-0.16	0.716	1SWASPJ202240.37-552744.7	4373.42	3602.62
165	-0.15	0.518	1SWASPJ202517.69-425505.5	6744.32	4592.57
166	-0.19	0.914	1SWASPJ203524.18-254301.7	5764.50	2501.38
167	-0.14	0.522	1SWASPJ204539.90-143913.6	9713.26	2457.24
168	-0.17	0.774	1SWASPJ210140.48-385855.5	6260.14	3938.12
169	-0.24	1.196	1SWASPJ210346.68-535356.5	5755.79	4650.56
170	-0.15	0.682	1SWASPJ210720.59-085004.1	5643.70	866.76
171	-0.15	0.566	1SWASPJ211154.51+225509.8	6293.00	-2450.72
172	-0.22	1.092	1SWASPJ212013.38-210420.1	2563.75	921.79
173	-0.20	1.016	1SWASPJ212148.82-003636.6	6210.70	66.14
174	-0.18	0.692	1SWASPJ212516.69-413643.3	8114.23	5388.52
175	-0.21	1.020	1SWASPJ213047.81-075924.4	7632.03	1060.87
176	-0.21	0.986	1SWASPJ213819.57+100010.8	15410.26	-2676.76
177	-0.23	1.086	1SWASPJ214215.40-482620.8	9811.79	7341.68
178	-0.18	0.754	1SWASPJ214306.37+080331.9	4965.90	-696.17
179	-0.19	0.770	1SWASPJ214440.94+181417.8	6101.69	-1909.64
180	-0.21	1.040	1SWASPJ214619.44-425048.9	3038.79	2066.50
181	-0.23	1.126	1SWASPJ220421.42-452505.1	5046.19	3594.14
182	-0.17	0.694	1SWASPJ220935.39-402550.6	10162.17	6590.45
183	-0.20	0.920	1SWASPJ221203.02-084545.6	4639.15	706.74
184	-0.16	0.520	1SWASPJ221211.60-163433.7	13588.49	3876.62
185	-0.16	0.578	1SWASPJ221329.19-404331.5	3260.95	2127.56
186	-0.16	0.616	1SWASPJ221611.32+262739.4	7415.25	-3304.15
187	-0.21	1.062	1SWASPJ221742.14+064359.8	6564.31	-769.65
188	-0.18	0.836	1SWASPJ222000.85-182240.2	9880.24	3115.07
189	-0.21	1.030	1SWASPJ222620.21-405928.1	6119.39	4013.97
190	-0.22	1.136	1SWASPJ223338.68-333523.8	6626.62	3666.15
191	-0.13	0.338	1SWASPJ224145.16+370716.1	2330.35	-1406.37
192	-0.15	0.622	1SWASPJ225255.83+291517.4	6081.04	-2971.77
193	-0.22	1.058	1SWASPJ225629.65-273915.8	6883.46	3194.87
194	-0.15	0.606	1SWASPJ230920.88+010557.8	8117.18	-155.74
195	-0.15	0.488	1SWASPJ231802.34+484658.3	1006.09	-756.80
196	-0.22	1.070	1SWASPJ232007.02+160406.9	1534.91	-424.85
197	-0.20	0.878	1SWASPJ232218.02-420524.0	2849.92	1910.29
198	-0.18	0.804	1SWASPJ233217.76-172348.6	2594.39	775.69
199	-0.14	0.448	1SWASPJ234023.78-154507.7	4488.20	1218.44
200	-0.13	0.534	1SWASPJ234855.86-414045.7	6138.97	4082.18

Appendix 32 – RRAB stars showing Blazhko effect

Known Blazhko effect - confirmed	
Known in SIMBAD and GCVS	
Object Id	GCVS Name
1SWASPJ003338.28-152914.7	RX Cet
1SWASPJ010510.70+341306.2	DR And
1SWASPJ014535.00+312249.8	UX Tri
1SWASPJ020751.97-265157.7	SS For
1SWASPJ031113.21-262858.8	RX For
1SWASPJ040638.89+552959.6	AH Cam
1SWASPJ041116.80-135054.0	XY Eri
1SWASPJ045314.41-374915.8	U Cae
1SWASPJ061314.73-371500.6	RX Col
1SWASPJ091348.80-091908.8	SZ Hya
1SWASPJ091906.03+290356.0	RW Cnc
1SWASPJ093629.77+040640.7	UU Hya
1SWASPJ114856.21-102628.4	X Crt
1SWASPJ120447.27-274043.2	IK Hya
1SWASPJ121346.95+305907.6	TU Com
1SWASPJ123030.50-260251.1	SV Hya
1SWASPJ124945.38+434625.2	Z CVn
1SWASPJ132333.32-163957.8	AM Vir
1SWASPJ134815.94+395403.0	SS CVn
1SWASPJ142734.95+360244.6	SW Boo
1SWASPJ142739.07-005405.9	ST Vir
1SWASPJ150923.77-481937.1	FU Lup
1SWASPJ153039.23+354704.3	ST Boo
1SWASPJ153330.81+024637.9	AR Ser
1SWASPJ163531.60+575023.1	RW Dra
1SWASPJ172022.44+143039.1	DL Her
1SWASPJ175944.23+515301.7	AV Dra
1SWASPJ181953.81+315854.7	MW Lyr
1SWASPJ190942.60+645132.1	XZ Dra
1SWASPJ193229.30+562317.5	XZ Cyg
1SWASPJ210128.87-151346.1	RV Cap
1SWASPJ215158.43-455906.3	RT Gru
1SWASPJ225301.03+154716.6	BH Peg
1SWASPJ231312.52+365404.4	GV And

WASP object shows Blazhko effect	
Known in SIMBAD and GCVS	
Object Id	GCVS Name
1SWASPJ000003.66+352146.1	GM And
1SWASPJ000035.58+263949.6	GV Peg
1SWASPJ000248.10-245643.1	RU Scl
1SWASPJ030830.88+102645.2	X Ari
1SWASPJ030904.77+531136.2	TU Per
1SWASPJ115507.14-443134.0	KW Cen
1SWASPJ125245.86-101536.4	AS Vir
1SWASPJ141539.60-253957.3	GS Hya
1SWASPJ142809.81+063243.9	AF Vir
1SWASPJ144600.67-285133.9	HO Hya
1SWASPJ154330.77-292201.5	CU Lib
1SWASPJ163818.04+374804.8	GY Her
1SWASPJ170539.90+213058.5	V0365 Her
1SWASPJ171450.69+415122.7	V0759 Her
1SWASPJ174543.74+111956.0	V0869 Oph
1SWASPJ191420.77-305220.3	V0871 Sgr
1SWASPJ200911.06-414951.1	V2239 Sgr
1SWASPJ224445.87-422142.3	WZ Gru
1SWASPJ224553.07+240837.0	BF Peg
1SWASPJ233656.58-372219.3	AK Scl

WASP object shows Blazhko effect	
Known in SIMBAD (not GCVS)	
Object Id	
1SWASPJ004753.93+114216.7	
1SWASPJ004757.06+114223.5	
1SWASPJ010949.43-441853.3	
1SWASPJ012848.26-112712.6	
1SWASPJ030830.17+102623.3	
1SWASPJ034307.03-192624.4	
1SWASPJ040010.75-194936.9	
1SWASPJ090448.55+053008.1	
1SWASPJ112541.38-013001.7	
1SWASPJ112613.77-140439.7	
1SWASPJ112613.84-140407.5	
1SWASPJ113218.92+031713.3	
1SWASPJ125245.27-101613.9	
1SWASPJ132922.47-055259.2	
1SWASPJ143927.36-032736.7	
1SWASPJ143947.53-040805.5	
1SWASPJ145315.45-143556.4	
1SWASPJ151157.68-165203.6	
1SWASPJ151316.95-144556.0	
1SWASPJ152153.11-120646.2	
1SWASPJ155229.33+100834.1	
1SWASPJ161255.64-082727.6	
1SWASPJ170641.06+154032.5	
1SWASPJ171245.62+322540.1	
1SWASPJ172811.65+382218.6	
1SWASPJ181953.34+191601.8	
1SWASPJ195958.34-392254.6	
1SWASPJ204315.74-090928.4	
1SWASPJ212258.23+235304.4	
1SWASPJ212433.22-571203.9	
1SWASPJ221822.47+220810.5	
1SWASPJ224441.55-315807.2	
1SWASPJ225519.22+174459.6	
1SWASPJ231039.05-033628.0	
1SWASPJ231549.92-290012.7	
1SWASPJ231806.60+155258.7	
1SWASPJ232030.71-144757.0	
1SWASPJ234158.75+181301.5	

WASP object shows Blazhko effect	
Unknown	
Object Id	
1SWASPJ000157.75-364042.4	
1SWASPJ000409.77-410810.8	
1SWASPJ000551.77+424258.3	
1SWASPJ000823.86+263323.3	
1SWASPJ031112.59-262823.4	
1SWASPJ041115.24-445028.3	
1SWASPJ044849.38-372825.9	
1SWASPJ051511.77-352335.3	
1SWASPJ091348.03-091944.6	
1SWASPJ093657.67-133711.9	
1SWASPJ142548.41-300214.0	
1SWASPJ150526.03-191503.5	
1SWASPJ152058.03-324518.9	
1SWASPJ154343.80-304722.4	
1SWASPJ182910.98+210432.3	
1SWASPJ192157.17-432820.4	
1SWASPJ192818.86-415115.7	
1SWASPJ192931.53+445623.8	
1SWASPJ195348.19-335546.2	
1SWASPJ204431.46-342324.4	
1SWASPJ211437.86+073728.1	
1SWASPJ213502.37+195628.0	
1SWASPJ213807.29+272659.7	
1SWASPJ215709.65-294303.3	
1SWASPJ222220.80-343007.9	
1SWASPJ224621.78-125522.2	
1SWASPJ224624.44-125447.1	
1SWASPJ235643.15+490916.8	

Known Blazhko effect - Not confirmed	
Known in SIMBAD and GCVS	
Object Id	GCVS Name
1SWASPJ002343.08+292403.6	SW And
1SWASPJ004119.42+052046.8	SW Psc
1SWASPJ012642.43+340407.1	XY And
1SWASPJ040327.05+475952.0	FM Per
1SWASPJ043442.90+214621.9	BR Tau
1SWASPJ092741.34+365822.5	Y LMi
1SWASPJ110505.30+232109.0	AH Leo
1SWASPJ130507.98+231642.2	RY Com
1SWASPJ143333.21+314516.6	RS Boo
1SWASPJ190827.29+384846.2	NR Lyr
1SWASPJ191800.43+504518.0	V1104 Cyg
1SWASPJ205229.63+222552.6	FK Vul
1SWASPJ212111.54+321128.7	DM Cyg
1SWASPJ222721.53+164816.8	AE Peg

Appendix 33 – Difference of the amplitudes in Blazhko stars

SuperWASP Object Id	Known Blazhko	Flux		Magnitude (Vmag)		
		Min. flux	Max. flux	Max. Mag.	Min. Mag.	Mag. Diff.
1SWASPJ003338.28-152914.7	Yes	32.0	43.0	11.24	10.92	0.32
1SWASPJ010510.70+341306.2	Yes	13.0	21.0	12.22	11.69	0.52
1SWASPJ014535.00+312249.8	Yes	5.2	8.6	13.21	12.66	0.55
1SWASPJ020751.97-265157.7	Yes	140.0	190.0	9.63	9.30	0.33
1SWASPJ031113.21-262858.8	Yes	20.0	28.0	11.75	11.38	0.37
1SWASPJ040638.89+552959.6	Yes	20.0	30.5	11.75	11.29	0.46
1SWASPJ041116.80-135054.0	Yes	9.0	19.0	12.61	11.80	0.81
1SWASPJ045314.41-374915.8	Yes	22.0	30.0	11.64	11.31	0.34
1SWASPJ061314.73-371500.6	Yes	8.4	11.6	12.69	12.34	0.35
1SWASPJ091348.80-091908.8	Yes	40.0	64.0	10.99	10.48	0.51
1SWASPJ091906.03+290356.0	Yes	17.0	23.0	11.92	11.60	0.33
1SWASPJ093629.77+040640.7	Yes	20.0	28.0	11.75	11.38	0.37
1SWASPJ114856.21-102628.4	Yes	36.0	38.0	11.11	11.05	0.06
1SWASPJ120447.27-274043.2	Yes	100.0	170.0	10.00	9.42	0.58
1SWASPJ121346.95+305907.6	Yes	3.8	6.0	13.55	13.05	0.50
1SWASPJ123030.50-260251.1	Yes	110.0	150.0	9.90	9.56	0.34
1SWASPJ124945.38+434625.2	Yes	20.0	32.0	11.75	11.24	0.51
1SWASPJ132333.32-163957.8	Yes	32.0	40.0	11.24	10.99	0.24
1SWASPJ134815.94+395403.0	Yes	30.0	54.0	11.31	10.67	0.64
1SWASPJ142734.95+360244.6	Yes	16.0	23.0	11.99	11.60	0.39
1SWASPJ142739.07-005405.9	Yes	50.0	66.0	10.75	10.45	0.30
1SWASPJ150923.77-431937.1	Yes	7.5	12.0	12.81	12.30	0.51
1SWASPJ153039.23+354704.3	Yes	75.0	90.0	10.31	10.11	0.20
1SWASPJ153330.81+024637.9	Yes	25.0	30.0	11.51	11.31	0.20
1SWASPJ163531.60+575023.1	Yes	30.0	50.0	11.31	10.75	0.55
1SWASPJ172022.44+143039.1	Yes	20.0	26.0	11.75	11.46	0.28
1SWASPJ175944.23+515301.7	Yes	7.5	11.0	12.81	12.40	0.42
1SWASPJ181953.81+315854.7	Yes	8.5	11.0	12.68	12.40	0.28
1SWASPJ190942.60+645132.1	Yes	100.0	135.0	10.00	9.67	0.33
1SWASPJ193229.30+562317.5	Yes	175.0	275.0	9.39	8.90	0.49
1SWASPJ210128.87-151346.1	Yes	65.0	85.0	10.47	10.18	0.29
1SWASPJ215158.43-455906.3	Yes	11.0	15.0	12.40	12.06	0.34
1SWASPJ225301.03+154716.6	Yes	80.0	105.0	10.24	9.95	0.30
1SWASPJ231312.52+365404.4	Yes	3.6	6.5	13.61	12.97	0.64
1SWASPJ000003.66+352146.1	No	8.5	11.0	12.68	12.40	0.28
1SWASPJ000035.58+263949.6	No	5.4	9.4	13.17	12.57	0.60
1SWASPJ000248.10-245643.1	No	155.0	185.0	9.52	9.33	0.19
1SWASPJ030830.88+102645.2	No	190.0	230.0	9.30	9.10	0.21
1SWASPJ030904.77+531136.2	No	15.0	19.0	12.06	11.80	0.26
1SWASPJ115507.14-443134.0	No	4.0	5.8	13.49	13.09	0.40
1SWASPJ125245.86-101536.4	No	24.0	42.0	11.55	10.94	0.61
1SWASPJ141539.60-253957.3	No	12.0	17.0	12.30	11.92	0.38
1SWASPJ142809.81+063243.9	No	44.0	64.0	10.89	10.48	0.41
1SWASPJ144600.67-285133.9	No	6.0	8.4	13.05	12.69	0.37
1SWASPJ154330.77-292201.5	No	6.0	10.0	13.05	12.50	0.55
1SWASPJ163818.04+374804.8	No	14.5	25.0	12.10	11.51	0.59
1SWASPJ170539.90+213058.5	No	5.0	8.8	13.25	12.64	0.61
1SWASPJ171450.69+415122.7	No	2.5	5.5	14.01	13.15	0.86
1SWASPJ174543.74+111956.0	No	10.5	13.5	12.45	12.17	0.27
1SWASPJ191420.77-305220.3	No	4.0	5.2	13.49	13.21	0.28
1SWASPJ200911.06-414951.1	No	6.0	9.0	13.05	12.61	0.44

Appendix 33 continued…

SuperWASP Object Id	Known Blazhko	Flux		Magnitude (Vmag)		
		Min. flux	Max. flux	Max. Mag.	Min. Mag.	Mag. Diff.
1SWASPJ224445.87-422142.3	No	4.0	6.0	13.49	13.05	0.44
1SWASPJ224553.07+240837.0	No	9.0	14.0	12.61	12.13	0.48
1SWASPJ233656.58-372219.3	No	5.5	8.5	13.15	12.68	0.47
1SWASPJ004753.93+114216.7	No	15.0	22.0	12.06	11.64	0.42
1SWASPJ004757.06+114223.5	No	20.0	34.0	11.75	11.17	0.58
1SWASPJ010949.43-441853.3	No	7.0	10.5	12.89	12.45	0.44
1SWASPJ012848.26-112712.6	No	7.0	11.0	12.89	12.40	0.49
1SWASPJ030830.17+102623.3	No	170.0	210.0	9.42	9.19	0.23
1SWASPJ034307.03-192624.4	No	4.0	5.8	13.49	13.09	0.40
1SWASPJ040010.75-194936.9	No	10.0	14.5	12.50	12.10	0.40
1SWASPJ090448.55+053008.1	No	10.0	16.0	12.50	11.99	0.51
1SWASPJ112541.38-013001.7	No	4.0	6.5	13.49	12.97	0.53
1SWASPJ112613.77-140439.7	No	8.0	12.0	12.74	12.30	0.44
1SWASPJ112613.84-140407.5	No	9.0	13.0	12.61	12.22	0.40
1SWASPJ113218.92+031713.3	No	90.0	175.0	10.11	9.39	0.72
1SWASPJ125245.27-101613.9	No	18.0	30.0	11.86	11.31	0.55
1SWASPJ132922.47-055259.2	No	25.0	40.0	11.51	10.99	0.51
1SWASPJ143927.36-032736.7	No	10.0	15.0	12.50	12.06	0.44
1SWASPJ143947.53-040805.5	No	7.0	10.0	12.89	12.50	0.39
1SWASPJ145315.45-143556.4	No	8.0	13.0	12.74	12.22	0.53
1SWASPJ151157.68-165203.6	No	3.6	5.6	13.61	13.13	0.48
1SWASPJ151316.95-144556.0	No	11.2	15.0	12.38	12.06	0.32
1SWASPJ152153.11-120646.2	No	8.0	15.5	12.74	12.02	0.72
1SWASPJ155229.33+100834.1	No	9.0	18.0	12.61	11.86	0.75
1SWASPJ161255.64-082727.6	No	5.0	13.0	13.25	12.22	1.04
1SWASPJ170641.06+154032.5	No	3.8	4.8	13.55	13.30	0.25
1SWASPJ171245.62+322540.1	No	2.8	5.0	13.88	13.25	0.63
1SWASPJ172811.65+382218.6	No	2.6	3.8	13.96	13.55	0.41
1SWASPJ181953.34+191601.8	No	1.2	2.6	14.80	13.96	0.84
1SWASPJ195958.34-392254.6	No	2.2	4.0	14.14	13.49	0.65
1SWASPJ204315.74-090928.4	No	4.6	8.4	13.34	12.69	0.65
1SWASPJ212258.23+235304.4	No	3.2	5.0	13.74	13.25	0.48
1SWASPJ212433.22-571203.9	No	4.0	9.5	13.49	12.56	0.94
1SWASPJ221822.47+220810.5	No	5.0	7.4	13.25	12.83	0.43
1SWASPJ224441.55-315807.2	No	5.5	9.0	13.15	12.61	0.53
1SWASPJ225519.22+174459.6	No	2.4	4.2	14.05	13.44	0.61
1SWASPJ231039.05-033628.0	No	3.6	6.2	13.61	13.02	0.59
1SWASPJ231549.92-230012.7	No	8.5	14.0	12.68	12.13	0.54
1SWASPJ231806.60+155258.7	No	8.5	11.5	12.68	12.35	0.33
1SWASPJ232030.71-144757.0	No	6.5	10.5	12.97	12.45	0.52
1SWASPJ234158.75+181301.5	No	11.0	17.5	12.40	11.89	0.50
1SWASPJ000157.75-364042.4	No	3.4	5.0	13.67	13.25	0.42
1SWASPJ000409.77-410810.8	No	2.4	4.0	14.05	13.49	0.55
1SWASPJ000551.77+424258.3	No	3.0	4.8	13.81	13.30	0.51
1SWASPJ000823.86+263323.3	No	2.4	3.8	14.05	13.55	0.50
1SWASPJ031112.59-262823.4	No	15.0	24.0	12.06	11.55	0.51
1SWASPJ041115.24-445028.3	No	1.0	2.5	15.00	14.01	0.99
1SWASPJ044849.98-372825.9	No	2.0	3.6	14.25	13.61	0.64
1SWASPJ051511.77-352335.3	No	9.0	18.0	12.61	11.86	0.75
1SWASPJ091348.03-091944.6	No	30.0	54.0	11.31	10.67	0.64
1SWASPJ093657.67-133711.9	No	2.2	4.0	14.14	13.49	0.65

Appendix 33 continued...

SuperWASP Object Id	Known Blazhko	Flux		Magnitude (Vmag)		
		Min. flux	Max. flux	Max. Mag.	Min. Mag.	Mag. Diff.
1SWASPJ142548.41-300214.0	No	3.6	8.0	13.61	12.74	0.87
1SWASPJ150526.03-191503.5	No	0.9	3.6	15.11	13.61	1.51
1SWASPJ152058.03-324518.9	No	1.2	3.0	14.80	13.81	0.99
1SWASPJ154343.80-304722.4	No	2.5	3.8	14.01	13.55	0.45
1SWASPJ182910.98+210432.3	No	24.0	29.0	11.55	11.34	0.21
1SWASPJ192157.17-432820.4	No	14.0	17.0	12.13	11.92	0.21
1SWASPJ192818.86-415115.7	No	2.8	4.2	13.88	13.44	0.44
1SWASPJ192931.53+445623.8	No	15.2	17.4	12.05	11.90	0.15
1SWASPJ195348.19-335546.2	No	2.8	4.5	13.88	13.37	0.52
1SWASPJ204431.46-342324.4	No	6.5	9.4	12.97	12.57	0.40
1SWASPJ211437.86+073728.1	No	3.4	5.4	13.67	13.17	0.50
1SWASPJ213502.37+195628.0	No	11.5	14.5	12.35	12.10	0.25
1SWASPJ213807.29+272659.7	No	3.2	4.2	13.74	13.44	0.30
1SWASPJ215709.65-294303.3	No	3.0	7.0	13.81	12.89	0.92
1SWASPJ222220.80-343007.9	No	2.6	4.0	13.96	13.49	0.47
1SWASPJ224621.78-125522.2	No	4.6	7.0	13.34	12.89	0.46
1SWASPJ224624.44-125447.1	No	11.0	16.0	12.40	11.99	0.41
1SWASPJ235643.15+490916.8	No	1.0	1.7	15.00	14.42	0.58
				Minimum		0.06
				Maximum		1.51
				Mean		0.49
				Median		0.51
				Mode		0.47

---------- The End ----------